MEDICAL RADIOLOGY

Diagnostic Imaging

A. L. Baert
M. Knauth

Head and Neck Cancer Imaging

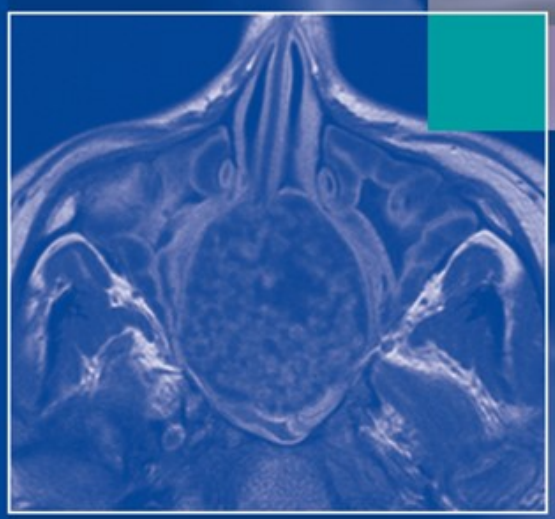

R. Hermans
Editor

Springer

MEDICAL RADIOLOGY
Diagnostic Imaging

Softcover Edition

Editors:
A.L. Baert, Leuven
L.W. Brady, Philadelphia
H.-P. Heilmann, Hamburg
M. Knauth, Göttingen
M. Molls, Munich
C. Nieder, Bodø
K. Sartor, Heidelberg

Robert Hermans (Ed.)

Head and Neck Cancer Imaging

With Contributions by

C. Castaigne · J. A. Castelijns · V. F. H. Chong · E. E. Coche · F. De Keyzer · P. R. Delaere
F. Dubrulle · T. Duprez · D. Farina · P. Flamen · R. L. M. Haas · R. Hermans · M. Keberle
K. Muylle · S. Nuyts · F. A. Pameijer · S. Robinson · I. M. Schmalfuss · R. Souillard
M. W. M. van den Brekel · V. Vandecaveye · V. Vander Poorten

Foreword by
A. L. Baert

With 353 Figures in 665 Separate Illustrations, 52 in Color and 30 Tables

Springer

Robert Hermans, MD, PhD
Professor, Department of Radiology
University Hospitals Leuven
Herestraat 49
3000 Leuven
Belgium

Medical Radiology · Diagnostic Imaging and Radiation Oncology
Series Editors: A. L. Baert · L. W. Brady · H.-P. Heilmann · M. Knauth · M. Molls
C. Nieder · K. Sartor

Continuation of Handbuch der medizinischen Radiologie
Encyclopedia of Medical Radiology

ISBN 978-3-540-68439-8 eISBN 978-3-540-33066-0
DOI 10.1007/978-3-540-33066-0

Hard cover, alk. paper: ISBN 978-3-540-22027-5

Library of Congress Control Number: 2005930273

© Springer-Verlag Berlin Heidelberg 2006, 2008

This work is subject to copyright. All rights are reserved, whether the whole or part of the material is concerned, specifically the rights of translation, reprinting, reuse of illustrations, recitations, broadcasting, reproduction on microfilm or in any other way, and storage in data banks. Duplication of this publication or parts thereof is permitted only under the provisions of the German Copyright Law of September 9, 1965, in its current version, and permission for use must always be obtained from Springer-Verlag. Violations are liable for prosecution under the German Copyright Law.

The use of general descriptive names, trademarks, etc. in this publication does not imply, even in the absence of a specific statement, that such names are exempt from the relevant protective laws and regulations and therefore free for general use.

Product liability: The publishers cannot guarantee the accuracy of any information about dosage and application contained in this book. In every case the user must check such information by consulting the relevant literature.

Medical Editor: Dr. Ute Heilmann, Heidelberg
Desk Editor: Ursula N. Davis, Heidelberg
Cover-Design and Typesetting: Verlagsservice Teichmann, Mauer

Printed on acid-free paper

5 4 3 2 1 0

springer.com

To my wife, *Isabelle*

And our children,
Simon, Lies, Thomas and *Tim*

Bob Hermans

Foreword

Progress in the management of cancer in the head and neck region depends to a great extent on the results from surgery or radiotherapy or a combination of both techniques. The successful outcome of these treatment modalities, however, will be largely determined by the precise choice of indications and judicious selection of the patients to be treated based on the nature of the lesion, its local extension and the stage of the tumor.

The role of the radiologist is of primordial importance in this respect. Indeed, mature, sophisticated imaging techniques such as multidetector CT, MRI and PET-CT are now available allowing exquisite morphological display of the extent of the disease in the head and neck region. The radiologist will thus be able to fully assume her/his role as a key member of the multidisciplinary team responsible for the global treatment strategy and the management of the patient with head and neck cancer.

This volume offers a comprehensive, detailed, up-to-date review of our current knowledge in the field. The eminently readable text is complemented by numerous and superb illustrations.

The editor, R. Hermans, of the radiological department at Leuven University, is a very well known and internationally recognized expert in head and neck radiology who has published widely, especially in the field of head and neck oncology. The authors of the individual chapters were invited to contribute because of their outstanding personal experience in a specific anatomic area and their major contributions to the radiological literature on the topic.

I would like to thank the editor and the authors and to congratulate them most sincerely for their superb efforts which have resulted in this excellent volume.

This book will be of great interest not only for general and specialized neuro- or head and neck radiologists but also for oncologists and ENT surgeons. I am confident that it will meet the same success with the readers as the previous volumes published in this series.

Leuven

Albert L. Baert

Preface

"To teach is to learn twice"
Joseph Joubert
(French philosopher, 1754-1824)

The head and neck is a region of considerable anatomical and functional complexity, making the accurate staging of a head and neck neoplasm a challenging task. The clinician often detects pathology, but may not appreciate, based on the physical examination, the entire submucosal tumor extension, nor the possible regional and distant disease spread.

The introduction of CT and MRI has revolutionized head and neck radiology. Current radiological modalities provide a reliable visualization of the head and neck structures to an unprecedented level of detail. If carefully performed and interpreted, modern radiological techniques allow a comprehensive evaluation of the extent of pathological processes.

The technological evolution has made the radiologist an important member of the multidisciplinary team managing head and neck cancer patients. Recent and ongoing research is enforcing the impact of imaging in oncologic patient care. These new developments are not only focusing on technical advances, such as PET-CT or diffusion-weighted MRI. The added value of existing imaging techniques in treatment choice and in monitoring tumor response to treatment is now also scientifically established.

This purpose of this book is to provide a comprehensive review of state-of-the-art head and neck cancer imaging. Several distinguished head and neck radiologists have contributed to this book, allowing full coverage of advanced imaging in the head and neck cancer patient.

Clinical-diagnostic techniques, as well as therapeutic strategies, have also seen significant changes over the past years; in this regard I would like to thank my fellow clinicians from Leuven who contributed to this book. Care has been taken to explain the role of imaging within these developments.

The ultimate goal of all medical intervention is to provide our patients with the best possible care for their health problems. Hopefully, this book contributes to achieving this purpose.

Leuven

Robert Hermans

Contents

1 Introduction: Epidemiology, Risk Factors, Pathology, and Natural History of Head and Neck Neoplasms

Vincent Vander Poorten

CONTENTS

The most frequent malignant head and neck neoplasms can be grouped under two major headings. The most abundant are the epithelial malignancies of the mucous membranes of the upper aerodigestive tract, so-called head and neck squamous cell carcinoma (HNSCC), accounting for about 90% of all head and neck neoplasms (Greenlee et al. 2001). The second largest group of neoplasms can be described as "glandular neoplasms", the majority arising in the thyroid, a minority in the salivary glands.

Skin cancer is generally considered a separate entity, and so is skin cancer of the head and neck, mainly including squamous cell carcinoma and basal cell carcinoma. Less frequent head and neck neoplasia includes localized lymphoma, soft tissue and bone tumours (sarcomas), and neuroectodermal tissue tumours (paraganglioma, olfactory neuroblastoma, neuroendocrine carcinoma, malignant melanoma). For information on these tumour types, the reader is referred to specific head and neck oncology literature.

V. Vander Poorten, MD, MSc, PhD
Professor, Department of Otorhinolaryngology, Head and Neck Surgery, University Hospitals Leuven, Herestraat 49, 3000 Leuven, Belgium

In this introductory chapter the first paragraph deals with epidemiology and risk factors of head and neck neoplasms. An overview of the pathology and natural history of the most frequent benign and malignant head and neck neoplasms will be outlined in the second paragraph.

1.1 Epidemiology and Risk Factors

1.1.1 Epidemiology: Incidence

Head and neck cancer, excluding skin cancer and Hodgkin and non-Hodgkin lymphoma, is the sixth most frequent cancer worldwide. The world incidence of epithelial malignancies of the mucous membranes is about 500,000 cases per year (laryngeal cancer: 136,000 new cases and 73,500 deaths yearly; oral and pharyngeal cancer: 363,000 new cases and 200,000 deaths yearly) (Parkin et al. 1999). Thus 6% of the global world incidence of cancer can be attributed to these neoplasms. Likewise, in the European Union 5% of the global cancer burden encountered in 1997 was caused by oral, pharyngeal and laryngeal cancer, and 1% by thyroid cancer (IARC CancerBase N°4 1999). Comparing these two largest groups, HNSCC and thyroid cancer, a definite gender difference is apparent regarding the incidence. As an example, the incidence of laryngeal SCC shows a male: female ratio of 10:1 (Boffetta and Trichopoulos 2002), whereas for incidence of thyroid cancer, the odds are in the opposite direction with a male:female ratio of 1:3. The incidence of salivary gland cancer is at the subpercentual level when looking at cancer in general, but is responsible for between 1% and 7 % of head and neck cancer incidence (Kane et al. 1991; Spiro and Spiro 2001).

There is an important geographical variation in incidence of head and neck cancer. The incidence of hypopharyngeal cancer is typically very high

in Northern France (10/100,000 males per year) as compared to e.g. the US (2/100,000 males per year). The incidence of laryngeal cancer in Northern Spain (20/100,000/year) is about 200 times as high as compared to certain regions is China (0.1/100,000/year) (IARC 1997). Besides probable differences in genetic susceptibility, a different prevalence of strong risk factors (e.g. Calvados drinking, smoking habits) is undoubtedly a large part of the explanation of these differences for HNSCC. In the same way differences in incidence among races can be observed [higher incidence in African versus Caucasian Americans (Day et al. 1993), and among men and women, largely attributable to differences in risk factor exposure (De Rienzo et al. 1991)].

1.1.2 Risk Factors for the Development of Head and Neck Malignancies

1.1.2.1 Risk Factors for Development of HNSCC

The most important established risk factor is chronic use of tobacco and alcohol (Fig. 1.1). The reason why these two factors are so important is twofold: there is a strong association with the disease on the one hand, and a very high prevalence of the factors among the population on the other. They are two independent risk factors that have been shown clearly to act in a multiplicative way when used in combination. Figure 1.2 shows that a 5.8-fold increased risk for development of oral and pharyngeal cancer is observed in non-smokers who consume 30 or more units of alcohol per week, a 7.4-fold increased risk is associated with smokers not consuming alcohol but with a history of 40 or more pack-years (smoking 20 cigarettes per day over a period of 40 years), whereas the person combining these two has a 38-fold increased risk (Blot et al. 1988). Conversely, after cessation of the use of tobacco, the risk of oral mucosal dysplasia and cancer falls to the level in the population that never smoked after 15 years (Morse et al. 1996).

Fig. 1.1. Smoking is the most prevalent and most powerful risk factor for the development of HNSCC. A doubled incidence of Warthin's tumor of the parotid gland has also been observed

The carcinogens in tobacco are nitrosamines, polycyclic aromatic hydrocarbons and aldehydes. Nitrosamines are alkylating agents that induce mutational events. Alcohol acts as a solvent and thus enhances permeability of the mucosa for the toxic substances in tobacco. A direct effect of alcohol is ascribed to mucosal enzymatic formation (alcohol dehydrogenase) of the carcinogenic acetaldehyde. The sites that are most at risk for alcohol induced carcinogenesis are the oro- and hypopharyngeal mucosal surfaces (Brugere et al. 1986), much more than the glottic larynx, for example, where only very high alcohol intakes can be shown to independently increase HNSCC risk.

Indirectly alcohol over consumption is associated with intake of non-alcoholic carcinogenic compounds contained in alcoholic drinks, e.g. nitroso dimethylamine in beer and tannin in wine. Furthermore, high intake of these beverages goes along with nutritional deficiencies, which in turn also confer an increased risk of HNSCC development. With poor nutrition, the proven protective effect of high intake of fruits and vegetables is lost. Indeed, a diet rich in fresh fruit and vegetables is associated with a 50%–70% reduction in the incidence of HNSCC (De Stefani et al. 1999). Especially dark yellow vegetables, citrus fruits (rich in vitamin C) and the carotene-rich vegetables (fresh tomatoes, carrots, pumpkins) are strongly protective. A crucial role is ascribed to antioxidant micronutrients in these vegetables such as vitamin C, vitamin E, beta carotene, and flavonoids (La Vecchia et al. 1997). Less proven but also suggested protective effects have been ascribed to use of olive oil (Franceschi et al. 1996) and high fibre intake (De Stefani et al. 1999).

Given the factors enumerated above, it is understandable that socioeconomic status is strongly associated with the development of HNSCC. Of this patient group, 75% live in the lower social classes, in terms of level of education and income. One in three patients has no partner and one in six patients is unemployed at the time of diagnosis. This social situation is a risk factor for having the combination of the direct risk factors tobacco, alcohol and poor dietary

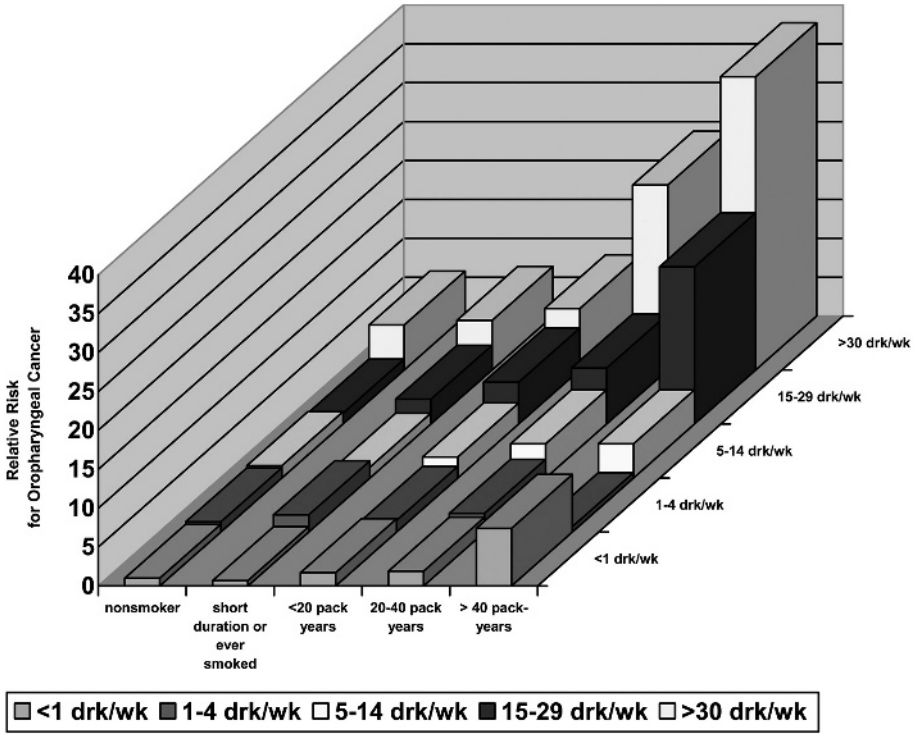

Fig. 1.2. Relative risk for oropharyngeal cancer for males according to amount of tobacco and alcohol use. (Based on data from Blot et al. (1988), with permission)

habits. There is also a lower level of oral hygiene. Once cancer is established, people in lower socioeconomic groups will seek medical help later, because of less education and more difficult access to the health system, and thus will present with more advanced stages of disease. Another reason for advanced disease at presentation lies in the fact that often a significant part of the intake of calories is provided for by alcohol and thus symptoms such as dysphagia for solid food will become problematic later. Stage at presentation is the strongest negative prognostic factor for outcome of treatment in HNSCC. Treatment of this disease, especially of the advanced stages, has often a serious impact on physical and psychological functioning of the patient. A great deal of effort is needed to become adapted to the resulting altered body image, to get integrated back into society, and also to achieve the change in lifestyle needed to prevent occurrence of second primary HNSCC. Unfortunately, immediately following treatment, patients in lower social classes are often isolated in facing this difficult challenge. Return to occupation thus becomes an illusion for the majority of these patients (Lefebvre et al. 2001). It is clear that a lower socioeconomic environment is a strong negative prognostic factor for the oncologic results following treatment, and also for survival in general because of the impact of many of the comorbidities that result from the previous way of living (pulmonary insufficiency, atherosclerosis, liver disease, etc.).

Viral infections have also been implicated in the carcinogenesis of HNSCC (Franceschi et al. 1996). Human papilloma virus DNA is prevalent in about 50% of oral cancer case series. Relative risks up to 6.2 for development of oral cancer have been reported. Epstein-Barr virus (EBV) has also been strongly associated with nasopharyngeal cancer. EBV antibody titers are much higher in cases than in controls, and biopsy specimens of undifferentiated nasopharyngeal carcinoma patients are 100% EBV positive and monoclonal as to this virus (Jeannel et al. 1999). EBV titers following treatment are used to monitor patients for disease recurrence. Patients infected with the human immunodeficiency virus (HIV) are at higher risk of developing HNSCC and Kaposi's sarcoma.

Among environmental factors, chronic sun exposure has been proven to induce development of skin and lip cancer. Occupational factors have been implied in HNSCC development. Working in industry that is associated with higher exposure to aromatic amines and phenoxy herbicides confides an elevated

risk for all sites. A specific and strong association has been repeatedly described between working in specific industries and the development of sinonasal cancer. The rate of development of SCC of the sinonasal tract has been observed to be increased 250 times in workers exposed to nickel (Pedersen et al. 1973). Working with wood in environments where there is no aspiration system for the dust particles has been found to result in a 500- to 1000-fold increase in the baseline incidence of sinonasal "intestinal type" adenocarcinoma and has led in several countries to the recognition of this cancer as an occupational disease and to the introduction of stringent safety precautions to minimize dust exposure (Acheson et al. 1968).

1.1.2.2 Risk Factors for Development of Glandular Neoplasms

Radiation exposure is the only firmly established environmental risk factor for the development of thyroid carcinoma. The information comes from scrutinized follow-up of atomic bomb survivors in Japan and atomic disaster survivors in Chernobyl (UNSCEAR: The United Nations Scientific Committee on the Effects of Atomic Radiation 2000) Typically a low dose exposure (e.g. about 3 Gy) results in the development of mainly papillary thyroid carcinoma, some 5–10 years later. The risk follows a linear dose–effect relationship and the incidence can be increased by more than 30 times.

Radiation exposure has also been observed to result in an increased incidence of both benign (Warthin's tumour) and malignant (mucoepidermoid carcinoma) salivary gland tumours in follow-up studies (Saku et al. 1997) in the same cohorts. For Warthin's tumour, also a doubled incidence has been observed in smokers versus non-smokers (Gallo and Bocciolini 1997). Epstein-Barr virus has been implicated in the genesis of bilateral Warthin's tumours and undifferentiated carcinoma of the salivary gland (Gallo 2001).

1.2 Pathology and Natural History of Frequent Benign and Malignant Head and Neck Neoplasms

With regard to tumour pathology, tumour typing is the first important subject. Within the different tumour types, the second subject is then detection of features with prognostic significance, such as grading, perineural or vascular invasion, and the assessment of radicality of resection margins. Regarding histological typing of head and neck neoplasms, it has already been mentioned that a great majority consists of primary epithelial neoplasms of the mucous membranes of the upper aerodigestive tract. A detailed discussion of all different tumour types that can be encountered in the head and neck area is beyond the scope of this introductory chapter and for this the reader is referred to surgical and pathological literature. What follows is an overview of the clinical course and pathological specificities of the most frequent tumour types.

1.2.1 Epithelial Neoplasms of the Mucous Membranes

1.2.1.1 Tumour Typing and Clinical Behaviour

1.2.1.1.1 Benign Lesions

Benign papillary lesions do occur, albeit that they are less frequently a reason for seeking medical attention than the malignant and premalignant lesions. Oral, pharyngeal and laryngeal sites can display squamous papillomas, which are white lesions with a wart-like appearance that have no signs of invasion of the deeper structures. A viral etiology in a part of these lesions (e.g. juvenile laryngeal papillomatosis) has been ascribed to HPV (type 6 and 11). Sinonasal papillomas are also called Schneiderian papillomas and can be exophytic, endophytic (inverted) or oncocytic in presentation. Especially the inverted type papilloma is considered a premalignant condition (Fig. 1.3). Most of the symptomatic epithelial neoplasms of the mucous membranes of the upper aerodigestive tract that bring patients to the doctor will turn out to be premalignant or malignant.

1.2.1.1.2 Premalignant Lesions

Premalignant lesions will often not be visualized on routine imaging studies. On the macroscopic level we consider leukoplakia and related lesions: homogeneous leukoplakia versus non-homogeneous leukoplakia (nodular leukoplakia, erythroplakia, proliferative verrucous leukoplakia; Fig. 1.4). On the

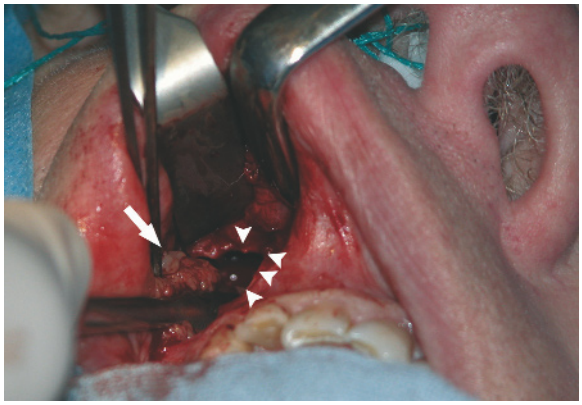

Fig. 1.3. Inverted papilloma (*arrow*) of the maxillary sinus being removed by Caldwell-Luc approach (antrostomy: *arrowheads*)

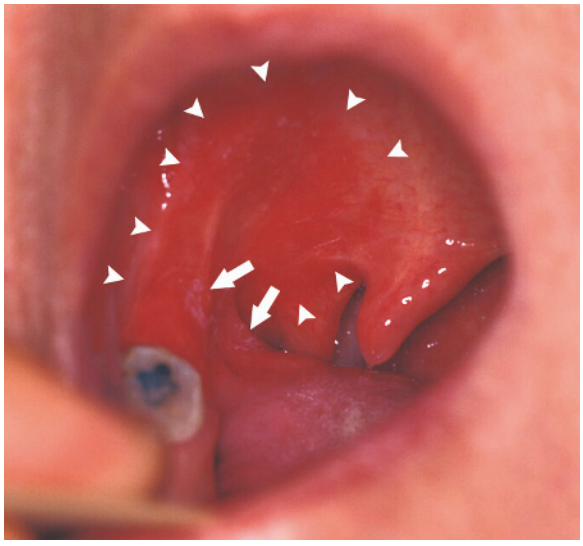

Fig. 1.4. Erythroplakia (*arrowheads*) with areas of nodular leukoplakia (*arrows*) of the tonsil, glossotonsillar sulcus, anterior tonsillar pillar, and hard and soft palate

microscopic level epithelial hyperplasia, dysplasia and carcinoma in situ can be discerned.

Leukoplakia is a descriptive clinical term use to describe "a white plaque or patch that cannot be characterized, clinically or histopathologically, as any other disease" (World Health Organization Collaborating Centre for Oral Precancerous Lesions 1978). Furthermore, in order to be designated as leukoplakia, the lesion should not be associated with any known physical (frictional keratosis, candidal leukoplakia) or chemical causal agent, except with the use of tobacco. It should also be impossible to scrape off the lesion.

Homogeneous leukoplakia is histologically either hyperortho- or hyperparakeratosis and rarely shows associated dysplasia. Less frequently we are dealing with non-homogeneous leukoplakia (nodular leukoplakia, erythroplakia, proliferative verrucous leukoplakia), which is usually associated with dysplasia and thus much more at risk for becoming real malignant disease (Batsakis 2003). Dysplasia can be "mild", meaning there is an increased number of mitotic figures and an abnormal cytologic appearance (loss of an orderly nuclear mosaic pattern: decreased nuclear/cytoplasmatic ratio and an irregular random nuclear placement) only in the basal layer of the epithelium, whereas suprabasal mitosis and cytologic abnormality indicates "moderate" dysplasia. In "severe" dysplasia the atypical cells with mitotic activity can be observed everywhere from the basal to the most superficial layers. The yearly rate of malignant transformation of homogeneous leukoplakia is estimated to be between 2% and 6% in the Western world, and is higher as the patient is older, female, and as the lesion persists for a longer time. The rate of malignant transformation in non-homogeneous (speckled) leukoplakia and erythroplakia can be more than 50% (Silverman et al. 1996).

1.2.1.1.3 Malignant Lesions

Less frequent entities with a specific clinical behaviour are verrucous carcinoma, papillary SCC, basaloid squamous cell carcinoma and sarcomatous SCC, increasingly aggressive in that order. Verrucous carcinoma is an exophytic papillomatous SCC that is a low grade tumour, very well differentiated, without known potential for regional or distant metastasis (Medina et al. 1984). Papillary SCC displays an exophytic growth with a poorly differentiated cell layer lining a central fibrovascular core. The behaviour of this type of tumour is more aggressive than verrucous carcinoma in that metastasis is observed. Basaloid SCC and sarcomatoid SCC are highly aggressive variants of SCC.

Most of the malignancies of the mucous membranes are simply called "invasive squamous cell carcinoma" and can be graded into well-, moderately- and poorly-differentiated SCC, paralleling the amount of keratin formation by cells. SCC cells by definition produce intercellular bridges (Figs. 1.5 and 1.6). Absence of these intercellular bridges is one of the features of undifferentiated carcinoma of the upper aerodigestive tract. This type of tumour occurs most frequently in the nasopharynx and is often

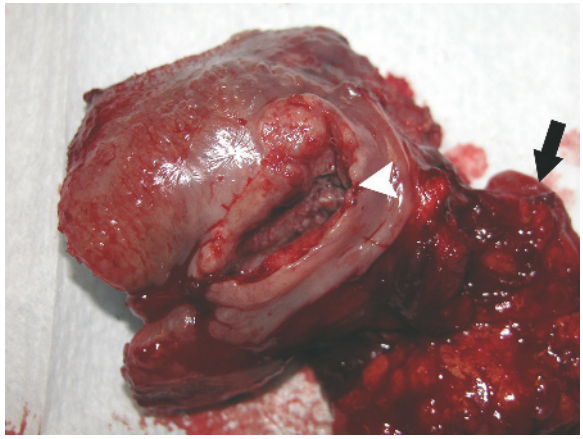

Fig. 1.5. Hemiglossectomy for ulcerative and deeply invasive well differentiated squamous cell carcinoma of the lateral tongue (*arrowhead*). Specimen in continuity with radical neck dissection (*arrow*)

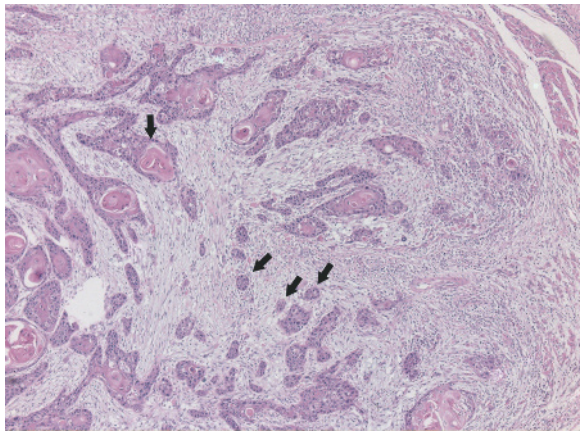

Fig. 1.6. Microscopical appearance of the same tumour. Note the diffuse infiltrative aspect of the tumour islets (*arrows*), the dense mononuclear inflammatory reaction, and the formation of keratin pearls (*vertical arrow*). (Courtesy Raf Sciot, MD, PhD)

diagnosed because of the massive neck lymph node metastasis already present at initial diagnosis, frequently bilaterally, and involving the posterior neck (region V).

1.2.1.1.4
Natural History Before and At Diagnosis

As pointed out under "risk factors", many patients with oral and pharyngeal cancer will present at an advanced stage of their disease, because of the late occurrence of symptoms and the social situation with more difficult access to the medical system. Patients with glottic laryngeal cancer tend to present at earlier stages, given the rapid effect of even a small vocal cord lesion on the voice quality. Early glottic laryngeal cancer is also not very likely to result in regional metastasis and thus often has a good prognosis following radiotherapy or surgery, with 5-year survival rates of 70%–100% (Lydiatt and Lydiatt 2001). Advancing stage and origin of SCC in most other anatomical subsites of the upper aerodigestive tract, are associated with lesser chances for successful treatment, and for the specifics the reader is referred to specific head and neck oncological literature.

1.2.1.1.5
Natural History Following Diagnosis and Successful Treatment of Malignant HNSCC

The annual incidence of second primary cancer following successful treatment of an index SCC in the head and neck area is 3%–7%. A known feature in HNSCC is the observation of field cancerization of the upper aerodigestive tract: several synchronous and also metachronous primary carcinomas and areas of moderate to severe dysplasia – carcinoma in situ are observed with areas of normal mucous membranes in between. This is caused by exposure of the entire upper aerodigestive tract to the same carcinogens – usually combined alcohol and tobacco. Patients are especially at risk of developing lung cancer, esophageal and gastric cancer, and a new localization of HNSCC. As already discussed under "risk factors", a change of lifestyle is essential to decrease the incidence of second primaries, but this is often difficult to achieve given the social context of the patient.

1.2.1.1.6
Microscopical Findings with Negative Prognostic Impact for Malignancy of the Mucous Membranes

The most important findings that are to be determined following resection of a primary head and neck SCC and the regional lymph nodes are listed in Table 1.1. They are routinely determined during microscopical analysis because they are known to carry a worse prognosis and thus contribute to decision making regarding the need for further therapy, i.e. postoperative radiotherapy. Many of these parameters (cTNM classification, perineural growth, tumour thickness, extracapsular spread in metastatic lymph nodes) can already be strongly suspected based on a high quality imaging study before the resection.

Table 1.1. Histopathological negative prognostic factors in HNSCC

(p)TNM classification (size of primary tumor, number/laterality of positive nodes, size of largest node)
Vascular invasion
Perineural growth
Resection margins (e.g. less than 5 mm is considered "close margins" in oral cancer)
Thickness
Invasive front
Differentiation
Exophytic versus endophytic growth pattern
Field cancerization
Mitotic index
Presence of extracapsular spread in metastatic lymph nodes

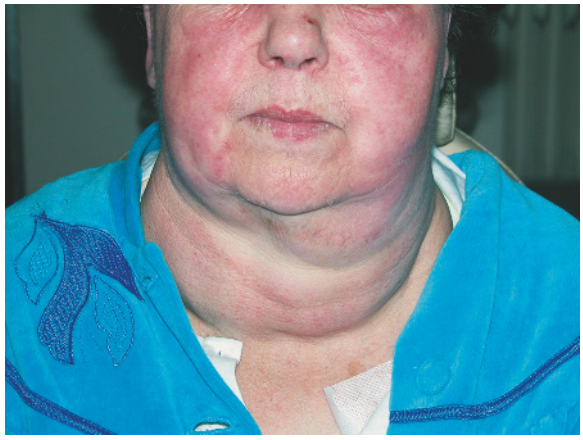

Fig. 1.7. Large multinodular goitre with pharyngeal, esophageal and tracheal compression

1.2.2 Glandular Neoplasms

1.2.2.1 Thyroid Neoplasia

1.2.2.1.1 Benign Disease: Multinodular Enlargement

Benign multinodular enlargement (multinodular goitre) is very frequently observed and is estimated to affect almost one in three persons worldwide (Delange 2000). Iodine deficiency is the most frequent contributory factor. In areas where iodine supply is sufficient, the prevalence of clinically detectable goitres is usually less than 4%, and thought to result from elevated thyroid stimulating hormone (TSH) levels or from elevated stimulation of the TSH receptor (such as in Graves' disease and non-atrophic Hashimoto's goitres). Most patients with this condition are asymptomatic, and medical concerns mostly arise when compressive symptoms appear (Fig. 1.7), when autonomous hyperfunction becomes apparent, or when presence of malignancy is feared. The latter is the case in rapidly enlarging goitres, suspicion of enlarged lymph nodes, a history of prior radiotherapy to the neck, or when fine needle aspiration cytology (FNAC) of dominant nodules indicates papillary carcinoma or a microfollicular lesion. A microfollicular lesion can be follicular carcinoma in about one in ten patients.

Macroscopically, following thyroidectomy, we usually see a polynodular, soft, and globally enlarged thyroid gland (Fig. 1.8). There may be one or more dominant larger nodules which deserve subsequent

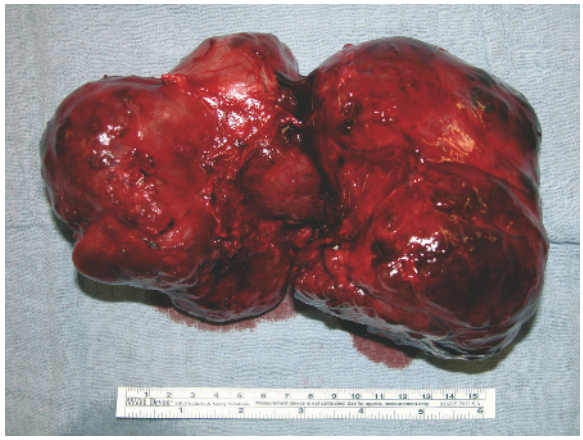

Fig. 1.8. The same goitre as in Fig. 1.7, following resection.

microscopical analysis. Up to 70% of hyperplastic nodules are clonal, neoplastic proliferations (Kopp et al. 1994). Microscopically, within the different nodules, there is a varied pattern of large and small follicles, usually with abundant colloid. There is an often oedematous stroma with fibrosis, macrophages, hemosiderin, and calcifications.

1.2.2.1.2 Benign Disease: Uninodular Enlargement – the Solitary Thyroid Nodule

Any clinically visible or palpable nodule, and "any discrete macroscopic intrathyroidal lesion that is clearly distinguishable from the adjacent normal thyroid parenchyma" (Hay and Klee 1993) on ultrasonography or Technetium scanning, should lead to action to estimate the chance of malignancy and to determine

subsequent action. The next step will be to do an ultrasound guided FNAC. A solitary thyroid nodule can be due to degenerative lesions such as cysts or degenerative colloid nodules on one hand, or to neoplastic lesions on the other. The latter can be benign or malignant. The global incidence of cancer in patients with a thyroid nodule is 10%, but this increases to 30% for women older than 50 and to 45% for men older than 50 (Tezelman and Clark 1995).

The rest will be benign lesions, where nine out of ten will be follicular adenomas, the remainder being mostly Hürthle cell adenomas. Macroscopically, adenomas are well demarcated from the adjacent parenchyma, and fleshy and pale, sometimes cystic or hemorrhagic on cut surface. The microscopic appearance of a solitary adenomatous nodule displays large and small follicles with a lot of colloid and a stromal component with hemosiderin, macrophages, fibrotic changes and often calcifications. A Hürthle cell variant displays oncocytic cells, with an intensely eosinophylic cytoplasm due to a lot of abnormal mitochondria, and large vesicular nuclei.

1.2.2.1.3 Malignant Disease

An important issue in suspected malignant thyroid disease is the avoidance of iodine containing contrast medium in imaging studies for thyroid lesions. "Differentiated thyroid cancer" (vide infra) are tumours that retain the ability to concentrate iodine, and hence can be effectively and very selectively treated with radioactive iodine. This treatment, however, will be delayed by 3 months following an imaging study using iodine contrast medium, due to saturation of the iodine binding capacity of the targeted thyroid cancer cells.

Generally a distinction is made between "differentiated thyroid cancer" with a relatively good (papillary carcinoma, follicular carcinoma, mixed papillary follicular carcinoma) to intermediate (Hürthle cell carcinoma) prognosis, and "other" cancers, with worse (medullary thyroid cancer) to fatal prognosis (anaplastic thyroid cancer). Of human malignant tumours, the thyroid harbours both the tumours with the best (papillary carcinoma) and the worst (anaplastic carcinoma of the thyroid) prognosis.

1.2.2.1.4 Papillary Thyroid Cancer

Papillary thyroid cancer is the most frequent thyroid cancer (four out of five thyroid cancers belong to this group). Overall women are affected three times as frequently as men. The clinical picture is usually a symptomless swelling in the thyroid area, although enlarged lymph nodes may be the primary presenting feature (Fig. 1.9). Indeed, regional metastasis to the paratracheal (level VI) and cervical (level II, III, and IV) lymph nodes is observed in one out of two patients at presentation (Fig. 1.10). Distant metastasis occurs usually late in the disease course.

Following thyroidectomy, macroscopically typical features are multifocality and bilaterality, which may

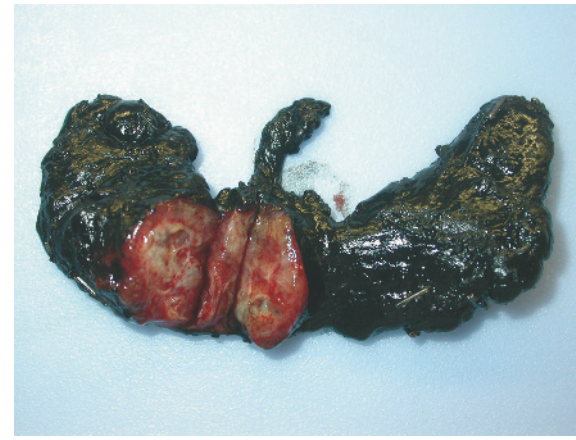

Fig. 1.9. Thyroidectomy specimen showing papillary carcinoma on cut surface in the left lobe and the isthmus. Posterior view. The specimen is inked to assess resection margins

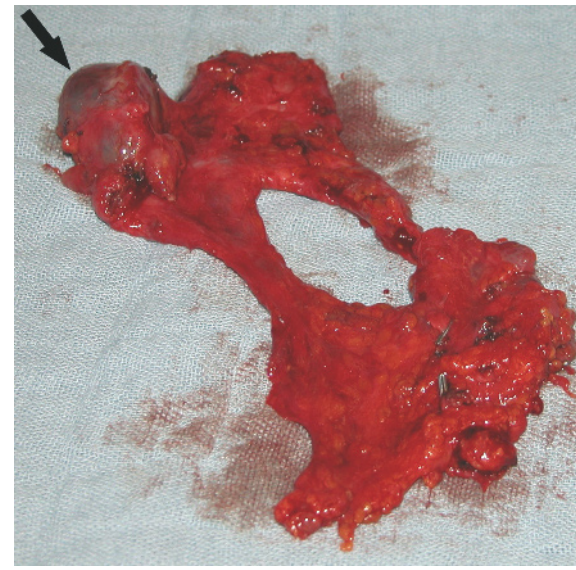

Fig. 1.10. Functional neck dissection specimen showing a typical black cystic metastatic neck node of papillary thyroid carcinoma (*arrow*)

occur in up to 87% of thyroid specimens (Russell et al. 1963). Lymph node metastasis is often cystic and dark bluish in appearance (Fig. 1.10).

Microscopically only 3% is true papillary carcinoma and 97% is "follicular variant of papillary carcinoma". Both forms have an equally good prognosis, with overall up to 95% of patients surviving 20 years following treatment (Hay and Klee 1993).

Essential for the diagnosis are the papillae with a central fibrovascular core and an epithelial lining showing the typical nuclear features with overlapping nuclei and nuclear grooves, making it possible to get the diagnosis from a fine needle aspiration cytology. Psammoma bodies, calcific concretions with concentric laminations, can be observed in about one in two of these tumours, and when present can also already be recognized on FNAC (Fig. 1.11).

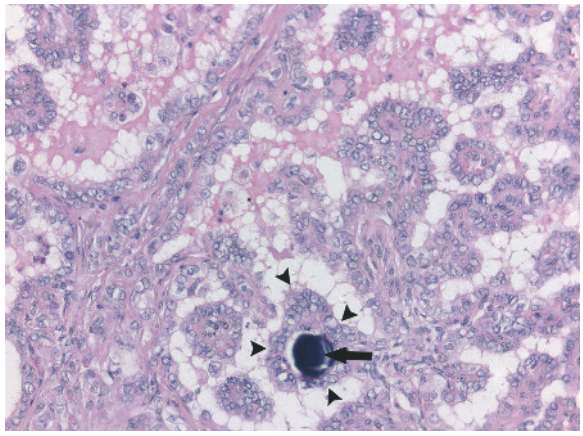

Fig. 1.11. Microscopical appearance of papillary thyroid cancer. Psammoma body (*arrow*) and papillary growth pattern (*arrowheads*). (Courtesy Raf Sciot, MD, PhD)

1.2.2.1.5 Follicular Thyroid Cancer

About one in ten thyroid malignancies are follicular carcinomas. These are macroscopically solitary, encapsulated tumours. The features discriminating them from follicular adenomas, their benign counterparts, are microscopical: the presence of vascular invasion and full thickness capsular invasion into the adjacent normal thyroid parenchyma. To be able to search the entire capsule for areas of invasion all solitary nodules, where FNAC results in the diagnosis "follicular lesion", should be completely excised with capsule and surrounding thyroid tissue. The degree of capsular invasion allows for the definition of a subgroup of minimally invasive follicular carcinomas, behaving essentially as follicular adenomas. The tendency for vascular invasion in invasive follicular carcinoma explains that metastasis is primarily haematogenous to the lungs and the bones, rather than to the cervical lymph nodes, as observed in papillary thyroid cancer. Prognosis is somewhat less than for papillary carcinoma, with an overall 20-year survival of 81% (Shaha et al. 1995).

1.2.2.1.6 Hürthle Cell Carcinoma

Hürthle cell carcinomas are also solitary, encapsulated tumours that are distinguished from their benign counterparts by the presence of capsular and vascular invasion. They have an intermediate prognosis of about 65% 20-year survival (Shaha et al. 1995).

1.2.2.1.7 Medullary Thyroid Cancer

Somewhat less than one in ten thyroid carcinomas are medullary thyroid carcinomas (MTC). MTC is a malignant tumour of the calcitonin-secreting parafollicular C cells of the thyroid.

These cells are embryologically maximally located in the upper two thirds of the thyroid gland and this explains that tumours are usually found in that upper part of the gland.

The tumours can occur in a sporadic form, which is usually unifocal, and presents in the age group of 40–60 years. This sporadic form is responsible for about 80% of MTC. An autosomal dominant hereditary form, due to a mutation in the retinoblastoma (RET) proto-oncogen, can occur within the framework of multiple endocrine neoplasia syndromes (MEN 2a: MTC, phaeochromocytoma, and parathyroid hyperplasia and MEN 2b: MTC, phaeochromocytoma and multiple mucosal neurinomas) or as familial medullary thyroid cancer (FMTC) without associated endocrinopathy. These hereditary forms usually occur earlier in life and are often multifocal and present in both thyroid lobes. In patients with MTC, lymph node metastasis, often bilateral, is frequently present at diagnosis and has a negative prognostic impact.

Microscopically the diagnosis is suggested by the presence of amyloid and confirmed by immunostaining for calcitonin, chromogranin an carcinoembryonic antigen (CEA). The 20-year survival following adequate treatment of MTC is about 65% (Moley 1995).

1.2.2.1.8 Anaplastic Thyroid Cancer

About 5% of thyroid cancers are anaplastic carcinomas. This is a highly lethal variant of thyroid cancer which is rapidly progressive and almost universally fatal. Patients are usually 60- to 75-years-old and present with a suddenly appeared and rapidly enlarging mass in the neck. Frequently at presentation there are already signs of local invasion of the surrounding structures: hoarseness due to recurrent laryngeal nerve paralysis, respiratory obstruction following tracheal compression or invasion, dysphagia due to esophageal invasion. Surgical treatment is almost never satisfactory and can only exceptionally be considered in the rare patient where disease is still intrathyroidal. Most patients are treated with radiotherapy with or without chemotherapy and survival is usually measured in months (Fig. 1.12).

The clinical diagnosis can sometimes be confirmed by FNAC, but often an incisional biopsy under local anaesthesia will be performed to rule out thyroid lymphoma. Macroscopically, the surgeon performing an incisional biopsy sees a grey, hard, necrotic and hemorrhagic tumour. Microscopically there is a high mitotic index, marked cellular pleomorphism, necrosis and tumour extension in blood vessels.

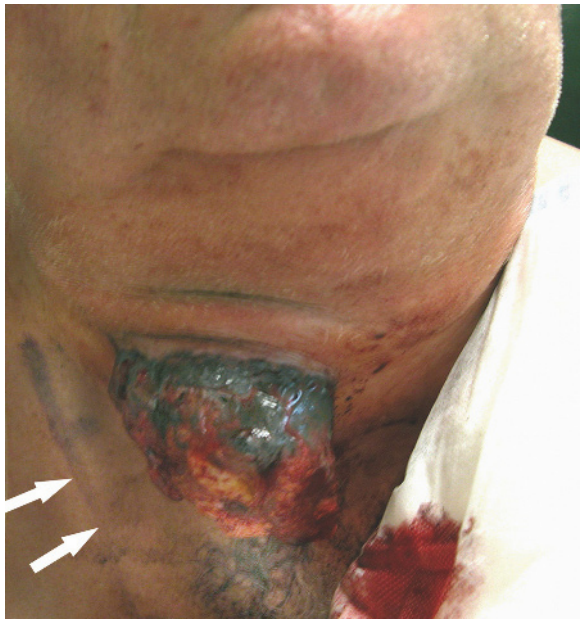

Fig. 1.12. Anaplastic thyroid carcinoma, growing through the dehiscent incision of the previous biopsy, during the radiotherapy. Note the tattoo on the skin of the patient demarcating the radiation field (*arrows*)

1.2.2.2 Salivary Gland Neoplasia

A distinction is made between the paired major salivary glands (parotid, submandibular, and sublingual) and the minor salivary glands. The latter are the seromucous glands that are found throughout the entire upper aerodigestive tract: 500–1000 of these glands are located in the oral cavity including lips, floor of mouth, cheek mucosa, tongue, soft and posterior hard palate, but also the nasal cavity, paranasal sinuses, nasopharynx, middle ear, Eustachian tube, oropharynx, hypopharynx and even trachea (Ellis and Auclair 1996a). The majority of tumours (64%–80%) arise in the parotid glands, 15%–32% of which are malignant. Between 7% and 11% arise in the submandibular glands, 41%–45% being malignant. Less than 1% of salivary gland tumours occur in the sublingual gland, most of these (70%–90%), however, are malignant. Minor salivary gland tumours form 9%–23% of the entire group, one in two being malignant (Ellis and Auclair 1996b). This observation has been the basis for the didactic rule "the smaller the salivary gland, the less frequent a tumour arises in it, but the more frequently malignancy is involved".

1.2.2.2.1 Tumour Typing and Clinical Behaviour

The extensive list of tumour types that can occur in the salivary glands is listed in Table 1.2, that is based on the 1991 World Health Organization Classification (Seifert and Sobin 1992). With time, the number of consistently identifiable light microscopically diverse types is still increasing. Among other new entities are hyalinizing clear cell adenocarcinoma (Batsakis et al. 1994), oncocytic mucoepidermoid carcinoma (Deveci et al. 2000) and even primary chondrosarcoma (Maruya et al. 2001). The key features of the most frequent benign and malignant types are shortly presented.

1.2.2.2.2 Benign Tumours

1.2.2.2.2.1 Pleomorphic Adenoma

Pleomorphic adenoma is definitely the most frequently occurring salivary gland tumour and accounts for up to 70% of parotid tumours, 50% of submandibular salivary gland tumours, 35% of the minor salivary gland tumours, and 6% of sublingual tumours (Ellis and Auclair 1996a).

Table 1.2 The WHO 1991 histologic classification of benign and malignant salivary gland tumors (Seifert and Sobin 1992)

Adenomas
1. Pleomorphic adenoma
2. Myoepithelioma (myoepithelial adenoma)
3. Basal cell adenoma
4. Warthin's tumor (adenolymphoma)
5. Oncocytoma (oncocytic adenoma)
6. Canalicular adenoma
7. Sebaceous adenoma
8. Ductal papilloma
8.1. Inverted ductal papilloma
8.2. Intraductal papilloma
8.3. Sialadenoma papilliferum
9. Cystadenoma
9.1. Papillary cystadenoma
9.2. Mucinous cystadenoma
Carcinomas
1. Acinic cell carcinoma
2. Mucoepidermoid carcinoma
3. Adenoid cystic carcinoma
4. Polymorphous low-grade adenocarcinoma (terminal duct adenocarcinoma)
5. Epithelial myoepithelial carcinoma
6. Basal cell adenocarcinoma
7. Sebaceous carcinoma
8. Papillary cystadenocarcinoma
9. Mucinous adenocarcinoma
10. Oncocytic carcinoma
11. Salivary duct carcinoma
12. Adenocarcinoma
13. Malignant myoepithelioma (myoepithelial carcinoma)
14. Carcinoma in pleomorphic adenoma (malignant mixed tumor)
15. Squamous cell carcinoma
16. Small cell carcinoma
17. Undifferentiated carcinoma
18. Other carcinomas

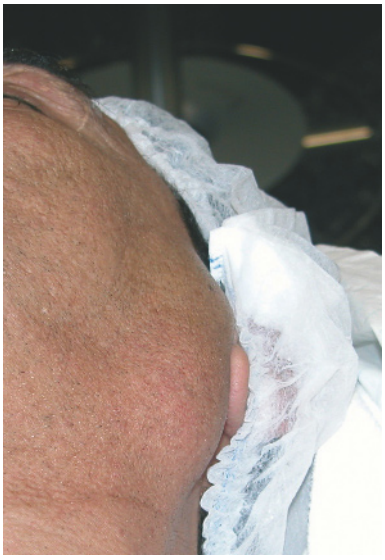

Fig. 1.13. Typical picture of a long-standing symptomless swelling in the left parotid region, following excision the diagnosis of pleomorphic adenoma was confirmed

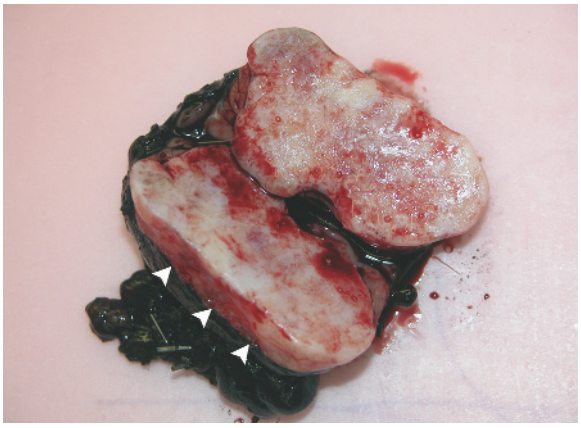

Fig. 1.14. Pleomorphic adenoma of the submandibular gland with a mainly mesenchymal – chondroid differentiation. Grey to white and lobulated on cut surface. Specimen inked for assessment of resection margins. Note the tumour looks easy to "shell out" (*arrowheads* demarcating the normal submandibular gland parenchyma that spontaneously retracts upon bisection of the gland)

Patients typically present with a long-standing, painless swelling that is usually well circumscribed towards the surrounding structures (Fig. 1.13). Macroscopically the tumours is well delineated from the normal salivary tissue, and this explains the old, bad surgical habit of thinking the tumour can be shelled out. It is grey to white and lobulated on cut surface (Fig. 1.14). Microscopically, a "mixture" of epithelial and mesenchymal (stromal) components in a varying combination are observed, an observation explaining the name of the tumours, "pleomorphic" adenoma or "mixed" tumour (Fig. 1.15). The tumour is notorious for its capacity to recur, often in a multinodular way, following inadequate surgical treatment. A 2%–23% rate of becoming malignant, the so-called carcinoma ex pleomorphic adenoma, has been reported (Gnepp 1993). The rate of malignant degeneration increases with time of presence of the lesion (Eneroth and Zetterberg 1974).

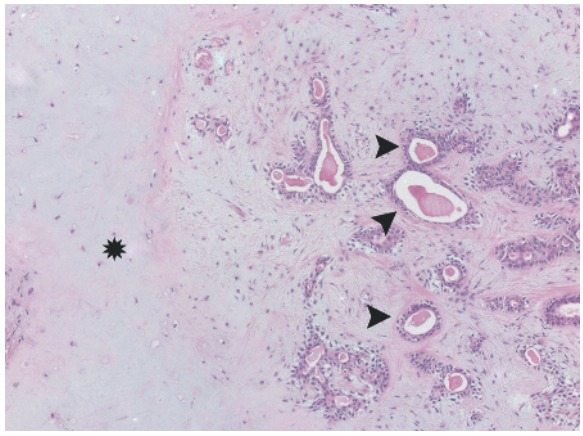

Fig. 1.15. Microscopical appearance of the same pleomorphic adenoma as in Fig. 1.14. Note the chondromyxoid matrix (*asterisk*), in which ductal structures (*arrows*) can be noted. (Courtesy Raf Sciot, MD, PhD)

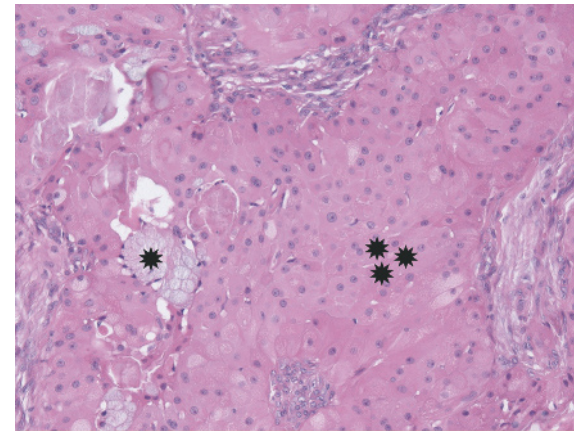

Fig. 1.16. Intermediate grade mucoepidermoid carcinoma of the parotid gland. Epithelial solid tumour (three *asterisks*) with some islands of mucinous cells (*asterisk*). (Courtesy Raf Sciot, MD, PhD)

1.2.2.2.2.2
Warthin's Tumour

Warthin's tumour is the second most frequent benign salivary gland tumour. It occurs exclusively in the parotid gland and the immediately adjacent level II lymph nodes. Between 6%–10% of parotid tumours are Warthin's tumours (Ellis and Auclair 1996a). There is a male to female preponderance of 5 to 1. Warthin's tumours can occur bilaterally in about 10% of patients (Heller and Attie 1988). Microscopically there is typically a two-layered eosinophylic epithelium and a lymphoid stroma, hence the name adenolymphoma.

1.2.2.2.3
Malignant Tumours

1.2.2.2.3.1
Mucoepidermoid Carcinoma

About one in six (Vander Poorten et al. 2003) to one in three (Spiro 1986) malignant salivary gland tumours are mucoepidermoid carcinomas. Macroscopically the cut surface is solid but can contain cysts. Microscopically the tumour consists of a variable combination of glandular cells lining cystic spaces and epidermoid basaloid type cells forming solid areas (Fig. 1.16). A histological grading system is based on the relative proportion of mucinous versus epidermoid cells. Tumours containing 90% solid area made up of epidermoid cells are designated high grade (Seifert and Sobin 1992) and are associated with a 72% disease specific death rate versus only 6%–8% disease specific death rate in low grade, more mucus containing, low grade tumours (Healey et al. 1970).

1.2.2.2.3.2
Adenoid Cystic Carcinoma

Adenoid cystic carcinoma accounts for about one out of six parotid carcinomas (Vander Poorten et al. 2003). It occurs more frequently in other salivary gland sites with about 45% of submandibular and minor salivary gland carcinomas being of this type (Vander Poorten et al. 1999a) (Vander Poorten et al. 2000). Macroscopically it is a frequently infiltrating, rather hard tumour with an irregular extension pattern. The tumour is notorious for extension via major cranial nerves and in this respect MRI imaging is often an essential imaging modality to determine the real anatomical extent. It is also a tumour with a well known capacity for distant metastasis in about 40% of patients (Spiro and Huvos 1992), mostly to the lungs (Fig. 1.17), and in this case a protracted clinical course can result in disease related deaths even after more than 10 years following the initial diagnosis (Vander Poorten et al. 1999b; Spiro and Huvos 1992). Microscopically the tumour is often composed of cylindrical cystic spaces separated by solid septae of tumour cells, and this is called the "cribriform pattern" of appearance (Fig. 1.18).

1.2.2.2.3.3
Acinic Cell Carcinoma

About one in five parotid carcinomas is diagnosed as acinic cell carcinoma (Vander Poorten et al. 2003). The majority of these tumours have a clinically low grade course, and following adequate resection, low stage tumours are not considered to need additional radiotherapy (Armstrong et al. 1990). Macroscopically acinic cell carcinomas are

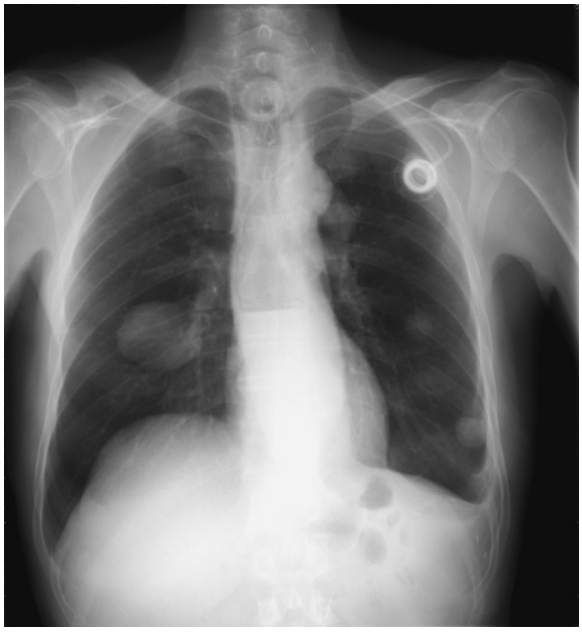

Fig. 1.17. Diffuse lung metastasis in a patient with subglottic adenoid cystic carcinoma diagnosed 10 years earlier

solitary, well circumscribed, multilobular masses. Microscopically typically acinar cells with cytoplasmic periodic acid Schiff's reagent positive glycogen granules are the main component of the tumour. A more aggressive [papillocystic (Spiro et al. 1978), microcystic (Colmenero et al. 1991)] subgroup is increasingly being distinguished, making up about 15% of acinic cell carcinomas (Hoffman et al. 1999) and requiring more aggressive treatment.

1.2.2.2.3.4

Adenocarcinoma Not Otherwise Specified (NOS)

Quite frequently a salivary gland adenocarcinoma lacks specific features allowing the pathologist to make a more specific diagnosis. About one in four salivary gland carcinomas cannot be accommodated in the other specific subtypes (Vander Poorten et al. 2003). Microscopically they range from well-differentiated and low grade to high grade, invasive lesions, displaying perineural growth (Fig. 1.19).

Acknowledgement

The author would like to express his sincere gratitude to Raf Sciot, MD PhD, for providing the illustrative microscopic images corresponding to the clinical examples displayed in this chapter.

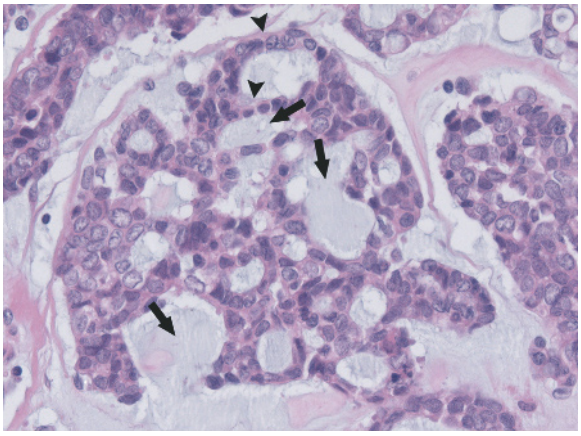

Fig. 1.18. Adenoid cystic carcinoma of the tongue base. Strands of tumour cells (*arrowheads*) grow in a cribriform pattern on a mucinous background (*arrows*) thus shaped as pseudolumina. (Courtesy Raf Sciot, MD, PhD)

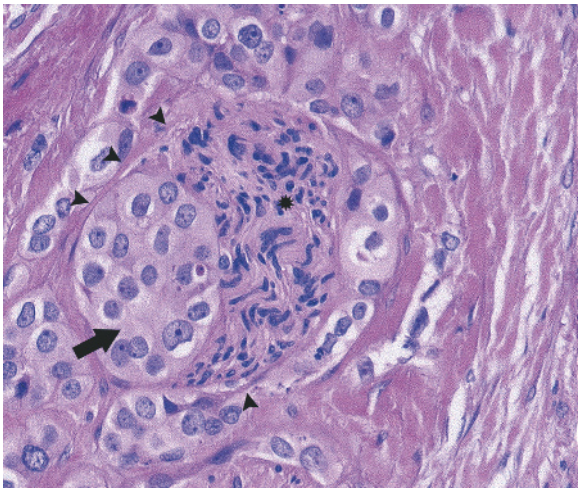

Fig. 1.19. Perineural growth in a high grade adenocarcinoma (not otherwise specified) of the parotid gland. *Arrowheads* demarcate perineurium, stretched by tumour cells (*arrow*), compressing the nerve bundles (*asterisk*). (Courtesy Raf Sciot, MD, PhD)

References

Acheson ED, Cowdell RH, Hadfield E et al (1968) Nasal cancer in woodworkers in the furniture industry. Br Med J 2:587–596

Armstrong JG, Harrison LB, Spiro RH et al (1990) Malignant tumors of major salivary gland origin. A matched-pair analysis of the role of combined surgery and postoperative radiotherapy. Arch Otolaryngol Head Neck Surg 116:290–293

Batsakis JG (2003) Clinical pathology of oral cancer. In: Shah JP, Johnson NW, and Batsakis JG (eds) Oral cancer, 1st

edn. Martin Dunitz, Taylor and Francis Group, London, pp 77–123
Batsakis JG, el Naggar AK, Luna MA (1994) Hyalinizing clear cell carcinoma of salivary origin. Ann Otol Rhinol Laryngol 103:746–748
Blot WJ, McLaughlin JK, Winn DM et al (1988) Smoking and drinking in relation to oral and pharyngeal cancer. Cancer Res 48:3282–3287
Boffetta P, Trichopoulos D (2002) Cancer of the lung, larynx and pleura. In: Adami HO, Hunter D, Trichopoulos D (eds) Textbook of cancer epidemiology. Oxford University Press, Oxford, pp 268–272
Brugere J, Guenel P, Leclerc A et al (1986) Differential effects of tobacco and alcohol in cancer of the larynx, pharynx, and mouth. Cancer 57:391–395
Colmenero C, Patron M, Sierra I (1991) Acinic cell carcinoma of the salivary glands. A review of 20 new cases. J Craniomaxillofac Surg 19:260–266
Day GL, Blot WJ, Austin DF et al (1993) Racial differences in risk of oral and pharyngeal cancer: alcohol, tobacco, and other determinants. J Natl Cancer Inst 85:465–473
De Rienzo DP, Greenberg SD, Fraire AE (1991) Carcinoma of the larynx. Changing incidence in women. Arch Otolaryngol Head Neck Surg 117:681–684
De Stefani E, Ronco A, Mendilaharsu M et al (1999) Diet and risk of cancer of the upper aerodigestive tract – II. Nutrients. Oral Oncol 35:22–26
Delange F (2000) Iodine deficiency. In: Braverman LE, Utiger RD (eds) Werner and Ingbar's the thyroid, 8th edn. Lippincott, Williams and Wilkins, Philadelphia, pp 295–296
Deveci MS, Deveci G, Gunhan O (2000) Oncocytic mucoepidermoid carcinoma of the parotid gland: report of a case with DNA ploidy analysis and review of the literature. Pathol Int 50:905–909
Ellis GL, Auclair PL (1996a) Salivary gland tumors: general considerations: site specific tumor differences. In: Ellis GL, Auclair PL (eds) Tumors of the salivary glands. Third Series. Armed Forces Institute of Pathology, Washington DC, p 32
Ellis GL, Auclair PL (1996b) The normal salivary glands. In: Ellis GL, Auclair PL (eds) Tumors of the salivary glands. Third Series. Armed Forces Institute of Pathology, Washington DC, pp 1–23
Eneroth CM, Zetterberg A (1974) Malignancy in pleomorphic adenoma. A clinical and microspectrophotometric study. Acta Otolaryngol 77:426–432
Franceschi S, Munoz N, Bosch XF et al (1996) Human papillomavirus and cancers of the upper aerodigestive tract: a review of epidemiological and experimental evidence. Cancer Epidemiol Biomarkers Prev 5:567–575
Gallo O (2001) Aetiology and molecular changes in salivary gland tumours. In: Mc Gurk M, Renehan AG (eds) Controversies in the management of salivary gland tumours, 1st edn. Oxford University Press, Oxford, pp 13–23
Gallo O, Bocciolini C (1997)Warthin's tumour associated with autoimmune diseases and tobacco use. Acta Otolaryngol 117:623–627
Gnepp DR (1993) Malignant mixed tumors of the salivary glands: a review. Pathol Annu 28:279–328
Greenlee RT, Hill-Harmon MB, Murray T et al (2001) Cancer statistics, 2001. CA Cancer J Clin 51:15–36
Hay ID, Klee GG (1993) Thyroid cancer diagnosis and management. Clin.Lab Med 13:725–734
Healey WV, Perzin KH, Smith L (1970) Mucoepidermoid carcinoma of salivary gland origin. Classification, clinicalpathologic correlation, and results of treatment. Cancer 26:368–388
Heller KS, Attie JN (1988) Treatment of Warthin's tumor by enucleation. Am J Surg 156:294–296
Hoffman HT, Karnell LH, Robinson RA et al (1999) National Cancer Data Base report on cancer of the head and neck: acinic cell carcinoma. Head Neck 21: 297–309
IARC (1997) Cancer incidence in five continents, vol. VII. IARC Sci Publ (143):i–xxxiv, 1–1240
IARC CancerBase N°4. EUCAN (1999) Cancer incidence, mortality and prevalence in the European Union 1997, version 4.0. IARC Press, Lyon
Jeannel D, Bouvier G, Hubert A (1999) Nasopharyngeal cancer. In: Newton R, Beral V, Weiss RA (eds) Infections and human cancer. Cold Spring Harbor Press, Plainview, New York, pp 125–156
Kane WJ, McCaffrey TV, Olsen KD et al (1991) Primary parotid malignancies. A clinical and pathologic review. Arch Otolaryngol Head Neck Surg 117:307–315
Kopp P, Kimura ET, Aeschimann S et al (1994) Polyclonal and monoclonal thyroid nodules coexist within human multinodular goiters. J Clin Endocrinol Metab 79:134–139
La Vecchia C, Tavani A, Franceschi S et al. (1997) Epidemiology and prevention of oral cancer. Oral Oncol. 33:302–312
Lefebvre J, Lartigau E, Kara A et al (2001) Oral cavity, pharynx and larynx cancer. Environment-related prognostic factors. In: Gospodarowicz MK, Henson DE, Hutter RVP, O'Sullivan BO, Sobin LH,Wittekind Ch (eds) UICC prognostic factors in cancer, 2nd edn. Wiley-Liss, New York, pp 151–165
Lydiatt WM, Lydiatt DD (2001) The larynx: early stage disease. In: Shah JP (ed) Cancer of the head and neck, 1st edn. BC Decker Inc., Hamilton, London, pp 169–184
Maruya S, Kurotaki H, Fujita S et al (2001) Primary chondrosarcoma arising in the parotid gland. ORL J Otorhinolaryngol Relat Spec 63:110–113
Medina JE, Dichtel W, Luna MA (1984) Verrucous-squamous carcinomas of the oral cavity. A clinicopathologic study of 104 cases. Arch Otolaryngol 110:437–440
Moley JF (1995) Medullary thyroid cancer. Surg Clin North Am 75:405–420
Morse DE, Katz RV, Pendrys DG et al (1996) Smoking and drinking in relation to oral epithelial dysplasia. Cancer Epidemiol Biomarkers Prev 5:769–777
Parkin DM, Pisani P, Ferlay J (1999) Global cancer statistics. CA Cancer J Clin 49:33–64, 1
Pedersen EA, Hogetveit C, Andersen A (1973) Cancer of respiratory organs among workers at a nickel refinery in Norway. Int J Cancer 12:32–41
Russell WO, Ibanez ML, Clark RL (1963) Thyroid carcinoma. Classification, intraglandular dissemination, and clinicopathological study based upon whole organ sections of 80 glands. Cancer 16:1425–1460
Saku T, Hayashi Y, Takahara O et al (1997) Salivary gland tumors among atomic bomb survivors, 1950–1987. Cancer 79:1465–1475
Seifert G, Sobin LH (1992) The World Health Organization's histological classification of salivary gland tumors. A commentary on the second edition. Cancer 70:379–385
Shaha AR, Loree TR, Shah JP (1995) Prognostic factors and risk group analysis in follicular carcinoma of the thyroid. Surgery 118:1131–1136

Silverman S Jr, Gorsky M, Kaugars GE (1996) Leukoplakia, dysplasia, and malignant transformation. Oral Surg Oral Med Oral Pathol 82:117

Spiro JD, Spiro RH (2001) Salivary tumors. In: Shah JP, Patel SG (eds) Cancer of the head and neck, 1st edn. Decker BC Inc, Hamilton, London, pp 240–250

Spiro RH (1986) Salivary neoplasms: overview of a 35-year experience with 2,807 patients. Head Neck 8:177–184

Spiro RH, Huvos AG (1992) Stage means more than grade in adenoid cystic carcinoma. Am J Surg 164:623–628

Spiro RH, Huvos AG, Strong EW (1978) Acinic cell carcinoma of salivary origin. A clinicopathologic study of 67 cases. Cancer 41:924–935

Tezelman S, Clark OH (1995) Current management of thyroid cancer. Adv Surg 28:191–221

UNSCEAR (2000) The United Nations Scientific Committee on the Effects of Atomic Radiation. Health Phys 79: 314

Vander Poorten VLM, Balm AJM, Hilgers FJM et al (1999a) Prognostic factors for long term results of the treatment of patients with malignant submandibular gland tumors. Cancer 85:2255–2264

Vander Poorten VLM, Balm AJM, Hilgers FJM et al (1999b) The development of a prognostic score for patients with parotid carcinoma. Cancer 85:2057–2067

Vander Poorten VLM, Balm AJM, Hilgers FJM et al (2000). Stage as major long term outcome predictor in minor salivary gland carcinoma. Cancer 89:1195–1204

Vander Poorten VLM, Hart AA, van der Laan BF et al. (2003) Prognostic index for patients with parotid carcinoma: external validation using the nationwide 1985–1994 Dutch Head and Neck Oncology Cooperative Group database. Cancer 97:1453–1463

World Health Organization Collaborating Centre for Oral Precancerous Lesions (1978) Definitions of leukoplakia and related lesions: an aid to studies on oral precancer. Oral Surg Oral Med Oral Pathol 46:518–539

2 Clinical and Endoscopic Examination of the Head and Neck

Pierre Delaere

CONTENTS

2.1 Introduction

Head and neck neoplasms present with variable signs and symptoms, depending on their site of origin and extension pattern. Thorough clinical examination, aided by modern endoscopic devices, is a cornerstone of the pre- and posttherapeutic evaluation of the patient suffering head and neck cancer. This chapter reviews the possibilities, but also the limitations of the clinical examination for each of the major subsites in the head and neck region.

2.2 Neck

Clinical examination still remains an important method of assessing regional lymph nodes. The presence of a clinically palpable, unilateral, firm, enlarged lymph node in the adult should be considered metastatic until proven otherwise. External examination of the neck represents an important starting point in the examination of the patient. It is important to remember that some cervical masses may escape the very best surgical palpation. It is essential that an orderly and systematic examination of the lymphatic fields on both sides of the neck is performed (Stell and Maran 1972).

Regional lymphatic drainage from the mucosa of the upper aerodigestive tract, salivary glands, and the thyroid gland occurs to specific regional lymph node groups (Shah 1990). They should be appropriately addressed in treatment planning for a given primary site. The major lymph node groups of the head and neck are shown in Fig. 2.1. Cervical lymph nodes in the lateral aspect of the neck primary drain the mucosa of the upper aerodigestive tract. These include the submental and submandibular group of lymph nodes located in the submental and submandibular triangles of the neck. Deep jugular lymph nodes include the jugulodigastric, jugulo-omohyoid, and supraclavicular group of lymph nodes adjacent to the internal jugular vein. Lymph nodes in the posterior triangle of the neck include the accessory chain of lymph nodes located along the spinal accessory nerve and the transverse cervical chain of lymph nodes in the floor of the posterior triangle of the neck. The retropharyngeal lymph nodes are at risk of metastatic dissemination from tumors of the pharynx. The central compartment of the neck includes the delphian lymph node overlying the thyroid cartilage in the midline draining the larynx, and the perithyroid lymph nodes adjacent to the thyroid gland. Lymph nodes in the tracheoesophageal groove provide primary drainage to the thyroid gland as well as the hypopharynx, subglottic larynx, and cervical esophagus. Lymph nodes in the anterior superior mediastinum provide drainage to the thyroid gland and the cervical esophagus.

The localisation of a palpable metastatic lymph node often indicates the potential source of a primary tumor. In Fig. 2.1 the regional lymph node groups draining a specific primary site as first echelon lymph nodes are depicted.

P. Delaere, MD, PhD
Professor, Department of Otorhinolaryngology, Head and Neck Surgery, University Hospitals Leuven, Herestraat 49, 3000 Leuven, Belgium

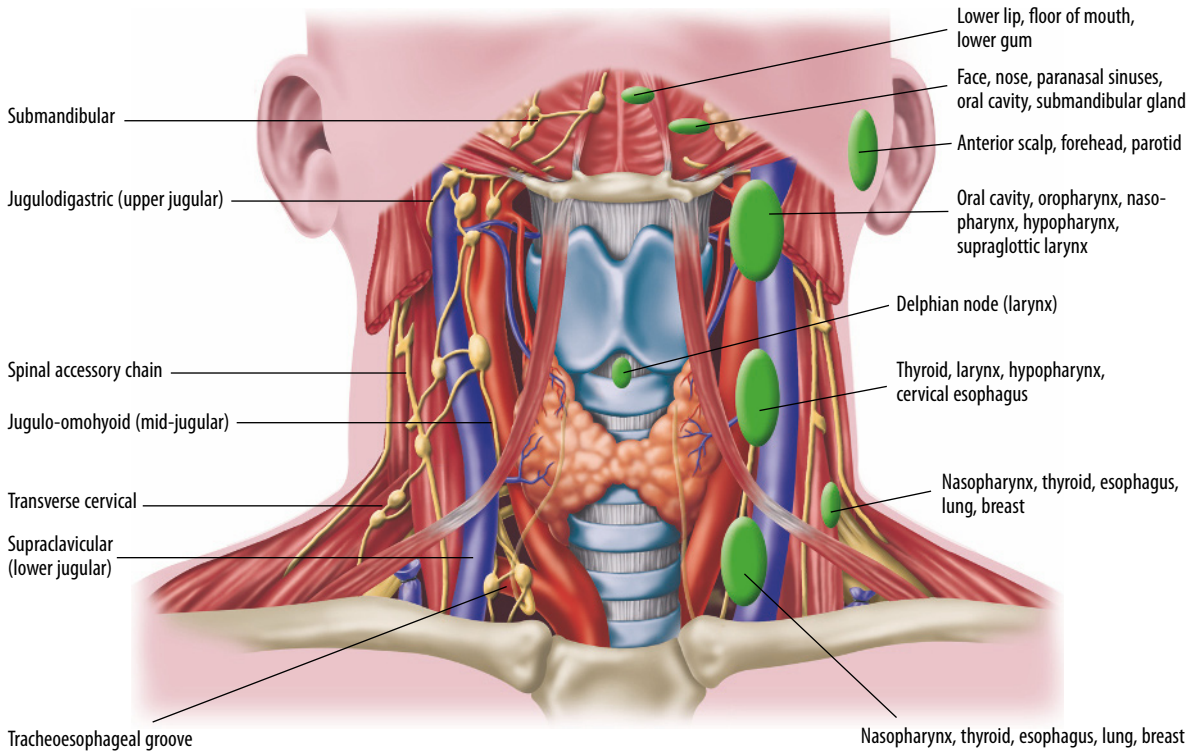

Fig. 2.1. The regional lymph nodes of the head and neck region; the major regional lymphatic chains are annotated on the *left*. These regional lymph node groups drain a specific primary site as first echelon lymph nodes (indicated on *right*)

In order to establish a consistent and easily reproducible method for description of regional cervical lymph nodes, providing a common language between the clinician, the pathologist, and radiologist, the Head and Neck Service at Memorial Sloan-Kettering Cancer Center has described a leveling system of cervical lymph nodes (Fig. 2.2). This system divides the lymph nodes in the lateral aspect of the neck into five nodal groups or levels. In addition, lymph nodes in the central compartment of the neck are assigned levels VI and VII.

- Level I: Submental group and submandibular group. Lymph nodes in the triangular area bounded by the posterior belly of the digastric muscle, the inferior border of the body of the mandible, and the hyoid bone.
- Level II: Upper jugular group. Lymph nodes around the upper portion of the internal jugular vein and the upper part of the spinal accessory nerve, extending from the base of the skull up to the bifurcation of the carotid artery or the hyoid bone. Surgical landmarks: base of skull superiorly, posterior belly of digastric muscle anteriorly, posterior border of the sternocleidomastoid muscle posteriorly, and hyoid bone inferiorly.
- Level III: Mid-jugular group. Lymph nodes around the middle third of the internal jugular vein. Surgical landmarks: hyoid bone superiorly, lateral limit of the sternohyoid muscle anteriorly, the posterior border of sternocleidomastoid muscle posteriorly, and the caudal border of the cricoid cartilage inferiorly.
- Level IV: Lower jugular group. Lymph nodes around the lower third of the internal jugular. Surgical landmarks: cricoid superiorly, lateral limit of the sternohyoid muscle anteriorly, posterior border of the sternocleidomastoid muscle posteriorly, and clavicle inferiorly.
- Level V: Posterior triangle group. Lymph nodes around the lower portion of the spinal accessory nerve and along the transverse cervical vessels. It is bounded by the triangle formed by the clavicle, posterior border of the sternomastoid muscle, and the anterior border of the trapezius muscle.
- Level VI: Central compartment group. Lymph nodes in the prelaryngeal, pretracheal, (Delphian), paratracheal and tracheoesophageal groove. The boundaries are: hyoid bone to suprasternal notch and between the medial borders of the carotid sheaths.

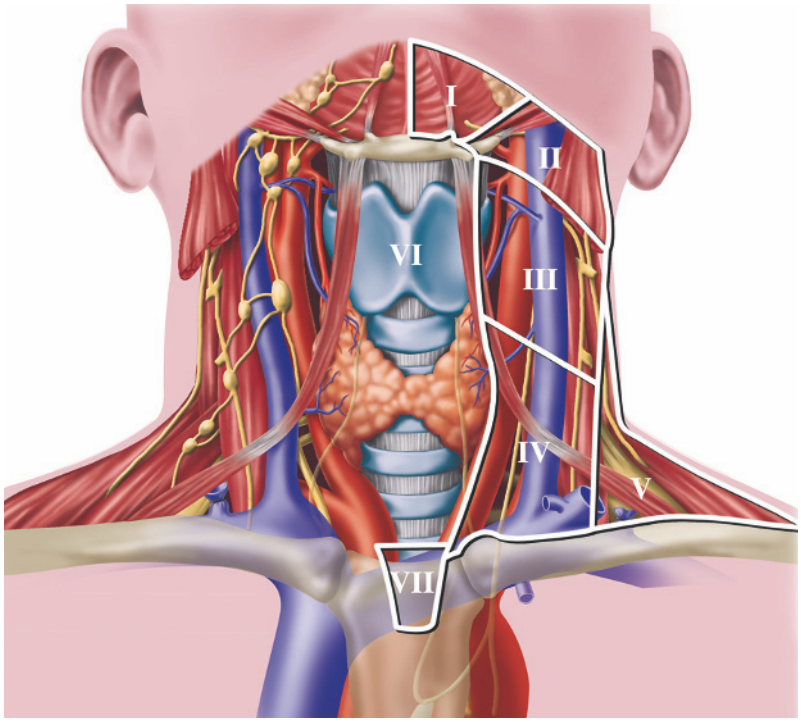

Fig. 2.2. Level system of cervical lymph nodes: 7 levels are distinguished (labeled *I* to *VII*)

- Level VII: Superior mediastinal group. Lymph nodes in the anterior superior mediastinum and tracheoesophageal grooves, extending from the suprasternal notch to the innominate artery.

Some nodes in the neck are more difficult to palpate than others. Thus the retropharyngeal and highest parajugular nodes are almost impossible to detect by palpation until they are very large.

Structures in the neck which may be mistaken for enlarged lymph nodes are the transverse process of the atlas, the carotid bifurcation and the submandibular salivary gland.

Physical examination of the neck for lymph node metastasis has a variable reliability (Watkinson et al. 1990). A meta-analysis comparing computed tomography (CT) with physical examination (PE) yielded the following results: sensitivity, 83% (CT) vs 74% (PE); specificity, 83% (CT) vs 81% (PE); and accuracy, 83% (CT) vs 77% (PE). Overall, PE identified 75% of pathologic cervical adenopathy; this detection rate increased to 91% with addition of CT (Merritt et al. 1997).

The American Joint Committee on Cancer and the International Union against Cancer has agreed upon a uniform staging system for cervical lymph nodes. The exact description of each N stage of lymph node metastasis from squamous carcinomas of the head and neck is described in Table 2.1. Squamous carcinomas of the nasopharynx and well-differentiated thyroid carcinomas have a different biology and cervical metastases from these tumors are assigned different staging systems.

An enlarged metastatic cervical lymph node may be the only physical finding present in some patients whose primary tumors are either microscopic or occult at the time of presentation. A systematic search for a primary tumor should be undertaken in these patients prior to embarking upon therapy for the metastatic nodes. If a thorough head and neck ex-

Table 2.1. N staging of lymph node metastasis from squamous cell carcinoma of the head and neck except nasopharynx and thyroid gland (AJCC/UICC, 2002)

Nx	Regional lymph nodes cannot be assessed
N0	No regional lymph node metastasis
N1	Metastasis in a single ipsilateral lymph node, < 3 cm in greatest dimension
N2a	Metastasis in single ipsilateral lymph node > 3 cm but < 6 cm in greatest dimension
N2b	Metastasis in multiple ipsilateral lymph nodes, none > 6 cm in greatest dimension
N3	Metastasis in a lymph node > 6 cm in greatest dimension

amination, including fiberoptic nasolaryngoscopy, CT or MRI study, and PDG-PET scan, fails to show a primary tumor, then the diagnosis of metastatic carcinoma to a cervical lymph node from an unknown primary is established.

2.3 Nose and Paranasal Sinuses

The nasal cavity is the beginning of the upper airway and is divided in the midline by the nasal septum. Laterally, the nasal cavity contains the nasal conchae, the inferior concha being part of the nasal cavity, and the superior and middle conchae being composite parts of the ethmoid complex. The nasal cavity is surrounded by air containing bony spaces called paranasal sinuses, the largest of which, the maxillary antrum, is present on each side. The ethmoid air cells occupy the superior aspect of the nasal cavity, and separate it from the anterior skull base at the level of the cribriform plate. Superoanteriorly, the frontal sinus contained within the frontal bone forms a biloculated pneumatic space. The sphenoid sinus at the superoposterior part of the nasal cavity is located at the roof of the nasopharynx. The adult ethmoid sinus is narrowest anteriorly in a section known as the ostiomeatal complex and this is the site of drainage of the maxillary and frontal sinuses (Fig. 2.3).

Since all of the paranasal sinuses are contained within bony spaces, primary tumors of epithelial origin seldom produce symptoms until they are of significant dimensions, causing obstruction, or until they have broken through the bony confines of the involved sinus cavity. Tumors of the nasal cavity often produce symptoms of nasal obstruction, epistaxis, or obstructive pansinusitis early during the course of the disease. Unilateral epistaxis, obstruction, or sinusitis should raise the index of suspicion regarding the possibility of a neoplastic process. Tumors of the maxillary antrum may present with symptoms of obstructive maxillary sinusitis. Swelling of the upper gum or loose teeth may be the first manifestation of a malignant tumor of the maxillary antrum. Locally advanced tumors may present with anesthesia of the skin of the cheek and upper lip, diplopia, proptosis, nasal obstruction, epistaxis, a mass in the hard palate or upper gum, or a soft tissue mass in the upper gingivobuccal sulcus. Advanced tumors may present with trismus and visible or palpable fullness of the check. Trismus usually is a sign of pterygoid musculature invasion. Epistaxis may be the first manifestation of tumors of the ethmoid or frontal sinus. This may be accompanied by frontal headaches or diplopia. Occasionally anosmia may be present in patients

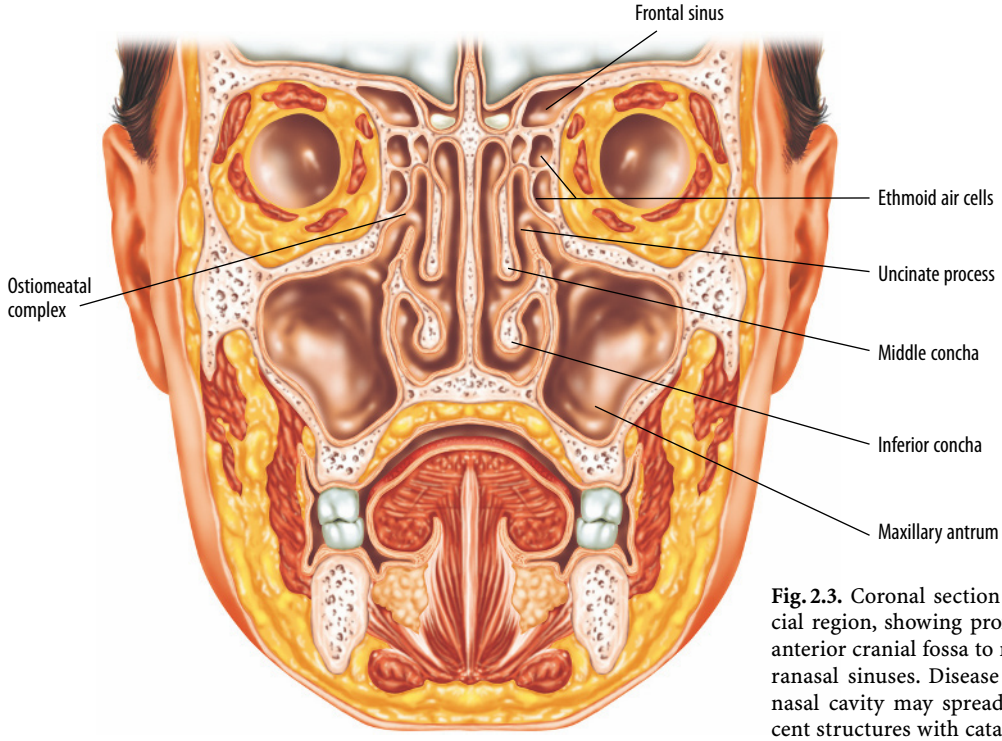

Fig. 2.3. Coronal section through maxillofacial region, showing proximity of orbit and anterior cranial fossa to nasal cavity and paranasal sinuses. Disease of the sinuses and nasal cavity may spread directly into adjacent structures with catastrophic results

with esthesioneuroblastoma. Anesthesia in the distribution of the fifth cranial nerve or paralysis of the third, fourth or sixth cranial nerve may be the first manifestation of a primary tumor of the sphenoid sinus. Although sinonasal malignancy is rare, persistent nasal symptoms should always be investigated, particularly if unilateral. Tumors of the nasal cavity and paranasal sinuses are the most challenging to stage. Endoscopic evaluation of the nasal cavity is crucial in accurate clinical assessment of an intranasal lesion. Fiber optic flexible endoscopy provides adequate visualization of the lower half of the nasal cavity. Therefore, lesions presenting in the region of the inferior turbinate, middle meatus, and the lower half of the nasal septum can be easily visualized by office endoscopy.

Rigid endoscopic evaluation with telescopes generally requires adequate topical anesthesia as well as shrinkage of the mucosal surfaces of the interior of the nasal cavity with the use of topical cocaine. A set of 0°, 30°, 70° and 90° telescopes should be available for appropriate evaluation of the interior of the nasal cavity (Fig. 2.4). Diagnostic nasal endoscopy allows the characterization of intranasal anatomy and identification of pathology not otherwise visible by traditional diagnostic techniques, such as the use of a headlight, speculum, and mirror (Bolger and Kennedy 1992; Levine 1990).

2.4 Nasopharynx

The nasopharynx is the portion of the pharynx bounded superiorly by the skull base and the sphenoid and laterally by the paired tori of the eustachian tubes, with the Rosenmüller's fossa. Anteriorly the posterior choanae form the limit of the space, and inferiorly an artificial line drawn at the level of the hard palate delimits the nasopharynx from the oropharynx.

Presenting symptoms of nasopharyngeal cancer may include a neck mass, epistaxis, nasal obstruction, otalgia, decreased hearing, or cranial neuropathies. Approximately 85% patients have cervical adenopathy and 50% bilateral neck involvement (Lindberg 1972). Serous otitis media may occur due to Eustachian tube obstruction. Cranial nerve VI is most frequently affected but multiple cranial nerves may be involved.

Nasopharyngeal carcinoma has a tendency for early lymphatic spread. The lateral retropharyngeal lymph node (of Rouvier) is the first lymphatic filter but is not palpable. The common first palpable node is the jugulodigastric and/or apical node under the sternomastoid which are second echelon nodes. Bilateral and contralateral lymph node metastases are not uncommon.

Nasendoscopy (Fig. 2.5) using the flexible scope gives a good view of the nasal floor, the walls of the nasopharynx and the fossa of Rosenmüller. Nasopharyngeal tumors in any quadrant including the fossa of Rosenmüller can be seen and accurately biopsied. For the nasopharynx, also rigid 0° and 30° sinus endoscopes can be similarly used in the clinical setting. Under anaesthesia, should this be necessary, these are the scopes of choice for visual assessment and biopsy.

Evidence of lower cranial nerve deficits may be apparent from palatal or glossal paralysis and atrophy. A full evaluation of the remaining cranial nerves

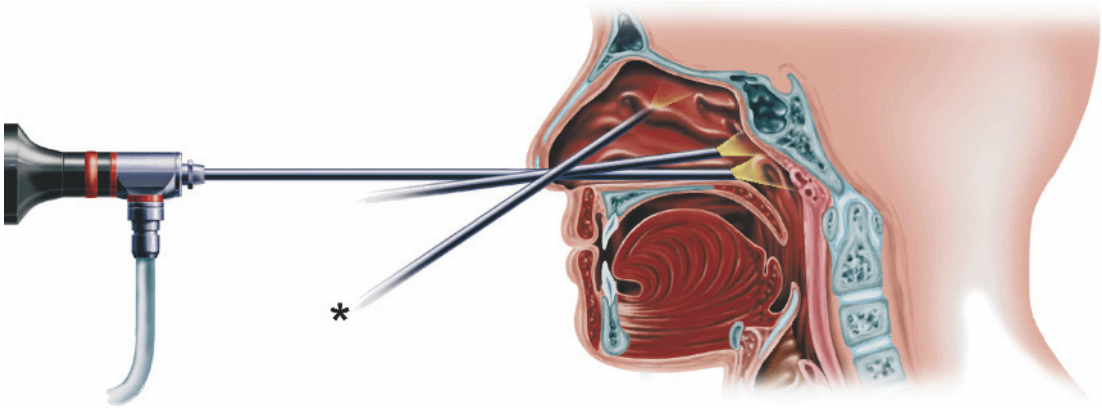

Fig. 2.4. The rigid endoscope allows for detailed examination of the nasal cavity. The scope can be rotated laterally under the middle turbinate into the posterior aspect of the middle meatus (*asterisk*). An excellent view of the middle turbinate, uncinate process, and surrounding mucosa can be obtained

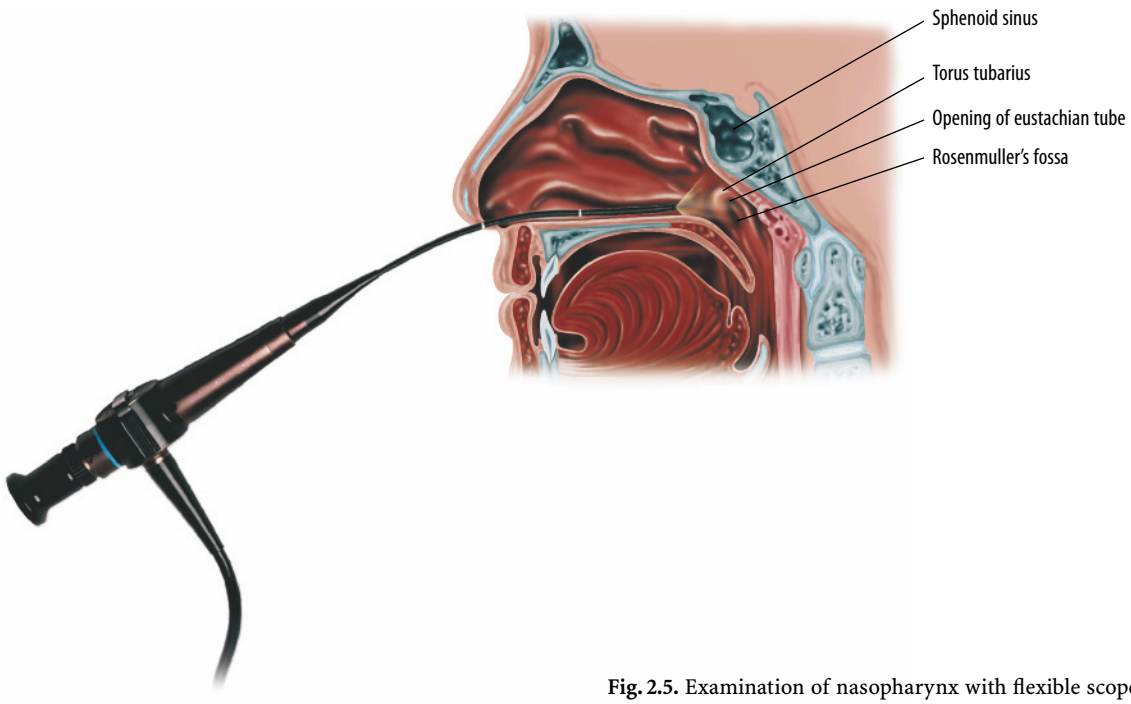

Fig. 2.5. Examination of nasopharynx with flexible scope

should include visual assessment and examination of the tympanic membranes.

2.5 Oral Cavity

The oral cavity extends from the vermilion borders of the lips to the junction of the hard and soft palates superiorly and to the line of the circumvallate papillae inferiorly. Within this area are the lips, buccal mucosa, alveolar ridges with teeth and gingiva, retromolar trigone, floor of mouth, anterior two-thirds of the tongue, and hard palate (Fig. 2.6).

All mucosal surfaces of the mouth require thorough and systematic examination. The oral cavity is lined by a mucous membrane which is a non-keratinizing stratified squamous epithelium and is therefore pink. It contains taste buds and many minor salivary glands. All mucosal surfaces should be examined using tongue blades under optimal lighting conditions.

The clinical features of the primary tumors arising in the mucosal surface of the oral cavity are variable. The tumor may be ulcerative, exophytic or endophytic, or it may be a superficial proliferative lesion. Most patients with a mouth cancer present with a painful ulcer. Squamous carcinomas with excessive keratin production and verrucous carcinomas present as white heaped-up keratotic lesions with varying degrees of keratin debris on the surface. Bleeding from the surface of the lesion is a characteristic for malignancy and should immediately raise the suspicion for a neoplastic process. Endophytic lesions have a very small surface component but have a substantial amount of soft tissue involvement beneath the surface.

Oral salivary tumors may present as a nodule, a non-ulcerative swelling or more usually as an ulcerative lesion. Metastatic tumors may also present as submucosal masses. Mucosal melanoma shows characteristic pigmentation.

Macroscopic lesions should be evaluated for mobility, tenderness and be palpated with the gloved finger to detect submucosal spread. This is particularly important in tongue lesions extending posteriorly into the posterior third and tongue base. The distance from the tumor to the mandible and the mobility of the lesion in relation to the mandible are critical elements in determining the management of perimandibular cancers. The indications for examination under anesthesia include an inadequate assessment of the extent of the disease by history and physical examination and imaging, or the presence of symptoms referable to the trachea, larynx, hypopharynx and esophagus that need endoscopic assessment. It is not cost-effective screening to perform panendoscopy on all patients with oral cavity cancer (Benninger et al. 1993; Hordijk et al. 1989).

Palpation of the neck is of course essential in the assessment of a patient with mouth cancer. Neck

nodal disease is the single most important factor determining the method of treatment, and also prognosis is determined by the presence of metastatic nodes. Full examination of the neck must be carried out to detect any lymph node metastases and each level must be carefully palpated, particularly the upper and middle deep cervical nodes deep to the sternomastoid, from behind the patient, using the tips of the fingers. Carcinoma of the oral tongue has the greatest propensity for metastasis to the neck among all oral cancers. The primary echelon of drainage is level II but other levels may be also involved.

2.6 Oropharynx

The oropharynx is that part of the pharynx which extends from the level of the hard palate above to the hyoid bone below. The anterior wall of the oropharynx is formed by the base or posterior third of the tongue bounded anteriorly by the v-shaped line of circumvallate papillae (Fig. 2.6). When present, the initial symptoms of oropharyngeal cancer are often vague and non-specific, leading to a delay in diagnosis. Consequently, the overwhelming majority of patients present with locally advanced tumors.

Presenting symptoms may include sore throat, foreign-body sensation in the throat, altered voice or referred pain to the ear that is mediated through the glossopharyngeal and vagus nerves. Over two-thirds of patients present with a neck lump. As the tumor grows and infiltrates locally, it may cause progressive impairment of tongue movement which affects speech and swallowing.

Most tumors of the oropharynx can be easily seen with good lighting, but those originating in the lower part of the oropharynx and tongue base are best viewed with a laryngeal mirror. The patient should be asked to protrude the tongue, to rule out injury to the hypoglossal nerve. Trismus is a sign of invasion of the masticator space. Sensory and motor function should be assessed, particularly mobility of the tongue as well as fixation. Fiberoptic nasopharyngeal endoscopy has greatly enhanced the ease of examination of these tumors, particularly in assessing the lower extent of the tumor and also the superior extent if the nasopharynx is involved. The extent of involvement is often underestimated on inspection, and bimanual palpation of the tumor must be undertaken in all patients. Careful palpation should be carried out to estimate the extent of infiltration, but this examination may be limited by patient tolerance; thorough palpation under general anaesthetic is advisable. Advanced tumors that cause trismus may also be better assessed under a general anesthetic. A detailed examination and biopsy under general anaesthetic may be the only accurate method of assessing the extent of tumors such as those of the tongue base that may be in a submucosal location.

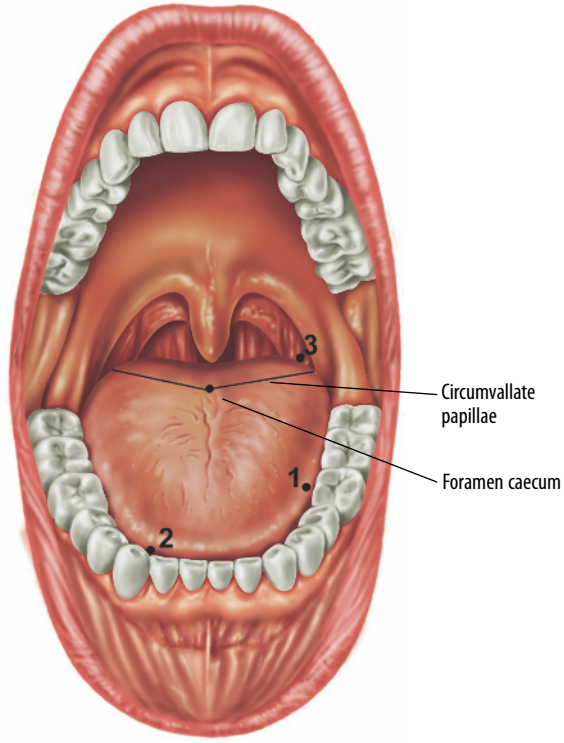

Fig. 2.6. Oral cavity and oropharynx. The posterior limits of the oral cavity are the anterior tonsillar pillars, the junction of the anterior two-thirds and posterior one-third of the tongue (i.e. the circumvallate papillae) and the junction of the hard and soft palate. The soft palate and the tonsil are therefore part of the oropharynx. Carcinoma of the anterior two-thirds of the tongue is the most frequent site for a mouth cancer and the lateral border (*1*) is the most common location. Carcinoma of the floor of the mouth most commonly occurs anteriorly either in the midline or more usually to one side of the midline (*2*). Carcinoma of the oropharynx most commonly occurs in the slit between tonsil and base of tongue, at the level of the anterior tonsillar pillar (*3*)

Examination of the neck must be carried out systematically and each level must be carefully palpated to detect lymph node enlargement or deep invasion of the tumor.

Nodal metastases from squamous cell carcinomas are typically hard and when small are generally mobile. As they enlarge, those in the deep cervical chain initially become attached to the structures in the carotid sheath and the overlying sternomastoid muscle

with limitation in vertical mobility, but later become attached to deeper structures in the prevertebral region with absolute fixation.

Lymphomas on the other hand have a rubbery consistency and are generally larger and multiple with matting together of adjacent nodes. Cystic degeneration in a metastatic jugulodigastric node from a squamous carcinoma of the oropharynx may have a similar presentation to a brachial cyst but the latter is a far less likely diagnosis in the older patient.

2.7 Larynx

The larynx communicates with the oropharynx above and the trachea below. Posteriorly it is partly surrounded by the hypopharynx. It may be functionally divided into three important areas. The supraglottis contains epiglottis, aryepiglottic folds, arytenoids, false cords and includes the laryngeal ventricle. The glottis includes the vocal cords and anterior com-

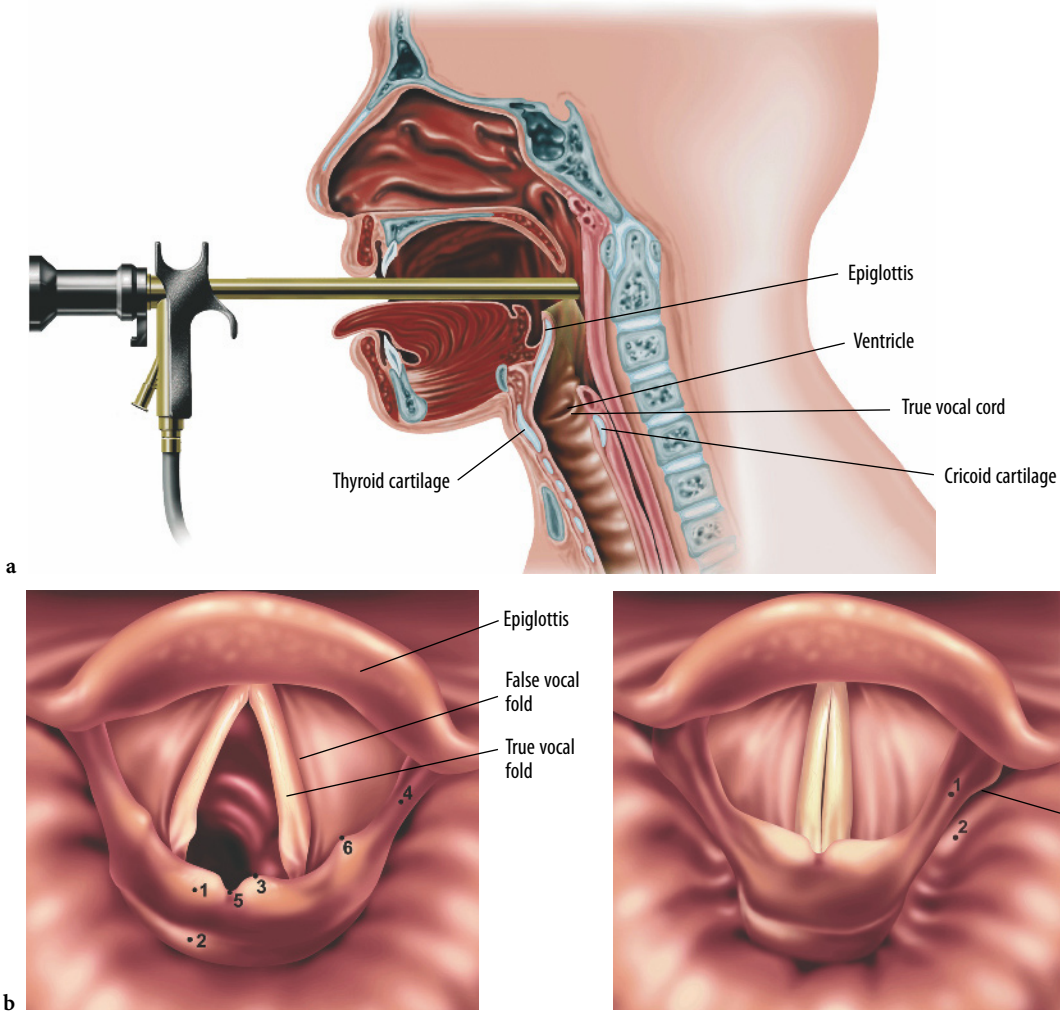

Fig. 2.7. a Indirect laryngoscopy with Hopkins rod telescope. Sagittal view. **b** View during quiet breathing. The arytenoid cartilages (*1*) articulate with facets on the superior surface of the posterior arch of the cricoid cartilage (*2*). A small mass of cartilage, the corniculate cartilage (*3*), usually articulates with the apex of the arytenoid and is located within the inferomedial part of the aryepiglottic fold (*4*). In the midline the mucosa forms a shallow notch between the two corniculate cartilages, known as the posterior commissure (*5*). On the lateral aspect of the corniculate cartilages, within the aryepiglottic folds, are the cuneiform cartilages (*6*). During laryngoscopy the corniculate and cuneiform cartilages appear as small paired swellings in the aryepiglottic folds lying on either side of the posterior commissure. **c** View during phonation. The aryepiglottic folds (*1*) define the anteromedial border of the pyriform fossae (*2*)

missure and posterior commissure. The subglottis is limited by the undersurface of the true cords to the inferior margin of the cricoid cartilage (Fig. 2.7a).

Patients with primary tumors of the larynx usually present with complaints of hoarseness of voice, discomfort in the throat, dysphagia, odynophagia, sensation of something stuck in the throat, occasional respiratory obstruction, hemoptysis, or with referred pain in the ipsilateral ear. Hoarseness is an early symptom of glottic cancer but may be seen later in advanced supraglottic or subglottic tumors indicating spread to the vocal cord, arytenoid or cricoarytenoid joint. Submucosal spread within the paraglottic space can occur from these sites to produce hoarseness without mucosal irregularity. Dyspnea and stridor occur with bulky supraglottic tumors or in the presence of vocal cord fixation. In most instances the diagnosis is made by a thorough clinical examination which includes mirror examination of the larynx for adequate assessment of the surface extent of the primary tumor and mobility of the vocal cords.

Examination must be carried out carefully to identify the possible spread of tumor beyond the larynx either directly or by metastasis to the regional lymph nodes. A neck mass almost always indicates lymphatic metastasis but may result from direct extension of the tumor into the soft tissues of the neck. The most frequent site of secondary deposits is the ipsilateral deep cervical chain, usually in the upper/middle region (level II, III). Glottic tumors rarely metastasize, while deposits in the lymph nodes are more frequent from supraglottic lesions. Examination must include an assessment of the number, mobility and level of the lymph nodes. Some anterior swelling of the larynx, by widening or by penetration of tumor through the cricothyroid membrane, may be felt.

The use of the 70° or 90° Hopkins rod telescope (Fig. 2.7a) allows a high resolution view of the larynx. It allows assessment of vocal cord function, high quality photography, and is the ideal instrument for videostroboscopy of the larynx. The clinical appearance of a normal larynx seen through a rigid telescope is shown in Figure 2.7b. This view of the normal larynx provides adequate visualization of all the anatomic sites of the supraglottic and glottic larynx as well as the hypopharynx. The dynamic function of the larynx should also be observed and recorded by asking the patient to phonate. During phonation, the vocal cords adduct while the pyriform sinuses are opening up, revealing their apices (Fig. 2.7c). Stroboscopy is useful for the differentiation of functional from anatomical defects (Sercarz et al. 1992) and has been employed in the early detection of glottic cancer. In the latter setting, preservation of the mucosal wave suggests that a lesion is not invasive (Zhao 1992).

Technological advance is producing increasingly smaller diameter fiberoptic endoscopes for examination of the human body. The flexible nasendoscope can be used to examine the postnasal space, pharynx and larynx, down to the level of the vocal cords. Flexible nasolaryngoscopy (Fig. 2.8) is generally carried out in a normal anatomical position and during normal respiration, unlike the rather distorted posi-

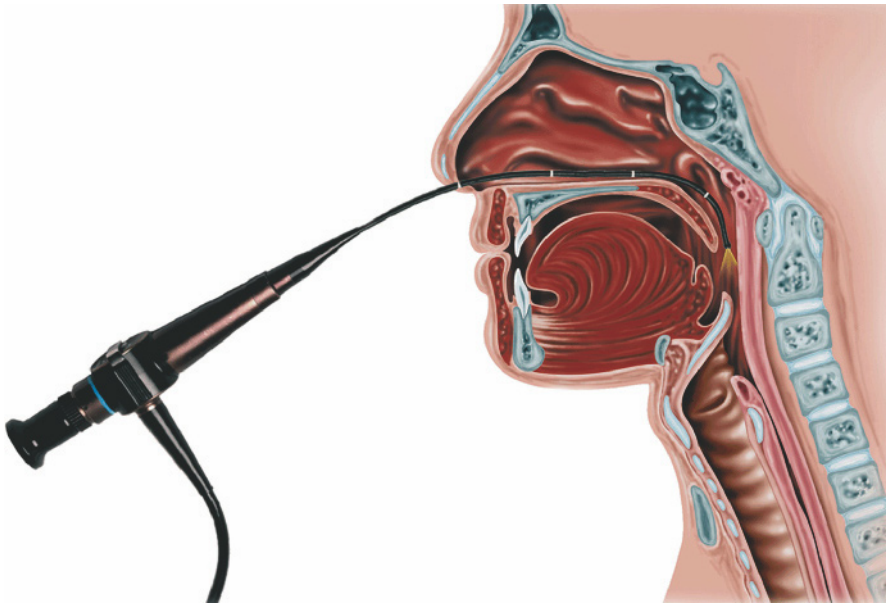

Fig. 2.8. Flexible laryngoscopy. Fiberoptic laryngeal nasendoscopy provides a clear image of the larynx, laryngopharynx and base of tongue

tion achieved by indirect laryngoscopy or the use of the Hopkins rods. Additionally, flexible endoscopy can be used to directly observe the pharyngeal phase of swallowing, giving complementary information to that obtained by videofluoroscopy. Test swallows of milk or coloured food can be examined (Logemann 1983).

Direct laryngoscopy under general anaesthesia is the only reliable way to assess mucosal lesions of the larynx and pharynx (Phelps 1992; Parker 1992), and more often enables adequate biopsies to be sampled than with flexible techniques (Ritchie et al. 1993). If a tumor is detected, its limits in all directions should be determined both by sight and palpation.

The introduction of the operating microscope has facilitated detailed examination of the larynx (Kleinsasser 1965) (Fig. 2.9). Use of various telescopes (0°, 30°, 70° and 120°) provide an excellent and detailed view of the lesion.

Clinical examination is limited by the fact that certain areas of the larynx are inaccessible to both visualization and palpation; nevertheless involvement of these structures has an important bearing on staging as well as on management. Information from radiological imaging and operative endoscopy must be utilized in conjunction with physical findings to obtain an accurate pretreatment TNM staging record. Particularly supraglottic tumors are frequently understaged because the pre-epiglottic and paraglottic spaces cannot be assessed clinically.

2.8 Hypopharynx and Cervical Esophagus

The hypopharynx links the oropharynx superiorly to the larynx and oesophagus below. Its boundaries are roughly the hyoid and valleculae above and the cricoid below. Common sites for squamous cell cancers are the pyriform sinuses, the posterior pharyngeal wall and the postcricoid space.

Patients with primary tumors of the hypopharynx usually present with the complaints of discomfort in the throat, dysphagia, odynophagia, sensation of something stuck in the throat, referred pain in the ipsilateral ear, hemoptysis, hoarseness of voice or shortness of breath. In most instances, diagnosis is made by a thorough clinical examination including mirror examination of the hypopharynx and larynx, as well as either rigid telescopic or fiberoptic nasolaryngopharyngoscopic examination for adequate clinical assessment of the primary tumor.

While clinical examination permits the diagnosis of a primary tumor of the hypopharynx, direct laryngoscopy and esphagoscopy under general anesthesia are essential for accurate assessment of the tumor extent and to obtain a biopsy for histologic diagnosis.

The important features to be assessed during endoscopic examination under anesthesia include the site of origin of the primary tumor, and its local extension to the other sites within the hypopharynx and adjacent regions.

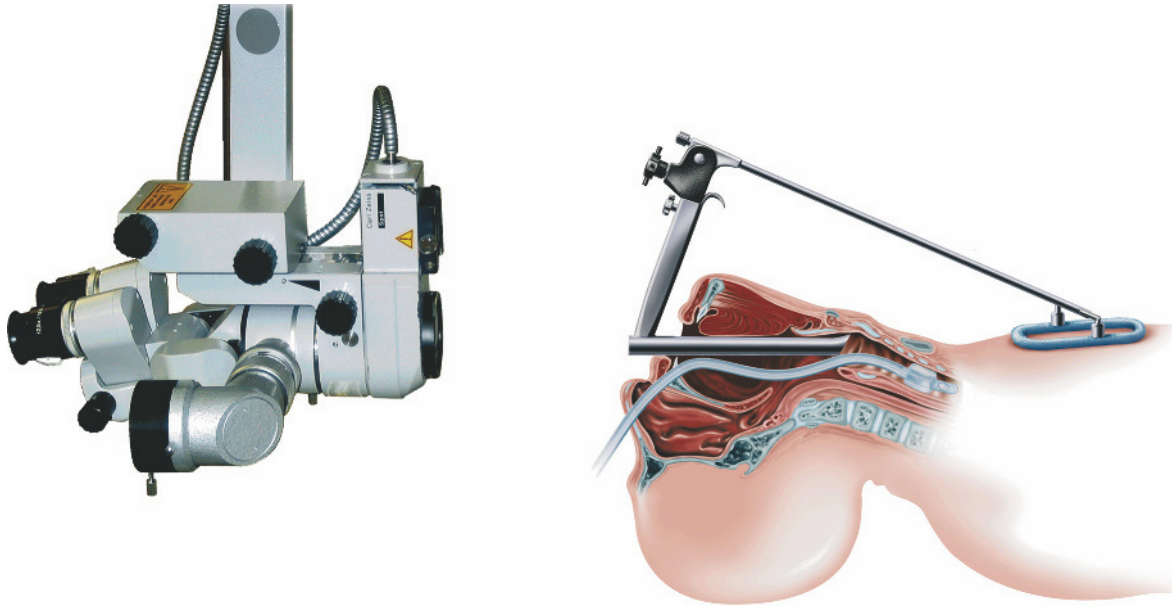

Fig. 2.9. The arrangement for stable microlaryngoscopy. After placement of the laryngoscope the laryngostat is attached and the tension tightened until the view is just adequate. The microscope is then brought into position and focused

In patients with a malignant tumor of the upper respiratory or upper digestive tract, it is advisable to perform flexible oesophagogastroduodenoscopy; the detection rate of a synchronous primary tumor is about 3%–13% (Levine and Nielson 1992).

2.9 Salivary Glands

The parotid glands are located in close proximity to the cartilage of the external auditory canal. Anteriorly the gland abuts both the lateral and posterior border of the ramus of the mandible and the overlying masseter muscle, while inferiorly it rests medially on the posterior belly of the digastric muscle, as well as the sternocleidomastoid muscle laterally. Medially the parotid is adjacent to the parapharyngeal space, while superiorly it reaches the arch of the zygoma. The facial nerve courses through the parotid gland. The parotid gland is arbitrarily divided into a 'superficial' and 'deep' lobe by the plane of the facial nerve. Numerous lymph nodes are localized within, and adjacent to, the capsule of the parotid gland, serving as the first echelon drainage for the temporal scalp, portions of the cheek, the pinna, and the external auditory canal. For this reason, the parotid gland may harbour metastatic cutaneous malignancy from these sites.

The submandibular glands are located in the anterior triangle of the neck, and are bounded superiorly and laterally by the body of the mandible. The mylohyoid muscle is located anterior to the gland, while the hyoglossus muscle lies medial to the gland. The submandibular (Wharton's) duct exists the gland medial to the mylohyoid muscle, then courses anteriorly and superiorly into the anterior floor of mouth (Fig. 2.10).

Located beneath the mucosa of the floor of the mouth, the small sublingual glands drain directly into the oral cavity through numerous small ducts.

The majority of neoplastic lesions of salivary glands appear as a lump without other symptoms.

Swellings in the retromandibular sulcus, the immediate preauricular region, and over the masseter are, in most cases, of parotid gland origin. Although about 10% of parotid gland tumors arise medial to the plane of the facial nerve in the deep 'lobe' of the gland, more than three-fourths of these deep lobe tumors will present as a typical parotid mass.

In the parotid gland pleomorphic adenomas present as round, firm, reasonable well-demarcated tumors, with a tendency to nodularity as they grow. Their site of election is between the ascending ramus of the mandible anteriorly, and the mastoid process and sternomastoid posteriorly, usually in

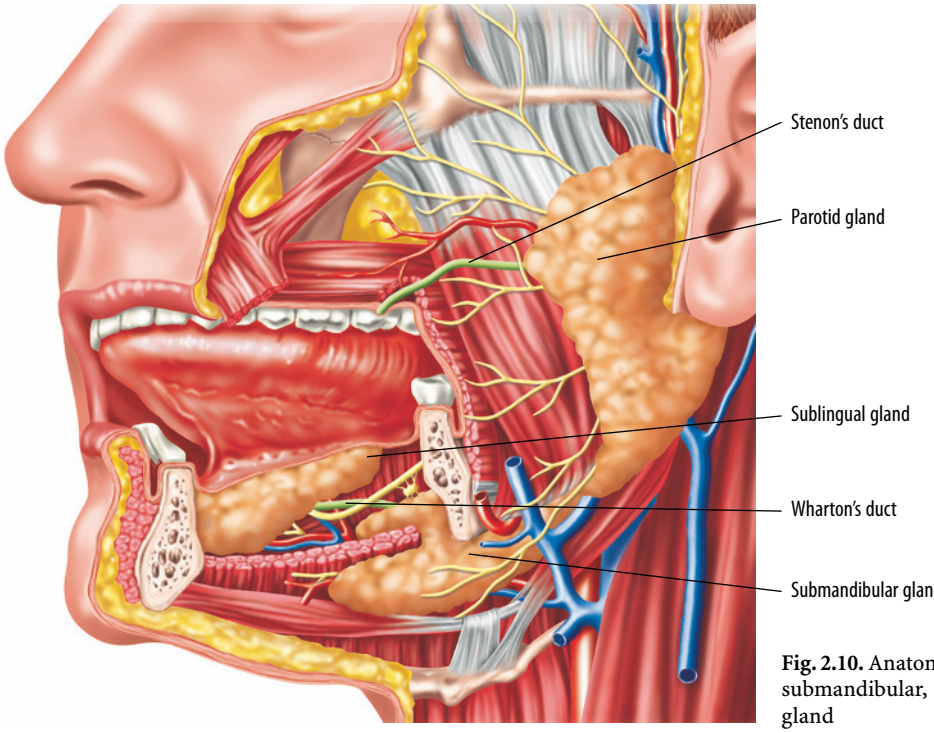

Fig. 2.10. Anatomic relations of the parotid, submandibular, and sublingual salivary gland

the tail of the gland. Occasionally they arise in the immediate preauricular region, where they tend to be small. Whartin's tumors lie almost invariably in the lower pole of the gland, are ovoid in shape, and vary in consistency between soft and firm, depending on whether or not they have been exposed to previous inflammation; these tumors can occur bilaterally.

Weakness or paralysis of the facial nerve in a previously untreated patient almost always indicates that a tumor is malignant (Spiro et al. 1975; Borthne et al. 1986). Careful assessment should be made of the facial nerve and the nerves traversing the nearby carotid space (cranial nerve IX and XII) if a deep lobe or parapharyngeal space tumor is suspected.

It is often difficult to distinguish between a tumor arising within the submandibular gland or an enlarged node close to the gland or on its outer surface. Bimanual palpation is essential to differentiate between the two, since a node lying on the outer surface of the salivary gland is unlikely to be palpated by a finger in the mouth, whereas a tumor of the gland itself is more readily compressible bimanually. Pleomorphic adenomas of the submandibular gland are usually large, quite hard, and nodular, but may be confused with a slowly growing malignancy such as an adenoid cystic carcinoma. Submandibular gland neoplasms also need evaluation of the lingual and hypoglossal nerves.

The assessment of intraoral minor salivary gland neoplasms depends on the location of the tumor. Palatal lesions are the most common, usually giving the appearance of being fixed, whether they are benign or malignant, because of the tight adherence of the mucous membrane to bone. Tumors of the hard or soft palate are often fusiform, firm to hard in consistency and nodular. Again the distinction between mixed tumor and adenoid cystic carcinoma may be difficult to make.

A salivary gland tumor arising from the deep lobe of the parotid gland, or from a minor salivary gland in the parapharyngeal space, may cause secondary displacement of the palatotonsillar region.

Swelling detectable both in the pharynx and parotid region indicates a very bulky tumor originating from within the deep lobe of the parotid gland. This parotid swelling can be visible externally, but the technique of bimanual palpation will elicit the characteristic sign of ballottement between the examining fingers, typical of masses occupying such a wide area. The absence of both a visible swelling in the parotid gland and ballottement suggests an origin exclusively in the parapharyngeal space.

2.10 Thyroid Gland

The thyroid gland lies within the pretracheal fascia in the front of the neck, and consists of two symmetrical lobes united in the midline by an isthmus that overlies the second to fourth tracheal rings (Fig. 2.1). There is often a pyramidal lobe, which may extend as high as the top of the thyroid cartilage.

The incidence of palpable thyroid nodules is estimated at only 4%–7% of the general adult population. They occur more frequently in women and they are increasing with age (Mazzaferri et al. 1988). Slightly less than 5% of thyroid nodules are found to be malignant (Gharib and Goellner 1993). Most patients with differentiated carcinoma present with a palpable nodule in the thyroid gland of varying size, consistency and local extent. The primary tumor may present as a solitary, well-defined, intrathyroidal discrete palpable nodule or it may manifest with diffuse involvement of the thyroid gland with or without extrathyroid extension and fixation to the structures in the central compartment of the neck, or it may present as multiple palpable nodules. The most common location of palpable metastatic lymph nodes from thyroid cancer is at levels III, IV or V in the lateral neck. Procedures commonly used for the initial evaluation of thyroid nodules are: ultrasound, radionuclide imaging, and fine-needle aspiration biopsy (FNAB).

Anaplastic carcinoma of the thyroid gland usually manifests in the older population with a very short history of a rapidly enlarging thyroid mass. Physical examination reveals a diffusely enlarged firm to hard ill-defined thyroid mass with significant extrathyroid extension to adjacent soft tissues. The mass appears fixed and inseparable from the laryngotracheal-esophageal complex.

2.11 Role of Imaging Studies

The clinical evaluation allows to appreciate the mucosal layer of the head and neck region quite well. However, the deep extent of potentially infiltrating lesions can only be judged indirectly. Some regions, such as the base of the skull, pterygopalatine and infratemporal fossa, orbits and brain are beyond clinical evaluation, but critical management decisions have to be made based on the involvement of these structures; imaging findings are of the utmost impor-

tance in such cases. Perineural and/or perivascular spread, eventually leading to tumor progression or recurrences at distance from the primary tumor can often only be detected by imaging.

Metastatic adenopathies can be identified, sometimes still in a subclinical stage or at places not accessible for clinical examination, such as the retropharyngeal or paratracheal lymph nodes. Also, information on extranodal tumor spread and the relation to critical structures such as the carotid arteries, is necessary for determining the optimal patient management, and can be deduced from imaging studies.

Imaging is needed in submucosal lesions, covered by an intact mucosa. The origin and extent of such lesions is often difficult to determine based on the clinical evaluation alone. Imaging may provide important clues to the diagnosis, as representative biopsies may be difficult to obtain in deep-seated lesions.

All these findings can profoundly influence the staging and management of the patient with head and neck cancer. Finally, imaging may be used to monitor tumor response and to try to detect recurrent or persistent disease before it becomes clinically evident, possibly with a better chance for successful salvage.

The single most important factor in the optimal use of all this information is the mutual co-operation between the radiologist and the physicians in charge of patient care.

References

Benninger MS, Enrique RR, Nichols RD (1993) Symptom-directed selective endoscopy and cost containment for evaluation of head and neck cancer. Head Neck 15:532–536

Bolger WE, Kennedy DW (1992) Nasal endoscopy in the outpatient clinic. Otolaryngol Clin North Am 25:791–802

Borthne A, Kaalhus O, Vermund H (1986) Salivary gland malignant neoplasms: treatment and prognosis. Int J Radiat Oncol Biol Phys 12:747–754

Gharib H, Goellner JR (1993) Fine needle aspiration biopsy of the thyroid: an appraisal. Ann Intern Med 118:282–289

Hordijk GJ, Bruggink T, Ravasz LA (1989) Panendoscopy: a valuable procedure? Otolaryngol Head Neck Surg 101:426–428

Kleinsasser O (1965) Weitere technische Entwicklungen und erste Ergebnisse der "endolaryngealen Mikrochirurgie". Laryngol Rhinol Otol 44:711–727

Levine B, Nielson EW (1992) The justifications and controversies of panendoscopy - a review. Ear Nose Throat J 71:335–343

Levine HL (1990) The office diagnosis of nasal and sinus disorders using rigid nasal endoscopy. Otolaryngol Head Neck Surg 102:370–373

Lindberg RD (1972) Distribution of cervical lymph node metastases from squamous cell carcinoma of the upper respiratory and digestive tracts. Cancer 29:1446–1450

Logemann JA (1983) Evaluation and treatment of swallowing disorders. College Hill Press, San Diego

Mazzaferri EL, de los Santos ET, Rofagha-Keyhani S (1988) Solitary thyroid nodule: diagnosis and management. Med Clin North Am 72:1177–1211

Merritt RM, Williams MF, James TH et al (1997) Detection of cervical metastasis. A meta-analysis comparing computed tomography with physical examination. Arch Otolaryngol Head Neck Surg 123:149–152

Parker R (1992) Laryngoscopy, microlaryngoscopy and laser surgery. In: McGregor IA, Howard DJ (eds) Rob and Smith's operative surgery: head and neck, part 2, 4th edn. Butterworth, Oxford, pp 451–463

Phelps PD (1992) Carcinoma of the larynx - the role of imaging in staging and pre-treatment assessments. Clinical Radiology 46:77–83

Ritchie AJ, McGuigan J, Stenvenson HM et al (1993) Diagnostic rigid and flexible oesophagoscopy in carcinoma of the oesophagus: a comparison. Thorax 48:115–118

Sercarz JA, Berke GS, Ming Y et al (1992) Videostroboscopy of human vocal fold paralysis. Ann Otol Rhinol Laryngol 101:567–577

Shah JP (1990) Patterns of nodal metastases from squamous carcinomas of the upper aerodigestive tract. Am J Surg 160:405–409

Spiro RH, Huvos AW, Strong EW (1975) Cancer of the parotid gland: a clinicopathologic study of 288 primary cases. Am J Surg 130:452–459

Stell PM, Maran AGD (eds) (1972) Pre-operative considerations. In: Head and neck surgery. William Heinnemann Medical, London, p 6

Zhao R (1992) Diagnostic value of stroboscopy in early glottic carcinoma. Chung Rua Ehr Pi Yan Hou Ko Tsa Chih 27:175–176

Watkinson JC, Johnston D, James D et al (1990) The reliability of palpation in the assessment of tumors. Clinical Otolaryngology 5:405–410

3 Imaging Techniques

Robert Hermans, Frederik De Keyzer, and Vincent Vandecaveye

CONTENTS

3.1 Introduction

Various imaging techniques are used in the evaluation of patients with head and neck cancer, before, during and after treatment. Each of these imaging techniques has its own advantages and disadvantages.

Many head and neck neoplasms arise from the mucosal lining; when a patient is referred for imaging, the histological diagnosis often was already established by endoscopic biopsy. Therefore, imaging should primarily supply information on the submucosal extension depth of the primary tumor, including its relation to surrounding structures, as well as on the presence of regional and/or distant metastasis.

The purpose of this chapter is to describe the various techniques available for imaging the head and neck cancer patient, and to provide general rules for their use. Specialized imaging applications are described in the following chapters where appropriate.

R. Hermans, MD, PhD
Professor, Department of Radiology, University Hospitals Leuven, Herestraat 49, 3000 Leuven, Belgium
F. De Keyzer, MSc; V. Vandecaveye, MD
Department of Radiology, University Hospitals Leuven, Herestraat 49, 3000 Leuven, Belgium

3.2 Plain Radiography

In the past, a variety of conventional methods were applied to stage head and neck cancer, including soft tissue views of the neck, plain films of the facial skeleton, xeroradiography, plain film tomography, laryngography and barium swallow. The value of these studies to stage head and neck cancer is very limited; these techniques are now replaced by cross-sectioning imaging modalities.

Plain radiography is still widely used in radiotherapy planning (see Chap. 18). Barium swallow remains an indispensable method in the early phase after pharyngeal surgery, to rule out or confirm the presence of fistulae. This technique is also essential in the evaluation of functional disorders (such as bolus retention, delayed passage and aspiration) after surgery or radiotherapy.

3.3 Ultrasonography

Ultrasonography is a widely used technique for the evaluation of the thyroid gland (see Chap. 14), neck lymph nodes (see Chap. 15) and salivary glands, as it offers visualization of these structures with high spatial resolution, at a low cost and without using ionizing radiation.

Ultrasonography in combination with fine needle aspiration cytology (FNAC) is the most accurate method for neck nodal staging in most head and neck cancers (van den Brekel et al. 1991). However, execution of this procedure is time consuming, and the obtained results are operator dependent (Takes

et al. 1996). Also, in a multicenter study where both computed tomography and ultrasound of the neck were applied for staging of head and neck cancer, the addition of ultrasound guided FNAC did not provide significant additional value (Takes et al. 1998).

3.4 Computed Tomography and Magnetic Resonance Imaging

Nowadays, in most patients computed tomography (CT) or magnetic resonance imaging (MRI) is performed for pretherapeutic staging of a head and neck malignancy. Both techniques can supply the information needed by the clinician for adequate treatment planning.

A common question is which of these techniques should be used in a particular patient. The most widely used technique is CT, as it has a number of important advantages over MRI:

- Wide availability
- Relative low cost
- Easy to execute, and this in a reproducible way
- Short examination time, resulting in less image quality degradation caused by motion, such as swallowing and respiration
- Superior bone detail
- High quality multiplanar imaging on multidetector CT systems
- Easy extension of the study into the upper thoracic cavity or intracranial cavity, if needed
- Easier interpretation, especially regarding nodal involvement (Curtin et al. 1998)

However, CT also has a number of disadvantages compared to MRI:

- Relative low soft tissue contrast resolution
- Administration of iodinated contrast agent is necessary
- Severe image quality degradation by dental fillings or other metallic foreign objects (Fig. 3.1)
- Radiation exposure

The advantages of MRI over CT in the evaluation of head and neck cancer are its superior soft tissue contrast resolution, and the absence of radiation exposure. Overall, the image quality is not or less hampered by the presence of dental fillings than in CT, but also MRI studies may be severely jeopardized by metallic implants (Fig. 3.2). The disadvantages of MRI are mainly related to the long acquisition time, making the technique sensible to motion artifacts which cause a non-diagnostic study (Fig. 3.3). It is also somewhat more difficult with MRI to properly stage both primary tumor and neck nodal disease in a single study. The lower availability of MRI, resulting in a longer waiting list, and its higher cost should also be taken into consideration.

In many institutions, CT is the preferred imaging method for evaluation of laryngeal and hypopharyngeal cancer, as well as of oral cavity and oropharyngeal cancer. These cancer sites constitute about 80%–85% of all head and neck malignancies (excluding skin cancer and lymphoma) in Europe and the USA. In most cases, a dedicated CT study will provide all answers needed by the clinician; in such a setting, MRI is used as a complementary tool to solve remaining questions.

Because of its higher contrast resolution, MRI is the preferred imaging method in rarer head and neck malignancies, such as nasopharyngeal cancer and sinonasal cancer. There is no consensus regarding the use of CT or MRI as primary imaging tool in salivary gland cancer, although there is a tendency among head and neck radiologists to choose MRI.

3.4.1 Computed Tomography

CT can be regarded as the 'workhorse' of head and neck cancer imaging. It is not possible to define the ideal imaging protocol, as available equipment varies. The minimal requirements for an optimal diagnostic study will be outlined.

3.4.1.1 Patient Positioning

The images are obtained with the patient supine and during quiet respiration. The neck should be in slight extension. The head is aligned in the cephalocaudal axis in order to make it possible to compare symmetric structures. Malposition may result in an appearance that simulates disease. Every effort should be made to make the patient feel comfortable; this will help the patient dropping the shoulders to a position as low as possible.

This patient-friendly position is applicable for all indications if multidetector spiral CT (MDCT) is used, as this modality allows retrospective high quality reformatting in every spatial plane. In case an incremental or single spiral CT technique has to be used, additional direct coronal imaging is needed

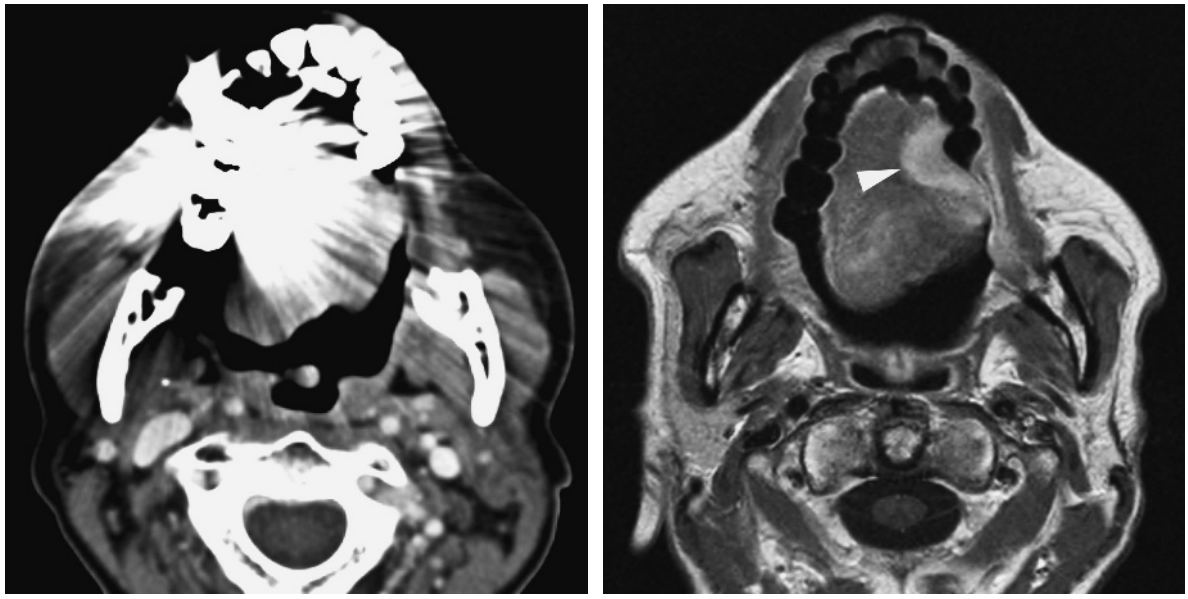

Fig. 3.1a,b. Patient suffering left-sided oral tongue cancer. **a** Axial contrast-enhanced CT image. As the image quality is severely hampered by artifacts arising from dental fillings, the primary tumor is not visible. A complementary MR study was advised. **b** Gadolinium-enhanced T1-weighted image, not affected by presence of dental fillings, clearly shows the primary tumor (*arrowhead*)

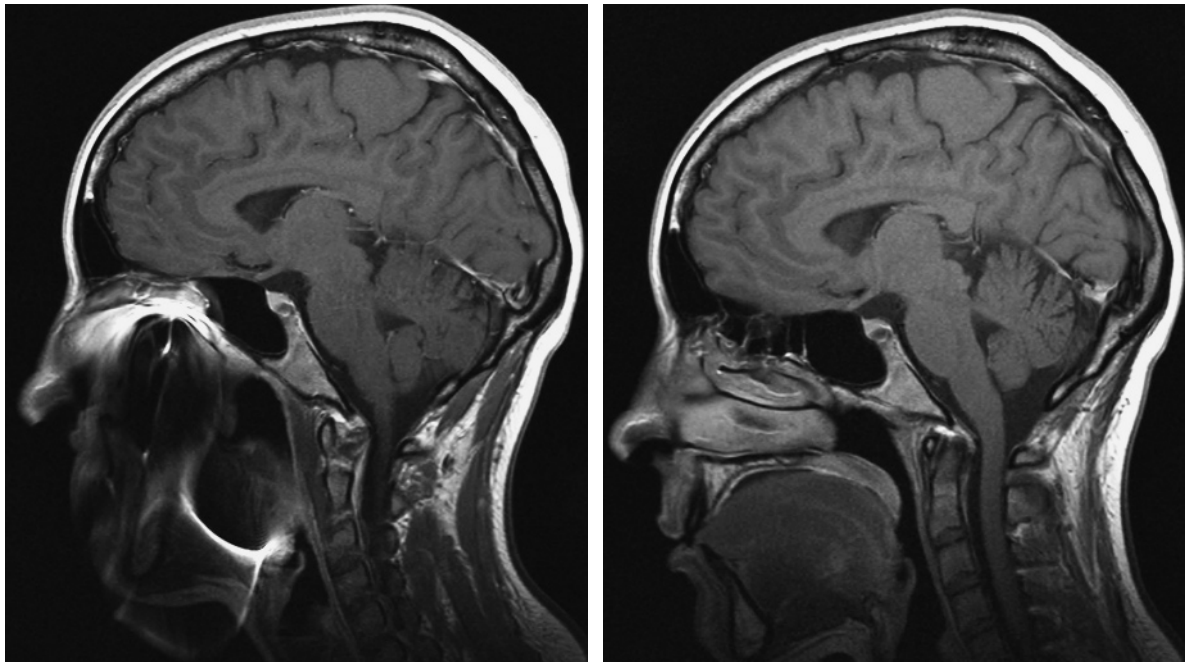

Fig. 3.2a,b. Patient referred for MR study of the maxillofacial region and skull base because of unilateral facial pain. **a** Initial MR study was inconclusive, as artifacts caused by fixed orthodontic material severely degrade image quality. **b** After removal of the orthodontic material by the dentist, optimal image quality was achieved

in the evaluation of sinonasal and skull base neoplasms. This can be realized by hyperextension of the neck, either in supine or prone position, and tilting the gantry to a position perpendicular to the hard palate.

3.4.1.2 Contrast Agent Injection

While evaluating a patient suffering head and neck cancer, a proper injection method of iodinated con-

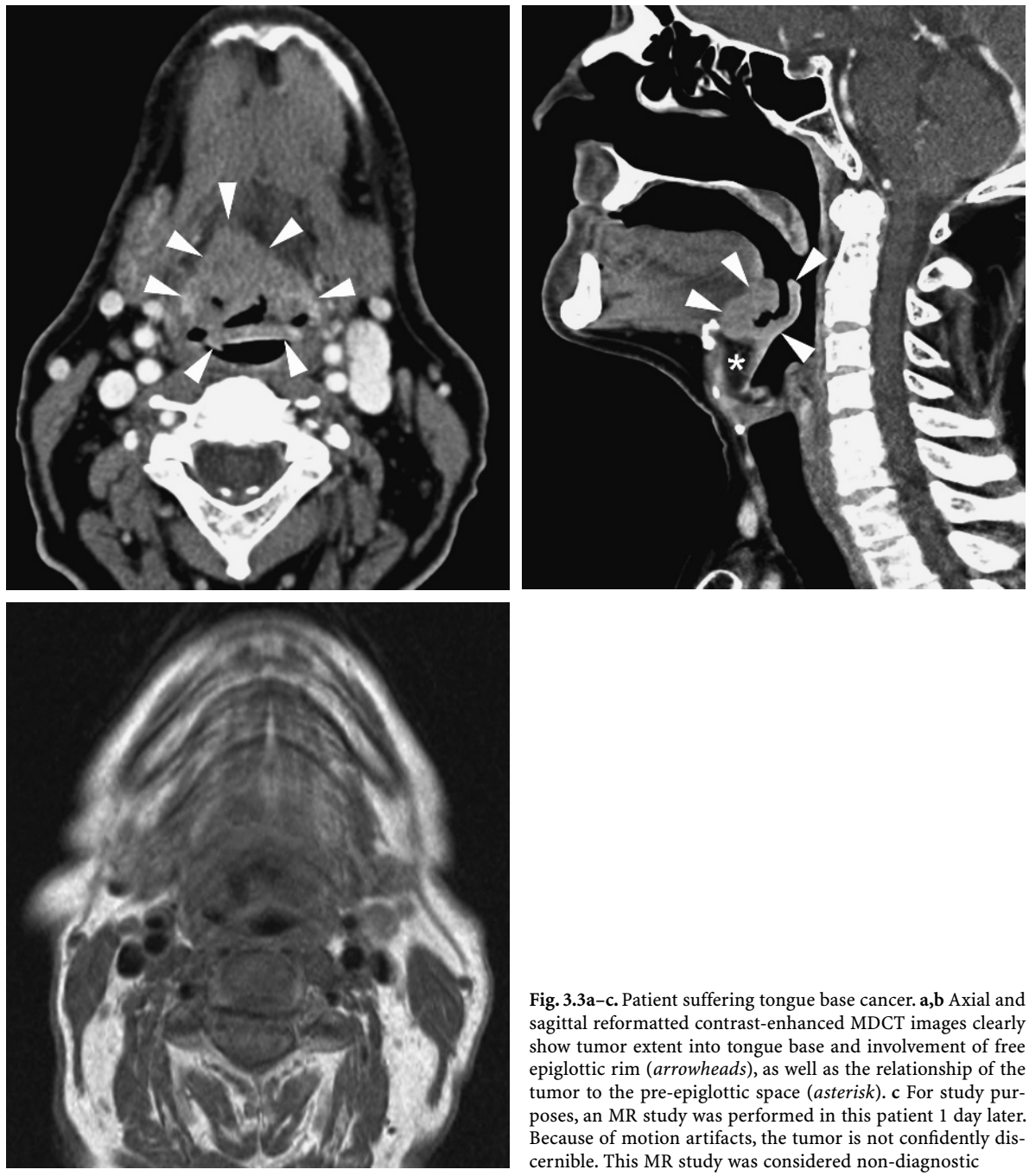

Fig. 3.3a–c. Patient suffering tongue base cancer. **a,b** Axial and sagittal reformatted contrast-enhanced MDCT images clearly show tumor extent into tongue base and involvement of free epiglottic rim (*arrowheads*), as well as the relationship of the tumor to the pre-epiglottic space (*asterisk*). **c** For study purposes, an MR study was performed in this patient 1 day later. Because of motion artifacts, the tumor is not confidently discernible. This MR study was considered non-diagnostic

trast agent is *crucial* to obtain state of the art CT images. Optimal tissue enhancement, allowing correct discrimination of tumoral from normal tissue, and a high neck vessel density must be realized at the same time. Several contrast agent injection protocols have been described, some of them being fairly complicated. For all practical purposes, a single bolus technique with an injection rate of 1 cc/s is appropriate on modern CT machines (Keberle et al. 2002). A total amount of 100 ml is sufficient in MDCT; a somewhat higher volume (up to 150 ml) may be required when an incremental or single slice spiral CT technique is used.

It is essential to wait 60 s before starting the acquisition, as the contrast agents needs some time to diffuse in the normal and pathologic soft tissues. If re-angulation of the gantry at the oral level is performed (see below), the contrast injection needs not

to be paused while changing the gantry angle. If one uses an MDCT machine, allowing a rapid entire neck examination without gantry angulation, the scan should be started only after injection of the entire contrast volume (i.e. after 100 s). A subsequent saline injection at the same injection rate is recommended.

3.4.1.3 Data Acquisition and Image Reconstruction

3.4.1.3.1 General Comments

On a lateral scout view, the area of interest is indicated. For a routine head and neck imaging study, images are acquired from the top of the sphenoid sinus to the lower border of the sternoclavicular joints. It makes sense to scan from cranial to caudal: this allows the contrast medium concentration in the subclavian vein, at the side of injection, to drop to a similar or only slightly higher level compared to other neck vessels, reducing artifacts at the level of the thoracic inlet.

When performing a routine study of the face, sinonasal region or skull base, images are acquired from the top of the frontal sinus to the submental region.

The field of view (FOV) must be as small as possible, to optimize spatial resolution. The recommended FOV for neck studies varies between 16 and 20 cm, depending on the size of the patient. The selected FOV also depends on the type of pathology: in a study performed for squamous cell cancer, the posterior part of the perivertebral space not necessarily needs to be included in the FOV as it is unlikely to encounter pathology in that region; however, for example in skin cancer and lymphoma, this part of the neck should also be visualized, as (sub)occipital adenopathies may be present.

The optimal display slice thickness for evaluation of neck structures is 3 mm; adjacent slices should be obtained. Somewhat thinner slices (2 mm) are apt for the evaluation of the facial bones, sinonasal cavities and orbits. In laryngeal and hypopharyngeal neoplasms, it is useful to reconstruct an additional series of images coned down to the laryngohypopharyngeal region, with a FOV of about 10 cm and a slice thickness of 2 mm. Also the evaluation of the temporal bone requires a coned down FOV (about 9 cm), and a thin slice thickness of 0.8–1 mm.

Image reconstruction is always done in a soft tissue algorithm. Additional images, reconstructed in a high resolution (bone detail) algorithm, are always generated in sinonasal cavity, skull base and temporal bone studies.

3.4.1.3.2 Incremental CT and Single-Slice Spiral CT

Even in this era of MDCT, studies of acceptable quality can be obtained using an incremental or single-slice spiral CT technique. The disadvantage of these techniques is the compromise that has to be made between slice thickness and acquisition time. As these techniques do not allow obtaining very high quality reformattings from the native images, the gantry angle should be changed at the mouth level. From the skull base down to the oral cavity, the image plane should be parallel to the hard palate, while from the oral cavity down to the thoracic inlet, the image plane should be parallel to the vocal cords. The vocal cord plane sometimes can be recognized on the lateral scout views; if this can not be seen, the gantry should be tilted parallel to the intervertebral disk space at the level of C4–C5 or C5–C6. Adherence to this protocol generates images reproducibly showing head and neck anatomy; furthermore, dental filling artifacts are avoided at the level of the oral cavity.

The CT examination is performed as contiguous 3-mm thick scans, or as a spiral study reconstructed as contiguous 3-mm sections. The spiral technique uses 3-mm thick scans with a 3- to 5-mm/s table speed, and a pitch of 1:1–1:1.6; these parameters may vary slightly according to the CT machine.

3.4.3.1.3 Multidetector Spiral CT

State-of-the-art CT of the head and neck requires the use of MDCT. The rapid acquisition results in a volumetric data set, reconstructed to a stack of thin and overlapping native images; this reduces partial volume averaging and motion artifacts. Furthermore, full advantage of the injected contrast agent is accomplished by optimal timing between injection and image acquisition. The disadvantage of this technique is the overall higher radiation exposure.

The data acquisition with MDCT is usually done with zero gantry tilt. However, in some patients, this causes problems at the level of the oral cavity when dental fillings are present. Also, in patients with short necks or a high position of the shoulders, the image quality may be suboptimal at the level of the larynx due to artifacts arising from the shoulder girdle. To avoid these problems, some head and neck radiologists continue to use gantry tilting in MDCT, as de-

scribed for the incremental and single slice spiral CT technique. Changing the gantry tilt increases the image study time, and makes it impossible to obtain reformatted images in the coronal or sagittal plane at the level of the oral cavity.

The native images can not routinely be used for display: the large amount of native images is difficult to handle, and the signal/noise level of these images is relatively low. Therefore, a new set of images needs to be reformatted from these native images for display. These images are routinely reformatted in the axial plane, mimicking the image display as is obtained in incremental or single slice spiral CT: for neck studies, adjacent 3-mm thick images are reformatted parallel to the hard palate from the skull base to the oral cavity, and parallel to the vocal cords from the oral cavity to the thoracic inlet (Fig. 3.4). Reformatting in other planes and/or with a thinner slice thickness is done according to the organ of interest (see above) and/or the findings on the axial images (Fig. 3.5).

More technical details on the MDCT parameters used currently in the University Hospitals of Leuven are summarized in Tables 3.1 and 3.2.

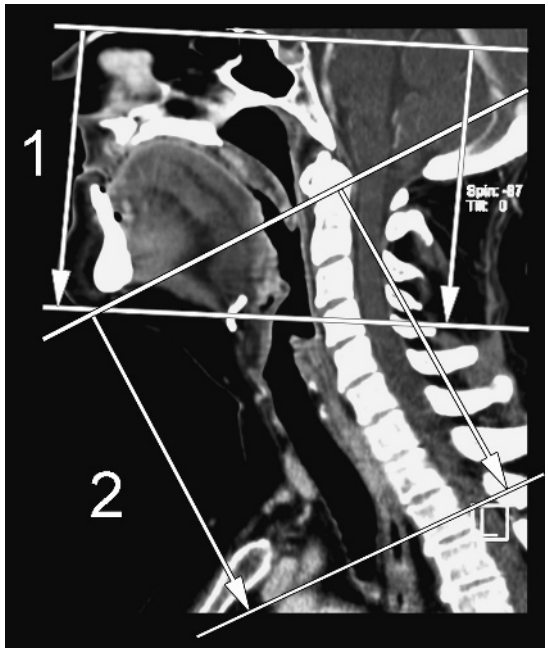

Fig. 3.4. Routine head and neck CT study. Midline sagittally reformatted image from native axial MDCT images. The data acquisition extended from just above the sphenoid sinus to the thoracic inlet. From the native images, two sets of axial images are routinely reformatted for display: the first set (*1*), parallel to the hard palate, from the skull base to the lower margin of the mandible; the second set (*2*), parallel to the vocal cords (or C4–C5/C5–C6 intervertebral space), from the oral cavity to the thoracic cavity. The two image sets should be overlapping

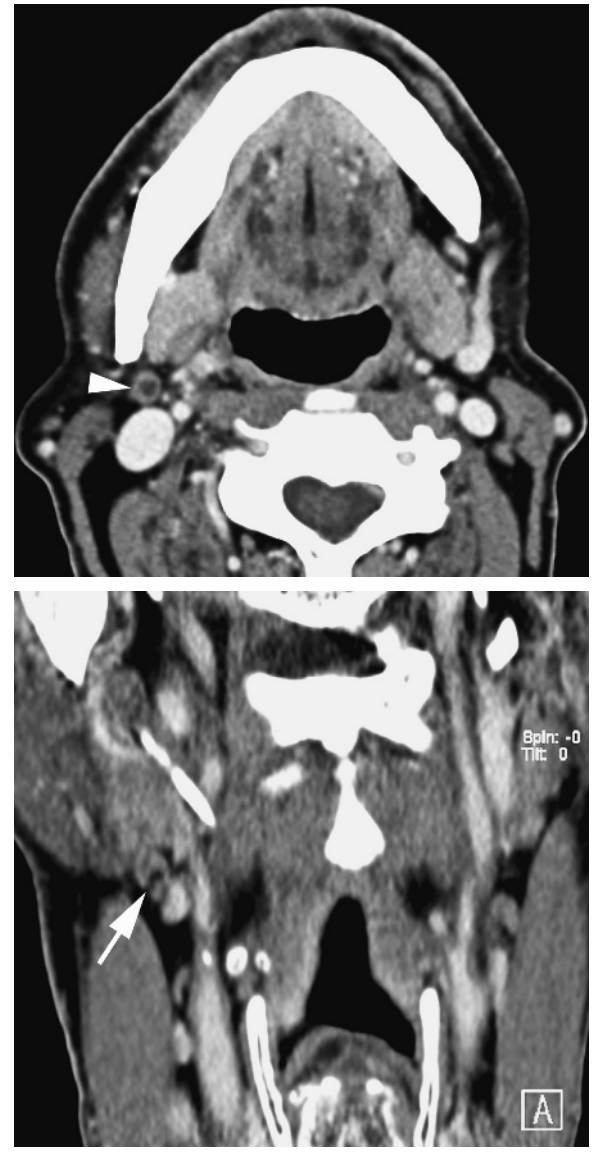

Fig. 3.5a,b. a Axial MDCT image (3-mm thick) shows lymph node on right side, appearing centrally hypodense (*arrowhead*): central necrosis or partial volume averaging of fatty nodal hilum? **b** Additionally, a thinner (1.5-mm) reformatting was made through this lymph node in the coronal plane. On this section, the hypodense nodal region shows fat density and communicates with the outer nodal border: fatty metaplasia in nodal hilum. Normal lymph node

3.4.1.4 Dynamic Maneuvers

The data acquisition is routinely performed while the patient continues breathing. Dynamic maneuvers during scanning can improve the visualization of particular anatomic structures. During prolonged phonation of [i], arytenoid mobility can be judged

Table 3.1. MDCT data acquisition and native image reconstruction parameters

		4-Row	16-Row	64-Row
	Collimation	4×1 mm	16×0.75 mm	64×0.6 mm
	Feed/rotation	4 mm	9.9 mm	34.5 mm
Neck[a]	Rotation time	0.75 s	1 s	1 s
Face[b]	KV	120	120	120
Sinonasal cavities[b]	mAs_{eff}	200[c]	250[c]	250[c]
	$Slice_{eff}$	2 mm	1.5 mm	1.5 mm
	Slice interval	1 mm	0.7 mm	0.7 mm
	Collimation	2×0.5 mm	2×0.6 mm	12×0.6 mm
	Feed/rotation	0.8 mm	1.2 mm	3.2 mm
Temporal bone[b]	Rotation time	1 s	1 s	1 s
Skull base[b]	KV	120	120	120
	mAs_{eff}	180[c]	220[c]	350[c]
	$Slice_{eff}$	0.5 mm	0.6 mm	0.6 mm
	Slice interval	0.2 mm	0.2 mm	0.2 mm

mAs_{eff}, effective mAs; $slice_{eff}$, effective slice thickness
[a]Soft tissue algorithm
[b]Both soft tissue and bone detail algorithm in tumoral pathology
[c]Effectively used mAs may be lower (determined by automatic exposure control system)

Table 3.2. MDCT image reformatting for display

	Slice thickness	Slice interval	Image plane
Neck	3 mm	3 mm	Axial (coronal + sagittal if needed)
Face, sinonasal cavities, skull base (soft tissue detail)	2 mm	4 mm (2 mm for skull base)	Axial + coronal (sagittal if needed)
Temporal bone, skull base (bone detail)	0.8 mm	1	Axial + coronal (sagittal if needed)

and a better visualization of the laryngeal ventricle can be achieved; the slight distention of the pyriform sinuses may also allow better delineation of the aryepiglottic folds (Lell et al. 2004). A modified Valsalva maneuver (blowing air against closed lips, puffing out the cheeks) produces substantial dilatation of the hypopharynx, allowing better visualization of the pyriform sinuses, including the postcricoid region (Robert et al. 1993) (Fig. 3.6). This modified Valsalva maneuver may also be of use in the evaluation of oral cavity tumors, as the inner cheek walls and gingivobuccal sulci become better visible.

The success rate of these dynamic maneuvers is variable, especially when an incremental CT technique is used, and is strongly dependent on patient cooperation. These problems are largely overcome by spiral CT and MDCT, as the patient has to perform the maneuver only once during one rapid acquisition.

Dynamic maneuvers are mainly helpful in showing superficial tumor spread, while the purpose of imaging is describing deep tumor extent. Also, abnormal mobility of the vocal cord is more accurately seen during clinical examination than on dynamic imaging studies. Therefore, the added value of acquiring images during a dynamic maneuver in staging head and neck neoplasms is, on average, limited.

3.4.1.5 Three-Dimensional Image Reformatting

Three-dimensional (3D) display of the data set is most often done to evaluate the bony structures of the maxillofacial skeleton in congenital abnormalities or traumatic lesions. Meaningful 3D display of the often subtle osteolytic changes seen in head and neck malignancies is rarely possible. However, in some cases of extensive bone destruction, 3D displays are helpful for the surgeon in planning bone resection (Fig. 3.7).

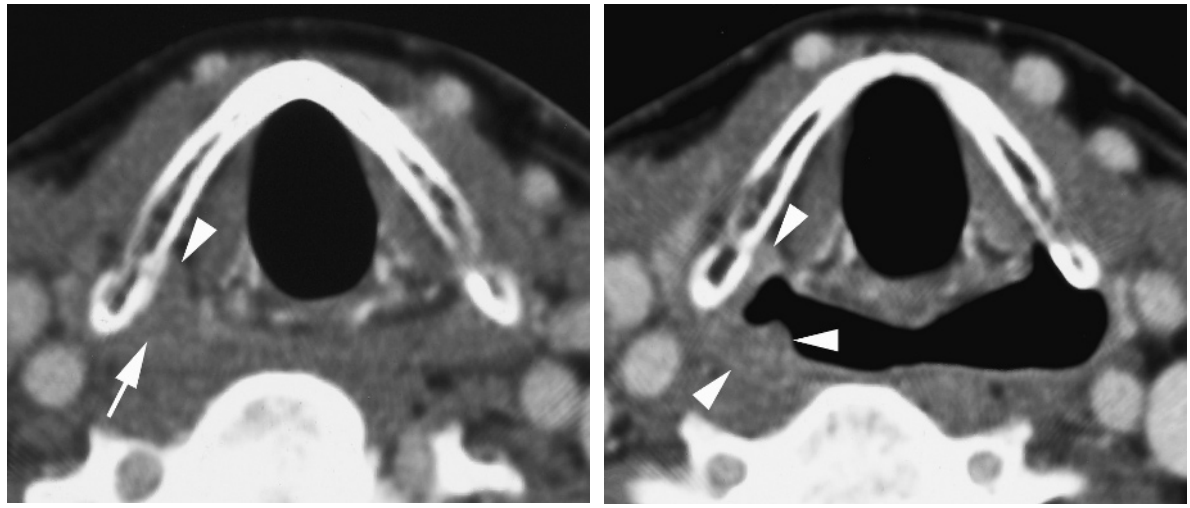

Fig. 3.6a,b. Contrast-enhanced single-slice spiral CT images in a patient suffering cancer of the pyriform sinus. **a** Axial image during quiet breathing shows subtle soft tissue thickening in the apex of the right pyriform sinus (*arrow*); some evidence of subtle infiltration or displacement of the paraglottic space fat is present (*arrowhead*). **b** Axial image obtained during modified Valsalva maneuver. The right pyriform sinus expands somewhat less than the opposite one; the mucosal irregularity produced by the cancer is now better visible (*arrowheads*)

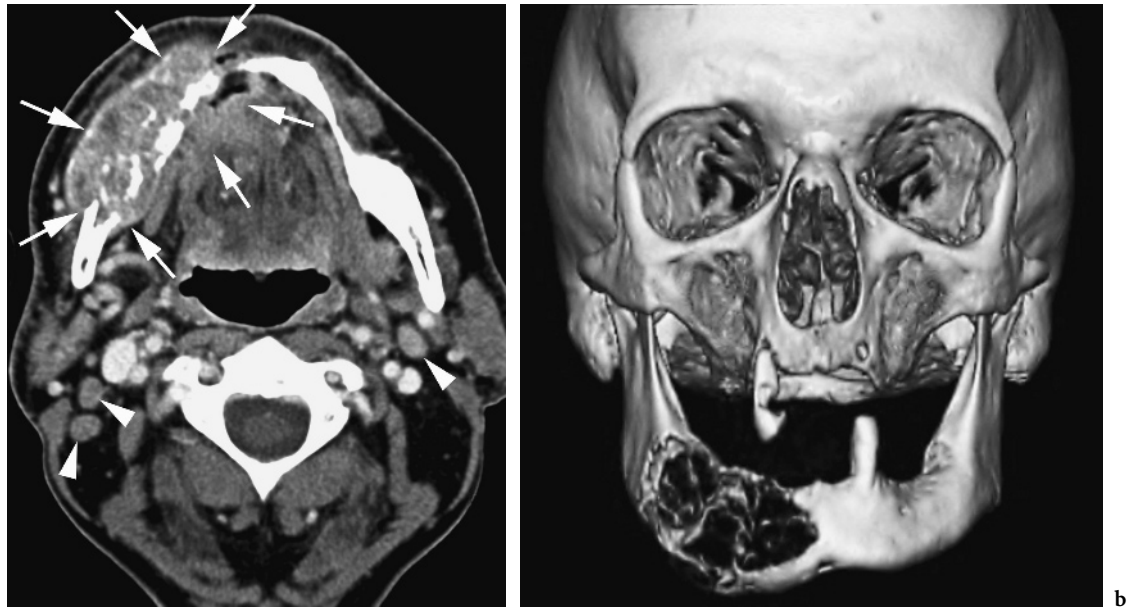

Fig. 3.7a,b. a Axial contrast-enhanced MDCT image. Large floor of the mouth cancer, massively invading the right side of the mandible (*arrows*). Several small but inhomogenously enhancing adenopathies are visible on both sides of the neck (*arrowheads*). **b** Extent of mandibular bone destruction can easily be appreciated on 3D reformatting

Virtual endoscopy of the larynx and hypopharynx has been studied; otolaryngologists rank such 3D images as more beneficial than radiologists, usually in bulky masses that precluded definitive direct endoscopic evaluation (Silverman et al. 1995). This technique does not show the adjacent soft tissues, and its clinical role is not exactly defined (Magnano et al. 2005).

3.4.2 Magnetic Resonance Imaging

MRI of the head and neck can be performed on low-field or high-field machines. At comparable measuring time, the high-field (≥ 1T) machines provide a better signal-to-noise ratio and a higher spatial

resolution. Currently, the experience on 3T systems regarding the investigation of head and neck tumors is limited.

3.4.2.1 Patient Positioning

Similar to CT, image acquisition is performed with the patient in supine position, and during quiet respiration. The head and neck should be aligned and symmetrically positioned. Every effort should be made to make the patient feel as comfortable as possible. The patient should be instructed not to move during the examination, and to try not to swallow or cough during the image acquisition.

3.4.2.2 Coils

The choice of the receiver coil is dictated by the localization of the disease process. If the tumor is localized in the oral cavity or infrahyoid part of the neck, the neck coil should be used. When the patient suffers neoplastic disease at the level of the skull base, sinonasal cavities, face, parotid glands, or nasopharynx, the head coil should be selected.

A disadvantage of using the head coil is that the neck lymph node regions are only partly covered; this is of particular importance in nasopharyngeal cancer, commonly associated with neck adenopathies throughout the neck. On modern MR machines, the head and neck coil can be combined, allowing comprehensive evaluation of the entire head and neck region. Alternatively, in the absence of a dedicated neck coil, one can opt to stage the primary tumor with MR, using the head coil, and perform an additional CT or neck ultrasound study to stage neck disease.

A possible drawback of using the combination of head and neck coils is that both coils have a distinctive coil design, inducing inhomogeneous recipient field characteristics at the crossover between the two coils, which translates into local signal loss, distortion and heterogeneous incomplete fat saturation. This drawback can be partially overcome by meticulous shimming, coil and patient position and the use of sequences with short echo-trains. The latest MR systems are equipped with large arrays of identical receiver coil elements, positioned in a homogeneous pattern on the patient, providing full receiver coil coverage with a homogeneous high signal to noise ratio and minimizing artifacts due to differential coil design.

3.4.2.3 Standard Sequences

After obtaining scout images, a standard examination of the head and neck should start with a T2-weighted turbo spin echo (TSE) sequence. Compared to a conventional T2-weighted spin echo (SE) sequence, a TSE sequence takes less time to perform, reducing motion artifacts and improving image quality. The high signal intensity of fat on a T2-weighted TSE sequence can be a disadvantage, as this may reduce the contrast between a tumor and the surrounding tissues. The contrast can be improved by performing the sequence with either a chemical shift-moderated fat suppression technique (chemical shift-selective fat suppression or water-selective excitation) or by applying an additional inversion recovery preparation pulse with a short inversion time (SPIR, SPAIR, STIR).

The high signal intensity of fat and bone marrow on a plain T1-weighted SE or TSE sequence is often very helpful to determine tumor extent, as it contrasts clearly with the low signal intensity of most tumors. Repetition of this sequence after injection of gadolinium-DTPA, and comparison with the pre-injection sequence, makes it possible to determine the areas of contrast enhancement and to differentiate these areas from fat.

A fat-saturated T1-weighted SE sequence after injection of gadolinium-DTPA may be helpful, as the contrast between enhancing tissue and fat is increased. However, such a sequence has a number of disadvantages. A fat-suppressed sequence is prone to susceptibility artifacts, commonly observed in the head and neck region because of the presence of numerous soft tissue-bone and tissue-air interfaces. Also, the conspicuity of anatomical structures is reduced, and the acquisition time is prolonged.

Depending on the investigated region, a slice thickness of 3–4 mm is optimal, with an interslice gap of 0%–50%. The FOV is similar to what is described above for CT. The imaging matrix should be at least 256×256; for lesions in and around the skull base and sinonasal cavities, a matrix of 512×512 should be used.

The plane of section is chosen according to the localization of the disease process. For most neck lesions, it is appropriate to start with a T2- and T1-weighted sequence in the axial plane, and to continue with a gadolinium-enhanced axial, coronal and sagittal T1-weighted sequence. In general, the axial plane should be, similar as for CT, parallel with the hard palate when dealing with suprahyoid pathology, and parallel with the vocal cords when dealing with infrahyoid pathology. In naso-ethmoidal neoplasms, it may

be more useful to start the study with a coronal T2- and T1-weighted sequence, in order to better evaluate potential spread to the anterior cranial fossa.

The use of very fast imaging such as single-shot techniques is not recommended in all but the newest systems. Single-shot techniques have in general a low signal to noise ratio and are very sensitive to magnetic field inhomogeneities (susceptibility effects), which are the two most persistent difficulties in head and neck MRI. When such sequences are used, patient positioning and shimming should be performed with the utmost precision. If patient movement is within limits, a segmented approach, probing the entire k-space into several separate acquisitions and thereby reducing the echo-train length, is preferable to minimize the above mentioned drawbacks. The use of parallel imaging grants the benefit of a reduced scan time with the same image quality, or a 'normal' scan time but with a better image quality. In practice this means that patient movement artifacts can be reduced and signal-to-noise ratio increased, making parallel imaging an ideal addition to head and neck MR imaging. However, as the parallel imaging reconstruction algorithm is very prone to both magnetic field and receiver coil homogeneity, a combined use of dedicated head and neck coils (see above) limits the application of parallel imaging. When using the newest systems with a large number of homogeneous receiver coils (see above), application of parallel imaging may allow comprehensive evaluation of the head and neck area.

3.4.2.4 Contrast Agents

In MR studies for head and neck neoplasms, obtaining sequences before and after injection of gadolinium-DTPA (at a dose of 0.1–0.2 mmol/kg body weight) is mandatory. Most neoplasms will show increased signal intensity after contrast agent injection. This will usually increase the contrast between the tumor and the surrounding lesions. However, tumors infiltrating bone marrow may become less well visible after contrast injection, as their signal intensity may become similar to that of the surrounding bone marrow; this problem can be solved by obtaining a fat-suppressed sequence (see above). Tumor necrosis becomes better visible after injection of gadolinium; this is of particular importance in staging the neck nodes (see Chap. 15).

Ultra-small superparamagnetic iron oxide (USPIO) particles are captured by macrophages in normally functioning lymph nodes. As a result, signal intensity reduction is observed in tissues accumulating these particles, because of the susceptibility effects of iron oxide. Metastatic lymph nodes show a hyperintensity on sequences weighted to these effects. Promising results have been obtained in the head and neck, but technical problems regarding motion, susceptibility artifacts and spatial resolution still need to be solved (Sigal et al. 2002).

3.4.2.5 Additional MRI Techniques

MRI is a very flexible imaging modality, and tailoring the study to the particular needs in the individual patient is possible. Although in most cases the standard sequences solve the diagnostic questions, in some instances additional sequences can further characterize pathological tissues or further refine the anatomical details visible on the study. Without aiming to be exhaustive, a number of possible additional MRI techniques are shortly described below.

Diffusion-weighted (DW) MRI is an imaging technique showing molecular diffusion, corresponding to the Brownian motion of the spins in biologic tissues. The apparent diffusion coefficient (ADC) is a parameter used to quantify DW-MRI. The ADC is in part determined by the molecular diffusion of water, the microcirculation of blood and the presence of structures on a microscopic scale (microvessels, tubuli, and others) (Le Bihan et al. 1988). Cell size, cell density and cell integrity influence the signal intensity seen on DW images, as well as the value of the ADC. The technique is promising to distinguish non-invasively different entities, such as benign and malignant tumor (Fig. 3.8) (Wang et al. 2001).

Volumetric interpolated breath-hold imaging (VIBE) is a 3D fat-saturated gradient-echo T1-weighted sequence that can be optimized for short acquisition times, providing high-quality MR angiograms if acquisition and contrast injection are properly synchronized. It can also be used to evaluate tumor perfusion, or as an alternative to T1-weighted SE sequences, as it combines excellent image contrast with minimal partial volume averaging (Farina and Borghesi 2005).

Heavily T2-weighted thin images are helpful for the visualization of the cisternal part of the cranial nerves; this can be achieved with gradient-echo or TSE sequences (Yousry et al. 2000). These sequences provide high-resolution anatomical images of the cranial nerves; however, involvement of the nerves by neoplasms is often best detected on gadolinium-enhanced images.

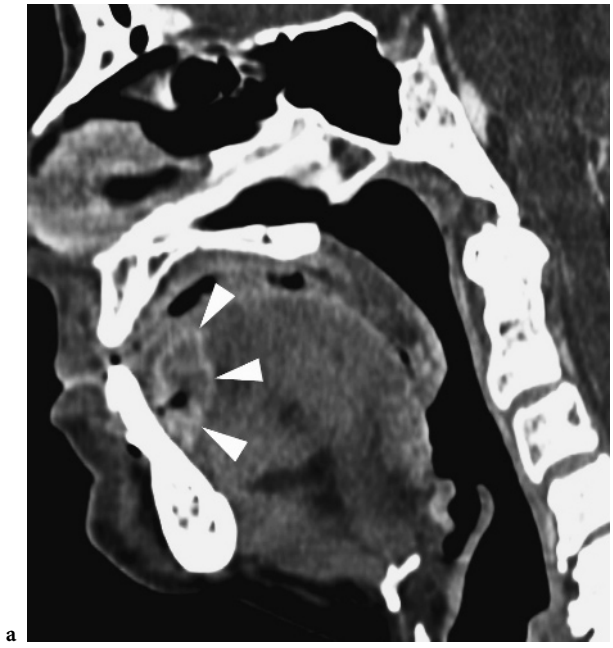

a

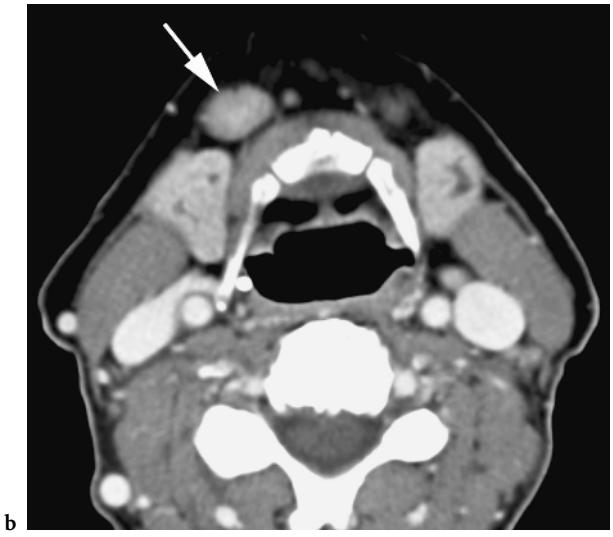

b

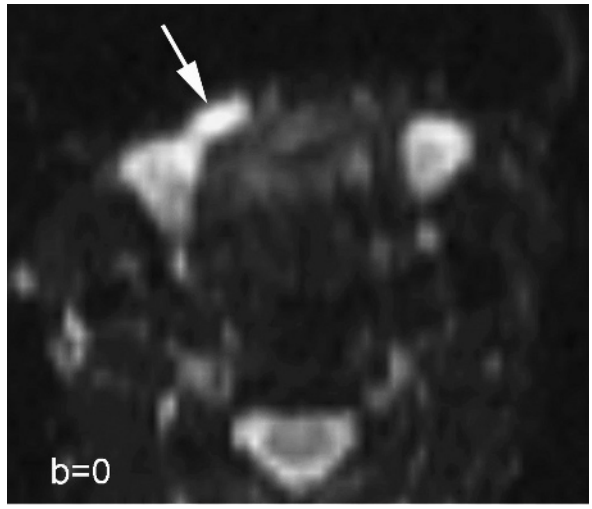

c

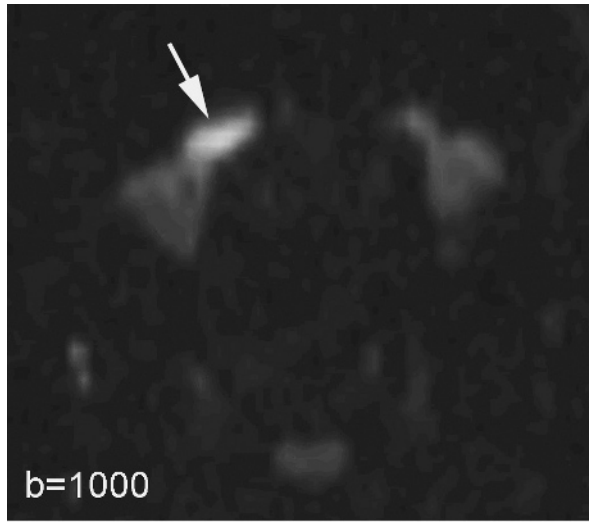

d

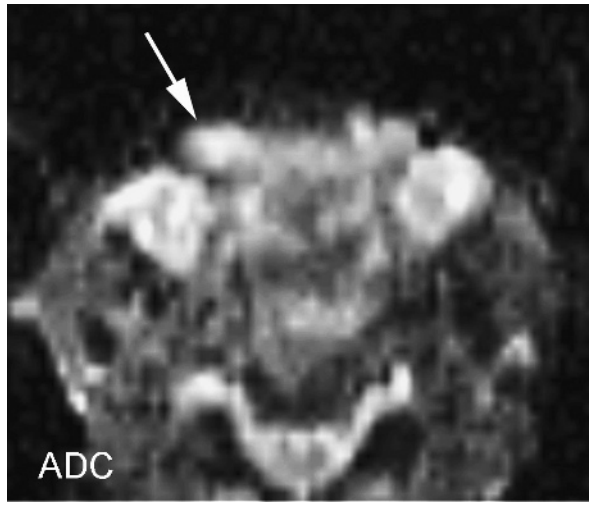

e

Fig. 3.8a–e. Patient suffering floor of the mouth cancer. **a** Sagittal contrast-enhanced MDCT image shows primary tumor at the junction of the floor of the mouth and oral tongue (*arrowheads*). **b** Axial MDCT image. Slightly enlarged lymph node (minimal axial diameter 12 mm) in the submandibular region (*arrow*): suspect for metastatic adenopathy. **c–e** Axial diffusion-weighted MR images. Compared to the *b=0* image (**c**), the signal clearly reduced in the adenopathy (*arrow*) on the *b=1000* image (**d**), indicating easy diffusion of water protons. The ADC map (**e**) shows a relatively high signal (ADC > 0.00130 mm^2/s). These findings are consistent with a benign adenopathy. After neck dissection, histologically no tumor was found in this lymph node

3.5 Nuclear Imaging

Nuclear imaging techniques, such as single photon emission computed tomography (SPECT) and positron emission tomography (PET), are increasingly being used in the evaluation of advanced head and neck cancer. Particularly PET and PET-CT, using fluorine-18-labeled 2-fluoro-2-deoxy-D-glucose (FDG) as tracer, have received a lot of attention in recent years.

PET can be used in the pretreatment staging process, during radiotherapy planning (see Chap. 18), and in the posttreatment work-up. Overall, PET has a higher sensitivity for detecting tumor compared to CT and MRI. However, this is achieved at a relatively low specificity. Physiological tracer uptake, e.g. in the thyroid gland, lymphoid tissue, salivary glands and in active muscles may cause confusion; tracer accumulation in inflammation, such as observed in therapy-induced tissue changes, may also cause false-positive results. Other pitfalls of PET imaging are the low spatial resolution, and the lack of tracer uptake in some neoplasms, causing false-negative results. The high cost of PET imaging is an important drawback.

A detailed description of the technical background and possibilities of nuclear imaging techniques is beyond the scope of this chapter. Detailed information on PET imaging in head and neck cancer is provided in Chap. 17.

References

Curtin HD, Ishwaran H, Mancuso AA et al (1998) Comparison of CT and MR imaging in staging of neck metastases. Radiology 207:123–130

Farina D, Borghesi A (2005) Techniques of radiological examination. In: Maroldi R, Nicolai P (eds) Imaging in treatment planning for sinonasal diseases. Springer, Berlin, p 5

Keberle M, Tschammler A, Hahn D (2002) Single-bolus technique for spiral CT of laryngopharyngeal squamous cell carcinoma: comparison of different contrast material volumes, flow rates, and start delays. Radiology 224:171–176

Le Bihan D, Breton E, Lallemand D, Aubin ML, Vignaud J, Laval-Jeantet M (1988) Separation of diffusion and perfusion in intravoxel incoherent motion MR imaging. Radiology 168:497–505

Lell MM, Greess H, Hothorn T, Janka R, Bautz WA, Baum U (2004) Multiplanar functional imaging of the larynx and hypopharynx with multislice spiral CT. Eur Radiol 14:2198–2205

Magnano M, Bongioannini G, Cirillo S et al (2005) Virtual endoscopy of laryngeal carcinoma: is it useful? Otolaryngol Head Neck Surg 13:776–782

Robert YH, Chevalier D, Rocourt NL et al (1993) Dynamic maneuver acquired with spiral CT in laryngeal disease. Radiology 189:298–299

Sigal R, Vogl T, Casselman J et al (2002) Lymph node metastases from head and neck squamous cell carcinoma: MR imaging with ultrasmall superparamagnetic iron oxide particles (Sinerem MR) – results of a phase-III multicenter clinical trial. Eur Radiol 12:1104–1113

Silverman PM, Zeiberg AS, Sessions RB, Troost TR, Zeman RK (1995) Three-dimensional imaging of the hypopharynx and larynx by means of helical (spiral) computed tomography. Comparison of radiological and otolaryngological evaluation. Ann Otol Rhinol Laryngol 104:425–431

Takes RP, Knegt P, Manni JJ et al (1996) Regional metastasis in head and neck squamous cell carcinoma: revised value of US with US-guided FNAB. Radiology 198:819–823

Takes RP, Righi P, Meeuwis CA et al (1998) The value of ultrasound with ultrasound-guided fine-needle aspiration biopsy compared to computed tomography in the detection of regional metastases in the clinically negative neck. Int J Radiat Oncol Biol Phys 40:1027–1032

van den Brekel MW, Castelijns JA, Stel HV et al (1991) Occult metastatic neck disease: detection with US and US-guided fine-needle aspiration cytology. Radiology 180:457–461

Wang J, Takashima S, Takayama F et al (2001) Head and neck lesions: characterization with diffusion-weighted echo-planar MR imaging. Radiology 220:621–630

Yousry I, Camelio S, Schmid UD et al (2000) Visualization of cranial nerves I–XII: value of 3D CISS and T2-weighted FSE sequences. Eur Radiol 10:1061–1067

4 Laryngeal Neoplasms

Robert Hermans

CONTENTS

R. Hermans, MD, PhD
Professor, Department of Radiology, University Hospitals Leuven, Herestraat 49, 3000 Leuven, Belgium

4.1 Introduction

The larynx is one of the most frequent head and neck cancer sites. Nearly all laryngeal malignancies are squamous cell carcinomas. Cigarette smoking and excessive alcohol consumption are well-known risk factors. An important factor in the treatment planning of laryngeal neoplasms is the accuracy of pretherapeutic staging. As most laryngeal tumors are mucosal lesions, they can often be seen directly or indirectly, but the limitations of clinical and endoscopic tumor evaluation are well recognized. The clinical and radiological evaluation of laryngeal tumors are complementary; the combination of the obtained information will lead to the most accurate determination of tumor extent. Imaging may be used to monitor tumor response and to detect recurrent or persistent disease as early as possible.

4.2 Normal Laryngeal Anatomy

Essentially the larynx consists of a supporting skeleton, a mucosal surface, and in between a soft tissue layer containing fat, some ligaments and muscular structures (Figs. 4.1–4.4).

4.2.1 Laryngeal Skeleton

The laryngeal skeleton is made up of cartilage and fibrous bands. The foundation of the larynx is the cricoid cartilage. The cricoid cartilage is the only complete cartilaginous ring in the airway. Its horizontal ring-shaped part is known as the arch (arcus), while the higher posterior part is called the lamina. Two paired facets are found at the upper margin of the lamina, allowing articulation with the arytenoid cartilages.

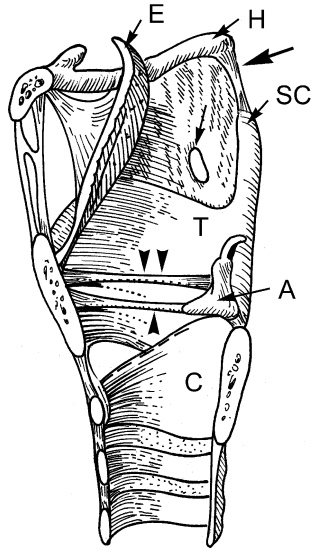

Fig. 4.1. Lateral diagram of the larynx showing the cartilaginous skeleton (mucosa, intrinsic laryngeal muscles and paraglottic fat removed). The vocal ligament (*single arrowhead*) stretches from the vocal process of the arytenoid (*A*) to the anterior thyroid cartilage. The ventricular ligament (*double arrowhead*) runs from the upper arytenoid to the anterior thyroid cartilage. *T*, thyroid lamina; *SC*, superior cornu (of thyroid). The superior cornua are attached to the hyoid by the thyrohyoid ligament (*unlabeled thick arrow*), which forms the posterior margin of the thyrohyoid membrane. *C*, cricoid cartilage; *E*, epiglottis; *H*, hyoid bone. Note: The small structure at the upper tip of the arytenoid is the corniculate cartilage. It has no clinical significance, but is occasionally seen on CT. The small hole (*unlabeled thin arrow*) in the thyrohyoid membrane transmits the internal branch of the superior laryngeal nerve that provides sensation to the laryngeal mucosa

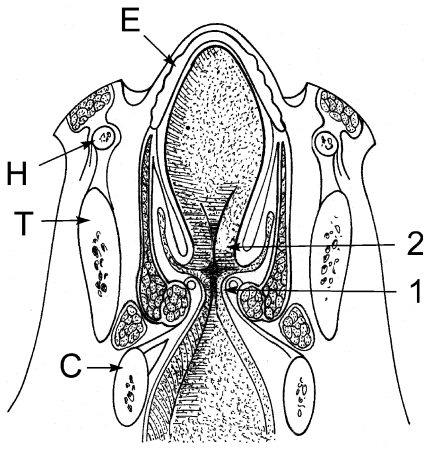

Fig. 4.3. Coronal diagram of the larynx showing the laryngeal subsites. *1*, True vocal cord (TVC) consist mainly of the bellies of the thyroarytenoid muscle. *2*, false vocal cord (FVC) consists mainly of fatty tissue. TVC and FVC are separated by the slitlike laryngeal ventricle (sinus of Morgagni), extending superolaterally as the sacculus laryngis or appendix. *E*, epiglottis; *H*, hyoid bone; *T*, thyroid cartilage; *C*, cricoid cartilage

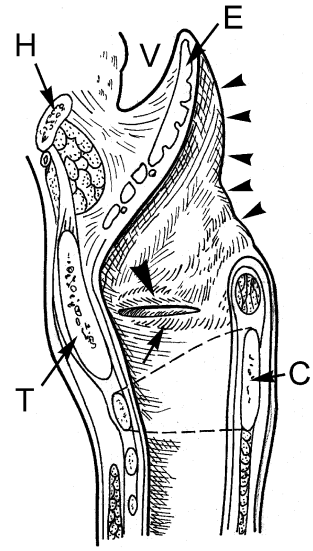

Fig. 4.2. Lateral diagram of the larynx sectioned sagittally in the midline. The slitlike ventricle separates true vocal cord (*unlabeled arrow*) and false vocal cord (*large arrowhead*). *Small arrowheads*, aryepiglottic fold; *T*, thyroid cartilage; *C*, cricoid cartilage (lamina); *dashed line*, projection of the arch of the cricoid cartilage; *E*: epiglottis; *H*, hyoid bone; *V*, vallecula

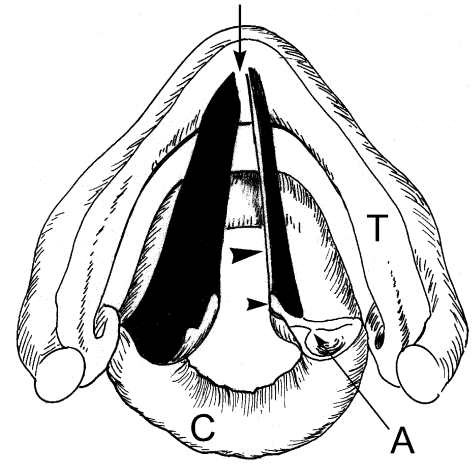

Fig. 4.4. Inner view of the larynx, seen from above, after removal of most soft tissues. *A*, arytenoid cartilage; *C*, cricoid lamina; *T*, thyroid cartilage. The bulk of the TVC is made up of the thyroarytenoid muscle (*in dark*) running from the inner aspect of the thyroid lamina to the arytenoid cartilage, paralleling the vocal ligament (*large arrowhead*). The thyroarytenoid muscle can be separated in two bellies. Only the medial portion (vocalis muscle) is seen on the right. The vocal ligament extends from the vocal process (*small arrowhead*) to the anterior commissure (*unlabeled arrow*)

The largest supporting cartilage is the thyroid cartilage, essentially consisting out of two wings or laminae. The teardrop-shaped epiglottis extends downward and attaches to the inner side of the thyroid cartilage. Only a small part of the epiglottis extends above the hyoid bone, the suprahyoid or free margin of the epiglottis.

The vocal ligament stretches from the vocal process of the arytenoid to the inner side of the thyroid cartilage; it forms the medial support of the true vocal cord. The ventricular ligament stretches from the upper arytenoid to the thyroid cartilage, forming the medial margin of the false cord. The epiglottis is held in place by the hyoepiglottic ligament, running through the fatty preepiglottic space.

Table 4.1. Subsites within the larynx (UICC 2002)

Supraglottis
Suprahyoid epiglottis (including tip, lingual and laryngeal surfaces)
Infrahyoid epiglottis
Aryepiglottic fold, laryngeal aspect
Arytenoid
Ventricular bands (false vocal cords)
Glottis
True vocal cords
Anterior commissure
Posterior commissure
Subglottis

4.2.2 Mucosal Layer and Deeper Laryngeal Spaces

All these structures are covered by mucosa; the inner larynx is dominated by two prominent parallel bands, the true and false cord, separated by a slitlike opening towards the laryngeal ventricle. The true cord largely consists of a muscle, running parallel and lateral to the vocal ligament, between the arytenoid and thyroid cartilage, hence known as the thyroarytenoid muscle. The false cord largely consists of fat. In between the cords, the ventricle is rising into the laryngeal tissue space between the mucosa and supporting skeleton. The relationship of pathological conditions to these three parallel structures is significant in the evaluation of laryngeal cancer.

Above the false cords, from the arytenoid cartilages, the mucosa reflects upwards towards the epiglottis, forming the aryepiglottic folds.

The part of the larynx at the level of the true vocal cords is called the glottis. The region beneath the undersurface of the true vocal cords until the undersurface of the cricoid cartilage is the subglottis. Above the level of the true vocal cords is the supraglottis. Within these different levels, further subsites are distinguished, important for staging purposes (Table 4.1).

The bare area between the anterior attachment of the true vocal cords, where no or only minimal soft tissue is present against the cartilage, is known as the anterior commissure. The area between the arytenoids is known as the posterior commissure.

The fat-containing space between the mucosa and the supporting skeleton is variable in size. The part of this deep space, anterior to the epiglottis, is known as the preepiglottic space. This preepiglottic space is continuous with the more lateral submucosal spaces, extending into the aryepiglottic folds and false vocal cords. These lateral spaces are known as the paraglottic spaces. At the level of the glottis, the paraglottic spaces are reduced to a very thin stripe of fat just lateral to the thyroarytenoidal muscles.

The paraglottic fat tissue is continuous with a thin infraglottic fat plane, bordered by the conus elasticus. The preepiglottic and paraglottic spaces together are sometimes called the paralaryngeal space (Sato et al. 1993).

4.2.3 Normal Radiological Anatomy

The normal radiological anatomy of the larynx is shown in Fig. 4.5.

The appearance of the laryngeal cartilages can vary considerably, depending on the degree of ossification and the amount of fatty marrow in the ossified medullar space. In children, the CT density of the laryngeal cartilages is similar to soft tissue. The (endochondral) ossification of hyaline cartilage starts early in the third decade of life. A high degree of variation exists between individuals (Yeager et al. 1982). The thyroid cartilage shows the greatest variability in ossification; its ossification may also occur in an asymmetrical fashion. The cricoid and arytenoids show less pronounced variability in ossification. The epiglottis and vocal process of the arytenoids are composed of yellow fibrocartilage; this type of cartilage usually does not ossify.

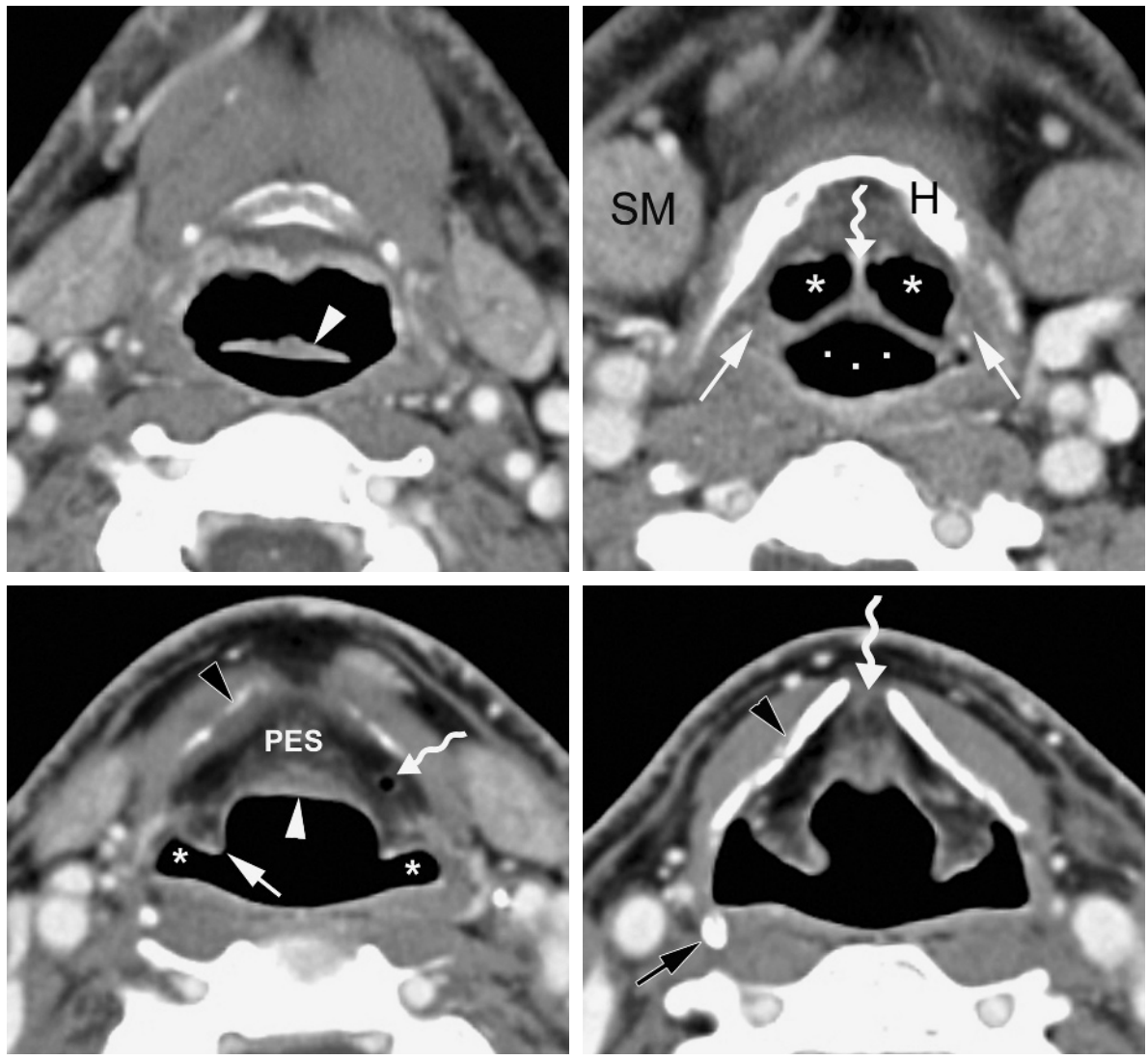

Fig. 4.5a-g. Axial CT images through normal appearing larynges (different patients), from cranial to caudal, illustrating normal radiological anatomy. **a** Level of the free epiglottic margin (*arrowhead*), at the superior edge of the hyoid bone. **b** Level of the hyoid bone (*H*). The glossoepiglottic ligament (*curved arrow*) separates both valleculae (*asterisks*). The epiglottis separates the oropharyngeal valleculae from the laryngeal vestibule (*dots*). The pharyngo-epiglottic folds (*arrows*) correspond to the

4.3 Squamous Cell Carcinoma

Squamous cell carcinoma, originating from the mucosal lining, is the most common malignant tumor in the larynx. Mucosal abnormalities can be far better evaluated by the clinician than with even sophisticated imaging methods such as CT or MRI. However, these tumors have the tendency to spread submucosally, and this extension into the deeply lying tissue planes may be difficult to evaluate by clinical examination alone.

The clinical criteria used for giving a tumor a particular T-classification are site-dependent; in the larynx involvement of different laryngeal subsites and reduced vocal cord mobility are important criteria. The local staging criteria for glottic, supraglottic and subglottic cancer are summarized in Tables 4.2–4.4. About 65%–70% of laryngeal cancers originate at the glottic level, and about 30% at the supraglottic level; laryngeal cancer originating from the subglottic region is rare.

The regional (neck) staging criteria for laryngeal cancer are similar to those for oro- and hypopharyngeal cancer and sinonasal cancer.

The validity of any classification is dependent on the diagnostic methods employed. It is recognized

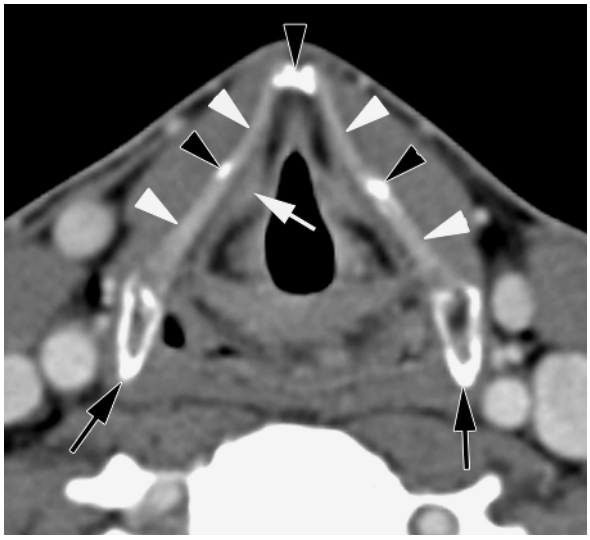

e

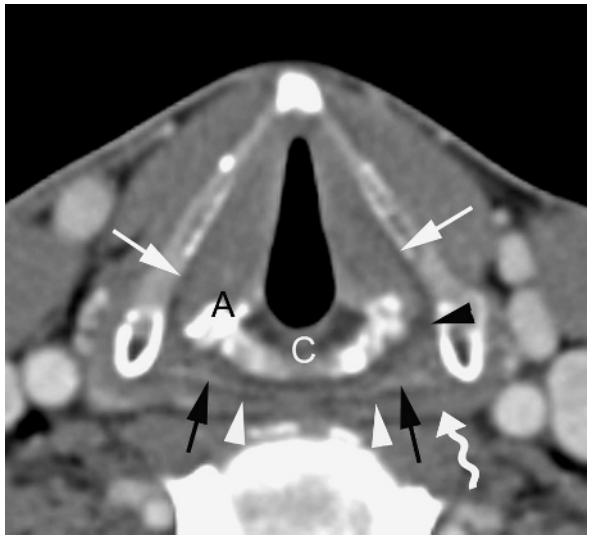

f

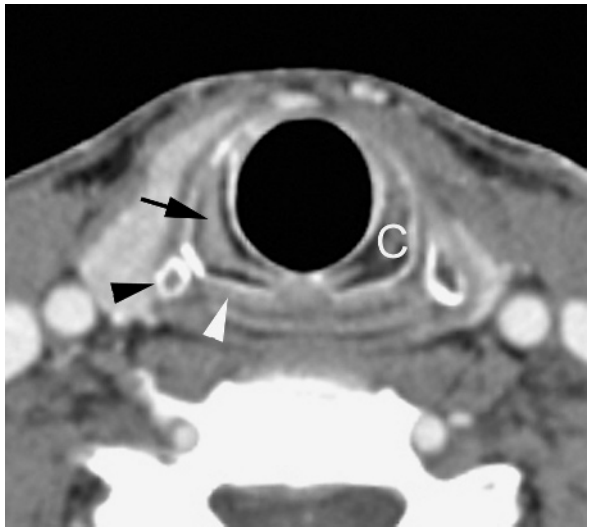

g

anterocranial margin of the piriform sinuses. Submandibular salivary gland (*SM*). **c** Level of superior margin of thyroid cartilage (*black arrowhead*). Epiglottis (*white arrowhead*), aryepiglottic fold (*arrow*), piriform sinuses (*asterisks*). The fatty space just in front to the epiglottis is the preepiglottic space (*PES*). The more lateral fatty spaces are called the paraglottic spaces; in the left paraglottic space, the air-containing tip of the laryngeal ventricle is seen (*curved arrow*). **d** Level of thyroid cartilage (*black arrowhead*). Thyroid notch (*curved arrow*). Superior thyroid cornu (*arrow*). **e** Level of false vocal cords. Within the fatty paraglottic space, some tissue with higher density can be seen, corresponding to intrinsic laryngeal muscles and the collapsed laryngeal ventricles (*white arrow*). The thyroid cartilage shows areas of calcification (*black arrowheads*), ossification (*black arrows*) and non-calcified cartilage (*white arrowheads*). **f** Level of true vocal cords. Arytenoid cartilage (*A*, partially ossified); lamina of cricoid cartilage (*C*). The fatty paraglottic spaces are reduced to a thin fatty line (*white arrows*) between the thyroid cartilage and vocal muscles. Posteriorly, the paraglottic spaces are continuous with the anterior submucosal fat plane in the retrocricoidal part of the hypopharynx (*black arrowhead*). Hypopharyngeal mucosa (*black arrows*), posterior submucosal fat plane in retrocricoidal hypopharynx (*white arrowheads*), pharyngeal constrictor muscle (*curved arrow*). **g** Level of subglottis. Arch of cricoid cartilage (*C*). The denser areas correspond to islands of non-ossified cartilage within the otherwise ossified cricoid. Inferior thyroid cornu (*black arrowhead*). Posterior cricoarytenoid muscle (*white arrowhead*)

that clinical classification of laryngeal cancer is insufficient when compared with pathologic classification (Pillsbury and Kirchner 1979). A marked improvement in accuracy is obtained when the results of CT or MRI are added to the clinical findings (Sulfaro et al. 1989; Katsantonis et al. 1986; Zbären et al. 1996). Imaging is mainly of benefit in detecting deep soft tissue extension, such as in the preepiglottic space, the laryngeal cartilages, and base of tongue. Findings from imaging studies frequently result in an upclassification of the disease.

For categorization of a given laryngeal tumor, the UICC and AJCC are not very precise regarding their recommendations for the use of imaging methods such as CT and MRI. The AJCC, for example, states that a variety of imaging procedures are valuable in evaluating the extent of disease, particularly for advanced tumors; these techniques include laryngeal tomograms, CT and MRI studies, but when to use either or all of these imaging methods is not indicated. Without further specification as to the type of imaging, the UICC recommends that imaging should be included in the diagnostic workup.

Although the benefit of CT in the classification of laryngeal cancer is already known for a long time, not all patients with clinically advanced cancer are being

Table 4.2. T staging of glottic cancer (UICC 2002)

T1	Tumor limited to vocal cord(s) with normal mobility (may involve anterior or posterior commissure)
	T1a: limited to one vocal cord
	T1b: involving both vocal cords
T2	Extension into supra- and/or subglottis, and/or with impaired vocal cord mobility
T3	Vocal cord fixation and/or invasion of paraglottic space, and/or minor thyroid cartilage erosion
T4	Extralaryngeal tumor spread
	T4a: tumor invading through thyroid cartilage, or tissues beyond the larynx (e.g. trachea, soft tissues of the neck, strap muscles, thyroid gland, esophagus)
	T4b: tumor invading prevertebral space, mediastinum, or encasing carotid artery

Table 4.3. T staging of supraglottic cancer (UICC 2002)

T1	Tumor limited to one subsite of supraglottis with normal vocal cord mobility
T2	Tumor invades mucosa of more than one adjacent subsite of supraglottis, glottis or region outside of supraglottis, without fixation of the larynx
T3	Vocal cord fixation or invasion of postcricoid area, preepiglottic and/or paraglottic space, and/or minor thyroid cartilage erosion
T4	Extralaryngeal tumor spread
	T4a: tumor invading through thyroid cartilage, or tissues beyond the larynx (e.g. trachea, soft tissues of the neck, strap muscles, thyroid gland, esophagus)
	T4b: tumor invading prevertebral space, mediastinum, or encasing carotid artery

Table 4.4. T staging of subglottic cancer (UICC 2002)

T1	Tumor limited to subglottis
T2	Tumor extends to vocal cord(s) with normal or impaired mobility
T3	Vocal cord fixation
T4	Extralaryngeal tumor spread
	T4a: tumor invading through cricoid or thyroid cartilage, and/or invades tissues beyond the larynx (e.g. trachea, soft tissues of the neck, strap muscles, thyroid gland, esophagus)
	T4b: tumor invading prevertebral space, mediastinum, or encasing carotid artery

examined with this tool; the reasons for this are not clear (Barbera et al. 2001).

In the United States, during the period 1990–1992 about 37% of patients with laryngeal cancer had a CT study (Shah et al. 1997). Large regional variation exist in the use of CT for staging purposes of laryngeal cancer. This variation can not always be attributed to the availability of these imaging modalities. In Ontario, about 20% of patients with glottic and 42% of patients with supraglottic cancer underwent CT during the period 1982–1995 (Barbera et al. 2001); in the same period, the overall rate of CT use varied between 10.4% to 50.5% among the regional cancer centers in this province.

One may argue that patients with clinically localized disease would benefit more from such a CT study, as upclassification of the cancer may result in a change of patient management. In The Netherlands, a national guideline states that all patients with a supraglottic carcinoma, and all patients with a glottic carcinoma (except T1 lesions limited to one vocal cord, not involving the anterior commissure) should undergo a high-quality CT or MRI study (Nationale werkgroep hoofd-halstumoren 2000).

4.3.1 General Imaging Findings

Criteria used for tumor involvement are abnormal contrast enhancement, soft tissue thickening, presence of a bulky mass, infiltration of fatty tissue (even without distortion of surrounding soft tissues), or a combination of these. Any tissue thickening between the airway and the cricoid arch is considered to represent subglottic tumor.

Several studies have compared the CT/MRI findings with the results of whole organ sectioning after total or partial laryngectomy, showing that both techniques are accurate methods to visualize laryngeal pathology (Zbären et al. 1996). These studies, correlating whole organ sectioning and imaging, have also revealed some pitfalls. Small foci of mucosal tumor may be difficult to detect or may be invisible, and associated inflammatory and edematous changes may cause overestimation of the tumor extent. Distortion of adjacent normal structures may mimic tumoral involvement.

Gross cartilage invasion can be detected with CT. Due to the large variability in the ossification pattern of the laryngeal cartilages, CT often fails to detect early cartilage invasion. Non-ossified hyaline cartilage shows more or less the same density values as tumor on CT images. Demonstration of tumor on the extralaryngeal side of the cartilage is a reliable, but late sign of cartilage invasion. Asymmetrical sclerosis, defined as thickening of the cortical margin and/or increased medullary density, comparing one arytenoid to the other, or one side of the cricoid or thyroid cartilage to the other side, is a sensitive but non-

specific finding on CT (Becker et al. 1995). Erosion or lysis has been found to be a specific criterion for neoplastic invasion in all cartilages. Other signs, such as cartilaginous blow-out or bowing, a serpiginous contour or obliteration of the medullary space are not very reliable for cartilage invasion. The combination of several diagnostic CT-criteria for neoplastic invasion of the laryngeal cartilages seems to constitute a reasonable compromise: when extralaryngeal tumor and erosion or lysis in the thyroid, cricoid and arytenoid cartilages was combined with sclerosis in the cricoid and arytenoid (but not the thyroid) cartilages, an overall sensitivity of 82%, an overall specificity of 79% and an overall negative predictive value of 91% was obtained (Becker et al. 1995).

The controversy on which modality should be preferred to image the larynx dealt for a great part with the accuracy to detect cartilage invasion. MRI was recommended to be the best method to determine the status of the cartilages in the presence of a laryngeal tumor (Becker et al. 1997a). MRI is a more sensitive technique than CT to detect cartilage abnormalities. Areas of cartilage abnormality will result in an increase in signal intensity on T2-weighted images and contrast-enhanced T1-weighted MRI images. However, due to its high sensitivity for intracartilaginous alterations MRI will yield in a considerable number of cases a false positive result, as distinction between true cartilage invasion and reactive inflammation, edema, fibrosis or ectopic red bone marrow is not possible (Becker et al. 1995). Peritumoral inflammatory changes without tumoral invasion are common coincidental findings in laryngeal cartilages, especially in the thyroid cartilage. The positive diagnosis of neoplastic invasion of the thyroid cartilage should be made with extreme caution on MRI; it has been suggested that one should rather talk about 'abnormal signal intensity in the cartilage' instead of 'invasion of cartilage' (Castelijns et al. 1996a).

4.3.2 Neoplastic Extension Patterns of Laryngeal Cancer

4.3.2.1 Glottic Cancer

4.3.2.1.1 Local Tumor Spread

The most common site of involvement is the anterior portion of the vocal cord, usually at the free margin or upper surface. Involvement of the anterior commissure is commonly present and such lesions may extend over the midline in the contralateral vocal cord. As the amount of normal soft tissue visible at the level of the anterior commissure is somewhat variable (Kallmes and Phillips 1997), radiological detection of subtle tumor spread into this structure by imaging can be challenging; however, usually the anterior commissure can be well evaluated during endoscopic examination.

Lesions limited to the anterior commissure are rarely seen (< 2%). Lesions involving the anterior commissure may directly invade the thyroid cartilage; involvement of the anterior subglottic region, lower preepiglottic space, as well as extralaryngeal spread through the cricothyroid ligament may occur (Fig. 4.9).

When the tumor arises from the posterior side of the vocal cord, posterior extension over the medial facet of the arytenoid cartilage, eventually involving the posterior commissure may occur (Fig. 4.10). The redundant mucosa at the level of the posterior commissure should not be misinterpreted as evidence for tumor spread. From the region of the posterior commissure, invasion of the cricoarytenoid joint may occur.

Obstruction of the opening of the ventricular orifice may be the cause of a fluid-filled laryngocele (also called a saccular cyst) (Fig. 4.10). Most laryngoceles are not caused by an obstructive mass, but an underlying neoplasm has to be excluded, both clinically and radiologically.

Extension into the subglottis may occur along the mucosal surface, or submucosally after penetration of the conus elasticus. As the upper airway wall gradually slopes from the free edge of the true vocal cords towards the inner side of the cricoid ring, the precise border between the undersurface of the true vocal cord and subglottic level is difficult to define on axial cross-sectional imaging. When soft tissue thickening is seen adjacent to a glottic neoplasm along the inner side of the cricoid, the lesion is extending into subglottis. Coronal images, either direct MR images or coronally reformatted CT images, may be helpful to evaluate more subtle subglottic tumor extension. A more precise manner to measure the inferior extent of glottic/subglottic cancer is by referring to the lateral free margin of the true vocal cord.

Lateral spread of the cancer causes infiltration of the vocal ligament and muscle. In a more advanced stage, the paraglottic space is infiltrated and the perichondrium of the thyroid cartilage is reached (Fig. 4.6). The tumor is diverted by the thyroid carti-

lage to grow further in the paraglottic space, extending cranially into the supraglottic region of the larynx, or caudally into the subglottic region. A glottic cancer growing inferiorly may be diverted by the conus elasticus, laterally and extralaryngeally, to grow through the opening between the thyroid and cricoid cartilage (Fig. 4.7).

Erosion and eventually break-through of the thyroid cartilage with extralaryngeal tumor spread are not commonly seen, being usually late phenomenons in advanced lesions (Figs. 4.7 and 4.8). Neoplastic cartilage involvement usually occurs in ossified parts of the laryngeal framework, most frequently at the inferior margin of the thyroid cartilage, upper margin of the cricoid cartilage or at the level of the anterior commissure (Kurita et al. 1985). These sites correspond to the attachment site of ligaments and membranes to the cartilages.

With extralaryngeal growth, tumor extension into non-fatty soft tissue structures surrounding the larynx may be present. Neoplastic invasion of the thyroid gland mostly occurs in glottic cancer showing subglottic extension or invading the thyroid cartilage (Dadas et al. 2001). Invasion of the subcutaneous layers and eventually skin may be seen in anteriorly spreading cancer. Posterior spread to the retrocricoid hypopharynx and eventually esophagus may occur (Fig. 4.11).

Rarely, glottic squamous cell carcinoma invading the anterior part of the thyroid cartilage presents as a prelaryngeal abscess. Presumably the neoplasm, or a combination of the neoplasm and an associated locally aggressive infection, erodes through the thyroid cartilage and offers bacteria a pathway to the prelaryngeal soft tissues (Fig. 4.12) (Op de Beeck et al. 2001). The main differential diagnosis in such cases

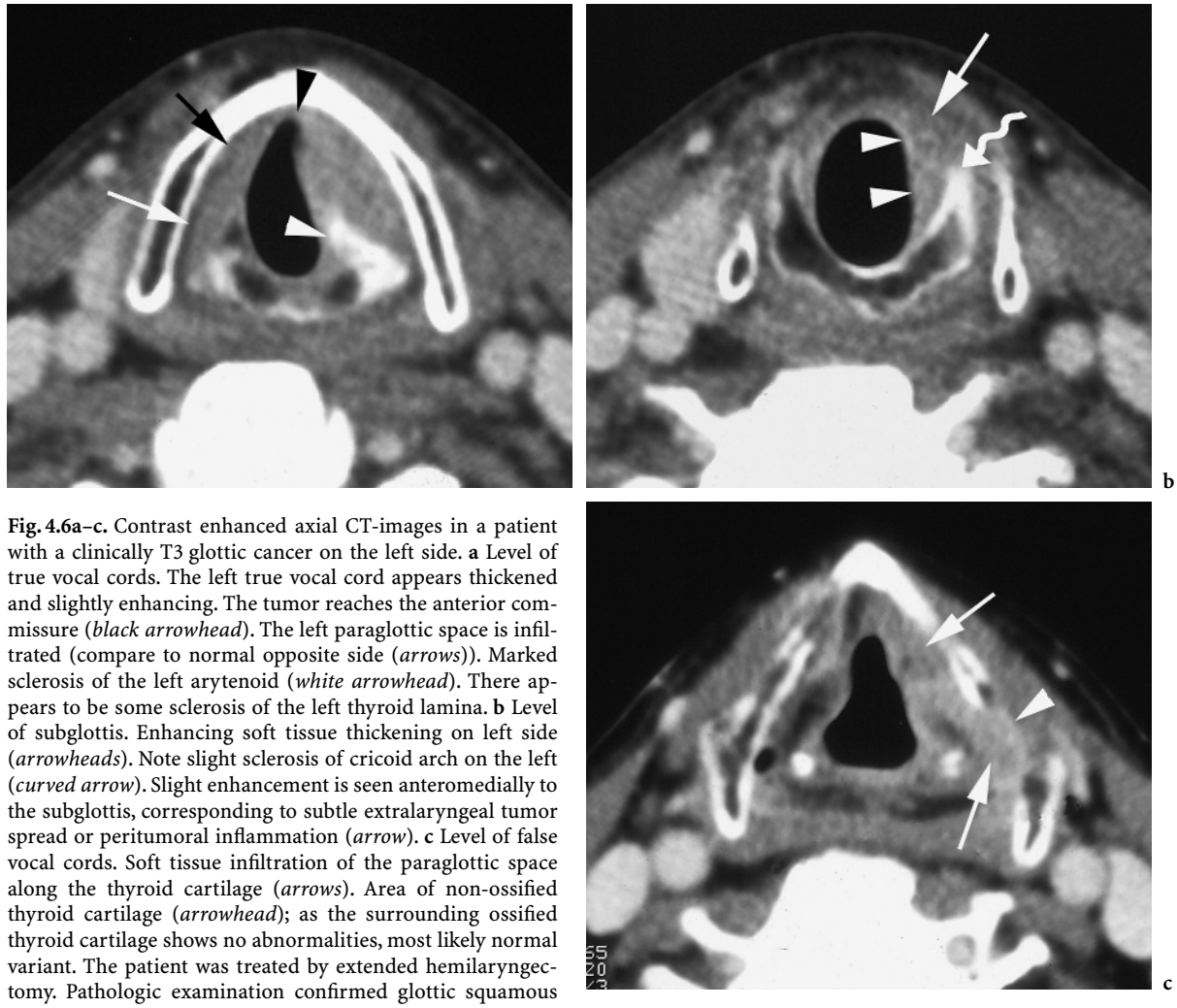

Fig. 4.6a–c. Contrast enhanced axial CT-images in a patient with a clinically T3 glottic cancer on the left side. **a** Level of true vocal cords. The left true vocal cord appears thickened and slightly enhancing. The tumor reaches the anterior commissure (*black arrowhead*). The left paraglottic space is infiltrated (compare to normal opposite side (*arrows*)). Marked sclerosis of the left arytenoid (*white arrowhead*). There appears to be some sclerosis of the left thyroid lamina. **b** Level of subglottis. Enhancing soft tissue thickening on left side (*arrowheads*). Note slight sclerosis of cricoid arch on the left (*curved arrow*). Slight enhancement is seen anteromedially to the subglottis, corresponding to subtle extralaryngeal tumor spread or peritumoral inflammation (*arrow*). **c** Level of false vocal cords. Soft tissue infiltration of the paraglottic space along the thyroid cartilage (*arrows*). Area of non-ossified thyroid cartilage (*arrowhead*); as the surrounding ossified thyroid cartilage shows no abnormalities, most likely normal variant. The patient was treated by extended hemilaryngectomy. Pathologic examination confirmed glottic squamous cell carcinoma extending in the subglottic and supraglottic region without evidence of extralaryngeal tumor extension. The arytenoid showed focal neoplastic invasion; in the other cartilages only inflammatory changes were noted

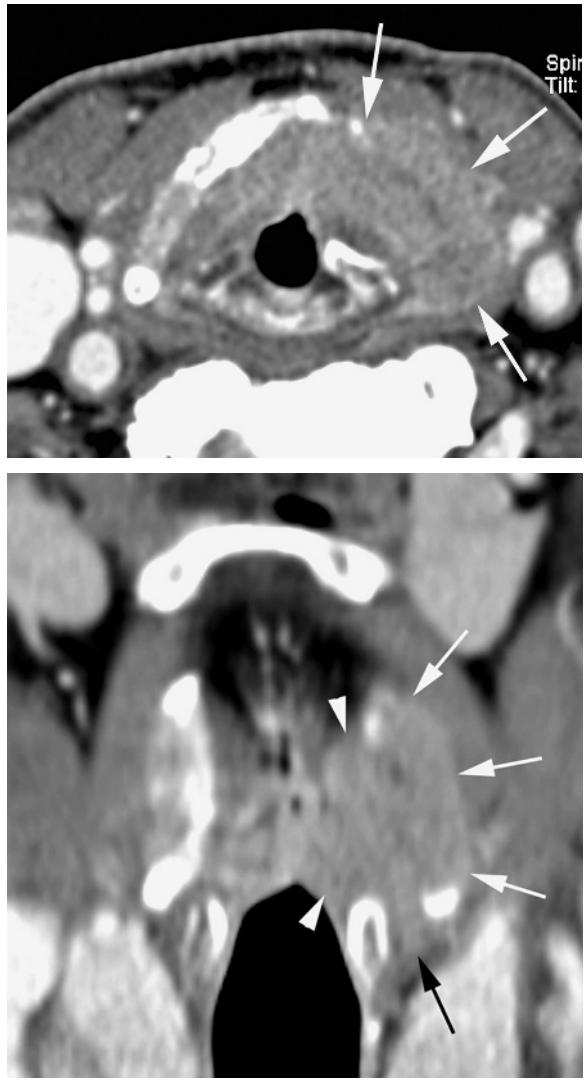

a

b

Fig. 4.7a,b. Contrast-enhanced CT-images in a patient with a large left-sided glottic squamous cell carcinoma. **a** Axial image. The tumor mass massively invades and destroys the left wing of the thyroid cartilage, growing into the extralaryngeal soft tissues (*arrows*). **b** Coronal reformatting. Involvement of the glottic and supraglottic laryngeal level (*arrowheads*) is seen, as well as massive destruction of left thyroid cartilage wing and extralaryngeal tumor spread (*white arrows*). Extralaryngeal extension also occurs through the lateral cricothyroid membrane (*black arrow*)

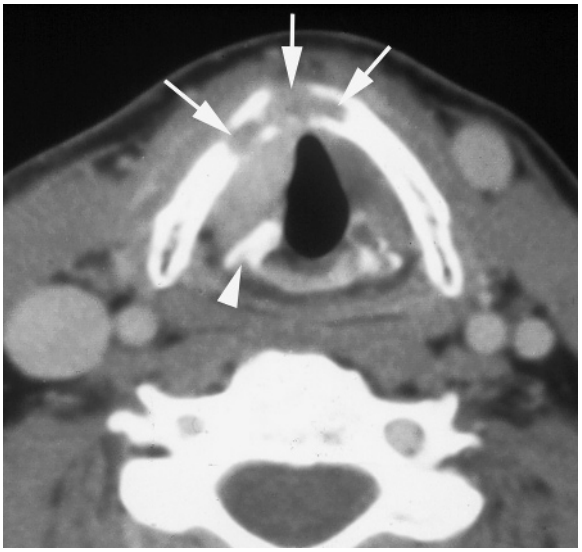

Fig. 4.8. Axial contrast-enhanced CT-image in a patient with a clinically T3 glottic cancer on the right side. Thickening and increased enhancement of the right true vocal cord. Sclerosis of the right arytenoid cartilage (*arrowhead*) and lysis of the anterior part of the thyroid cartilage, containing enhancing tissue (*arrows*). The patient was treated by definitive radiotherapy; long-term local tumor control was achieved

is infected thyroglossal duct cyst. Infection coexisting with malignancy complicates the clinical picture and may lead to a delayed diagnosis of malignancy. Therefore, careful follow-up after the initial treatment should be initiated if the etiology of the prelaryngeal infection remains obscure, especially in patients with an increased risk of developing head and neck cancer (alcohol and/or tobacco abusers). Repeated imaging studies may be helpful in coming to a correct diagnosis.

Cancer involving the glottic and supraglottic region is also called transglottic cancer. However, the definition of transglottic cancer varies from author to author. Usually, tumors crossing the laryngeal ventricle involving both the false and true vocal cord are called transglottic cancer; most agree that the use of this term also implies that the subglottic region is involved, and that the true vocal cord is fixed (Mancuso et al. 1989).

Verrucous carcinoma is a variant of squamous cell carcinoma, occurring in 1%–2% of patients with glottic cancer. The histologic diagnosis of this type of cancer is difficult, and must be correlated with the gross appearance of the tumor. Clinically, it appears as an accretion or papillary mass with a warty surface or filiform projections, and it may extend over a large area. It is often 'underdiagnosed' as a benign hyperplasia. Repeated and deep biopsy may be necessary to confirm the diagnosis. On CT and MR studies, verrucous carcinoma is difficult to differentiate from other types of squamous cell carcinoma, although an exophytic soft tissue mass originating from the true vocal cords, displaying an irregular surface and no or minimal submucosal extension, may suggest the diagnosis (Becker et al. 1998).

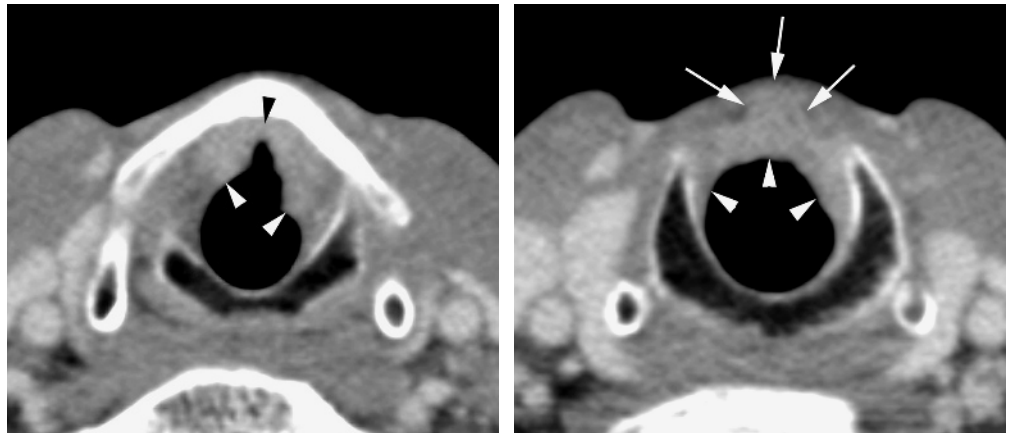

Fig. 4.9a,b. Axial contrast-enhanced CT-images in a patient with squamous cell carcinoma of the anterior glottic region. **a** Thickening and slightly increased enhancement of lower surface of true vocal cords (*white arrowheads*) and anterior commissure (*black arrowhead*) is seen. **b** Soft tissue thickening at the subglottic level (*arrowheads*); extralaryngeal extension (*arrows*) occurred, through the cricothyroid membrane

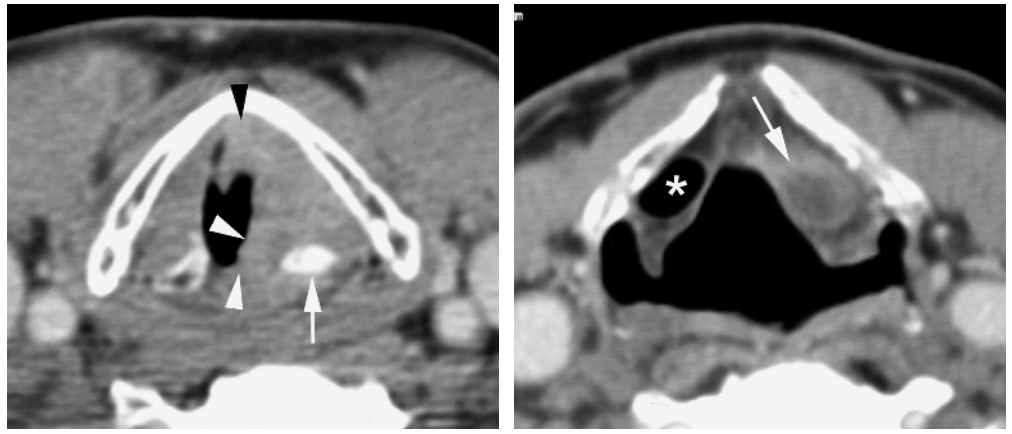

Fig. 4.10a,b. Axial contrast-enhanced CT-images in a patient with a clinically T3 glottic cancer on the left side. **a** Level of true vocal cords. The left true vocal cord is markedly thickened. The lesion extends into the anterior commissure (*black arrowhead*), and grows over the medial facet of the arytenoid into the posterior commissure (*white arrowheads*). The left paraglottic space is infiltrated. The left arytenoid cartilage appears sclerotic (*arrow*). **b** Level of the aryepiglottic folds. Secondary fluid-filled laryngocele (*arrow*). Air-filled ventricle in the right paraglottic space (*asterisk*). The patient was treated by total laryngectomy. Pathologic examination confirmed squamous cell carcinoma, invading the anterior commissure and spreading to the right true vocal cord. The left arytenoid cartilage was invaded by the neoplasm

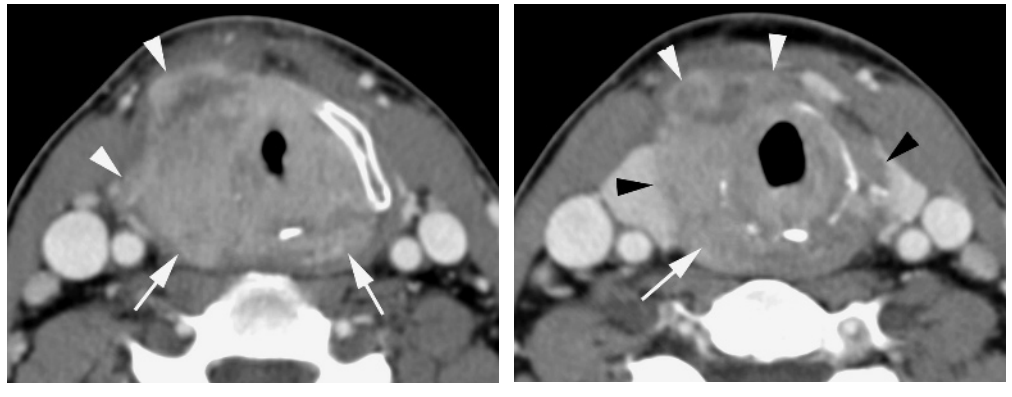

Fig. 4.11a,b. Axial contrast-enhanced CT-images in a patient with extensive glottic squamous cell carcinoma. **a** Level of true vocal cords. Circumferential neoplastic involvement of the glottis, with massive destruction of the thyroid cartilage and extralaryngeal spread into the soft tissue anterolateral to the larynx (*white arrowheads*). Posterior tumor spread into the hypopharynx is at this level visible on both sides (*arrows*). **b** Circumferential involvement of the subglottis, including massive lysis of cricoid cartilage. Extralaryngeal spread into the prelaryngeal soft tissues (*white arrowheads*), as well as in both lobes of thyroid gland (*black arrowheads*). Involvement of retrocricoidal part of hypopharynx on the right side (*arrow*)

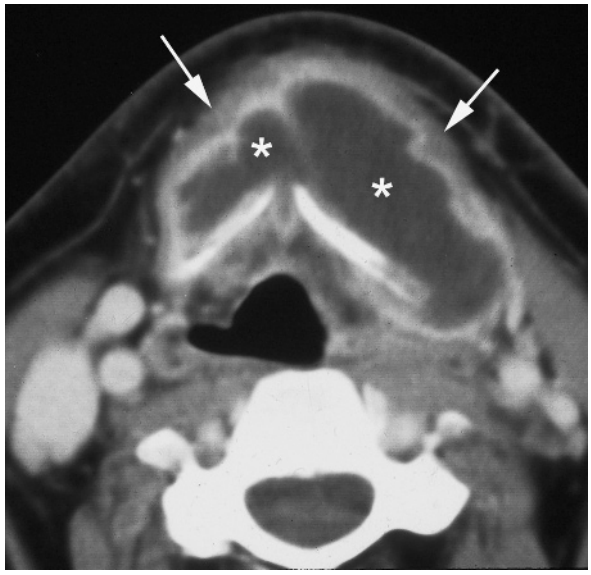

a

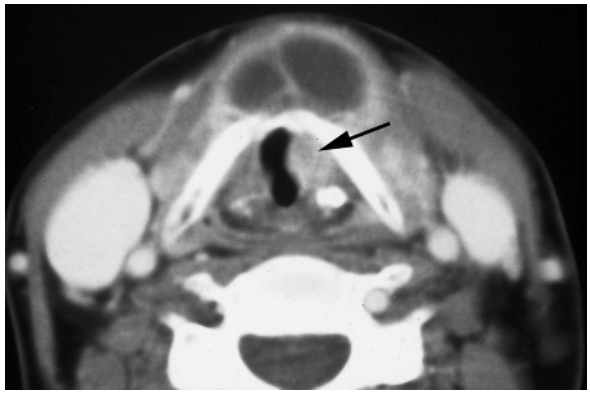

b

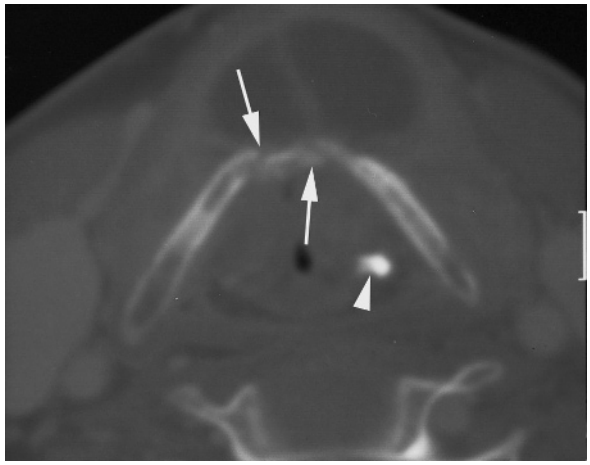

c

Fig. 4.12a–c. Axial contrast-enhanced CT images. **a** Supraglottic level. Large fluid collection (*asterisks*) with rim enhancement is seen in the prelaryngeal soft tissues, displacing the strap muscles (*arrows*) anteriorly. **b** Glottic level. The large fluid collection extends downwards to this level. Thickening and enhancement of the left true vocal cord (*arrow*). **c** Same level as (**b**), bone window. Fragmentation of the anterior part of the thyroid cartilage (*arrows*). Sclerosis of left arytenoid cartilage (*arrowhead*)

4.3.2.1.2 Lymphatic Spread

Usually, glottic cancer only metastasizes to the neck lymph nodes when growing beyond the glottic region. Level III is the most commonly affected level. Neck adenopathies are very uncommonly encountered in small (T1) lesions, but the risk increases to about 8% and 30% in respectively T2 and T3 lesions. Imaging studies may detect these adenopathies at an earlier stage than clinical examination alone (see also Chap. 15).

4.3.2.2 Supraglottic Cancer

Essentially, the radiological signs are similar to those in glottic cancer, but supraglottic cancers often show a larger tumor volume at first presentation.

Clinically visible tumor extension and radiological tumor volume are not always correlated, due to submucosal spread in the preepiglottic space and/or paraglottic space. Laryngeal cartilage invasion is rarely seen in supraglottic cancer.

4.3.2.2.1 Suprahyoid Epiglottis

Lesions of the suprahyoid epiglottis may grow exophytically. Others invade the epiglottic tip and spread to adjacent structures, such as the valleculae, tongue base and preepiglottic space; soft tissue ulceration and amputation of the epiglottic tip may be present (Fig. 4.13).

4.3.2.2.2 Infrahyoid Epiglottis

As the infrahyoid epiglottis contains tiny perforations, such lesions easily infiltrate the preepiglottic space; from this space, they may spread upwards towards the valleculae and tongue base, or downwards to the epiglottic petiolus. Invasion of the anterior commissure or subglottic spread are rare, but may be seen in advanced cases.

Extension into the aryepiglottic folds and false vocal cords may be seen; extension to the true vocal cords mostly occurs in advanced cases (Fig. 4.14).

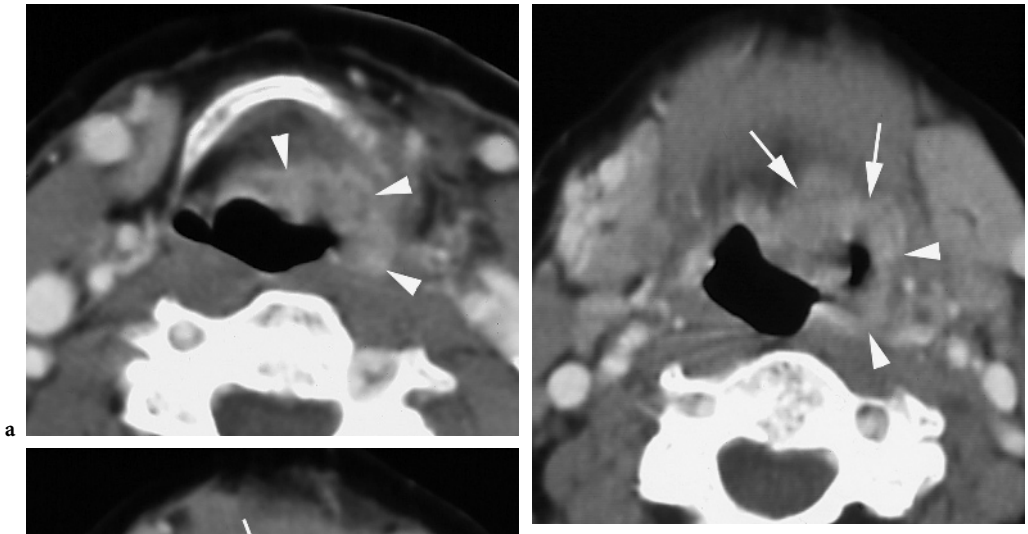

Fig. 4.13a–c. Contrast-enhanced axial CT images in a patient with a supraglottic squamous cell carcinoma. **a** Level of hyoid bone. Thickening and increased enhancement of the epiglottis, as well as infiltration of the preepiglottic and paraglottic space, with extension into the left aryepiglottic fold, is seen. Involvement of the upper part of the left piriform sinus can not be excluded. **b** Level of free epiglottic margin. The epiglottic tip (*arrowhead*) is amputated on the left side. The margins of the left vallecula are occupied by tumoral tissue (*arrows*), and there is extension into the posterolateral wall of the oropharynx (*posterior arrow*). **c** At a slightly higher level, invasion of the tongue base (*arrows*), as well as posterolateral oropharyngeal wall (*arrowheads*), is seen. Pathological neck lymph nodes are ipsilaterally present

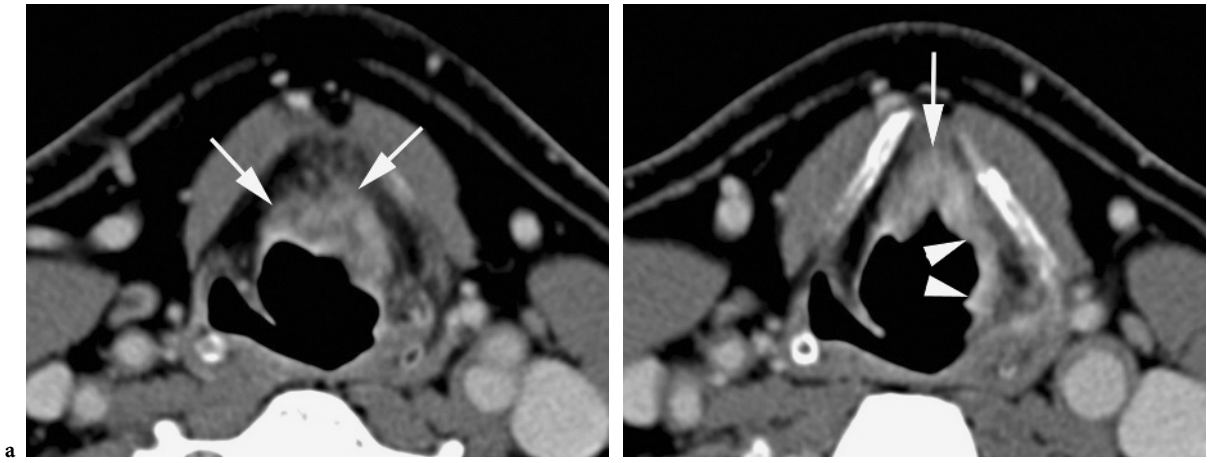

Fig. 4.14a–g. Contrast-enhanced CT images in a patient with supraglottic squamous cell carcinoma. **a** Axial image. Thickening and increased enhancement of the infrahyoid epiglottis, with infiltration of the preepiglottic space (*arrows*). **b** Axial image, more inferiorly, shows downwards tumor extension along the epiglottis and preepiglottic space (*arrow*), as well as posterolateral growth into the aryepiglottic fold (*arrowheads*). **c** Axial image, more inferiorly, shows tumoral infiltration of the left false vocal cord (*asterisk*). **d** Axial image, level of ventricle entrance. Tumoral soft tissue thickening just above the level of the anterior commissure (*arrowhead*), as well as just above the level of the true vocal cord (*arrow*). Sclerosis of left thyroid cartilage wing (*curved arrow*). **e** Axial image, level of true vocal cords. Apart from sclerosis of left arytenoid cartilage (*arrowhead*), no abnormalities are seen. **f** Coronal image. The tumor mass (*arrows*) extends throughout the left paraglottic space, abutting and slightly displacing downwards the upper margin of the true vocal cord. Normal right true vocal cord (*asterisk*), right laryngeal ventricle (*arrowhead*). **g** Sagittal image. Tumoral thickening of the infrahyoid epiglottis (*arrowheads*), extending down to the level just above the anterior commissure. True vocal cord (*arrow*)

4.3.2.2.3 Aryepiglottic Fold and Arytenoid

Aryepiglottic fold tumors may present as exophytic lesions, or infiltrative masses invading the paraglottic space. Along the paraglottic space, they may spread towards the false and eventually true vocal cords. Invasion of the cricoarytenoid joint may be seen. Extension towards the piriform sinus commonly occurs, and it may be difficult to distinguish between a primary piriform sinus cancer and supraglottic cancer.

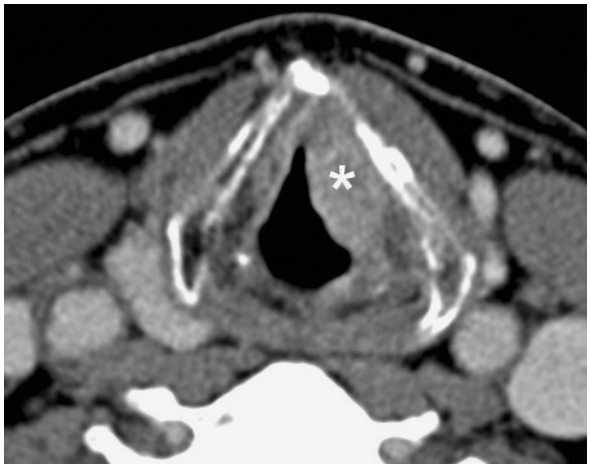

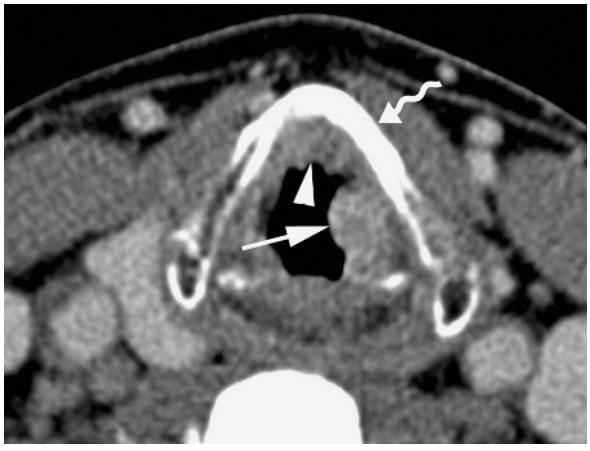

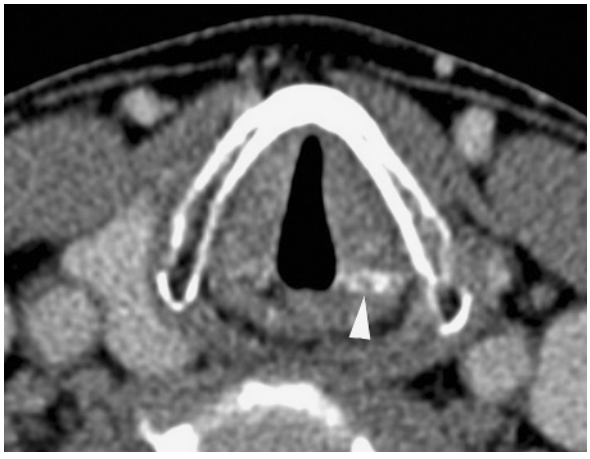

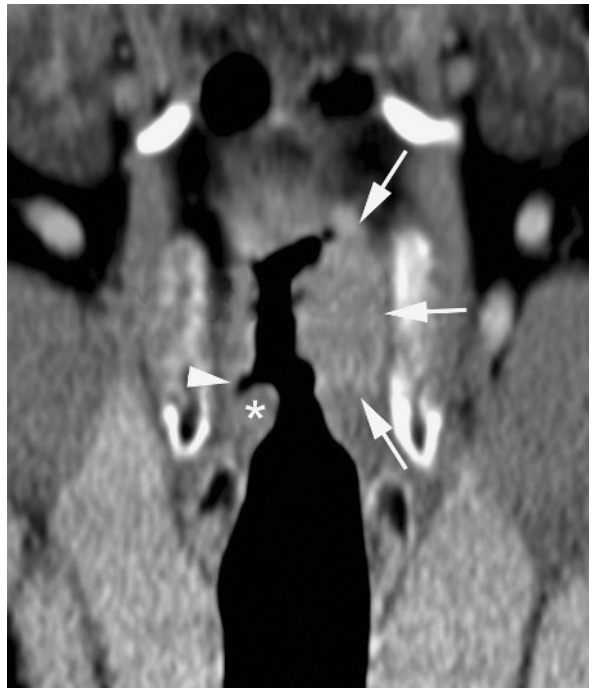

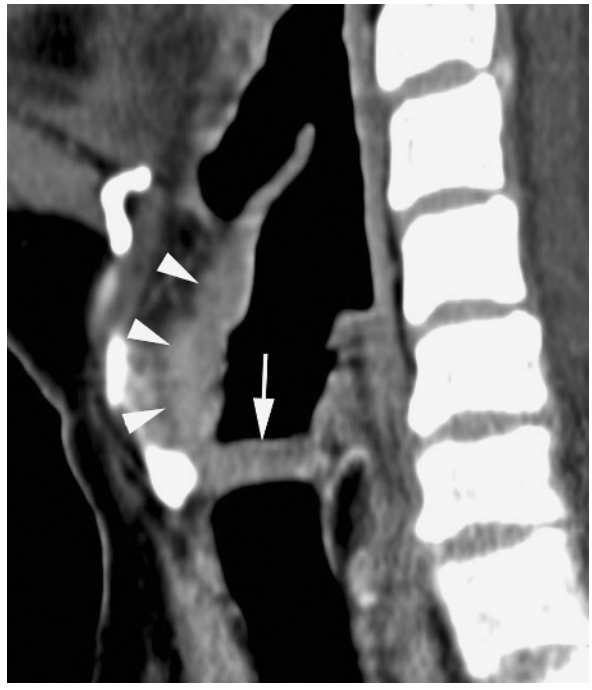

4.3.2.2.4 False Vocal Cords

Submucosal tumor spread is commonly present in these lesions, with involvement of the paraglottic space at the level of the infrahyoid epiglottis/ary-epiglottic fold and/or at the level of the true vocal cord (Fig. 4.15). Subglottic tumor spread is seen in advanced cases.

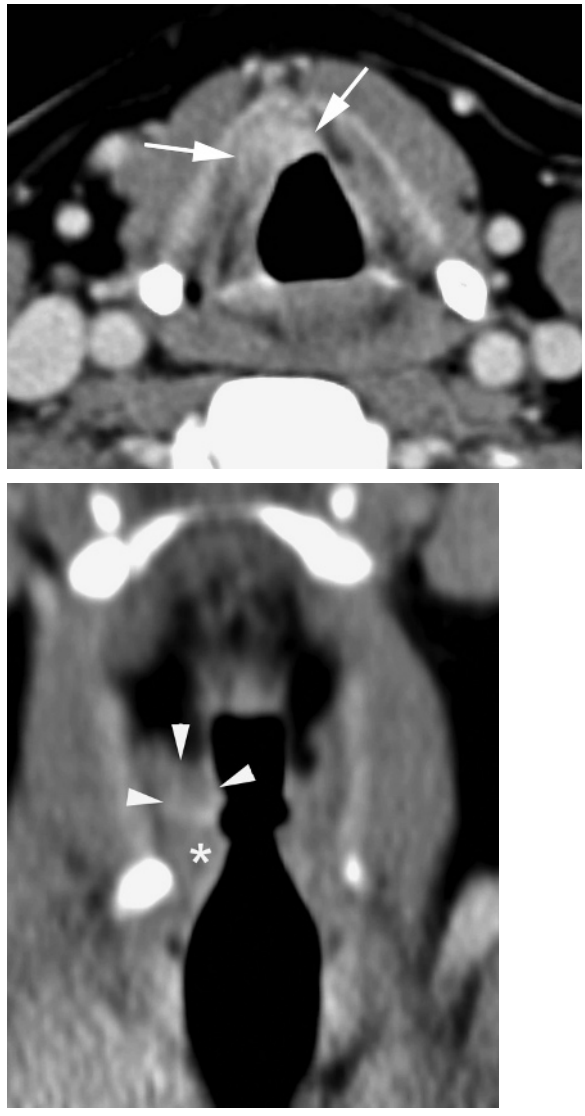

Fig. 4.15a,b. Patient presenting with hoarseness. Squamous cell carcinoma of the left false vocal cord. **a** Axial contrast-enhanced CT image shows small infiltrating lesion (*arrows*) in the right paraglottic space, at the level of the false vocal cords; the lesion extends into the anterior midline (lower part of preepiglottic space, level of epiglottic petiole). **b** Coronal reformatting. Enhancing soft tissue lesion in the right false vocal cord (*arrowheads*), just above the normal true vocal cord (*asterisk*)

4.3.2.2.5 Lymphatic Spread

As the supraglottic region has a rich network of lymphatic channels, lymphadenopathy is frequently present in supraglottic cancer. At presentation, about 50%–60% of patients with supraglottic cancer have clinically manifest lymphadenopathy. The incidence of neck metastasis is about 30% in T1 and T2 lesions, and about 70% in T3 and T4 lesions. Neck level II is most commonly affected, to a lesser extent level III.

4.3.2.3 Subglottic Cancer

Subglottic cancer is a rare malignant lesion. Apart from squamous cell carcinoma, also adenoid cystic

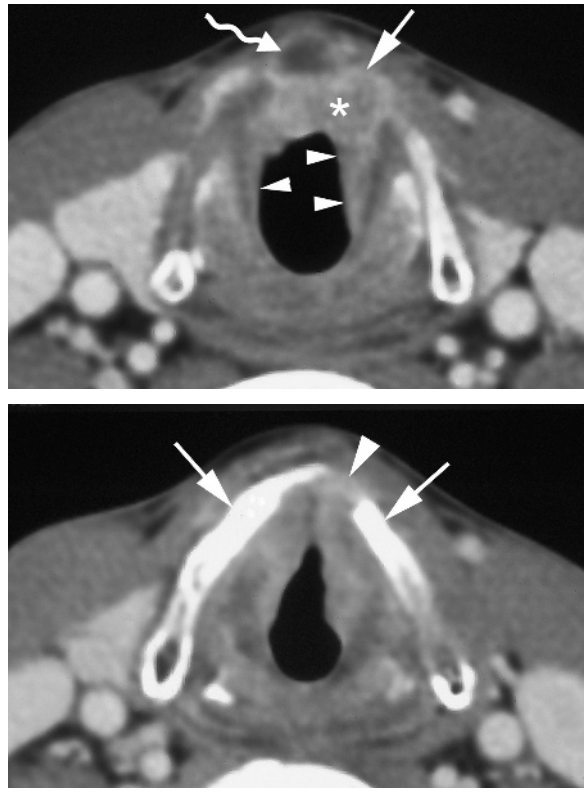

Fig. 4.16a,b. Patient suffering from subglottic squamous cell carcinoma. Axial contrast enhanced CT images. **a** Anterior subglottic soft tissue thickening (*asterisk*), with bilateral posterior spread along the subglottic wall (*arrowheads*). Extralaryngeal spread through the cricothyroid membrane (*arrow*). Centrally hypodense nodule (*curved arrow*), presumably corresponding to necrotic prelaryngeal ('Delphian') lymph node. **b** Section 9 mm cranial to (**a**). The soft tissue mass extends into the anterior commissure and both true vocal cords. Some sclerosis (*arrows*) of the thyroid cartilage is visible; the adjacent area of absent cartilage ossification (*arrowhead*) may correspond to lysis of previously ossified cartilage

carcinoma is frequently located at this level. By the time of diagnosis, subglottic cancer has usually invaded the true vocal cords, and it may be difficult to distinguish between a cancer originating in the glottis or subglottis. Subglottic cancer is commonly bilateral or even circumferential at presentation. Cricoid cartilage invasion occurs early; extralaryngeal extension, anteriorly through the cricothyroid membrane or inferiorly into the trachea, is also commonly present.

Lymphatic dissemination is seen in about 10% of cases; among the lymph nodes which may become involved are the Delphian node and paratracheal lymph nodes.

Imaging shows a subglottic soft tissue mass (normally no soft tissue is seen between the subglottic air column and the cricoid cartilage), more or less with circumferential extension along the cricoid cartilage. The findings may include cricoid cartilage alterations (sclerosis, lysis), intratracheal soft tissue thickening, and infiltration of the glottic and prelaryngeal soft tissues (Fig. 4.16).

4.4 Prognostic Factors for Local Outcome of Laryngeal Cancer

4.4.1 Treatment Options

4.4.1.1 Glottic Cancer

Carcinoma in situ can often be controlled by stripping the cord or laser treatment; radiotherapy is used after rapid or multiple recurrences of such superficial cancer (Million 1992).

In T1 and T2 tumors radiation treatment is usually preferred, as the voice quality is better than after partial laryngectomy, and fewer complications are encountered. Patients with well defined lesions, suitable for transoral laser excision with a good functional outcome, can be treated with either laser or radiotherapy (Mendenhall et al. 2004).

Favorable T3 and T4 tumors, confined to one side of the larynx without significant airway compromise, may be cured either with radiotherapy or total laryngectomy with possible postoperative irradiation. Failures after radiotherapy may be cured by salvage laryngectomy. Such a strategy yielded similar locoregional control rates and survival for T3 tumors either treated with radiotherapy alone with surgery in reserve, or with primary surgery (with or without adjuvant irradiation), but with a significantly higher likelihood of voice preservation in the first group (Mendenhall et al. 1992, 1997). This concept of 'radical radiotherapy with surgery for salvage' is a subject of discussion, as according to some authors this treatment policy means that a number of patients will die in order that others could save their larynx; furthermore the costs are thought to be higher than if surgery is used as first treatment, due to the intensive follow up and retreatment needed in a substantial fraction of patients (DeSanto 1984).

Patients with advanced disease are in the unfavorable group for radiotherapy and are advised to undergo total laryngectomy (Million 1992). Some patients who refuse total laryngectomy or are medically unsuited for this procedure may be cured by radiotherapy; Van den Bogaert et al. (1983) reported in advanced glottic cancer (T3 and T4 lesions) a 5-year local control rate of 23%.

Parsons et al. (1998) reported an overall 5-year local control of 52% in 43 T4 laryngeal tumors (26 supraglottic, 11 glottic and 6 subglottic cancers), treated by irradiation with curative intent. 'Non-bulky' tumors tended to have a better prognosis than 'bulky' ones (67% versus 38% local control rate); 'bulkiness' was assessed clinically and by CT. Of the patients in this study 20 (46%) were thought to be suitable for radical radiotherapy based on relative low tumor volume; it is unlikely that irradiation would produce a 50% rate of local control in all (unselected) T4 laryngeal cancers.

As in supraglottic carcinoma, there are indications that imaging is helpful in the selection of patients into the 'favorable' glottic carcinoma group, with a reasonable chance of voice sparing cure by radiotherapy (see below).

In selected patients with advanced glottic cancer, extended partial laryngectomy may still be feasible. Extended hemilaryngectomy with tracheal autotransplantation allows to remove half of the larynx, including the full height of the cricoid; the resection can be extended to include the apex of the piriform sinus. This allows to perform a partial laryngectomy in patients with arytenoid cartilage fixation and subglottic tumor extension reaching the upper border of the cricoid cartilage (Delaere et al. 2000; Delaere and Hermans 2003) (see below).

Verrucous carcinoma is not consistently responsive to irradiation; although debated, an anaplastic transformation may follow such a treatment (Ferlito et al. 1998). Therefore, in patients with this type of tu-

mor surgery is usually recommended as treatment of choice.

4.4.1.2 Supraglottic Cancer

Patients with a T1, T2 or a 'favorable' T3 lesion can be treated with either irradiation or supraglottic laryngectomy (Robbins et al. 1987; Lee et al. 1990; Million 1992). The selection is at the preference of the patient and the physician in charge. A 'favorable' T3 tumor is classified as T3 due to preepiglottic space involvement (visible on CT) or limited extension to the medial wall of the piriform sinus or postcricoid area, not due to vocal cord fixation which precludes supraglottic laryngectomy (Million 1992). Supraglottic laryngectomy probably produces a higher initial local control rate but, based on anatomic and coexisting medical considerations, is suitable for a smaller subset of patients and has a higher risk of complications compared with radiotherapy (Hinerman et al. 2002). Patients with pulmonary or cardiac disease are not good candidates for this procedure, as essentially all patients aspirate to some degree after the operation. The proportion of patients suitable for conservative surgery in an unselected population with supraglottic cancer is estimated to be about 15%–20%.

Of patients who undergo a supraglottic laryngectomy 50% or more will have a combined treatment with radiotherapy (Weems et al. 1987; Lee et al. 1990). Radiotherapy increases the morbidity of supraglottic laryngectomy (Steiniger et al. 1997). If such a combined treatment can be anticipated (clinically positive neck nodes), or the likelihood of conversion of partial to total laryngectomy during surgery is high, radical radiotherapy is preferred over surgery (Weems et al. 1987).

T3 cancers with a fixed vocal cord have lower local control rates after radiotherapy than those with normal mobility (Mendenhall et al. 1996).

Bulky, endophytic T3 lesions and most T4 lesions are considered unfavorable for radiotherapy; often they will show vocal cord fixation and/or airway compromise. Partial (if feasible) or total laryngectomy, with or without postoperative radiotherapy, is often recommended in these patients, as the local control rates are better for the surgically treated patients (Weems et al. 1987). Patients who are medically unfit for total laryngectomy or refuse this procedure are treated with radiotherapy; in T3 and T4 tumors anatomically unsuitable for conservation surgery, local control can be achieved by radiotherapy in 40%–63% of patients (Mendenhall et al. 1996).

There is a need for better selection of patients with a T3 lesion, medically suitable for partial laryngectomy, into the favorable group for radiotherapy; in this way a more informed treatment choice can be made. Imaging findings can be helpful to select patients in which radiotherapy has a good chance of success (see below).

Some selected T4 lesions may also be not as unfavorable for radiotherapy as is suggested by their staging: minimal cartilage invasion or minimal neck soft tissue extension may not influence the local outcome when treated by RT (Million 1992; Parsons et al. 1998).

Chemotherapy may be useful as concurrent therapy in patients with advanced tumors (Milas et al. 2003). CT-determined parameters, such as tumor volume, are helpful to select patients likely to benefit from such combined treatment (Mendenhall et al. 2003).

4.4.2 Impact of Imaging on Treatment Choice and Prognostic Accuracy

Very few studies are available on the impact of imaging on treatment choice and the accuracy of predicting treatment outcome in laryngeal cancer. Such an impact depends on the treatment policy of laryngeal cancer in a given centre (Barbera et al. 2001). Charlin et al. (1989) studied the impact of CT on management, working in an institution where at that time all cancers with a small to moderate tumor volume and no sign of deep infiltration were treated by radiotherapy alone, larger cancers and those with signs of deep infiltration by conservation surgery when local extension allowing it, and total laryngectomy with postoperative radiotherapy was performed for tumors with vocal cord fixation, cartilage destruction and other signs of deep major infiltration. Charlin et al. (1989) observed a change in therapeutic attitude with CT in 10 out of 66 consecutive patients (15.1%). In all ten patients radiotherapy was thought to be the best treatment after endoscopic evaluation; this was changed to conservative surgery in seven and total laryngectomy with postoperative irradiation in three patients.

In other centers, nearly all laryngeal cancers are treated by radical radiotherapy, surgery being used as a salvage procedure. In such institutions the impact of laryngeal imaging on initial treatment selection can be anticipated to be of less importance. However, the radiological findings may influence the definition of radiation portals, which require an exact knowl-

edge of the local extension of the tumor, the status of the neck lymph nodes, and the location of metastatic neck adenopathies.

In a retrospective multi-centre study, the incorporation of CT information did not improve the ability of the T classification for predicting local failure or cause-specific survival (Barbera et al. 2001). However, as noted by these authors, the ability of CT to improve the predictive value of the T-classification is constrained by the definitions of the T classifications, which do not take into account other prognostic information provided by CT.

Archer et al. (1984) have proposed a classification system of laryngeal cancer based on CT findings. This classification used the localization of the tumor mass relative to the arytenoid cartilage, as visible on CT studies. The rationale was that tumors with their plane of maximal size at or below the mid-body of the arytenoid cartilage have a much higher likelihood of cartilage invasion. In more than half of their cases such cartilage invasion was only detectable by microscopic study of the resection specimen. This alternative classification system has not been adopted.

4.4.3 Use of Imaging Parameters as Prognostic Factors for Local Outcome Independently from the TN Classification

4.4.3.1 Predicting Local Outcome After Radiotherapy

4.4.3.1.1 Tumor Volume and Deep Tissue Infiltration

Success in controlling a tumor by radiotherapy depends on killing all clonogenic cells. The probability of cure depends, among other factors, on the initial number of clonogenic cells. There are indications that the clonogen number increases linearly with tumor volume (Johnson et al. 1995).

Large primary tumor volume is already for a long time known to be a reason of poor local outcome of laryngeal cancer after definitive radiation treatment (Fletcher et al. 1975). Clinical estimation of tumor volume in various advanced head and neck cancers treated in a multicenter EORTC trial, correlated with survival and locoregional control after radiation treatment (Van den Bogaert et al. 1995), but the volume classes defined in this study (< 10 cc, 10–30 cc, 30–100 cc, > 100 cc) are too rough to be applicable to less advanced head and neck cancers. Overgaard et al. (1986) reported laryngeal tumor diameter (< 2 cm, 2–3.9 cm, > 4 cm) to be of significant importance to both probability of local control and survival in glottic and supraglottic tumors. However, tumor diameters are a rough and potentially inaccurate estimation of tumor volume due to invisible deep tumor extension (Marks et al. 1979; Van den Bogaert et al. 1983).

Three-dimensional tumor visualization, as offered by modern cross sectional imaging techniques, allows more accurate estimation of the tumor volume. To determine the volume of a particular structure, its borders are traced on consecutive images, either manually or with some (semi-)automated method. The segmented surface on each image is then calculated. This procedure can be done on the screen of a workstation, using a mouse-controlled cursor, or indirectly using a digitizer. The obtained surfaces are then multiplied by the slice interval. The summation of all these obtained volumes represents the total volume of the structure of interest. This technique is called the summation-of-areas technique (Breiman et al. 1982).

Gilbert et al. (1987) have been the first to report the prognostic value of CT-determined laryngeal tumor volume for outcome after definitive radiation therapy. Their study consisted of 37 patients with T2–T4 laryngeal cancer (both from glottic and supraglottic origin). The mean tumor volume for patients failing radiotherapy in their study was 21.8 ml, and for patients primarily controlled this was 8.86 ml; tumor volume significantly predicted disease-free interval and outcome with radiotherapy.

Glottic and supraglottic tumors should be considered separately in such studies, as the anatomic situation, and correlated extension pattern, is very different for glottic versus supraglottic tumors. Freeman et al. (1990) and Mancuso et al. (1999) were able to identify those patients with T1–T4 supraglottic carcinomas who had a higher likelihood of local control based on pretreatment CT volumetric analysis (tumors < 6 ml had a probability of 89% of local control, while tumors > 6 ml had only a control rate of 40%). In another study, a significant difference in local outcome after radiotherapy was found in supraglottic cancer, with local control rates for tumors with volumes greater than or less than 8 ml being 20% and 70%, respectively (Kraas et al. 2001).

Lee et al. (1993) and Pameijer et al. (1997) could stratify in a similar way patients with T3 glottic carcinoma into groups with different likelihood of local control (tumors of ≤ 3.5 ml had a local control probability of 85%, while tumors of > 3.5 ml had

only a local control rate of 22%). On the other hand, Mukherji et al. (1995), in a study on 28 patients with T2 glottic carcinoma, were not able to distinguish groups with significantly different local control rates using CT-determined tumor volume. However, in another study in patients with a T2 laryngeal cancer, a tumor volume of > 4 ml predicted a significantly worse local outcome rate (Lo et al. 1998).

The results of the studies by Hermans et al. (1999a,b) corroborate well these previous findings. Both for glottic and supraglottic cancer, tumor volume was found to be a significant prognostic indicator of local control. In glottic cancer, failure probability analysis showed a clear relation between larger tumor volume and increasing risk for local failure (Fig. 4.17); a tumor volume of 3.5 ml correlated with a risk for local failure of approximately 50%. From the graph published by Pameijer et al. (1997), an approximately 40% chance of local failure in T3 glottic cancer with a similar tumor volume can be inferred. Also for supraglottic cancer, Hermans et al. (1999b) found a significant relation between tumor volume and risk for local failure (Fig. 4.18). Compared to glottic cancer, larger supraglottic tumor volumes were found for similar local control rates; similar results can be inferred from other publications (Mancuso et al. 1999). The reason for this different critical tumor volume between glottic and supraglottic cancer is not clear; it might be related to a different local environment in the glottic and supraglottic region, but also (and maybe predominantly) to the more exophytic growth pattern exhibited by supraglottic tumors.

However, tumor volume was not found to be a independent predictor of local outcome when a multivariate analysis was performed. In glottic carcinoma, involvement of the paraglottic space at the level of the true vocal cord and involvement of the preepiglottic space were found to be independent predictors of local outcome (Hermans et al. 1999a). Deep involvement of the paraglottic space at the glottic level, as seen on imaging studies, is also called the 'adjacent sign'. This sign was found to the only independent predictor of local outcome and survival in a series of 130 patients suffering T1–T2 glottic cancer (Murakami et al. 2005).

In supraglottic carcinoma, involvement of the preepiglottic space and subglottic extension were the strongest independent predictors of local control (Hermans et al. 1999b).

Tumor volume and degree of involvement of the laryngeal deep tissues are correlated to some extent. However, these descriptive CT parameters may also reflect a more aggressive tumoral behavior, which could explain their stronger association with local recurrence. Fletcher and Hamberger (1974) stated that the preepiglottic space is poorly vascularized; they suggested that the anoxic compartment of

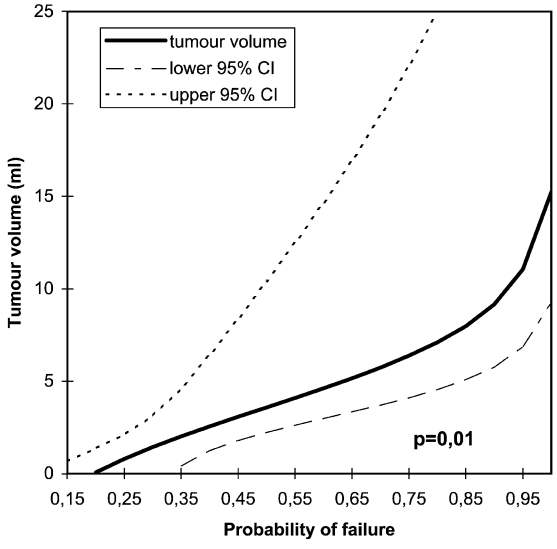

Fig. 4.17. Glottic cancer: probability of local failure after definitive radiation therapy versus CT-determined primary tumor volume. Local failure rate is significantly higher with larger primary tumor volume. The 95% confidence intervals for tumor volume are indicated. [From Hermans et al. (1999a), with permission]

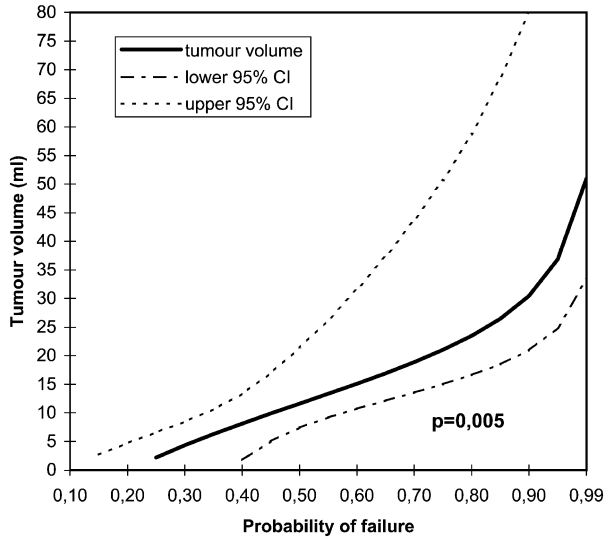

Fig. 4.18 Supraglottic cancer: probability of local failure after definitive radiation therapy versus CT-determined primary tumor volume. As for glottic cancer, local failure rate is significantly higher with larger primary tumor volume. The 95% confidence intervals for tumor volume are indicated. [From Hermans et al. (1999b), with permission]

tumors invading this space must be significant, and thus relatively radioresistant.

4.4.3.1.2 Cartilage Involvement

Laryngeal cartilage invasion is often considered to predict a low probability of radiation therapy alone to control the primary tumor site, and to indicate an increased risk of late complications, such as severe edema or necrosis (Lloyd et al. 1981; Castelijns et al. 1990).

Before the era of computer assisted cross sectional imaging only gross cartilage destruction, usually occurring in large volume laryngeal tumors, could be detected clinically or by conventional radiography. More limited laryngeal cartilage invasion can be detected with modern cross-sectional imaging methods (Becker et al. 1995). Earlier studies described an association between CT depicted cartilage involvement in laryngeal carcinoma and poor outcome after radiation therapy (Silverman 1985; Isaacs et al. 1988). However, according to others involvement of laryngeal cartilage is not necessarily associated with a reduced success rate of radiation therapy (Million 1989). More recent studies correlating laryngeal cartilage abnormalities, detected on CT, with local outcome after radiotherapy seem to corroborate this last point of view.

The cartilage most often showing abnormalities is the arytenoid cartilage; usually this cartilage appears sclerotic. An abnormal appearance of this cartilage was not found to be associated with poorer local control, and may be unimportant in terms of prognosis (Tart et al. 1994; Hermans et al. 1999a). The majority of sclerotic arytenoid cartilages do not contain tumor within ossified bone marrow, which can help to explain why radiation therapy is efficient in a large percentage of patients with isolated arytenoid sclerosis on CT (Becker et al. 1997b).

Pameijer et al. (1997) found a lower probability of local control in patients with T3 glottic carcinoma, when both arytenoid and cricoid showed sclerosis. These authors assume that if both the arytenoid and cricoid cartilage are sclerotic, the probability of microscopic cartilage invasion will increase. Hermans et al. (1999b) did also find that cricoid cartilage abnormalities in glottic carcinoma yielded a statistically significant lower control rate. Ten out of the 13 patients with sclerosis of the cricoid in this study had also sclerosis of the arytenoid cartilage, corresponding with the 'double sclerosis' situation described by Pameijer et al. (1997). However, the multivariate analysis performed in the study by Hermans et al. (1999a) showed that an abnormal appearing cricoid cartilage is not an independent predictor of poor local control in glottic carcinoma: it lost significance when paraglottic and preepiglottic space involvement were entered in the statistical model. Even relatively subtle cartilage abnormalities, as detected in this study population (sclerosis of the cartilage being the most frequent alteration seen), seem to be correlated with deep tumor extension. More destructive cartilage changes are associated with very bulky tumors, which are not selected for radiation therapy.

There are only few data available on the correlation between thyroid cartilage abnormalities as seen on CT and local outcome of glottic cancer after definitive radiation therapy. Some studies explicitly excluded patients showing evidence of thyroid cartilage involvement (Mukherji et al. 1995; Pameijer et al. 1997). In the study by Hermans et al. (1999a), where tumor visible on both sides of the cartilage and lysis of ossified cartilage were used as signs of thyroid cartilage invasion, only a limited number of patients with glottic carcinoma had an abnormal appearance of this cartilage. No evidence was found that thyroidal cartilage involvement on itself as seen on CT is associated with a poorer local outcome after definitive radiation therapy but, as said, the number of patients in this study with signs of neoplastic involvement of this cartilage was small.

No conclusions can be drawn concerning cricoid or thyroid cartilage abnormalities on CT in supraglottic carcinoma, due to the limited number of patients selected for radiation therapy with abnormalities of these cartilages.

On MRI, cartilage involvement in patients with small sized tumors (under 5cc) is not correlated with tumor recurrence; abnormal MR signal pattern in cartilage combined with large tumor volume (above 5cc) worsens the prognosis significantly (Castelijns et al. 1996b). Consequently abnormal MR signal pattern in laryngeal cartilage should not automatically imply laryngectomy, especially in lesions with smaller volumes. It is incorrect to postulate that radiotherapy can not cure a substantial number of lesions with cartilage involvement on MRI. Castelijns et al. (1995, 1996a) agree with Million (1989), that minimal cartilage involvement in patients with low staged tumors does not imply a bad prognosis. Similar to CT, the presence of cartilage abnormalities on MRI studies may be just reflecting a large tumor volume and deep tumor spread, and as such being only indirectly correlated with local outcome after radiotherapy (Ljumanovic et al. 2004).

4.4.3.1.3 Imaging of the Tumoral Micro-Environment

Multiple factors determine the resistance of tumors against radiation treatment and chemotherapy. Tumors may show an intrinsic, genetically determined inherent resistance. However, extrinsic physiological (environmental) factors are also important. Most critical is the presence of less or inadequate and heterogeneous vascular networks leading to chronic 'diffusion-limited' tumor hypoxia.

There is strong evidence that for some human tumors treatment may fail due to the presence of hypoxia (Overgaard and Horsman 1996). The presence of tumor hypoxia needs to be identified and quantified, not only as predictor of outcome, but also to select patients for concomitant radiosensitising therapy to overcome the hypoxia effect. Treatments such as hyperbaric oxygen or carbogen (95%–98% O_2 with 2%–5% CO_2) breathing during radiotherapy have been extensively investigated and initiated in clinics (Kaanders et al. 2002). The adequate appreciation of tumor hypoxia may also lead to the efficient use of hypoxia-directed treatments such as bioreductive drugs or gene therapy.

Direct quantification of tumor oxygenation can thus be expected to be of important prognostic and therapeutic value. Until now one has to rely on invasive methods, e.g. biopsy-based immunohistochemistry techniques, or the use of Eppendorf oxygen-sensitive electrodes to screen tumors for hypoxia. However, oxygen-sensitive needle electrodes can only to a certain extent be used, as some primary tumors (such as laryngeal cancers) are deeply seated and difficult to reach.

There is a clear need for non-invasive methods to investigate the tumoral micro-environment. Nuclear imaging methods (such as PET imaging) may provide important information on tumor physiology (see Chap. 17). There is increasingly more evidence that CT and MR studies, classically used to demonstrate the anatomic position and extent of tumors, are able to provide additional, biological information (Rijpkema et al. 2001, 2002; Hermans et al. 2003).

For example, breathing a hyperoxic hypercapnic gas mixture may have an effect on both blood flow and oxygenation. To study these effects in the clinic a combination of blood oxygen level dependent (BOLD)-MRI and dynamic contrast enhanced MRI techniques seems suitable. The effects of breathing a hyperoxic hypercapnic gas mixture (98% O_2 + 2% CO_2) were assessed by functional MRI techniques in patients with head and neck tumors (Rijpkema et al. 2002). The main conclusion of this study was that breathing this gas mixture improved tumor blood oxygenation. No changes in tumor vascularity were found as assessed by the gadolinium uptake rate (Rijpkema et al. 2001). Functional MRI proved to be a promising tool to investigate both tumor oxygenation and vascularity and might be developed into a predictive tool for treatments using hyperoxygenation for other types of tumors as well.

4.4.3.2 Predicting Local Outcome After Surgery

One study addressed the correlation between volume of supraglottic cancer, as assessed on imaging studies, and outcome after surgical therapy. This study examined a small population with few local recurrences; patients with a tumor volume over 16 ml were found to have a significantly worse local outcome than those with smaller volumes (Mukherji et al. 2000). The threshold tumor volume in this surgical series is greater than threshold tumor volumes reported for supraglottic cancer treated by radiotherapy (see above). This can be expected as during laryngectomy the tumor is resected en bloc. The endolaryngeal soft tissues of the larynx are contained within a cartilaginous framework; the primary tumor should therefore be completely contained within the resected specimen in a successfully performed laryngectomy. Large tumors are more likely invading the laryngeal framework and grow extralaryngeally (Mukherji et al. 2000).

It is often suggested that cartilage involvement precludes voice-sparing partial laryngectomy (Tart et al. 1994, Becker et al. 1995, Castelijns et al. 1996a). However, a recent study indicated that cartilage alterations, as seen on preoperative CT, are not correlated with the local outcome of patients treated by a speech-preserving surgical technique: no increased local failure rate was observed in the patients with cartilage alterations (1 of 11) over those without cartilage abnormalities (1 of 5) (Thoeny et al. 2005). The used surgical technique in this study (extended hemilaryngectomy with tracheal autotransplantation) allows resection of the hemilarynx, including half of the cricoid cartilage. Therefore, areas of possible neoplastic cartilage involvement are very likely to be included in the resection specimen. The inability of other speech-preserving surgical techniques to adequately resect areas of laryngeal framework invasion may falsely lead to the belief that cartilage involvement, in itself, is a contraindication for partial laryngectomy (Thoeny et al. 2005).

4.4.3.3
Towards Risk Profiles Incorporating Imaging Findings

As staging procedures, CT and MRI have an important function in corroborating clinical findings and ruling out more extensive disease. Accurate staging is critical in decision making in oncology (Barbera et al. 2001). However, to what extent CT or MRI influence treatment decisions in laryngeal cancer is currently not very clear, and likely varies from institute to institute. This influence depends on the conducted treatment policy, more precisely on the relative role of radiotherapy and surgery as primary treatment modality in more advanced laryngeal cancer.

The parameters defined in the T-classification are mainly based on clinical examination; the addition of modern imaging methods in staging laryngeal cancer may influence the prognostic information of the T-classification itself, by causing stage migration (Piccirillo and Lacy 2000). Furthermore, imaging-derived parameters such as tumor volume and depth of invasion in the deep tissues are stronger related to local outcome than the T categories.

Pure morphologic criteria can not explain entirely the biologic behavior of a tumor and its response to treatment. Ongoing research focuses on the evaluation with radiological methods of tumor microvascularisation, perfusion and oxygenation, factors known to be of important prognostic value.

New classification systems should be conceived, incorporating not only morphologic tumor extent as within the present TNM system, but also including other variables with independent prognostic significance. Piccirillo et al. (1995) anticipated this will be developed as computer software staging packages, not only calculating prognosis, but also estimating the accuracy of this prognosis based on the amount of information used to generate it.

4.5
Post-treatment Imaging in Laryngeal Cancer

4.5.1
Expected Findings After Treatment

After treatment of a head and neck cancer, a number of tissue changes become visible on CT and MR images of the neck. These expected alterations should be known, so that they are not misinterpreted as evidence of persistent or recurrent tumor.

Imaging may be used to monitor tumor response and to try to detect recurrent or persistent disease before it becomes clinically evident, possibly with a better chance for successful salvage.

Treatment complications, such as soft tissue or cartilage/bone necrosis, are less frequent than tumor recurrences, but these conditions may sometimes be clinically difficult to distinguish. Although definitive distinction between necrosis and recurrent tumor may also radiologically be difficult, imaging findings may be helpful in guiding the choice of treatment and assessing the response to specific treatment.

4.5.1.1
Expected Tissue Changes After Radiotherapy

Within the first 2 weeks after radiotherapy, there is an acute inflammatory reaction within the deep tissues. Increased permeability, due to detachment of the lining endothelial cells within small blood and lymphatic vessels, results in interstitial edema. After this initial period of a few weeks, there is progressive thickening of the connective tissue. Endothelial proliferation is also seen, eventually resulting in complete obstruction of the vessels. The reduction in venous and lymphatic drainage results in further accumulation of interstitial fluid. Then the fibrosis becomes progressively more advanced, but the interstitial edema may be reduced by formation of collateral capillary and lymphatic channels. The changes visible on post-treatment CT and MR images depend on the radiation dose and rate, the irradiated tissue volume, and the time elapsed since the end of radiation therapy (Mukherji et al. 1994a; Nömayr et al. 2001). Changes which may be seen include (Fig. 4.19):

- Thickening of the skin and platysma muscles
- Reticulation of the subcutaneous fat and the deep tissue fat layers
- Edema in the retropharyngeal space
- Increased enhancement of the major salivary glands, followed by size reduction of these glands: postirradiation sialadenitis
- Atrophy of lymphatic tissue, in both the lymph nodes and Waldeyer's ring
- Thickening and increased enhancement of the pharyngeal walls
- Thickening of the laryngeal structures, with increased density of the fat in the preepiglottic and paraglottic spaces.

These tissue changes are most pronounced during the first few months after the end of radiation

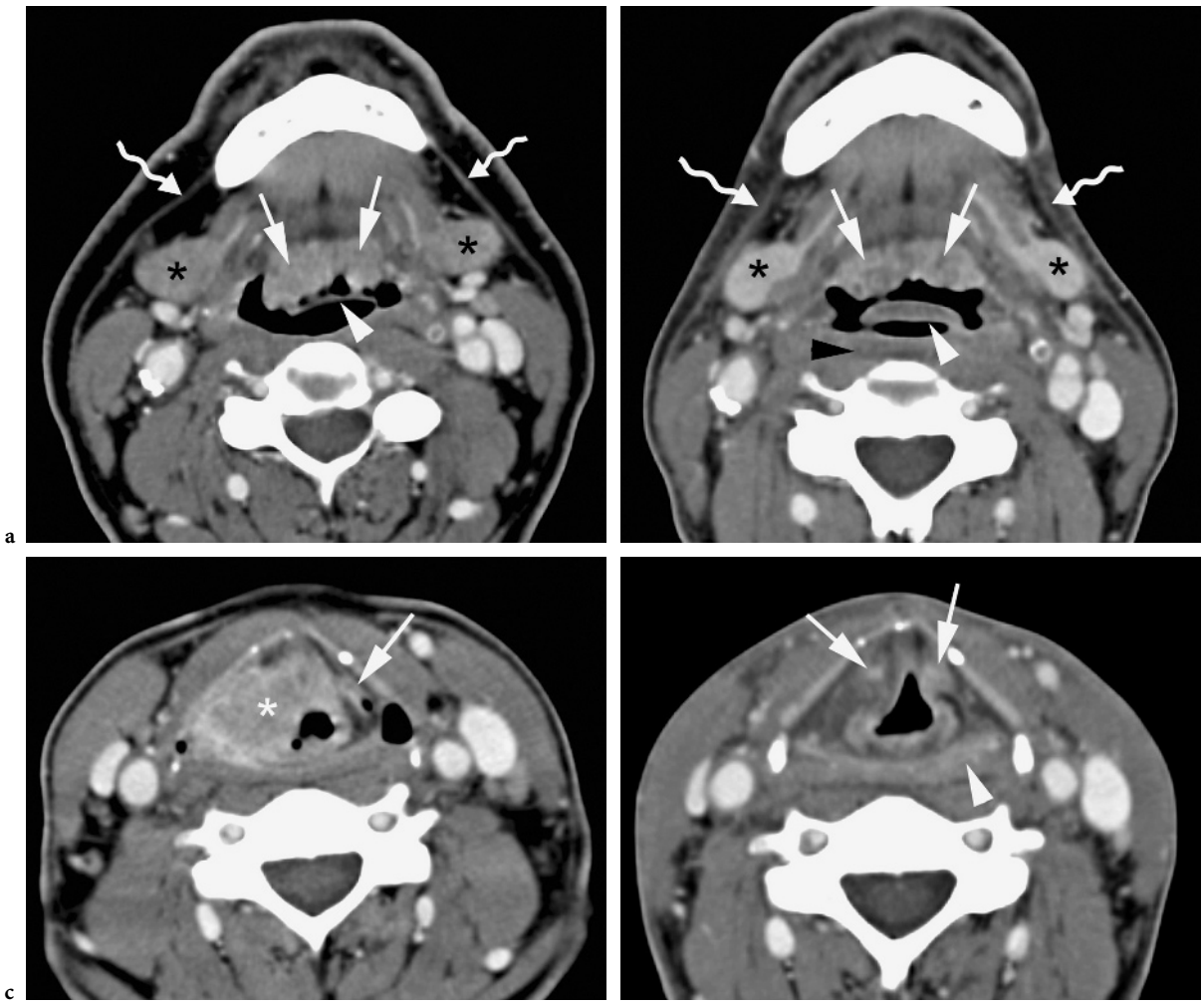

Fig. 4.19a–d. Patient with supraglottic squamous cell carcinoma, staged T3N0, treated by definitive radiotherapy. Axial contrast-enhanced CT images are shown, obtained just before and 3 months after completion of radiation treatment. **a,b** Level of lingual tonsil. After radiotherapy (**b**), apart from diffuse increased attenuation of the neck fatty tissue, thickening of the free edge of the epiglottis (*white arrowhead*), platysma muscles (*curved arrows*), and oropharyngeal walls is seen. Slight amount of retropharyngeal edema is present (*black arrowhead*). Note also increased enhancement of the submandibular salivary glands (*asterisks*), corresponding to radiation sialadenitis, and volume reduction of lingual tonsil (*arrows*). **c,d** Level of supraglottis. Before radiotherapy (**c**), a large supraglottic tumor mass (*asterisk*) is seen, infiltrating the preepiglottic and right paraglottic space; normal left ventricle, containing air bubble, in left paraglottic space (*arrow*). After radiotherapy (**d**), the tumor mass disappeared; increased attenuation of the paraglottic fat spaces, somewhat more pronounced in former tumor bed; no mass lesion can be recognized. Laryngeal ventricle is now visible on both sides (*arrows*). Thickening and increased enhancement of the hypopharyngeal walls (*arrowhead*)

therapy, and diminish or even resolve with time. It is important to note that the expected tissue changes after radiation therapy appear symmetrical, unless the neck was irradiated using asymmetric radiation portals.

The laryngeal cartilages do not show changes after irradiation. Reduction in the degree of cartilage sclerosis in the neighborhood of the tumor has been described, and this appears to correlate with local control (Pameijer et al. 1999).

4.5.1.2 Expected Findings After Laryngeal Surgery

The limits of surgical therapy are determined by the balance between obtaining cure by radical resection of the tumor, and leaving the patient in a functionally and esthetically acceptable situation. More extensive resections are possible by the introduction of various reconstructive materials, such as pedicled or free soft tissue flaps, grafts and protheses.

4.5.1.2.1 Laser Resection

The expected findings after transoral laser excision of a laryngeal cancer depend on the amount of tissue resected. The laryngeal soft tissues may appear normal, or show a focal tissue defect (Fig. 4.20). After a more extensive resection, the laryngeal soft tissue may be replaced by scar, appearing as homogenous but relatively dense tissue with a straighter inner border (Maroldi et al. 2001); in such cases, differentiation with recurrent tumor may be difficult and correlation with endoscopic findings is necessary. In case of doubt, biopsy is warranted.

4.5.1.2.2 Partial Laryngectomy

The aim of partial laryngectomy is to combine radical tumor resection with preservation of laryngeal function. This requires continuity and patency of the airway, separation of the airway and digestive tract, and sparing or reconstruction of the glottic phonation function.

Traditional partial laryngectomies include horizontal supraglottic laryngectomy and vertical hemilaryngectomy, but more complex surgical techniques are also being employed (Maroldi et al. 1997; Maroldi et al. 2001; Delaere and Hermans 2003). The postoperative radiological findings depend on the technique employed. Changes in the laryngeal framework offer landmarks for interpreting postoperative findings. However, a somewhat different appearance for the same technique may be encountered among different patients, depending on technical adaptations needed for adequate tumor resection. The postoperative soft tissue changes are less predictable, depending on individual differences in healing, and variations in amount of edema and scarring (Maroldi et al. 2001). The differentiation between redundant or hypertrophic mucosa, as well as scar tissue, from recurrent cancer, may be difficult.

Horizontal supraglottic laryngectomy can be performed in supraglottic cancer staying above the level of the ventricles; this procedure is not performed when the tumor infiltrates both arytenoids (one arytenoid can be resected), the posterior commissure, the postcricoid area, the apex of the sinus piriformis, the glottis or the thyroid cartilage. Minimal tongue base invasion is not a contra-indication. Almost all of the larynx above the level of the ventricles is removed. The residual thyroid cartilage is pulled upwards and sutured to the hyoid bone.

Limited glottic cancer can be treated by vertical hemilaryngectomy. The most limited variant of this procedure is a cordectomy, where the entire vocal cord is removed from the anterior commissure to the vocal process of the arytenoid. In a frontolateral laryngectomy, the true and false vocal cord is removed, as well as the greatest part of the ipsilateral thyroid cartilage, including the angle to encompass the anterior commissure; the vocal process of the arytenoid can also be included. In a frontal laryngectomy, the anterior portion of both vocal cords is removed, together with the anterior commissure; a modified frontal laryngectomy is Tucker's "near-total" technique, using the epiglottis as reconstructive tissue (Fig. 4.24).

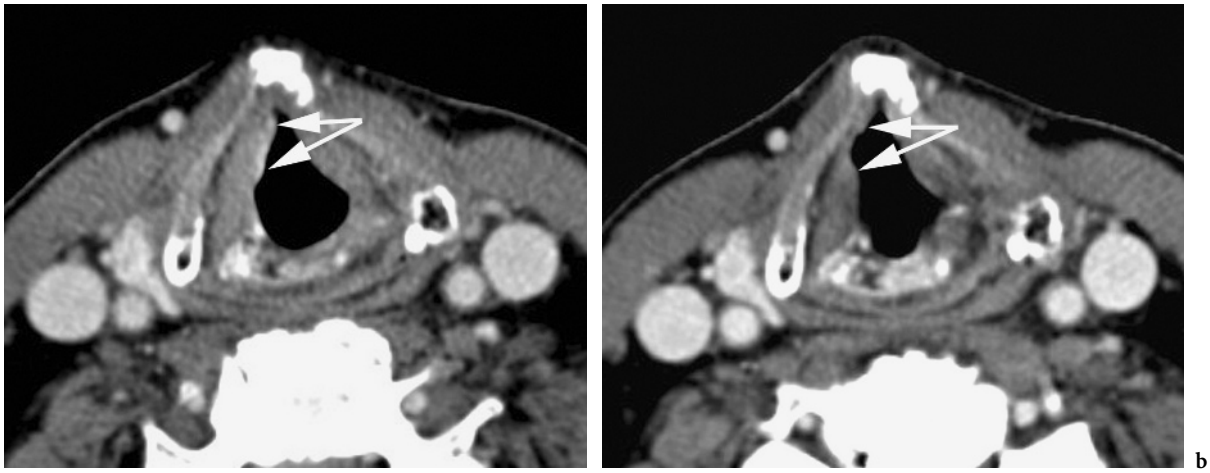

a **b**

Fig. 4.20. a Recurrent glottic squamous cell cancer, presenting as soft tissue thickening (*arrows*), 2 years after radiotherapy for a right-sided glottic cancer (T2N0). **b** Situation 7 months after partial cordectomy by transoral laser resection: a soft tissue defect is seen in the anterior half of the right true vocal cord (*arrows*); no evidence for recurrent cancer

If more extensive involvement of the arytenoid is present (possibly with involvement of the cricoarytenoid joint) and/or subglottic extension is present, these procedures are not performed. Extended hemilaryngectomy may then be an alternative. During this procedure, half of the larynx, including half of the cricoid cartilage, is removed. The large defect in the larynx is reconstructed with a tracheal patch, revascularized by a freely transplanted radial forearm soft tissue flap. Full height cricoid defects can be closed using this patch in a position comparable to unilateral laryngeal paralysis. This is a functional reconstruction, allowing the patient to breathe and speak through his larynx, and swallow without aspiration (Delaere et al. 2000; Delaere and Hermans 2003) (Fig. 4.25).

Some advanced glottic and supraglottic cancer can be treated by supracricoid partial laryngectomy (SPL), entailing en bloc resection of all tissues between the upper margin of the cricoid cartilage and the inferior margin of the hyoid bone, including the true and false vocal cords. Only the arytenoid on the less involved site is left in place. For glottic cancers without involvement of the supraglottis, the upper two thirds of the epiglottis can be preserved; this variant is known as SPL with cricohyoidoepiglottopexy (CHEP) (Gavilan 2000).

4.5.1.2.3 Total Laryngectomy

Complete removal of the larynx may be required as primary treatment of extensive laryngeal cancer or for salvage of tumor recurrence after radiation treatment or failed partial laryngectomy.

When the larynx is removed, the airway and upper digestive tract become completely separated. The airway will then end at a tracheostomy in the base of the neck. If, following the laryngectomy, not sufficient hypopharyngeal tissue is left for creating a neopharyngeal lumen of acceptable diameter, a soft tissue flap is used to create a wider lumen. A pedicled pectoralis major musculocutaneous flap is commonly used for this purpose (Fig. 4.21). The pectoralis major flap has an excellent blood supply. The skin of the flap borders the lumen, while the bulk of the flap fills the soft tissue neck defect, creating a more acceptable aesthetic appearance. On imaging studies, the pectoralis major flap appears initially as a bulky soft tissue structure, showing the characteristics of muscle; gradually, denervation atrophy appears, causing volume loss and fatty replacement of the muscle. At the time of imaging, the muscle de-

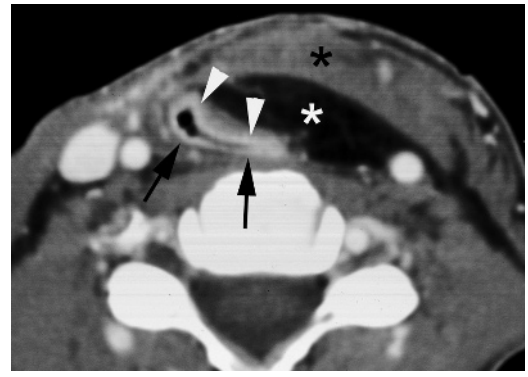

Fig. 4.21. Axial contrast-enhanced CT image. Situation after total laryngectomy. The neopharynx is reconstructed by residual pharyngeal tissue (*arrows*) and a musculocutaneous soft tissue flap (pectoralis major flap), containing skin (*arrowheads*), subcutaneous fat (*white asterisk*) and muscle (*black asterisk*)

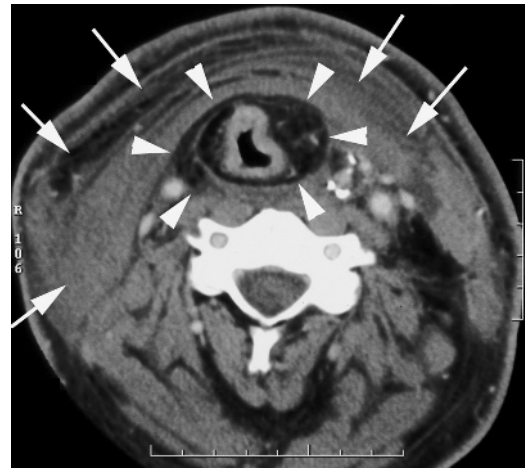

Fig. 4.22. Axial contrast-enhanced CT image, in a patient treated by total laryngectomy. The neopharynx is reconstructed by a free radial forearm flap (*arrowheads*; inner enhancing rim is skin); the soft tissues are anteriorly covered by a pedicled pectoralis major flap (*arrows*)

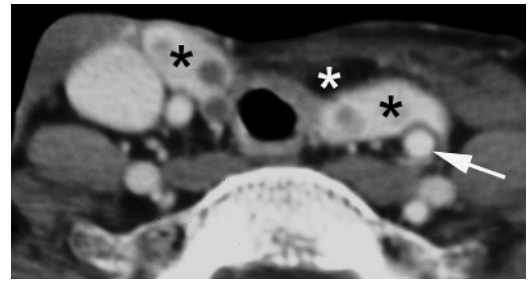

Fig. 4.23. Axial contrast-enhanced CT image. The neopharynx is seen lying between both thyroid lobes (*black asterisks*). The thyroid isthmus was resected during the laryngectomy. The inhomogeneous appearance of the thyroid lobes is caused by nodular hyperplasia. Absence of left internal jugular vein along the common carotid artery (*arrow*), resected during radical neck dissection. Soft tissue flap (*white asterisk*)

nervation may be incomplete; fiber-like structures with muscle density within the flap should not be confused with tumor recurrence. Sometimes a radial forearm flap is used to create a neopharynx (Fig. 4.22), or an intestinal structure is transplanted to function as neopharynx.

Commonly during laryngectomy, tissue of the thyroid gland is removed. Unilateral thyroidectomy may be performed, to facilitate surgical access to the larynx and to remove at the same time a site of potential direct spread of the cancer. Another option is to remove the isthmus of the thyroid gland, leaving the two thyroid lobes. This remnant thyroid tissue is usually easy to recognize because it shows a high density, related to the high iodine concentration in the gland and its strong vascularisation. However, as the normal shape of the thyroid gland is lost, these remnants usually show a rounded or oval appearance. Thyroid tissue may appear inhomogeneous due to the presence of nodular hyperplasia, adenomas or cysts. It is important that these thyroid remnants are not confused with recurrent cancer; unlike recurrent cancer, they have well-defined borders (Fig. 4.23).

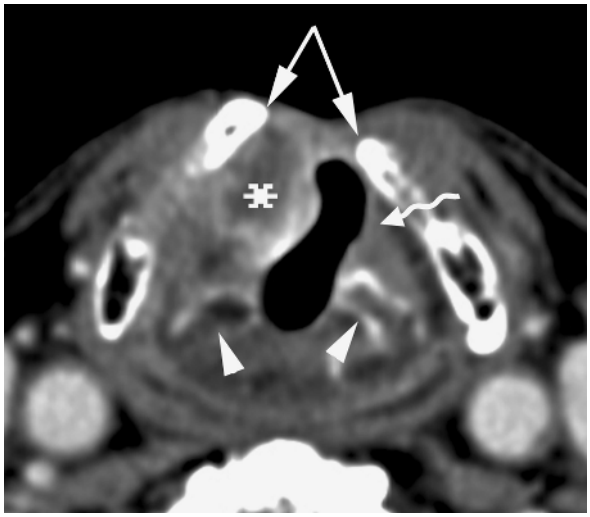

a

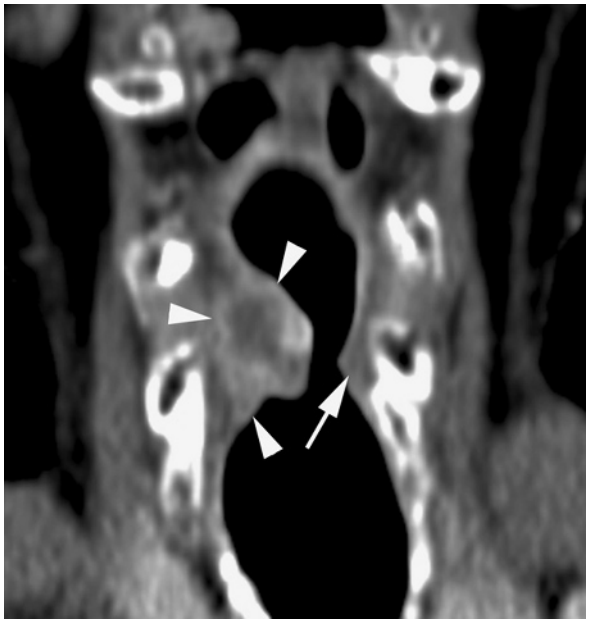

b

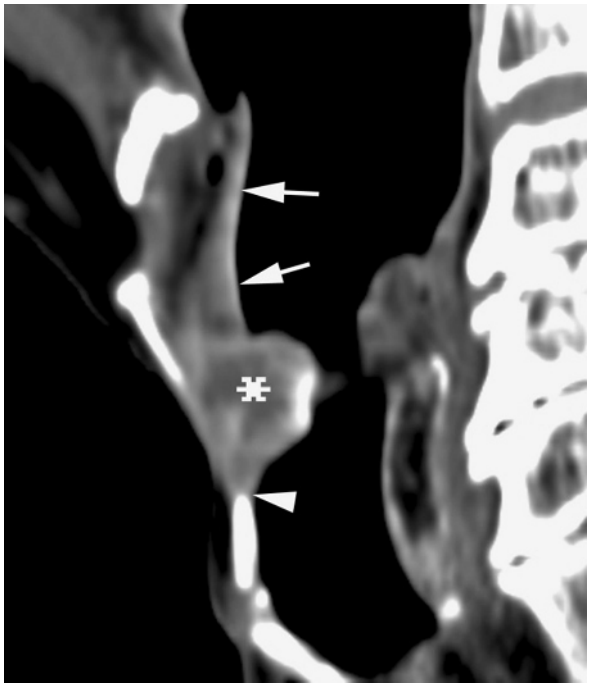

c

Fig. 4.24a–c. Contrast-enhanced CT images in a patient who was treated by a frontal laryngectomy (according to Tucker) for a carcinoma in the anterior commissure. At 3 years later, the patient presents with increasing dysphonia. Clinically, swelling of the right false vocal cord is noted with an intact mucosa. **a** Axial section at the level of the arytenoid cartilages (*arrowheads*). Defect in the anterior part of the thyroid cartilage (*arrows*); the anterior part of the left true vocal cord (*curved arrow*) has been resected. On the right side, a centrally necrotic soft tissue mass is seen (*asterisk*), indicating tumor recurrence. **b** Coronal reformatting. Level of true vocal cord is indicated on left side by arrow. The recurrent tumor on the right (*arrowheads*) grows from the false vocal cord region into the true vocal cord; early subglottic extension may be present (*lower arrowhead*). **c** Sagittal reformatting. The upper part of the epiglottis (*arrows*) has a more anterior course as normally expected, as this structure was used to close the thyroid cartilage defect. The recurrent tumor (*asterisk*) abuts the upper margin of the arch of the cricoid cartilage, appearing sclerotic (*arrowhead*). No neoplastic cartilage invasion was present histologically

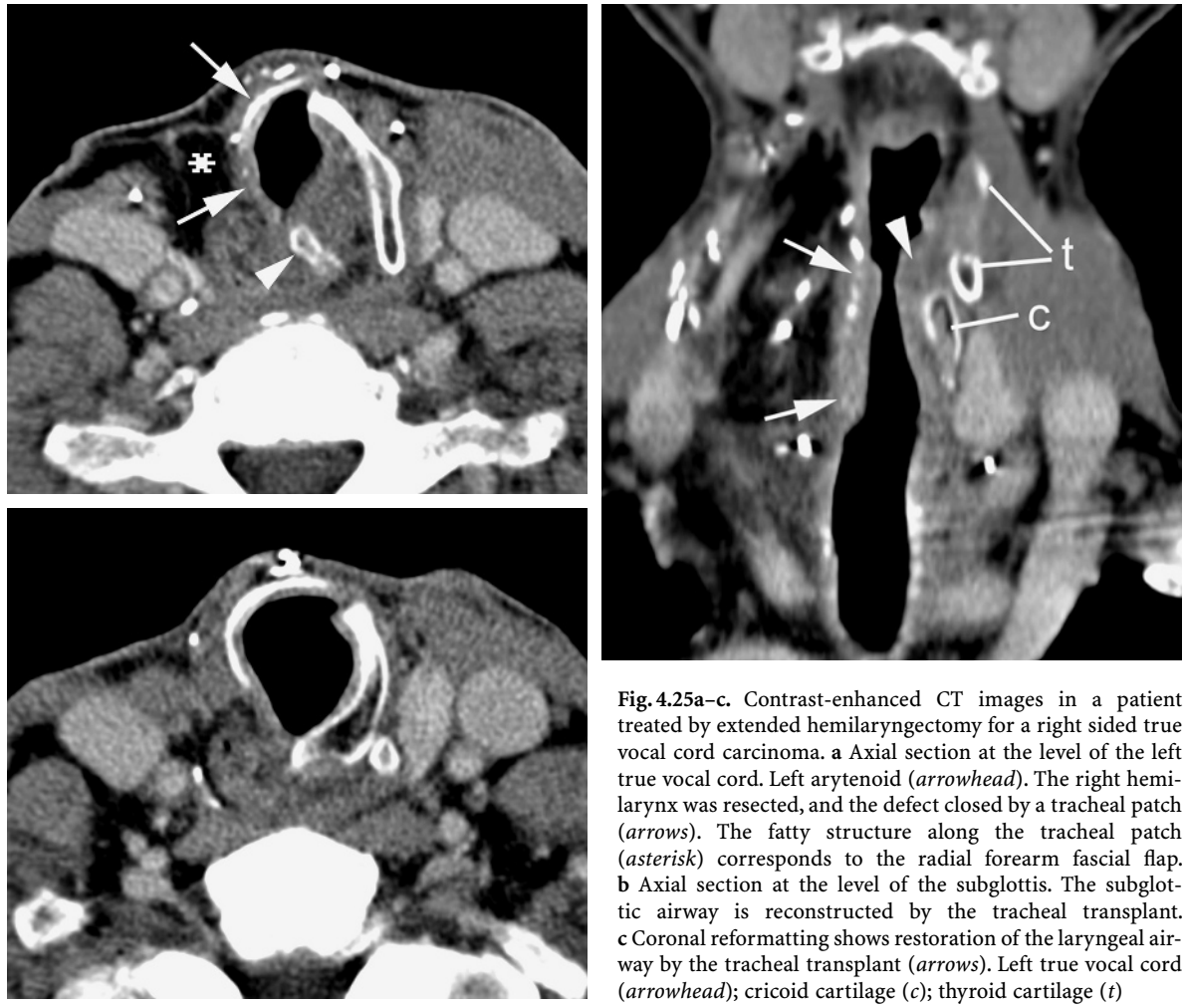

Fig. 4.25a–c. Contrast-enhanced CT images in a patient treated by extended hemilaryngectomy for a right sided true vocal cord carcinoma. **a** Axial section at the level of the left true vocal cord. Left arytenoid (*arrowhead*). The right hemilarynx was resected, and the defect closed by a tracheal patch (*arrows*). The fatty structure along the tracheal patch (*asterisk*) corresponds to the radial forearm fascial flap. **b** Axial section at the level of the subglottis. The subglottic airway is reconstructed by the tracheal transplant. **c** Coronal reformatting shows restoration of the laryngeal airway by the tracheal transplant (*arrows*). Left true vocal cord (*arrowhead*); cricoid cartilage (*c*); thyroid cartilage (*t*)

4.5.2 Persistent or Recurrent Cancer

4.5.2.1 Imaging Strategies and Findings

Post-treatment imaging is useful to confirm the presence of clinically suspected tumor recurrence.

On CT or MRI, tumor recurrence appears after radiation therapy as a soft tissue mass at the primary site and/or as an enlarged (and/or centrally liquefied) neck adenopathy. After surgical treatment, the most reliable imaging finding in recurrent tumor is an enhancing soft tissue mass (Fig. 4.24, Fig. 4.26); after partial laryngectomy, destruction of residual laryngeal cartilage may be seen.

Early tumor recurrence may be difficult to distinguish from tissue changes induced by therapy. Therefore, it is recommended to obtain a follow-up

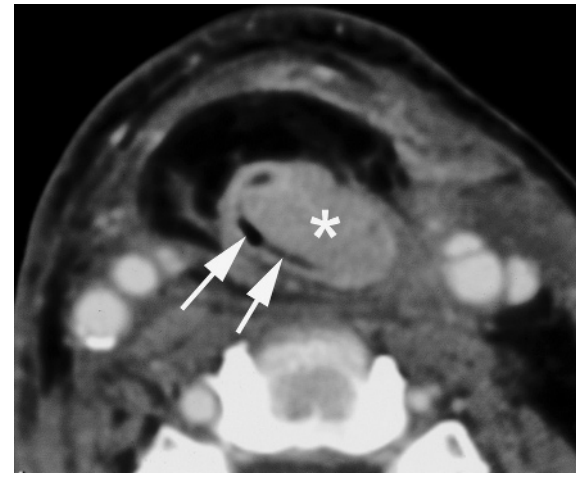

Fig. 4.26. Axial contrast-enhanced CT image, after total laryngectomy for squamous cell carcinoma. Enhancing soft tissue mass (*asterisk*) at the anterolateral side of the neopharyngeal lumen (*arrows*): recurrent cancer

CT or MR study after surgical, radiation or combined treatment for a laryngeal neoplasm with high-risk profile (Hermans et al. 2000a; Schwartz et al. 2003). Probably the best time to obtain such a baseline study is about 3–6 months after the end of treatment. Such a baseline study allows treatment-caused changes in the head and neck tissues to be documented. By comparing subsequent studies with the baseline study, it becomes possible to detect with more confidence tumor recurrences or treatment complications, and this at an earlier stage than is possible with clinical follow-up alone (Fig. 4.27). In patients with laryngeal cancer, CT is an adequate imaging modality for pre- and post-treatment imaging.

There is evidence that the baseline study after radiotherapy carries important predictive information

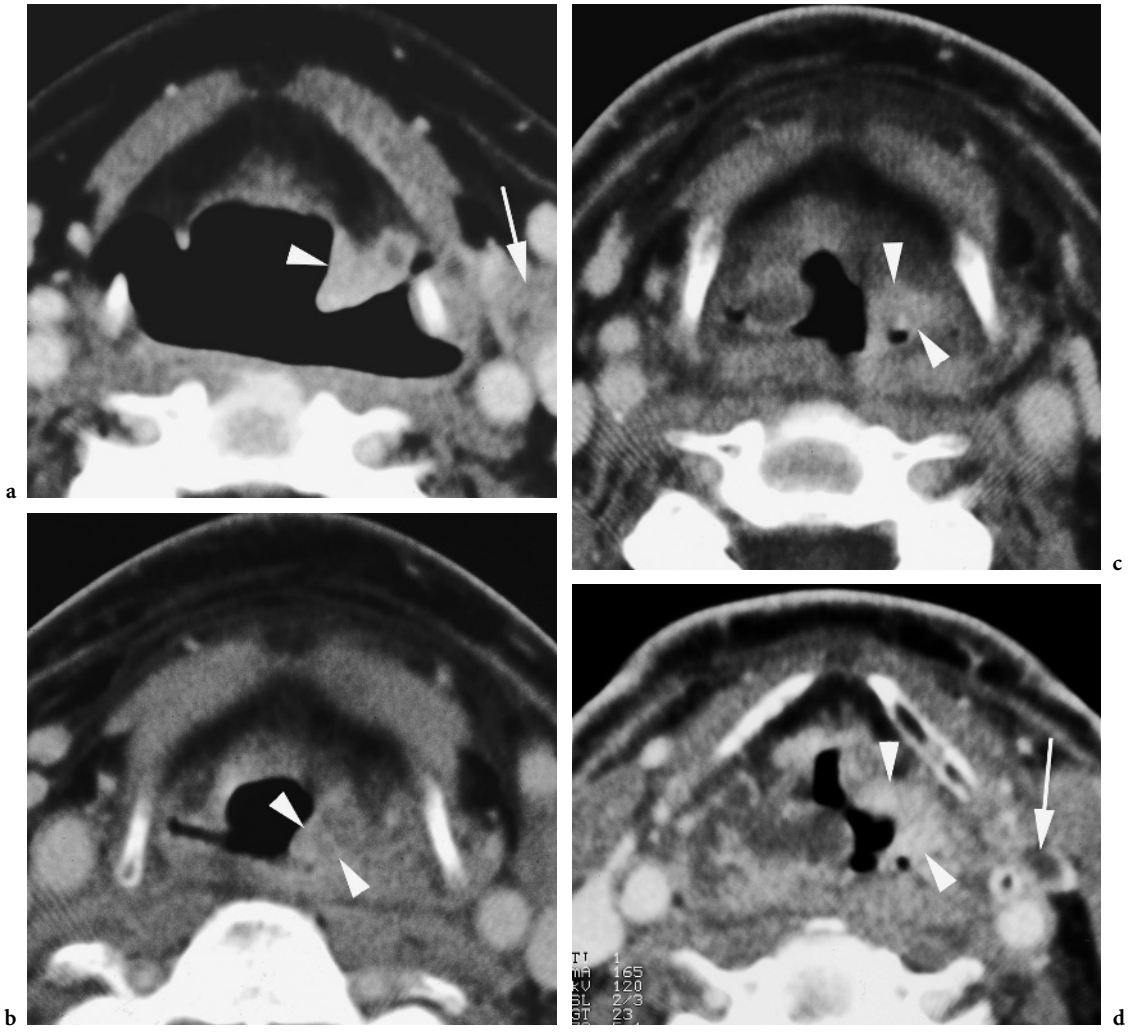

Fig. 4.27a–d. a Pretreatment CT image of patient with T2 supraglottic squamous cell carcinoma, shows infiltrating lesion within the left aryepiglottic fold (*arrowhead*). A pathologic lymph node is seen along the left internal jugular vein (*arrow*). **b** At 3 months after radiation treatment, clinical examination showed pronounced laryngeal edema, but no evidence of tumor. On CT, thickening of the supraglottic soft tissues is seen, more pronounced in the left aryepiglottic fold (*arrowheads*); the density within the left aryepiglottic fold is also somewhat higher than in the surrounding tissues. This is a non-specific finding (score 2), warranting further imaging follow-up. **c** At 9 months after radiation treatment. Clinically favourable evolution. However, CT shows more pronounced enhancement in the left aryepiglottic fold compared to the previous study (*arrowheads*). This was reported as suspicious for tumor recurrence. Direct laryngoscopy was performed but showed no mucosal abnormalities; biopsies were negative. **d** At 1 year after radiation treatment. Apart from increasing generalized laryngeal edema, the enhancing mass in the aryepiglottic fold is now extending more anteriorly into the left paraglottic space (*arrowheads*). Also note appearance of small necrotic lymph node in the left neck (*arrow*). Direct laryngoscopy, performed after the CT study, showed caking of necrotic tissue over the left aryepiglottic fold, suspect for tumor recurrence. Biopsy revealed squamous cell carcinoma. The patient died with progressive locoregional disease 7 months later

regarding the eventual local outcome: several studies show that CT may be useful in the early differentiation of treatment responders from non-responders in irradiated laryngeal and hypopharyngeal cancer (Hermans et al. 2000a; Mukherji et al. 1994b). In this regard, the value of MRI is less well established.

Based on the appearance of the larynx/hypopharynx on an early post-radiotherapy CT study, a prediction of long-term local outcome can be made according to the following scores: 1 = expected post-radiotherapy changes, i.e. complete resolution of the tumor at the primary site and symmetrically appearing laryngeal and hypopharyngeal tissues, as described above; 2 = focal mass with a maximal diameter of < 1 cm and/or asymmetric obliteration of laryngeal tissue planes; 3 = focal mass with a maximal diameter of > 1 cm, or < 50% estimated tumor volume reduction (Pameijer et al. 1999; Hermans et al. 2000a).

The post-radiotherapy CT score 1 was shown to be a very strong predictor of long-term local control; patients with such findings on post-radiotherapy CT will probably not benefit from further follow-up imaging studies. Conversely, patients with a first follow-up examination classified as CT score 3 do very poorly; almost all these patients will develop a local failure (Pameijer et al. 1999). Further exploration in such post-radiotherapy CT score 3 patients is warranted. FDG or thallium PET or SPECT imaging may prove to be a useful intermediate step in cases where biopsy is considered too risky, or if a biopsy result is returned as negative (Fig. 4.28). Indeed, the predictive value of a negative biopsy for local control is reported to be only 70% (Keane et al. 1993); this is likely due to sampling error, as tumor recurrences initially develop submucosally and can therefore not be accurately targeted. In cases of contradiction between the clinical findings, CT findings, results of radionuclide studies and/or biopsy, close clinical follow-up and repeat imaging studies are needed.

The local outcome of patients initially classified as post-radiotherapy CT score 2 is indeterminate. Unless clinical examination is already suspect for local failure, further follow-up CT studies are needed in these patients; a time interval of 3–4 months is recommended, to be continued up to 2 years after completion of radiation treatment.

Some authors recommend FDG-PET as the initial baseline study, in patients treated with advanced disease with low clinical suspicion of recurrence, and in patients with non-specific symptoms that could indicate recurrence but without a clinically obvious mass; cross-sectional imaging should then be performed for an equivocal or positive PET study, or as the initial study in patients with a suspicious palpable mass or biopsy proved recurrent tumor (Mukherji and Wolf 2003). Further study is needed to elucidate the most efficient use of PET and CT/MR in posttreatment situations; also the potential role of combined PET-CT systems has be evaluated.

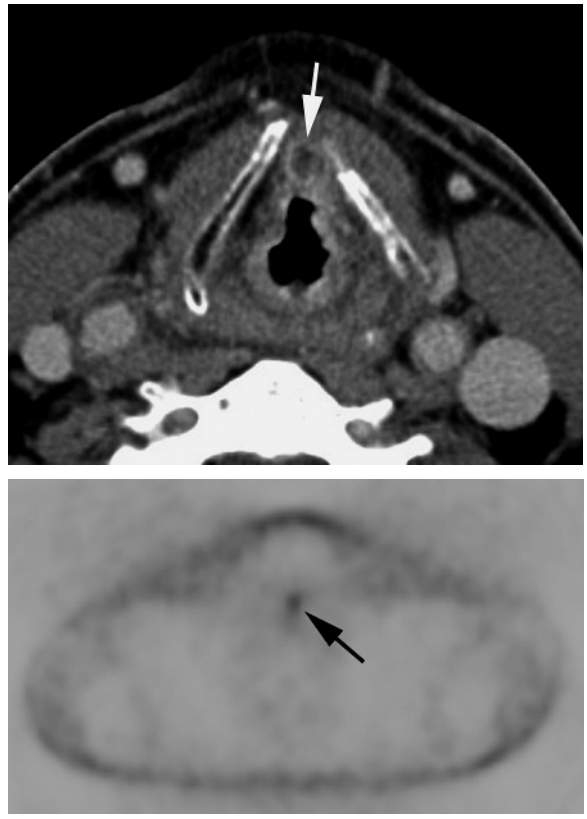

Fig. 4.28a,b. Same patient as in Fig. 4.14. At 6 months after radiotherapy, clinical suspicion of tumor recurrence. Axial contrast-enhanced CT image shows centrally hypodense nodular lesion in the preepiglottic space (*arrow*) suggesting necrotic tumor. Biopsies were negative. FDG-PET image shows faint tracer accumulation at the level of the supraglottis. Total laryngectomy was performed; histological analysis of the resection specimen confirmed presence of squamous cell carcinoma

4.5.2.2 Potential Value of Imaging Surveillance

Use of this imaging-based information could lead to more prompt salvage surgery and potentially improve the survival of these patients (Hermans et al. 2000a). However, few data regarding the value of posttreatment surveillance in patients with head and neck cancer are available. Some authors argue that routine follow-up is indispensable, as patients with asymptomatic locoregional recurrences, discovered during

surveillance, have a significant better post-recurrence survival than those patients in whome recurrent disease was found by symptoms (de Visscher and Manni 1994). Other authors point out that the apparently longer survival of patients with recurrent tumor diagnosed by testing, may be due to lead time bias (i.e. early diagnosis falsely appears to prolong survival) (Schwartz et al. 2003). This statement probably is true for patients treated by combined-modality therapy for advanced head and neck cancer, who are known to do extremely poorly after relapse and rarely have an effective treatment option available (Cooney and Poulsen 1999). However, in single modality treated patients, in whome a reasonable chance of salvage exists after locoregional recurrence (e.g. 35%–60% surgical salvage rate for irradiated laryngeal cancer), imaging surveillance may be worthwhile to add to the clinical follow-up in order to further improve the salvage rate. More studies are required to elucidate this question.

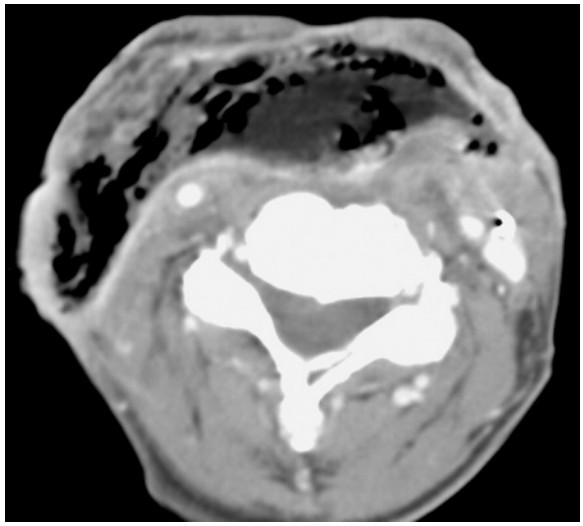

Fig. 4.29. Axial contrast-enhanced CT image. A few weeks before this CT study, total laryngectomy was performed, with neopharyngeal reconstruction by a pectoralis major flap. The patient suffers now from persistent fistulization. Throughout the pectoralis major flap, large, confluent gas bubbles are visible, indicating flap necrosis. Flap necrosis was surgically confirmed

4.5.3 Treatment Complications

4.5.3.1 Complications After Surgery

Most surgical complications occur early after treatment, and are dealt with on a clinical basis. Imaging may be required in the detection and follow-up of a fistula after partial or total laryngectomy. Many of these fistulas will close spontaneously, but some may need reintervention.

After conservative surgery, swallowing coordination may be impaired. The postoperative swallowing function can be analyzed by videofluoroscopy or videofluorography, providing information allowing the planning of rehabilitation (Maroldi et al. 2001). In some cases, surgical intervention may be required; in case of severe aspiration, total laryngectomy may be necessary.

Imaging may also be of use in the confirmation of flap failure due to necrosis (Fig. 4.29).

4.5.3.2 Complications After Radiotherapy

4.5.3.2.1 Laryngeal Necrosis

Acute effects of radiotherapy (skin and mucosal reactions) occur during or immediately after treatment, and usually settle spontaneously.

Persisting severe edema and radionecrosis of the larynx are uncommon treatment complications, with an incidence of about 1%. The occurrence of laryngeal necrosis peaks during the 12 months following treatment, which is more or less contemporaneous with the peak incidence of tumor recurrence. However, cases of laryngeal necrosis more than 10 years after radiation treatment do occur (O'Brien 1996). These late effects after radiation treatment are largely due to impaired vascular and lymphatic flow, caused by endothelial damage and fibrosis (Alexander 1963). Cartilage itself is resistant to the effect of irradiation (see above). Cartilage changes usually occur when the perichondrium is broached by trauma or tumor, exposing the underlying irradiated cartilage to microorganisms in the airway (Keene et al. 1982); this may lead to infectious perichondritis, possibly resulting in necrosis and laryngeal collapse.

Patients with laryngeal necrosis often have neck and/or ear pain, some degree of dysphagia, and anterior neck swelling. Hoarseness and dyspnea are caused by increasing edema with impairment of vocal cord mobility, resulting in cord fixation. Inflammatory changes in the overlying skin, or cutaneous fistulae may be present. Palpation of the laryngeal region usually is painful. On imaging studies,

a variable degree of laryngeal soft-tissue swelling is seen (Hermans et al. 1998). These soft tissue changes surrounding the necrotic cartilage can be very pronounced and may be the only visible abnormality, making the differentiation with recurrent tumor very difficult. Furthermore, laryngeal necrosis and tumor recurrence may occur simultaneously. In laryngeal necrosis, some fluid may be seen surrounding the cartilages (Fig. 4.30). Cartilaginous abnormalities are often visible, but in some patients they may only become apparent on follow-up CT studies.

Necrosis of the thyroid cartilage may cause fragmentation and collapse of this cartilage with or without gas bubbles visible adjacent to or in it. Patients with arytenoid cartilage necrosis may show anterior dislocation of this cartilage; this could be due to crico-arytenoidal joint effusion, secondary to inflammation or infection. Progressive lysis of the arytenoid is possible, showing a crumbly aspect evolving to complete disappearance (De Vuysere et al. 1999). Also, sloughing of the arytenoid cartilage into the airway has been described (Hermans et al. 1998). The adjacent part of the cricoid cartilage may appear sclerotic. Cricoidal sclerosis or destruction may be also seen in association with lysis of the thyroid cartilage (Fig. 4.31).

On MR studies, laryngeal necrosis may appear as focal swelling of the laryngeal soft tissues, loss of the normal high signal in the medullary space of ossified laryngeal cartilage on T1-weighted images, and enhancement of the affected cartilage after injection of gadolinium (Bousson et al. 1995).

In some cases, the imaging findings allow better differentiation between tumor recurrence and chondronecrosis than clinical examination alone. Studies on post-radiotherapy surveillance of laryngeal and hypopharyngeal cancer (Mukherji et al. 1994b; Pameijer et al. 1999) showed that progressive cartilage alterations on post-radiotherapy CT studies predicted poor local outcome, either due to tumor recurrence or chondroradionecrosis. In these studies gas bubbles in the vicinity of cartilage and cartilage collapse were not observed in cases of tumor recurrence. Such findings can be regarded as suggestive of radionecrosis; nevertheless, a co-existent tumor recurrence may be difficult to exclude, depending on the associated tissue alterations (Fig. 4.30).

It has been suggested that FDG-PET may allow differentiation between tumor recurrence and tissue necrosis as complication of therapy (Anzai et al. 1996; McGuirt et al. 1998). However, false positive results may occur as tissue necrosis may be associated with

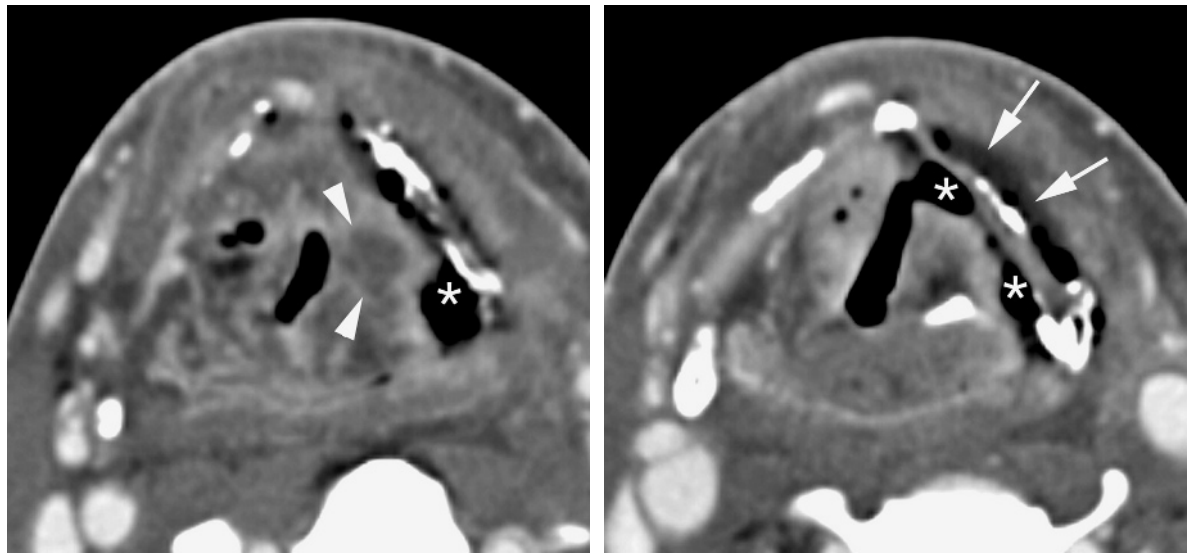

a b

Fig. 4.30a,b. Axial contrast-enhanced CT images. Patient treated 5 months earlier by irradiation for T3 supraglottic cancer, suffering from progressive dysphagia. Laryngoscopy showed a fixed left vocal cord, suspect for tumor recurrence. **a** On a background of expected changes after radiation therapy, a centrally hypodense nodular area of soft tissue thickening is seen in the left aryepiglottic fold (*arrowheads*). Furthermore, a large soft tissue defect (*asterisk*), connecting the left piriform sinus with the denuded thyroid cartilage lamina, is seen. The thyroid lamina appears slightly irregular, and is abutted by air. **b** At a lower level, soft tissue defects are seen to connect to the left piriform sinus, as well as to the laryngeal ventricle (*asterisks*). Fluid layer at the outer side of the thyroid cartilage (*arrows*). A FDG-PET study was strongly positive at the level of the supraglottis. Because of a rapidly deteriorating clinical situation, total laryngectomy was performed. Histologic examination revealed extensive tissue necrosis, but no laryngeal tumor recurrence

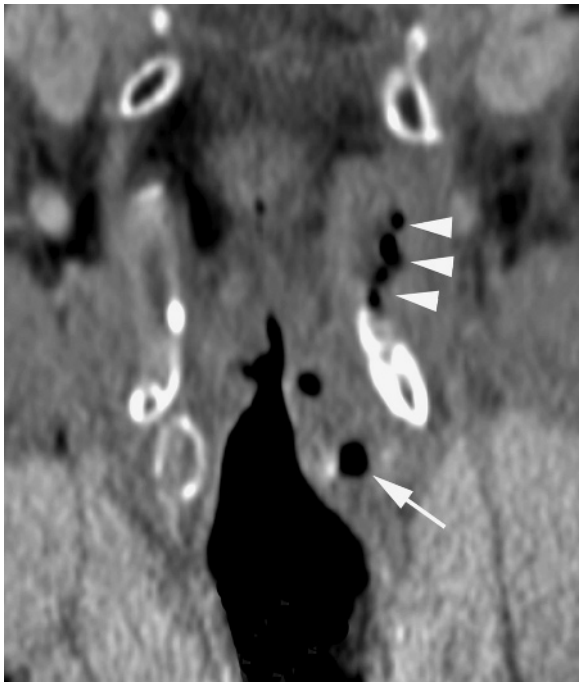

Fig. 4.31. Coronal reformatting of contrast-enhanced laryngeal CT study. The patient was treated 2 years earlier with radiotherapy for a T2 glottic carcinoma, and now presented with increasing breathing and swallowing difficulties. Laryngeal soft tissue thickening is seen, more pronounced on the left side. Lysis of the left part of the cricoid arcus, with presence of an intracartilaginous gas bubble (*arrow*); also the upper part of the left thyroid cartilage wing appears lytic and contains several gas bubbles (*arrowheads*). The image is suggestive for extensive laryngeal necrosis. Total laryngectomy was performed; histopathologic study confirmed extensive radionecrosis, without evidence of tumor recurrence

an important inflammatory reaction, increased metabolism and thus increased uptake of the tracer, suggesting tumor recurrence.

4.5.3.2.2 Other Complications After Radiotherapy

Fibrosis after radiotherapy may lead to contraction and hardening of the cervical tissues. Fibrosis-induced laryngeal dysfunction may lead to aspiration due to immobilization of the epiglottis and/or delayed closure of the laryngeal vestibulum and glottis; secondary aspiration may be caused by ineffective clearance of the pharynx. Dysphagia may be caused by pharyngeal stenosis, which is most often seen in the neopharynx after total laryngectomy.

Fibrosis of the masticatory muscles may occur, particularly if they were involved by the cancer. The MRI signal characteristics of fibrosis are variable; often, follow-up studies are needed to rule out tumor recurrence with a sufficient degree of confidence.

Other long-term complications of radiotherapy include arteriopathy, delayed central nervous system reaction, radiation myelopathy, cranial nerve palsy and secondary tumors (Becker et al. 1997b).

4.6 Non-squamous Cell Laryngeal Neoplasms

The vast majority of laryngeal mass lesions are squamous cell carcinomas, and most of them clinically show mucosal alterations. Non-squamous cell carcinomas typically grow beneath an intact mucosal layer. Clinical and endoscopic diagnosis of a submucosal laryngeal mass lesion is more difficult, and the initial biopsy results of such lesions may be returned as inconclusive or negative.

CT and MR studies demonstrate the presence and extension of such submucosal mass lesion. However, the radiological differentiation between a benign and malignant submucosal mass may be difficult. Signs suggesting malignancy include cartilage destruction, the presence of adenopathies, and a multifocal appearance and/or widely infiltrating behavior.

A variety of epithelial non-squamous neoplasms, and non-epithelial neoplasms can be encountered within the larynx (De Foer et al. 1996). The following discussion is limited to malignant lesions.

4.6.1 Minor Salivary Gland Neoplasms

Minor salivary glands are found throughout the mucosa of the oral and upper respiratory tract. In the larynx, these glands are located in the supra- and subglottic region; the glottis is devoid of minor salivary glands. The incidence of malignant tumors is considerably higher in minor salivary glands than in the large salivary glands; adenoid cystic carcinoma is the most frequent neoplasm of the minor salivary glands, but also adenocarcinoma and muco-epidermoid carcinoma arise from these glands.

Adenoid cystic carcinoma is a misleading name as macroscopic cystic structures are unusual in this tumor. It is sometimes called cylindroma, an old name which is better abandoned as it includes several non-related types of neoplasms.

About 25%–35% of minor salivary gland tumors are adenoid cystic carcinomas. This tumor is mainly seen in the fourth, fifth and sixth decade of life.

The radiographic characteristics of adenoid cystic carcinoma are non-specific. In the larynx, these tumors usually present as a submucosal soft tissue mass in the subglottis (Fig. 4.36). As they grow submucosally, they are often locally more extensive than clinically suspected.

4.6.2 Mesenchymal Malignancies

4.6.2.1 Chondrosarcoma

Chondrosarcomas are the most frequent laryngeal sarcomas. Cartilaginous tumors of the larynx account for less than 1% of all laryngeal tumors. Both chondroma and chondrosarcoma are encountered in the larynx, with 70% arising from the cricoid cartilage, and the thyroid cartilage being the next most common site of origin.

These cartilaginous tumors may be asymptomatic, or present with hoarseness, dyspnea or dysphagia. At presentation, the lesion is usually less than 2–3 cm in diameter. On pathological examination, a lobular growth pattern with low cellularity is seen; nuclear atypia and mitoses are not encountered (Devaney et al. 1995).

True chondromas of the larynx are probably very rare. It is difficult to firmly establish the diagnosis of benign laryngeal chondroma on a small amount of tissue obtained by biopsy. Low-grade chondrosarcoma may also show a lobular growth pattern. Compared to chondroma, low-grade chondrosarcoma may display only minimally increased cellularity and nuclear atypia, a pattern overlapping with benign chondromas; there is also no appreciable degree of mitotic activity in such lesions (Devaney et al. 1995).

On CT studies, cartilaginous tumors of the larynx appear as hypodense, well circumscribed masses centered within the laryngeal cartilage, with coarse or stippled calcification within the lesion (Wang et al. 1999) (Fig. 4.32). The imaging findings do not allow to distinguish between a benign and malignant chondroid tumor, although in high-grade chondrosarcomas nodal metastasis in the head and neck may rarely be seen. MRI is less specific for diagnosing such a lesion as it does not depict the intratumoral calcifications as well as CT; on MRI, the tumor matrix shows a relative high signal intensity on T2-weighted images; the tumor enhancement after injection of gadolinium is variable (Fig. 4.33).

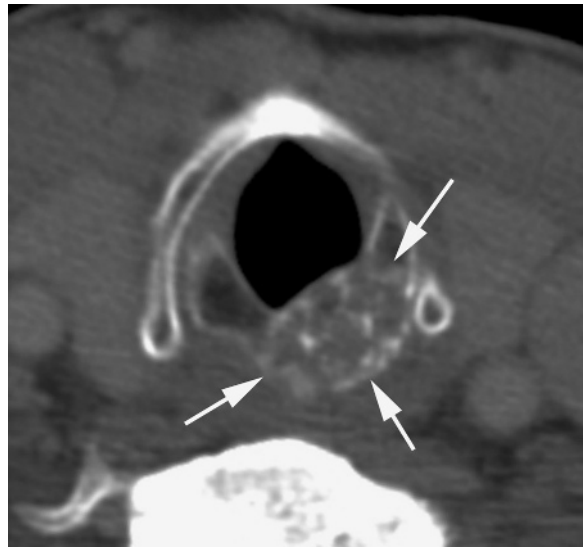

Fig. 4.32. Coincidentally discovered mass lesion in cricoid cartilage, on occasion of a MR study of the cervical spine. Clinical examination showed submucosal swelling underneath the left true vocal cord. Axial CT image (bone window) confirms an expansile lesion in the left posterolateral part of the cricoid arch; the lesion contains punctiform calcifications. The patient was treated by extended hemilaryngectomy; histological examination showed low-grade chondrosarcoma

Cystic-appearing chondrosarcomas have been reported, and may mimic a fluid-filled laryngocele when originating from the thyroid cartilage (De Foer et al. 1996).

Surgery is the only curative modality in laryngeal cartilaginous tumors. Low-grade chondrosarcomas may locally recur if incompletely resected, but have only limited risk of metastatic disease. Therefore, in all laryngeal cartilaginous tumors a conservative approach is followed whenever possible, directed towards voice-sparing partial laryngectomy. However, total laryngectomy may be the appropriate treatment in lesions involving larger portions of the cricoid cartilage, interfering with surgical reconstruction of a functional larynx, or when the diagnosis of high grade chondrosarcoma is established (Devaney et al. 1995; Wang et al. 1999).

4.6.2.2 Other Mesenchymal Malignancies

Other types of laryngeal sarcomas are extremely rare. These include osteosarcoma, malignant fibrous histiocytoma, fibrosarcoma, liposarcoma (Fig. 4.34), angiosarcoma, synovial sarcoma, rhabdomyosarcoma,

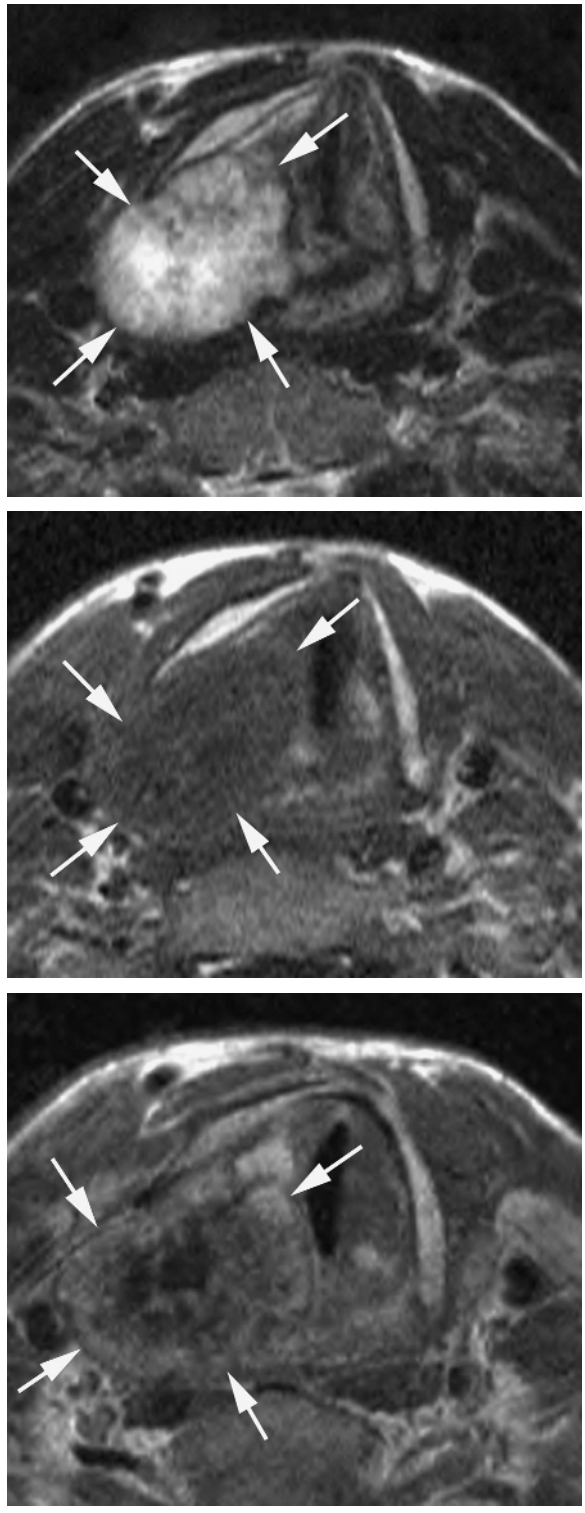

Fig. 4.33a–c. MR appearance of a large low-grade chondrosarcoma originating from the cricoid cartilage. **a** Axial T2-weighted spin echo image shows a lobulated mass (*arrows*) with high signal intensity. **b** Axial T1-weighted spin echo image. **c** Gadolinium-enhanced axial T1-weighted spin echo image shows irregular enhancement of the mass lesion

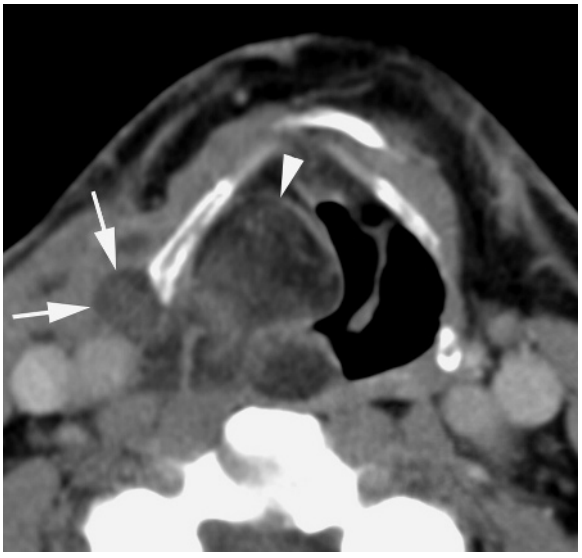

Fig. 4.34. Axial contrast-enhanced CT image. Soft tissue mass centered in the right paraglottic space (*arrowhead*), extending into the hypopharynx as well as extrapharyngeally (*arrows*). The tumor appears inhomogeneously, consisting of tissue with negative and positive density values. Liposarcoma

leiomyosarcoma and Kaposi's sarcoma. These tumors usually appear radiologically as a huge and infiltrating supraglottic mass lesion.

4.6.3 Hematopoietic Malignancies

4.6.3.1 Lymphoma

Non-Hodgkin lymphoma is a heterogeneous group of neoplasms originating from lymphocytes or their derivatives. Non-Hodgkin lymphoma has varying clinical presentations and different courses and prognoses (see Chap. 16).

Non-Hodgkin lymphoma is a disease of the middle-aged and elderly, with only few cases occurring before the age of 40. It represents about 5% of head and neck malignancies. About 11% of non-Hodgkin lymphomas present with lesions in this region, and about 50% of patients with head and neck disease have systemic disease.

Non-Hodgkin lymphoma can involve virtually any site in the extracranial head and neck. Nodal involvement is common, but in several studies extranodal spread is reported to occur more frequently than nodal enlargement. In the head and neck, two distinct extranodal sites are recognized: extranodal

lymphatic spread or involvement of Waldeyer's ring, and extranodal extralymphatic spread. Extranodal extralymphatic non-Hodgkin lymphoma occurs most commonly in the sinonasal cavities and orbits, but it may infiltrate any tissue of the head and neck, such as the deep spaces, skeletal structures, larynx (Fig. 4.35) and thyroid gland. Whenever an infiltrating mass is present in the extracranial head and neck region, lymphoma is a possible cause (Hermans et al. 1994).

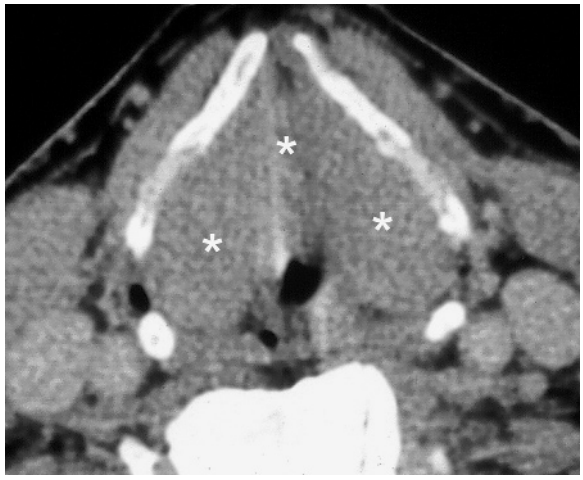

Fig. 4.35. Axial contrast-enhanced CT image shows diffuse soft tissue infiltration of the deep fatty laryngeal spaces (paraglottic and preepiglottic space), corresponding to non-Hodgkin lymphoma

4.6.3.2 Plasma Cell Neoplasms

Plasma cell neoplasms are relatively unusual malignancies of the head and neck region. Multiple myeloma, solitary plasmacytoma of bone, and extramedullary plasmacytoma are plasma cell neoplasms. Multiple myeloma is a fatal disease with a mean survival of 2–3 years. Progression to multiple myeloma is the most important prognostic factor for solitary plasmocytoma of bone and extramedullary plasmocytoma; extramedullary plasmocytoma has a better prognosis than solitary plasmacytoma of bone.

The incidence of laryngeal plasmacytoma with respect to all malignant tumors of the larynx is small (Maniglia and Xue 1983). Approximately 6%–18% of extramedullary plasmocytomas in the head and neck region occur in the larynx. The most common laryngeal sites are the epiglottis, followed by the vocal cords, false cords, ventricles, and subglottis. Laryngeal plasmacytomas are generally submucosal lesions, but can also be polypoid and may involve multiple contiguous sites of the larynx (Nofsinger et al. 1997).

The imaging findings of extramedullary plasmocytoma in the larynx are non-specific. The major role of imaging is to confirm the presence of a tumor mass and show the extent of the lesion.

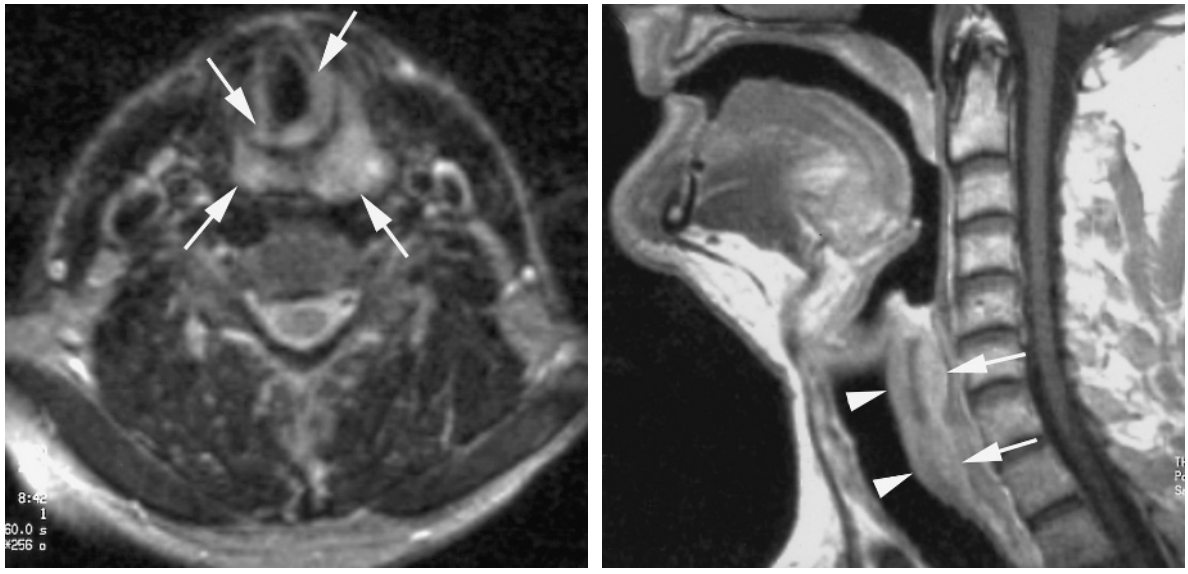

a b

Fig. 4.36a,b. Patient presenting with hoarseness; endoscopically, a submucosal mass lesion is suspected. The axial T2-weighted MR image (**a**) shows a hyperintense mass lesion (*arrows*) in the subglottis and distal hypopharynx. On the sagittal gadolinium-enhanced T1-weighted image (**b**), the mass is seen to infiltrate the larynx (*upper arrowhead*), proximal trachea (*lower arrowhead*), distal hypopharynx (*upper arrow*) and proximal oesophagus (*lower arrow*). [From Hermans (2000b), with permission]

4.6.3.3 Metastasis

The larynx is a rare site for metastasis. In most cases, the metastasis involves the supra- or subglottic submucosa, or the ossified laryngeal framework. The most common primary tumors are malignant melanoma, renal cell carcinoma, gastrointestinal cancer, breast cancer and pulmonary cancer (Batsakis et al. 1985; Nicolai et al. 1996). Laryngeal metastasis may be asymptomatic, or cause symptoms similar to primary laryngeal tumors (Fig. 4.37).

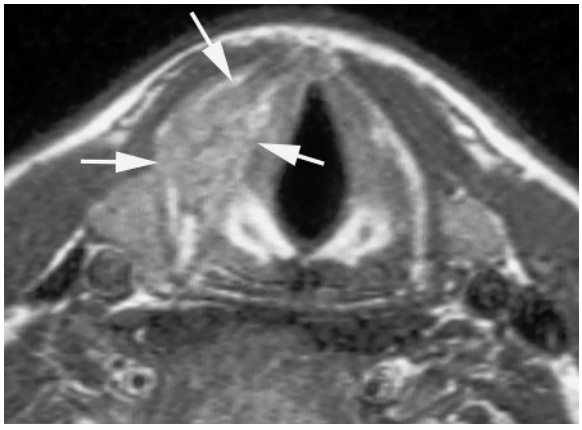

Fig. 4.37. Patient known with localized bladder cancer, treated by endoscopic resection. Because of pain during swallowing, an imaging study of the neck was performed. Gadolinium-enhanced axial T1-weighted spin echo image shows enhancing and expansile mass lesion (*arrows*) in the right thyroid cartilage wing. Resection was performed; pathologic examination revealed urothelial cancer, histologically similar to the previously removed bladder tumor: metastasis. The patient died a few months later due to widespread and rapidly progressive metastatic disease

References

Alexander FW (1963) Micropathology of radiation reaction in the larynx. Ann Otol Rhinol Laryngol 72:831–841

Anzai Y, Carroll WR, Quint DJ et al (1996) Recurrence of head and neck cancer after surgery or irradiation: prospective comparison of 2-deoxy-2-(F-18)fluoro-D-glucose PET and MR imaging diagnoses. Radiology 200:135–141

Archer CR, Yeager VL, Herbold DR (1984) Improved diagnostic accuracy in laryngeal cancer using a new classification based on computed tomography. Cancer 53:44–57

Barbera L, Groome PA, Mackillop WJ, Schuze K, O'Sullivan B, Irish JC, Warde PR, Schneider KM, Mackenzie RG, Hodson DI, Hammond JA, Gulavita SPP, Eapen LJ, Dixon PF, Bissett RJ (2001) The role of computed tomography in the T classification of laryngeal carcinoma. Cancer 91:394–407

Batsakis JG, Luna MA, Byers RM (1985) Metastases to the larynx. Head Neck Surg 7:458–460

Becker M, Zbären P, Laeng H, Stoupis C, Porcellini B, Vock P (1995) Neoplastic invasion of the laryngeal cartilage: comparison of MR imaging and CT with histopathologic correlation. Radiology 194:661–669

Becker M, Zbären P, Delavelle J et al (1997a) Neoplastic invasion of the laryngeal cartilage: reassessment of criteria for diagnosis at CT. Radiology 203:521

Becker M, Schroth G, Zbären P et al (1997b) Long-term changes induced by high-dose irradiation of the head and neck region: imaging findings. Radiographics 17:5–26

Becker M, Moulin G, Kurt AM, Zbaren P, Dulgerov P, Marchal F, Zanaret P, Lehmann W, Rufenacht DA, Terrier F (1998) Atypical squamous cell carcinoma of the larynx and hypopharynx: radiologic features and pathologic correlation. Eur Radiol 8:1541–1551

Bousson V, Marsot-Dupuch K, Lashiver X et al (1995) Nécrose post-radique du cartilage cricoïde: un cas inhabituel. J Radiol 76:517–520

Breiman RS, Beck JW, Korobkin M, Glenny R, Akwari OE, Heaston DK, Moore AV, Ram PC (1982) Volume determinations using computed tomography. AJR Am J Roentgenology 138:329–333

Castelijns JA, Golding RP, van Schaik C, Valk J, Snow GB (1990) MR findings of laryngeal cartilage invasion by laryngeal cancer: value in predicting outcome of radiation therapy. Radiology 174:669–673

Castelijns JA, van den Brekel MWM, Smit EMT, Tobi H, van Wagtendonk FW, Golding RP, Venema HW, van Schaik C, Snow GB (1995) Predictive value of MR imaging-dependent and non-MR imaging dependent parameters for recurrence of laryngeal cancer after radiation therapy. Radiology 196:735–739

Castelijns JA, Becker M, Hermans R (1996a) The impact of cartilage invasion on treatment and prognosis of laryngeal cancer. Eur Radiol 6:156–169

Castelijns JA, van den Brekel MWM, Tobi H, Smit EMT, Golding RP, van Schaik C, Snow GB (1996b) Laryngeal carcinoma after radiation therapy: correlation of abnormal MR imaging signal pattern in laryngeal cartilage with the risk of recurrence. Radiology 198:151–155

Charlin B, Brazeau-Lamontagne L, Guerrier B, Leduc C (1989) Assessment of laryngeal cancer: CT scan versus endoscopy. J Otolaryngol 18:283–288

Cooney TR, Poulsen MG (1999) Is routine follow-up useful after combined-modality therapy for advanced head and neck cancer? Arch Otolaryngol Head Neck Surg 125:379–382

Dadas B, Uslu B, Cakir B, Ozdogan HC, Calis AB, Turgut S (2001) Intraoperative management of the thyroid gland in laryngeal cancer surgery. J Otolaryngol 30:179–183

De Foer B, Hermans R, Van der Goten A, Delaere PR, Baert AL (1996) Imaging features in 35 cases of submucosal laryngeal mass lesions. Eur Radiol 6:913–919

de Visscher AVM, Manni JJ (1994) Routine long-term follow-up in patients treated with curative intent for squamous cell carcinoma of the larynx, pharynx and oral cavity. Arch Otolaryngol Head Neck Surg 120:934–939

De Vuysere, Hermans R, Delaere P et al (1999) CT findings in laryngeal chondroradionecrosis. J Belge Radiol 82:16–18

Delaere P, Vander Poorten V, Vanclooster C, Goeleven A, Hermans R (2000) Results of larynx preservation surgery for

advanced laryngeal cancer through tracheal autotransplantation. Arch Otolaryngol Head Neck Surg 126:1207–1215

Delaere PR, Hermans R (2003) Tracheal autotransplantation as a new and reliable technique for the functional treatment of advanced laryngeal cancer. Laryngoscope 113:1244–1251

DeSanto LW (1984) T3 glottic cancer: options and consequences of the options. Laryngoscope 94:1311–1315

Devaney KO, Ferlito A, Silver CE (1995) Cartilaginous tumors of the larynx. Ann Otol Rhinol Laryngol 104:251–255

Ferlito A, Rinaldo A, Mannara GM (1998) Is primary radiotherapy an appropriate option for the treatment of verrucous carcinoma of the head and neck? J Laryngol Otol 112:132–139

Fletcher GH, Hamberger AD (1974) Causes of failure in irradiation of squamous-cell carcinoma of the supraglottic larynx. Radiology 111:697–700

Fletcher GH, Lindberg RD, Hamberger A, Horiot JC (1975) Reasons for irradiation failure in squamous cell carcinoma of the larynx. Laryngoscope 85:987–1003

Freeman DE, Mancuso AA, Parsons JT, Mendenhall WM, Million RR (1990) Irradiation alone for supraglottic larynx carcinoma: can CT findings predict treatment results? Int J Radiation Oncology Biol Phys 19:485–490

Gavilan J (2000) Cancer of the glottis. In: Ferlito A (ed) Diseases of the larynx. Arnold, London, p 615

Gilbert RW, Birt D, Shulman H, Freeman J, Jenkin D, MacKenzie R, Smith C (1987) Correlation of tumor volume with local control in laryngeal carcinoma treated by radiotherapy. Ann Otol Rhinol Laryngol 97:514–518

Hermans R, Horvath M, De Schrijver T, Lemahieu SF, Baert AL (1994) Extranodal non-Hodgkin lymphoma of the head and neck. J Belge Radiol 77:72–77

Hermans R, Pameijer FA, Mancuso AA et al (1998) Computed tomography findings in chondroradionecrosis of the larynx. Am J Neuroradiol 19:711–718

Hermans R, Van den Bogaert W, Rijnders A, Doornaert P, Baert AL (1999a) Predicting the local outcome of glottic cancer treated by definitive radiation therapy: value of computed tomography determined tumor parameters. Radiother Oncol 50:39–46

Hermans R, Van den Bogaert W, Rijnders A, Baert AL (1999b) Value of computed tomography determined tumor parameters as outcome predictor of supraglottic cancer treated by definitive radiation therapy. Int J Radiat Oncol Biol Phys 44:755–765

Hermans R, Pameijer FA, Mancuso AA et al (2000a) Laryngeal or hypopharyngeal squamous cell carcinoma: can follow-up CT after definitive radiotherapy be used to detect local failure earlier than clinical examination alone? Radiology 214:683–687

Hermans R (2000b) Head and Neck Imaging. In: Pettersson H, Allison D (eds.). The NICER Institute, Oslo, part VI

Hermans R, Meijerink M, Van den Bogaert W, Rijnders A, Weltens C, Lambin P (2003) Tumor perfusion rate determined noninvasively by dynamic computed tomography predicts outcome in head-and-neck cancer after radiotherapy. Int J Radiat Oncol Biol Phys 57:1351–1356

Hermans R (2004) Post-treatment imaging of head and neck cancer. Cancer Imaging 4:1–10. DOI:10.1102/1470–7330.2004.0007

Hinerman RW, Mendenhall WM, Amdur RJ, Stringer SP, Villaret DB, Robbins KT (2002) Carcinoma of the supraglottic larynx: treatment results with radiotherapy alone or with planned neck dissection. Head Neck 24:456–467

Isaacs JH, Mancuso AA, Mendenhall WM, Parsons JT (1988) Deep spread patterns in CT staging of T2–4 squamous cell laryngeal carcinoma. Otolaryngol Head Neck Surg 99:455–464

Johnson CR, Thames HD, Huang DT, Schmidt-Ullrich RK (1995) The tumor volume and clonogen number relationship: tumor control predictions based upon tumor volume estimates derived from computed tomography. Int J Radiat Oncol Biol Phys 33:281–287

Kaanders JH, Bussink J, van der Kogel AJ (2002) ARCON: a novel biology-based approach in radiotherapy. Lancet Oncol 3:728–737

Kallmes DF, Phillips CD (1997) The normal anterior commissure of the glottis. AJR Am J Roentgenol 168:1317–1379

Katsantonis GP, Archer CR, Rosenblum BN, Yeager VL, Friedman WH (1986) The degree to which accuracy of preoperative staging of laryngeal carcinoma has been enhanced by computed tomography. Otolaryngol Head Neck Surg 95:52–62

Keane TJ, Cummings BJ, O' Sullivan B et al (1993) A randomized trial of radiation therapy compared to split course radiation therapy combined with Mitomycin C and 5 Fluorouracil as initial treatment for advanced laryngeal and hypopharyngeal squamous carcinoma. Int J Radiat Oncol Biol Phys 25:613–618

Keene M, Harwood AR, Bryce DP et al (1982) Histopathological study of radionecrosis in laryngeal carcinoma. Laryngoscope 92:173–180

Kraas JR, Underhill TE, D'Agostino RB Jr, Williams DW 3rd, Cox JA, Greven KM (2001) Quantitative analysis from CT is prognostic for local control of supraglottic carcinoma. Head Neck 23:1031–1036

Kurita S, Hirano M, Matsuoka H, Tateishi M, Sato K (1985) A histopathological study of carcinoma of the larynx. Auris Nasus Larynx 12[Suppl 2]:S172–177

Lee NK, Goepfert H, Wendt CD (1990) Supraglottic laryngectomy for intermediate-stage cancer: U.T. M.D. Anderson Cancer Center experience with combined therapy. Laryngoscope 100:831–836

Lee WR, Mancuso AA, Saleh EM, Mendenhall WM, Parsons JT, Million RR (1993) Can pretreatment computed tomography findings predict local control in T3 squamous cell carcinoma of the glottic larynx treated with radiotherapy alone? Int J Radiat Oncol Biol Phys 25:683–687

Ljumanovic R, Langendijk JA, Schenk B et al (2004) Supraglottic carcinoma treated with curative radiation therapy: identification of prognostic groups with MR imaging. Radiology 232:440–448

Lloyd GAS, Michaels L, Phelps PD (1981) The demonstration of cartilaginous involvement in laryngeal carcinoma by computerized tomography. Clin Otolaryngol 6:171–177

Lo SM, Venkatesan V, Matthews TW, Rogers J (1998) Tumor volume: implications in T2/T3 glottic/supraglottic squamous cell carcinoma. J Otolaryngol 27:247–251

Mancuso AA, Harnsberger HR, Dillon WP (1989) Workbook for MRI and CT of the head and neck, 2nd edn. William & Wilkins, Baltimore, p. 183

Mancuso AA, Mukherji SK, Schmalfuss I, Mendenhall W, Parsons J, Pameijer F, Hermans R, Kubilis P (1999) Preradiotherapy computed tomography as a predictor of local control in supraglottic carcinoma. J Clin Oncol 17:631–637

Maniglia A, Xue JW (1983) Plasmacytoma of the larynx. Laryngoscope 93:903–906
Maroldi R, Battaglia G, Nicolai P, Maculotti P, Cappiello J, Cabassa P, Farina D, Chiesa A (1997) CT appearance of the larynx after conservative and radical surgery for carcinomas. Eur Radiol 7:418–431
Maroldi R, Farina D, Battaglia G, Palvarini L, Maculotti P (2001) Imaging after laryngeal surgery. In: Hermans R (ed) Imaging of the larynx. Springer, Berlin Heidelberg New York, pp 124–125
McGuirt WF, Greven KM, Keyes JW Jr et al (1998) Laryngeal radionecrosis versus recurrent cancer: a clinical approach. Ann Otol Rhinol Laryngol 107:293–296
Mendenhall WM, Parsons JT, Stringer SP, Cassisi NJ, Million RR (1992) Stage T3 squamous cell carcinoma of the glottic larynx: a comparison of laryngectomy and irradiation. Int J Radiat Oncol Biol Phys 23:725–732
Mendenhall WM, Parsons JT, Mancuso AA, Stringer SP, Cassisi NJ (1996) Radiotherapy for squamous cell carcinoma of the supraglottic larynx: an alternative to surgery. Head Neck 18:24–35
Mendenhall WM, Parsons JT, Mancuso AA, Pameijer FJ, Stringer SP, Cassisi NJ (1997) Definitive radiotherapy for T3 squamous cell carcinoma of the glottic larynx. J Clin Oncol 15:2394–2402
Mendenhall WM, Morris CG, Amdur RJ, Hinerman RW, Mancuso AA (2003) Parameters that predict local control after definitive radiotherapy for squamous cell carcinoma of the head and neck. Head Neck 25:535–542
Mendenhall WM, Werning JW, Hinerman RW, Amdur RJ, Villaret DB (2004) Management of T1–T2 glottic carcinomas. Cancer 100:1786–1792
Milas L, Mason KA, Liao Z, Ang KK (2003) Chemoradiotherapy: emerging treatment improvement strategies. Head Neck 25:152–167
Million RR (1989) The myth regarding bone or cartilage involvement by cancer and the likelihood of cure by radiotherapy. Head Neck 11:30–40
Million RR (1992) The larynx...so to speak: everything I wanted to know about laryngeal cancer I learned in the last 32 years. Int J Radiat Oncol Biol Phys 23:691–704
Mukherji SK, Mancuso AA, Kotzur IM et al (1994a) Radiologic appearance of the irradiated larynx. Part I. Expected changes. Radiology 193:141–148
Mukherji SK, Mancuso AA, Kotzur IM et al (1994b) Radiologic appearance of the irradiated larynx. Part II. Primary site response. Radiology 193:149–154
Mukherji SK, Mancuso AA, Mendenhall W, Kotzur IL, Kubilis P (1995) Can pretreatment CT predict local control of T2 glottic carcinomas treated with radiation therapy alone? AJNR Am J Neuroradiol 16:655–662
Mukherji SK, O'Brien SM, Gerstle RJ, Weissler M, Shockley W, Stone JA, Castillo M (2000) The ability of tumor volume to predict local control in surgically treated squamous cell carcinoma of the supraglottic larynx. Head Neck 22:282–287
Mukherji SK, Wolf GT (2003) Evaluation of head and neck squamous cell carcinoma after treatment (editorial). AJNR Am J Neuroradiol 24:1743–1746
Murakami R, Nishimura R, Baba Y, Furusawa M, Ogata N, Yumoto E, Yamashita Y (2005) Prognostic factors of glottic carcinomas treated with radiation therapy: value of the adjacent sign on radiological examinations in the sixth edition of the UICC TNM staging system. Int J Radiat Oncol Biol Phys 61:471–475
Nationale werkgroep hoofd-halstumoren (2000) Richtlijn Larynxcarcinoom. Kwaliteitsinstituut voor de Gezondheidszorg, Utrecht
Nicolai P, Puxeddu R, Cappiello J, Peretti G, Battocchio S, Facchetti F, Antonelli AR (1996) Metastatic neoplasms to the larynx: report of three cases. Laryngoscope 106:851–855
Nofsinger YC, Mirza N, Rowan PT, Lanza D, Weinstein G (1997) Head and neck manifestations of plasma cell neoplasms. Laryngoscope 107:741–746
Nömayr A, Lell M, Sweeney S et al (2001) MRI appearance of radiation-induced changes of normal cervical tissues. Eur Radiol 11:1807–1817
O'Brien P (1996) Tumor recurrence or treatment sequelae following radiotherapy for larynx cancer. J Surg Oncol 63:130–135
Op de beeck K, Hermans R, Delaere PR, Van den Bogaert W, Marchal G (2001) Laryngeal squamous cell carcinoma presenting as a prelaryngeal neck abscess: report of two cases. Eur Radiol 11:2479–2483
Overgaard J, Hansen HS, Jørgensen K, Hjelm-Hansen M (1986) Primary radiotherapy of larynx and pharynx carcinoma – an analysis of some factors influencing local control and survival. Int J Radiat Oncol Biol Phys 12:515–521
Overgaard J, Horsman MR (1996) Modification of hypoxia-induced radioresistance in tumors by the use of oxygen and sensitizers. Semin Radiat Oncol 6:10–21
Pameijer FA, Mancuso AA, Mendenhall WM, Parsons JT, Kubilis MS (1997) Can pretreatment computed tomography predict local control in T3 squamous cell carcinoma of the glottic larynx treated with definitive radiotherapy? Int J Radiat Oncol Biol Phys 37:1011–1021
Pameijer FA, Hermans R, Mancuso AA et al (1999) Pre- and post-radiotherapy computed tomography in laryngeal cancer: imaging-based prediction of local failure. Int J Radiat Oncol Biol Phys 45:359–366
Parsons JT, Mendenhall WM, Stringer SP, Cassisi NJ (1998) T4 laryngeal carcinoma: radiotherapy alone with surgery reserved for salvage. Int J Radiation Oncology Biol Phys 40:549–552
Piccirillo JF, Lacy PD (2000) Classification and staging of laryngeal cancer. In: Ferlito A (ed) Diseases of the larynx. Arnold, London, pp 563–564, 574
Pillsbury HR, Kirchner JA (1979) Clinical vs histopathologic staging in laryngeal cancer. Arch Otolaryngol 105:157–159
Rijpkema M, Kaanders JH, Joosten FB, van der Kogel AJ, Heerschap A (2001) Method for quantitative mapping of dynamic MRI contrast agent uptake in human tumors. J Magn Reson Imaging 14:457–463
Rijpkema M, Kaanders JH, Joosten FB, van der Kogel AJ, Heerschap A (2002) Effects of breathing a hyperoxic hypercapnic gas mixture on blood oxygenation and vascularity of head-and-neck tumors as measured by magnetic resonance imaging. Int J Radiat Oncol Biol Phys 53:1185–1191
Robbins KT, Davidson W, Peters LJ, Goepfert H (1987) Conservation surgery for T2 and T3 carcinomas of the supraglottic larynx. Arch Otolaryngol Head Neck Surg 114:421–426
Sato K, Kurita S, Hirano M (1993) Location of the preepiglottic space and its relationship to the paraglottic space. Ann Otol Rhinol Laryngol 102:930–934
Schwartz DL, Barker J, Chansky K et al (2003) Postradio-

therapy surveillance practice for head and neck squamous cell carcinoma – too much for too little? Head Neck 25:990–990

Shah JP, Karnell LH, Hoffman HT, Ariyan S, Brown GS, Fee WE, Glass AG, Goepfert H, Ossoff RH, Fremgen A (1997) Patterns of care for cancer of the larynx in the United States. Arch Otolaryngol Head Neck Surg 123:475–483

Silverman PM (1985) Medullary space involvement in laryngeal carcinoma. Arch Otolaryngol 111:541–542

Steiniger JR, Parnes SM, Gardner GM (1997) Morbidity of combined therapy for the treatment of supraglottic carcinoma: supraglottic laryngectomy and radiotherapy. Ann Otol Rhinol Laryngol 106:151–158

Sulfaro S, Barzan L, Querin F, Lutman M, Caruso G, Comoretto R, Volpe R, Carbone A (1989) T staging of the laryngohypopharyngeal carcinoma. Arch Otolaryngol Head Neck Surg 115:613–620

Tart RP, Mukherji SK, Lee WR, Mancuso AA (1994) Value of laryngeal cartilage sclerosis as a predictor of outcome in patients with stage T3 glottic cancer treated with radiation therapy. Radiology 192:567–570

Thoeny HC, Delaere PR, Hermans R (2005) Correlation of local outcome after partial laryngectomy with cartilage abnormalities on CT. AJNR Am J Neuroradiol 26:674–678

UICC, International Union Against Cancer (2002) TNM classification of malignant tumors, 6th edn. Wiley-Liss, New York, p 36

Van den Bogaert W, Ostyn F, Van der Schueren E (1983) The primary treatment of advanced vocal cord cancer: laryngectomy or radiotherapy? Int J Radiation Oncology Biol Phys 9:329–334

Van den Bogaert W, van der Schueren E, Horiot JC, De Vilhena M, Schraub S, Svoboda V, Arcangeli G, de Pauw M, van Glabbeke M (1995) The EORTC randomized trial on three fractions per day and misonidazole in advanced head and neck cancer: prognostic factors. Radiother Oncol 35:100–106

Wang SJ, Borges A, Lufkin RB et al (1999) Chondroid tumors of the larynx: computed tomography findings. Am J Otolaryngol 20:379–382

Weems DH, Mendenhall WM, Parsons JT, Cassisi NJ, Million RR (1987) Squamous cell carcinoma of the supraglottic larynx treated with surgery and/or radiation therapy. Int J Radiati Oncol Biol Phys 13:1483–1487

Yeager VL, Lawson C, Archer CR (1982) Ossification of the laryngeal cartilages as it relates to computed tomography. Invest Radiol 17:11–19

Zbären P, Becker M, Laeng H (1996) Pretherapeutic staging of laryngeal cancer: clinical findings, computed tomography and magnetic resonance imaging versus histopathology. Cancer 77:1263–1273

5 Neoplasms of the Hypopharynx and Proximal Esophagus

Ilona M. Schmalfuss

CONTENTS

5.1 Introduction

Cancers of the hypopharynx and proximal esophagus represent one of the most difficult diseases for head and neck surgeons to manage as they pose a significant diagnostic challenge. The trend of these cancers to grow in submucosal fashion, combined with the complex functions of the hypopharynx, esophagus and adjacent larynx, requires detailed mapping of the tumor boundaries to yield the most optimal treatment selection, determine the extent of possible surgical resection and subsequent reconstructive surgery. Consequently, cross-sectional imaging plays a critical role in evaluation of hypopharyngeal and esophageal cancers.

Computer tomography (CT) is a well-established and in most institutions preferred method for the evaluation of the hypopharynx and the cervical esophagus. The short acquisition time is the main advantage of CT over magnetic resonance (MR) imaging (Wenig et al. 1995). Up to 16% of MR studies focusing on hypopharynx and cervical esophagus have been reported to be non-diagnostic secondary to claustrophobia or motion artifacts (Becker 1998). MR has also shown to be inadequate in evaluation of patients with recurrent tumor or following radiation therapy (Castelijns et al. 1988). MR imaging is however superior in the evaluation of the esophageal verge and cervical esophagus as a result of better soft tissue delineation and lack of obscuration of these structures by beam-hardening artifacts caused by the shoulders as seen with CT. Multi-planar capabilities of MR play a minor advantage over CT since the introduction of multi-slice helical CT scanners and the wide use of interactive picture archive computer systems.

5.2 Anatomy

5.2.1 Descriptive Anatomy

The hypopharynx is the portion of the pharynx that extends from the oropharynx to the esophageal verge. It continues inferiorly as the cervical esophagus to the level of the thoracic inlet. The anterior boundary of the hypopharynx and the cervical esophagus is formed by the larynx and the trachea, respectively. The retropharyngeal space forms the posterior boundary. There is no clear anatomical barrier between the hypopharynx and the oropharynx, nor between the hypopharynx and the cervical esophagus.

I. M. Schmalfuss, MD
Department of Radiology, Malcolm Randall VA Medical Center and University of Florida College of Medicine, Gainesville, Florida, USA

The hypopharynx is divided into three distinct regions: pyriform sinus, post-cricoid region and posterior hypopharyngeal wall. The pyriform sinus (one on each side) is formed by the anterior, medial and lateral walls and resembles an inverted pyramid. The base of the pyramid at the level of the pharyngoepiglottic folds constitutes the entrance of the pyriform sinus. The pyriform sinus apex, located at the inferior margin of the cricoid cartilage, represents the tip of the inverted pyramid. The aryepiglottic folds separate the pyriform sinus posteriorly from the larynx anteromedially. More inferiorly, the pyriform sinus abuts the posterior margin of the paraglottic space. This close anatomical proximity explains the frequently seen involvement of the larynx in patients diagnosed with pyriform sinus cancer. The thyrohyoid membrane forms the boundary between the pyriform sinus medially and the lateral neck compartment laterally. The superior laryngeal neurovascular bundle courses through the thyrohyoid membrane. The sensory axons of the superior laryngeal nerve continue superiorly to join the Arnold nerve within the jugular foramen, giving rise to referred otalgia seen in patients with pyriform sinus cancer. In addition, the superior laryngeal neurovascular bundle causes a "weak" point within the thyrohyoid membrane facilitating tumor spread out of the visceral compartment into the extrapharyngeal soft tissues. The postcricoid region represents the anterior wall of the hypopharynx extending from the posterior surface of the arytenoid cartilage to the esophageal verge. The posterior hypopharyngeal wall forms the posterior boundary of the hypopharynx stretching from the aryepiglottic folds superiorly to the esophageal verge inferiorly. There is no defined boundary of the hypopharyngeal wall towards the oropharynx superiorly and towards the esophagus inferiorly. The retropharyngeal space separates the vertebral and paravertebral structures from the posterior hypopharyngeal wall and allows the pharynx to move freely during swallowing.

The wall of the hypopharynx consists of four layers: the outer fascial layer originating from the buccopharyngeal fascia, the muscular layer, the fibrous layer arising from the pharyngeal aponeurosis and the mucosal lining of stratified squamous epithelium over loose stroma that can be identified on cross-sectional images as a thin fat plane (see Sect. 5.2.2). The muscular layer is formed by the posterior cricoarytenoid muscle anteriorly and the middle or inferior constrictor muscles posteriorly. The inferior constrictor muscle continues inferiorly to blend with the cricopharyngeus muscle, forming the upper esophageal sphincter at the esophageal verge. The esophageal verge assumes a round to oval shape, slightly more inferiorly establishing the cervical esophagus. At the cervical esophagus level, the muscular layer consists of inner circular and outer longitudinal muscle fibers that is protected on the inside by nonkeratinizing squamous epithelium over loose areolar tissue. Externally, the muscular layer is covered by a fascial sheath. The cervical esophagus is located posterior to the trachea where it often causes an impression upon the posterior fibrous wall of the trachea. A thin layer of fatty tissue separates the fibrous wall of the trachea from the esophagus and may be referred to as the "common wall". Laterally, the cervical esophagus abuts the tracheoesophageal (TE) groove. It houses the recurrent laryngeal nerve and the TE groove lymph nodes as part of the group VI nodal group. Occasionally, the parathyroid and/or the thyroid gland extend into the TE groove.

5.2.2 Imaging Anatomy

On cross-sectional images, all three portions of the hypopharynx are seen posterior to the arytenoid and cricoid cartilages, while only the pyriform sinuses and the posterior pharyngeal wall constitute the hypopharynx above the arytenoid cartilage level. The hypopharyngeal cross-sectional anatomy posterior to the cricoid cartilage is therefore very complex: the post-cricoid region lies directly posterior to the cricoid cartilage, the inferior portion of the pyriform sinuses laterally on each side and the posterior hypopharyngeal wall posteriorly. The fact that the hypopharynx is typically collapsed during cross-sectional imaging, bringing the mucosa of the postcricoid region and of the posterior hypopharyngeal wall in direct contact to form a single mucosal layer, complicates the already difficult hypopharyngeal anatomy at that level. Therefore, knowledge of the normal appearance and of normative data is essential for detection of abnormalities (Schmalfuss et al. 2000).

The anteroposterior (AP) dimensions of the postcricoid portion of the hypopharynx show little variations from the upper to lower margin of the cricoid cartilage. However, an AP diameter over 10 mm should be considered abnormal (Schmalfuss et al. 2000). The post-cricoid area is usually slightly thinner than the posterior pharyngeal wall with 2.5 and 3.5 mm on average, respectively. In contrast to the AP measurements, the transverse dimension of the postcricoid portion of the hypopharynx tapers from

the upper to the lower margin of the cricoid cartilage. Therefore, lack of normal tapering should raise the suspicion for an underlying abnormality and initiate a search for additional abnormal findings such as obscuration of the intramural or surrounding fat planes (see below). The esophageal diameter depends upon the amount of intraluminal air and is therefore not a useful indicator for underlying pathology. The thickness of the esophageal wall, however, is relatively constant with less than 5 mm and consequently a key marker for detection of an underlying lesion. In addition, the internal attenuation of the esophageal wall is helpful as it should be homogeneously isointense to the surrounding musculature on CT and T2-weighted images (Fig. 5.1) and show no enhancement following contrast administration (Schmalfuss et al. 2000; Quint et al. 1985).

The assessment of intramural and surrounding fat planes is critical in the work-up of patients with suspected hypopharyngeal or upper esophageal abnormality as obliteration of these fat planes might be the only sign of an underlying cancer (Fig. 5.2). Overall, the fat planes are more frequently seen with CT than with MR. The gradient-echo T2-weighted images are superior to the T1- or T2-weighted images in the visibility of the intramural fat planes while there are no preferences between the various MR sequences for the surrounding fat planes (Schmalfuss et al. 2000).

In the postcricoid portion of the hypopharynx, the visibility of the intramural fat planes decreases from the upper to the lower cricoid cartilage level with 85%–30%, respectively. The intramural fat planes are usually symmetric in appearance at the upper cricoid cartilage level but show marked asymmetry at the mid and lower cricoid cartilage levels in approximately one third of the patients (Fig. 5.3). Typically, the left intramural fat plane is more obvious which might be due to the commonly seen left-sided location of the esophagus (Schmalfuss et al. 2000).

The surrounding fat planes lateral to the postcricoid portion of the hypopharynx and cervical esophagus are most constantly seen. The left surrounding fat plane is markedly more commonly visible than the right while the posterior fat plane is least frequently appreciated (Fig. 5.4a). In addition, the visibility of the surrounding fat planes varies by location with best visibility around the esophageal verge (Fig. 5.4b). The fat planes of the TE groove contain a subset of group VI lymph nodes. These lymph nodes are considered by several authors as normal if homogenous in attenuation and less than 1 cm in largest diameter (Schmalfuss et al. 2000; Glazer et al. 1985). However, normal lymph nodes are infrequently seen at this level. Therefore, the classically used cut-off value of 1 cm may not be applicable to these nodes; small but round appearing TE nodes, especially when enhancing inhomogeneously, should

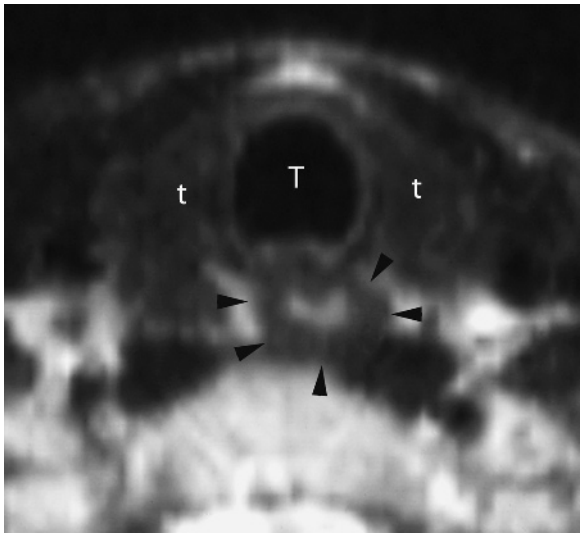

Fig. 5.1. Axial T2-weighted image through the cervical esophagus demonstrating the normal homogenous low attenuation of the muscular wall of the esophagus (*arrowheads*) in comparison to the hyperintense mucosa centrally and the paraesophageal fat planes laterally. *T*, trachea, *t*, thyroid

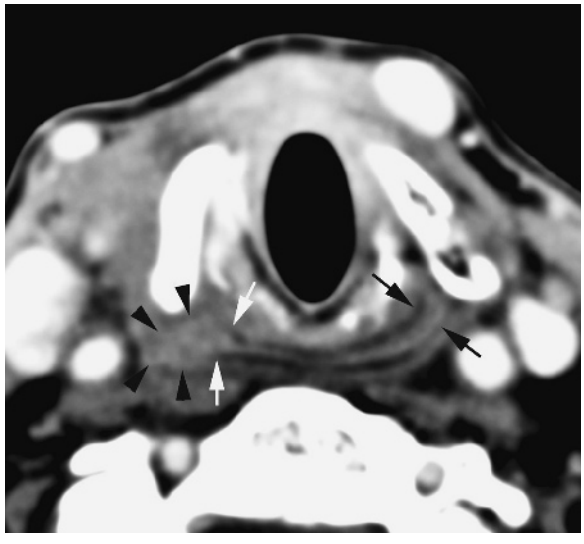

Fig. 5.2. Axial contrast-enhanced CT image through the postcricoid region shows normal submucosal fat planes on the left (*black arrows*) and abrupt cut-off of the submucosal fat planes on the right (*white arrows*) caused by a small pyriform sinus tumor on the right (*arrowheads*)

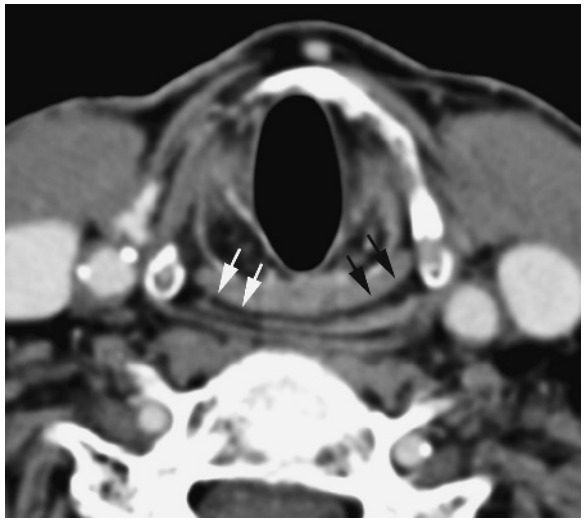

Fig. 5.3. Axial contrast-enhanced CT image through the mid cricoid level demonstrate asymmetric appearance of the submucosal fat planes. As in this patient, the submucosal fat planes are usually more prominent on the left (*black arrows*) than on the right (*white arrows*) which might be related to the preferred left-sided location of the cervical esophagus (not demonstrated)

be considered suspicious in the presence of a hypopharyngeal or esophageal cancer.

The common wall of the trachea and esophagus is formed by the fibrous wall of the posterior trachea, anterior esophageal wall and adipose tissue in between (Figs. 5.5 and 5.6). The common wall is more frequently seen with MR than with CT. Contrast enhanced T1-weighted images are superior to other MR sequences (Fig. 5.6). In addition, its different components can be most distinctly separated at the esophageal verge with a gradual decline more inferiorly. Evaluation of the common wall of the trachea and the esophagus is an essential step in the surgical treatment planning process of patients with cancer arising from the esophagus, trachea or adjacent anatomical structures such as the thyroid gland.

5.3 Pathology

The hypopharynx and cervical esophagus are in the vast majority involved by squamous cell malignancies, followed by infiltration by surrounding tumors such as thyroid gland and bronchogenic carcinomas. Other types of tumors are very rare.

5.3.1 Non-squamous Cell Malignancies

Non-squamous cell malignancies of the hypopharynx and cervical esophagus are extremely rare and include various sarcomas, lymphoma and malignant minor salivary gland tumors (Becker 1998; Matsuki et al. 1999; De Campora et al. 1987; Tom et al. 1981; Miyazaki et al. 2004; Mouret 1999; Artico et al. 2004; Kitamoto 2003).

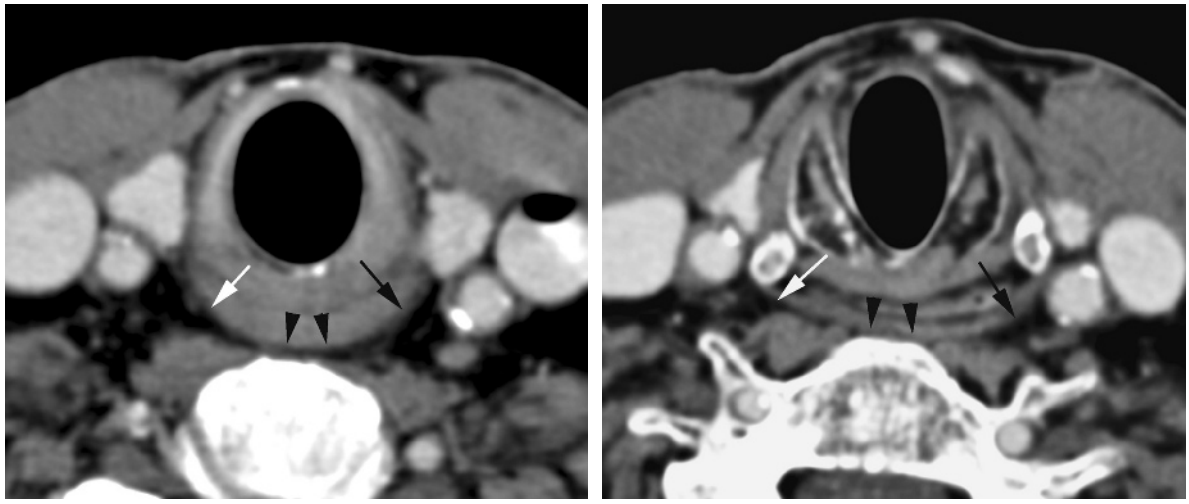

a b

Fig. 5.4a,b. Axial contrast-enhanced CT images through the mid (**a**) and lower cricoid cartilage (**b**) show the typically seen variable size of the different surrounding fat planes. The left surrounding fat plane is usually the largest (*black arrows*) and the posterior fat plane is the least appreciable (*arrowheads*). At the esophageal verge (**b**), the surrounding fat planes are usually much easier to see than at adjacent levels. *White arrow*, right-sided surrounding fat plane

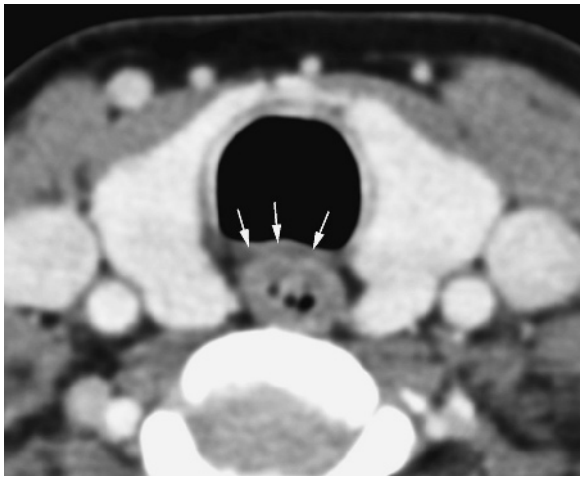

Fig. 5.5. Axial contrast-enhanced CT image demonstrates the normal appearance of the common wall of the trachea and esophagus with a thin layer of fat (*arrows*) visualized between the trachea anteriorly and the esophagus posteriorly

Lipo- and synovial sarcomas are the most commonly reported types of sarcomas involving the hypopharynx and cervical esophagus (Mouret 1999; Artico et al. 2004). Hypopharyngeal liposarcoma most commonly involves older males. Patients typically present with local symptoms and rarely with nodal or distant metastasis. The prognosis does not seem to be affected by the tumor size but rather by the grade of the tumor. Low grade liposarcomas are less locally aggressive but still show a high local recurrence rate and rarely metastasize. In contrast, high grade tumors show a much more aggressive growth pattern and metastasize frequently. The imaging findings vary dependent upon the grade and differentiation of the tumor, with well-differentiated low grade tumors almost resembling benign lipoma, while high grade undifferentiated tumors may be indistinguishable to squamous cell malignancies. Synovial hypopharyngeal sarcoma is the second most common sarcoma type involving the hypopharynx. Only 3% of the synovial sarcomas involve the head and neck region with the hypopharynx being most commonly involved (Rangheard et al. 2001). Typically, they affect young adults and adolescents. Although synovial sarcomas are often seen adjacent to joints they do not originate from synovial tissue but rather from pluripotential mesenchymal cells located near articular surfaces, tendons, tendon sheaths, juxta-articular membranes and facial aponeuroses. They are characterized by a reciprocal translocation between chromosomes X and 18 and are divided into a monophasic and biphasic form (Artico et al. 2004; Rangheard et al. 2001). The monophasic form is more common and is constituted of one cell type (epithelial or spindle cells), whereas the biphasic form is very rare and is composed of epithelial and spindle cells. As liposarcomas, they usually present with local symptoms and rarely with nodal or distant metastatic disease. On cross-sectional imaging studies, synovial sarcomas classically display a well-defined, multilocular mass with heterogeneous enhancement (Fig. 5.7) (Quint et al. 1985). No significant imaging differences have been reported between the mono- and biphasic form. The tumor size primaily influences patient's

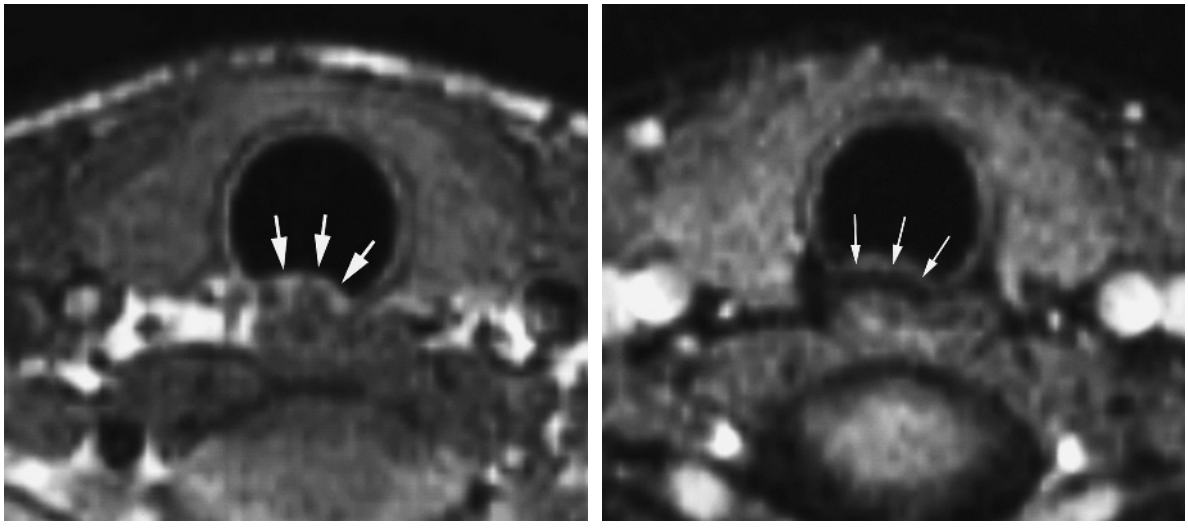

a **b**

Fig. 5.6a,b. Axial non-enhanced T1- (**a**) and gradient echo T2-weighted (**b**) images illustrate the dependency of visibility on the thin layer of fat within the common wall of the trachea and esophagus (*arrows*), with this fat plane more completely visible on the gradient echo T2 image (*arrows* in **b**)

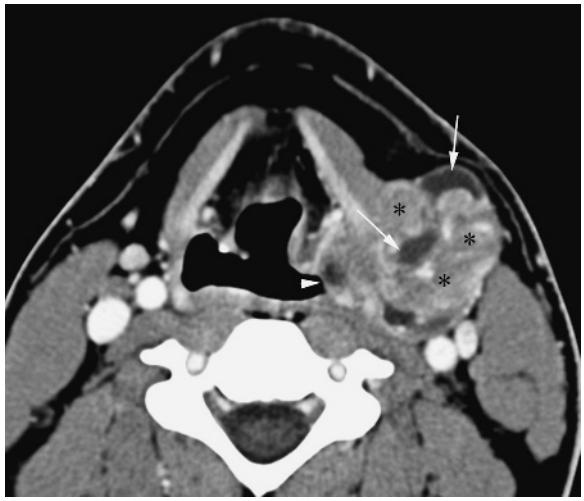

Fig. 5.7. Axial contrast-enhanced CT image through the upper thyroid cartilage level shows a large mass arising from the lateral wall of the pyriform sinus on the left (*arrowhead*) with gross extension into the lateral compartment of the neck. This mass has heterogeneous density with solid (*asterisks*) and cystic (*arrows*) portions that is characteristic for synovial sarcoma but not typically seen with squamous cell carcinoma

prognosis. Presence of calcifications is also a favorable prognostic factor (Hirsch et al. 1997; Bukachevsky et al. 1992; Mamelle et al. 1986). Wide excision with post-operative radiation therapy is currently considered the optimal treatment of the different sarcoma types.

Lymphoma involving the hypopharynx and cervical esophagus is extremely rare (Miyazaki et al. 2004; Kitamoto et al. 2003). Mucosa-associated lymphoid tissue (MALT) lymphoma – a non-Hodgkin lymphoma – is the most commonly reported subtype of lymphoma in those regions. None of the published case reports refers to cross-sectional imaging findings; however, the reported cases describe a smooth-surfaced, submucosal mass rather than a mucosal lesion as suggested by its name (Miyazaki et al. 2004; Kitamoto et al. 2003). MALT lymphoma of other regions have been described to show increased signal intensity on T2, decreased attenuation on T1-weighted images and strong, rapid enhancement following intravenous contrast administration (Takahara et al. 2005; Espinosa et al. 2005). Therefore, MALT lymphoma should be considered in the differential diagnosis if such MR imaging findings are seen in a patient with a submucosal lesion of the hypopharynx and/or cervical esophagus.

Salivary gland malignancies are also rare in the hypopharynx and cervical esophagus. Mucoepidermoid and adenoid cystic carcinomas are the most commonly reported subtypes (Matsuki et al. 1999; De Campora et al. 1987; Tom et al. 1981). Adenoid cystic tumors typically arise in salivary gland tissue and minor salivary glands; however, some authors also suggested their origin in common mucosal glands. When arising in common mucosal glands, as this would be the case in the hypopharynx and cervical esophagus, adenoid cystic carcinomas have been shown to be particular malignant with a high incidence of local recurrence and distant metastatic disease. The cross-sectional imaging findings of adenoid cystic carcinoma arising from the salivary gland tissue or minor salivary glands have been reported; however, it is uncertain if the more aggressive subtype of adenoid cystic carcinoma arising from the common mucosal glands follows the same imaging characteristics. Mucoepidermoid carcinoma is composed of signet-ring and squamous cells. None of the published cases mentions the cross-sectional imaging findings of mucoepidermoid carcinoma of the hypopharynx and/cervical esophagus; however, as these tumors range between low and high grade malignancies their imaging features would be expected to range from a well defined lesion to an aggressive, locally advanced malignancy. The prognosis is also variable and certainly depends upon the grade of the tumor; however, there seems to be also a difference by location with a reported overall 5-year survival rate of 77% for the hypopharyngeal mucoepidermoid carcinoma and 0% 2-year survival rate for the esophagus (Matsuki et al. 1999; Damiani et al. 1981).

5.3.2 Squamous Cell Malignancies

5.3.2.1 Risk Factors

Chronic tobacco and alcohol abuse represent the main risk factors. Therefore, older males are most commonly involved by this type of tumor, with slowly increasing incidence in females as tobacco use in females is still on the rise. Postcricoid area cancers, however, represent an exception. They occur most commonly in females and are associated with Plummer–Vinson syndrome that is rarely seen in the US or continental Europe, but more commonly encountered in the UK (Zbären and Egger 1997). Postcricoid region hypopharyngeal tumors are hypothesized to be caused by food stasis resulting from hypopharyngeal or esophageal webs as seen with Plummer–Vinson syndrome. In addition, these patients present with iron deficiency anemia.

5.3.2.2 Clinical Presentation

Most commonly patients with hypopharyngeal and/or cervical esophageal cancer present with a neck mass, secondary to metastatic nodal involvement, and/or dysphagia, odynophagia, globus sensation and otalgia. Weight loss and a characteristic change in voice to a "hot potato" voice can also be seen. Typically, these cancers present at a locally advanced stage; they also have a high tendency to metastasize to the draining nodal chains early on. Therefore, it is not surprising that up to 75% of patients have nodal metastatic disease at presentation. In addition, elective dissection in patients with clinically N0 neck have shown a high incidence of occult nodal metastasis with a frequency of 30%. Between 20% and 40% of patients also have distant metastasis at the time of presentation (Million 1994; Kraus et al. 1997).

5.3.2.3 Growth Pattern

Hypopharyngeal malignancies like to spread in submucosal fashion that is often undetectable on clinical and/or endoscopic examination (Million 1994; Saleh et al. 1993). Nevertheless, the different subtypes of hypopharyngeal malignancies show distinct grows patterns, as described below.

Postcricoid region cancers like to invade the posterior aspect of the larynx, causing vocal cord paralysis and hoarseness. The cricoarytenoid joint itself is usually not involved. In addition, these tumors have a high propensity to grow posterolateral to involve the pyriform sinuses (100%) and inferiorly to involve the trachea (71%) and/or cervical esophagus (71%) (Aspestrand et al. 1990). Tracheal or esophageal invasion is not detectable by endoscopic evaluation in half of the patients.

The growth pattern of pyriform sinus cancers depends on their site of origin or involvement. Tumors arising from or infiltrating the lateral wall of the pyriform sinus like to invade the posterior aspect of the thyroid cartilage, extend into the soft tissues of the lateral compartment of the neck, and the paraglottic space of the true vocal cord (Fig. 5.8) (Zbären and Egger 1997). Direct infiltration of the intrinsic laryngeal muscles is rarely seen. In contrast, tumors arising from or infiltrating the medial wall of the pyriform sinuses show early laryngeal invasion and vocal cord fixation in 60% of the patients (Figs. 5.9 and 5.10) (Becker 1998; Zbären and Egger 1997; Nowak et al. 1999). They also have a high propensity for contralateral tumor extension with 87%, higher frequency of submucosal tumor spread than the other tumor subtypes with 56%, and perineural tumor invasion in almost 45% of patients (Figs. 5.9 and 5.10) (Zbären and Egger 1997).

Posterior hypopharyngeal wall cancers like to grow in craniocaudal direction with potential extension from the nasopharynx all the way to the esophagus (Nowak et al. 1999). As the craniocaudal extension of these tumors may solely be superficial, the full extent of the tumor may not be detectable on cross-sectional examination; therefore, correlation with clinical findings is critical for staging and treatment planning purposes. Rarely, these tumors cause infiltration of the prevertebral fascia or musculature at the time of presentation. Even when there is obliteration of the prevertebral fat planes on CT and/or MR studies, the diagnosis of prevertebral fascia or muscle invasion cannot be made as the accuracy of CT in predicting prevertebral musculature involvement has been reported to be low at 55% (Righi et al. 1996). Therefore, surgical exploration has to be done for definitive diagnosis. In contrast, preservation of the prevertebral fat planes is helpful as the negative predicative value for prevertebral musculature involvement is high with 82% (Righi et al. 1996).

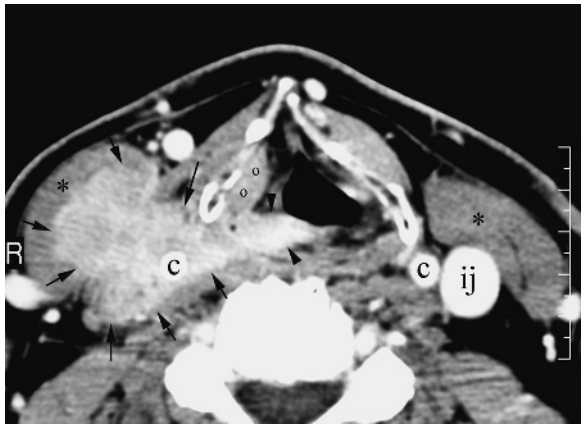

Fig. 5.8. Axial contrast-enhanced CT image through the mid thyroid cartilage level shows a large squamous cell carcinoma arising from the pyriform sinus on the right (*arrowheads*) with huge extension into the lateral compartment of the neck (*arrows*) causing marked flattening and lateral displacement of the sternocleidomastoid muscle (*asterisk* on right) when compared to its normal appearance on the left (*asterisk* on left). In addition, this mass results in complete occlusion of the internal jugular vein on the right when compared to the left side (*ij* on left). The common carotid artery (*c*) is also surrounded by the mass on the right (*c* on right) when compared to its normal appearance on the left (*c* on left). Please note also the submucosal involvement of the false vocal cord on the right (*o*)

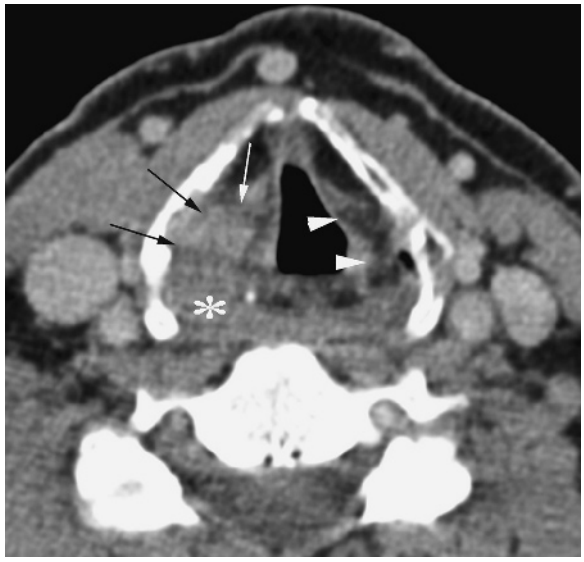

Fig. 5.9. Axial contrast-enhanced CT image through the false vocal cord level shows submucosal extension of a right pyriform sinus tumor (*asterisk*) into the right false vocal cord (*arrows*) that is seen as obliteration of the paraglottic fat plane when compared to the normal appearance on the left (*arrowheads*). This portion of the tumor was not appreciable on endoscopic examination

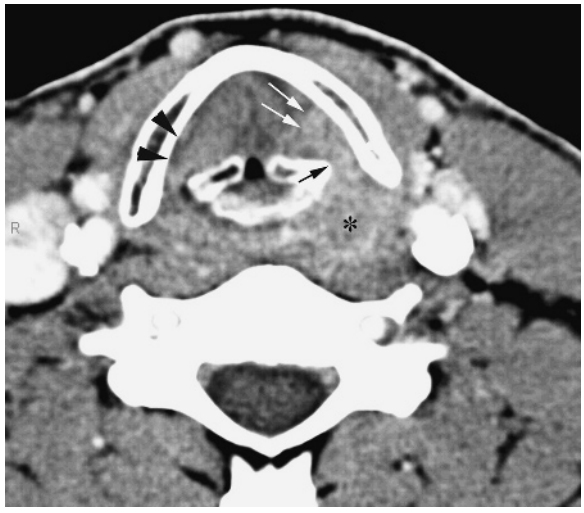

Fig. 5.10. Axial contrast-enhanced CT image through the true vocal cord level demonstrates a large pyriform sinus cancer on the left (*asterisk*) that is extending in submucosal fashion into the left true vocal cord (*white arrows*). The extension into the true vocal cord is slightly higher in density than the normal vocal cord tissues; also the slight widening of the distance between the arytenoid and thyroid cartilage (*black arrow*), the disorganization of the intrinsic vocal cord musculature and the obliteration of the paraglottic fat plane provide additional clues to the glottic extent of the primary tumor. Note that the normal paraglottic fat plane (*arrowheads* on right) at the true vocal cord level are significantly thinner than at the false vocal cord level (compare with Fig. 5.9)

Cervical esophageal tumors like to infiltrate adjacent anatomical structures, such as the trachea, TE groove housing the recurrent laryngeal nerve, and adjacent vasculature (Figs. 5.11 and 5.12). In addition, they are inclined to spread in a submucosal fashion to involve the hypopharynx (Fig. 5.12c).

The exact assessment of the craniocaudal extension of hypopharyngeal tumors into the cervical esophagus and vice versa is crucial for planning of surgical resection (limited versus extensive resection) (Fig. 5.12). Since hypopharyngeal tumors can spread in a superficial or submucosal pattern, a combination of clinical examination and cross-sectional study should be used in the treatment planning process.

5.3.2.4 Nodal Chain Involvement

The different hypopharyngeal tumor subtypes and the cervical esophagus have slightly different lymphatic drainage pathways: the postcricoid area tumors primarily drain into group III, IV and VI lymph nodes; the pyriform sinus tumors tend to metastasize into group II, III, and V lymph nodes; the posterior hypopharyngeal wall cancers like to involve the retropharyngeal lymph nodes and secondarily the internal jugular chain lymph nodes. Retropharyngeal lymph nodes are only rarely involved with the other hypopharyngeal cancer subtypes and seen in 15% of patients, however, only when there is concomitant involvement of the lateral nodal chain groups (Million 1994). Cervical esophageal cancer drains into group VI and mediastinal lymph nodes. The group VI lymph nodes are involved in 71% of patients at presentation (Weber et al. 1993).

5.3.2.5 TNM Classification

The staging system of the primary hypopharynx and cervical esophageal cancers and associated nodal metastatic disease is outlined in Tables 5.1 and 5.2, respectively (American Joint Committee on Cancer 2002). The recommended staging of cervical esophageal lesions is identical to that of the intrathoracic esophagus.

5.3.3 Secondary Involvement by Other Tumors

Infiltration of the hypopharynx and cervical esophagus by surrounding tumors is rare. It may occur

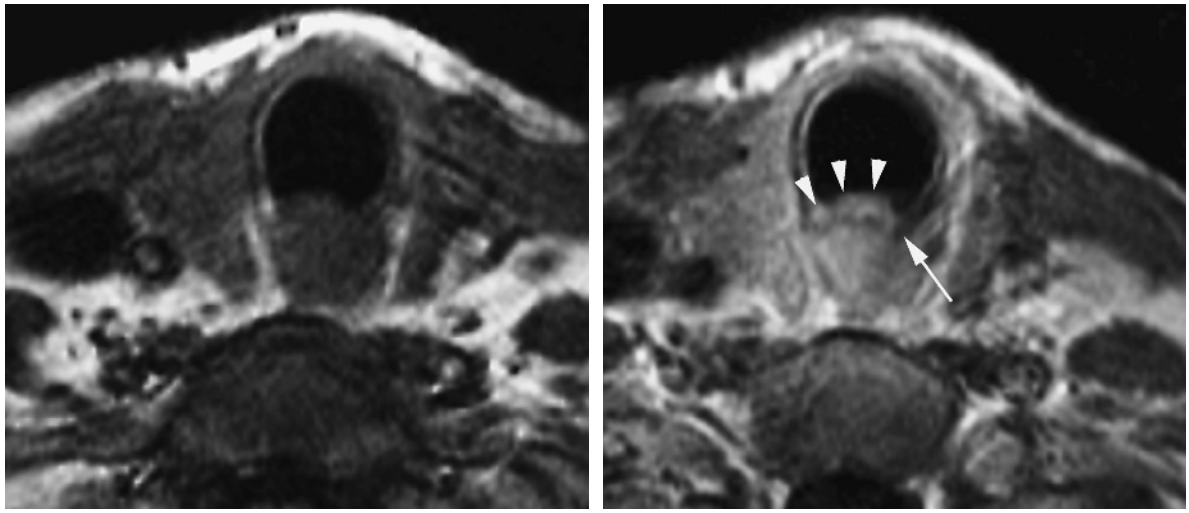

Fig. 5.11a,b. Axial non-enhanced T1- (**a**) and contrast enhanced T1- (**b**) weighted images through the upper esophagus show lack of patent esophageal lumen caused by an esophageal cancer that is difficult to appreciate on the non-enhanced T1-weighted image (**a**). The contrast-enhanced T1-weighted image clearly shows gross involvement of the common wall of the trachea and esophagus (*arrowheads*) that enhances in comparison to the non-enhancing normal tracheal wall (*arrows*); this provides critical clues to the correct diagnosis

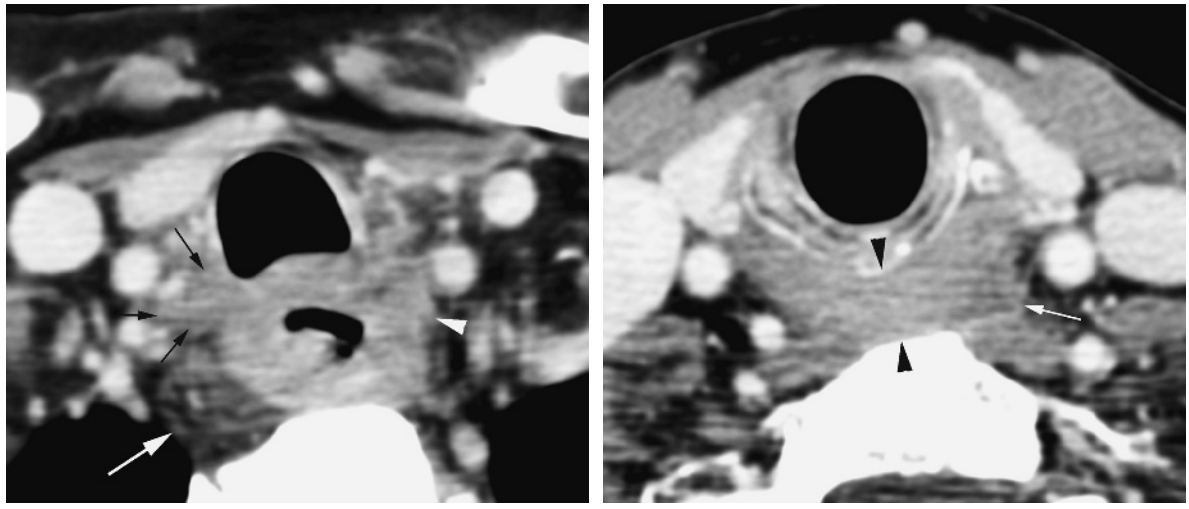

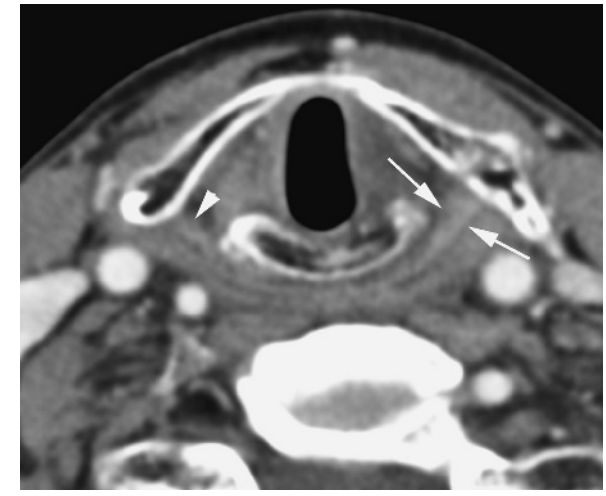

Fig. 5.12a–c. Axial contrast-enhanced CT images through the cervical esophagus (**a**), esophageal verge (**b**) and post-cricoid level (**c**) show marked wall thickening of the upper esophagus caused by a large esophageal cancer with clear signs of tumor growth beyond the serosal layer, delineated as indistinct appearance of the outer esophageal margin (*arrowhead* in **a**), "dirty" appearance of the paraesophageal fat on right (*white arrow*) and gross extension into the TE groove on the right (*black arrows* in **a**). Superiorly, the tumor is involving the esophageal verge which is slightly larger in anteroposterior diameter (between *arrowheads* in **b**) than typically seen. In addition, there is partial obscuration of the left-sided surrounding fat plane (*arrow* in **b**) consistent with extra-esophageal tumor growth, providing an additional clue for involvement of the esophageal verge. The tumor continues superiorly to involve the post-cricoid region on the left (*arrows* in **c**), when compared to the normal appearance on the right (*arrowhead* in **c**)

Table 5.1. Staging of primary tumors of the hypopharynx (American Joint Committee on Cancer 2002)

Primary tumor	
Tis	Carcinoma in situ
T1	Tumor limited to one subsite of hypopharynx and 2 cm or less in greatest dimension
T2	Tumor invades more than one subsite of hypopharynx or an adjacent site, or measures more than 2 cm but not more than 4 cm in greatest diameter without fixation of hemilarynx
T3	Tumor more than 4 cm in greatest dimension or with fixation of the hemilarynx
T4	Tumor invades thyroid/cricoid cartilage, hyoid bone, thyroid gland, esophagus, or central compartment soft tissues[a]
Regional lymph nodes	
NX	Regional lymph nodes cannot be assessed
N0	No regional lymph node metastasis
N1	Metastasis in a single ipsilateral lymph node, 3 cm or less in greatest dimension
N2	
N2a	Metastasis in a single ipsilateral lymph node more than 3 cm but not more than 6 cm in greatest dimension
N2b	Metastasis in multiple ipsilateral lymph nodes, none more than 6 cm in greatest dimension
	Metastasis in bilateral or contralateral lymph nodes, none more than 6 cm in greatest dimension
N2c	
N3	Metastasis in a lymph node more than 6 cm in greatest dimension

[a]Central compartment soft tissues includes prelaryngeal strap muscles and subcutaneous fat.

Table 5.2. Staging of primary tumors of the cervical esophagus (American Joint Committee on Cancer 2002)

Primary tumor	
Tis	Carcinoma in situ
T1	Tumor invades the lamina propria or submucosa
T2	Tumor invades muscularis propria
T3	Tumor invades adventitia
T4	Tumor invades adjacent structures
Regional lymph nodes	
NX	Regional lymph nodes cannot be assessed
N0	No regional lymph node metastasis
N1	Regional lymph node metastasis

with advanced head and neck tumors, thyroid tumors, tracheal and bronchogenic carcinomas (Roychowdhury et al. 2000). MR is more sensitive than CT for detection of hypopharyngeal and/or esophageal invasion by an adjacent malignancy due to its better soft tissue definition. Focal areas of increased T2 signal intensity raise the suspicion for invasion (Fig. 5.13). Focal enhancement following contrast administration might also be a sign of infiltration; however, it is not as specific as the T2 changes (Fig. 5.13b,c). Circumferential mass at the level of the cervical esophagus has been reported to be the most sensitive and specific sign of invasion (accuracy, 100%). In contrast, intact adjacent fat planes, absence of wall thickening, and normal T2 wall signal intensity indicate no invasion with a very high degree of confidence (Fig. 5.1) (Roychowdhury et al. 2000).

5.4 Cross-Sectional Imaging

Cross-sectional imaging with CT and MR is critical in the evaluation of patients with hypopharyngeal and/or cervical esophagus malignancies (Wenig et al. 1995; Becker 1998; Aspestrand et al. 1990; Nowak et al. 1999; Prehn et al. 1998; Thabet et al. 1996). Overall, it has been shown that the clinical tumor stage increases in up to 90% of patients with cross-sectional imaging. Changes in T-stage account for two thirds of primary tumor up-staging due to detection of lateral soft tissue involvement in 88%, and bone or cartilage invasion in 23% of patients. In one third of patients the N-stage was responsible for the tumor up-staging. Comparison of the accuracy of tumor staging with pathological findings revealed that the clinical examination is less accurate with 58% than CT and MR imaging with 80% and 85% accuracy, respectively. These facts emphasize the essential role of cross-sectional imaging in staging of hypopharyngeal and esophageal cancer. Interestingly, none of the other cancers of the head and neck region shows such a significant impact of cross-sectional imaging upon staging.

CT and MR imaging is, however, only helpful when performed with an appropriate protocol covering the potential sites of tumor spread, utilizing the appro-

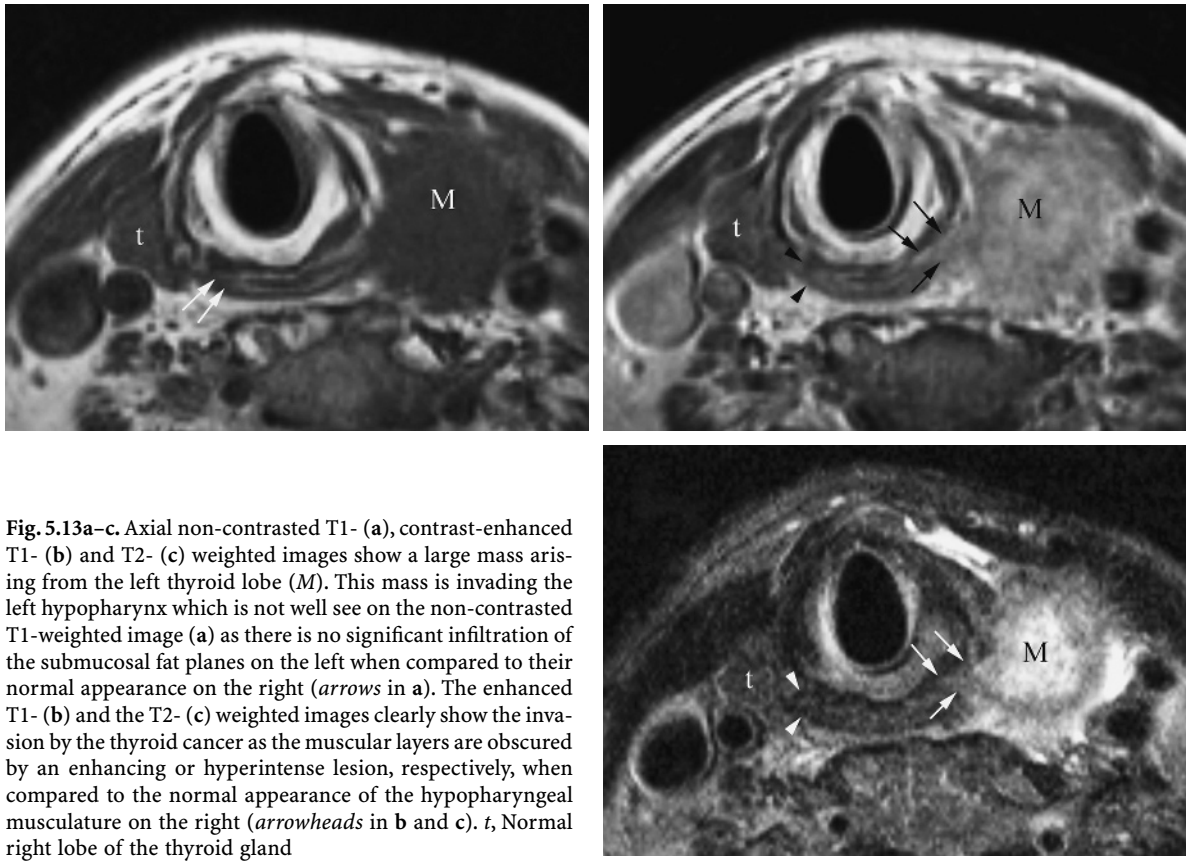

Fig. 5.13a–c. Axial non-contrasted T1- (**a**), contrast-enhanced T1- (**b**) and T2- (**c**) weighted images show a large mass arising from the left thyroid lobe (*M*). This mass is invading the left hypopharynx which is not well see on the non-contrasted T1-weighted image (**a**) as there is no significant infiltration of the submucosal fat planes on the left when compared to their normal appearance on the right (*arrows* in **a**). The enhanced T1- (**b**) and the T2- (**c**) weighted images clearly show the invasion by the thyroid cancer as the muscular layers are obscured by an enhancing or hyperintense lesion, respectively, when compared to the normal appearance of the hypopharyngeal musculature on the right (*arrowheads* in **b** and **c**). *t*, Normal right lobe of the thyroid gland

priate imaging study, sequence and window display. Although each radiologist has personal preferences and there are vendor related variations in hardware and software, the subsequent generic imaging guidelines should be followed:

1. Image the patient in supine position with the neck slightly hyperextended to elongate the airway. Use dedicated neck coil for MR imaging to improve the spatial resolution and signal-to-noise ratio.
2. Perform images in axial plane aligned parallel to the true vocal cords from the body of the mandible to the thoracic inlet. Increase the upper extent to the skull base if posterior pharyngeal wall cancer is suspected to capture the entire possible extent of the tumor and to include all retropharyngeal lymph nodes.
3. Utilize a slice thickness of ≤ 3 mm for CT and contiguous 3-mm images for MR imaging for adequate display of the pertinent anatomical structures. Consider even thinner slices for CT if multi-planar reformations are desired.
4. Use a field-of-view of ≤ 16 cm through the neck. Additional reconstructions of the CT images through the hypopharynx with a field-of-view of 10 cm are recommended to increase spatial resolution. Magnification of the images performed with the larger field-of-view are not sufficient as the special resolution will stay the same.
5. Use image matrix of at least 256×256 for MR and 512×512 for CT for optimal spatial resolution.
6. Inject intravenous contrast for better tumor border delineation and detection of nodal metastatic foci.
7. MRI: A minimum of non-contrasted and contrast T1-weighted images and fast spin-echo T2-weighted images should be performed to emphasize soft tissue detail. Other sequences may be included to better evaluate certain structures such as the intramural fat planes (see Sect. 5.2.2).
8. CT: Reconstruction of the images through the laryngeal cartilages in bone algorithm is helpful for detection of subtle cartilage destruction and or sclerosis.
9. Utilize the multi-planar capabilities of both imaging modalities to facilitate the assessment of craniocaudal tumor extension.

5.5 Radiologist's Role

5.5.1 Pre-treatment

The radiologist's pre-treatment role is multifold: detection of the subsite of origin of the primary tumor, delineation of the extent of the primary tumor, assessment of the nodal status and detection of a second primary cancer. When the full extent of the primary tumor is assessed and reported, the following pertinent issues have to be emphasized as they may influence the T staging of the tumor:

5.5.1.1 Submucosal Spread

As mentioned before, hypopharyngeal and or esophageal cancers like to grow in a submucosal fashion and, therefore, remain undetectable in a significant number of patients on clinical and endoscopic examination (Saleh et al. 1993). Occasionally, the entire tumor is submucosal in location and difficult or impossible to biopsy endoscopically. In such cases, the radiologist may offer percutaneous biopsy under CT guidance.

5.5.1.2 Cartilage Involvement

Cartilage involvement may be studied with CT and MR. Both modalities struggle with the problem of lack of ossification of the different cartilages in the younger patient and inhomogeneous as well as variable ossification with advanced age (Yeager et al. 1982). This is in particular true for the thyroid cartilage. Since the different cartilages tend to ossify in a symmetric fashion, asymmetric attenuation might be a helpful hint for presence of cartilage invasion and needs to be included in the pre-treatment assessment of CT and or MR studies (Fatterpekar et al. 2004).

The role of CT and MR in detection of cartilage involvement has been studied extensively in the past decade as it has been shown that non-removal of an abnormal-appearing cartilage carries a risk of 50%–60% of leaving tumor behind. The overall consensus is that MR is the most sensitive imaging modality in detection of cartilage involvement; however, it suffers from low specificity as inflammation, edema and sclerosis can show similar MR findings as tumor invasion (Wenig et al. 1995; Becker 1998; Becker et al. 1995; Castelijns et al. 1988; Zbären et al. 1996). For CT, the reported sensitivity is lower but the overall specificity is higher than for MR (Becker et al. 1997). Therefore, a combination of both studies might be the most effective strategy in the evaluation process of cartilage invasion by cancer (Yousem and Tufano 2002). In addition, the specificity of both imaging modalities depends upon the cartilage type. The thyroid cartilage has the lowest specificity due to its variable ossification and the arytenoid cartilage has the highest. Therefore, the diagnosis of thyroid cartilage involvement by tumor should only be made with caution with both imaging modalities.

Cartilage involvement can manifest as cartilage sclerosis (Fig. 5.14), cortical erosions or lysis (Fig. 5.15) and bone marrow replacement (Fig. 5.16). Cartilage sclerosis is discernible as increased density on CT and decreased attenuation on all MR sequences with lack of enhancement following contrast administration (Fig. 5.14). It has been shown to be the most sensitive criterion for cartilage invasion; however, it often corresponds to "benign" reactive inflammation caused by the adjacent tumor or occasionally to a normal anatomical variation as reported for the arytenoid cartilage (Schmalfuss et al. 2000; Becker et al. 1997; Munoz et al. 1993). Therefore, it is not surprising that the positive predictive value of cartilage sclerosis for tumor invasion has been reported to be only about 50%. Cartilage erosion or lysis manifests as serpiginous or gapping cartilage contour while bone marrow replacement shows increased density on CT and decreased signal intensity on T1-weighted images in relation to the uninvolved fatty replaced bone marrow seen in older patients with marked enhancement following contrast administration (Figs. 5.15 and 5.16). None of the criteria alone showed sufficient sensitivity and specificity for cartilage invasion and therefore, the highest degree of accuracy could only be reached when combining sclerosis, erosions or lysis and extralaryngeal tumor extension together. Since not all of these criteria are present in each patient simultaneously, a significant false negative rate would be expected. Nevertheless, cross-sectional imaging is valuable as an excellent negative predictor for cartilage invasion with reported high negative predictive values of 92%–100% (Becker 1998; Castelijns et al. 1988; Becker et al. 1995; Zbären et al. 1996).

5.5.1.3 Tumor Volume

In recent years, focus has been placed on stratifying patients in high- or low-risk groups to help with the

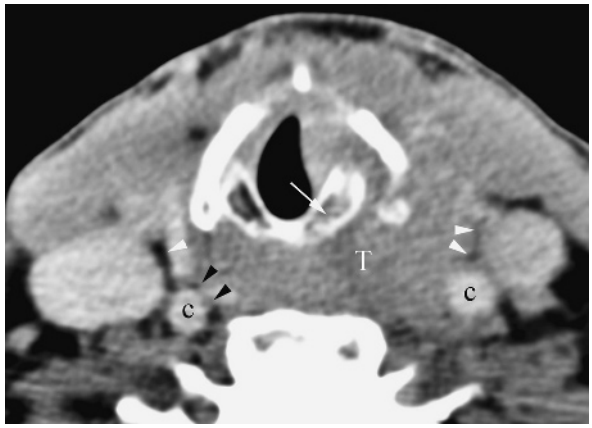

a

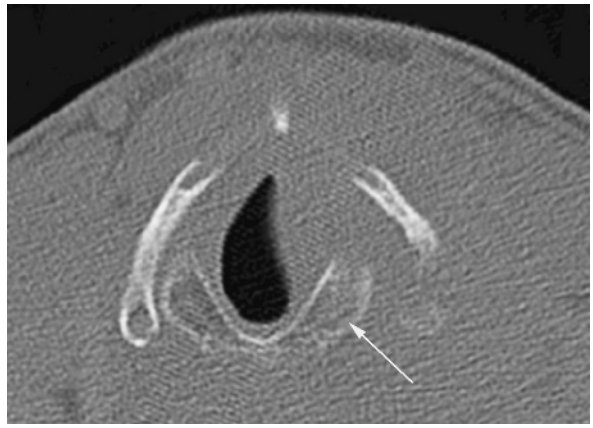

b

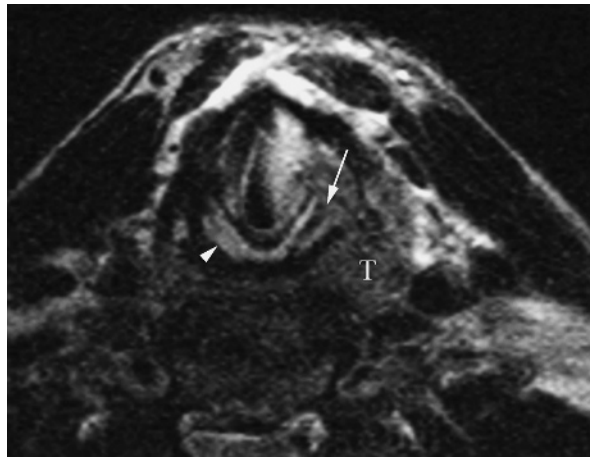

c

Fig. 5.14a–c. Axial contrast-enhanced CT images displayed in soft tissue (**a**) and bone (**b**) windows show a large pyriform sinus mass on the left (*T*) that is causing subtle sclerosis of the left cricoid cartilage (*white arrow* in **a** and **b**). The T2-weighted (**c**) image at the same level confirms the sclerosis as the normally seen high signal intensity of the cricoid cartilage (*arrowhead* in **c**) is replaced by dark signal intensity on the left (*arrow* in **c**). In addition, this mass partially obliterates the left lateral surrounding fat plane (*white arrowheads* on left in **a**) when compared to its normal appearance on the right (*white arrowhead* on right in **a**). There is also obliteration of the normally seen fat plane around the common carotid artery (*c* in **a**) on the left when compared to its normal appearance on the right (*black arrowheads* in **a**)

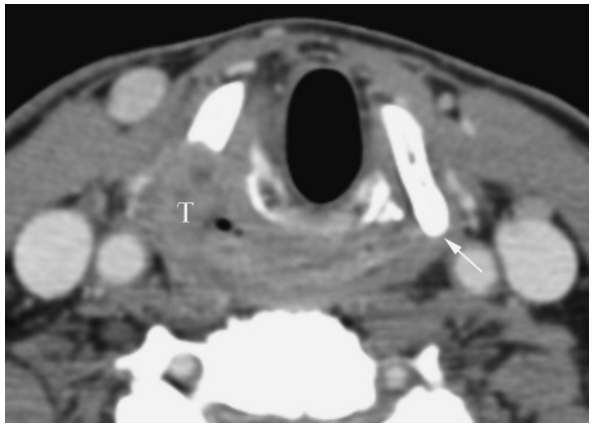

a

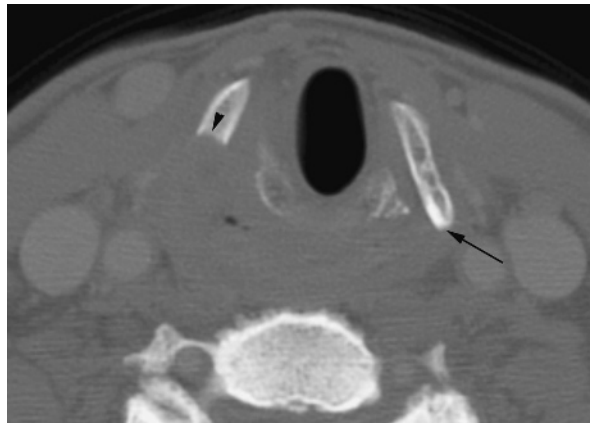

b

Fig. 5.15a,b. Axial contrast-enhanced CT images displayed in soft tissue (**a**) and bone (**b**) windows show severe foreshortening of the posterior thyroid cartilage caused by extensive pyriform sinus cancer (*T*) involvement on the right, when compared to its normal length on the left (*arrow*)

selection of the most optimal treatment plan based on outcome measures. Beside cartilage invasion, tumor volume and amount of disease at the pyriform sinus apex have been identified to be critical prognostic factors in patients with T1 and T2 stage pyriform sinus cancer (Pameijer et al. 1998). A tumor volume of 6.5 ml demarcated the threshold between favorable and non-favorable to reach control at the primary site with radiation therapy alone. Similar threshold criteria were also detected in regard to

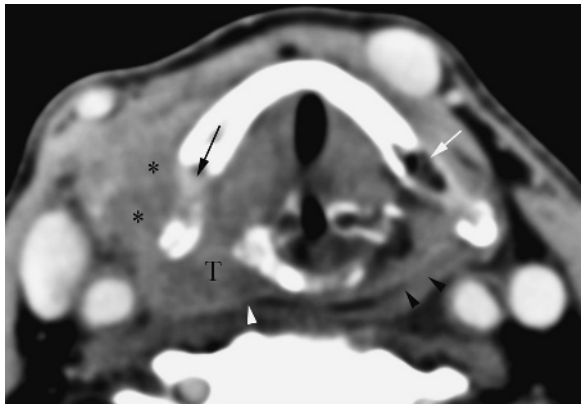

Fig. 5.16. Axial contrast-enhanced CT image through the arytenoid cartilage level shows replacement of the normally seen fatty bone marrow (*white arrow*) by soft tissue density (*black arrow*) caused by bone marrow replacement of this portion of the thyroid cartilage by a pyriform sinus cancer on the right (*T*). Note the abrupt cut-off of the submucosal fat planes caused by the tumor on the right (*white arrowhead*) when compared to their normal appearance on the left (*black arrowheads*). The tumor also wraps around the posterior border of the thyroid cartilage to involve the strap muscles (*asterisks*)

pyriform sinus apex involvement. A tumor diameter of < 10 mm at the level of the base of the arytenoid cartilage and upper 3 mm of the cricoid cartilage (= "minimal apical disease") has been shown to have a favorable prognosis to reach control at the primary site with radiation therapy alone, in contrast to tumor diameter of ≥ 10 mm (= "bulky apical disease") (Pameijer et al. 1998). The results of tumor volume and apical disease combined, classified the patients in different risk groups with the following criteria and local control rates if treated with radiation therapy alone:

- Low-risk group: Tumor volume < 6.5 ml and no or minimal pyriform apex disease resulted in a control rate of 94% (Fig. 5.17).
- Moderate risk group: Tumor volume of < 6.5 ml and bulky apical disease or tumor volume ≥ 6.5 ml and no or minimal pyriform apex disease demonstrated local control rates of 50% (Fig. 5.18).
- High-risk group: Tumor volume of ≥ 6.5 ml and bulky apical disease yielded a local control rate of 0% (Fig. 5.19).

Therefore, tumor volume and extent of disease at the pyriform apex level should be included in the radiological report for all T1 and T2 stage pyriform sinus cancers. Thresholds for tumor volume and/or extent of pyriform apex disease for other types of hypopharyngeal and/or other T stages are still unknown.

5.5.2 During Treatment

At present, the radiologist is only rarely involved during the treatment phase of patients with hypopharyngeal or cervical esophageal cancer, unless the patient develops complications related to the therapy, such as fistula and abscess formation or vascular rupture requiring percutaneous intervention. Advances in current, and development of new, treatment regimes will, however, require that the radiologist assumes a more active role in the therapy delivery in the foreseeable future. Intra-arterial administration of supradose of Cisplatin directly into the tumor bed combined with concurrent radiation therapy ("RADPLAT protocol") has already been shown to be a promising treatment option in patients with advanced head and neck cancer (Robbins et al. 2000). The preliminary results show a significantly higher rate of local control in advanced head and neck tumors (80%) and an improved 5-year disease-specific and overall survival rate (54% and 39%, respectively). The results of RADPLAT applied specifically to pyriform sinus cancer demonstrated a complete local response rate of 92% and 76% at the nodal site with a 5-year disease-specific and overall survival rate of 50% and 23%, respectively (Samant et al. 1999). Although these survival rates are similar or only slightly higher than reported for other treatment regimes, RADPLAT has shown a higher organ preservation rate (88%) with adequate voice preservation and acceptable swallowing abilities. A shift of the disease progression from local recurrence to distant metastasis has been noted in patients with head and neck cancers treated with RADPLAT protocol (Samant et al. 1999)[42]. No data regarding other sites of the hypopharynx or cervical esophagus are currently available.

5.5.3 Post Treatment

As it is true for the pretreatment evaluation of patients with hypopharyngeal or cervical esophageal cancer, cross-sectional imaging plays a crucial role in the detection of recurrent cancer. It has been reported that up to 40% of recurrent tumors are detected with cross-sectional imaging prior to their discovery on clinical examination (Hermans et al. 2000). This is on the one side due to the similarity of post-radiotherapy changes to recurrent tumor on clinical examination, and on the other side due to potential submucosal location of recurrent tumors. Therefore,

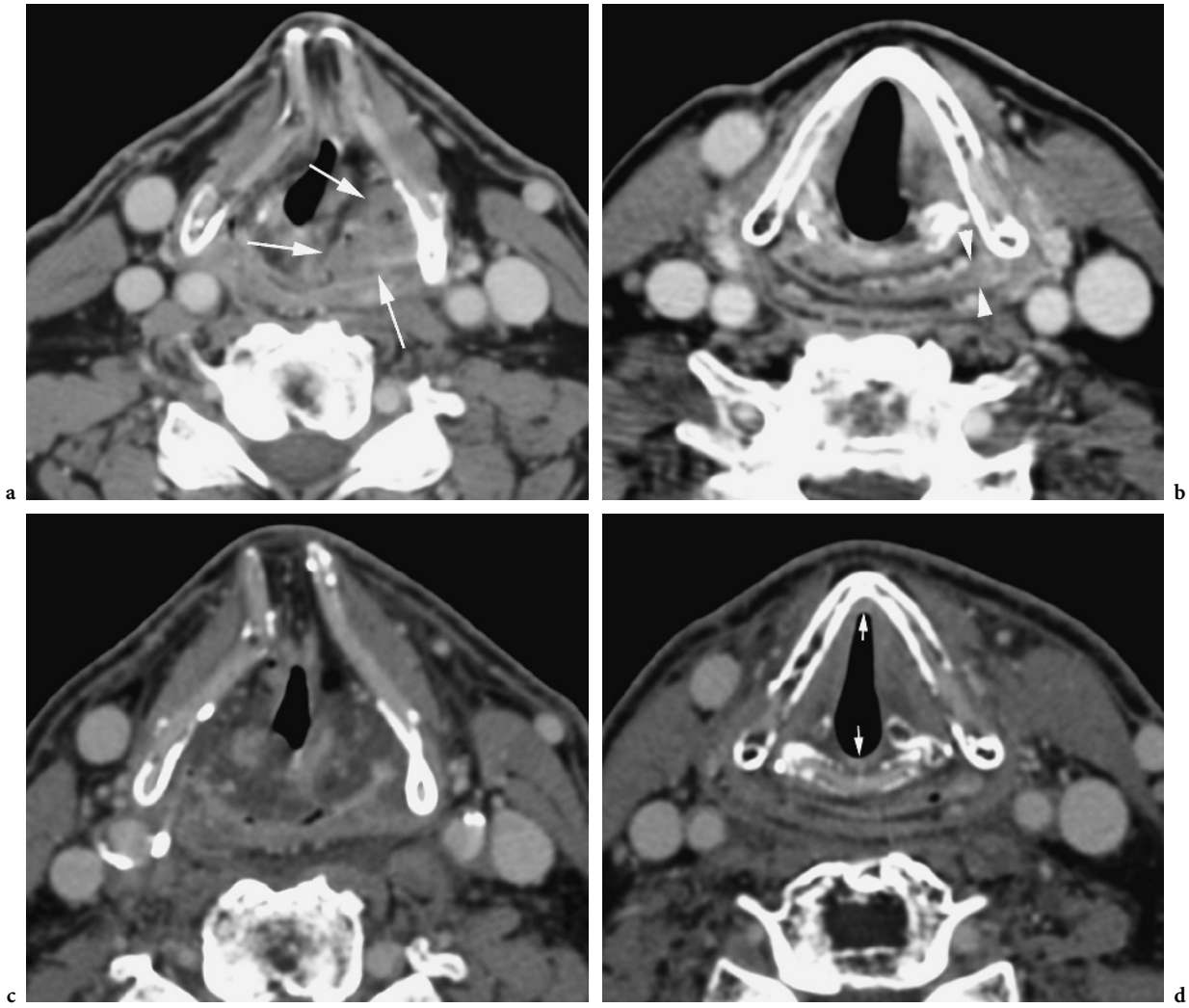

Fig. 5.17a–d. Axial contrast-enhanced CT images through the false (**a**) and true (**b**) vocal cord level demonstrate a pyriform sinus cancer (*arrows* in **a**) of < 6.5 ml with minimal involvement at the pyriform sinus apex (*arrowheads* in **b**) that carries a favorable prognosis to be controlled at the primary site with radiation therapy alone, as demonstrated on the matched post-treatment images (**c,d**). Note the diffuse swelling of the false vocal cords (**c**) as well as anterior and posterior commissure (*arrows* in **d**) that represent expected findings following radiation therapy

the referring physicians rely on imaging surveillance even more in patients with hypopharyngeal or cervical esophageal cancer than in patients with other head and neck tumor types. Since the treatment options of patients with tumors of the hypopharynx and cervical esophagus vary from radiation therapy alone to total pharyngectomy in combination with various reconstructive techniques and/or radiation therapy, the cross-sectional imaging findings significantly vary from patient to patient (Kraus et al. 1994). Superimposed post-treatment complications, such as abscess or fistula formation, may further complicate this issue. Therefore, to allow easier and faster detection of recurrent or persistent tumor, a CT and/or MR imaging study 3 to 4 months after completion of the treatment is recommended in all patients.

5.5.3.1 Post Surgery

Knowledge of the type of surgery and familiarity of expected post-surgical tissue changes in the different types of reconstructive techniques is critical in the assessment of radiological post-treatment studies. A jejunal free flap with microvascular anastomosis is the most commonly used reconstructive method for patients that require total pharyngectomy and show only limited invasion of the cervical esophagus. Since

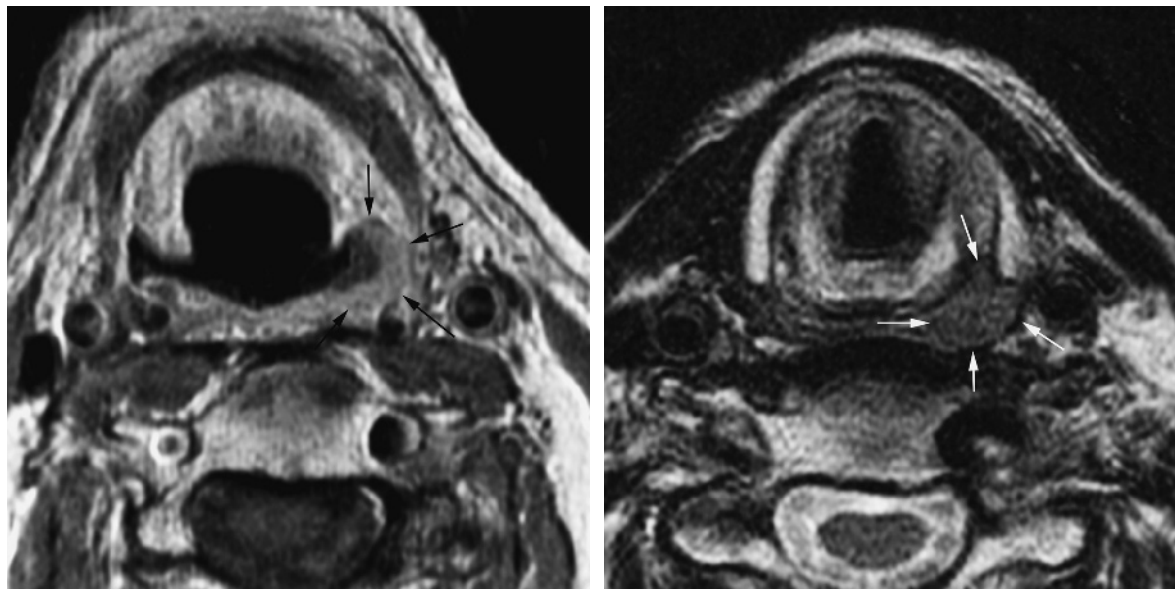

Fig. 5.18a,b. Axial contrast-enhanced T1- (**a**) and T2- (**b**) weighted image at the entrance site of the pyriform sinus (**a**) and pyriform sinus apex (**b**) level shows a small pyriform sinus cancer (*arrows* in **a**). The small volume is favorable for reaching control at the primary site with radiation therapy along. However, since there is bulky apical involvement (*arrows* in **b**) that chance for the patient to be cured with radiation therapy alone decreases to about 50%

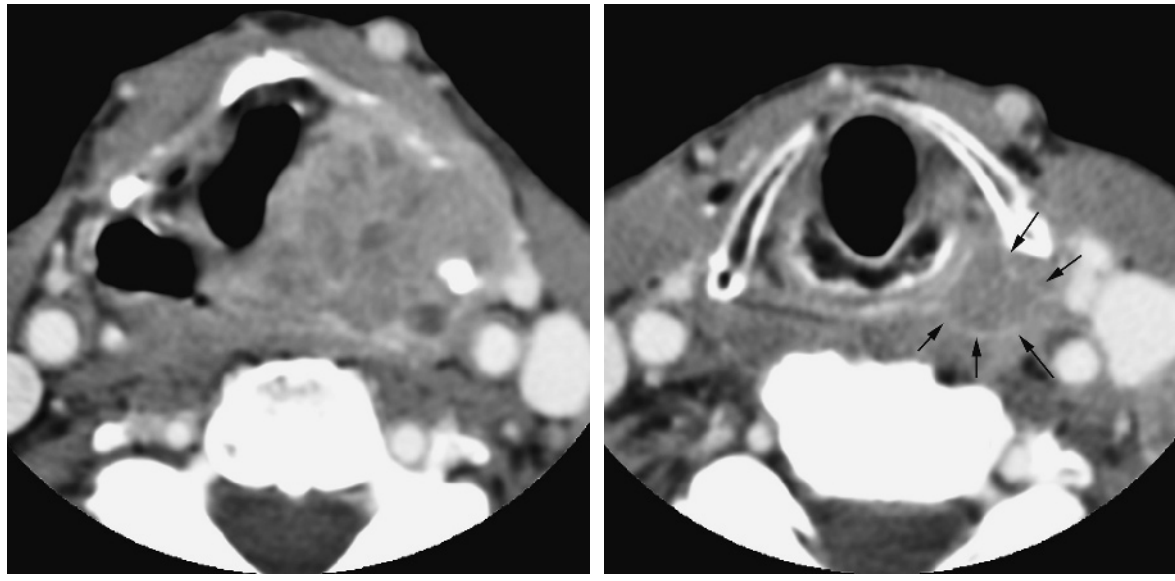

Fig. 5.19a,b. Axial contrast-enhanced CT images through the upper thyroid (**a**) and mid cricoid (**b**) cartilage levels show a huge pyriform sinus cancer on the left with bulky disease at the pyriform sinus apex (*arrows* in **b**). Because of the size and the bulky apical disease this patient has extremely poor chances to be cured with radiation therapy alone, and therefore surgical resection should be the preferred treatment choice

the jejunum is already a tube only two anastomotic sutures are required during surgery. This decreases the risk of post-operative stricture and fistula formation (Reece et al. 1995). In addition, it tolerates post-surgical radiation therapy better than gastric or colonic interposition (Uppaluri and Sunwoo 2005). However, if the jejunal conduit is chosen too long, a kink in the "neopharynx" may develop causing dysphagia and stasis symptoms. Gastric pull-up is the reconstruction method of choice in patients with longer esophageal involvement. It has a low frequency of fistula formation, but the patients often complain

of dumping and reflux symptoms. On cross-sectional studies, the jejunal interposition has a thin and regular wall while the gastric interposition shows polypoid folds of redundant mucosa. Both conduits should be surrounded by a "clean" fat plane. Colonic interposition is currently the least favorable method of hypopharyngeal reconstruction as it is associated with the highest rate of morbidity and mortality with 70% and 20%, respectively (Surkin et al. 1984). Therefore, it is only rarely performed at present.

Pectoralis major myocutaneous and radial forearm flaps may be used for subtotal hypopharyngeal defects in which a posterior stripe of mucosa remains intact (Uppaluri and Sunwoo 2005). The lack of pliability and the bulky nature of the pectoralis flap make circumferential tubing difficult, especially in obese or muscular patients (Schuller 1980). In contrast, the radial forearm flap offers thin, flexible tissue that is easy to form. It has also the tendency to remodel over time allowing better swallowing function than with other reconstructive surgeries, including jejunal interposition (Anthony et al. 1994). The radial forearm flap is a well-vascularized free flap with a large-caliber donor vessel and long vascular pedicle that is connected as end-to-end or end-to-side anastomoses to the external carotid artery or its branches, as also done with the jejunal conduit (Fig. 5.20) (Uppaluri and Sunwoo 2005). The vascular anastomosis might be seen on contrast enhanced CT images. In contrast, the pectoralis major myocutaneous flap does not require a vascular anastomosis as the myocutaneous flap does not represent a free flap but is formed by rotation of the pectoralis major muscle superiorly with subsequent transposition over the clavicle through a widely undermined subcutaneous tunnel. Typically, the pectoralis major muscle can therefore be fol-

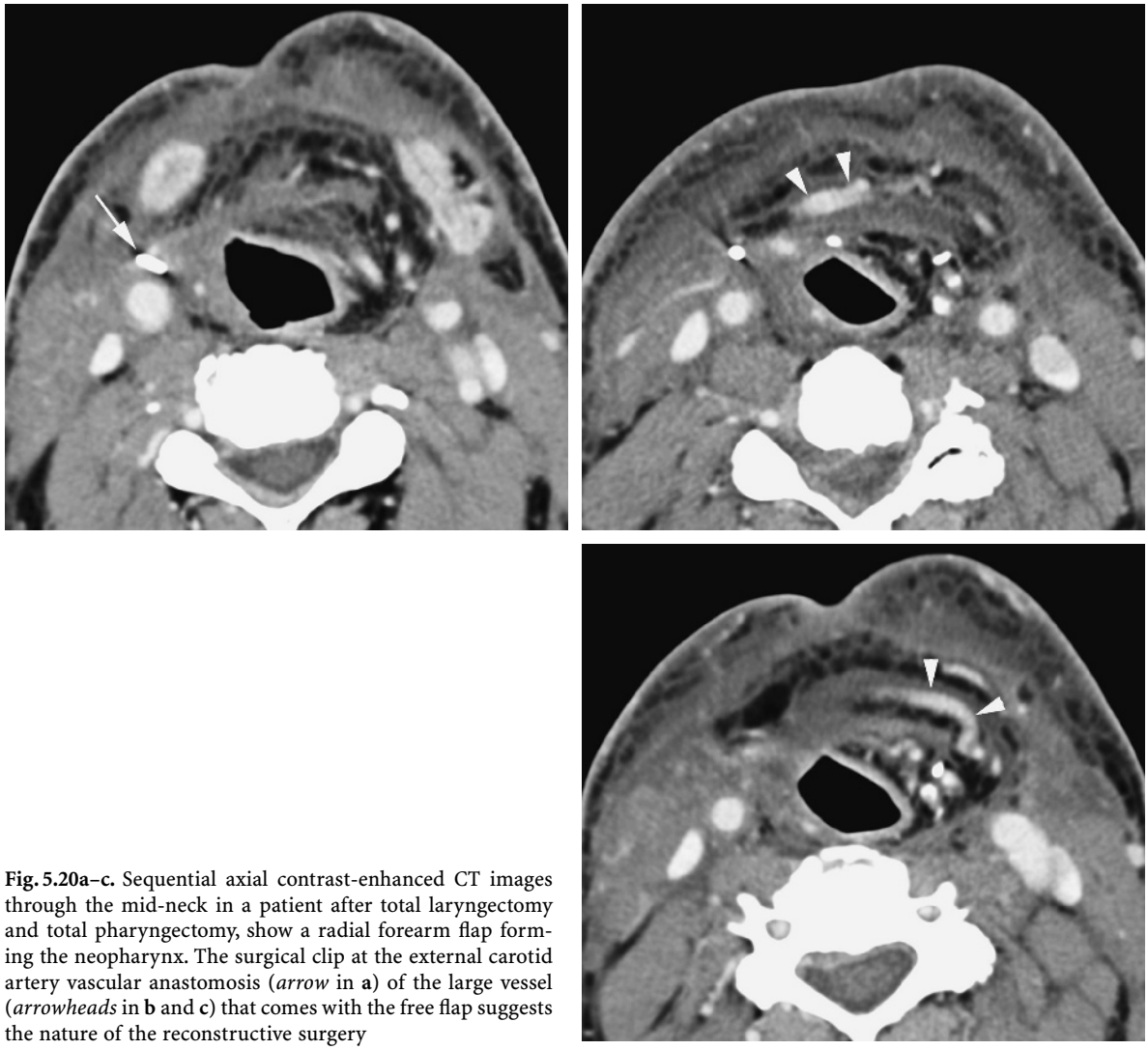

Fig. 5.20a–c. Sequential axial contrast-enhanced CT images through the mid-neck in a patient after total laryngectomy and total pharyngectomy, show a radial forearm flap forming the neopharynx. The surgical clip at the external carotid artery vascular anastomosis (*arrow* in **a**) of the large vessel (*arrowheads* in **b** and **c**) that comes with the free flap suggests the nature of the reconstructive surgery

lowed to the upper chest on cross-sectional imaging (Fig. 5.21). If the type of reconstructive surgery is not known, this muscular connection might provide a helpful hint.

After surgery, recurrent tumors typically occur at the margins of the resection or within the deep tissues of the neck (Fig. 5.22). On cross-sectional images, the appearance of the mucosa is not very helpful in evaluating recurrent tumor because single or multiple irregular-appearing folds are typically seen with gastric pull-up and less commonly with jejunal interposition. The evaluation of cross-sectional imaging studies should therefore focus on regular thickness and attenuation of the muscular wall and on smooth outer border of the neopharyngeal wall (Becker 1998).

5.5.3.2 Post-radiation therapy

The post-radiation therapy changes can be divided into general, localized to the primary site and related to the laryngeal cartilages. The general post-radiation therapy changes within the neck have been described in detail by Mukherji et al. (1994a) (Fig. 5.17c,d).

In contrast, the work of Hermans et al. (2000) focuses on changes at the primary tumor specific site as seen on the 3- to 4-month follow-up CT examinations. Based on the response of the tumor and the clinical outcome three groups of patients were stratified:

1. Patients with complete resolution of the tumor and symmetric-appearing soft tissues planes on the CT examination at 3–4 months following completion

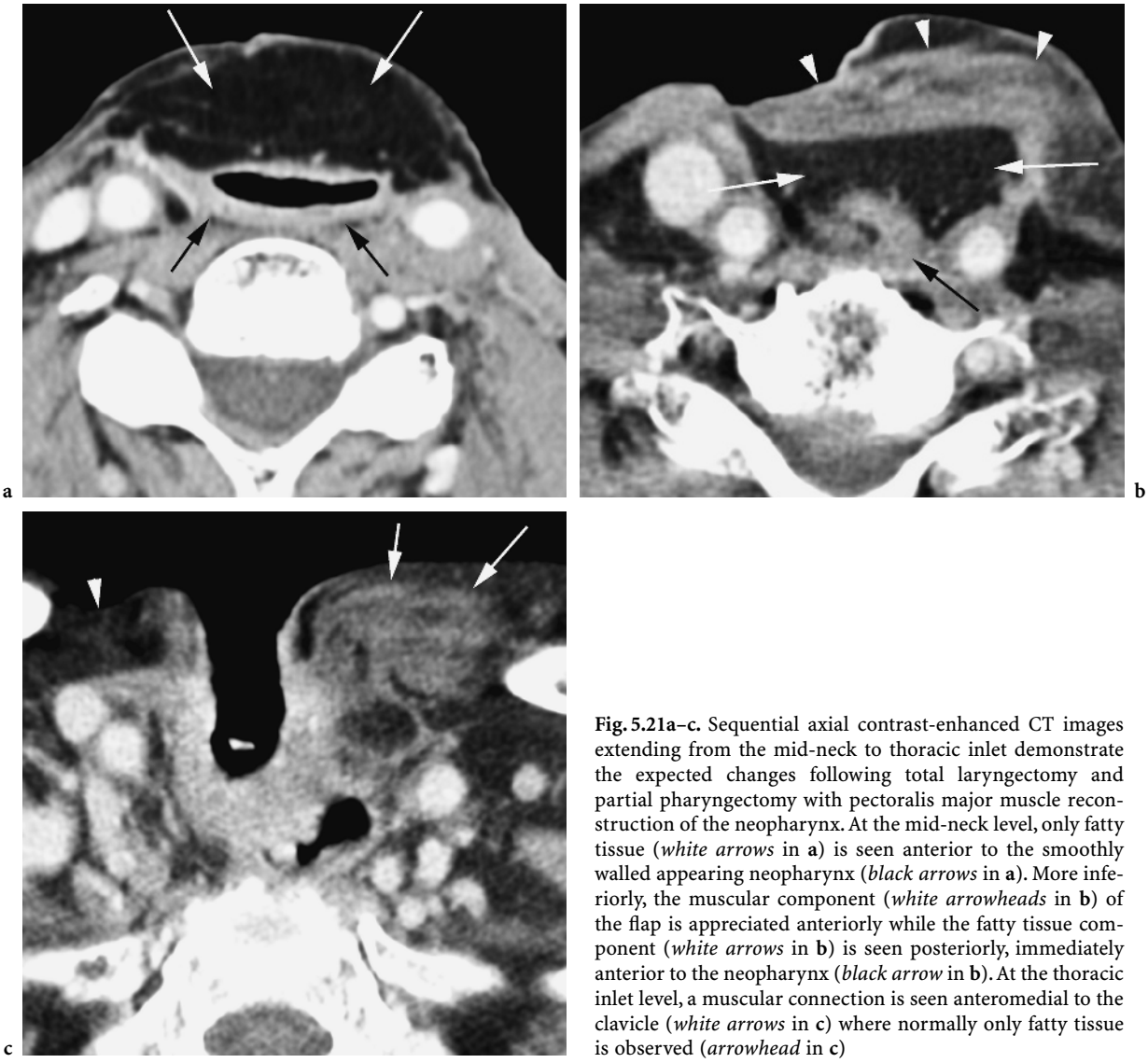

Fig. 5.21a–c. Sequential axial contrast-enhanced CT images extending from the mid-neck to thoracic inlet demonstrate the expected changes following total laryngectomy and partial pharyngectomy with pectoralis major muscle reconstruction of the neopharynx. At the mid-neck level, only fatty tissue (*white arrows* in **a**) is seen anterior to the smoothly walled appearing neopharynx (*black arrows* in **a**). More inferiorly, the muscular component (*white arrowheads* in **b**) of the flap is appreciated anteriorly while the fatty tissue component (*white arrows* in **b**) is seen posteriorly, immediately anterior to the neopharynx (*black arrow* in **b**). At the thoracic inlet level, a muscular connection is seen anteromedial to the clavicle (*white arrows* in **c**) where normally only fatty tissue is observed (*arrowhead* in **c**)

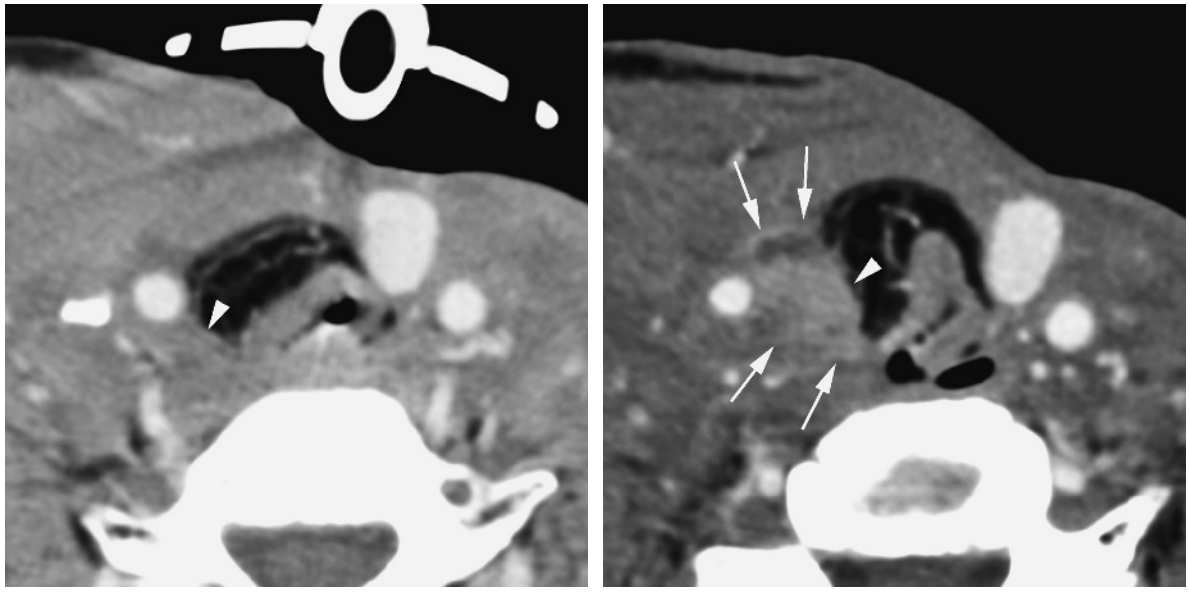

Fig. 5.22a,b. Axial contrast-enhanced CT images of a patient after total laryngectomy and partial pharyngectomy with pectoralis major flap reconstruction; imaging was performed immediately post surgery (**a**) and 3 months later (**b**); a large recurrent tumor along the lateral margin of the surgical bed is seen 3 months after surgery (*arrows* in **b**). Note the changes in the contour of the fatty component of the pectoralis major flap with convex appearance (*arrowhead* in **b**) on the follow-up study and concave appearance on the immediate post-surgical examination (*arrowhead* in **a**). Sometimes this contour change may be the only hint for recurrent disease

of radiation therapy showed an excellent clinical outcome as none of the patients presented with local recurrence over an at least 2-year follow-up period (Fig. 5.17c,d). Therefore, this patient group requires clinical follow-up and cross-sectional imaging only if suspicion for recurrent tumor is raised on the clinical examination.

2. Patients with tumor volume reduction of less than 50% or a persistent mass of ≥ 1 cm in diameter have a high likelihood of local failure (Fig. 5.23). Therefore, in these patients immediate further investigation is warranted (Hermans et al. 2000; Mukherji et al. 1994b).
3. Patients with a residual mass of < 1 cm in diameter and or asymmetry of the soft tissue planes have an intermediate prognosis and, therefore, cross-sectional follow-up at 3- to 4-month intervals should be performed if there is no clinical suspicion for recurrent tumor (Fig. 5.24). Two consecutive stable studies after the baseline study are consistent with control at the primary site.

Hermans et al. (2000) also described post-radiation alterations of the cartilages and its significance for recurrent disease in the same study. Based on their results, cartilage alteration associated with a persistent mass of ≥ 1 cm in diameter should be considered as local failure and appropriate salvage surgery needs to be considered. Cartilage alteration associated with only minimal soft tissue asymmetry requires close follow-up as it can be related to recurrent tumor or minimal chondronecrosis.

5.5.4 Detection of Second Primary

The radiologist is required to search for a second primary in patients with hypopharyngeal or cervical esophagus cancer as these patients have a higher incidence of a second primary (15%) than the remainder of head and neck malignancies (Million 1994). Interestingly, in only 25% of the patients a second primary is found at the time of the diagnosis of the hypopharyngeal or cervical esophageal cancer (synchronous lesions) while the majority is discovered on follow-up studies (metachronous lesion). Therefore, search for a second primary has to be conducted on every study performed in patients with a history of hypopharyngeal or cervical esophageal cancer.

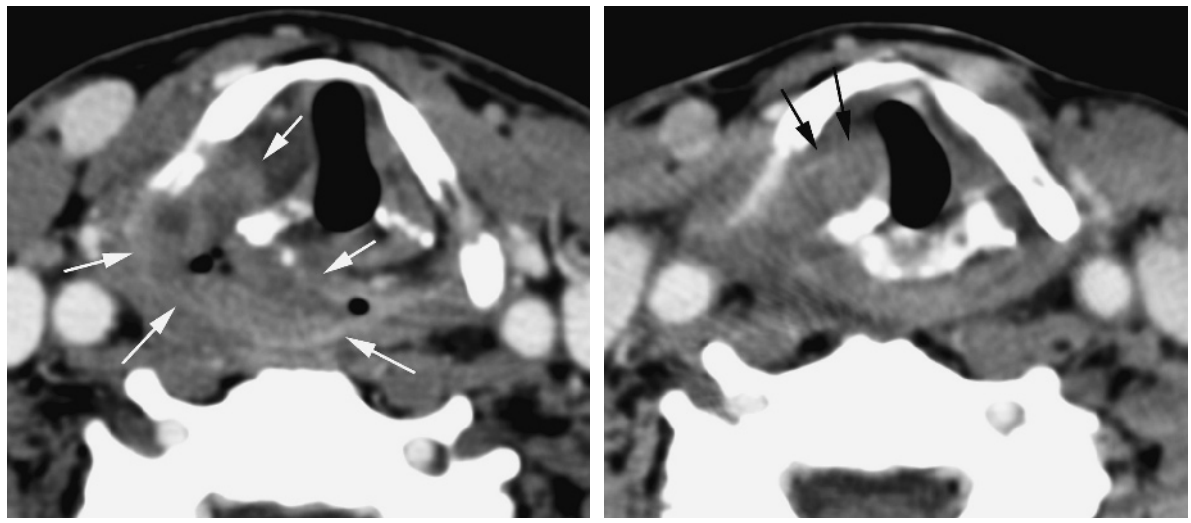

Fig. 5.23a,b. Axial contrast-enhanced CT images pre (**a**) and post (**b**) radiation therapy for a large pyriform sinus cancer on the right (*arrows* in **a**) show marked decrease of the tumor at the pyriform sinus level with persistent mass in the right true vocal cord (*arrows* in **b**) that is over 1 cm in largest diameter. Such an appearance is strongly suspicious for persistent disease and the patient should undergo biopsy and/or FDG positron emission tomography

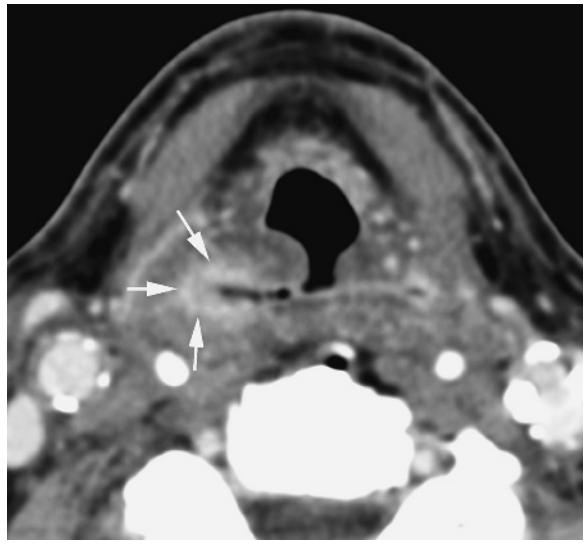

Fig. 5.24. Axial contrast-enhanced CT image performed 3 months following completion of radiation therapy shows asymmetric thickening of the mucosa in the upper pyriform sinus on the right (*arrows*) when compared to the left that is less than 1 cm in thickness. Since the pyriform sinus tumor did not completely resolve, a 3- to 4-month follow-up CT study is warranted to exclude persistent tumor; this appearance can also be caused by asymmetric radiation-induced mucositis or non-viable tumor. Biopsy is recommended if there is also clinical suspicion for persistent tumor

References

American Joint Committee on Cancer (2002) AJCC cancer staging manual, 6th edn. Springer, New York

Anthony JP, Singer MF, Mathes SJ (1994) Pharyngoesophageal reconstruction using the tubed free radial forearm flap. Clin Plast Surg 21:137–147

Artico R, Bison E, Brotto M (2004) Monophasic synovial sarcoma of hypopharynx: case report and review of the literature. Acta Otorhinolaryngol Ital 24:33–36

Aspestrand F, Kolbenstvendt A, Boysen M (1990) Carcinoma of the hypopharynx: CT staging. J Comput Assist Tomogr 14:72–76

Becker M (1998) Larynx and hypopharynx. Radiol Clin North Am 36:891–920

Becker M, Zbären P, Laeng H, Stoupis C, Porcellini B, Vock P (1995) Neoplastic invasion of the laryngeal cartilage: comparison of MR imaging and CT with histopathologic correlation. Radiology 194:661–669

Becker M, Zbären P, Delavelle J, Kurst AM, Egger C, Rufenacht DA, Terrier F (1997) Neoplastic invasion of the laryngeal cartilage: reassessment of criteria for diagnosis at CT. Radiology 203:521–532

Bukachevsky RP, Pincus RL, Shechtman FG, Sarti E, Chodsh P (1992) Synovial sarcoma of the head and neck. Head Neck 14:44–48

Castelijns JA, Gerritsen GJ, Kaiser MC, Valk J, van Zanten TE, Golding RG, Meyer CJ, van Hattum LH, Sprenger M,

Bezemer PD (1988) Invasion of laryngeal cartilage by cancer: comparison of CT and MR imaging. Radiology 167:199–206

Damiani JM, Damiani KK, Hauck K, Hyams VJ (1981) Mucoepidermoid-adenosquamous carcinoma of the larynx and hypopharynx: a report of 21 cases and a review of the literature. Otolaryngol Head Neck Surg 89:235–243

De Campora E, Croce A, Biocciolo G, Radici M (1987) Adenoid-cystic carcinoma (cylindroma) of the pyriform sinus in pediatric age. Int J Pediatr Otorhinolaryngol 14:235–242

Espinosa LA, Daniel BL, Jeffrey SS, Nowels KW, Ikeda DM (2005) MRI features of mucosa-associated lymphoid tissue lymphoma in the breast. AJR Am J Roentgenol 185:199–202

Fatterpekar GM, Mukherji SK, Rajgopalan P, Lin Y, Castillo M (2004) Normal age-related signal changes in the laryngeal cartilages. Neuroradiology 46:678–681

Glazer GM, Gross BH, Quint LE, Francis IR, Bookstein FL, Orringer MB (1985) Normal mediastinal lymph nodes: number and size according to American Thoracic Society mapping. AJR Am J Roentgenol 144:261–265

Hermans R, Pameijer FA, Mancuso AA, Parson JT, Mendenhall WM (2000) Laryngeal and hypopharyngeal squamous cell carcinoma: can follow-up CT after definitive radiation therapy be used to detect local failure earlier than clinical examination alone? Radiology 214:683–687

Hirsch RJ, Yousem DM, Loevner LA, Montone KT, Chalian AA, Hayden RE, Weinstein GS (1997) Synovial sarcomas of the head and neck: MR findings. AJR Am J Roentgenol 169:1185–1188

Kitamoto Y, Hasegawa M, Ishikawa H, Saito J, Yamakawa M, Kojima M, Nakano T (2003) Mucosa-associated lymphoid tissue lymphoma of the esophagus: a case report. J Clin Gastroenterol 36:414–416

Kraus DH, Pfister DG, Harrison LB, Shah JP, Spiro RH, Armstrong JG, Fass DE, Zelefsky M, Schantz SP, Weiss MH (1994) Larynx preservation with combined chemotherapy and radiation therapy in advanced hypopharyngeal cancer. Otolaryngol Head Neck Surg 111:31–37

Kraus DH, Zelefsky MJ, Brock HA, Huo J, Harrison LB, Shah JP (1997) Combined surgery and radiation therapy for squamous cell carcinoma of the hypopharynx. Otolaryngol Head Neck Surg 116:637–641

Mamelle G, Richard J, Luboinski B, Schwaab F, Eschwege F, Micheau C (1986) Synovial sarcoma of the head and neck: an account of four cases and review of the literature. Eur J Surg Oncol 12:347–349

Matsuki A, Nishimaki T, Suzuki T, Kanda T, Hatakeyama K (1999) Esophageal mucoepidermoid carcinoma containing signet-ring cells: three case reports and a literature review. J Surg Oncol 71:54–57

Million RR (1994) Pharyngeal walls, pyriform sinus, postcricoid pharynx. In: Million RR (ed) Management of head and neck cancer. JB Lippincott, Philadelphia, pp 502–532

Miyazaki T, Kato H, Masuda N, Nakajima M, Manda R, Fukuchi M, Tsukada K, Kojima M, Nakajima T, Kuwano H (2004) Mucosa-associated lymphoid tissue lymphoma of the esophagus: case report and review of the literature. Hepatogastroenterology 51:750–753

Mouret P (1999) Liposarcoma of the hypopharynx. A case report and review of the literature. Rev Laryngol Otol Rhinol 120:39–42

Mukherji SK, Mancuso AA, Kotzur IM, Mendenhall WM, Kubilis PS, Tart RP, Lee WR, Freeman D (1994) Radiologic appearance of the irradiated larynx. Part I. Expected changes. Radiology 183:141–148

Mukherji SK, Mancuso AA, Kotzur IM, Mendenhall WM, Kubilis PS, Tart RP, Freeman D, Lee WR (1994) Radiologic appearance of the irradiated larynx. Part II. Primary site response. Radiology 183:149–154

Munoz A, Ramos A, Ferrando J et al (1993) Laryngeal carcinoma: sclerotic appearance of the cricoid and arytenoids cartilage – CT-pathological correlation. Radiology 189:433–437

Nowak B, Di Martino E, Janicke S, Cremerius U, Adam G, Zimny M, Reinartz P, Bull U (1999) Diagnostic evaluation of malignant head and neck cancer by F-18-FDG PET compared to CT/MRI. Nuklearmedizin 38:312–318

Pameijer FA, Mancuso AA, Mendenhall WM, Parson JT, Mukherji SK, Hermans R, Kubilis PS (1998) Evaluation of pretreatment computed tomography as a predictor of local control in T1/T2 pyriform sinus carcinoma treated with definitive radiotherapy. Head Neck 20:159–168

Prehn RB, Pasic TR, Harari PM, Brown WD, Ford CN (1998) Influence of computed tomography on pretherapeutic tumor staging in head and neck cancer patients. Otolaryngol Head Neck Surg 119:628–633

Quint L, Glazer G, Orringer M (1985) Esophageal imaging by MR and CT: study of normal anatomy and neoplasms. Radiology 156:727–731

Rangheard AS, Vanel D, Viala J, Schwaab G, Casiraghi O, Sigal R (2001) Synovial sarcomas of the head and neck: CT and MR imaging findings of eight patients. AJNR Am J Neuroradiol 22:851–857

Reece GP, Schusterman MA, Miller MJ, Kroll SS, Robb GL, Baldwin BJ, Luethcke DR (1995) Morbidity and functional outcome of free jejunal transfer reconstruction for circumferential defects of the pharynx and cervical esophagus. Plast Reconstr Surg 96:1307–1316

Righi PD, Kelley DJ, Ernst R, Deutsch MD, Gaskill-ShipleyM, Wilson KM, Gluckman JL (1996) Evaluation of the prevertebral muscle invasion by squamous cell carcinoma. Can computed tomography replace open neck exploration? Arch Otolaryngol Head Neck Surg 122:660–663

Robbins KT, Kumar P, Wong FS, Hartsell WF, Flick P, Palmer R, Weir AB, Neill HB, Murry T, Ferguson R, Hanchett C, Vieira F, Busch A, Howell SB (2000) Targeted chemoradiation for advanced head and neck cancer: analysis of 213 patients. Head Neck 22:687–693

Roychowdhury S, Loevner LA, Yousem DM, Chalian A, Montone KT (2000) MR imaging for predicting neoplastic invasion of the cervical esophagus. AJNR Am J Neuroradiol 21:1681–1687

Saleh E, Mancuso AA, Stringer S (1993) Relative roles of computed tomography and endoscopy for determining the inferior extent of pyriform sinus carcinoma: correlative histopathologic study. Head Neck 15:44–52

Samant S, Kumar P, Wan J, Hanchett C, Vieira F, Murry T, Wong FS, Robbins KT (1999) Concomitant radiation therapy and targeted cisplatin chemotherapy for the treatment of advanced pyriform sinus carcinoma: disease control and preservation of organ function. Head Neck 21:595–601

Schmalfuss IM, Mancuso AA, Tart R (2000) Postcricoid region and cervical esophagus: normal appearance at CT and MR imaging. Radiology 214:237–246

Schuller DE (1980) Limitations of the pectoralis major myocutatenous flap in head and neck cancer reconstruction. Arch Otolaryngol 106:709–714

Surkin MI, Lawson W, Biller HF (1984) Analysis of the methods of pharyngoesophageal reconstruction. Head Neck 6:953–970

Takahara Y, Kawashima H, Han YS, Sugimura N, Nakatani T, Tanaka K, Hino M (2005) Primary mucosa-associated lymphoid tissue (MALT) lymphoma of the urinary bladder. Hinyokika Kiyo 51:45–48

Thabet HM, Sessions DG, Gado MH, Gnepp DA, Harvey JE, Talaat M (1996) Comparison of clinical evaluation and computed tomographic diagnostic accuracy for tumors of the larynx and hypopharynx. Laryngoscope 106:589–594

Tom LW, Wurzel JM, Wetmore RF, Lowry LD (1981) Mucoepidermoid carcinoma of the hypopharynx. Otolaryngol Head Neck Surg 89:753–757

Uppaluri R, Sunwoo JB (2005) Neoplasms of the hypopharynx and cervical esophagus. In: Cummings CW (ed) Otolaryngology – head and neck surgery. Elsevier Mosby, Philadelphia; pp 1899–1859

Weber RS, Marvel J, Smith P, Hankins P, Wolf O, Goepfert H (1993) Paratracheal lymph node dissection for carcinoma of the larynx, hypopharynx, and cervical esophagus. Otolaryngol Head Neck Surg 108:11–17

Wenig BL, Ziffra KL, Mafee MF, Schild JA (1995) MR imaging of squamous cell carcinoma of the larynx and hypopharynx. Otolaryngol Clin North Am 28:6009–6019

Yeager VL, Lawson C, Archer CR (1982) Ossification of laryngeal cartilages as it relates to computed tomography. Invest Radiol 17:11–19.

Yousem DW, Tufano RP (2002) Laryngeal imaging. Magn Reson Imaging Clin N Am 10:451–465

Zbären P, Begger M, Laeng H (1996) Pretherapeutic staging of laryngeal cancer: clinical findings, computed tomography and magnetic resonance imaging versus histopathology. Cancer 77:1263–1273

Zbären P, Egger C (1997) Growth pattern of piriform sinus carcinomas. Laryngoscope 107:511–518

6 Neoplasms of the Oral Cavity

Marc Keberle

CONTENTS

6.1 Anatomy

Predominantly, oral cavity lesions are clinically apparent. Except for important information on the differential diagnosis, cross-sectional imaging provides the clinician with the crucial pretherapeutic information on deep tumor infiltration. In this regard, the clinician needs to know exactly which anatomic structures (Figs. 6.1–6.6) are involved.

The oral cavity is the most anterior part of the aerodigestive tract. Its borders are the lips ventrally, the mylohyoid muscle caudally, the gingivobuccal regions laterally, the circumvallate papillae and the anterior tonsillar pillar dorsally, and the hard palate cranially. The center of the oral cavity is filled out by the tongue.

M. Keberle, MD
Diagnostic Radiology, Medizinische Hochschule Hannover, Carl-Neuberg-Str. 1, 30625 Hannover, Germany

6.1.1 The Floor of the Mouth

The floor of the mouth is considered the space between the mylohyoid muscle and the caudal mucosa of the oral cavity. The mylohyoid muscle has the form of a hammock which is attached to the mandible ventrally and laterally on both sides but with a free dorsal margin. Coronal planes nicely demonstrate the anatomy of the mylohyoid as well as the geniohyoid muscles (Figs. 6.4, 6.5). The geniohyoid muscles are paired sagittally orientated slender muscles on the superior surface of the mylohyoid muscle. In the median, they arise from the inner surface of the mandible and pass dorsally to insert onto the anterior surface of the hyoid bone. Above these muscular landmarks is the primarily fat-filled bilateral sublingual space. It comprises the following important paired structures: the sublingual gland, the hyoglossus muscle, the lingual artery, vein, and nerve, Wharton's (submandibular) duct, and dorsally the tip of the submandibular gland as it surrounds the dorsal margin of the mylohyoid muscle. Anatomically noteworthy is that in the sagittal plane the hyoglossus muscle separates Wharton's duct and the hypoglossal and lingual nerves, which course laterally, from the lingual artery and vein, which lie medially (compare Figs. 6.1 and 6.5).

6.1.2 The Tongue

While the posterior third of the tongue – located dorsally of the circumvallate papillae – forms part of the oropharynx, the two anterior thirds of the tongue belong to the oral cavity. The tongue contains a complex mixture of various intrinsic and extrinsic

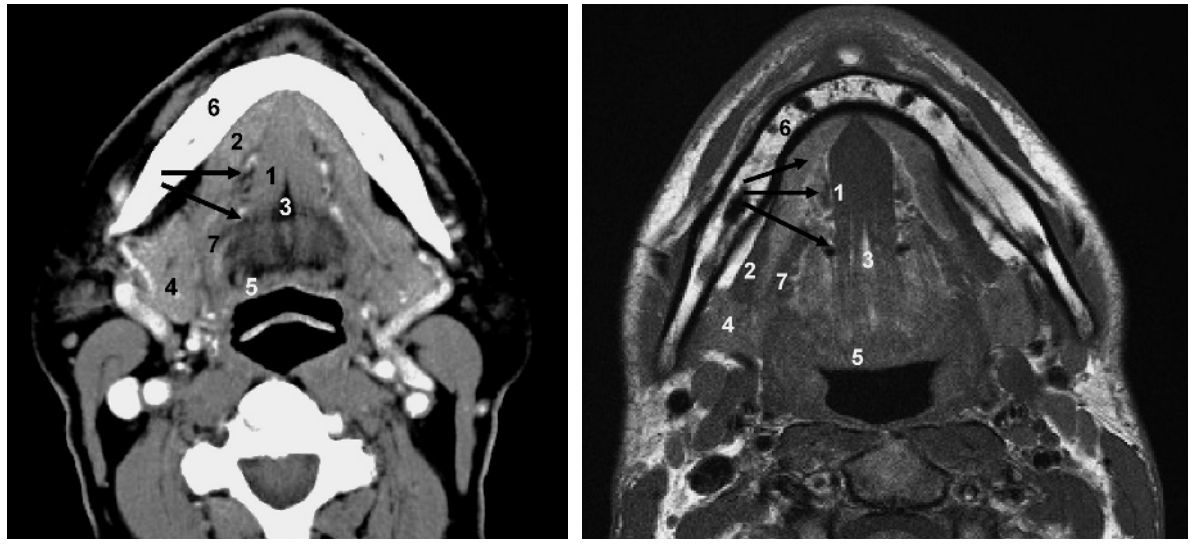

a b

Fig. 6.1a,b. Axial CT (**a**) and MRI (**b**) of the floor of the mouth. *1*, geniohyoid muscle; *2*, mylohyoid muscle; *3*, fatty lingual septum; *4*, submandibular gland; *5*, base of the tongue; *6*, mandible; *7*, hyoglossus muscle; *arrows*, sublingual (fat) space with lingual artery and vein

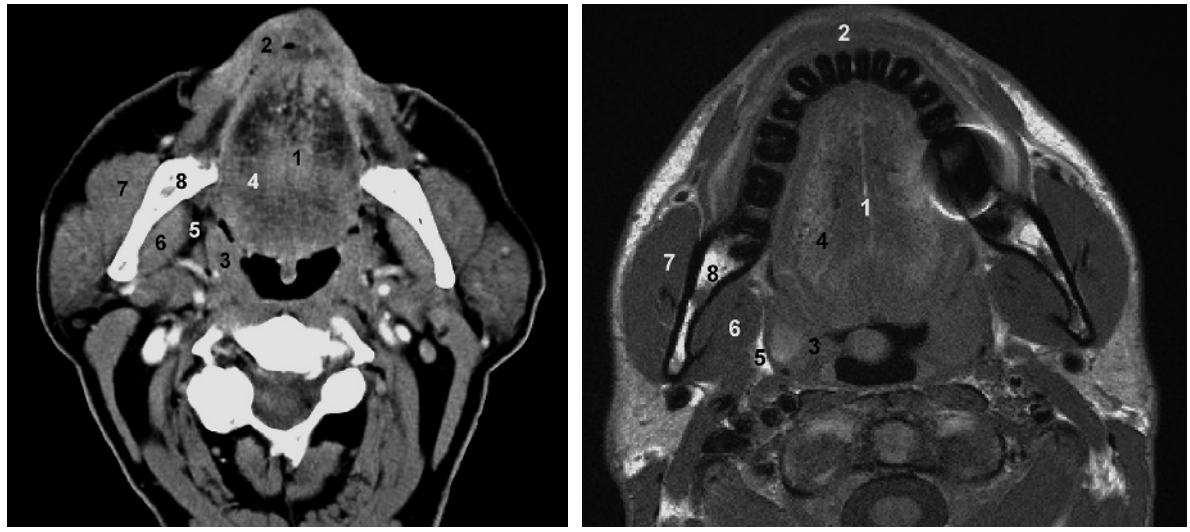

a b

Fig. 6.2a,b. Axial CT (**a**) and MRI (**b**) at the level of the tongue. *1*, tongue with fatty lingual septum; *2*, (lower) lip; *3*, palatopharyngeal muscles and palatopharyngeal arch; *4*, intrinsic lingual muscles fibers; *5*, parapharyngeal fat space; *6*, medial pterygoid muscle; *7*, masseter muscle; *8*, mandible

muscles. Intrinsic muscles are made up by longitudinal, transverse, vertical, and oblique fibers which are not connected with any structure outside the tongue (Figs. 6.2, 6.4, and 6.5). The extrinsic muscles have their origin external to the tongue (Figs. 6.1 and 6.4): the genioglossus (chin), hyoglossus (hyoid bone), and styloglossus (styloid process) muscles. Both intrinsic and extrinsic muscles of the tongue receive their innervation from the (XII) hypoglossus nerve. Sensory fibers are carried by the lingual nerve, a branch of the (V3) mandibular nerve (Fig. 6.6). The tongue is sagittally divided in two halves by a fatty midline septum (Figs. 6.1–6.5).

6.1.3 The Lips and Gingivobuccal Regions

Externally, the lips are covered by keratinizing stratified squamous epithelium, and internally, by nonke-

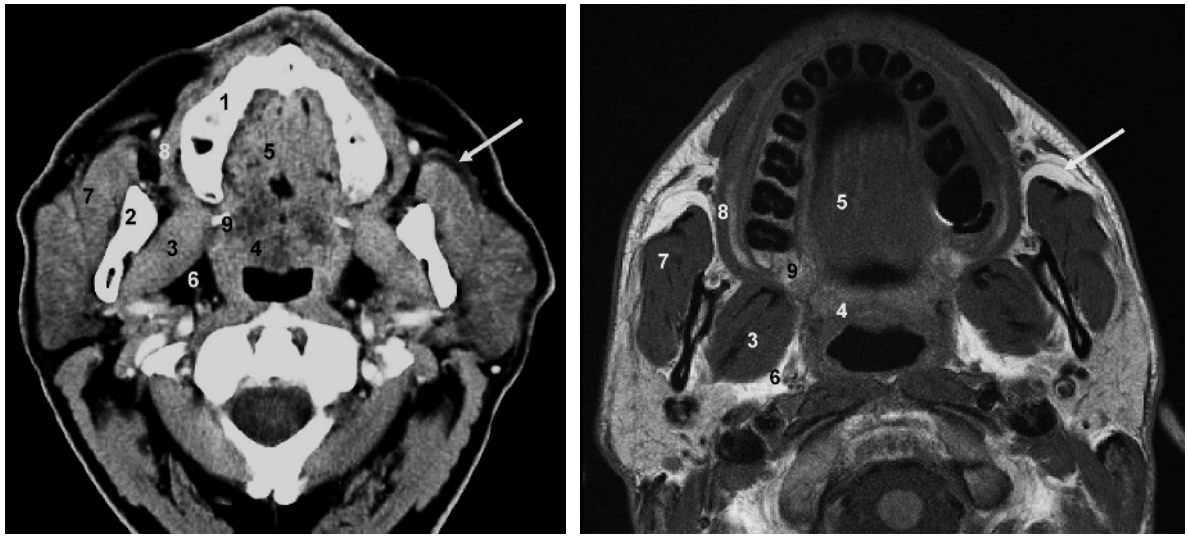

Fig. 6.3a,b. Axial CT (**a**) and MRI (**b**) at the level of the maxilla. *1*, maxilla; *2*, mandible; *3*, lateral pterygoid muscle; *4*, soft palate; *5*, tongue; *6*, parapharyngeal fat space; *7*, masseter muscle; *8*, buccinator muscle; *9*, area of the retromolar trigone (with bony pterygoid process on CT); *arrows*, (Stensen's) parotid duct

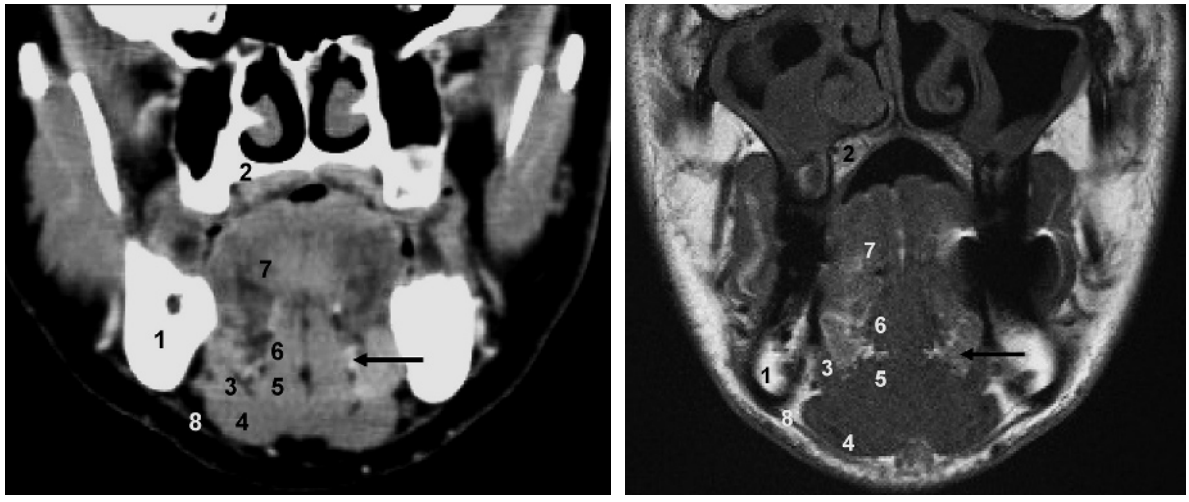

Fig. 6.4a,b. Coronal CT (**a**) and MRI (**b**) at more anterior aspects of the oral cavity. *1*, mandible; *2*, (maxillary) hard palate with a tiny nerval canal; *3*, mylohyoid muscle; *4*, anterior belly of digastric muscle; *5*, geniohyoid muscle; *6*, genioglossus muscle; *7*, intrinsic lingual muscles; *8*, submandibular fat space; *arrows*, sublingual fat space with lingual artery and vein

ratinizing stratified squamous mucosa. The vestibule of the mouth separates lips and cheeks from the alveolar processes of the mandible and maxilla. The gingiva is the mucosa on both the lingual and the buccal aspects of the alveolar processes. The junction of the gingival with the buccal mucosa is called gingivobuccal region. At the level of the second maxillary molar tooth Stensens' (parotid) duct opens within the buccal mucosa (Fig. 6.3). Moreover, minor salivary glands are relatively frequent in the gingivobuccal regions. Dorsally, the vestibules open into the dorsal part of the oral cavity.

6.1.4 The Hard Palate and the Region of the Retromolar Trigone

While the soft palate is part of the oropharynx, the mucosal layer beneath the hard palate belongs to the oral cavity. There are several openings for palatine nerves piercing the hard palate (compare Figs. 6.4 and 6.6). The strategic region posterior to the last maxillary molar tooth is called the retromolar trigone (Fig. 6.3). The retromolar trigone has a connection to the buccinator space laterally, to the anterior tonsillar

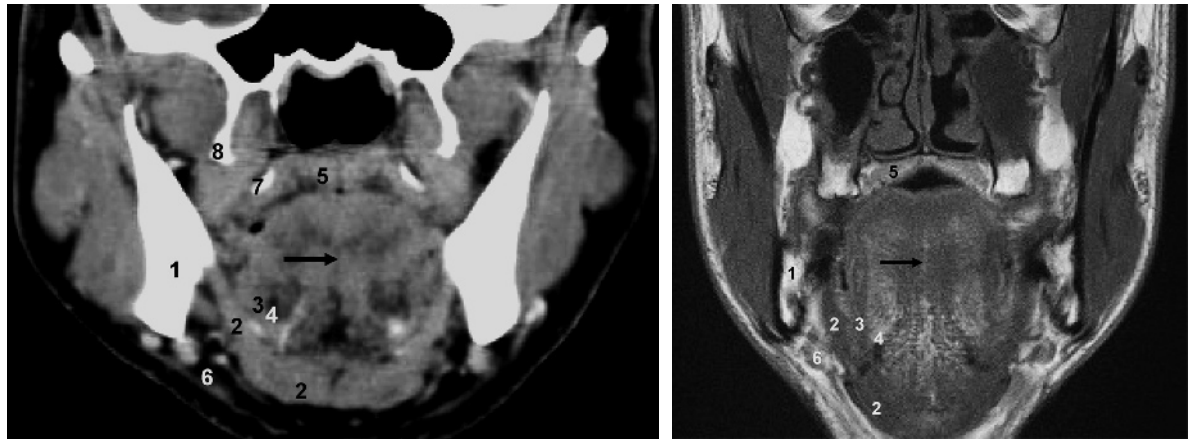

a b

Fig. 6.5a,b. Coronal CT (**a**) and MRI (**b**) at more posterior aspects of the oral cavity. *1*, mandible; *2*, mylohyoid muscle; *3*, hyoglossus muscle; *4*, sublingual fat space (with lingual artery and vein); *5*, soft (on CT) and hard (on MRI) palate; *6*, submandibular fat space; *7*, medial pterygoid process; *8*, lateral pterygoid process; *arrow*, fatty lingual septum

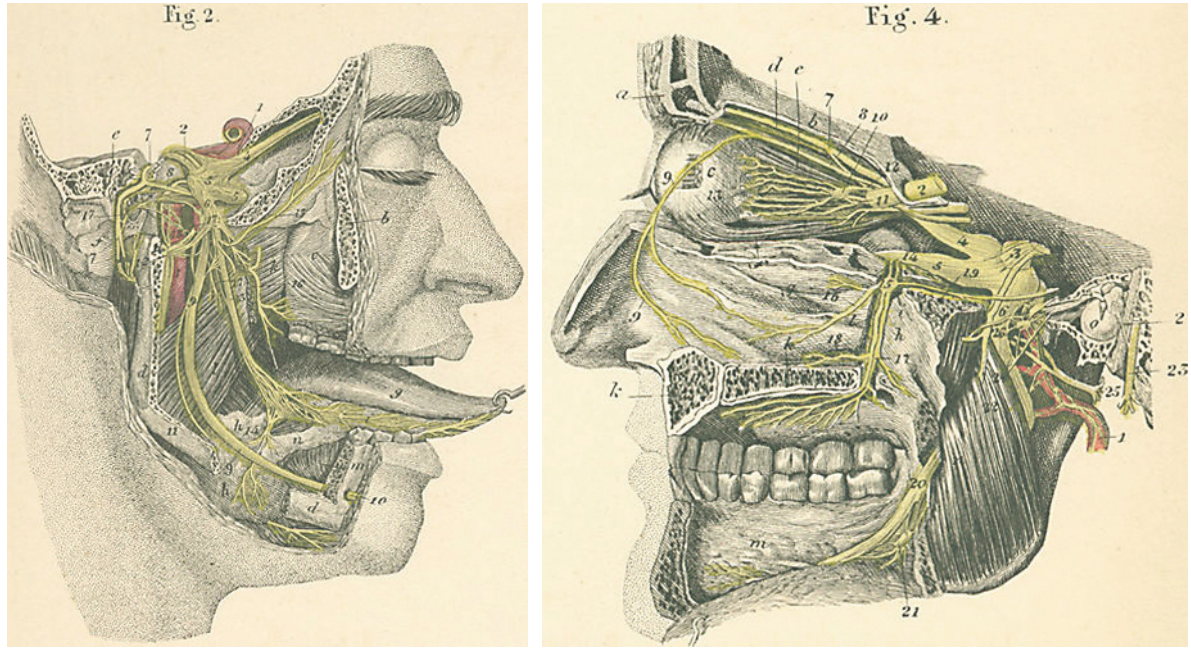

a b

Fig. 6.6a,b. Anatomic views of the trigeminal nerve (from Bergman and Afifi 2002, with permission). **a** *a*, Greater wing of the sphenoid bone; *b*, zygomatic bone; *c*, maxilla; *d*, mandible; *e*, petrous part of temporal bone; *f*, mastoid process; *g*, tongue; *h*, submandibular gland; *i*, sublingual gland; *k*, medial pterygoid muscle, *l*, lateral pterygoid muscle; *m*, genioglossus muscle; *n*, hyoglossus muscle. *1*, internal carotid artery; *2*, trigeminal nerve; *3*, trigeminal ganglion; *4*, trigeminal nerve (V/1, ophthalmic division); *5*, trigeminal nerve (V/2, maxillary division); *6*, trigeminal nerve (V/3, mandibular division); *7*, facial nerve; *8*, great superficial petrosal nerve; *9*, inferior alveolar nerve; *10*, mental nerve; *11*, mylohyoid nerve; *12*, anterior auricular nerve (with middle meningeal artery); *13*, lingual nerve; *14*, submandibular ganglion; *15*, deep temporal nerve; *16*, buccinator nerve; *17*, chorda tympani; *18*, internal carotid plexus (sympathetic nerves). **b** *a*, Frontal bone (frontal sinus); *b*, roof of the orbit (frontal bone); *c*, ocular bulb; *d*, M. levator palpbrae superioris; *e*, M. ocular superior rectus; *f*, M. ocular inferior rectus; *g*, wall of the nasal cavity; *h*, pterygoid process; *i*, sphenopalatine foramen; *k*, hard palate; *l*, pterygopalatine canal; *m*, mandible; *n*, medial pterygoid muscle; *o*, tympanic membrane (with an auditory bone). *1*, maxillary artery; *2*, optic nerve; *3*, trigeminal nerve with trigeminal ganglion; *4*, trigeminal nerve (V/1, ophthalmic division); *5*, trigeminal nerve (V/2, maxillary division); *6*, trigeminal nerve (V/3, mandibular division); *7*, frontal nerve; *8*, nasal nerve; *9*, ethmoidal nerve; *10*, ciliary ganglion; *11*, ciliary ganglion, short ciliary nerves; *12*, ciliary ganglion, long ciliary nerves; *13*, ciliary ganglion and ciliary nerves; *14*, pterygopalatine nerves; *15*, pterygopalatine ganglion; *16*, posterior superior nasal nerves; *17*, pterygopalatine nerve; *18*, posterior inferior nasal nerves; *19*, greater superficial petrosal nerve; *20*, lingual nerve; *21*, submandibular ganglion; *22*, pterygoid nerve; *23*, facial nerve in the facial canal; *24*, chorda tympani; *25*, anterior auricular nerve; *26*, otic ganglion

pillar (part of the oropharynx), the mandible, and to the pterygomandibular space dorsally (and this way to the anterior parts of the parapharyngeal space and the skull base cranially), and to the palate medially.

6.1.5 Lymphatic Drainage

The lips predominantly drain to the submental and/or submandibular (level 1) lymph nodes. The major lymphatic drainage of the floor of the mouth is to the submental, submandibular, and/or internal jugular nodes (levels 1 and 2). The oral tongue drains mainly to the submandibular and internal jugular nodes (levels 1 and 2), often with bilateral involvement in case of a carcinoma of the tongue.

6.2 Preferred Imaging Modalities

In children, due to radiation exposure, ultrasound and MRI are the methods of first choice. In contrast to more cranial parts of the oral cavity and of the oropharynx, the floor of the mouth, the base of the tongue, and the neck can be evaluated with ultrasound (compare Figs. 6.11 and 6.19). High frequency transducers should be used. For the evaluation of the most ventral part of the floor of the mouth the transducer has to be tilted accordingly. Contrast-enhanced MRI offers several diagnostic advantages over ultrasound; it allows covering of the entire oral cavity and has a higher diagnostic accuracy, especially regarding the exact evaluation of the extension and differential diagnosis of a lesion.

In adults, CT and MRI are the most frequently used imaging modalities. The administration of intravenous contrast agent is a rule. Only in rare circumstances, such as the detection of calculi, an initial (or sole) native CT may be necessary (or sufficient). The most frequent diagnostic problem of CT are dental filling artifacts, whereas the interpretation of MRI is most frequently limited by motion artifacts due to swallowing. As a result of these diagnostic drawbacks, one can recommend using CT for lesions which are primarily located in the floor of the mouth and the base of the tongue because the latter structures can be scanned without disturbing artifacts from dental fillings. On the other hand, MRI can generally be recommended for lesions predominantly involving the tongue and the palate. However, to specifically answer the question of bone involvement (hard palate, mandible) CT is generally regarded to be slightly superior over MRI so that sometimes both methods add up to the final diagnosis.

6.3 Pathology

6.3.1 Benign Lesions

6.3.1.1 Congenital Lesions

6.3.1.1.1 Vascular Malformations

Although vascular malformations are predominantly present at birth, they can manifest with symptoms later on. Generally, vascular malformations tend to involve muscle and bone (Figs. 6.7 and 6.8). They usually grow slowly, however, rapid growth can be linked with endocrine changes during life. In contrast to hemangiomas, vascular malformations do not involute during childhood (Mulliken 1988) (Figs. 6.7 and 6.8). Main therapeutic options are steroid injection, embolization, laser therapy, and/or surgical resection (if possible). Based on the predominant type of anomalous vessel involved, capillary (e.g. nevus flammeus in Sturge-Weber syndrome), venous, or arterial malformations are distinguished (Baker et al. 1993). In rare circumstances, they may appear as "lymphatic" malformations which can also be secondary after infection, tumor, or trauma, such as surgery (Kennedy 1989, Smoker 2003).

In the oral cavity, venous malformations are the most frequent vascular malformations (Figs. 6.7 and 6.8). In contrast to arterial malformations, these are slow-flow malformations. On CT, they are usually isodense to muscle (however phleboliths are characteristic) and demonstrate variable contrast enhancement. On MR they are isointense to muscle on T1-weighted images but quite hyperintense on T2; contrast enhancement is usually inhomogeneous, often with rather strongly enhancing components (Fig. 6.7). Arterial malformations are high-flow lesions with tortuous and enlarged vessels and usually show flow-voids (Baker et al. 1993). Some vascular malformations comprise both slow- and high-flow components. In lymphatic malformations, on the other hand, only septae and/or cyst walls enhance.

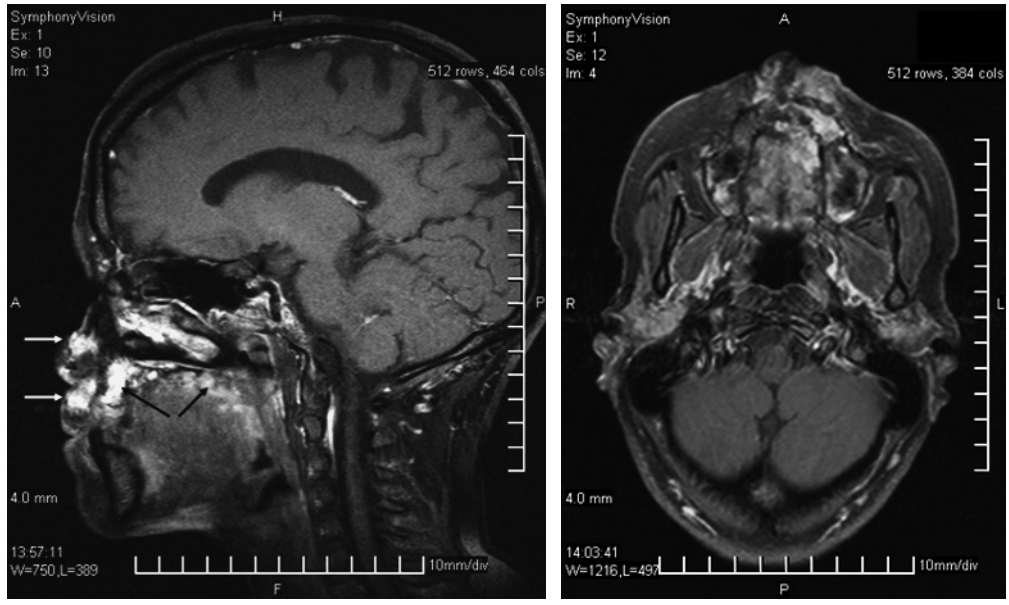

a b

Fig. 6.7a,b. MRI of a venous vascular malformation in a 25-year-old man. Fat-saturated sagittal (**a**) and axial (**b**) post-contrast T1-weighted images reveal an inhomogeneous rather strongly contrast enhancing mass at the upper lip, hard and soft palate, maxilla, and the nose

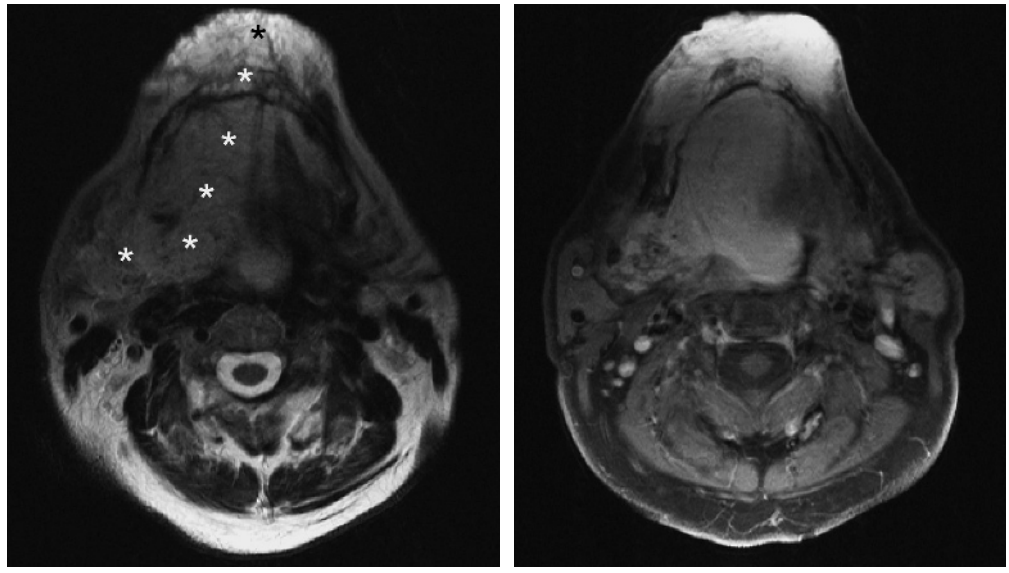

a b

Fig. 6.8a,b. MRI of a venous malformation with hardly any flow voids in a 65-year-old male. The lesion shows diffuse extension through the mandible and the mylohyoid muscle into the lower lip and the submandibular region. Moreover, there is midline crossing and extension to the base of the tongue. On T2, the lesion is quite hyperintense (**a**) and on the post-contrast image there is a rather homogeneous strong contrast enhancement (**b**)

6.3.1.1.2 (Epi-)Dermoid Cysts

When epithelial remnants become enclaved during early midline closure of the first and second branchial arches, (epi-)dermoid cysts can be the result (King et al. 1994). These lesions occur in or close to the midline (Figs. 6.9 and 6.10), both cranial and caudal to the mylohyoid muscle. Coronal or sagittal slices are useful to show their relation to the latter muscle because the surgical approaches differ (Vogl et al. 1993).

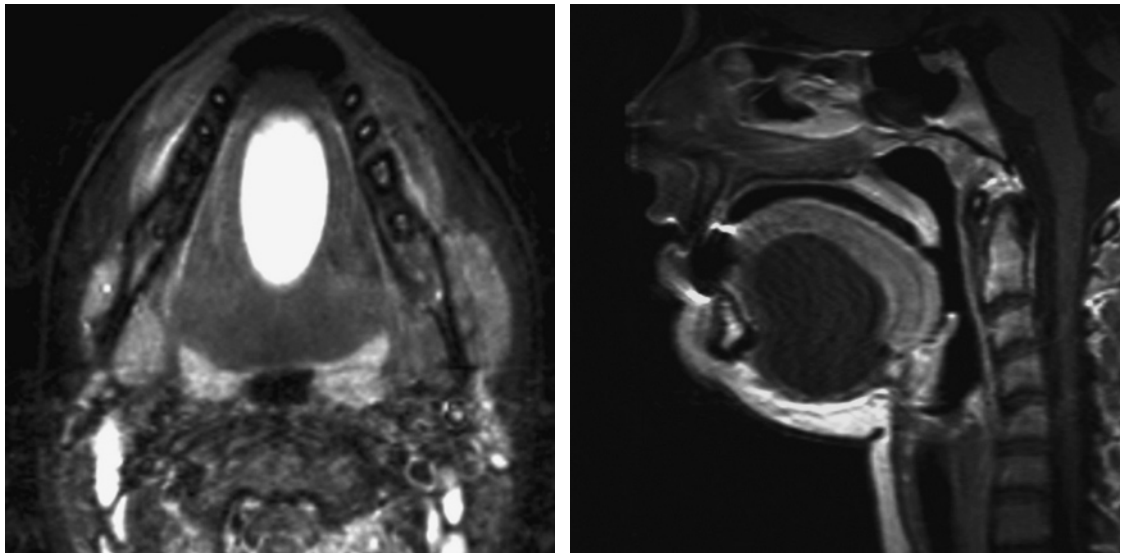

Fig. 6.9a,b. MRI of an epidermoid of the floor of the mouth and the tongue in a 21-year-old female. The lesion is strictly located in the midline. On T2, it presents well delineated with a very bright homogeneous signal (**a**). On post-contrast T1, there is no enhancement – the sagittal image nicely shows the relation of the epidermoid to the more caudal mylohyoid muscle. (Courtesy of Nicole Freling, MD, Amsterdam, The Netherlands)

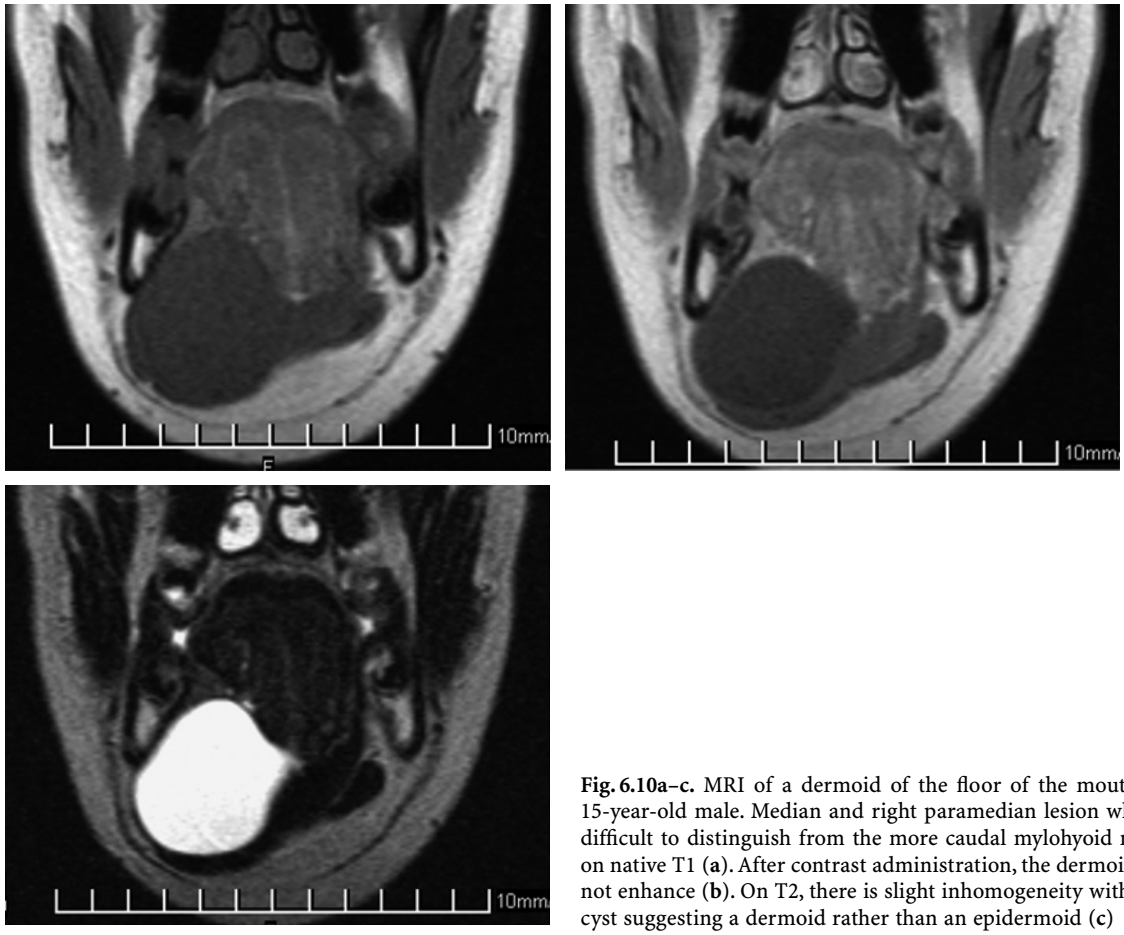

Fig. 6.10a–c. MRI of a dermoid of the floor of the mouth in a 15-year-old male. Median and right paramedian lesion which is difficult to distinguish from the more caudal mylohyoid muscle on native T1 (**a**). After contrast administration, the dermoid does not enhance (**b**). On T2, there is slight inhomogeneity within the cyst suggesting a dermoid rather than an epidermoid (**c**)

Fatty contents (either as fat drops or as a fat-fluid level) are pathognomonic for dermoid cysts (Fig. 6.10). However, without fatty contents a differentiation is not possible (Koeller et al. 1999). In case of an epidermoid cyst (Fig. 6.9), an entirely fluid-filled lesion is visible (CT: <20 HU; MR: hypointense signal on T1 and hyperintense on T2). A slight rim enhancement around these cysts can sometimes be noted.

In contrast to epidermoid cysts, dermoid cysts have malignant potential (King et al. 1994).

6.3.1.1.3 Lingual Thyroid

If the thyroid gland does not descend from the foramen cecum, the midline dorsum of the tongue is the most common location for an ectopic thyroid gland (Fig. 6.11), whereas thyroglossal duct cysts predominantly occur at the level of the hyoid bone or below (Douglas and Baker 1994). Mostly, women are affected. Lingual thyroids are usually small and discovered incidentally. In larger symptomatic cases surgery is the first therapeutical option. However, in more than 50% of the patients no other functioning thyroid tissue is present, so that complete resection may be problematic.

Comparable to a thyroid gland in its normal location, a lingual thyroid is hyperdense on precontrast CT. On precontrast MRI, it may be only slightly hyperintense on both T1- and T2-weighted images. Thyroid tissue, generally, shows strong contrast enhancement (Johnson and Coleman 1989).

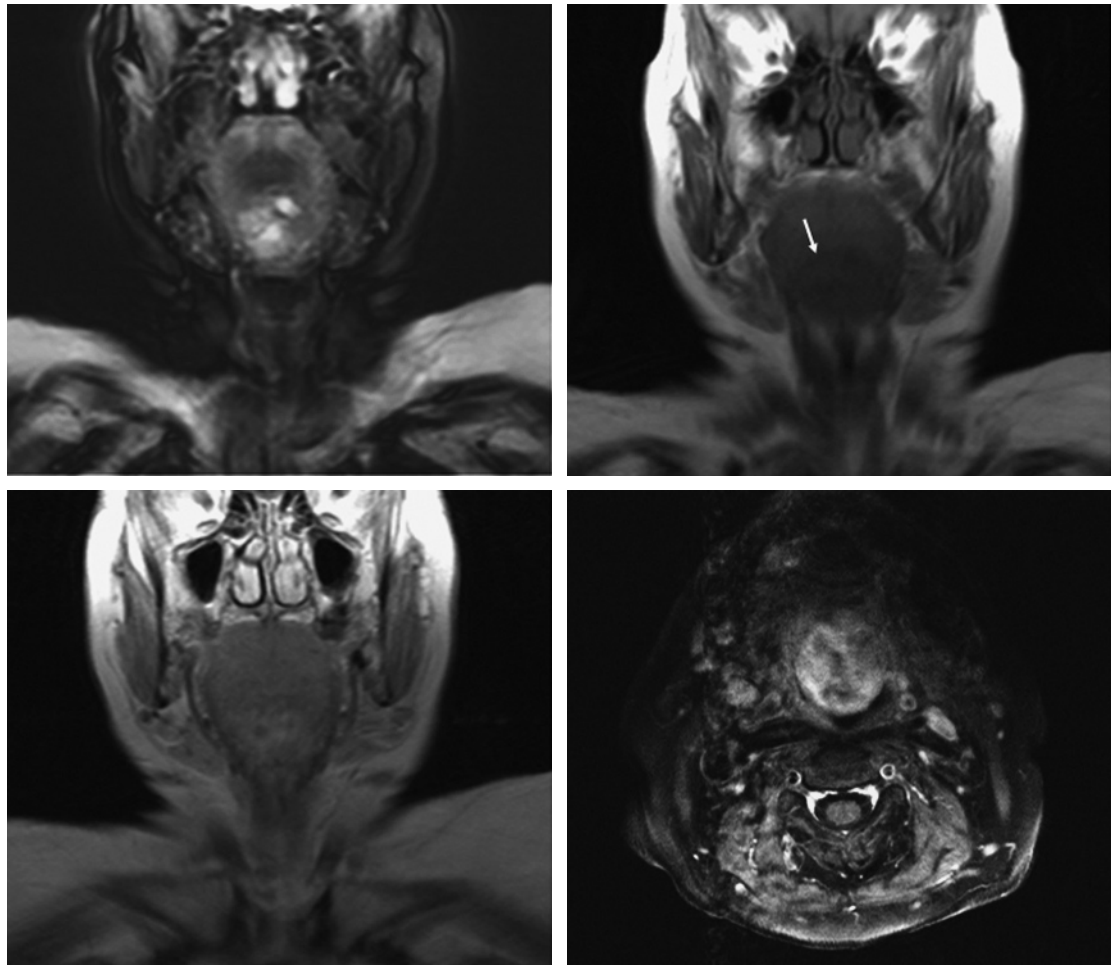

Fig. 6.11a–d. MRI of a 65-year-old female with a large lingual thyroid affecting the tongue as well as the floor of the mouth. The T2-weighted image (**a**) reveals an inhomogeneous mass with some very hyperintense cysts. On the native T1-weighted image, the mass is slightly hypointense compared to the tongue (**b**). After contrast agent has been given, the respective coronal (**c**) and fat-saturated axial (**d**) images show irregular rather strong enhancement of the lesion. Histology after laser resection revealed a lingual thyroid with regressive cystic changes (goitre). The lesion has been present since childhood but enlarged after orthotopic strumectomy

6.3.1.2 Inflammatory Conditions

6.3.1.2.1 Cervical Phlegmon and Abscess (and Sialolithiasis)

Dental infection or ductal obstruction of the salivary glands are the main causes of oral inflammations, both mainly involving the sublingual and/or submandibular spaces (Smoker 2003; Yousem et al. 2000). Phlegmons are diffuse inflammatory processes which in contrast to abscesses do not contain central necrotic components and/or air. Native CT and MRI show edematous changes, contrast enhancement is diffuse. If Wharton's duct is obstructed (e.g. in the case of sialolithiasis) the respective submandibular gland as well as the duct can be enlarged (Fig. 6.12). Either native CT or a bone-window setting of a post-contrast CT best unveil hyperdense calculi which may be missed in a soft-tissue window setting after contrast enhancement or with other modalities. A clinically important issue is the exclusion of osteomyelitis (Fig. 6.13). In mild cases, CT is known to be superior in the evaluation of the mandibular cortex, whereas MRI appears better regarding medullar bone involvement.

6.3.1.2.2 Ranulas

In the case of obstruction of the duct of the sublingual gland patients can present with a ranula, a true epithelium-lined "mucus retention cyst". They are located above the mylohyoid muscle, fill out the sublingual space and, thus, mostly have an oval configuration (Fig. 6.14). But they can also grow to an enormous size and then have a more roundish shape. In contrast to a "simple ranula", a ranula can present ruptured and extend dorsally (or caudally through gaps in the mylohyoid muscle) into the submandibu-

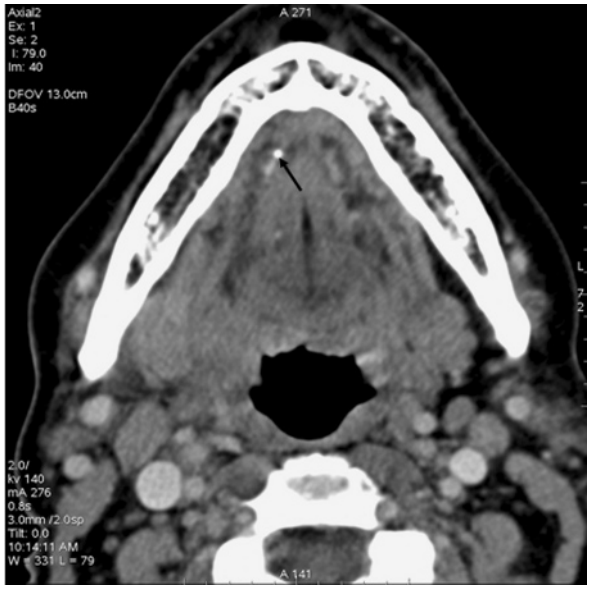

a

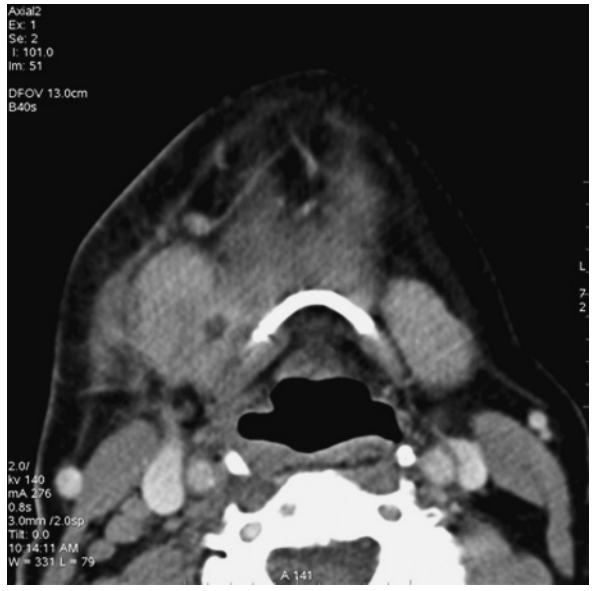

b

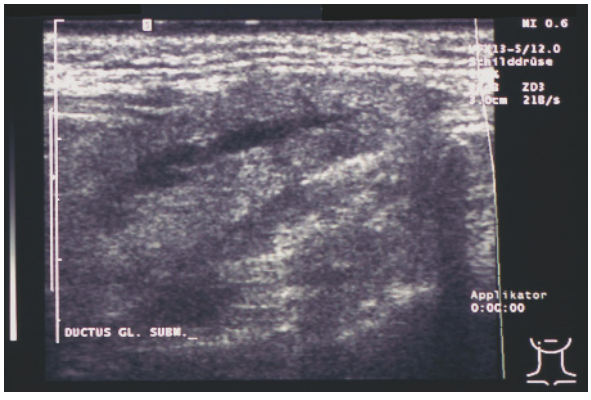

c

Fig. 6.12a–c. CT of a submandibular abscess due to an obstruction of Wharton's (submandibular) duct by a stone (female, 57 years). In the anterior right floor of the mouth, a small stone can be seen at the level of the aperture of the duct (**a**). The right submandibular duct is swollen and contains an abscess right at its tip behind the mylohyoid muscle (**b**); the surrounding fat contains inflammatory edematous streaks. An ultrasound image of the enlarged submandibular gland showing the dilated duct (**c**)

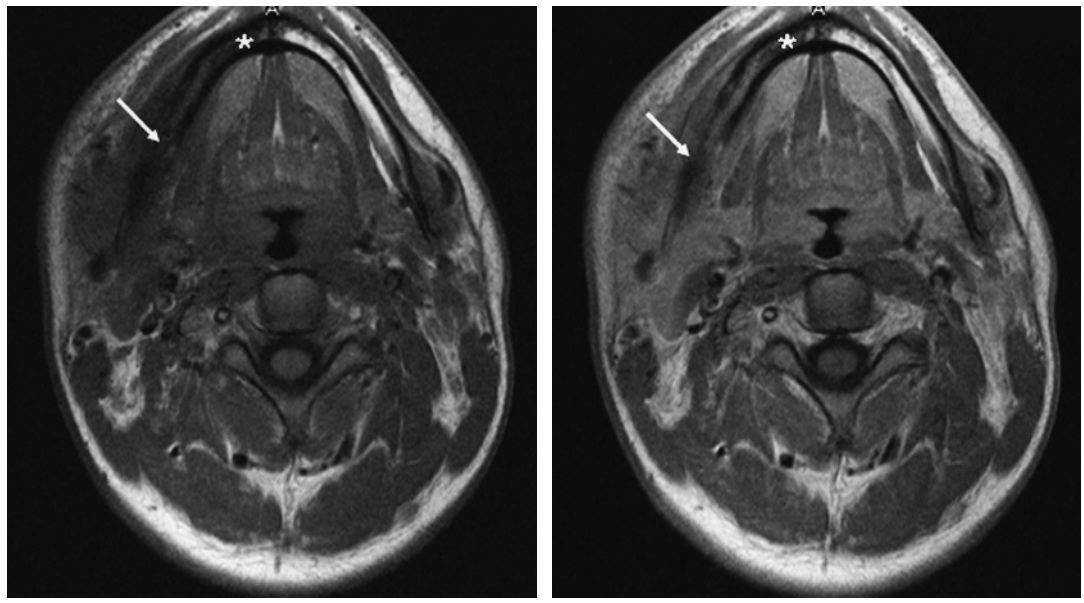

a b

Fig. 6.13a,b. Axial MRI of a 23-year-old man with multifocal osteomyelitis (Sapho-Syndrome). The pre-contrast (**a**) as well as the post-contrast (**b**) images show a diffuse (contrast enhancing) lesion within and on both sides of the mandible. The cortex is partly eroded (*arrow* on both images) and the bone marrow yields hypointense signal alterations due to inflammatory edema (*asterisk* on both images)

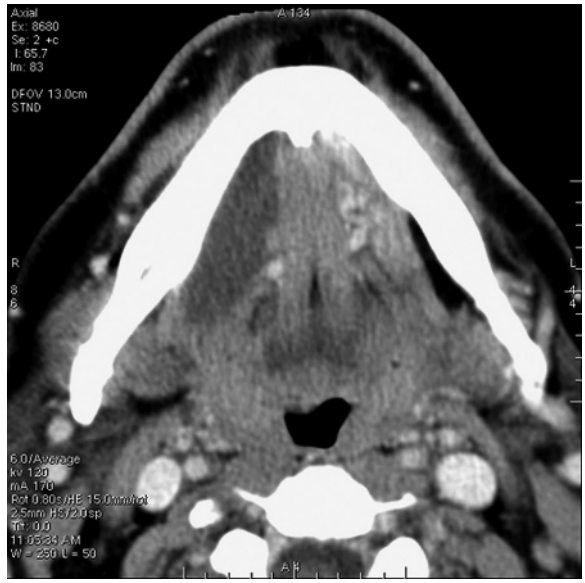

Fig. 6.14. CT of a 57-year-old male who noted a swelling at the right floor of the mouth. The typical simple ranula is hypodense (18 HU), well delineated and without contrast enhancement

lar space and then is called a diving or plunging ranula (Coit et al. 1987). The bulk of the latter typically lies – more posteriorly – medial to the submandibular gland with a typical anterior extension to the sublingual space (suggesting its sublingual origin).

On CT, ranulas present as hypodense, non-enhancing, thin-walled, solitary, paramedian lesions (Coit et al. 1987). Accordingly, on MR, ranulas have homogeneous high signal on T2 and low signal on T1. However, plunging ranulas, as these are pseudocysts, are to a various extent surrounded with granulation tissue so that a slight circular enhancement may be present on post-contrast images.

6.3.1.3 Benign Tumors

6.3.1.3.1 Pleomorphic Adenoma

In adults, pleomorphic adenomas are the most common benign neoplasms of the oral cavity. On histology, pleomorphic adenomas contain epithelial as well as fibromyxoid tissue, and with increasing size, there are often cystic changes, central necrosis and/or calcifications (Som and Brandwein 2003). As pleomorphic adenomas can originate from the sublingual glands as well as from minor salivary glands, these tumors can be found throughout the oral cavity. Complete resection is recommended because pleomorphic adenomas tend to reoccur.

The varying mixture of epithelial and fibromyxoid tissues as well as possible degenerative changes of this tumor result in their "pleomorphic" inhomogeneous

imaging appearance with a varying signal on T2 and varying contrast enhancement (especially concerning larger tumors) (Okahara et al. 2003; Keberle et al. 2005). In contrast to malignant tumors, pleomorphic adenomas show a rather slow growth pattern and are well circumscribed tumors (Fig. 6.15).

6.3.1.3.2 Lipoma

Other benign neoplasms are much rarer. Of all mesenchymal tumors, lipoma is the most common in the oral cavity (Smoker 2003). To some extent, lipomas can contain other tissues and present as fibro-, angio-, myxo-, or chondrolipomas. Lipomas occur virtually all over the oral cavity with the cheek as the most common location. Imaging features are pathognomonic with homogeneous low-density values of around –100 HU on CT, no contrast enhancement, and high signal intensity on T1-weighted MR images. Lipomas are clearly defined tumors, sometimes separated by thin septae and do not infiltrate neighboring anatomic structures.

6.3.1.3.3 Rhabdomyoma

In contrast to rhabdomyosarcomas, rhabdomyomas are benign tumors. They originate from striated muscle and, within the oral cavity, they have a predilection for the floor of the mouth and the tongue (Smoker 2003). In adults, rhabdomyomas mostly affect middle-aged men. The second age group is early childhood (usually during the first 2 years of life). Like lipomas, they do not infiltrate and, thus, complete resection is rarely a problem.

On both native CT and T1-weighted MRI rhabdomyomas have the density/intensity of muscle; slight enhancement is seen on post-contrast images. They are usually only slightly hyperintense on T2-weighted MR images.

6.3.1.3.4 Hemangiomas

Hemangiomas only occur in early childhood (Mulliken and Glowacki 1982), and in this age group they are the most common benign tumors. They are true neoplasms mostly containing endothelial and fibrous tissues. They grow rapidly, and usually involute by adolescence. Only if hemangiomas are gravely symptomatic or are cosmetically problematic, therapy e.g. with laser is performed rather than a "wait-and-see policy". In this regard, color Doppler or MRI may be useful tools in order to show high-flow lesions which are more amenable to laser therapy than low-flow lesions.

It is a diagnostic challenge and not always possible to differentiate hemangiomas from vascular malformations. In opposition to the latter, hemangiomas are usually well defined subcutaneous tumors, which do not infiltrate bone or muscle. Like vascular malformations, they are isointense on T1-weighted, rather hyperintense on T2-weighted MR images (Baker et

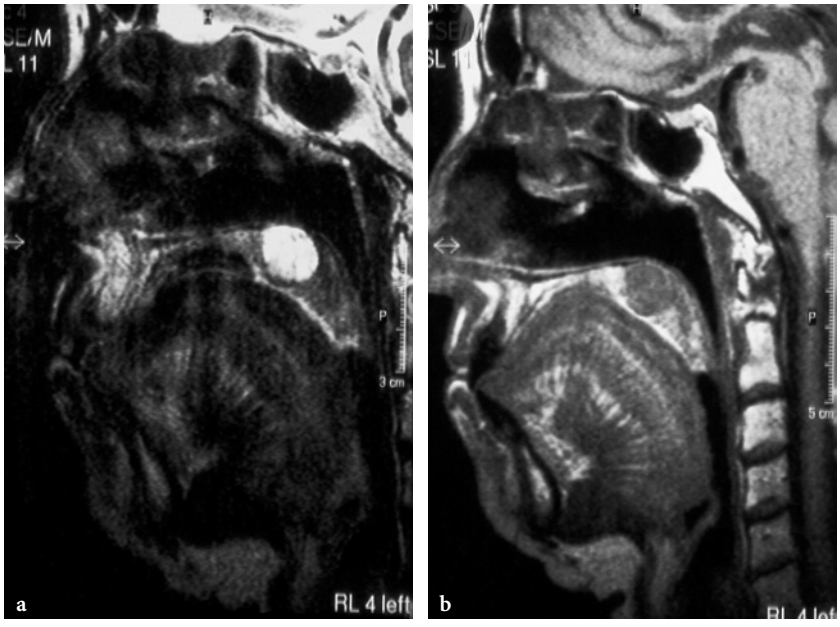

Fig. 6.15a,b. Sagittal MR images of a 34-year-old male showing a pleomorphic adenoma between hard and soft palate. On the T2-weighted image, the lesion is homogeneously hyperintense, round and well delineated (**a**). The post-contrast T1-weighted image shows only slight enhancement (**b**). (Courtesy of Nicole Freling, MD, Amsterdam, The Netherlands)

al. 1993), and on contrast-enhanced images, they usually show bright enhancement with a varying homogeneity; high-flow arteriovenous shunts can be seen as well.

6.3.1.3.5 Schwannomas

Schwannomas are rare benign tumors originating from nerve sheaths. Within the oral cavity they are most frequently found in the tongue of the adult population (Al-Ghamdi et al. 1992). Surgical excision is the treatment of choice.

They are usually isointense (isodense) on T1-weighted MR images (on CT). On T2, solid components of schwannomas are rather hyperintense. Moreover, cystic tumor components may be present. After the administration of contrast agent a "target-like" appearance is a characteristic sign (Beaman et al. 2004).

6.3.1.3.6 Miscellaneous Benign Tumors and Tumor-Like Lesions

Other benign tumors within the oral cavity are even rarer. For completion they are listed in Table 6.1. Some of them, such as an exostosis, are straight-forward diagnoses, others require tissue sampling for identification.

6.3.2 Squamous Cell Cancer

6.3.2.1 General Considerations

In adulthood, most lesions in the oral cavity sent for imaging are malignant. The most frequent question to answer is whether there is deep infiltration in already clinically detected and biopsied oral cancer. Squamous cell cancer (SCC) predominantly affects men between 50–70 years of age (Ferlay et al. 1999; Caswon 1998). Most important risk factors are a long history of tobacco and/or alcohol abuse. Oral SCC originate from the mucosa and, therefore, allow for an easy clinical access regarding detection and biopsy. This holds especially true for the lower lip which is the most often site for SCC of the oral cavity. Furthermore, local extension of a tumor of the lip can usually be sufficiently determined clinically so that cross-sectional imaging is only needed in very large tumors (e.g. to exclude mandibular infiltration). In

Table 6.1. List of oral cavity pathologies

- Benign lesions
  - Congenital
    - Vascular malformations
      - Venous
      - Arterial
      - Lymphatic
      - Capillary
    - (Epi-)Dermoid cysts
    - Lingual thyroid
    - Thyroglossal duct cyst
    - Digastric muscle aplasia
  - Inflammatory
    - Cervical phlegmon (e.g. odontogenic)
    - Abscess (+/– sialolithiasis)
    - Sialadenitis (+/– sialolithiasis)
    - Ranula
      - Simple
      - Plunging (or diving)
    - Ludwig's angina
  - Neoplastic
    - Pleomorphic adenoma
    - Lipoma
    - Rhabdomyoma
    - Hemangioma
    - Lymphangioma
    - Schwannoma
    - Leiomyoma
    - Neurofibromatosis
    - Fibroma
    - Aggressive fibromatosis
  - Others
    - Osseous lesions
    - Pseudotumor
      - Hemiatrophy of the tongue (or of other muscles)
- Malignant lesions
  - Squamous cell carcinoma (major sites in descending frequency)
    - Lips
    - Floor of the mouth
    - Retromolar trigone
    - Tongue
  - Adenoid cystic carcinoma
  - Mucoepidermoid carcinoma
  - Lymphoma
    - Non-Hodgkin lymphoma
    - Burkitt lymphoma
  - Sarcoma (rhabdomyo-, lipo-, fibro-, angio-, leiomyo-)
  - Adenocarcinoma
  - Malignant schwannoma
  - Metastases
  - Melanoma
  - Osseous malignancies (see Chap. 10)

addition to the lips, any intraoral mucosal surface can be affected; however, three specific intraoral sites are predominantly affected. In descending frequency, the floor of the mouth, the retromolar trigone, and the ventrolateral tongue are involved (Mashberg and Meyers 1976).

Small superficial T1 tumors are often not visible on both CT and MR images (Keberle et al. 1999). With increasing size, SCC infiltrate deeper submucosal structures. As a result, CT and MRI show a tumor mass and allow for an accurate evaluation of deep tumor infiltration (Kösling et al. 2000; Leslie et al. 1999). This results in the possibility of staging SCC of the oral cavity according to the TNM system (UICC 2002) (Table 6.2). In spite of the invasive character of SCC, bony structures and arteries resemble anatomic barriers and are infiltrated rather late in the course of the disease.

Table 6.2. Squamous cell carcinoma of the oral cavity: T staging (UICC 2002)

T1	Tumor ≤ 2 cm in greatest diameter
T2	Tumor > 2 cm but < 4 cm in greatest diameter
T3	Tumor ≥ 4 cm in greatest diameter
T4a	Oral cavity: Cortical bone, extrinsic muscles of the tongue, maxillary sinus, skin Lips: Cortical bone, inferior alveolar nerve, floor of the mouth, skin
T4b	Masticator space, pterygoid process, skull base, internal carotid artery

Regarding bony structures, cortical tumor infiltration can best be detected as erosion and/or lysis of the adjacent cortex on CT images with a bone-window setting (van Den Brekel et al. 1998; Mukherji et al. 2001). A soft tissue mass within the bony marrow is a direct sign and can be seen on both CT and MR images. Especially, pre-contrast in combination with fat-saturated post-contrast T1-weighted MR images are very helpful to detect bone marrow invasion (Fig. 6.16).

Furthermore, an important aspect regarding malignancies of the oral cavity is the invasion of nerves and vessels of neurovascular bundles, such as in the sublingual space (Mukherji et al. 1996, Smoker 2003). Whereas vascular invasion yields a greater risk of remote as well as lymph node metastases, nerve involvement can lead to tumor extension along nerve routes (perineural extension) far beyond the expected tumor margins (compare Figs. 6.6 and 6.17). Perineural extension may be asymptomatic and is often not easy to detect with all imaging modalities. Therefore, perineural extension results in a greater likelihood of positive resection margins and/or remote tumor remnants. As a consequence, it is crucial to look for direct or indirect signs for perineural tumor extension. Direct signs are thickened (Fig. 6.17) and contrast-enhanced nerves. Indirect signs are

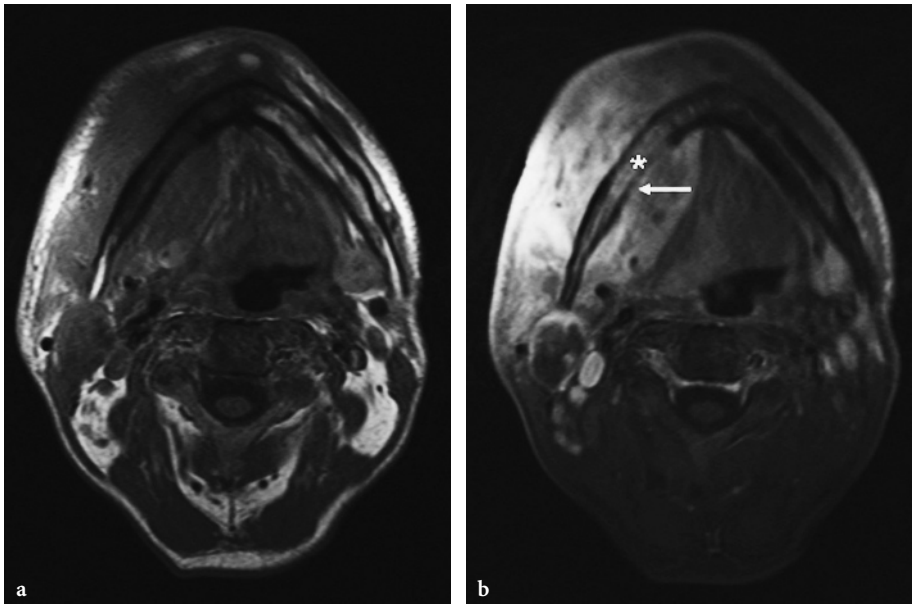

Fig. 6.16a,b. Pre-contrast (**a**) and post-contrast (**b**) T1-weighted axial MRI showing carcinomatous infiltration of the mandible. Erosion of the bony cortex (*arrow*). The post-contrast image differentiates between hypointense edema and hyperintense tumor infiltration (*asterisk* on **b**) of the bone marrow. (Courtesy of Bodo Kress, MD, Heidelberg, Germany)

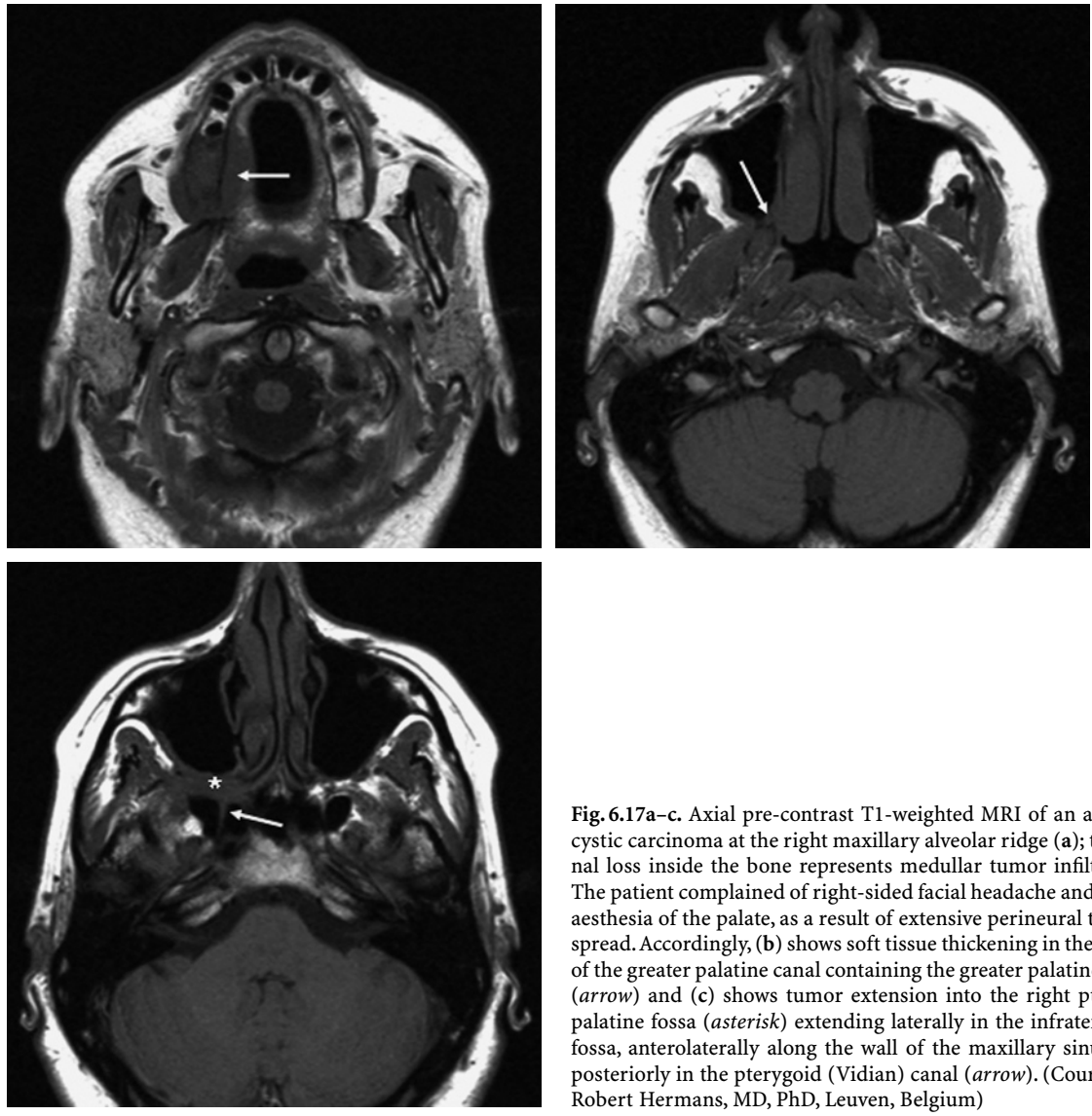

Fig. 6.17a–c. Axial pre-contrast T1-weighted MRI of an adenoid cystic carcinoma at the right maxillary alveolar ridge (**a**); the signal loss inside the bone represents medullar tumor infiltration. The patient complained of right-sided facial headache and an anaesthesia of the palate, as a result of extensive perineural tumour spread. Accordingly, (**b**) shows soft tissue thickening in the region of the greater palatine canal containing the greater palatine nerve (*arrow*) and (**c**) shows tumor extension into the right pterygopalatine fossa (*asterisk*) extending laterally in the infratemporal fossa, anterolaterally along the wall of the maxillary sinus, and posteriorly in the pterygoid (Vidian) canal (*arrow*). (Courtesy of Robert Hermans, MD, PhD, Leuven, Belgium)

invasion of sublingual space and widening of bony foramina or canals.

In general, SCC have a similar density to muscle on pre-contrast images (on both, CT and MR images) (Yasumoto et al. 1995; Keberle et al. 2002). Nonetheless, native T1-weighted MR images are of great value to delineate the tumor because the characteristic architecture of the tongue musculature is usually altered by the lesion. Furthermore, native T1-weighted images as well as post-contrast CT images yield the best contrast versus normal fat (e.g. the fatty tissue of the sublingual space). On T2 images, SCC are slightly hyperintense. On post-contrast images there is moderate enhancement, so that fat-saturated MR images have to be obtained. With increasing size, SCC (and respective metastases) often present with a central necrosis.

Cervical lymph node metastases occur in approximately 50% of the patients with SCC of the oral cavity (Magrin and Kowalski 2000; Smoker 2003). In tumors crossing the median (midline) there is often bilateral lymph node involvement. This holds especially true for tumors of the tongue. Lymph node involvement is generally accepted to be the single most important prognostic parameter (Magrin and Kowalski 2000). In addition to CT and MRI, ultrasound is known to be a very valuable tool regarding the detection and differentiation of cervical lymph nodes (see also Chap. 15).

In general, therapeutic options comprise surgery, radiation therapy, and chemotherapy. The latter is increasingly used as inductive chemotherapy in order to reduce the size of the tumor prior to surgery.

Furthermore, surgery and radiation therapy are often combined. Clear extension beyond the midline in tongue cancer often precludes surgical resection as this would imply total glossectomy; primary radiation therapy is usually performed in such circumstances. Whereas smaller tumors can be removed with laser or classic surgery, larger tumors often require extensive surgery with tissue reconstruction. An additional invasion of the mandibular cortex requires marginal (cortical) mandibulectomy. Invasion of the mandibular marrow instead requires complete mandibular resection of the infiltrated segment (segmental mandibulectomy) with local reconstruction.

As a result there is a large variety of therapeutic options so that for any individual an exact evaluation of the tumor extension is essential.

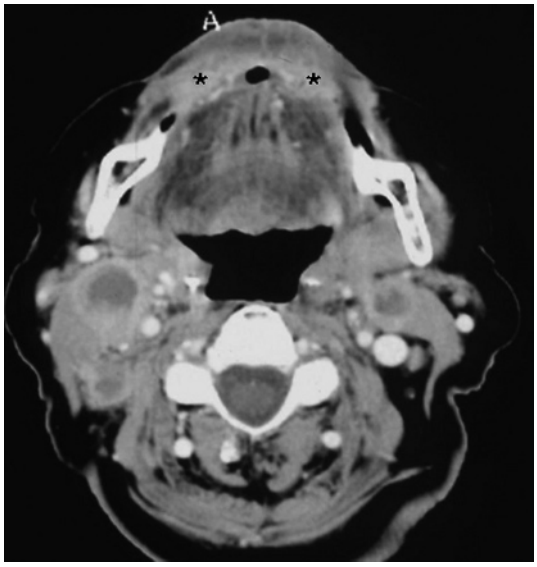

Fig. 6.18. CT in a 55-year-old pipe-smoking male with a squamous cell carcinoma of the lower lip. The contrast-enhancing mass is on both sides of the midline, the adjacent soft tissues are edematously swollen. In level II there are bilateral lymph node metastases with central necrosis

6.3.2.2 Lip Cancer

As already mentioned, the lips are the most frequent location regarding SCC of the oral cavity (Fig. 6.18). However, only very large tumors require local evaluation of deep tumor extension by CT or MRI. In this regard, pretherapeutically important anatomic structures are the mandibular cortex, the mandibular marrow, and the inferior alveolar and/or mental nerves (for the imaging criteria of perineural and mandibular infiltration see Chap. 5).

6.3.2.3 Floor of the Mouth Cancer

Most tumors of the floor of the mouth originate in its anterior aspects. Here small superficial tumors are readily diagnosed by clinical means. In order to evaluate a tumor's deep infiltration and for TN staging, cross-sectional imaging is needed (Figs. 6.19 and 6.20).

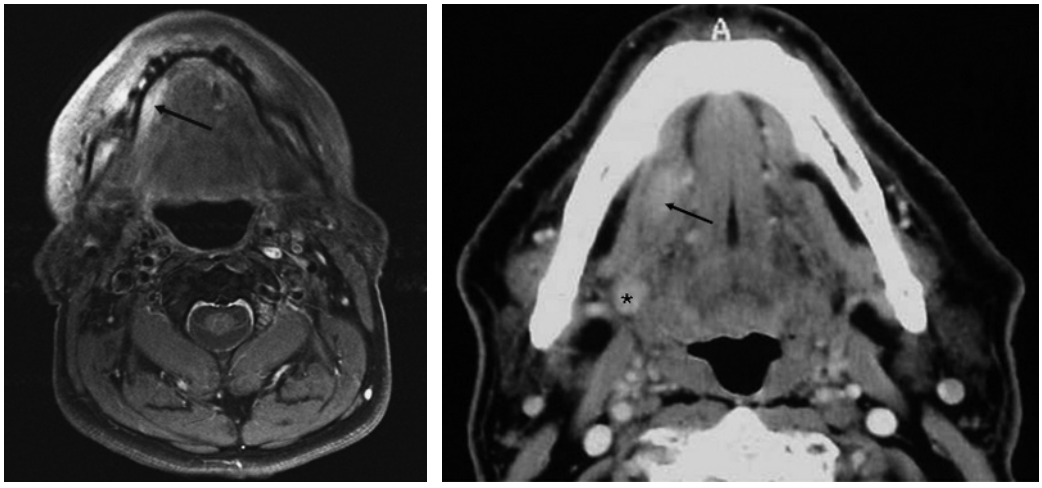

Fig. 6.19a,b. MRI of a 54-year-old man with a small T1 tumor (SCC) in the anterior part of the floor of the mouth (**a**). A fat-saturated axial T1-weighted MR image shows the small hyperintense mass adjacent to the attachment of the mylohyoid muscle at the inner mandibular surface. The cortex is intact. **b** A different patient (63-year-old male) presented with a squamous cell carcinoma of the right floor of the mouth. At CT, the small T1 tumor almost completely fills out the sublingual (fat) space and lies directly between the medially located ipsilateral neurovascular bundle (and hyoglossus muscle) and the laterally located mylohyoid muscle. A lymph node metastasis can be seen on the same slice (*asterisk*)

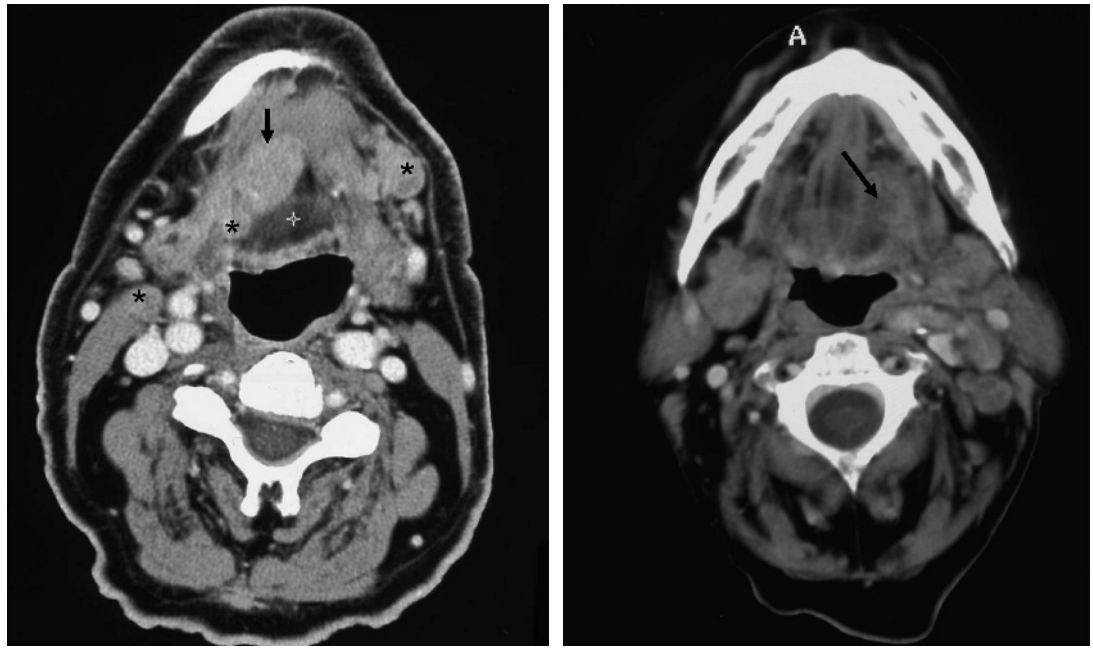

Fig. 6.20a,b. CT of a 62-year-old man with a squamous cell carcinoma lying more deeply in the floor of the mouth (**a**). The tumor is located between the mylohyoid muscle and the partially presented transverse (intrinsic) muscles of the tongue (*cross*). Note the bilateral lymph node metastases. Different patient (**b**) with a SCC with central necrosis on the left side of the floor of the mouth. At CT, the tumor (*arrow*) is located between the geniohyoid and the hyoglossus muscles. Note the ipsilateral lymph node metastasis with central necrosis

Considering the latter facts, in ultrasound, the transducer has to be tilted so that the anterior part of the floor of the mouth can be evaluated accordingly (Mende et al. 1996; Keberle et al. 2000). SCC of the floor of the mouth preferentially infiltrate the surrounding soft tissues first before the mandible and/or the mylohyoid muscle are invaded (Lenz and Hermans 1996). Medially, the tumor can cross the midline, invade the contralateral neurovascular bundle and if there is also cranial extension of the tumor the tongue can be involved. As previously mentioned, large tumor involvement of the contralateral tongue and/or neurovascular bundle often precludes radical surgical resection (Mukherji et al. 1997). Dorsally and caudally, SCC of the floor of the mouth can spread to deeper cervical tissues. Usually, it comes to a dorsal spread first along the mylohyoid muscle and the inner surface of the mandible which are natural borders. Dorsally, Wharton's duct or the submandibular gland itself can be infiltrated. Both can result in inflammatory changes of the gland due to duct obstruction (Yousem et al. 2000). Enlargement of the submandibular gland and dilatation of the duct are important indirect tumor signs. On the other hand, oropharyngeal tumors at the base of the tongue tend to infiltrate the floor of the mouth ventrally (resulting in a T4-oropharyngeal tumor if extrinsic muscles of the tongue are involved) (Fig. 6.21). The same tumor stage applies for oral cavity tumors in case of invasion of extrinsic muscles of the tongue and/or lateral (as well as anterior) infiltration of the mandible (Table 6.2). Interestingly, caudal infiltration of the mylohyoid muscle is not regarded a T4 stage according to UICC guidelines (Table 6.2). The coronal plane facilitates the evaluation of the mylohyoid as well as extrinsic tongue muscles (Lell et al. 1999).

Tumors of the anterior part of the floor of the mouth in particular result in submental (level I; best seen on coronal slices; Lell et al. 1999) and/or submandibular (also level I) lymph node metastases (Fig. 6.20a).

6.3.2.4 Retromolar Trigone Cancer

SCC of the retromolar trigone are localized in the superoposterior part of the oral cavity and often involve oropharyngeal subregions (Fig. 6.22). These tumors are rarer than tumors of the lips or of the floor of the mouth, however, they are more difficult to detect by clinical means. Dorsally, the cranial part of the tonsillar pillar, the lateral aspect of the soft palate, as well as the pharyngeal tonsil can be affected. Deeply, along

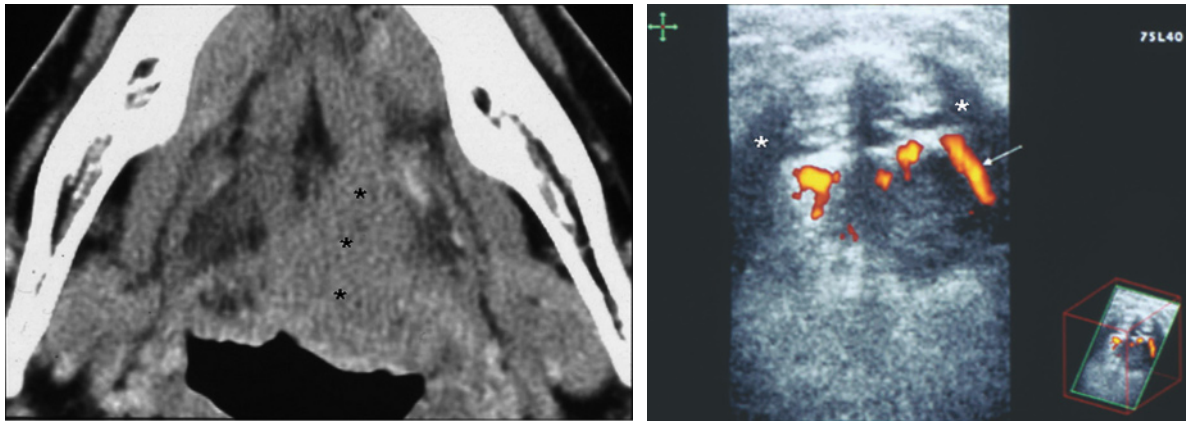

a b

Fig. 6.21a,b. CT of a 56-year-old man with an oropharyngeal (T4) squamous cell carcinoma of the base of the tongue and deep tumor infiltration into the geniohyoid and genioglossus muscles of the floor of the mouth (*stars*) and midline crossing (**a**). The corresponding ultrasound nicely shows the relation to the lingual artery (*arrow*, *asterisks* indicate the mylohyoid muscle on both sides)(**b**)

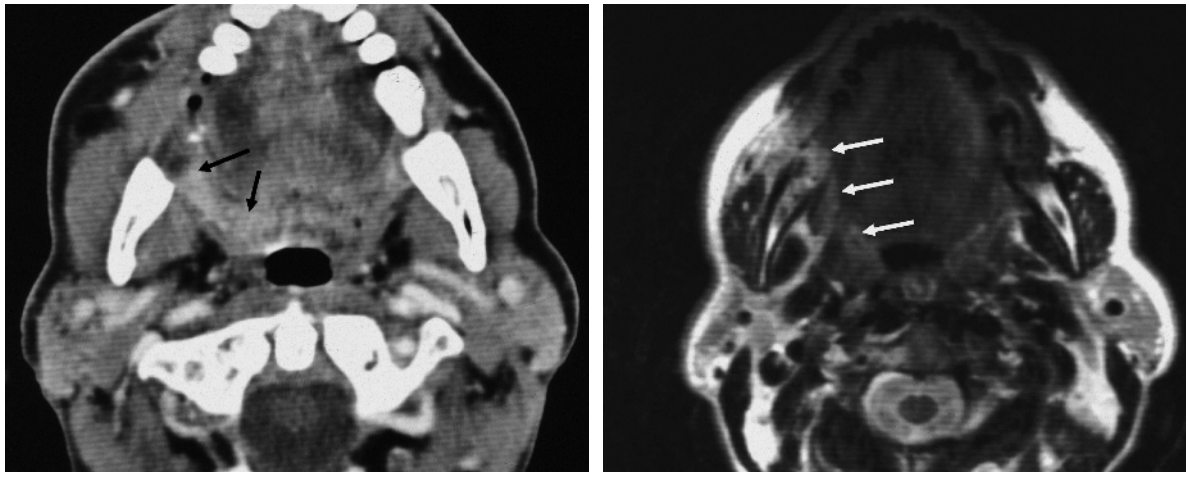

a b

Fig. 6.22a,b. Axial CT (**a**) and axial T2-weighted MRI (**b**) of a male patient with squamous cell carcinoma of the right retromolar trigone (*arrows*) extending medially to the soft palate. The contrast-enhancing (**a**) mass is hyperintense on the T2-weighted MR image (**b**). (Courtesy of Sabrina Kösling, MD, Halle, Germany)

the pterygomandibular space, the mandible, superior pharyngeal constrictor muscle, the pterygoid processes, the medial pterygoid muscle (eventually causing trismus), and the masticator and the parapharyngeal spaces (and this way even the skull base) can be infiltrated. Especially, in the case of tumor extension into the pterygopalatine fossa, one always has to watch for perineural tumor spread (Mukherji et al. 1997). Ventrally and cranially, the gingival and/or buccal mucosa as well as the maxillary alveolar ridge (the latter being a T4 stage) are possibly infiltrated (Table 6.2). Medially, the tumor may extend towards the hard palate; laterally, the buccinator space can be infiltrated.

6.3.2.5 Tongue Cancer

The ventrolateral surface of the tongue is involved more often than the rest of the tongue (Fig. 6.23). These tumors easily invade the intrinsic muscles of the tongue. The floor of the mouth with the ipsilateral neurovascular bundle (Fig. 6.24), the base of the tongue, the gingival mucosa and eventually the oropharyngeal tonsils, the soft palate, and the mandible may become invaded. Again, it is crucial to evaluate tumor extension in relation to the midline and to the contralateral neurovascular bundle and sublingual space.

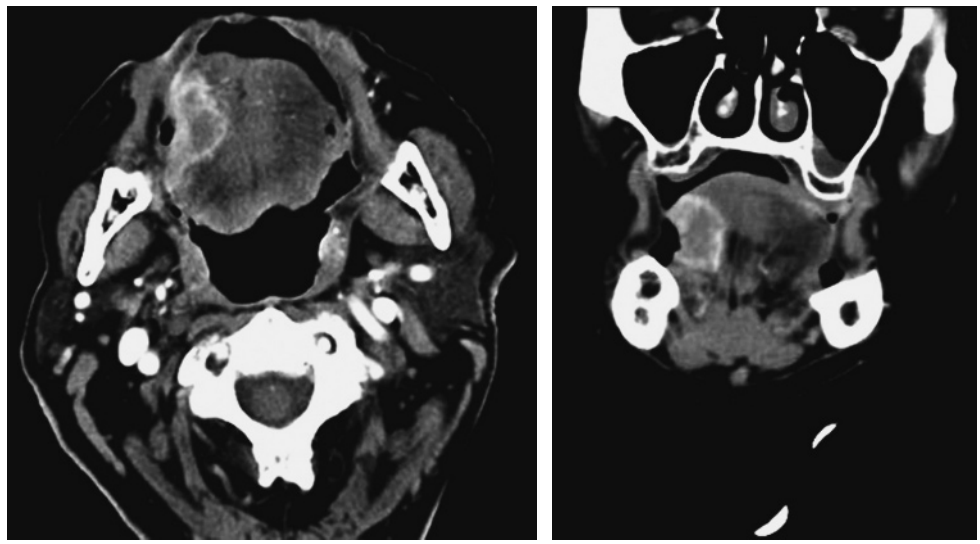

a b

Fig. 6.23a,b. CT with axial (**a**) as well as coronal reformation (**b**) in a 49-year-old male with a T2 squamous cell carcinoma of the ventrolateral tongue. The tumor does not cross the midline and, thus can more easily be removed than the masses shown in Figs. 6.21 and 6.24 (e.g. by hemiglossectomy)

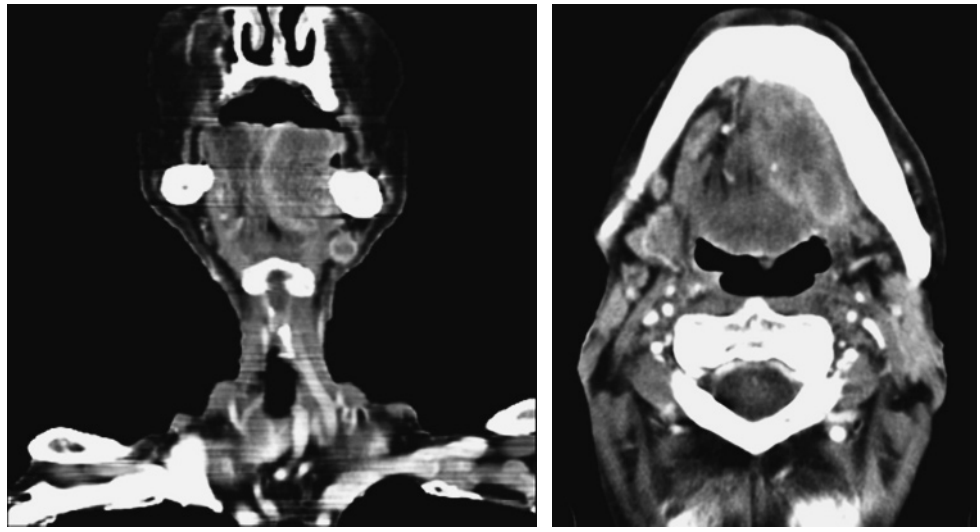

a b

Fig. 6.24a,b. CT with coronal (**a**) and axial (**b**) reconstructions of a 60-year-old male with a huge squamous cell carcinoma of the tongue. The tumor extends into the floor of the mouth and reaches the mandible as well as the midline but without crossing it. The tumor shows a strong rim enhancement and appears to surround the ipsilateral neurovascular bundle. Beneath the mylohyoid muscle is a small submandibular lymph node metastasis (level I)

6.3.2.6 Hard Palate, Gingival and Buccal Cancer

Tumor location at the mucosal layer beneath the hard palate eventually implies close evaluation of the adjacent bone (Fig. 6.25). This can best be achieved on coronal MR or CT images (bone window). Furthermore, the incisive canal and the greater and lesser palatine canals have to be inspected closely for potential perineural tumor spread along the respective palatine nerves (nerve V/2) towards the pterygopalatine fossa. Whereas CT can demonstrate asymmetric pathologic widenings (sometimes cortical erosions) of the respective bony canals, MRI superiorly displays perineural spread as thickening (Fig. 6.17) and/or contrast enhancement of the nerve.

SCC of the gingival or buccal mucosa may eventually invade the mandibular or maxillary cortex (Figs. 6.16 and 6.26), which is usually best seen on axial slices.

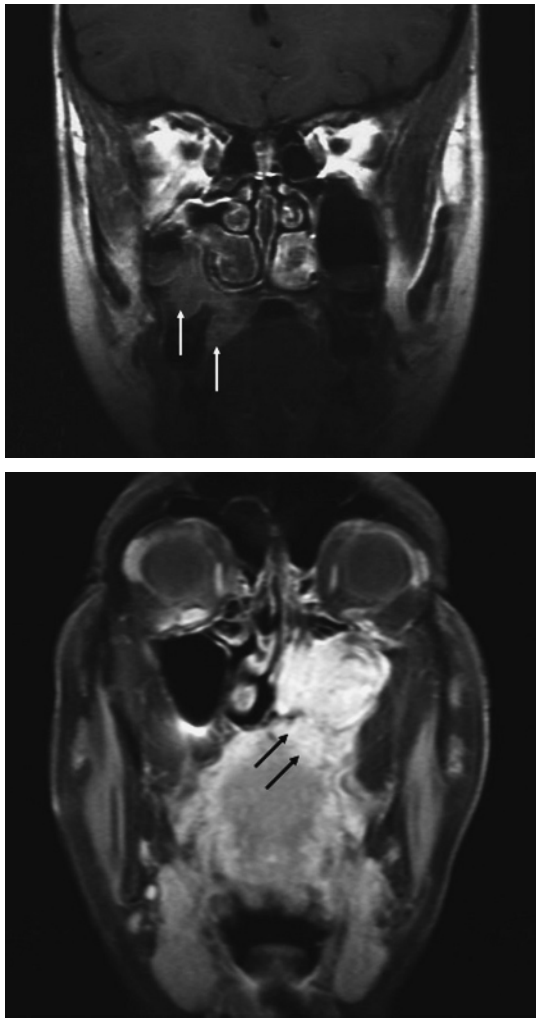

Fig. 6.25a,b. Coronal MRI (post-contrast T1-weighted) in a 72-year-old male showing a mildly enhancing squamous cell carcinoma of the hard palate with infiltration of bone and extension into the right maxillary sinus (**a**). **b** An adenoid cystic carcinoma in a 84-year-old female (fat-saturated T1-weighted post-contrast MRI) of the hard palate with severe extension into the maxillary sinus. Although adenoid cystic carcinoma is often associated with perineural infiltration, this patient did not present with the latter form of tumor spread

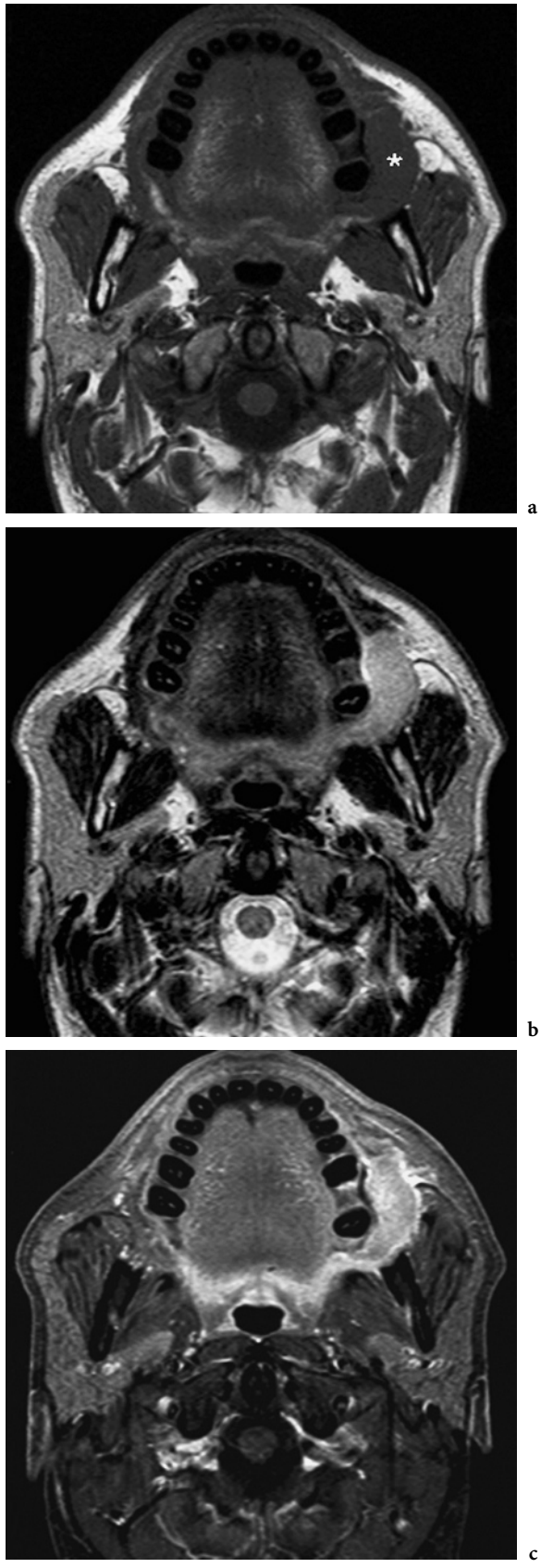

Fig. 6.26a–c. Axial MRI in a 60-year-old female with a swollen cheek and histologically proven squamous cell carcinoma of the gingival mucosa at the level of the left-sided 7th and 8th maxillary molar teeth. Isointense mass on native T1 (**a**), hyperintense mass on T2 (**b**), and homogeneously enhancing hyperintense mass on fat-saturated post-contrast T1 (**c**). The adjacent maxillary cortex is not invaded. The tumor grows behind the 8th molar into the region of the retromolar trigone. (Courtesy of Nicole Freling, MD, Amsterdam, The Netherlands)

6.3.3 Other Malignant Tumors

6.3.3.1 Adenoid Cystic Carcinoma

Malignant tumors other than SCC are quite rare. Adenoid cystic carcinoma (ACC) originates from the minor salivary glands which can be found everywhere in the oral cavity (Figs. 6.17, 6.25b, and 6.27) (Cawson 1998). They usually occur in the fifth to seventh decade of life, men and women are affected about equally. The long term prognosis is worse in comparison to SCC (Friedman et al. 1986). This is mainly due to the propensity of adenoid cystic carcinoma for perineural tumor spread and deep local invasion (Sigal et al. 1992; Parker and Harnsberger 1991). On the other hand, lymphatic metastases are much

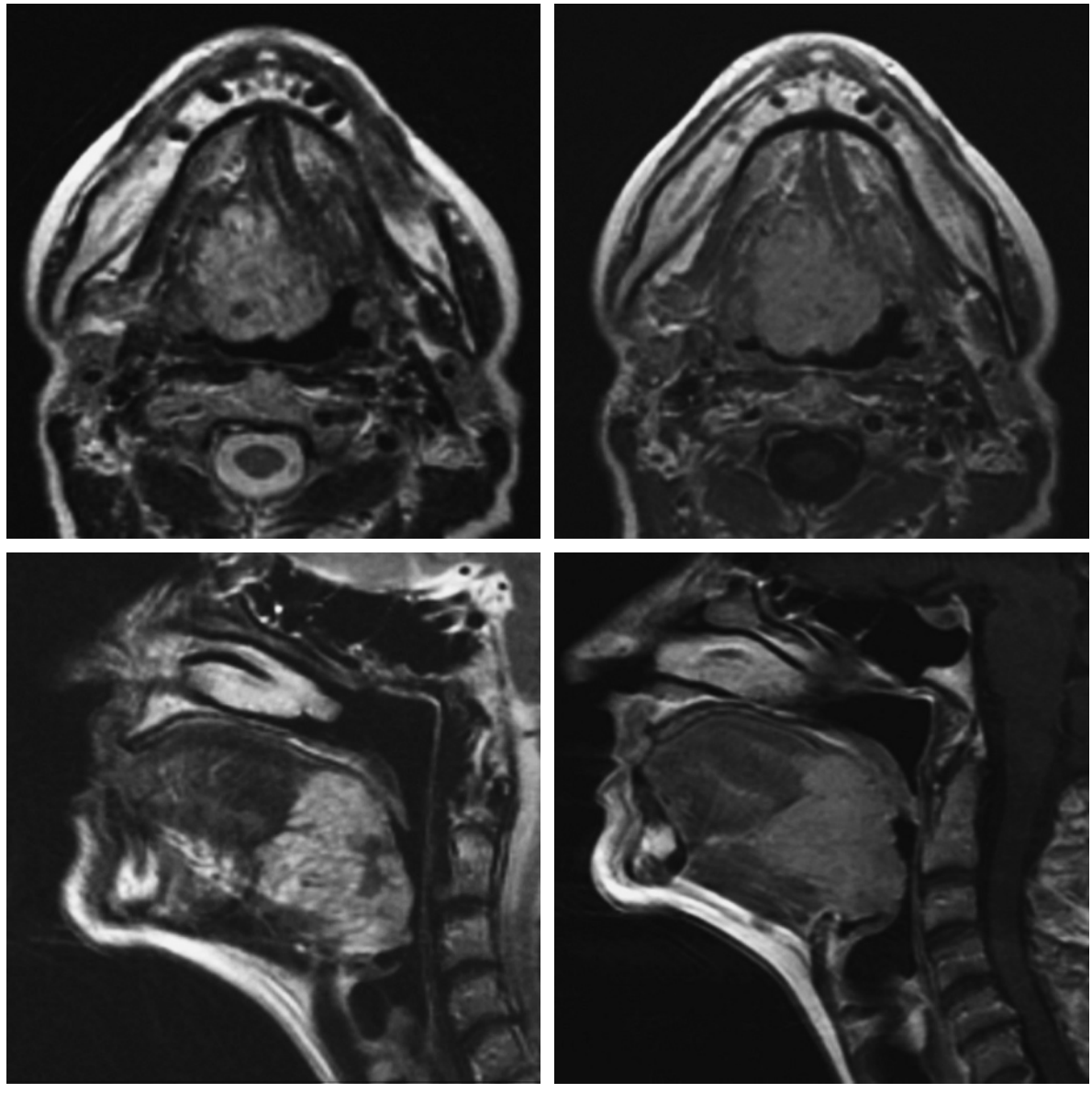

Fig. 6.27a–d. MRI of a 56-year-old female with a short history of dysphagia. Axial T2- (**a**) and post-contrast T1-weighted (**b**) images of an irregular, slightly inhomogeneous hyperintense adenoid cystic carcinoma of the tongue which infiltrates the floor of the mouth and clearly crosses the midline. Thus, there were no surgical options. Sagittal T2- (**c**) and post-contrast T1-weighted (**d**) images better show the entire longitudinal and sagittal extension of the tumor. Posteriorly, the tumor infiltrates the base of the tongue. (Courtesy of Nicole Freling, MD, Amsterdam, The Netherlands)

rarer than in SCC, but hematogenous spread, mainly to the lungs and liver, does occur. Perineural invasion mainly affects the maxillary (V2) and/or the mandibular (V3) nerves. To avoid underestimation of tumor spread, in this regard, the latter nerves, the pterygopalatine fossa (V2), the foramen rotundum (V2), the pterygoid canal (canal containing mixed para- and orthosympathic nerve entering the pterygopalatine canal), the foramen ovale (V3), and the cavernous sinus have to be inspected thoroughly. It is important to note that in some cases of ACC tumor-free areas ("skip areas") along the nerves have been reported. On CT images, perineural spread might be identified by enlargement of skull base foramina, whereas enlarged nerves are usually not directly visualized. On MR images, perineural tumor spread can directly be visualized as an enlarged nerve with a varying extent of contrast enhancement. The primary tumor itself cannot be distinguished form SCC by cross-sectional imaging (Becker et al. 1998); perineural spread can also occur in SCC. Thus, differentiation of ACC and SCC requires histopathologic analysis.

6.3.3.2 Mucoepidermoid Carcinoma

As adenoid cystic carcinoma, mucoepidermoid carcinoma arises from minor salivary glands. An important aspect to mucoepidermoid carcinoma is the wide range of histological subclassifications (Som and Brandwein 2003; Smoker 2003). Low-grade mucoepidermoid carcinoma have a very good prognosis. On imaging studies they appear as well-delineated solid tumors. Cystic tumor components and even calcifications can be present. On the other hand, high-grade mucoepidermoid carcinoma have a very poor prognosis. The latter tumors are ill-defined and have similar imaging characteristics as SCC or ACC.

6.3.3.3 Miscellaneous (see also Table 6.1)

Other malignancies in the oral cavity are extremely rare. However, lymphoma, especially non-Hodgkin lymphoma (NHL), merits some attention (see also Chap. 16). Extranodal involvement of the oropharynx by NHL or Burkitt lymphoma can reach a considerable size and, this way extend ventrally to affect the oral cavity. NHL tends to present with homogeneous masses, usually, originating from lymphatic tissues of the base of the tongue or the pharyngeal tonsils (Fig. 6.28). Necrotic tumor components are rare as opposed to carcinomas. This also applies to cervical lymph nodes and more remote tumor sites which are mostly present in NHL (Lee et al. 1987).

Other extremely rare malignancies include sarcoma (rhabdomyo-, lipo-, fibro-, angio-, and leiomyosarcoma). Among these, rhabdomyosarcoma merit further attention since these tumors are the most frequent malignancies during the first two decades of life (Peters et al. 1989). Several histopathologic subtypes occur in rhabdomyosarcomas, which have a predilection for the head and neck region. In the oral cavity, the floor of the mouth and the tongue are more frequently involved than the rest of the oral cavity. On precontrast images, they have the density of muscle. Mostly, there is inhomogeneous contrast enhancement. On MR, rhabdomyosarcomas may be slightly hyperintense on T2-weighted images. Both well- and ill-defined masses have been reported.

6.3.4 Recurrent Cancer

In the oral cavity, there are typical post-therapeutic imaging findings which should not be misinterpreted with recurrent tumor. After radiation therapy these alterations are generally unspecific and consist in mucosal thickening, edematous changes, and later fibrotic changes (for a more general description of tissue changes after radiotherapy, see Chap. 4).

A specific complication in the oral cavity after radiation therapy may be osteoradionecrosis (Fig. 6.29) which usually presents with local lysis, sclerosis and

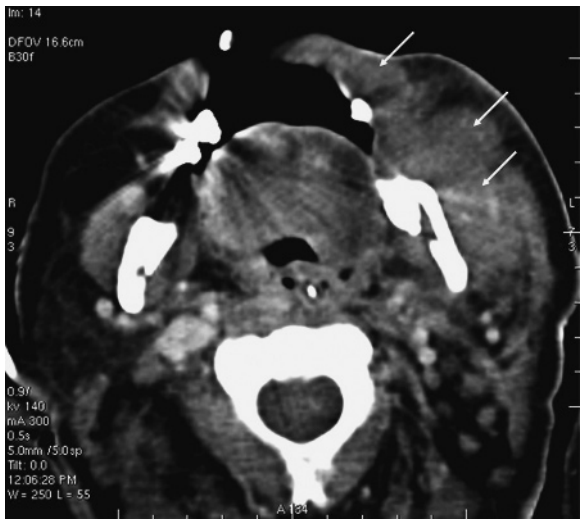

Fig. 6.28. CT of a 50-year-old female with multi-focal non-Hodgkin lymphoma also involving her left masseter muscle, cheek, and lip

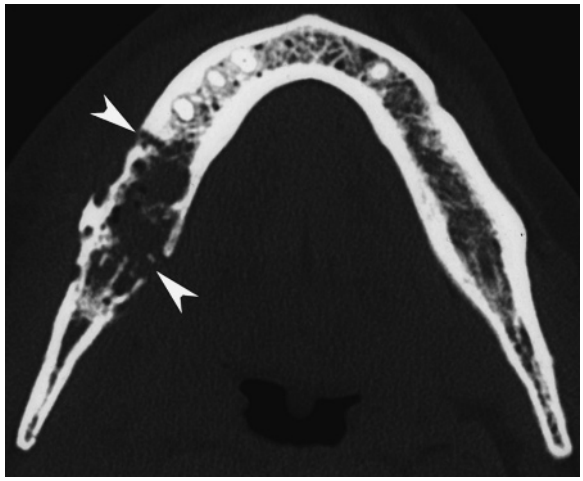

Fig. 6.29. Axial CT-image (*bone window*) of a patient treated by external irradiation 10 years earlier for a right-sided parotid malignancy, now presenting with oral pain and mucosal dehiscence. Extensive resorption of right-sided mandibular spongiosa and destruction of both lingual and buccal cortex, complicated by a pathologic fracture (*arrowheads*). Intra-osseous air bubbles are seen. Histopathologic examination showed necrotic bone with signs of osteomyelitis (Courtesy of Robert Hermans, MD, PhD, Leuven, Belgium)

eventually bone destruction (Hermans 2003; Weber et al. 2003). On the other hand, recurrent tumor may infiltrate the mandible or maxilla. Although sometimes difficult, CT is the imaging modality of choice to differentiate osteoradionecrosis and recurrent tumor with bony infiltration. An adjacent soft tissue mass suggests the presence of bony tumor infiltration, whereas a typical moth-eaten appearance and sequestrations favor the diagnosis of osteoradionecrosis.

Specific post-operative changes in the oral cavity can be seen after hemiglossectomy (Lell et al. 2000). Often the tip of the tongue is inverted towards the resected side. Sometimes soft tissue reconstructions (e.g. myocutaneous flaps) are performed to reduce functional impairment after surgery (Fig. 6.30) (Hudgins et al. 1994). Due to denervation, transformation of muscle into fat and eventually atrophy of the transplanted flap occur.

In contrast to primary carcinoma, which start out superficially, recurrent tumor mainly grows deeply so that for clinicians it is difficult to find recurrent tumor in an early stage (Fig. 6.31). However, because of the aforementioned expected post-therapeutic tissue changes and the possible presence of other post-therapeutic lesions (e.g. inflammatory changes, granulation tissue, etc.), it is challenging to find a recurrent cancer on imaging studies. In general, the signs for recurrent tumor are similar to the pretherapeutic situation.

There is a predisposition for local recurrences in the tongue (Fig. 6.32). The reason for this are the rather close resection margins in patients with tumors that are close to or just across the midline in order to avoid severe post-operative swallowing disorders (Keberle et al. 2003).

Rather than evaluating anatomic features associated with tumor growth, FDG-PET assesses abnormal metabolic activity of tumor and, this way, avoids some of the difficulties inherent in examining the post-treatment head and neck (Lapela et al. 1995). However, except for a high negative predictive value (91%) the positive predictive value is rather low (5%) (Goodwin 1998) (see also Chap. 17).

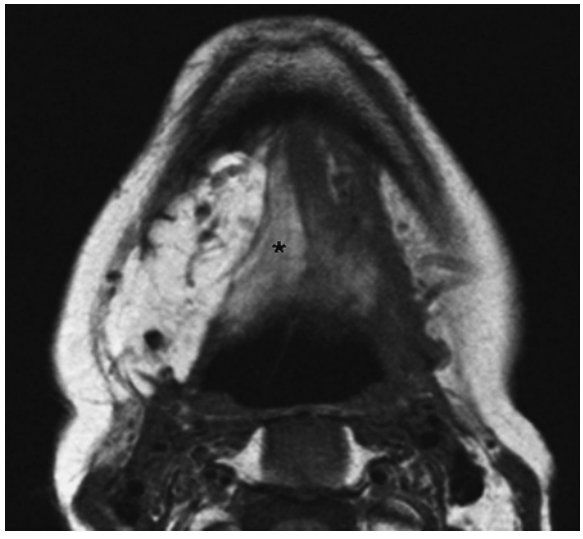

Fig. 6.30. Axial MRI of 63-year-old male patient after resection of a squamous cell carcinoma with flap reconstruction on the right side (**a**). On the one hand, note the flow-voids of the arterial supply and the fatty transformation of the myocutaneous flap itself. And on the other hand, note the fatty transformation of the muscles (*asterisk*) between the flap and the midline due to muscle denervation. The borders of the flap and of the anatomic structures are smooth, there is no recurrence

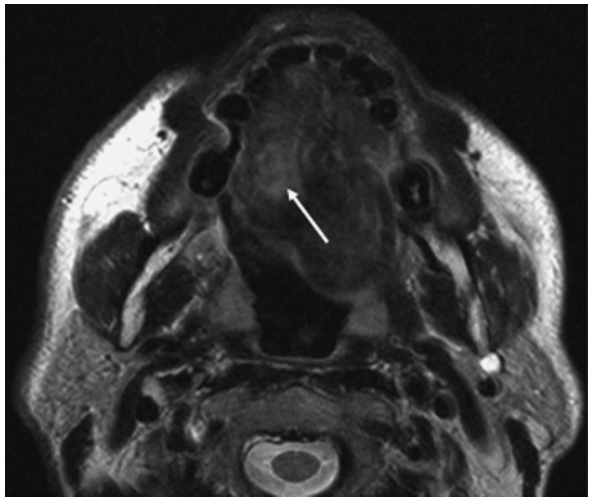

a

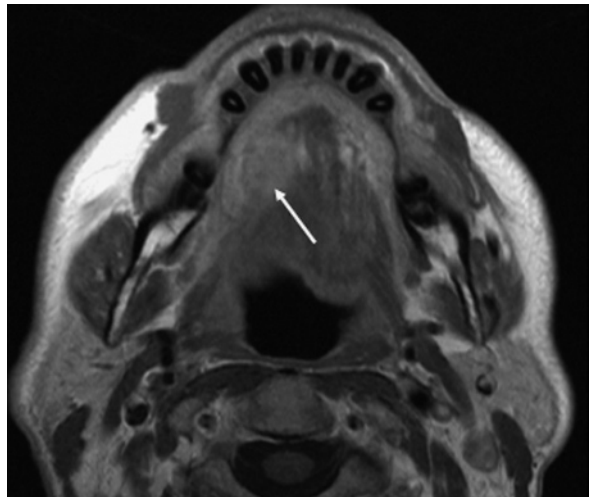

b

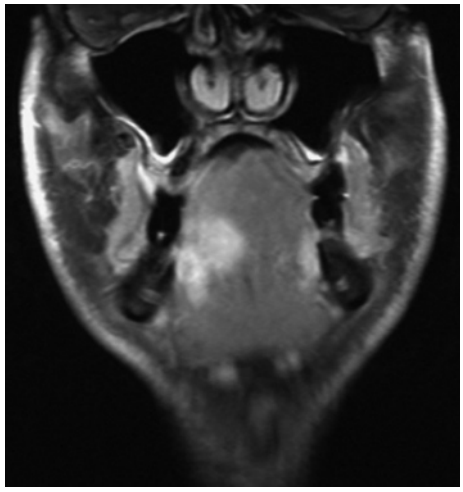

c

Fig. 6.31a–c. MRI of a 56-year-old man with a local recurrence after resection of a squamous cell carcinoma of the tongue and respective asymmetric changes of the anatomy. The T2-weighted image shows a small hyperintense lesion (*arrow*) deeply between floor of the mouth and tongue (**a**). The respective post-contrast axial (**b**) and coronal (**c**) T1-weighted images demonstrate contrast enhancement of that lesion

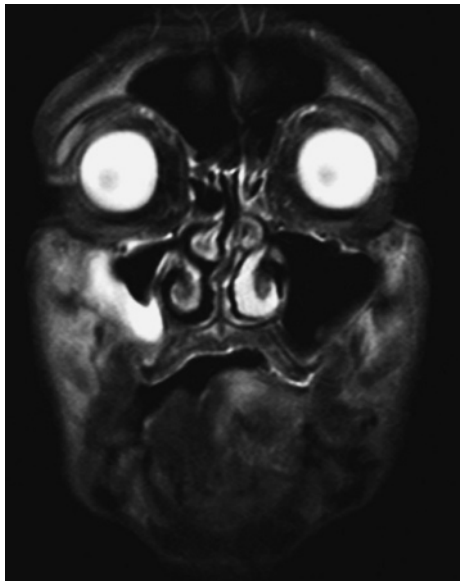

a

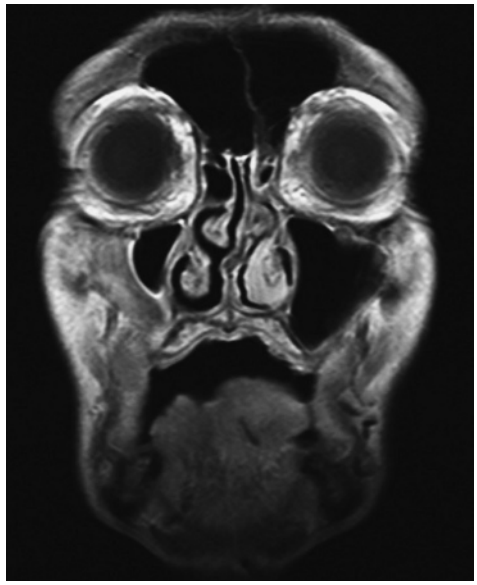

b

Fig. 6.32a,b. Coronal MRI of a 50-year-old male with a local recurrence at the left tongue. Both the T2-weighted (**a**) as well as the T1-weighted post-contrast (**b**) images show a hyperintense lesion

References

Al-Ghamdi S, Black MJ, Lafond G (1992) Extracranial head and neck schwannomas. J Otolaryngol 107:186–188

Baker LL, Dillion WP, Hieshima GB et al (1993) Hemangiomas and vascular malformations of the head and neck: MR characterization. AJNR Am J Neuroradiol 14:307–314

Beaman FD, Kransdorf MJ, Menke DM (2004) Schwannoma: radiologic-pathologic correlation. Radiographics 24:1477–1481

Becker M, Moulin G, Kurt A et al (1998) Non-squamous cell neoplasms of the larynx: radiologic-pathologic correlation. Radiographics 18:1189–1209

Bergman RA, Afifi AK (2002) Nerves of the eyes, nose, and mouth. Atlas of human anatomy. Copyright protected material used with permission of the authors and the University of Iowa's Virtual Hospital, www.vh.org

Cawson RA (1998) Lucas's pathology of tumors of the oral tissues, 5th edn. Churchill Livingstone, Harcourt Brace & Co Ltd, Edinburgh

Coit WE, Harnsberger HR, Osborn AG et al (1987) Ranulas and their mimics. Radiology 263:211–216

Douglas PS, Baker AW (1994) Lingual thyroid. Br J Oral Maxillofac Surg 32:123–124

Ferlay J, Bray F, Sankila R et al (1999) EUCAN: cancer incidence, mortality and prevalence in the European Union 1995, version 2.0. IARC CancerBase No. 4., Lyon, IARCPress

Ferner H, Staubesand J (1982) Sobotta – atlas of human anatomy. Urban & Schwarzenberg, Munich

Friedman M, Levin B, Grybauskas V et al (1986) Malignant tumors of the major salivary glands. Otolaryngol Clin North Am 19:625–636

Goodwin WJ (1998) PET and recurrent squamous cell carcinoma of the head and neck: a surgeon's view. AJNR Am J Neuroradiol 19:1189–1196

Hermans R (2003) Imaging of mandibular osteoradionecrosis. Neuroimaging Clin N Am 13:597–604

Hudgins PA, Burson JG, Gussack GS et al (1994) CT and MR appearance of recurrent malignant head and neck neoplasms after resection and flap reconstruction. AJNR Am J Neuroradiol 15:1698–1694

Johnson JC, Coleman LL (1989) Magnetic resonance imaging of a lingual thyroid gland. Pediatr Radiol 19:461–462

Keberle M, Kenn W, Tschammler A et al (1999) Current value of double-contrast pharyngography and of computed tomography for the detection and for staging of hypopharyngeal, oropharyngeal and supraglottic tumors. Eur Radiol 9:1843–1850

Keberle M, Jenett M, Kessler C et al (2000) New possibilities in the diagnosis and documentation using 3D power Doppler ultrasound with carcinoma of the floor of the mouth as illustration. Ultraschall Med 21:26–31

Keberle M, Tschammler A, Hahn D (2002) Single-bolus technique for spiral CT of laryngopharyngeal squamous cell carcinoma: comparison of different contrast material volumes, flow rates, and start delays. Radiology 22:171–176

Keberle M, Hoppe F, Dotzel S et al (2003) Prognostic value of pretreatment CT regarding local control in oropharyngeal cancer after primary surgical resection. Fortschr Röntgenstr 175:61–66

Keberle M, Ströbel P, Relic A (2005) Simultaneous pleomorphic adenomas of the parotid and the submandibular gland. Fortschr Röntgenstr 177:436–438

Kennedy TL (1989) Cystic hygroma-lymphangioma: a rare and still unclear entity. Laryngoscope 99:1–10

King RC, Smith BR, Burk JL (1994) Dermoid cysts in the floor of the mouth. Review of the literature and case reports. Oral Surg Oral Med Oral Pathol 78:567–576

Koeller KK, Alamo L, Adair CF et al (1999) Congenital cystic masses of the head and neck: radiologic-pathologic correlation. Radiographics 19:121–146

Kösling S, Schmidtke M, Vothel F et al (2000) The value of spiral CT in the staging of carcinomas of the oral cavity and of the oro- and hypopharynx. Radiologe 40:632–639

Lapela M, Grenman R, Kurki T et al (1995) Head and neck cancer: detection of recurrence with PET and 2-(F-18)Fluoro-2-deoxy-D-glucose. Radiology 197:205–211

Lee YY, van Tassel P, Nauert C et al (1987) Lymphomas of the head and neck: CT findings at initial presentation. AJNR Am J Neuroradiol 8:665–671

Lell M, Baum U, Koester M et al (1999) The morphological and functional diagnosis of the head-neck area with multiplanar spiral CT. Radiologe 39:932–938

Lell M, Baum U, Greess H et al (2000) Head and neck tumors: imaging recurrent tumor and post-therapeutic changes with CT and MRI. Eur J Radiol 33:239–247

Lenz M, Hermans R (1996) Imaging of the oropharynx and the oral cavity. Part II: pathology. Eur Radiol 6:536–549

Leslie A, Fyfe E, Guest P et al (1999) Staging of squamous cell carcinoma of the oral cavity and oropharynx: a comparison of MRI and CT in T- and N-staging. J Comput Assist Tomogr 23:43–49

Magrin J, Kowalski L (2000) Bilateral radical neck dissection: results in 193 cases. J Surg Oncol 75:232–240

Mashberg A, Meyers H (1976) Anatomical site and size of 222 early asymptomatic oral squamous cell carcinomas. Cancer 37:2149–2157

Mende U, Zöller J, Dietz A et al (1996) The sonography in the primary staging of head and neck tumors. Radiologe 36:207–216

Mukherji SK, Weeks SM, Castillo M et al (1996) Squamous cell carcinomas that arise in the oral cavity and tongue base: can CT help predict perineural or vascular invasion? Radiology 198:157–162

Mukherji SK, Pillsbury HR, Castillo M (1997) Imaging squamous cell carcinomas of the upper aerodigestive tract: what clinicians need to know? Radiology 205:629–646

Mukherji SK, Isaacs DL, Creager A et al (2001) CT detection of mandibular invasion by squamous cell carcinoma of the oral cavity. AJR Am J Roentgenol 177:237–243

Mulliken JB (1988) Vascular malformations of the head and neck. In: Mulliken JB, Young AE (eds) Vascular birthmarks, hemangiomas and malformations. WB Saunders, Philadelphia, pp 301–342

Mulliken JB, Glowacki J (1982) Hemangiomas and vascular malformations in infants and children: a classification based on endothelial characteristics. Plast Reconstr Surg 69:412–420

Okahara M, Kiyosue H, Hori Y et al (2003) Parotid tumors: MR imaging with pathological correlation. Eur Radiol 13[Suppl 4]:L25–33

Parker GD, Harnsberger HR (1991) Clinical-radiologic issues in perineural tumor spread of malignant diseases of the extracranial head and neck. Radiographics 11:383–399

Peters E, Cohen M, Altini M et al (1989) Rhabdomyosarcoma of the oral and paraoral region. Cancer 63:963–966

Sigal R, Monnet O, de Baere T et al (1992) Adenoid cystic carcinoma of the head and neck. Radiology 184:95–101

Sigal R, Zagdanski A, Schwaab G et al (1996) CT and MR imaging of squamous cell carcinoma of the tongue and floor of the mouth. Radiographics 16:787–810

Smoker WRK (2003) The oral cavity. In: Som PM, Curtin HD (eds) Head and neck imaging, 4th edn.. Mosby, St. Louis, pp 1377–1464

Som PM, Brandwein MS (2003) Salivary glands: anatomy and pathology. In: Som PM, Curtin HD (eds) Head and neck imaging, 4th edn. Mosby, St. Louis, pp 2005–2133

UICC Union international contre le cancer (2002) TNM atlas. Springer, Berlin Heidelberg New York

van den Brekel MWM, Runne RW, Smeele LE et al (1998) Assessment of tumour invasion into the mandible: the value of different imaging techniques. Eur Radiol 8:1552–1557

Vogl TJ, Steger W, Ihrer S et al (1993) Cystic masses in the floor of the mouth: value of MR imaging in planning surgery. AJR Am J Roentgenol 161:183–186

Weber AL, Kaneda T, Scrivani SJ et al (2003) Jaw: cysts, tumors, and nontumorous lesions. In: Som PM, Curtin HD (eds) Head and neck imaging, 4th edn. Mosby, St. Louis, pp 930–994

Yasumoto M, Shibuya H, Takeda M et al (1995) Squamous cell carcinoma of the oral cavity: MR findings and value of T1- versus T2-weighted fast spin-echo images. AJR Am J Roentgenol 164:981–987

Yousem DM, Kraut MA, Chalian AA (2000) Major salivary gland imaging. Radiology 216:19–29

7 Neoplasms of the Oropharynx

Robert Hermans

CONTENTS

7.1 Introduction

Head and neck cancer commonly originates from the oropharynx. As in most head and neck sites, squamous cell cancer is the most frequently encountered malignant disease. Cigarette smoking and excessive alcohol consumption are well-known risk factors. The accuracy of pretherapeutic staging is an important factor in the treatment planning of oropharyngeal neoplasms; clinical examination and imaging studies are complementary in precisely evaluating tumor extent. As an adjunct to clinical surveillance, imaging can be used to monitor tumor response and to detect recurrent or persistent disease as early as possible.

R. Hermans, MD, PhD
Professor, Department of Radiology, University Hospitals Leuven, Herestraat 49, 3000 Leuven, Belgium

7.2 Normal Anatomy

The pharynx is divided in three sections: the nasopharynx lies behind the nasal cavity, the oropharynx behind the oral cavity, and the hypopharynx merging with the proximal oesophagus at the lower level of the cricoid bone, behind the larynx.

The pharyngeal constrictor muscles compose the posterior and lateral wall of the pharynx. They all insert on a midline localised fibrous raphe. This posterolateral wall of the pharynx is a continuous structure, without markings allowing separation in a naso-, oro- or hypopharyngeal level.

The soft palate separates the nasopharynx from the oropharynx. On imaging studies, often one uses a line extending the level of the hard palate as demarcation line on the lateral and posterior wall; an alternative is to use a horizontal line through the C1–C2 articulation (Chong et al. 1999). Direct sagittal MR images, or sagittally reformatted CT images are well suited for defining the border between the naso- and oropharynx.

The oropharynx is separated from the hypopharynx by the pharyngoepiglottic folds. The border between the oropharynx and oral cavity is more complex, being ring-like and composed by several structures. The upper part of this ring is formed by the junction between the hard and soft palate; therefore, the hard palate is a structure belonging to the oral cavity, while the soft palate is an oropharyngeal structure (actually only its lower surface – the upper surface belongs to the nasopharynx). A mucosal fold, known as the anterior tonsillar pillar, forms the lateral part of the ring. This mucosal fold marks the anterior border of the tonsillar fossa. The lower part of the ring is formed by a row of small structures on the back of the tongue, the circumvallate papillae. These papillae are on a V-shaped line, with the tip of the V pointing posteriorly. By definition, the posterior third of the tongue (called tongue base) is part of the oropharynx, and not of the oral cavity (Hermans and Lenz 1996).

The soft palate is a complex structure, composed of muscles, some fat and lymphoid tissue. Two muscles, arising from the skull base, take part in the formation of the soft palate. The more medial one is known as the levator veli palatini, the more lateral one as the tensor veli palatini. These muscles have an important role during deglutition and phonation. They also form a functional unit with the Eustachian tube; their action opens the Eustachian tube fissure during swallowing and yawning. Dysfunction of the Eustachian tube causes serous otitis, a common finding in nasopharyngeal cancer.

The anterior and posterior tonsillar pillar define the triangular tonsillar fossa. Both pillars are mucosal folds produced by underlying muscular structures. The anterior muscle is the palatoglossal muscle, connecting the soft palate with the tongue base. The posterior muscle is the palatopharyngeal muscle, which takes part in the formation of the muscular pharyngeal wall. Oropharyngeal cancers commonly arise on the anterior tonsillar pillar, using this muscle and the overlying mucosa as a pathway to spread into the soft palate and tongue base. The tonsillar fossa harbours the palatine tonsil, consisting of encapsulated lymphoid tissue. The palatine tonsil is one of the major tonsils in the lymphoid ring of Waldeyer; the other major tonsils are the lingual tonsil in the tongue base, and the pharyngeal tonsil in the roof of the nasopharynx.

The pit between the tongue base and the free edge of the epiglottis is divided by a median mucosal fold running from the base of the tongue to the epiglottis; this fold is known as the glossoepiglottic fold, and separates both valleculae. The valleculae are part of the oropharynx. Anatomically, the lingual side of the free epiglottic margin is the posterior border of the valleculae. For staging purposes, it is important to know that the entire epiglottis is considered as part of the larynx.

Underneath the vallecular floor a laryngeal fat plane is present, known as the preepiglottic fat plane; this fatty tissue is sometimes used by oropharyngeal tumours to dive into the larynx, an extension that is occult to the examining clinician.

The different subsites of the oropharynx, important for staging purposes, are summarized in Table 7.1.

The largest part of the tongue base is composed of muscles, both intrinsic and extrinsic muscles. On axial imaging, these intrinsic muscular fibres may produce a relative high density in the tongue base on CT images, which should not be confused with an infiltrating mass lesion; the regular and symmetric appearance of these normal muscles allows avoidance of this pitfall.

Table 7.1. Subsites within the oropharynx (UICC 2002)

Anterior wall
– Base of tongue (posterior to circumvallate papillae or posterior third)
– Vallecula
Lateral wall
– Tonsil
– Tonsillar fossa and tonsillar (faucial) pillars
– Glossotonsillar sulci
Posterior wall
Superior wall
– Inferior surface of soft palate
– Uvula

The lingual artery is the main arterial supply to the tongue. It is a branch of the external carotid artery, arising just distal from the superior thyroid artery and proximal to the facial artery. Three segments can be distinguished (Portugalli et al. 2003):

- A proximal segment, running anterosuperior from the external carotid artery, entering the tongue base just above the hyoid bone, medial to the hyoglossal muscle. The hypoglossal nerve crosses the origin of the lingual artery, but runs lateral to the hyoglossal muscle.
- A middle segment, running along the medial side of the hyoglossal muscle.
- A branching distal segment, dividing into the deep lingual artery and sublingual artery.

The lingual nerve, a branch of the third portion of the trigeminal nerve, enters the tongue at a higher level than the lingual artery; this nerve enters the tongue from the parapharyngeal space, lateral to the stylohyoid and hyoglossal muscle. The lingual nerve contains sensitive and sensory (via the chorda tympani, branch of the facial nerve) fibres for the anterior two-thirds of the tongue. The sensory and sensitive innervation of the tongue base is via the glossopharyngeal nerve.

The lymphoid tissue within the ring of Waldeyer can appear prominent in younger subjects, prolapsing into the pharyngeal lumen. The amount of the lymphoid tissue decreases with age. Patients older than 40 years are not expected to have a significant amount of residual lymphatic tissue, but small tags of tissue may persist. The volume of the tonsils may increase due to an upper respiratory tract infection, but also due to an extranodal lymphoma localisation. A persistent or asymmetric appearing lingual tonsil can cause problems, as differentiation with a malignant tumour is not always possible. Clues, which may help to differentiate,

are air-filled crypts and the presence of small calcifications within the lymphatic tissue. Lymphatic tissue does not invade the deeper structures (Fig. 7.1; see also Fig. 7.9). One should however always stay prudent, and in the case of doubt, biopsies are warranted.

The parapharyngeal space runs from the skull base to the submandibular salivary glands. It essentially consists of fat and is bordered medially by the pharyngeal walls and laterally by the infratemporal space (containing the masticatory muscles). Contrary to the superficial tissues of the oropharynx, which may appear somewhat asymmetric, this deeper lying parapharyngeal space should always appear symmetric; any asymmetry should be treated with extreme caution (Farina et al. 1999). The parapharyngeal space has a small anterior extension between the oropharyngeal wall and the medial pterygoid muscle; this narrow space is known as the pterygomandibular space, reaching the mandible; it contains the lingual nerve. This small pterygomandibular space is actually a crossroads of several structures belonging to different spaces. The anterior tonsillar pillar, connecting the soft palate to the tongue base, and using the pterygomandibular space as access to the parapharyngeal space, is very close, as well as the retromolar trigonum of the mandible, a small triangular bony space, localised just

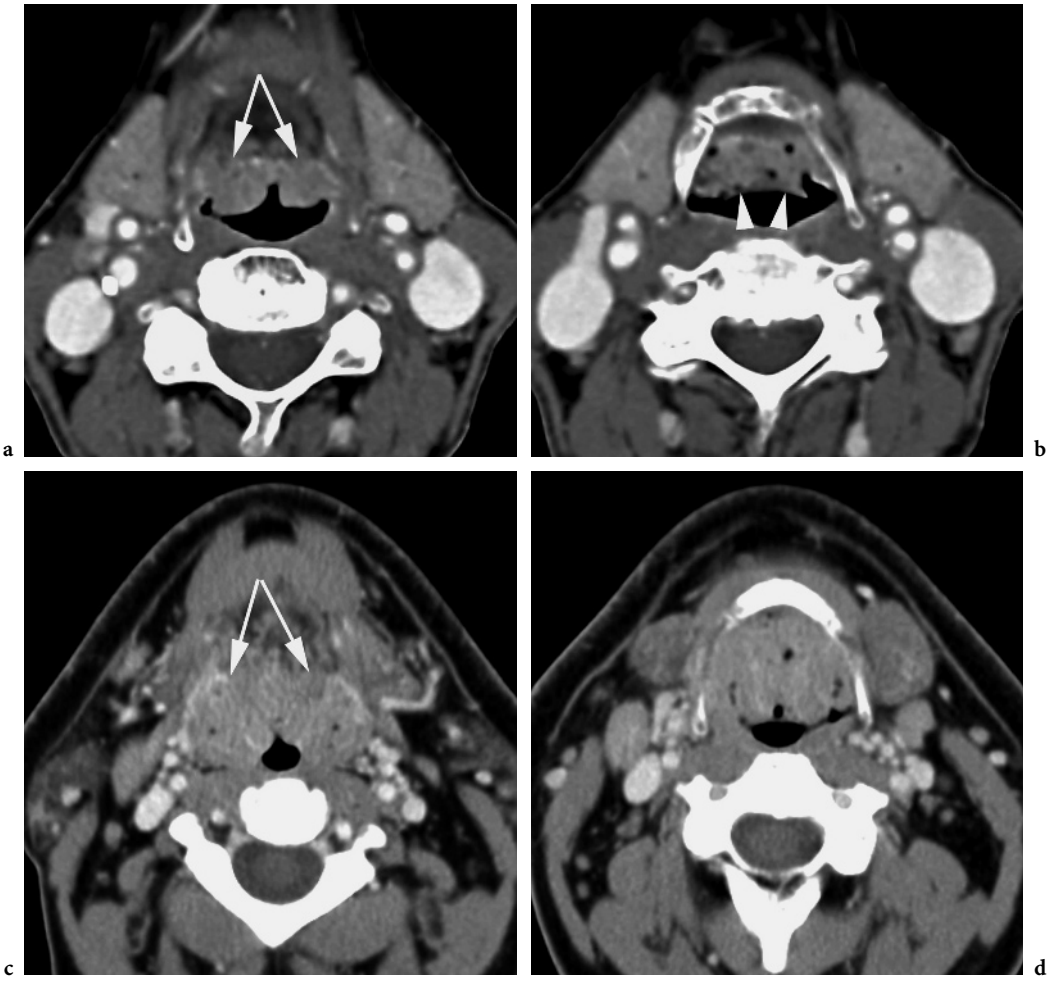

Fig. 7.1.a–d. Contrast-enhanced CT images in a 63-year-old patient (**a,b**). The study was performed because of a parotid tumor. The lingual tonsil appear prominent. The symmetric appearance, lack of invasion in the tongue base tissues (*arrows*, **a**), and the presence of air-filled crypts, as visible at the vallecular level (**b**), indicate benign enlargement of the tonsillar lymphoid tissue. Epiglottic rim, (*arrowheads*) (**b**). No biopsies were obtained. **c,d** Contrast-enhanced CT images in a 40-year-old patient complaining of globus sensation. Large volume of the lingual tonsil, narrowing the oropharyngeal airway, both at the level of the tongue base (**a**) and valleculae (**b**). The tissue appears symmetrical, does not invade the tongue base (*arrows*) and contains air-filled crypts, suggesting benign enlargement of the tonsillar lymphoid tissue. Because of the large size of this tonsil, and the associated symptoms, biopsies were obtained on three occasions over a period of 6 months: histological examination always showed follicular hyperplasia, without evidence of tumor

behind the third lower molar. The mucosal surface at the level of the retromolar trigone also covers the fibrous pterygomandibular raphe. On the posterior side of this raphe, part of the pharyngeal constrictor muscle originates, while on the anterior side, the buccinator muscle takes its origin, eventually forming the muscular substrate of the cheek.

The parapharyngeal space and its neoplastic pathology is discussed in detail in Chap. 9.

7.3 Squamous Cell Carcinoma

Squamous cell carcinoma is the most frequent malignant tumour of the oropharynx (90%). Most patients complain of sore throat, otalgia or dysphagia; more advanced, invasive tumours may cause severe pain and trismus.

The T staging is based on tumour size, and involvement of adjacent structures (Table 7.2). The most common site of origin of oropharyngeal cancer is the anterior tonsillar pillar.

7.3.1 Tonsillar Cancer

Nearly all tonsillar cancers originate from the anterior tonsillar pillar. These cancers commonly spread anteroinferiorly to the tongue base, and superomedially to the soft palate, both along the palatoglossal muscle. Anterolateral spread, along the pharyngeal constrictor muscle to the pterygomandibular raphe and retromolar trigone, is also commonly seen (Fig. 7.2). Advanced lesions may invade the mandible, spread along the pharyngeal wall to the hypo- and/or nasopharynx, or invade the parapharyngeal space through the pharyngeal wall (Figs. 7.3 and 7.4). Spread to the infratemporal space, with involvement of the muscles of mastication and neurovascular structures in this space may be seen in advanced cases (Fig. 7.5).

Lesions originating from the posterior tonsillar pillar are rare; these may spread inferiorly along the palatopharyngeal muscle.

Table 7.2. T staging of oropharyngeal carcinoma (UICC 2002)

Tis	Carcinoma in situ
T1	Tumour ≤ 2 cm in greatest dimension
T2	Tumour > 2 cm but ≤ 4 cm in greatest dimension
T3	Tumour measures > 4 cm in greatest dimension
T4a	Tumour invades any of the following : larynx, deep/extrinsic muscle of the tongue (genioglossus, hyoglossus, palatoglossus, and styloglossus), medial pterygoid, hard palate, and mandible
T4b	Tumour invades any of the following: lateral pterygoid muscle, pterygoid plates, lateral nasopharynx, skull base, or encases the carotid artery

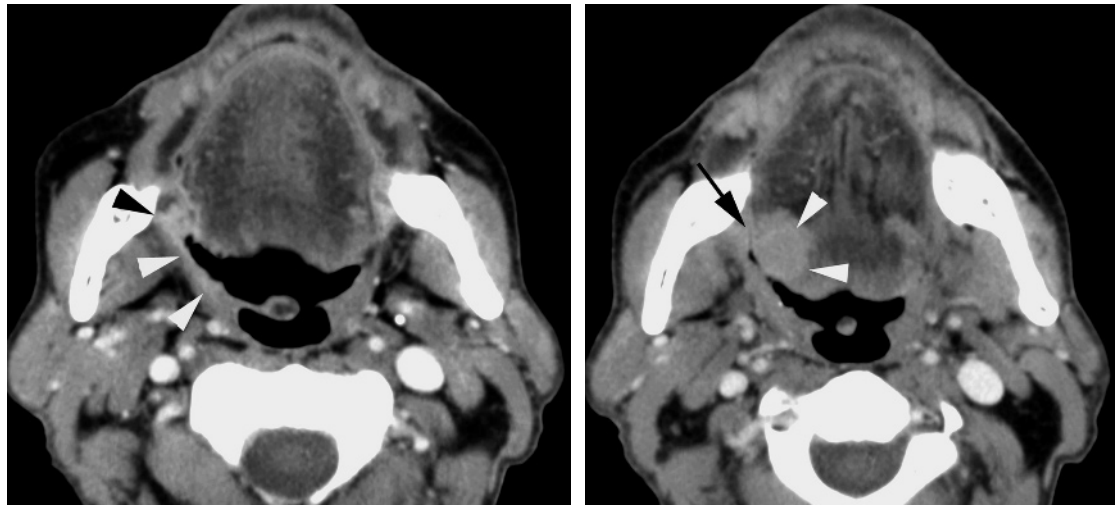

a b

Fig. 7.2a,b. Axial contrast-enhanced CT images in a patient with right-sided tonsillar cancer. **a** Soft tissue thickening and increased enhancement is seen in the right anterior tonsillar pillar (*white arrowheads*), extending into pterygomandibular raphe (*black arrowhead*). **b** The enhancing soft tissue mass extends along the glossotonsillar sulcus (*arrow*) into the tongue base (*arrowheads*)

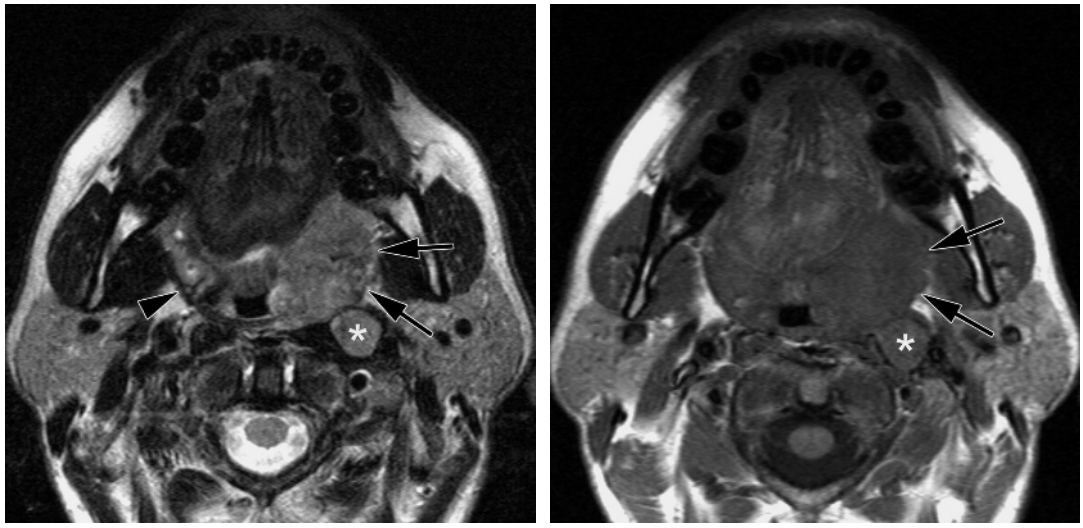

Fig. 7.3a,b. Axial T2-weighted (**a**) and plain T1-weighted spin echo image (**b**) in a patient with a left-sided tonsillar cancer. The soft tissue mass involves the palatine tonsil, grows through the pharyngeal constrictor muscle into the parapharyngeal space (*arrows*, compare to opposite side). The mass lesion reaches the retromolar trigone, and slightly compresses the tongue base. Retropharyngeal adenopathy (*asterisk*). Normal pharyngeal constrictor muscle on right side (*arrowheads*)

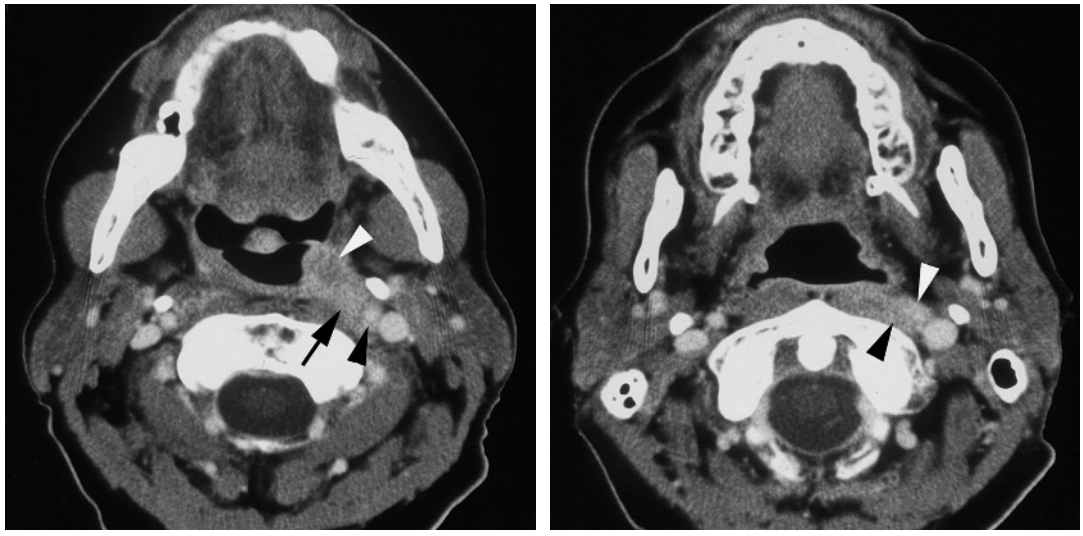

Fig. 7.4a,b. Patient presenting with left-sided otalgia. Clinical examination show left-sided tonsillar tumor. Axial contrast-enhanced CT images. **a** Level of oropharynx: enhancing mass lesion in left oropharyngeal tonsil (*white arrowhead*), extending into the retrostyloid compartment of the parapharyngeal space (*arrow*), encasing the internal carotid artery (*black arrowhead*). **b** Level of nasopharynx. Submucosal perivascular tumor extension (*black arrowhead*) along the internal carotid artery (*white arrowhead*)

7.3.2 Tongue Base Cancer

Cancer in the tongue base tends to grow silently and deeply, and is often larger than suspected at clinical examination. Tumours may spread along the palatoglossal muscle, cornering the glossotonsillar sulcus, to involve the anterior tonsillar pillar.

Anterior spread into the floor of the mouth and/or tongue body may occur, along the mylo- and/or hyoglossal muscle, and/or along the lingual neurovascular bundle (Fig. 7.6). Tongue base cancer may also grow in a retrograde fashion along the lingual vessels towards the external carotid artery (Dubin et al. 2002).Vascular and perineural tumor spread is associated with reduced local and regional tumor

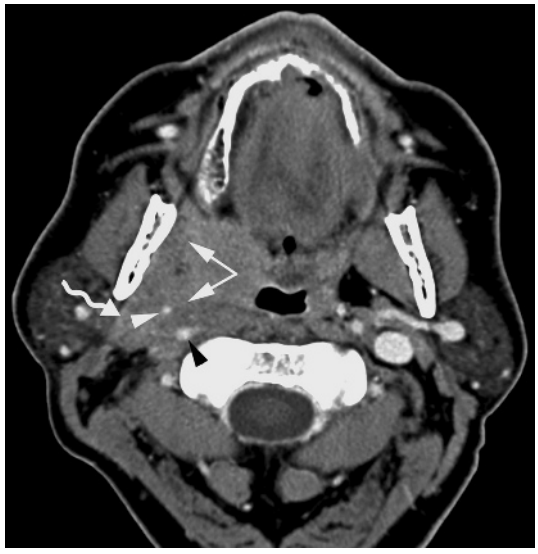

Fig. 7.5 Contrast-enhanced CT image in a patient with a right sided tonsillar cancer. The mass extends into the infratemporal space, parapharyngeal and carotid space (*arrows*). Encasement of the external carotid artery (*white arrowhead*), and partial encasement of the internal carotid artery (*black arrowhead*). Laterally, the mass is bordered by the posterior belly and the digastric muscle (*curved arrow*) and parotid gland

control and reduced patient survival. A tumor mass with a overall diameter of more than 2 cm on imaging predicts vascular and perineural tumor spread (Mukherji et al. 1996). Infiltration of the normal fatty tissue planes in the base of the tongue, of the fat in the sublingual space, as well as irregular tumor margins are also associated with an increased risk of vascular and perineural tumor spread. Such findings are related to overall tumor bulk.

Spread to the valleculae and piriform sinuses, and into the preepiglottic space may be seen. Retrograde tumor growth sometimes occurs along the styloid musculature (Fig. 7.7).

Extension of a tongue base cancer across the midline usually precludes surgical cure, as one lingual neurovascular pedicle needs to be conserved for sufficient functional recovery to allow safe swallowing (Fig. 7.8).

Differentiation of tongue base cancer from normal lymphoid tissue on the surface of the tongue base may be difficult on imaging studies; the only reliable criterion to diagnose cancer is infiltration of the deeper soft tissue structures (see above) (Fig. 7.9).

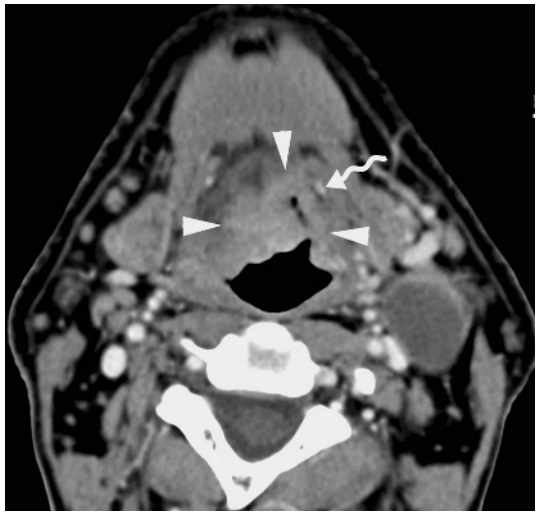

a

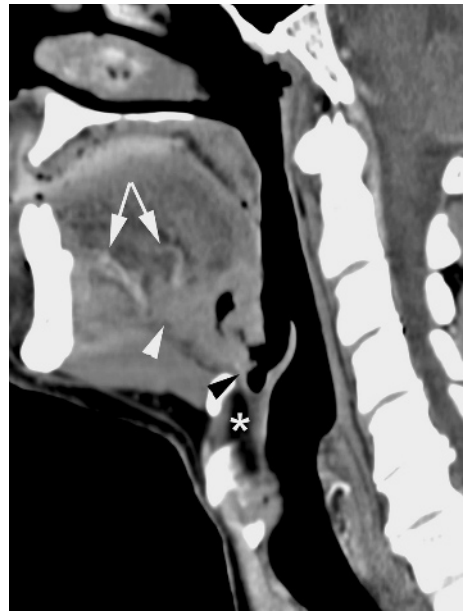

b

Fig. 7.6a,b. Contrast-enhanced CT images in a patient with tongue base cancer. **a** Axial image. An ulcerated, contrast-enhancing soft tissue mass is seen in the base of the tongue (*arrowheads*). Irregular tumor margins are present. The lesion crosses the midline, and approaches the left lingual artery (*curved arrow*). Large, necrotic adenopathy on left side. **b** Sagittal reformatted image (paramedian section on *left side*). The anterior spread in the floor of the mouth can be well appreciated (*white arrowhead*); again, close relationship to the proximal part of the lingual artery is seen (distal branches indicated by *arrows*). The lesion extends into the vallecula (*black arrowhead*); the preepiglottic space (*asterisk*) is not involved

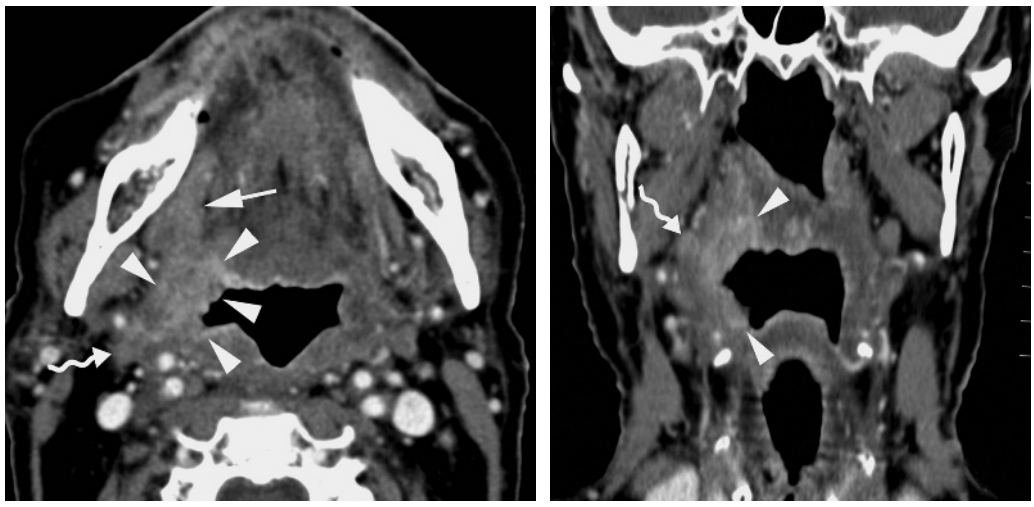

Fig. 7.7a,b. Patient treated by irradiation for right-sided tonsillar cancer 5 years earlier; clinically an area suspicious for recurrent cancer is seen on the right tonsil. **a** Axial contrast-enhanced CT image. Area of soft tissue thickening and increased enhancement in right tonsillar area, extending into tongue base (*arrowheads*): recurrent cancer. Some anterior extension along the hyoglossus muscle is suspected (*arrow*). The lesion abuts the styloglossal muscle, which has a slightly irregular contour (*curved arrow*). The fat planes surrounding the external and internal carotid artery are obliterated, but do not show increased enhancement: probably post-radiotherapy. **b** Coronal reformatted image. The cancer is extending into the soft palate (*upper arrowhead*) and down to the pharyngoepiglottic fold (*lower arrowhead*). Obliteration of fat planes along the styloglossal muscle, showing increased enhancement: perimuscular tumor extension

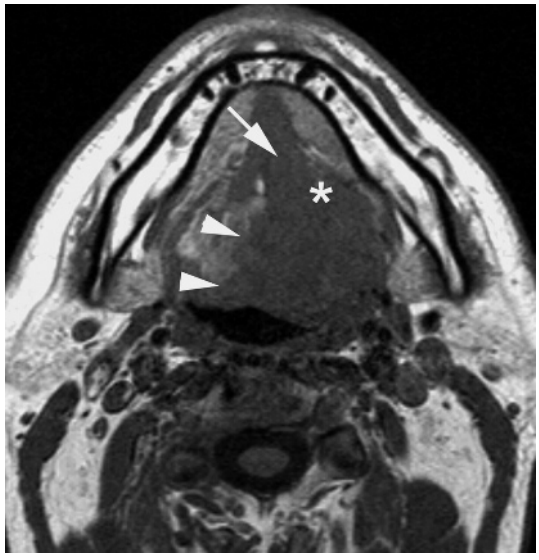

Fig. 7.8. Patient with a left-sided tongue base cancer. Axial plain T1-weighted spin echo image shows soft tissue mass growing over the midline (*arrowheads*), involving the left sublingual space (*asterisk*) and genioglossus/geniohyoid muscles (*arrow*)

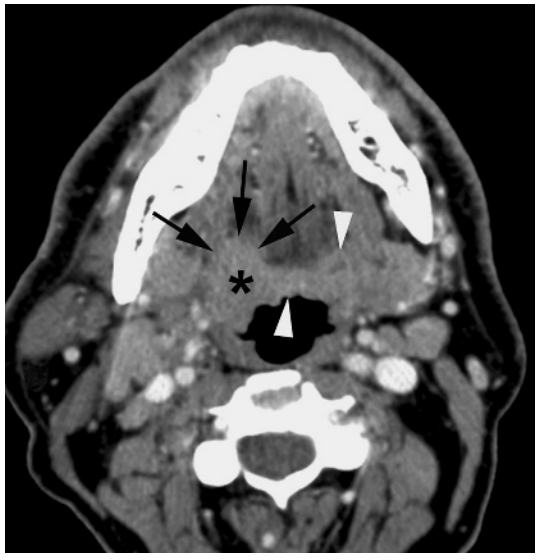

Fig. 7.9. Axial contrast-enhanced CT image in a patient with a right-sided tongue base cancer (*asterisk*). The lesion shows the same density as the lingual tonsil (*arrowheads*), but can be identified because it infiltrates the deeper tissues of the tongue base (*arrows*, compare to opposite side)

7.3.3 Soft Palate Cancer

Soft palate cancer may spread laterally and inferiorly along the tonsillar pillars. Superior spread to the nasopharynx occurs in advanced disease (Fig. 7.10). Carcinoma of the soft palate may occasionally spread perineurally along palatine branches of the maxillary nerve (Ginsberg and DeMonte 1998).

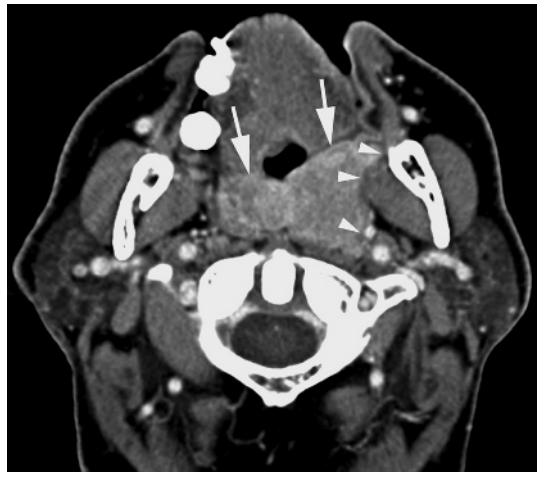

a

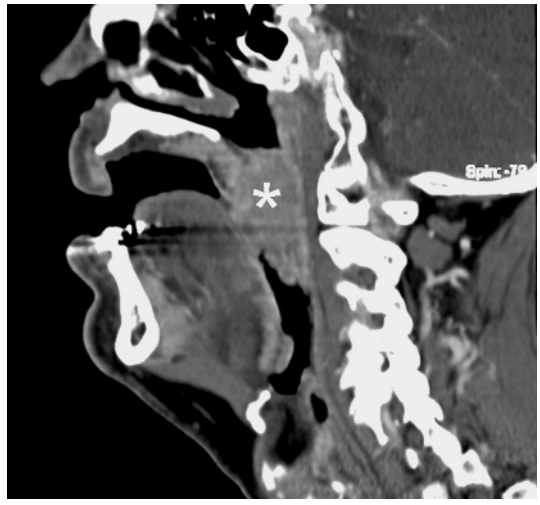

b

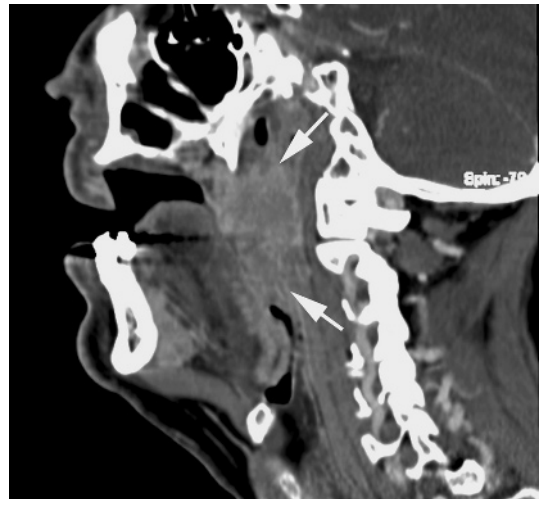

c

Fig. 7.10a–c. Contrast-enhanced CT images in a patient with soft palate cancer. **a** Axial image. Pronounced thickening and increased enhancement of the soft palate (*arrows*); the mass extends into the region of the retromolar trigone, and pushes the left lateral pharyngeal wall towards to parapharyngeal space (*arrowheads*). **b,c** Sagittal reformatted images (**c** more lateral than **a**), showing the soft palate tumor (*asterisk*); superior extension into the lower part of the nasopharynx (*upper arrow*) and into the lateral oropharyngeal wall (*lower arrow*) is seen

7.3.4 Posterior Oropharyngeal Wall Cancer

Isolated cancer in the posterior oropharyngeal wall is rare (Fig. 7.11); more commonly, this wall is invaded by cancers originating from the lateral oropharyngeal wall. Along the posterior wall, mucosal or submucosal spread to the hypopharynx and/or nasopharynx is possible.

Fixation to or direct invasion of the prevertebral fascia precludes the possibility of surgical resection of pharyngeal cancer, and is associated with a poor prognosis. The absence of prevertebral space involvement is reliably predicted on CT and MR images by demonstrating the preservation of the retropharyngeal fat plane. The negative predictive value of this sign varies between 82% and 97.5% (Righi et al. 1996; Hsu et al. 2005). However, cross-sectional imaging is poor in predicting involvement of the prevertebral space. Obliteration of the retropharyngeal fat plane, asymmetric enlargement of the prevertebral muscles (on CT studies), and thickening and signal abnormalities (on MR studies) are all unreliable signs to diagnose extension into this space (Righi et al. 1996; Loevner et al. 1998; Hsu et al. 2005) (Fig. 7.11). Open neck exploration with direct evaluation of the prevertebral muscles is superior to CT and MRI and should be considered in these patients. However, the decision to surgical resection is influenced in these patients by a number of factors in addition to involvement of the prevertebral space, including carotid artery encasement, perineural spread, retropharyngeal adenopathy and overall patient performance status. Also, the majority of lesions on the posterior pharyngeal wall are treated by radiotherapy or combined chemotherapy and radiotherapy, as the reported cure rates are similar to those of surgery alone or combined surgery and radiotherapy (Million et al. 1994). Nevertheless, as surgical reconstruction methods improve, resection with postoperative radiotherapy can be considered in selected cases (Julieron et al. 2001).

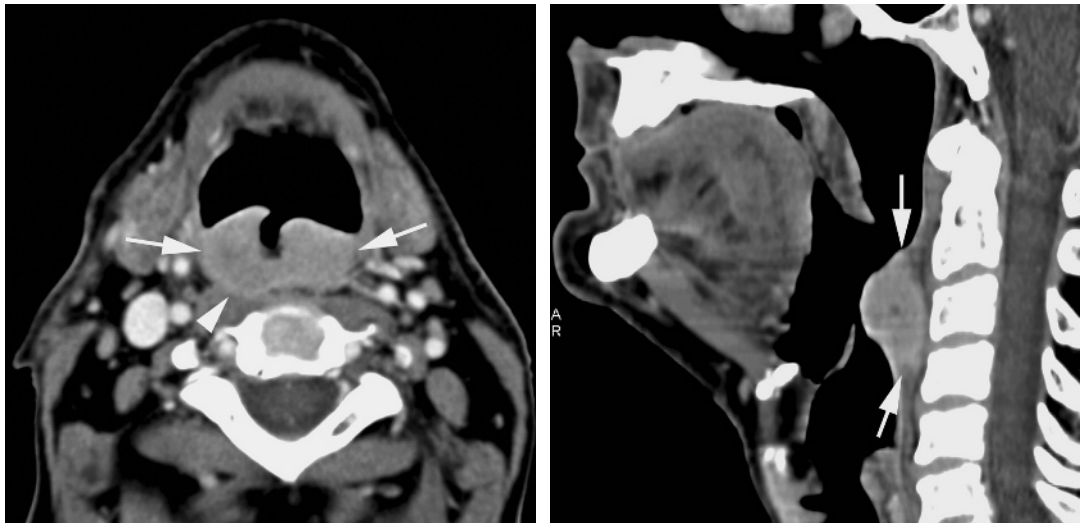

Fig. 7.11a,b. Contrast-enhanced CT images in a patient with cancer of the posterior oropharyngeal wall. **a** Axial image. Contrast-enhancing soft tissue mass (*arrows*), showing ulceration. On the right side, the lesion obliterates the retropharyngeal fat plane and abuts the prevertebral muscle (*arrowhead*); invasion of this muscle can not be excluded. **b** Coronal reformatted image, showing the craniocaudal extent of the lesion (*arrows*). The mass remains limited to the oropharyngeal level. The patient was treated by radiotherapy

7.3.5 Lymphatic Spread

Lymphatic spread usually occurs in a predictable way, from superior to inferior, the upper parajugular lymph nodes (level II) being the first echelon at risk. Retropharyngeal adenopathy is relatively common and usually associated with lymphadenopathy in other neck levels; isolated retropharyngeal adenopathy without involvement of other lymph nodes also occurs, particularly in posterior oropharyngeal wall cancer.

Bilateral adenopathies are commonly seen in soft palate cancer, as well in base of the tongue cancer.

The imaging criteria for diagnosing metastatic neck adenopathy are described in Chap. 15.

7.4 Treatment

Oropharyngeal cancer is treated with curative intent by radiotherapy, surgery or a combination of both modalities. Depending on anatomical localisation, small lesions (T1 or T2) are treated by either radiotherapy or surgery; cancer of the soft palate or uvula is treated by irradiation, as surgery of these structures interferes with palatal function. Larger lesions (T3 or T4) are, if possible, surgically treated, with postoperative radiotherapy. Inoperable oropharyngeal cancer is treated by concomitant chemoradiotherapy.

Several studies indicated, in glottic, supraglottic, hypopharyngeal and nasopharyngeal squamous cell carcinoma, the value of CT-determined primary tumour volume as prognostic parameter for local outcome after radiation treatment; increasing volume of the primary tumour indicates an increased likelihood of local failure (Mukherji et al. 2004). Such imaging-derived information allows better stratification of patients in a low- or high-risk group for local failure than clinical examination alone. This opens perspectives for more optimized treatment modulation in patients with head and neck squamous cell carcinoma. It also allows the identification of a patient group potentially benefiting from frequent post-therapy imaging surveillance, in order to identify tumour persistence or recurrence at an early stage.

However, studies on oropharyngeal cancer in general (Nathu et al. 2000), and tonsillar cancer in particular (Hermans et al. 2001), revealed an only marginal impact of CT-determined primary tumour volume on local outcome, while T category was very significantly correlated with local outcome. Despite the pronounced variability within each T category, tumour volume could not be used to separate patients within the same T category in groups with different local outcome (Hermans et al. 2001). Why the relation between tumour volume and local outcome is less pronounced in oropharyngeal cancer compared

to other head and neck sites, is not clear. Clinically, a relation between the growth pattern of a cancer and its response to radiotherapy has been noted, with exophytically growing cancers generally being more radiosensitive than infiltrating cancers. This may be related to a larger anoxic compartment in deeply growing cancers, as was suggested by Fletcher and Hamberger (1974) in a study on supraglottic cancer. In this context, the variable degree of deep tissue infiltration by oropharyngeal cancer may dilute the volume effect.

7.5 Post-treatment Imaging

The expected neck tissue changes after radiotherapy are described in Chap. 4. Within the oropharyngeal region, mainly thickening of the muscular pharyngeal walls, reduced volume of the tonsillar lymphoid tissue, some degree of retropharyngeal edema, and increased attenuation of the fatty tissue planes is expected. After successful irradiation, the tumor bed is expected to show similar characteristics as the surrounding normal tissues (Fig. 7.12).

Although currently no hard data are available on the value of surveillance imaging for oropharyngeal cancer after radiotherapy, obtaining a baseline follow-up CT or MR study 3–6 months after the end of therapy can be considered. In a number of cases, local failure can be detected at an earlier stage than by clinical examination alone. Persisting or recurring tissue asymmetry and/or increased tissue enhancement after therapy, are suspect for persisting or recurring tumor (Fig. 7.13). Such findings need further exploration; when no clinical correlate is apparent, it is safe to perform an additional nuclear imaging study or to obtain a follow-up CT/MR study about 4 months later. In case of persisting or progressive tissue changes, tissue sampling is required.

When an oropharyngeal cancer is treated primarily by surgery, often extensive removal of soft tissues, and possibly also mandibular bone is needed to obtain oncologically safe resection margins. To reconstruct the created tissue defects, and to obtain a better functional and/or cosmetic result, tissue transfer from a body donor site to the oropharyngeal region may be required. These flaps are vascularized by local vessels, anastomosed to the flap by microvascular techniques. Different kinds of free flaps are in use, for example cutaneous flaps to reconstruct defects in the oropharyngeal cavity, or osseous flaps (e.g. fibula) to reconstruct mandibular defects (Fig. 7.14). A CT or MR study, obtained about 4 months after the end of such a complex procedure, may be helpful as a baseline study allowing earlier diagnosis of subsequent tumor recurrence.

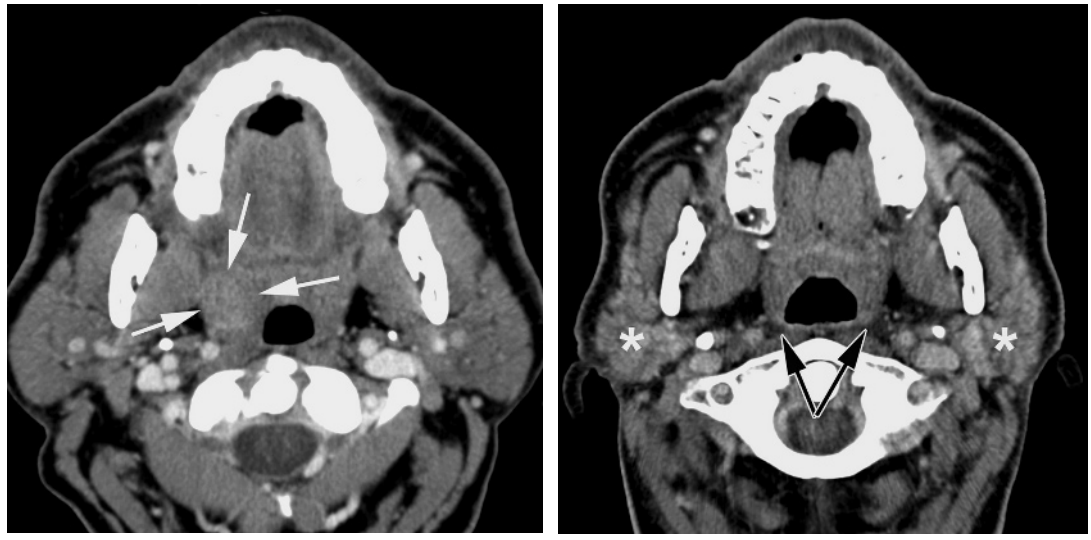

Fig. 7.12a,b. Patient with a right-sided T3 oropharyngeal tonsillar cancer, treated by definitive radiotherapy. Anatomically corresponding axial contrast-enhanced CT images are shown, obtained just before and 6 months after completion of radiation treatment. Before treatment (**a**), part of the oropharyngeal cancer is seen (*white arrows*). After radiotherapy (**b**), the oropharyngeal tissues appear symmetrical. Volume reduction and increased enhancement of the parotid salivary glands (*asterisks*) correspond to radiation sialadenitis. Slight retropharyngeal edema (*black arrows*)

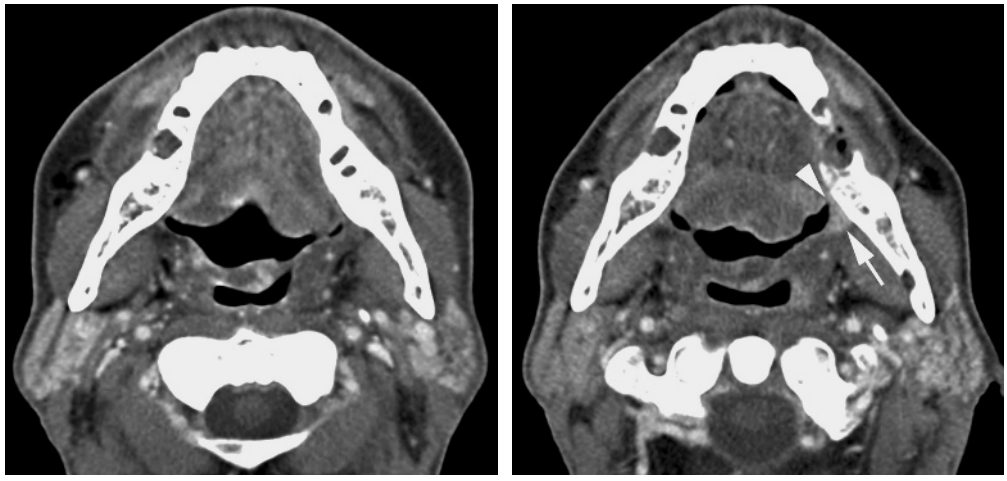

Fig. 7.13a,b. Axial contrast-enhanced CT image (**a**), obtained 4 months after completion of radiotherapy for a T2N1 oropharyngeal cancer. Expected changes after radiotherapy are seen, no evidence for local disease. **b** Because of left-sided odynophagia and otalgia, a new CT study was obtained 2 months later. Slight soft tissue thickening and increased enhancement is seen in the left anterior tonsillar pillar (*arrow*) extending into glossotonsillar sulcus (*arrowhead*) (compare with **a**). Clinically, this abnormality corresponded to a small granulomatous lesion. Biopsy revealed squamous cell cancer

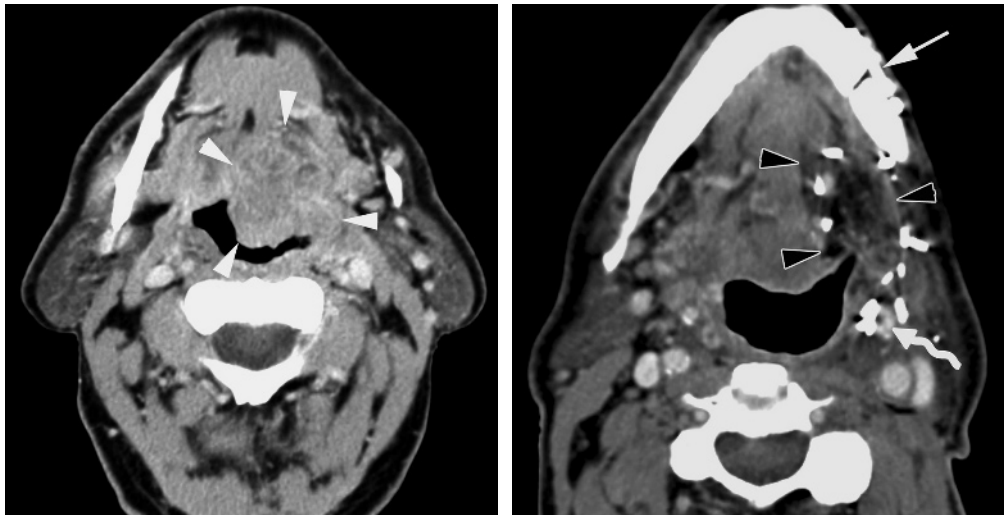

Fig. 7.14a,b. Contrast-enhanced CT images in patient with a T3 squamous cell cancer of the tongue base. **a** Large tumour mass, slightly extending over the midline and growing into the lateral pharyngeal wall (*arrowheads*). **b** CT study obtained 1 year after surgical resection and post-operative radiotherapy. The tumor was approached after splitting the mandible (osteotomy site and osteosynthetic plate, *white arrow*). The soft tissue defect was closed by a radial forearm flap (*black arrowheads*), whose vascular pedicle was anastomosed to the external carotid artery (*curved arrow*). The high density opacities correspond to surgical clips

7.6. Other Neoplastic Disease

7.6.1 Non-Hodgkin Lymphoma

Due to the abundant lymphoid tissue in the oropharynx (lingual and palatine tonsils), non-Hodgkin lymphoma occurs in this region as extranodal lymphatic disease. The diagnosis of lymphoma can often be suggested based on the imaging findings, as these tumours frequently appear large and homogenous on imaging studies. Also, adenopathies may be present at sites unusual for an untreated carcinoma (Fig. 7.15), or the oropharyngeal lesion may be associated with another extranodal neck lymphoma localisation (Hermans et al. 1994). Such findings, occurring in patients without risk factors for head and neck carcinoma, are suggestive for lymphoma.

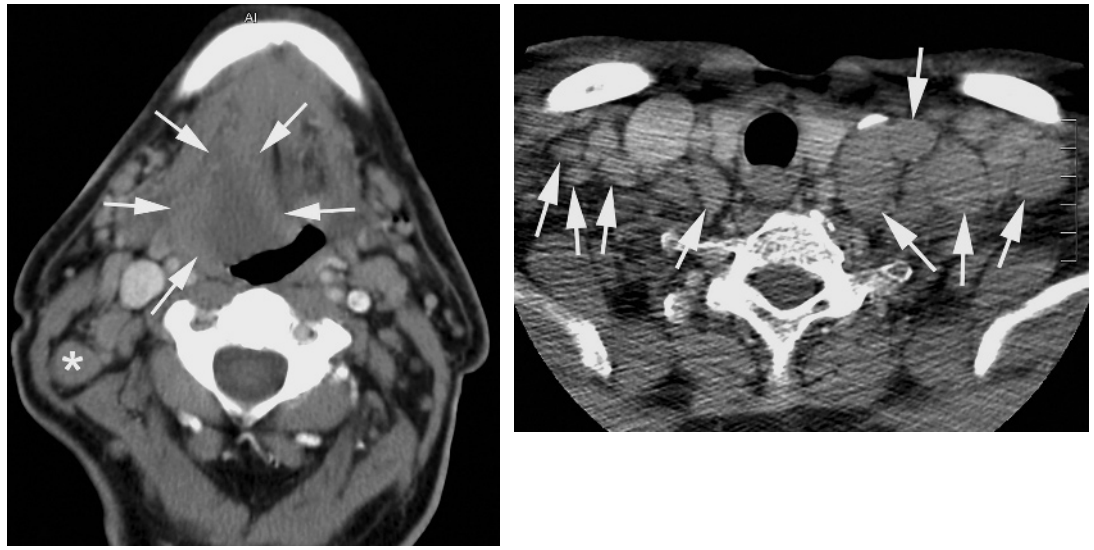

Fig. 7.15a,b. Axial contrast-enhanced CT images. **a** Infiltrating soft tissue mass (*arrows*) in the right tongue base. Ipsilaterally, a slightly enlarged lymph node is seen in level II (*asterisk*). Several of such lymph nodes were seen throughout both sides of the neck. **b** Bilaterally in the neck base, homogenous adenopathies are present, larger on the left side. The distribution of the adenopathies is atypical for tongue base cancer, making the imaging findings suspect for non-Hodgkin lymphoma; this was confirmed histologically

Neck lymphoma is described in more detail in Chap. 16.

7.6.2 Salivary Gland Tumors

These oropharyngeal neoplasms originate from minor salivary glands. In the soft palate, these are often benign pleiomorphic adenomas, but in other oropharyngeal sites malignant tumors, such as mucoepidermoid and adenoid cystic carcinoma, predominate (Watkinson et al. 2000) (Fig. 7.16).

7.6.3 Other

The thyroid gland is formed during embryologic life as an epithelial proliferation from the ventral pharyngeal wall; this proliferation is known as the medial thyroid anlage and the place where it arises corresponds later to the foramen caecum, at the border between the oral tongue and the tongue base. This medial thyroid anlage migrates downwards along the neck midline to its final position. Ectopic thyroid tissue can be found anywhere along this tract, but most commonly in the tongue. Patients with a lingual thyroid gland have no thyroid tissue in the neck in 70%–80% of the cases (Fig. 7.17). Ectopic thyroid is subject to the same diseases as the anatomically correct positioned thyroid, such as nodular hyperplasia and rarely neoplastic degeneration (Fig. 7.18). Development of a mass lesion is often the reason why this ectopic thyroid tissue becomes symptomatic.

Other benign tumoral lesions, such as hemangioma or schwannoma, may be encountered in the oropharynx. As these masses occur submucosally,

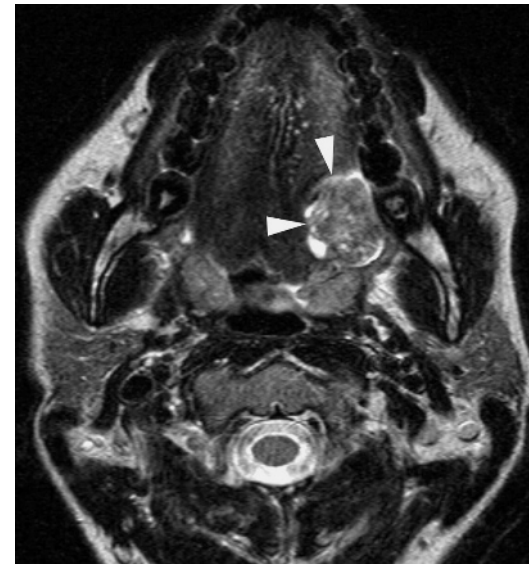

Fig. 7.16. Axial T2-weighted spin echo image. Well demarcated hyperintense soft tissue mass (*arrowhead*) posterolaterally in the tongue base. Biopsy revealed mucoepidermoid carcinoma

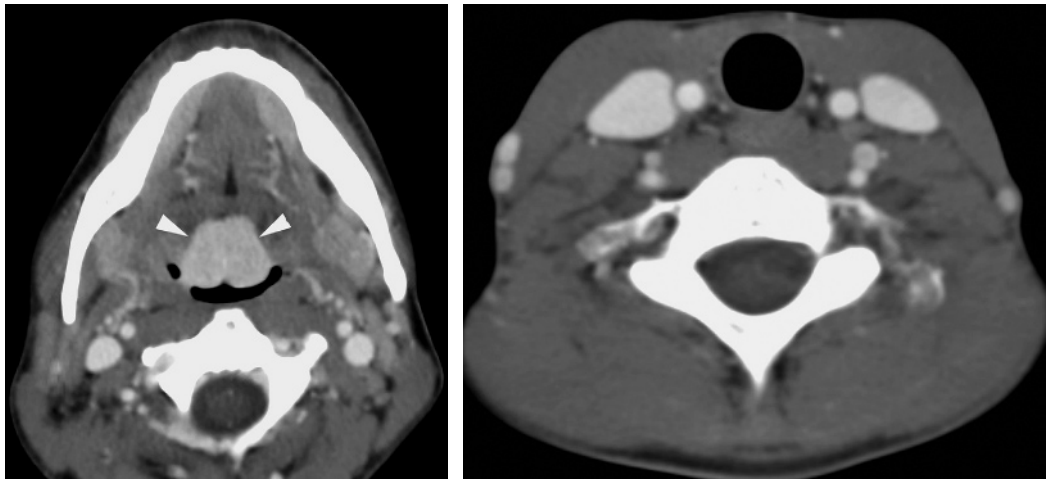

Fig. 7.17a,b. Axial contrast-enhanced CT images in a patient with progressive dysphagia. **a** Strongly enhancing soft tissue mass (*arrowheads*) in tongue base midline, compatible with ectopic thyroid tissue. **b** Absence of thyroid gland at its normal position

imaging is required to estimate their extent. A specific soft tissue diagnosis is usually not possible based on imaging findings, and tissue sampling is required for diagnosis (Fig. 7.19).

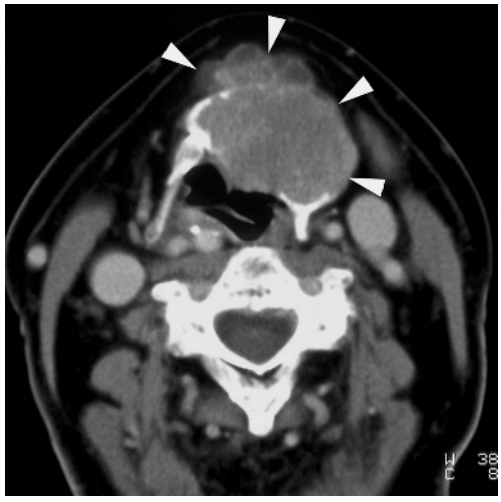

Fig. 7.18. Axial contrast-enhanced CT image in a patient with a progressive neck swelling. Mass lesion (*arrowheads*) centered in and destroying the hyoid bone, with extension to surrounding structures, causing narrowing of the oropharyngeal airway. The lesion was resected; pathological study revealed papillary thyroid carcinoma, presumably arising from ectopic thyroid tissue. There was no evidence for a primary cancer in the thyroid gland

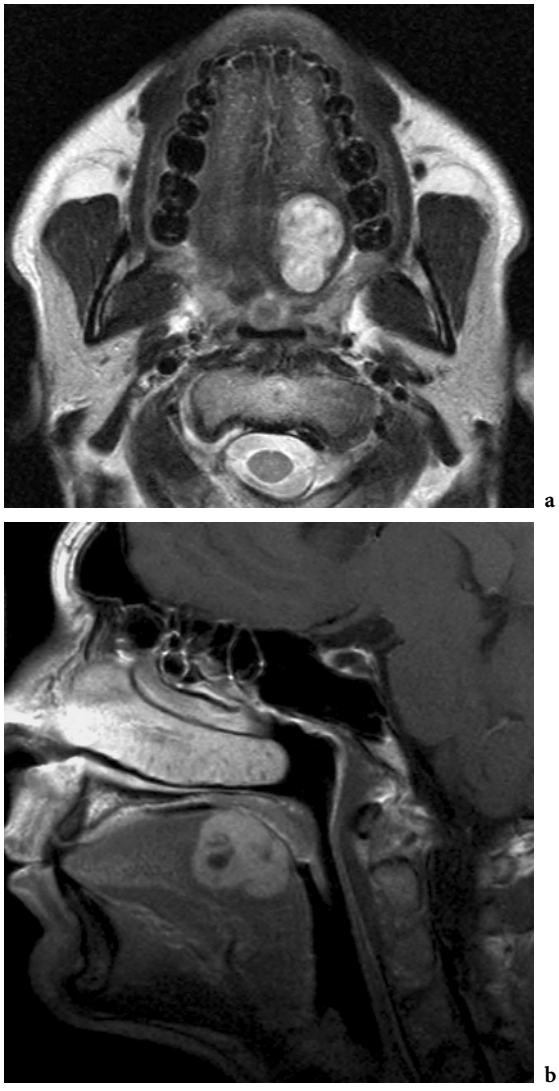

Fig. 7.19a,b. Axial T2-weighted spin echo image (**a**) in a 32-year-old patient shows a sharply demarcated, hyperintense mass in the tongue base on the left side. The sagittal gadolinium-enhanced T1-weighted spin echo image (**b**) shows homogenous lesion enhancement, with some areas of liquefaction. Biopsy revealed schwannoma

References

Chong VFH, Mukherji SK, Ng SHH, et al. (1999) Nasopharyngeal carcinoma: review of how imaging affects staging. JCAT 23:984–993

Dubin MG, Ebert CS, Mukherji SK, Pollock HW, Amjadi D, Shockley WW (2002) Computed tomography's ability to predict sacrifice of hypoglossal nerve at resection. Laryngoscope 112:2181–2185

Farina D, Hermans R, Lemmerling M, et al. (1999) Imaging of the parapharyngeal space. J Belge Radiol 82:234–239

Ginsberg LE, DeMonte F (1998) Imaging of perineural tumor spread from palatal carcinoma. AJNR Am J Neuroradiol 19:1417–1422

Hermans R, Lenz M (1996) Imaging of the oropharynx and oral cavity. Part I: normal anatomy. Eur Radiol 6:362–368

Hermans R, Horvath M, De Schrijver T, et al. (1994) Extranodal non-Hodgkin lymphoma of the head and neck. J Belge Radiol 77:72–77

Hermans R, Op de beeck K, Van den Bogaert W, et al. (2001) The relation of CT-determined tumor parameters and local and regional outcome of tonsillar cancer after definitive radiation treatment. Int J Radiat Oncol Biol Phys 50:37–45

Hsu WC, Loevner LA, Karpati R, et al. (2005) Accuracy of magnetic resonance imaging in predicting absence of fixation of head and neck cancer to the prevertebral space. Head Neck 27:95–100

Julieron M, Kolb F, Schwaab G, et al. (2001) Surgical management of posterior pharyngeal wall carcinomas: functional and oncologic results. Head Neck 23:80–86

Loevner LA, Ott IL, Yousem DM, et al. (1998) Neoplastic fixation to the prevertebral compartment by squamous cell carcinoma of the head and neck. AJR Am J Roentgenol 170:1389–1394

Million RR, Cassisi NJ, Mancuso AA (1994) Hypopharynx: pharyngeal walls, pyriform sinus, postcricoid pharynx. In: Million RR, Cassisi NJ (eds) Management of head and neck cancer: a multidisciplinary approach. J.B. Lippincott Co, Philadelphia, p 516

Mukherji SK, Weeks SM, Castillo M, et al. (1996) Squamous cell carcinomas that arise in the oral cavity and tongue base: can CT help predict perineural or vascular invasion? Radiology 198:157–162

Mukherji SK, Schmalfuss IM, Castelijns J, Mancuso AA (2004) Clinical applications of tumor volume measurements for predicting outcome in patients with squamous cell carcinoma of the upper aerodigestive tract. AJNR Am J Neuroradiol 25:1425–1432

Nathu RM, Mancuso AA, Zhu TC, Mendenhall WM (2000) The impact of primary tumor volume on local control for oropharyngeal squamous cell carcinoma treated with radiotherapy. Head Neck 22:1–5

Portugalli V, Borghesi A, Mossi F, Farina D, Maroldi R (2003) VIBE sequence in the diagnostic work-up of malignant neoplasms of the oropharynx. Scientific poster ECR 2003. http://epos.myecr.org/

Righi PD, Kelley DJ, Ernst R, et al. (1996) Evaluation of prevertebral muscle invasion by squamous cell carcinoma. Can computed tomography replace open neck exploration? Arch Otolaryngol Head Neck Surg 122:660–663

UICC, International Union Against Cancer (2002) TNM classification of malignant tumours, 6th edn. Wiley-Liss, New York, p 27, 29

Watkinson JC, Gaze MN, Wilson JA (2000) Stell and Maran's head and neck surgery, 4th edn. Butterworth Heinemann, Oxford, p 322, 338

8 Neoplasms of the Nasopharynx

Vincent F. H. Chong

CONTENTS

V. F. H. Chong, MD, MBA
Department of Diagnostic Radiology, National University Hospital, Yong Loo Lin School of Medicine, National University of Singapore, 5 Lower Kent Ridge Road, Singapore 119074, Singapore

8.1 Introduction

The nasopharyngeal mucosa consists of epithelium that is largely squamous in adult life, with foci of pseudostratified respiratory type surface epithelium, lymphoid submucosal stroma and seromucinous glands. A wide variety of malignant neoplasms can theoretically originate from the nasopharyngeal mucosa but regardless of geographic distribution, undifferentiated carcinoma is the most common form of malignancy, accounting for up to 98% of all nasopharyngeal malignancies in the Orient (Shanmugaratnam et al. 1979). Nasopharyngeal carcinoma (NPC) is a unique malignancy, representing the outcome of interactions of genetic factors, environmental factors and the Epstein-Barr virus (EBV). Patients with NPC show consistently high levels of antibodies to EBV antigens and these antibodies are very useful diagnostic markers.

NPC also shows a unique geographical distribution. The highest incidence rates (up to 50 per 100,000 population) are found in Southern China and Hong Kong followed by Singapore and US Chinese (Parkin et al. 1997). Intermediate incidence rates are seen in Eskimos, Polynesians and North Africans (Nielson et al. 1977). The incidence rates in Whites are very low (less than 1 per 100,000 population). NPC may affect children and adolescents but is much more frequently seen in the middle-aged (Seow et al. 2004). This malignancy is more common in males with a male to female ratio of 2.5:1.

NPC is distinct from the other squamous cell tumors of the head and neck. It shows aggressive local infiltration and a high frequency of cervical nodal metastasis despite apparently early primary lesions. Systemic failure is also common in patients with locally advanced disease (Ahmad and Stefani 1986). Radiation therapy is the mainstay of treatment. Chemotherapy is usually used for recurrent or metastatic disease but in recent years, a combination of radiation and chemotherapy has been tried for treatment of locally advanced disease. Surgery plays only

a minor role and is limited to resection of residual or recurrent disease in the nasopharynx and neck nodes.

8.2 Normal Anatomy

The nasopharynx is a fibromuscular sling suspended from the skull base. The boundaries of the nasopharynx are as follows: superiorly, the floor of the sphenoid sinus and the clivus; anteriorly, the nasal choanae; inferiorly, the oropharynx; posteriorly, the prevertebral musculature; and, laterally the parapharyngeal space (PPS) (Fig. 8.1).

The lateral pharyngeal recess (fossa of Rosenmüller) is located superior and posterior to the torus tubarius. The inverted J-configuration of the torus tubarius explains why the fossa of Rosenmüller appears posterior (on axial images) and superior (on coronal images) to the eustachian tube orifice. The eustachian tube enters the nasopharynx through the sinus of Morgagni, a defect in the pharyngobasilar fascia. The pharyngobasilar fascia (a tough aponeurosis), is the cranial extension of the superior constrictor muscle. It begins at the level of the soft palate and superiorly it is attached to the skull base.

The PPS separates the wall of the nasopharyngeal visceral space from the masticator space (MS). NPC frequently extends across the PPS resulting in the infiltration of the muscles of mastication and potential perineural spread along the mandibular nerve into the intracranial cavity (Chong et al. 1996a). Anatomically, the retrostyloid PPS, containing the carotid space (CS), is at risk for invasion by NPC (see also Chap. 9).

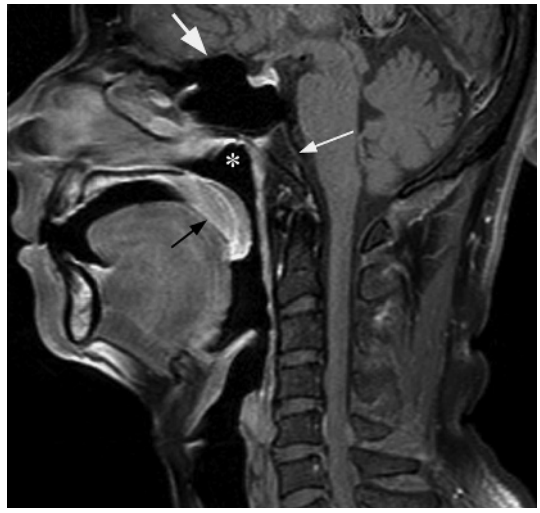

a

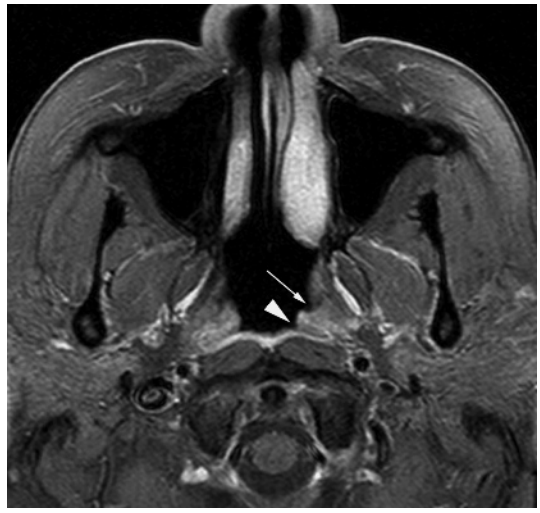

b

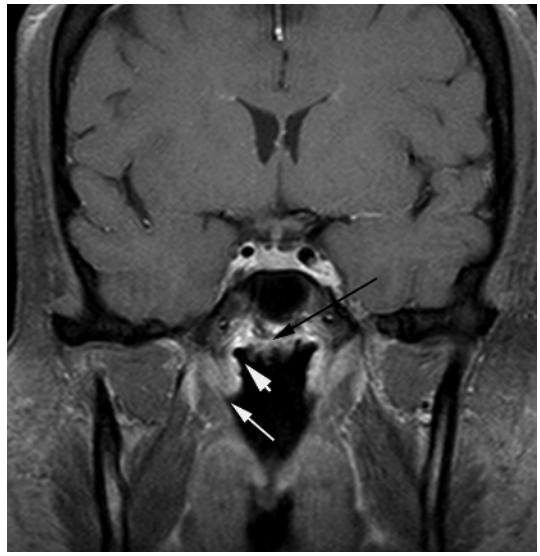

c

Fig. 8.1a–c. Normal anatomy of the nasopharynx. **a** Sagittal contrast-enhanced MR image shows nasopharynx (*asterisk*), sphenoid sinus (*big white arrow*), clivus (*small white arrow*) and soft palate (*black arrow*). **b** Axial contrast-enhanced MR image shows left eustachian tube opening (*arrow*) and left fossa of Rosenmüller (*arrowhead*). **c** Coronal contrast-enhanced MR image shows right fossa of Rosenmüller (*thick arrowhead*) and eustachian tube opening (*thin white arrow*). Note normal remnant adenoid tissue (*black arrow*)

Between the nasopharynx and the vertebral bodies are the retropharyngeal (RPS) and prevertebral spaces. Within the RPS are the lateral retropharyngeal (LRP) nodes of Rouviere. These nodes are the first echelon nodes in the lymphatic drainage of the nasopharynx and may be identified as discrete 3–5 mm nodules. However, in up to 35% of patients with NPC, cervical lymphadenopathy was seen without any demonstrable LRP nodal enlargement (Chong et al. 1995a).

The foramen lacerum and foramen ovale are potential pathways for tumor extension into the intracranial cavity. The foramen lacerum is superolateral to the fossa of Rosenmüller and is located within the attachment of the pharyngobasilar fascia to the skull base. Cartilage fills the inferior portion of the foramen lacerum. The foramen ovale is located lateral to the attachment of the pharyngobasilar fascia to the skull base.

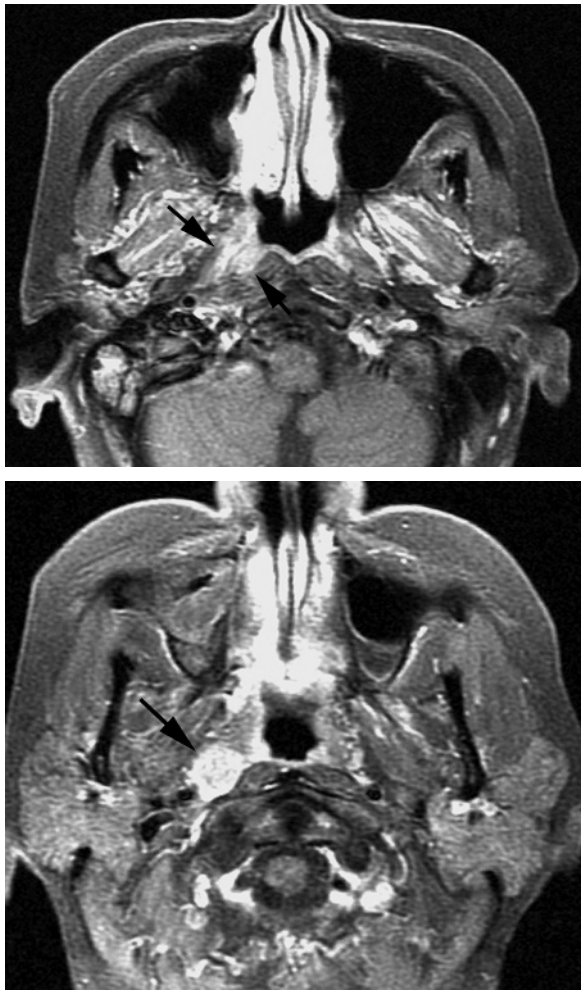

Fig. 8.2a,b. Early NPC. **a** Axial contrast-enhanced MR image shows enhancing tumor in right fossa of Rosenmüller (*opposing arrows*). Note inflammatory changes in right mastoid secondary to eustachian tube obstruction. **b** Axial contrast-enhanced MR image shows associated right retropharyngeal lymphadenopathy (*arrow*)

8.3 Pathologic Anatomy

Most tumors originate in the fossa of Rosenmüller (Fig. 8.2). Tumors tend to spread submucosally with early infiltration of the palatal muscles, in particular, the levator veli palatine (Sham et al. 1990a). This muscle is responsible for opening the eustachian tube orifice during swallowing. Muscular dysfunction leads to disequilibrium in the air pressure in the middle ear and the nasopharynx. The tumor may also obstruct the orifice of the eustachian tube, or spread along the this tube into the middle ear (Fig. 8.3). These factors commonly result in serous otitis media.

NPC spreads along well-defined routes and these routes are well reflected in the TNM staging system (Sobin and Wittekind 2002).

8.3.1 Anterior Spread

Tumors often spread anteriorly into the nasal fossa and this may be associated with erosion into the maxillary sinus (Chong et al. 1995b). From the nasal fossa, the tumor may infiltrate the pterygopalatine fossa (PPF) through the sphenopalatine foramen. The earliest sign of involvement of the PPF is obliteration of the normal fat content. Once the tumor gains access into the PPF, it can extend along the maxillary nerve and through the foramen rotundum into the cranium (Chong and Fan 1996a). Tumor in the PPF may spread further superiorly into the inferior orbital fissure and the orbital apex (Fig. 8.4). From the orbital apex, tumor can readily extend intracranially through the superior orbital fissure (Chong et al. 1998).

8.3.2 Lateral Spread

This is the most common direction of spread and can be recognized by infiltration of the fat-filled PPS (Fig. 8.5). Further lateral spread involves the MS and infiltration of the muscles of mastication (Fig. 8.6) (Chong 1997). Once the tumor is within the MS, the mandibular nerve is vulnerable to perineural

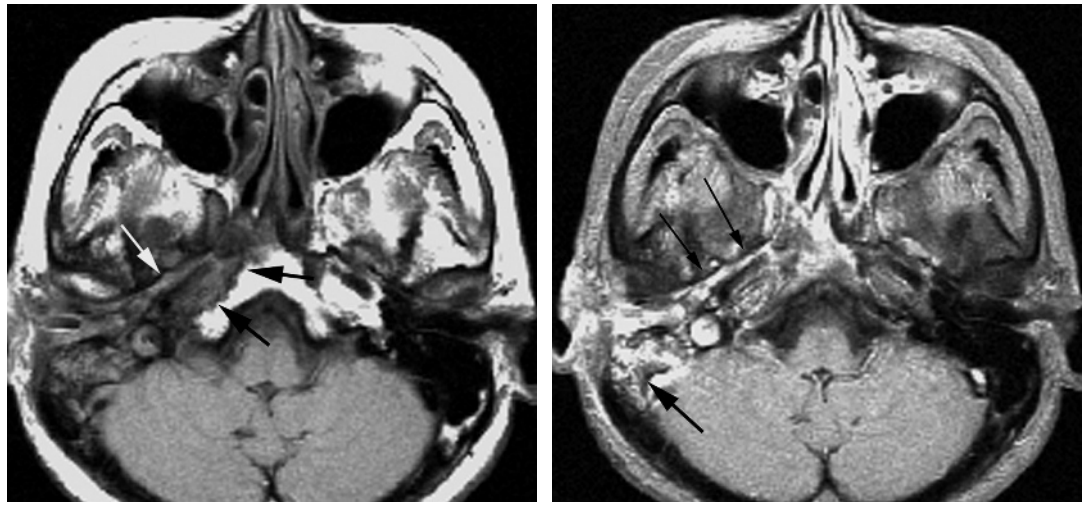

Fig. 8.3a,b. NPC spread along eustachian tube. **a** Axial T1-weighted MR image shows intermediate signal intensity tumor in eustachian tube (*white arrow*) and tumor eroding clivus (*black arrows*). **b** Axial contrast-enhanced MR image shows enhanced tumor in eustachian tube (*thin arrows*). Note secondary inflammatory changes in mastoid cells (*thick arrow*)

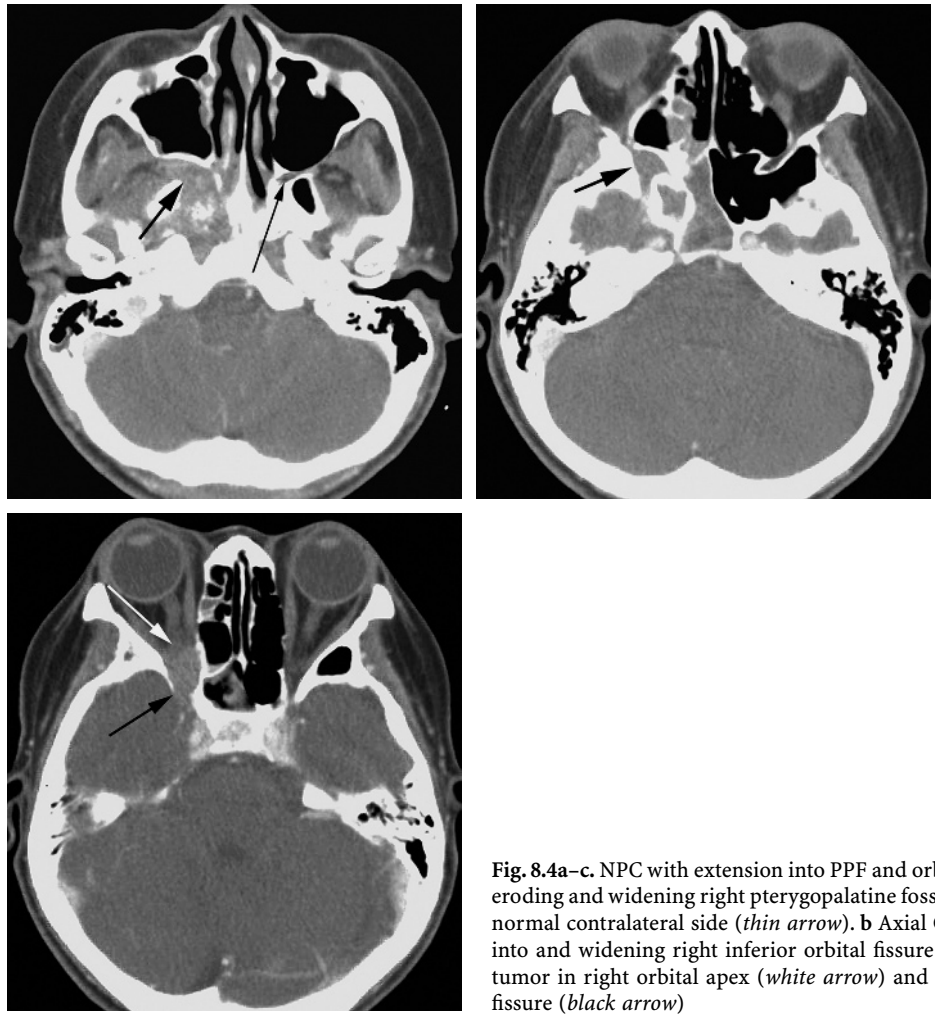

Fig. 8.4a–c. NPC with extension into PPF and orbit. **a** Axial CT shows tumor eroding and widening right pterygopalatine fossa (*thick arrow*); compare to normal contralateral side (*thin arrow*). **b** Axial CT shows tumor extending into and widening right inferior orbital fissure (*arrow*). **c** Axial CT shows tumor in right orbital apex (*white arrow*) and erosion of superior orbital fissure (*black arrow*)

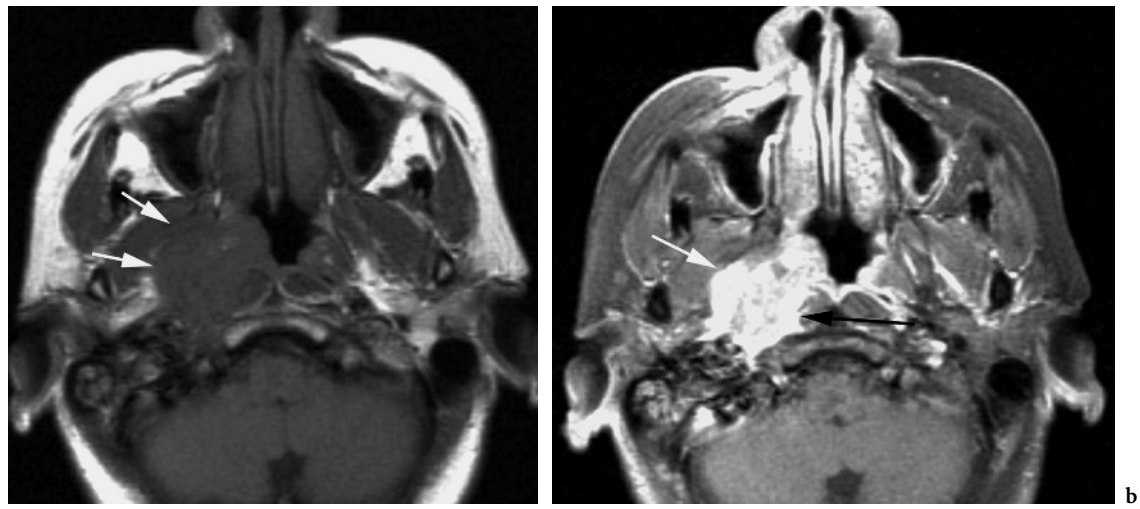

Fig. 8.5a,b. NPC with parapharyngeal spread. **a** Axial T1-weighted MR image shows tumor extending into right parapharyngeal space (*arrows*). **b** Axial fat-suppressed contrast-enhanced MR image shows enhanced tumor displacing lateral pterygoid muscle (*white arrow*) and invading right prevertebral muscle (*black arrow*)

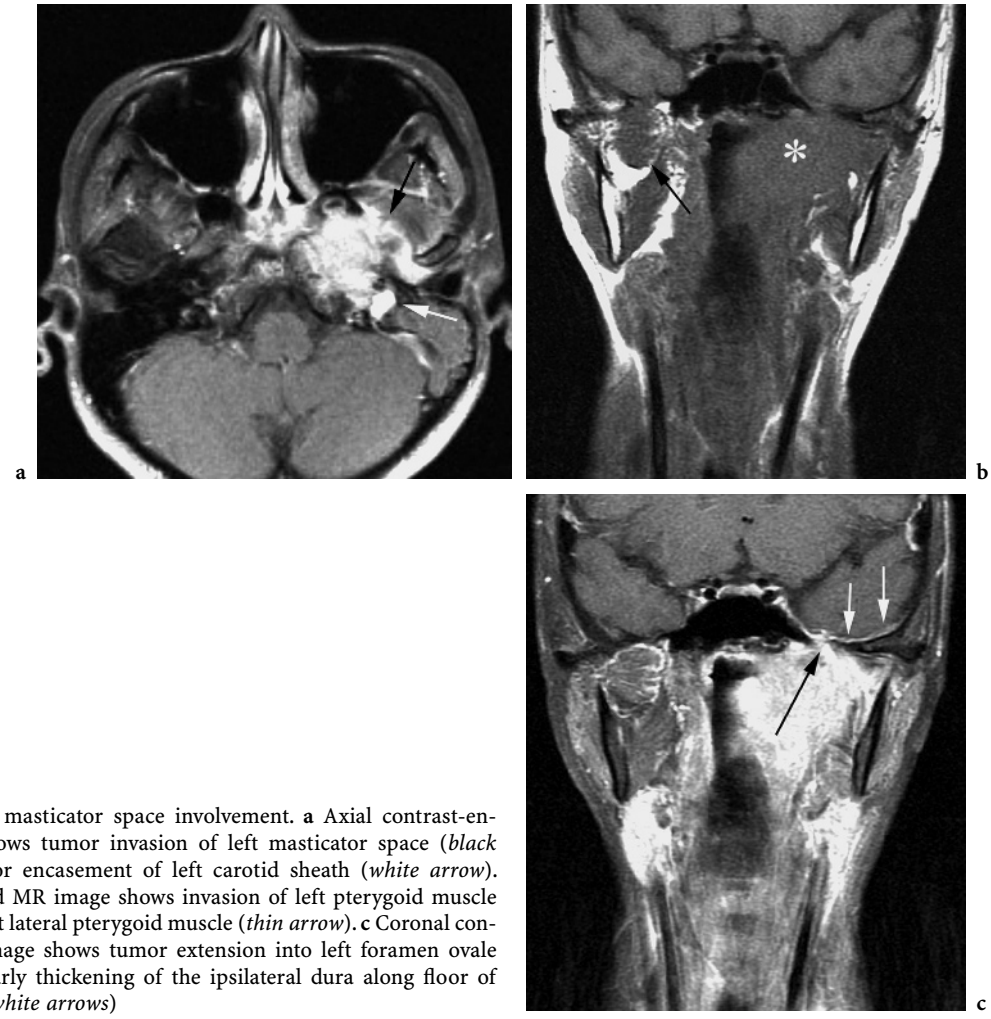

Fig. 8.6a–c. NPC with masticator space involvement. **a** Axial contrast-enhanced MR image shows tumor invasion of left masticator space (*black arrow*). There is tumor encasement of left carotid sheath (*white arrow*). **b** Coronal T1-weighted MR image shows invasion of left pterygoid muscle (*asterisk*). Normal right lateral pterygoid muscle (*thin arrow*). **c** Coronal contrast-enhanced MR image shows tumor extension into left foramen ovale (*black arrow*). Note early thickening of the ipsilateral dura along floor of middle cranial fossa (*white arrows*)

infiltration and subsequent intracranial extension. Denervation changes are readily demonstrated on MR images (Fig. 8.7).

Changes in the skeletal muscles following denervation can be divided into three phases: acute, subacute and chronic. Animal models show that in the first 4 weeks, there is a decrease in the caliber of muscle fibers but no change in the total amount of tissue water. There is, however, a relative decrease in intracellular water associated with a relative increase in extracellular water. In the chronic phase, muscle atrophy associated with fatty infiltration takes place. A mixture of features seen in the acute and chronic stages characterises the subacute phase. In addition, there is a relative increase in the perfusion of muscles following denervation.

In the acute to subacute phases, T2-weighted images show high signals thus producing an edema-like appearance (Chong et al. 2004a). This is because T2 of extracellular water is longer than the T2 of intracellular water. In addition, there is a relative increase in perfusion and increased accumulation of contrast in the extracellular spaces in denervated muscles resulting in increased contrast enhancement (Fig. 8.7). In the chronic phase, there is muscle atrophy and increased signals on T1 and fast spin echo T2 weighted images due to fat accumulation.

The MRI features may be confused with tumor infiltration of the muscles concerned. It should be noted that malignant infiltration produces an increase in size of the affected muscles, whereas, denervation atrophy shows a decrease in muscle bulk. Additionally, the signal changes in denervation atrophy are generalised and higher in signal intensity. Malignant infiltration of the muscles on the other hand is more localised and lower in signal intensity.

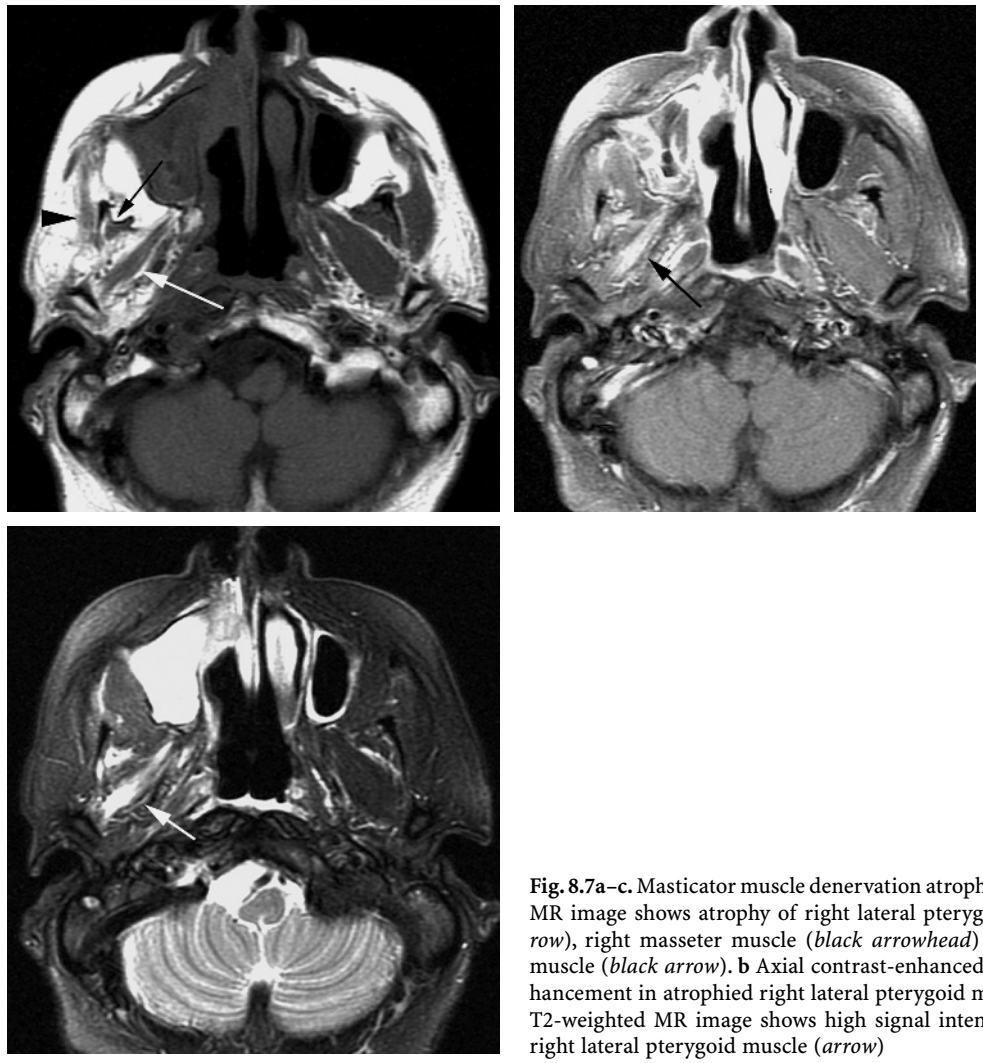

Fig. 8.7a–c. Masticator muscle denervation atrophy. **a** Axial T1-weighted MR image shows atrophy of right lateral pterygoid muscle (*white arrow*), right masseter muscle (*black arrowhead*) and right temporalis muscle (*black arrow*). **b** Axial contrast-enhanced MR image shows enhancement in atrophied right lateral pterygoid muscle (*arrow*). **c** Axial T2-weighted MR image shows high signal intensity within atrophied right lateral pterygoid muscle (*arrow*)

8.3.3 Posterior Spread

NPC can extend posteriorly infiltrating the RPS and prevertebral muscles (Fig. 8.5). Destruction of the vertebral bodies and involvement of the spinal canal is occasionally seen in neglected patients. Posterolateral spread results in the encasement or infiltration of the carotid sheath (Fig. 8.6). Posterosuperior extension may involve the jugular foramen and the adjacent hypoglossal canal thus endangering the cranial nerves IX–XII (Fig. 8.8) (Chong and Fan 1998). Subsequent spread into the posterior cranial fossa is not uncommon.

Involvement of the hypoglossal nerve results in hypotonia and atrophy of the tongue musculature (Fig. 8.9). The earliest clinical sign is muscle fasciculation; atrophy may not be obvious. At this stage, radiological signs of atrophy and fatty infiltration may be subtle. However, the affected side of the tongue can be seen to drop backwards in axial images; this is a helpful sign, easily seen in lower sections showing the posterior aspect of the tongue (Chong and Fan 1998). It is important to note that posterior displacement of the tongue may give the impression of an apparent increase in its length. MRI may show contrast enhancement and high T2 signal intensity changes in the tongue as a result of perineural infiltration or encasement of the hypoglossal nerve. The findings are similar to those observed in the muscles of mastication following tumor infiltration of the mandibular nerve.

8.3.4 Inferior Spread

Some tumors show preferential inferior spread along the pharyngeal wall. This may take place submucosally and thus escapes endoscopic detection. Submucosal spread into the oropharynx can readily be detected on imaging studies. The oropharyngeal wall shows subtle to gross wall thickening (Fig. 8.10). Tumor may also spread along the retropharyngeal space. Hence, imaging plays an important role in accurate tumor staging and mapping. However, in advanced cases, the tumor in the oropharynx may be clearly seen during clinical examination.

8.3.5 Superior Spread

When NPC spreads superiorly it may erode the clivus, sphenoid sinus floor, petrous apex, and the foramen lacerum. Skull base erosion is detected in up to one-third of the patients. The frequency of intracranial abnormalities on CT is 12% and on MRI 31% (Chong et al. 1996a; Sham et al. 1991a). This difference can be explained by the higher sensitivity of MRI.

For a long time, NPC was believed to spread intracranially mainly through the foramen lacerum (Neel 1986). CT studies however showed that the most common manner of intracranial spread was by direct skull base erosion (Curtin and Hirsch 1991; Sham et al. 1991b). However, on MRI the most

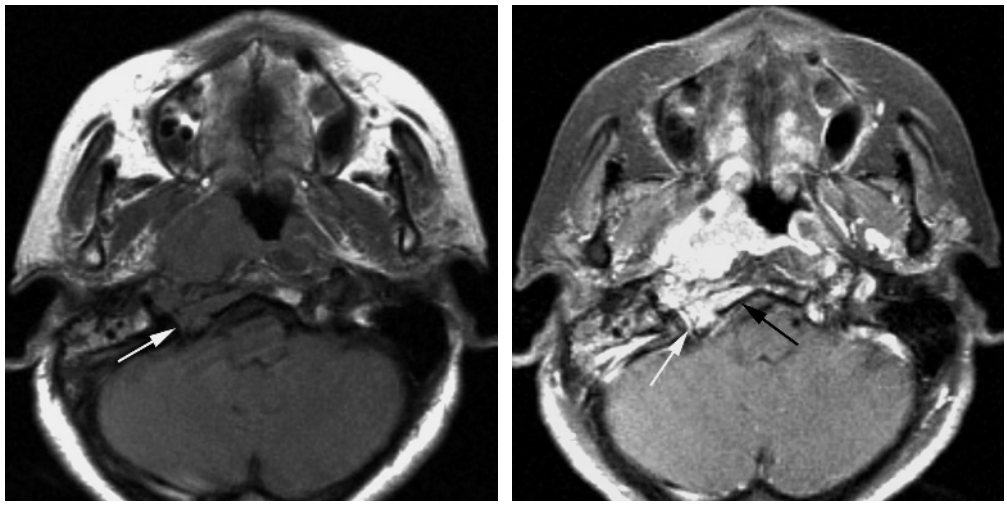

Fig. 8.8a,b. NPC showing posterolateral spread. **a** Axial T1-weighted MR image shows a large right nasopharyngeal tumor with extension into right hypoglossal canal (*arrow*). **b** Axial contrast-enhanced MR image shows tumor enhancement (*white arrow*). Note tumor involvement of clivus marrow (*black arrow*)

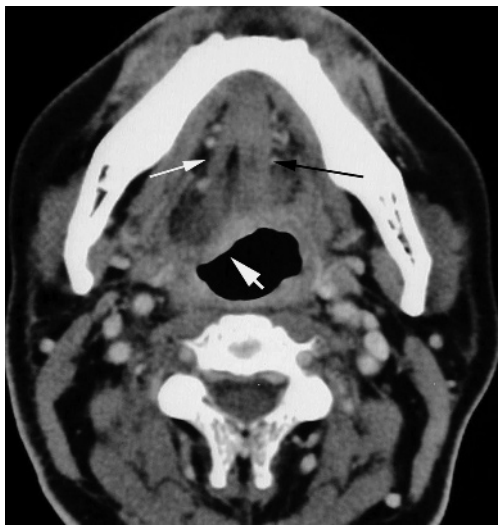

Fig. 8.9. Hypoglossal nerve palsy. Axial contrast-enhanced CT shows right hemitongue atrophy with fatty infiltration. Note posterior displacement of right tongue base (*thick white arrow*), atrophied right geniohyoid-genioglossus complex (*thin white arrow*) and compensatory hypertrophy of right geniohyoid-genioglossus complex (*black arrow*)

common route involves the foramen ovale (Fig. 8.11) (Chong et al. 1996a; Su and Lui 1996). Dural thickening along the floor of the middle cranial fossa may be the first sign of intracranial infiltration and this feature can be detected on MRI (Fig. 8.6). It should be noted that dural thickening itself does not constitute conclusive of malignant infiltration. It is known that dura thickening may be due to reactive hyperplasia. Tumor may also be seen infiltrating the mandibular nerve, gasserian ganglion, trigeminal nerve and pons (Chong 1996). This often results in denervation atrophy of the muscles of mastication. Intracranial extension usually involves the cavernous sinus thus placing the III, IV, ophthalmic division of V, and VI nerves at risk.

8.4 Metastasis

8.4.1 Nodal Metastasis

Cervical nodal metastasis is common in NPC. Often, it is the enlarged neck nodes that prompt initial medical consultation. In all, 75% of patients have enlarged cervical nodes at presentation (Chong et al. 1996b). Bilateral cervical lymphadenopathy may be seen in up to 80% of patients. Nodal metastasis shows an orderly inferior spread and the affected nodes are larger in the upper neck (Sham et al. 1990b). LRP lymphadenopathy may be seen in 65% of patients with cervical metastasis. Although the LRP nodes are considered first echelon nodes, 35% of metastasis bypasses the LRP nodes to reach the cervical nodes (Chong et al. 1995a).

8.4.2 Distant Metastasis

NPC shows a high frequency of distant metastasis compared with other tumors of the head and neck.

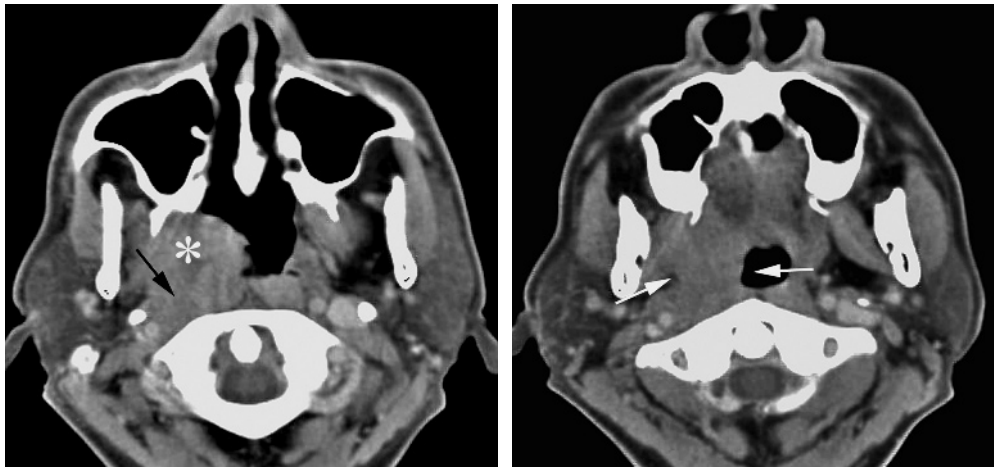

a **b**

Fig. 8.10a,b. NPC with inferior spread to oropharynx. **a** Axial contrast-enhanced CT shows a large NPC (*asterisk*). Note also tumor infiltration of right retropharyngeal space and prevertebral muscle (*black arrow*). **b** Axial contrast-enhanced CT shows tumor extension in right pharyngeal wall (*opposing arrows*)

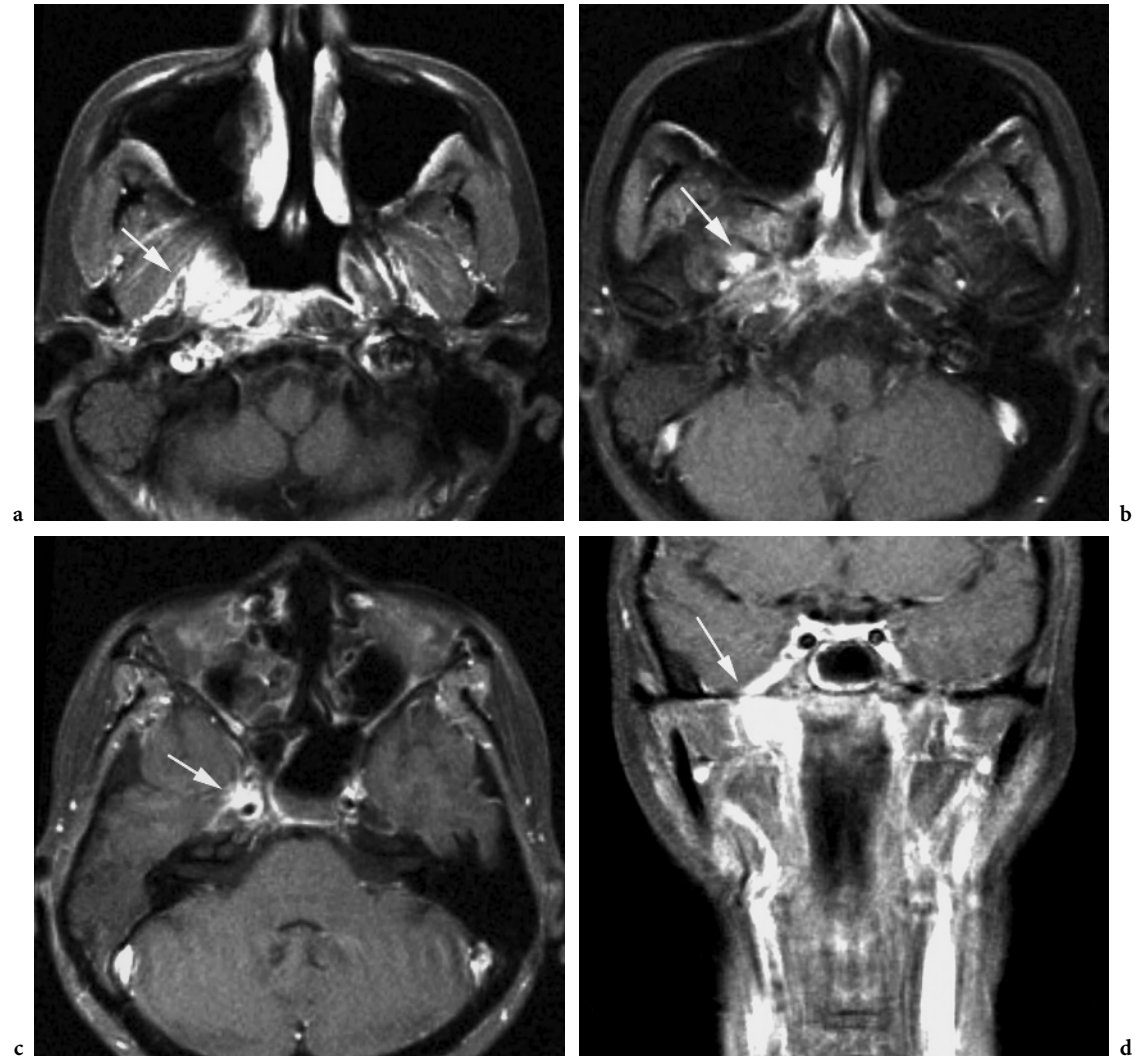

Fig. 8.11a–d. NPC with intracranial extension. **a** Axial contrast-enhanced MR image shows enhanced right nasopharyngeal tumor (*arrow*). **b** Axial contrast-enhanced MR image shows dense enhancement in the right foramen ovale (*arrow*). **c** Axial contrast-enhanced MR image shows intracranial tumor adjacent to the right internal carotid artery (*arrow*). **d** Coronal contrast-enhanced MR image shows right NPC extending through the foramen ovale (*arrow*)

The frequency of distant spread varies between 5% and 41% compared with 5%–24% in other head and neck tumors. Patients with low cervical lymphadenopathy, especially in the supraclavicular fossa, have a significantly higher risk of distant metastasis (Lee et al. 1996). This observation can be explained by the nature of the lymphatic drainage of the head and neck. Lymph flows down the neck and the supraclavicular nodes form the last defensive barrier to the spread of malignant cells within the lymphatic vessels. Malignant cells upon escaping the supraclavicular nodes enter the thoracic duct and subclavian vein resulting in systemic dissemination. Alternatively, tumor cells upon spreading into the PPS enter the parapharyngeal venous plexus resulting in systemic spread (Cheng et al. 2005). Common sites of metastasis include bone (20%), lung (13%) and liver (9%) (Sham et al. 1990c).

8.5 TNM Staging System

Before 1997, the main staging system used in East Asia was that of Ho's classification. In addition, staging systems for NPC have proliferated in the absence of an international consensus. The 5th edition (1997) of the

UICC TNM Classification (published in collaboration with the American Joint Committee on Cancer) introduced prominent modifications in the stage classification for NPC. This was made in response to a need for an updated and new staging system to facilitate the sharing of knowledge and the comparison of data. No significant changes to the NPC staging (Tables 8.1 and 8.2) were introduced in the 6th edition (2002) (Sobin and Wittekind 2002; Green et al. 2002).

The TNM system was originally constructed to assess only three basic indicators of anatomic spread (tumor, node, metastasis). However, over the years, non-anatomic factors were included to further refine prognostic accuracy (Sobin 2003; Gospodarowicz et al. 2004). In recent years, efforts were directed at elucidating the relationship between the TNM system and tumor volume in stratifying patients into prognostic groups.

Many investigators working in the field of NPC research have shown that tumor volume is an independent prognostic indicator. Tumor volume was consistently shown to be more accurate than the TNM system in predicting NPC treatment outcome (Chua et al. 1997; Willner et al. 1999; Chen et al. 2004; Sze et al. 2004). With the development of new tumor volume measuring tools and further validation studies, tumor volume could in future be incorporated into NPC TNM staging system (Chong et al. 2004b,c).

Table 8.1. Nasopharyngeal carcinoma: 6th edition TNM Classification (2002)

T – Primary Tumor	
TI	Tumor confined to nasopharynx
T2	Tumor extends to soft tissue of oropharynx and/or nasal fossa
	T2a Without parapharyngeal extension
	T2b With parapharyngeal extension
T3	Tumor invades bony structures and/or paranasal sinuses
T4	Tumor with intracranial extension and/or involvement of cranial nerves, infratemporal fossa, hypopharynx, or orbit
N – Regional Lymph Nodes	
NX	Regional lymph nodes cannot be assessed
N0	No regional lymph node metastasis
N1	Unilateral metastasis in lymph node(s), 6 cm or less in greatest dimension, above supraclavicular fossa
N2	Bilateral metastasis in lymph node(s), 6 cm or less in greatest dimension, above supraclavicular fossa
N3	Metastasis in lymph node(s)
	(a) Greater than 6 cm in dimension
	(b) In the supraclavicular fossa

Table 8.2. Nasopharyngeal carcinoma: stage grouping

Stage 0	Tis	N0	M0
Stage I	T1	N0	M0
Stage IIA	T2a	N0	M0
Stage IIB	T1	N1	M0
	T2a	N1	M0
	T2b	N0, N1	M0
Stage III	T1	N2	M0
	T2a, T2b	N2	M0
	T3	N0, N1, N2	M0
Stage IVA	T4	N0, N1, N2	M0
Stage IVB	Any T	N3	M0
Stage IVC	Any T	Any N	M1

8.5.1 T Staging

8.5.1.1 T1 Tumors

T1 tumors are limited to the nasopharynx and confined within the pharyngobasilar fascia (Fig. 8.2). There are two points worth noting. Firstly, a T1 tumor should not spread into the nasal cavity. In cross-section imaging, a line joining the posterior free margins of the medial pterygoid plates can be used to demarcate the nasopharynx from the nasal cavity. Secondly, involvement of the prevertebral muscles is, anatomically speaking, spread beyond the nasopharynx. However, this by itself is not given a higher T classification and is still considered a T1 tumor.

8.5.1.2 T2 Tumors

T2 tumors extend beyond nasopharynx into the oropharynx or into the nasal fossa. T2 tumors are subdivided into T2a (without parapharyngeal extension) and T2b (with parapharyngeal extension).

There is a need to define the radiologic boundary between the nasopharynx and the oropharynx. This issue may require attention in future staging definitions. Using the soft palate (which slopes posteroinferiorly during imaging studies) as a demarcating structure can be difficult. The hard palate is a possible alternative landmark. There is, however, one important potential difficulty. NPC spreads into the oropharynx posteriorly. Extrapolating the hard palate posteriorly may produce inconsistent results, as the slope of the hard palate is dependent on the degree of flexion or extension of the neck. Generally speaking an adopted landmark should be as close to the tumor as possible and as such the C1/C2 level appears more appropriate.

In the TNM staging system, parapharyngeal involvement is defined as "posterolateral infiltration beyond the pharyngobasilar fascia" (Sobin and Wittekind 2002). There is still a lack of consensus about the significance of parapharyngeal extension. Nevertheless, parapharyngeal involvement is currently categorized as T2b to facilitate future review.

Although the TNM system defined parapharyngeal spread as "posterolateral infiltration beyond the pharyngobasilar fascia", it is not entirely clear to a diagnostic radiologist what this actually means. This problem is compounded by the presence of two definitions of PPS within the diagnostic radiology circle. The first definition includes two components: the "prestyloid parapharyngeal space" which is fat-filled and the "retrostyloid parapharyngeal space" containing the carotid sheath. The second definition designates the above two components as "parapharyngeal space" (excluding the carotid space) and "carotid space" (a more detailed discussion on the anatomic nomenclature concerning the PPS is in Chap. 9). The TNM definition appears to refer only to the "retrostyloid parapharyngeal space".

8.5.1.3 T3 Tumors

Tumors that invade bony structures and the paranasal sinuses are classified T3 lesions. There are no separate sub-classifications for involvement of the various sinuses, bony structures or the skull base. Some investigators have shown that bone erosion in itself (without associated cranial nerve involvement) does not appear to be an important prognostic indicator. However, subdivisions may be required following further validation studies (Lu et al. 2001; Roh et al. 2004).

8.5.1.4 T4 Tumors

Tumors with intracranial extension, involvement of cranial nerves, infratemporal fossa, hypopharynx and orbit are classified as T4 tumors.

Involvement of the infratemporal fossa is defined as "extension of tumor beyond the anterior surface of the lateral pterygoid muscle or lateral extension beyond the posterolateral wall of the maxillary antrum and pterygomaxillary fissure" (Sobin and Wittekind 2002). This definition of infratemporal fossa involvement will present difficulties to a radiologist unless he is familiar with the term as specifically used in NPC staging classification. Furthermore, the 2002 edition of TNM included the masticator space under T4 classification without any definition of masticator space. Future editions of TNM should clarify the definitions of infratemporal fossa, the masticator space and their relationship.

Involvement of the orbit is classified T4 disease. In most instances, tumor spreads to the orbit via the PPF and the inferior orbital fissure. It remains unclear whether infiltration of the PPF or the inferior orbital fissure themselves should be classified T4 as these areas are not mentioned specifically.

8.5.2 N Staging

The distribution and prognosis of nodal metastasis is sufficiently different from other head and neck tumors to justify the use of a different N classification system. In NPC, nodal size of 6 cm is used to separate N1 and N2 disease in contrast to 3 cm in other head and neck malignancies. The level of nodal involvement is also important and a new term, the supraclavicular fossa, is now introduced in N staging.

The supraclavicular fossa is an unfamiliar staging term outside Asia. The supraclavicular fossa is formed by three points: (1) the superior margin of the sternal end of the clavicle; (2) the superior margin of the lateral end of the clavicle; (3) the point where the neck meets the shoulder. Nodes in the supraclavicular fossa will include caudal portions of levels IV and V.

It should be noted that involvement of the LRP nodes does not appear to affect prognosis in NPC. Hence, there is insufficient evidence for an N1 classification when LRP nodes are demonstrated, regardless of the nodal size. In contrast, in other head and neck tumors, LRP lymphadenopathy signifies a poor prognostic outcome.

8.6 Imaging Technique

The technique for CT will vary slightly depending on the scanner used. In general 3-mm axial sections through the skull base and nasopharynx should be obtained preceded by axial 5-mm sections through the neck. The volume of contrast injected also varies from institutions to institutions. Administration of 100–150 ml of contrast appears adequate for opacify-

ing vessels and lesions in present generation of CT scanners. In all cases, images obtained through the skull base are reconstructed using a high-resolution bone algorithm. Although desirable, routine coronal sections need not be obtained.

For MRI, following sequences are adequate: 4-mm sections with 1.5-mm spacing using spin echo axial and coronal T1-weighted pre-contrast images and fast spin echo fat-suppressed axial T2-weighted images; following administration of gadolinium, fat-suppressed axial and coronal T1-weighted images are obtained.

8.7 Imaging Modalities

Compared with the pre-CT era, the post-CT period witnessed a dramatic improvement in treatment outcome of NPC. This was initially largely attributed to improvements in tumor staging and definition of tumor extent. Subsequent improvement in radiation treatment and chemotherapy techniques further improved the treatment results. The place of CT in the evaluation of NPC is now extensively documented. CT remains the most commonly used modality for staging in regions where NPC occur with high frequencies, as access to MRI is still limited.

MRI is superior to CT in demonstrating the tumor soft tissue extent (Mukherji et al. 1997). It was generally accepted that CT was superior to MRI in detecting skull base involvement. It is now known that MRI is more sensitive to CT in detecting skull base marrow changes (Chong and Fan 1996b; Ng et al. 1997). CT often underestimates the frequency and extent of skull base involvement (Fig. 8.12). These marrow changes could represent tumor infiltration, inflammation or both. Hence, although MRI is more sensitive to CT in detecting marrow changes, the specificity of this observation remains unknown. This is because, unlike laryngeal cartilage signal abnormalities in patients with squamous cell carcinoma, histopathologic verification of skull base lesions cannot be easily performed. The nasopharynx is a relatively inaccessible place. Furthermore, the mainstay of treatment is radiation therapy. As a result, surgical verification of abnormalities detected by imaging studies is difficult.

Perineural tumor spread in head and neck cancers is well documented. The most commonly affected nerves in NPC are the maxillary and mandibular nerves. Perineural infiltration may lead to retrograde spread to the cavernous sinus, Meckel's cave and the trigeminal nerve. MRI is far more sensitive than CT in detecting perineural tumor spread. It is clear that MRI may upstage many tumors staged with CT. This may introduce potential problems when comparing the results of treatment outcome.

Cervical lymphadenopathy is better studied with CT especially for nodal necrosis and extracapsular

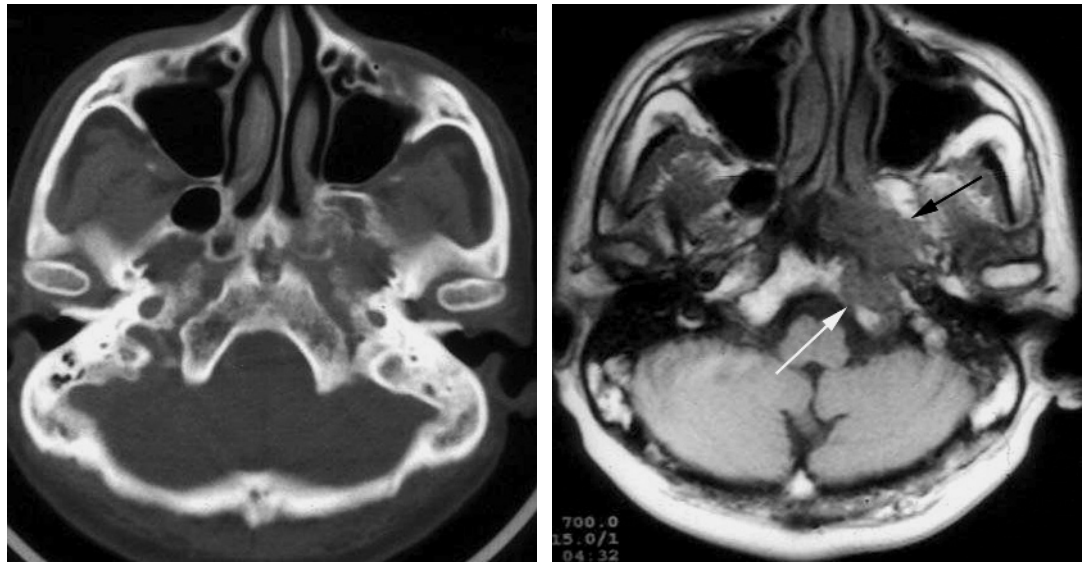

Fig. 8.12a,b. NPC with clivus involvement. **a** Axial CT (*bone window*) shows unremarkable appearances in clivus. No erosion seen in the clivus. **b** Axial T1-weighted MR image shows infiltration (*white arrow*) replacing high signal intensity marrow in the clivus. Note intermediate signal intensity NPC involving the left petrous apex

spread. Although much has been written on the superiority of CT over MRI in the assessment of nodal metastasis, both modalities are adequate in routine clinical practice. It is uncommon for CT to provide additional information over MRI resulting in a change of treatment strategy.

MRI is, however, the recommended modality in the assessment of recurrence. Although MRI has limitations in separating post radiation fibrosis from tumor recurrence, it is superior to CT in identifying submucosal infiltration, skull base marrow replacement and intracranial spread (Chong and Fan 1997).

8.8 Imaging Strategies

Three groups of patients require imaging of the nasopharynx. The first group presents with cervical lymphadenopathy but without endoscopic evidence of a nasopharyngeal lesion. The second group presents with a nasopharyngeal mass for radiologic evaluation or staging. The third group presents for post-treatment assessment for suspected treatment complications, tumor surveillance or mapping of tumor extent.

8.8.1 Occult Malignancy

NPC may show submucosal spread with normal or relatively normal endoscopic findings. These patients usually present clinically with metastatic cervical lymphadenopathy. Serologic studies may reveal elevated antibodies against EBV antigens. Radiologic evaluation for such patients is mandatory especially in populations with high frequencies of NPC. MRI should be performed as it is superior to CT in delineating submucosal abnormalities.

Residual nasopharyngeal lymphoid tissue may occasionally mimic neoplasms (Fig. 8.1). The adenoids decrease in volume with age but may persist as tags of tissue into adulthood. CT and T1-weighted MRI cannot separate lymphoid tissues from the underlying muscles with a high degree of confidence. However, T2-weighted images show good contrast between the high signal intensity lymphoid tissue and the low signal intensity muscles. Lymphoid tissues enhance following gadolinium administration. They are located superficially and never penetrate the underlying muscle.

8.8.2 Staging

Most patients undergo imaging evaluation because of an endoscopically demonstrated nasopharyngeal mass. MRI is again the preferred imaging modality. As most current radiation therapy techniques utilize relatively large fields to cover potential areas of microscopic spread, CT staging is adequate for most patients. However, with the advent of 3D conformal radiation therapy and intensity modulated radiation therapy (IMRT), MRI should be used for more accurate tumor mapping.

The increasing use of MRI in tumor staging has given rise to problems related to tumor staging and treatment planning. The basic issue to be resolved is the significance of skull base marrow changes seen on MRI. If these changes are considered tumor involvement, then MRI will upstage a certain number of patients. In clinical practice, skull base with marrow changes (detected by MRI) are included within the radiation treatment field.

The detection of distant metastasis alters prognosis and treatment planning. Chest X-ray and abdominal (liver) ultrasound are performed as part of the overall staging procedure. If these examinations present diagnostic issues, chest or abdomen CT are ordered for further evaluation. Similarly, bone scans are only done if there is a clinical suspicion of osseous metastases. If neck adenopathies are present in nasopharyngeal cancer, also a FDG-PET scan, if available, may be considered to search for occult distant disease.

8.8.3 Follow-up Issues and Problems

The aims of post-treatment imaging include the early detection of recurrence and treatment complications. Follow up studies are important because they may lead to early treatment of recurrent disease, thereby decreasing morbidity and improving survival rates.

8.8.3.1 Tumor Recurrence

There is usually complete tumor resolution within 3 months following radiation therapy, otherwise, the patient is considered to have residual disease. Hence, designation of tumor recurrence rests on the documentation of a disease free period. The distinction between residual and recurrent disease is relevant because it affects not only treatment plans but also

management policies. Persistent or residual disease may be due to firstly, a "geographic miss" on the irradiation plan; secondly, the relative radio-insensitivity of the tumor; thirdly, an insufficiently high radiation dose, and fourthly, the time taken to deliver the dose was too long.

Patients are often followed-up clinically at 1- to 2-monthly intervals in the first year, 2- to 3-monthly intervals in the second year and 3- to 4-monthly intervals in the third year. These patients can be seen at 6-monthly intervals subsequently. Tumor recurrence is usually detected by endoscopy and imaging is requested for the assessment of tumor extent (Sham et al. 1992). Imaging is also used to confirm deep recurrences not apparent on endoscopy but suspected on the basis of history and symptomology (Fig. 8.13).

Differentiating fibrosis from tumor recurrence is difficult on CT since the attenuation values of these tissues are similar. Separating tumor recurrence from fibrosis on MRI is only easier if the scar is mature. Early fibrous tissue is hypercellular and produces high signals on T2-weighted images. Both immature scar and tumor show contrast-enhancement on MRI and high signals on T2-weighted images. Mature scar, which is hypocellular, does not show contrast-enhancement and is characterized by low signal intensity on T2-weighted images.

The simultaneous dynamic processes of fibrosis and tissue reaction to irradiation often produce a confusing picture. Residual disease or recurrent tumor may be hypointense relative to granulation tissue in the early stage. Scar tissue may also show high signal intensity in T2-weighted images. Furthermore, areas of high signals on T2-weighted images may be seen in corresponding areas showing no contrast enhancement. Differentiating tumor recurrence from fibrosis, therefore, can be a formidable task (Chong and Fan 1997).

To overcome the above mentioned problems, regular follow-up should be performed. It is important to obtain a baseline study around 6 months after radiation therapy and another scan 6 months later. These studies can be used for comparison with future yearly follow up studies over the next 3 years (and longer if required). A stable appearance can provide reassurance that the abnormality seen is most likely to be due to the effects of radiation.

Positron emission tomography (PET) using 2-[F-18] fluoro-2-deoxy-D-glucose (FDG) has demonstrated value in detecting NPC recurrence following radiotherapy (Kao et al. 1998; Tsai et al. 2002). The advent of PET CT has provided even more information by co-registering tracer uptake with anatomic information.

8.8.3.2 Treatment Complications

The complications of radiation therapy can be divided into neurological and non-neurological sequelae. Neurological complications include temporal lobe necrosis, encephalomyelopathy and cranial nerve palsies. Non-neurological complications include at-

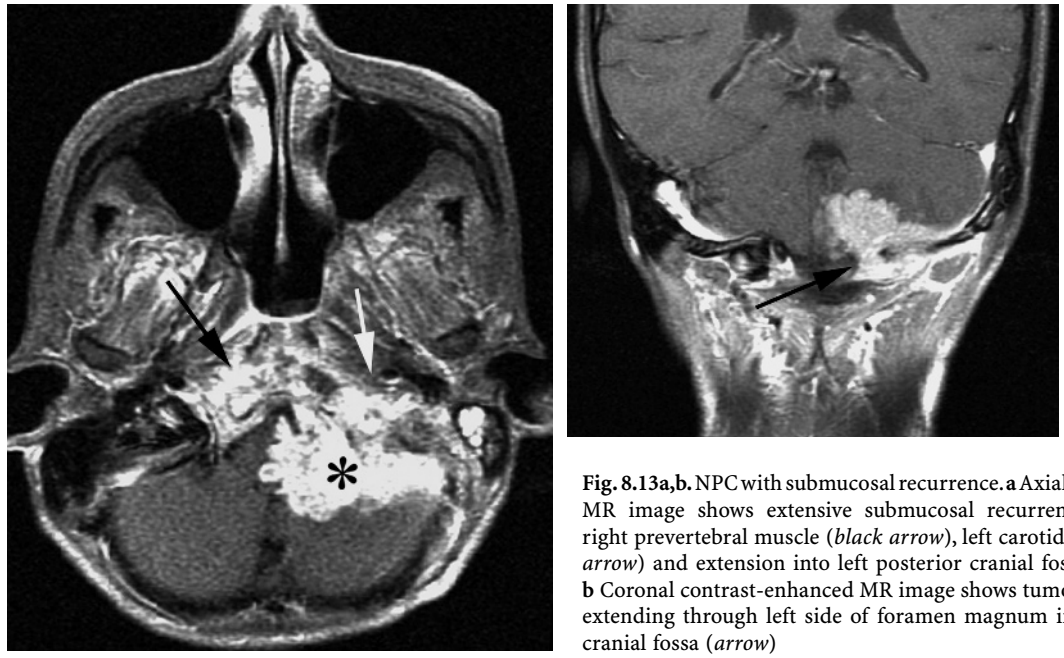

Fig. 8.13a,b. NPC with submucosal recurrence. **a** Axial T1-weighted MR image shows extensive submucosal recurrence involving right prevertebral muscle (*black arrow*), left carotid space (*white arrow*) and extension into left posterior cranial fossa (*asterisk*). **b** Coronal contrast-enhanced MR image shows tumor infiltrating extending through left side of foramen magnum into posterior cranial fossa (*arrow*)

rophy of salivary glands, muscles of mastication, and radiation associated tumors.

8.8.3.3 Neurological Complications

8.8.3.3.1 Temporal Lobe Necrosis (TLN)

NPC shows high frequencies of skull base erosion and intracranial extension and is frequently associated with perineural infiltration. The natural history of tumor spread requires adequate radiation treatment coverage of the skull base and the middle cranial fossa. Radiation doses below 6000 cGy at conventional 200 cGy daily are inadequate for tumor control. Hence, the effective radiation dose for the treatment of NPC exceeds the quoted tolerance limit for the neural tissues resulting in a substantial risk of radiation-induced brain damage. Lee et al. (1992) reported a 3% cumulative incidence of TLN in her series of 4527 patients. TLN is probably under diagnosed as 39% of patients had only vague symptoms while 16% had none at all. The latent interval ranged from 1.5 to 13 years (median, 5 years).

The inferior and medial portions of both temporal lobes are at risk as they are included in the target volume. Cerebral edema is the earliest radiologic sign. This is followed by foci of necrosis that may be located in the gray matter, white matter or both (Fig. 8.14). White matter lesions are characteristically associated with florid edema while gray matter lesions may show minimal or no edema (Chong et al. 2000). Early lesions may heal completely but ex-

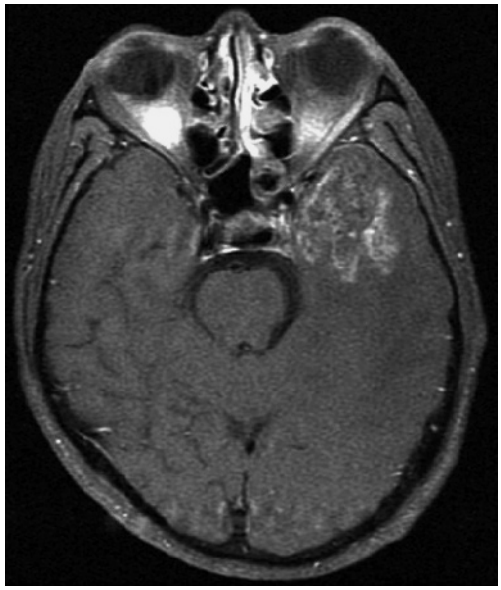

a

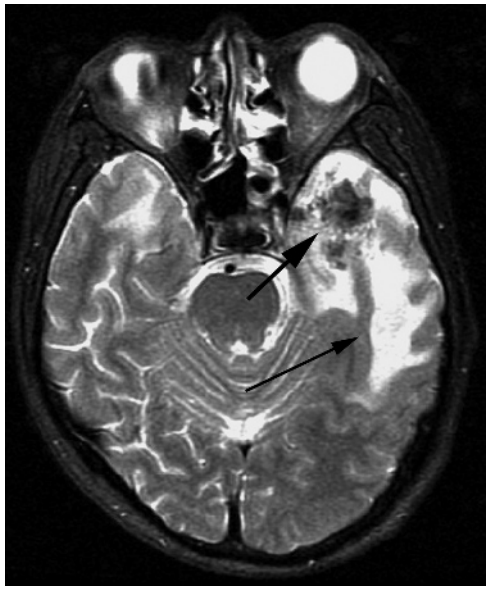

b

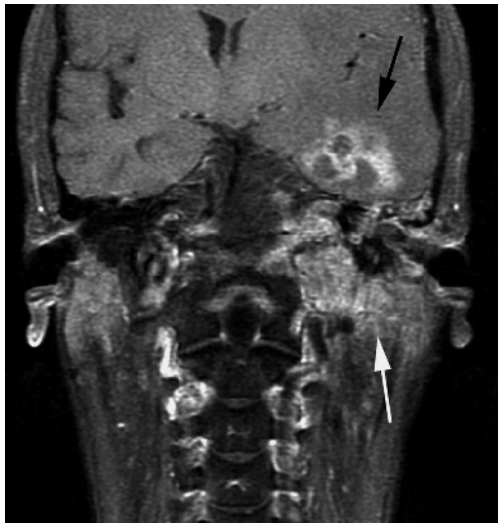

c

Fig. 8.14a–c. Radiation-induced temporal lobe necrosis (TLN). **a** Axial contrast-enhanced MR image shows heterogeneous enhancing lesion in left temporal lobe. **b** Axial T2-weighted MR image shows heterogeneous signal intensities in left temporal lobe. Low signal area due to hemosiderin deposition from hemorrhage associated with TLN (*thick arrow*). Note accompanying high signal intensity cerebral edema (*thin arrow*). **c** Coronal contrast-enhanced MR image shows intra-axial heterogeneously enhancing left TLN (*black arrow*). Note tumor recurrence in left skull base (*white arrow*)

tensive involvement frequently results in temporal lobe atrophy or macrocystic encephalomalacia. With the introduction of conformal and intensity modulated radiation therapy (IMRT), the frequency of TLN should gradually decrease.

The differential diagnosis of TLN includes intracranial tumor recurrence and cerebral metastasis. An important point of distinction is whereas recurrent tumor is almost always an extra-axial lesion, TLN is an intra-axial pathologic process. In addition, NPC with intracranial extension, unlike TLN, is usually not associated with cerebral edema. Cerebral metastases are exceedingly rare in NPC (Leung et al. 1991). In clinical practice, cerebral metastasis is seldom placed high on the list of differential diagnosis. If, there are difficulties in differentiating these entities, other modalities based on functional imaging may provided the additional information required for accurate diagnosis. These techniques include MR spectroscopy and PET imaging.

In recent years, MR spectroscopy is increasingly used to study the metabolic changes in the brain following radiation injury. MR spectroscopy in patients with radiation-induced changes in the temporal lobes showed reduced N-acetyl-aspartate levels and relatively stable creatine levels. However, the choline levels may be increased, normal or reduced. The increase choline levels may mimic the presence of primary brain tumor. However, given the known clinical setting, it is unlikely to confuse TLN with the presence of a primary brain neoplasm (Chong et al. 1999, 2001). In addition to MR spectroscopy, PET CT can be used to separate TLN from tumor recurrence. Brain necrosis typically shows no uptake of tracers while tumor recurrence will demonstrate increased metabolic activity.

8.8.3.3.2 Brainstem Encephalopathy

In the past it was widely known that radiation therapy could damage the brainstem and cervical spinal cord in up to 3% of patients (Mesic et al. 1981). The frequency is now considerably less with improved radiation techniques and shielding. Patients with radiation induced cord injury usually present with clinically unmistakable symptoms and signs of corticospinal tract damage. This major complication has a median latent interval of 3 years (range 0.4–9 years). There is no effective way of reverting or arresting this pathologic process. The majority of patients will develop severe motor disability (Lee and Yau 1997).

8.8.3.3.3 Cranial Nerves

Cranial nerves are relatively radioresistant. The reported frequencies of radiation-induced palsies range from 0.3% to 6% (Flores et al. 1986; Hoppe et al. 1976). This entity is diagnosed by exclusion, as the involved cranial nerves usually appear radiologically unremarkable. The XIIth cranial nerve is the most commonly affected nerve. The optic nerve is the second most commonly damaged nerve followed by the VIth cranial nerve. The IVth, Vth and VIIth nerves are usually involved as part of the brainstem damage syndrome.

8.8.3.4 Non-neurological Complications

8.8.3.4.1 Salivary Glands

Almost all patients have varying degrees of xerostomia and thickening of saliva. Subsequent development of dental caries is common. Radiologically, almost all salivary glands show atrophy. Imaging not infrequently reveals intense salivary gland enhancement. Rarely, patients show acute parotitis, which may develop rapidly over a few days. With the advent of IMRT, the frequency and severity of radiation induced parotitis has decreased.

8.8.3.4.2 Soft Tissue Fibrosis

Marked soft-tissue fibrosis in the neck is common following irradiation with large fractional doses. Although neck fibrosis per se rarely causes serious functional limitation, it may mask nodal recurrence. When the neck is woody hard, palpation is unreliable and the recommended strategy is to use CT to detect lymphadenopathy.

Trismus due to fibrosis around the temporomandibular joints and adjacent muscles of mastication

can result in feeding difficulties. This may be aggravated by pharyngeal mucositis and stricture.

8.8.3.4.3 Radiation Associated Tumors

The tumor induction potential of ionizing radiation is a well-recognized phenomenon. The term radiation-induced tumor is frequently used to describe second tumors appearing within previously irradiated fields. However, ascribing the second tumor as a direct consequence of irradiation is often difficult. This entity is better called radiation-associated tumors (RATs).

The criteria for diagnosing RATs include a history of irradiation; the second neoplasm occurring within irradiation field; a difference in the histology of the second neoplasm from the primary tumor; and finally, an arbitrary latency period of at least 5 years (Cahan et al. 1948).

The frequency of head and neck RATs is unknown although it has been estimated to occur between 0.4% to 0.7% (Steeves and Bataini 1981). The reported types of RATs include sarcomas (Fig. 8.15), meningiomas, schwannomas, gliomas, thyroid tumors and squamous cell carcinomas (Fig. 8.16) (Mark et al. 1993; Rubinstein et al. 1989; Bernstein and Laperriere 1991). The improvement of radiation therapy techniques has contributed to increased survival rates of patients with NPC. We can, therefore, expect to see more long-term complications like RATs (Goh et al. 1999) (Fig. 8.16).

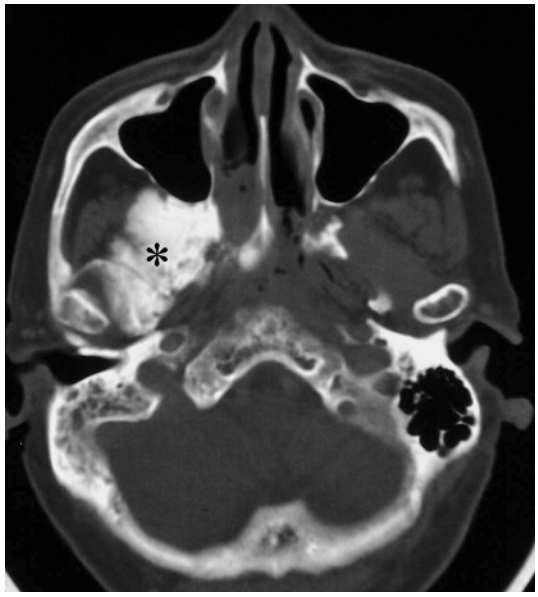

Fig. 8.15. Radiation associated tumor (RAT) – parosteal sarcoma. Patient had a history of irradiation for NPC (undifferentiated carcinoma) 11 years previously. Axial CT shows a large dense (*asterisk*) bone tumor arising from the right pterygoid process

8.9 Other Neoplasms of the Nasopharynx

In comparison with undifferentiated carcinoma, nasopharyngeal adenoid cystic carcinoma is rare (Mukherji and Chong 2004). The vast majority of adenoid cystic carcinomas are found in the salivary glands, the mucosa of the oral cavity, nasal fossa and the paranasal sinuses. This tumor affects patients in the middle age and there is no reported sex predilection. Unlike NPC, patients with adenoid cystic carcinomas rarely present with cervical lymphadenopathy.

Although lymphoid tissues are normally found in the nasopharynx, primary lymphomas in the nasopharynx are uncommon. These tumors are more commonly seen in conjunction with system disease. Nasopharyngeal lymphomas affect all age groups but are more commonly encountered in middle and old age. The majority of these tumors belong to the non-Hodgkin group. Nasopharyngeal involvement is usually detected during the staging process of known disease elsewhere.

Plasma cell neoplasms can be grouped into three categories: multiple myeloma, plasmacytoma of bone, and extramedullary plasmacytoma. Extramedullary plasmacytomas account for approximately 20% of all plasma cell neoplasms and 80% of these lesions are found in the head and neck. Plasmacytomas are most commonly seen in the sixth and seventh decades and have an 80% male preponderance. Plasmacytomas are most frequently seen in the upper airways such as the epiglottis, larynx and nasopharynx (Ching et al. 2002). Approximately 30% of patients with extramedullary plasmacytoma will have systemic disease after 20 years.

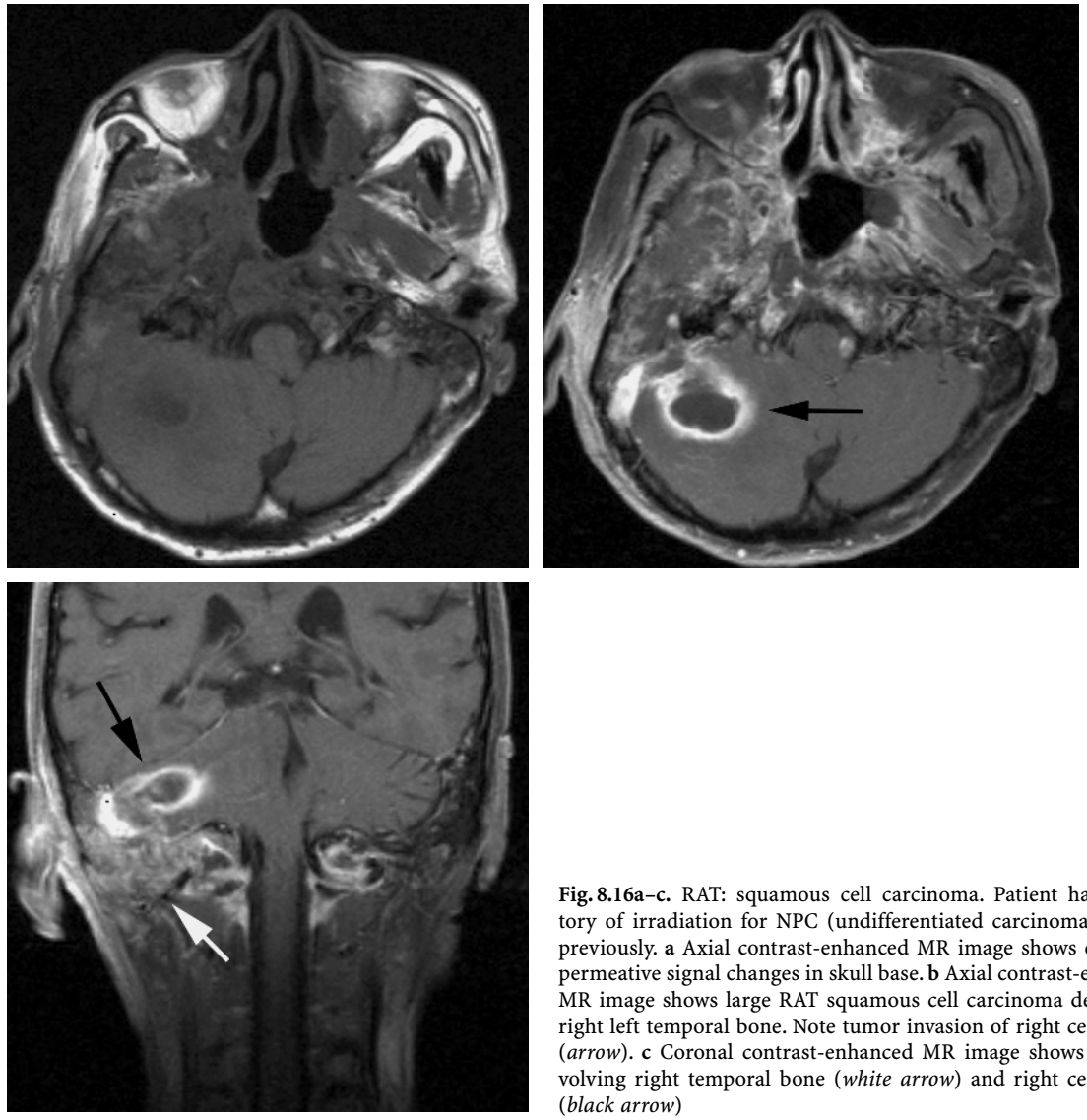

Fig. 8.16a–c. RAT: squamous cell carcinoma. Patient had a history of irradiation for NPC (undifferentiated carcinoma) 7 years previously. **a** Axial contrast-enhanced MR image shows extensive permeative signal changes in skull base. **b** Axial contrast-enhanced MR image shows large RAT squamous cell carcinoma destroying right left temporal bone. Note tumor invasion of right cerebellum (*arrow*). **c** Coronal contrast-enhanced MR image shows RAT involving right temporal bone (*white arrow*) and right cerebellum (*black arrow*)

References

Ahmad A, Stefani S (1986) Distant metastases of nasopharyngeal carcinoma. A study of 256 male patients. J Surg Oncol 33:194–197

Bernstein M, Laperriere N (1991) Radiation-induced tumors of the nervous system. In: Gutin PH, Leibel SA, Sheline GE (eds) Radiation injury to the nervous system. Raven Press, New York, pp 455–472

Cahan WG, Woodward HG, Higinbotham NL, Stewart FW, Coley L (1948) Sarcoma arising in irradiated bone: report of eleven cases. Cancer 1:3–29

Chen MK, Chen TH, Liu JP, et al. (2004) Better prediction of prognosis for patients with nasopharyngeal carcinoma using primary tumor volume. Cancer 100:2160–2166

Cheng SH, Tsai SYC, Yen KL, et al. (2005) The hypothesis of dissemination for Stage I-III nasopharyngeal carcinoma. Int J Radiat Oncol Biol Phys 61:456–465

Ching ASC, Khoo JBK, Chong VFH (2002) CT and MR imaging of solitary extramedullary plasmacytoma of the nasal tract. AJNR 23:1632–1636

Chong VFH (1996) Trigeminal neuralgia in nasopharyngeal carcinoma. J Laryngol Otol 110:394–396

Chong VFH (1997) Masticator space in nasopharyngeal carcinoma. Ann Otol Rhinol Laryngol 106:979–982

Chong VFH, Fan YF (1996a) Maxillary nerve involvement in nasopharyngeal carcinoma. AJR Am J Roentgenol 167:1309–1312

Chong VFH, Fan YF (1996b) Skull base erosion in nasopharyngeal carcinoma: Detection by CT and MRI. Clin Radiol 51:625–631

Chong VFH, Fan YF (1997) Detection of recurrent nasopharyngeal carcinoma: CT vs MR imaging. Radiology 202:453–470

Chong VFH, Fan YF (1998) Hypoglossal nerve palsy in nasopharyngeal carcinoma. Eur Radiol 8:939–945
Chong VFH, Fan YF, Khoo JBK (1995a) Retropharyngeal lymphadenopathy in nasopharyngeal carcinoma. Eur J Radiol 21:100–105
Chong VFH, YF Fan, KH Toh, Khoo JBK (1995b) MRI and CT features of nasopharyngeal carcinoma with maxillary sinus involvement. Australas Radiol 39:2–9
Chong VFH, Fan YF, Khoo JBK (1996a) Nasopharyngeal carcinoma with intracranial spread: CT and MRI characteristics. J Comput Assist Tomogr 20:563–639
Chong VFH, Fan YF, Khoo JBK (1996b) MRI features of cervical nodal necrosis in metastatic disease. Clin Radiol 51:103–109
Chong VFH, Fan YF, Mukherji SK (1998) Nasopharyngeal carcinoma. Sem Ultrasound CT MR 19:449–462
Chong VFH, Rumpel H, Aw YS, Ho GL, Fan YF, Chua EJ (1999) Temporal lobe necrosis following radiation therapy for nasopharyngeal carcinoma: proton MR spectroscopic findings. Int J Radiat Oncol Biol Phys 45:699–705
Chong VFH, Fan YF, Mukherji SK (2000) Radiation-induced temporal lobe changes: CT and MR imaging characteristics. AJR Am J Roentgenol 175:431–436, 89
Chong VFH Rumpel H, Fan YF, Mukherji SK (2001) Temporal lobe changes following radiation therapy: imaging and proton MR spectroscopic findings. Eur Radiol 11:317–324
Chong VFH, Khoo JBK, Fan YF (2004a) Nasopharynx and skull base. Neuroimag Clin North Am 14:695–719
Chong VFH, Zhou JY, Khoo JBK, J Huang, Lim TK (2004b) Tumor volume measurement in tongue carcinoma. Int J Radiat Oncol Biol Phys 59:59–66
Chong VFH, Zhou JY, Khoo JBK, J Huang, Lim TK (2004c) Tumor volume measurement in nasopharyngeal carcinoma. Radiology 231:914–921
Chua D, Sham J, Kwong D, Tai K, et al. (1997) Volumetric analysis of tumor extent in nasopharyngeal carcinoma and correlation with treatment outcome. Int J Radiat Oncol Biol Phys 39:711–719
Curtin HD, Hirsch WL (1991) Base of the skull. In: Atlas SW (ed) Magnetic resonance imaging of the brain and spine. Raven Press, New York, pp 669–707
Flores AD, Dickson RI, Riding K, Coy P (1986) Cancer of the nasopharynx in British Columbia. Am J Clin Oncol 9:281–291
Goh YH, Chong VFH, Low WK (1999) Temporal bone tumours in patients irradiated for nasopharyngeal neoplasms. J Laryngol Otol 113:222–228
Gospodarowicz MK, Miller D, Groome PA, Greene FL, Logan PA, Sobin LH (2004) The process for continuous improvement of the TNM classification. Cancer 100:1–5
Green FL, Page D, Morrow M, Balch C, Haller D, Fritz, Fleming I (eds) (2002) AJCC cancer staging manual 6th edn. Springer, New York
Hoppe RT, Goffinet DR, Bagshaw MA (1976) Carcinoma of the nasopharynx: eighteen years' experience with megavoltage radiation therapy. Cancer 37:2605–2612
Kao CH, ChangLai SP, Chieng PU, Yen RF, Yen TC (1998) Detection of recurrent or persistent nasopharyngeal carcinoma after radiotherapy with 18-fluoro-2-deoxyglucose positron emission tomography and comparison with computed tomography. J Clin Oncol 16:3550–3355
Lee AWM, Law SCK, Ng SH et al. (1992) Retrospective analysis of nasopharyngeal carcinoma treated during 1976–1985: late complications following megavoltage irradiation. Br J Radiol 65:918–928
Lee AWM, Foo W, Poon YF, et al. (1996) Staging nasopharyngeal carcinoma: evaluating of N-staging by Ho and UICC/AJCC systems. Clin Oncol 8:146–154
Lee AWN, Yau TK (1997) Complications of radiotherapy. In: Chong VFH, Tsao SY (eds) Nasopharyngeal carcinoma. Armour, Singapore, pp 114–127
Leung SF, Teo PM, Shiu W, Tsao SY, Leung WT (1991) Clinical features and management of distant metastases of nasopharyngeal carcinoma. J Otolaryngol 20:27–29
Lu TX, Mai WY, The BS, et al. (2001) Important prognostic factors in patients with skull base erosion from nasopharyngeal carcinoma after radiotherapy. Int J Radiat Oncol Biol Phys 51:589–598
Mark RJ, Bailet JW, Poen J, Tran LM, Calcaterra TC, Abemayor E, Fu YS, Parker RG (1993) Post-radiation sarcoma of the head and neck. Cancer 72:887–893
Mesic JB, Fletcher GH Goepfert H (1981) Megavoltage irradiation of epithelial tumors of the nasopharynx. Int J Radiat Oncol Biol Phys 7:447–452
Mukherji SK, Chong V (2004) Atlas of head and neck imaging. Thieme, New York
Mukherji SK, Pillsbury HR, Castillo M (1997) Imaging squamous cell carcinomas of the upper aerodigestive tract: what clinicians need to know. Radiology 205:629–646
Neel HM (1986) Malignant neoplasm of the nasopharynx. In: Schuller DE (ed) Otolaryngology: head and neck surgery, vol 2. CV Mosby, St Louis, p 1401
Ng SH, Chang TC, Ko SF, et al. (1997) Nasopharyngeal carcinoma: MRI and CT assessment. Neuroradiology 39:741–746
Nielson NH, Mikkelsen F, Hansen JP (1977) Nasopharyngeal cancer in Greenland: the incidence in an arctic Eskimo population. Acta Pathol Microbiol Scand 85:850–858
Parkin DM, Whelan DL, Ferley J, et al. (eds) (1997) Cancer incidence in five continents, vol. VII. IARC, Lyon, No 143
Roh JL, Sung MW, Kim KH, et al. (2004) Nasopharyngeal carcinoma with skull base invasion: A necessity of staging subdivision. Am J Otolaryngol 25:26–32
Rubinstein AB, Reichenthal E, Borohov H (1989) Radiation-induced schwannomas. Neurosurgery 24:929–932
Seow A, Koh WP, Chia KS, Shi LM, Lee HP, Shamugaratnam K (2004) Trends in cancer incidence in Singapore 1968–2002. Singapore Cancer Registry, Singapore
Sham JST, Wei WI, Zong YS, et al. (1990a) Detection of subclinical nasopharyngeal carcinoma by fiberoptic endoscopy and multiple biopsies. Lancet 335:371–374
Sham JST, Choy D, Wei WI (1990b) Nasopharyngeal carcinoma: orderly neck node spread. Int J Radiat Oncol Biol Phys 19:929–933
Sham JST, Cheung YK, Chan FL, et al. (1990c) Nasopharyngeal carcinoma: pattern of skeletal metastases. Br J Radiol 63:202–205
Sham JST, Cheung YK, Choy D, Chan FL Leong LLY (1991a) Nasopharyngeal carcinoma: CT evaluation of patterns of tumor spread. AJNR 12:265–270
Sham JST, Cheung YK, Choy D, et al. (1991b) Cranial nerve involvement and base of skull erosion in nasopharyngeal carcinoma. Cancer 68:422–426
Sham JST, Choy D, Wei WI, et al. (1992) Value of clinical follow-up for local nasopharyngeal carcinoma relapse. Head Neck 14:208–217

Shanmugaratnam K, Chan SH, de-The G, et al. (1979) Histopathology of nasopharyngeal carcinoma. Correlations with epidemiology, survival rates and other biological characteristics. Cancer 44:1029–1044

Sobin LH (2003) TNM: evolution and relation to other prognostic factors. Semin Surg Oncol 21:3–7

Sobin LH, Wittekind Ch (eds) (2002) UICC TNM classification of malignant tumors, 6th edn. Wiley-Liss, New York

Steeves RA, Bataini JP (1981) Neoplasms induced by megavoltage radiation in the head and neck region. Cancer 47:1770–1774

Su CY, Lui CC (1996) Perineural invasion of the trigeminal nerve in patients with nasopharyngeal carcinoma. Cancer 78:2063–2069

Sze WM, Lee AWM, Yau TK, et al. (2004) Primary tumor volume of nasopharyngeal carcinoma: prognostic significance of local control. Int J Radiat Oncol Biol Phys 59:21–27

Tsai MH, Shiau YC, Kao CH, Shen YY, Lin CC, Lee CC (2002) Detection of recurrent nasopharyngeal carcinoma with positron tomography using 18-fluoro-2-deoxyglucose in patients with indeterminate magnetic resonance imaging findings after radiotherapy. J Cancer Res Clin Oncol 128:279–282

van der Laan BF, Baris G, Gregor RT, Hilgers FJ, Balm AJ (1995) Radiation-induced tumors of the head and neck. J Laryngol Otol 109:346–349

Willner J, Baier K, Pfreunder L, et al. (1999) Tumor volume and local control in primary radiotherapy of nasopharyngeal carcinoma. Acta Oncol 38:1025–1030

9 Parapharyngeal Space Neoplasms

Robert Hermans and Davide Farina

CONTENTS

9.1 Introduction

The parapharyngeal space (PPS) is a deep space of the neck shaped as a tilted up pyramid with its base attaching to the skull base and the apex reaching the level of the hyoid bone, and almost exclusively containing fat. Primary neoplasms arising in this space are quite rare, accounting for only 0.5% of all head and neck tumors (Olsen 1994; Miller et al. 1996; Pang et al. 2002), whereas the PPS is more commonly displaced or infiltrated by lesions arising in the adjacent spaces, including the pharyngeal mucosal, masticator, parotid, and retropharyngeal spaces. Approximately 70%–80% of the tumors originating from the PPS itself are benign (Luna-Ortiz et al. 2005).

Small tumors of the PPS, with a size of less than 2.5 cm, are often incidental findings. Larger tumors produce aspecific signs and symptoms, including sore throat, ear fullness, dysphagia and, less frequently, jaw pain combined with cranial nerves palsy. These last two symptoms may be caused by a malignant lesion. Clinical assessment of tumors in this region is often difficult, commonly causing a delay between the onset of clinical manifestations and the diagnosis. Bulging of the lateral nasopharyngeal wall may be appreciated, associated with displacement of the soft palate and palatine tonsil. When a PPS lesion grows laterally, facial swelling may result at the level of the parotid or submandibular region. Rarely, the mandible will be displaced by a slowly growing tumor (Farina et al. 1999).

Physical examination may not allow differentiation between a PPS neoplasm and a parotid gland lesion originating in the deep lobe. Before the advent of cross-sectional imaging techniques, such as CT and MR, treatment was performed via a transparotid approach. Nowadays, when a CT or MR study demonstrates the lesion to be in the PPS, most patients are operated via a transcervical approach, with or without resection of the deep lobe of the parotid gland. In large tumors, mandibulotomy may be required to remove the tumor. In selected small tumors, a transoral approach may be sufficient. The use of imaging studies has resulted in a significant decrease of transient or permanent damage to the facial nerve (Stell et al. 1985; Olsen 1994; Miller et al. 1996; Luna-Ortiz et al. 2005).

Lesions arising from the adjacent spaces displace the PPS in a particular way, allowing the radiologist to identify precisely the space of origin. Combining the imaging characteristics of the lesion with a limited space-specific differential diagnosis often allows a precise diagnosis. Knowledge of the anatomy is, therefore, the key to unlock the PPS and its related spaces.

9.2 Anatomy

9.2.1 Fascial Layers and Compartments

Medially, the PPS is in close contact with the pharyngeal mucosal space, bordered by the middle layer of

R. Hermans, MD, PhD
Professor, Department of Radiology, University Hospitals Leuven, Herestraat 49, 3000 Leuven, Belgium
D. Farina, MD
Department of Radiology, University of Brescia, Piazzale Spedali Civili 1, 25123 Brescia, BS, Italy

the deep cervical fascia (also known as buccopharyngeal fascia), which curves around the posterior and lateral side of the pharyngeal mucosal space, surrounding the constrictor muscles (Figs. 9.1 and 9.2). Superiorly, the pharyngeal constrictor muscle does not reach the skull base; at that level, the lumen of the nasopharynx is held open by the thick pharyngobasilar fascia. This fascia lies within the middle layer of the deep cervical fascia. The pharyngobasilar fascia is interrupted at the level of the sinus of Morgagni, an opening through which the cartilaginous part of the Eustachian tube and the levator veli palatini muscle enter the nasopharynx. This area should be carefully inspected on imaging studies of the nasopharynx, as it is a common route of spread for nasopharyngeal carcinomas from the mucosal space to the skull base (see Chap. 8). Just posterior to the Eustachian tube is the fossa of Rosenmüller, a mucosal recess where most of the nasopharyngeal carcinomas arise.

The superficial layer of the deep cervical fascia is lateral to the PPS, separating this space from the masticator space. This fascia curves around the medial surface of the pterygoid muscles and extends from the mandible to the skull base, where it attaches just medial to the foramen ovale. As a consequence, the mandibular nerve (V3), as it courses through this foramen, directly enters the masticator space.

In its posterolateral portion, the PPS is in contact with the deep lobe of the parotid gland. The existence of a fascial layer at this level is controversial.

The anterior border of the PPS is the pterygomandibular raphe. Inferiorly, the PPS gradually becomes narrower and ends at the level of the hyoid bone and superior margin of the submandibular salivary gland.

The posterior border of the PPS is the most complex and controversial; different descriptions are found in the literature. Some authors consider the PPS completely separate from the more posterior carotid space: the anterior surface of the carotid sheath (made up of the three layers of deep cervical fascia) draws the borderline between the two spaces. From a radiological point of view such a separation allows a precise and reliable space-specific differential diagnosis (Som and Curtin 1995). Others, in contrast, consider the carotid sheath and, consequently, the carotid space to be part of the PPS (Mukherji and Castillo 1998).

Three more fascial structures are described, acting as anatomical landmarks subdividing the PPS. The tensor-vascular-styloid fascia (TVS) is a layer that extends from the inferior border of the tensor veli palatini muscle, posterolaterally and inferiorly to the styloid process and muscles (Fig. 9.2). Anteriorly, it reaches the pterygomandibular raphe and there-

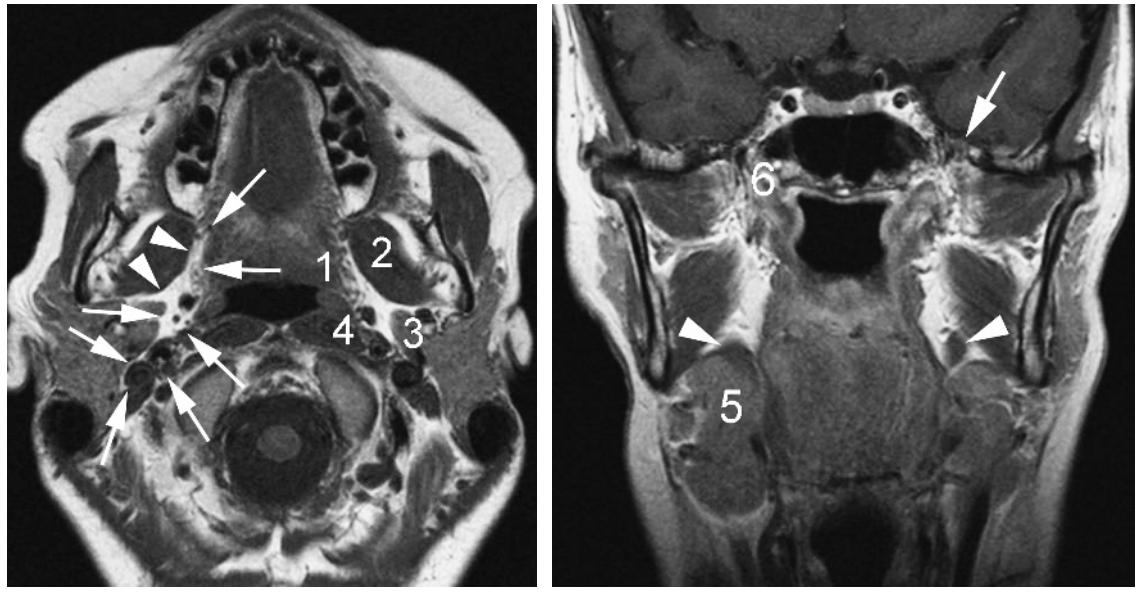

a b

Fig. 9.1a,b. Axial T1-weighted spin-echo image (**a**) at the level of the soft palate. The boundaries of the parapharyngeal space (PPS) (including prestyloid and retrostyloid compartment) are indicated by *arrows* and *arrowheads* on the right. On the left, the adjacent spaces are labeled: *1*, pharyngeal mucosal space; *2*, masticator space; *3*, parotid space; *4*, retropharyngeal/prevertebral space. **b** Coronal T1-weighted spin-echo images through prestyloid compartment of the PPS. Inferiorly, this space is closed by the submandibular gland (*5*), while superiorly, it reaches the skull base (*6*). The foramen ovale (*arrow*), through which exits the mandibular nerve, communicates with the masticator space. The styloglossal muscles run through the PPS (*arrowheads*)

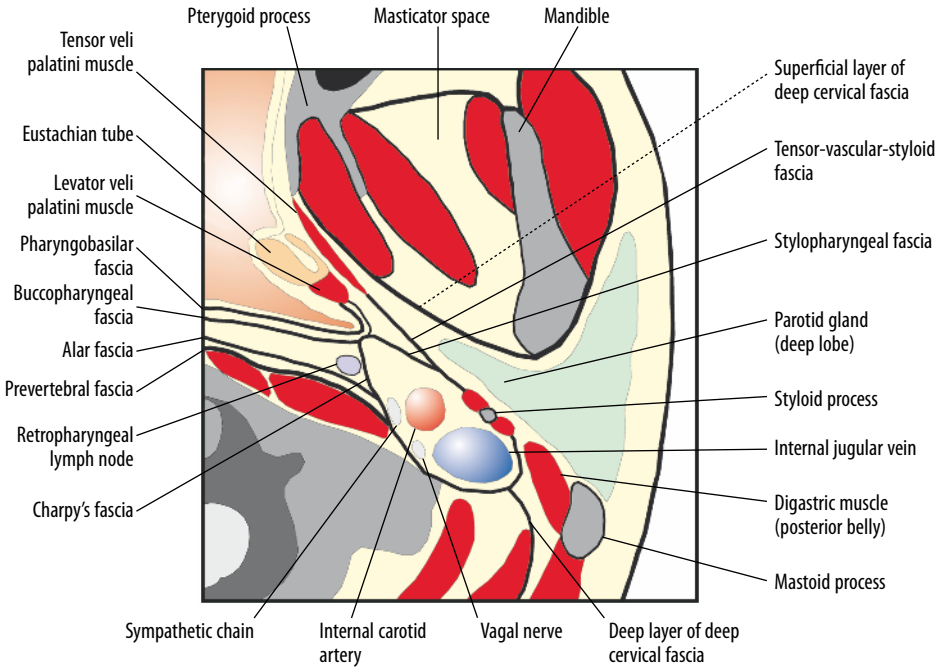

Fig. 9.2. Topographical anatomy of the PPS in the axial plane, including the different fascial layers at this level

fore it closes the gap between the skull base, the tensor veli palatini muscle and the styloid process (Som and Curtin 1995). The stylopharyngeal fascia splits on a coronal plane connecting the styloid process to the pharyngobasilar fascia, at the level of the fossa of Rosenmüller. In this same site a third layer, Charpy's fascia, also known as the '*cloison sagittale*', arises, oriented on a sagittal plane and posteriorly reaching the prevertebral fascia where it attaches to the lateral cervical processes.

The TVS fascia allows further subdivision of the parapharyngeal space into two compartments: the prestyloid compartment, lying between the pterygoid muscles and the TVS fascia, and the retrostyloid compartment, just medial to the TVS fascia itself and including the carotid space (Maroldi et al. 1994; Nasser and Attia 1990).

The PPS mainly contains fat tissue and loose connective tissue. In the prestyloid compartment ectopic minor salivary glands and vascular structures (pharyngeal ascending and internal maxillary artery, pharyngeal venous plexus) are found. The retrostyloid PPS contains the internal carotid artery (ICA), the internal jugular vein (IJV), the cranial nerves IX–XII, and the sympathetic plexus. Lymph nodes of the deep cervical chain, known as the jugulodigastric lymph nodes, are present in the retrostyloid compartment, below the level of the posterior belly of the digastric muscle (Grégoire et al. 2003).

9.2.2 Radiological Anatomy

When dealing with pathology at the level of the PPS, MRI has an advantage over CT because of its higher contrast resolution. CT better demonstrates subtle bone erosion. However, MR yields unique information about the medullary bone, which normally has a hyperintense signal on the unenhanced T1-weighted images (due to its fatty content). This signal will become hypointense on the same sequence when the medullary bone is replaced by neoplastic tissue. This signal decrease is a very sensitive sign for neoplastic infiltration, but it is rather aspecific, because edema and inflammatory bone reactions also cause a signal decrease in the medullary bone on T1-weighted images.

In the axial plane the prestyloid compartment of the PPS is recognized as a triangular fat-filled space (Fig. 9.1) with maximum width at the level of the soft palate. While CT is unable to display the pharyngobasilar fascia, this fascia is visible on MRI as a hypointense line (Fig. 9.3).

The sinus of Morgagni is not visible with MR, but the Eustachian tube, particularly at the torus tubarius, where it opens in the nasopharyngeal lumen, can be used as an anatomical landmark.

The TVS, stylopharyngeal and Charpy's fascia can not be routinely identified on MR. Their course can be

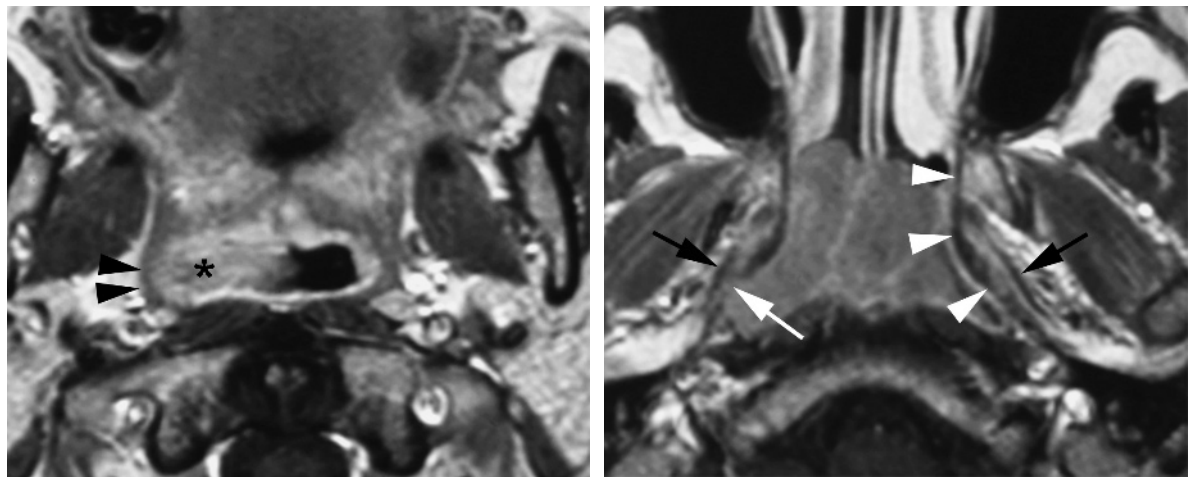

Fig. 9.3a,b. Axial gadolinium-enhanced T1-weighted spin-echo images, showing the relationship between the superior constrictor muscle, the pharyngobasilar fascia and a nasopharyngeal cancer. **a** Axial section at level of soft palate. The superior constrictor muscle (*arrowheads*) is surrounding the nasopharynx; the tumor (*asterisk*) is confined to the nasopharyngeal lumen. **b**. At a higher level, the nasopharyngeal lumen is bordered by the pharyngobasilar fascia (*arrowheads*). Bilaterally, the tensor veli palatini muscle (*black arrow*) is visible on the outer side of this fascial layer. On the right, the tumor extends into the PPS through the pharyngobasilar fascia (*white arrow*); this site likely corresponds to the sinus of Morgagni

mentally outlined on axial scans by using the tensor veli palatini muscle and styloid process as anatomical landmarks. This last structure, easily detected with CT, is seen on MR with a characteristic 'target' appearance: hypointense external cortical rim with hyperintense bone marrow in its center.

The lateral fascial border of the PPS is not identified, but its cranial attachment lies just medial to foramen ovale (Fig. 9.1). MR is able to depict the course of the mandibular nerve – from Meckel's cave, through the foramen ovale – and also the proximal segment of the main terminal branch, the inferior alveolar nerve, as it runs to the entrance of the mandibular canal.

The ICA and IJV, just medial to the styloid process, appear hyperdense on enhanced CT, while they generally show a flow void on T1- and T2-weighted MR sequences. High or inhomogeneous signal is often seen in the jugular vein due to turbulent or slow flow and should not be mistaken for a strongly enhancing mass (e.g. glomus jugulare tumor).

9.3 Imaging of Parapharyngeal Space Lesions

The role of imaging in lesions at the level of the PPS can be summarized in two key points:

- To precisely identify the space of origin; this allows to reduce the differential diagnostic list to a limited number of possibilities.
- To identify hypervascular neoplasms in order to avoid biopsy and its possible complications.

9.3.1 Primary Lesions of the Parapharyngeal Space

Primary lesions of the PPS are rare and most are benign. These lesions can be classified based on histology (three main groups: salivary, neurogenic, paragangliomas), or according to the compartment of origin (prestyloid or retrostyloid).

9.3.2.1 Prestyloid Lesions

The overwhelming majority of neoplasms in the prestyloid compartment are salivary gland tumors. Most other lesions in this compartment are related to anomalies of the branchial apparatus.

Pleomorphic adenoma is the most frequent salivary tumor. These tumors may arise from ectopic minor salivary glands, localised in the prestyloid compartment along the embryological growth path of the parotid gland, but much more often they originate from the deep lobe of the parotid gland. Making the differentiation between a primary prestyloid PPS lesion and a neoplasm of the deep lobe of the parotid gland is important, because, in the latter case, the deep lobe of the parotid gland also needs to be resected.

The most reliable sign of a primary PPS tumor is the presence of a fat layer separating the tumor from the deep lobe of the gland. A deep parotid lobe tumor appears as a more or less dumbbell-shaped mass, connected to the parotid gland, potentially widening the stylomandibular tunnel, and displacing anteromedially the PPS fat (Fig. 9.4).

Pleomorphic adenomas usually show the following MR appearance: hyperintense signal intensity on T2-weighted sequences, related to their myxoid component, and often pronounced enhancement with focal areas of hypointensity on T1-weighted sequences. However, various signal intensities due to haemorrhage, calcifications and necrosis may be seen within such a tumor (Fig. 9.5).

Although pleomorphic adenoma is a benign tumor, it may recur locally if the thin capsule is interrupted during surgical resection. Most frequently, these relapses are multifocal and appear very hyperintense on T2-weighted sequences.

Salivary malignancies are infrequent, with mucoepidermoid and adenoid cystic carcinoma being the most common histologic types. CT and MR characteristics do not allow differentiation of a malignant from a benign lesion, only the presence of infiltration of adjacent structures suggests malignancy.

Much rarer neoplasms in the prestyloid compartment are lipomas (Kakani et al. 1992) and muscular neoplasms (rhabdomyomas and rhabdomyosarcomas).

Anomalies of the second branchial apparatus represent a spectrum of manifestations, ranging from a fistula to an isolated cyst. One end of the spectrum is a fistula between the anterior side of the sternocleidomastoid muscle and the pharyngeal wall at the level of the palatine tonsil. The other end of the spectrum is a cyst, potentially localised anywhere along this tract. The most typical localisation of such a cyst is just below the mandibular angle, posterior to the submandibular salivary gland, lateral to the vessels and anterior to the sternocleidomastoid muscle. As the trajectory of such a branchial apparatus anomaly runs through the PPS, such cysts may also occur within the PPS (Fig. 9.6). Thickened, irregular walls may be seen in branchiogenic cysts that are, or have been infected. In the absence of a history of inflammation, an atypical cystic lesion should also raise the possibility of a cystic (retropharyngeal) adenopathy, as can be seen with papillary thyroid carcinoma (Fig. 9.7) (Lombardi et al. 2004).

A possible imaging pitfall in the prestyloid compartment is an hypertrophic pterygoid venous plexus mimicking a vascular lesion; in these cases imaging techniques will demonstrate the presence of multiple serpiginous flow voids (on MR) or enhancing vessels (on CT) just medial to the medial pterygoid muscle.

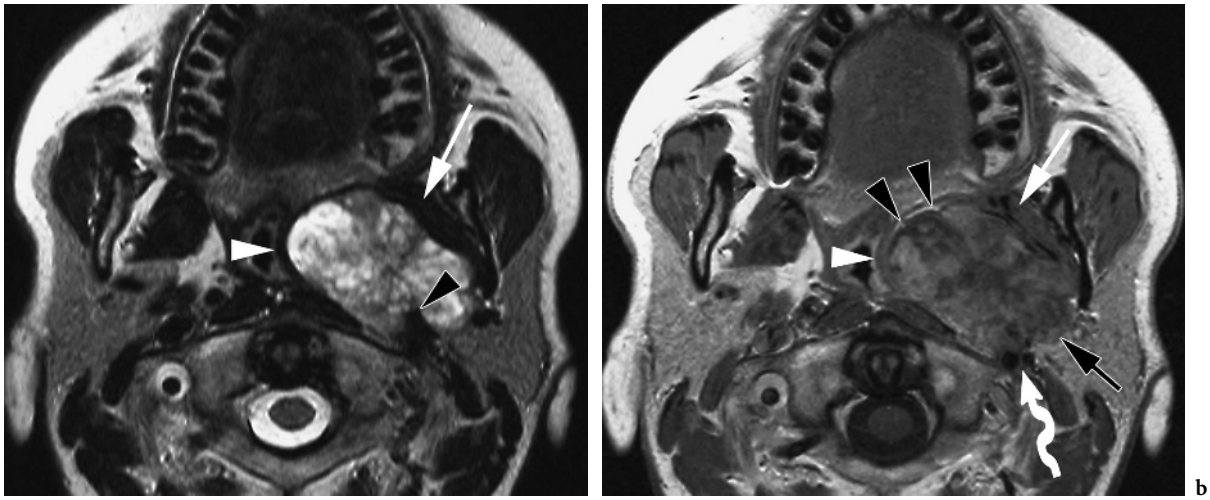

a b

Fig. 9.4a,b. Axial T2-weighted (**a**) and gadolinium-enhanced T1-weighted spin-echo image (**b**) in a patient with a coincidentally discovered PPS tumor. The lesion can not be separated from the deep lobe of the parotid gland (*black arrow*), and largely fills the prestyloid compartment; a thin layer of fat is still visible at the anteromedial margin of the tumor (*black arrowheads*, **b**). The pharyngeal wall (*white arrowheads*) and medial pterygoid muscle (*white arrow*) are displaced. The large vessels (*curved arrow*) are displaced posteriorly. The styloid musculature produces an indentation in the posterior tumor margin (*black arrowhead*, **a**). The tumor was removed via a cervical approach, with resection of the deep parotid lobe. Pathologic examination showed pleomorphic adenoma

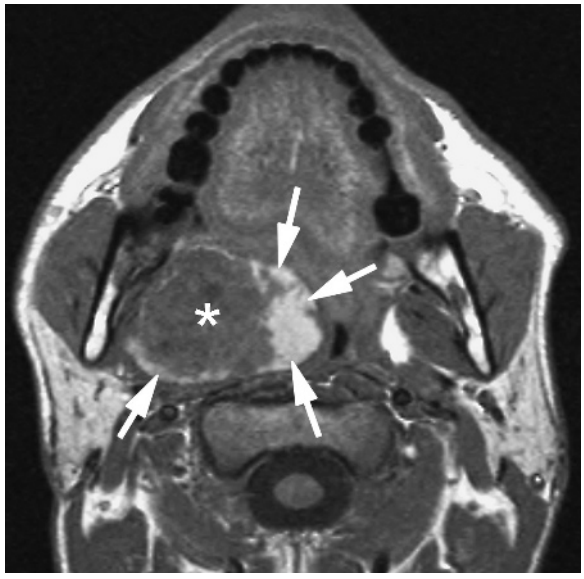

Fig. 9.5. Axial plain T1-weighted spin-echo image in a patient with a peritonsillar swelling on the right, rapidly increasing over a few hours time. A soft tissue mass (*asterisk*) is seen in the prestyloid compartment of the PPS; the mass periphery, mainly on the tonsillar side, shows spontaneous hyperintensity, compatible with recent hemorrhage (*arrows*). The mass was resected; pathologic examination showed pleomorphic adenoma

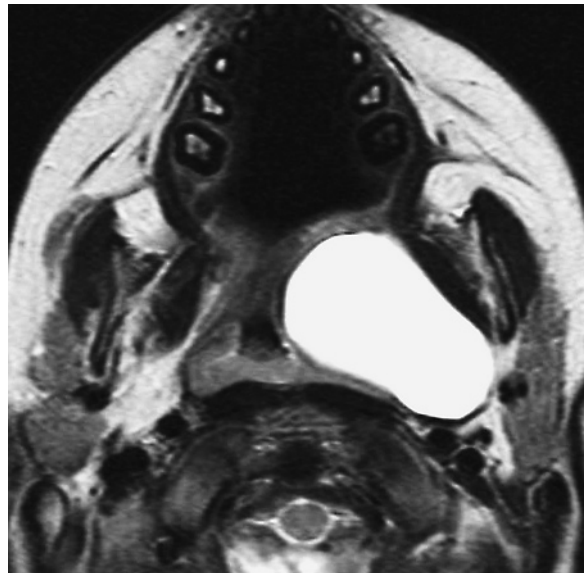

Fig. 9.6. A 3-year-old patient presenting with peritonsillar swelling. Axial T2-weighted spin-echo image shows a cystic mass in the prestyloid compartment of the PPS, displacing the pharyngeal wall. The cyst was resected and confirmed to be a branchiogenic cyst

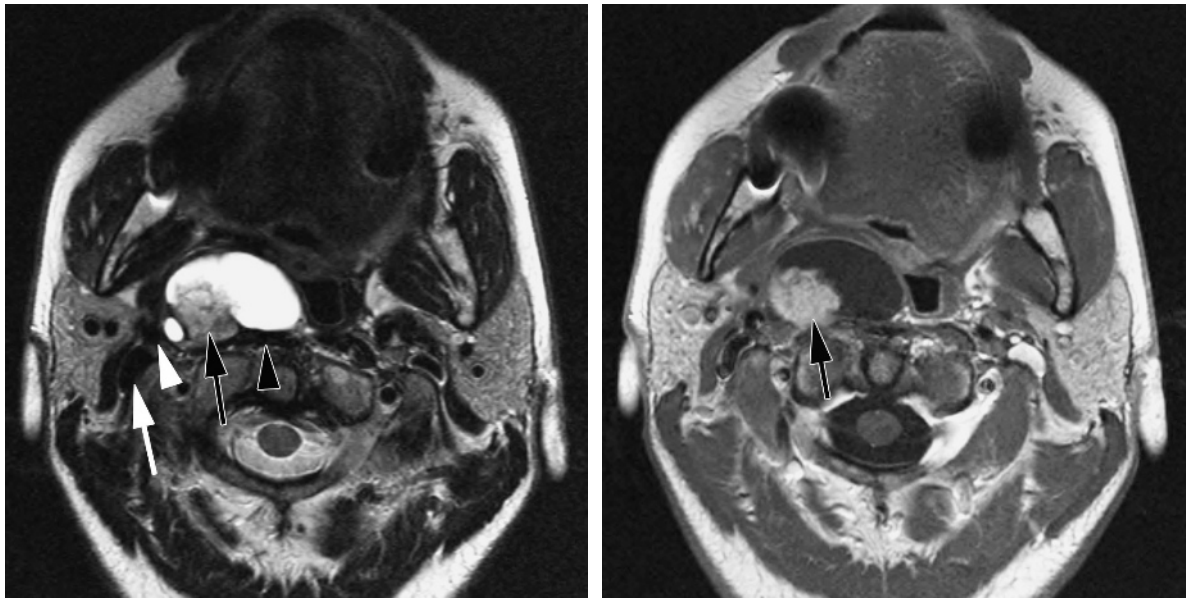

a **b**

Fig. 9.7a,b. An asymptomatic, 42-year-old female patient, with coincidentally discovered peritonsillar swelling on right side. Axial T2-weighted (**a**) and gadolinium-enhanced T1-weighted (**b**) spin-echo images show largely cystic lesion, filling the prestyloid compartment of the PPS. The mass is centered between the prevertebral muscle (*black arrowhead*) and internal carotid artery (*white arrowhead*), a typical localisation for retropharyngeal adenopathy. The internal carotid artery, as well as the internal jugular vein (*white arrow*) are displaced posterolaterally. The cystic mass contains a solid component (*black arrow*), showing enhancement. A lesion showing such appearance, especially in a young female patient, should raise the possibility of metastatic papillary thyroid cancer. Cytologic examination of the cyst content was compatible with (although not conclusive for) metastatic papillary thyroid cancer. Resection of the thyroid gland eventually confirmed papillary cancer in the right lobe; after subsequent resection of the retropharyngeal mass, metastatic thyroid cancer was histologically proven also at this level

9.3.2.2 Retrostyloid Lesions

A retrostyloid tumor can easily be identified when an anterior displacement of the ICA, and possibly the styloid process, is present. These lesions also displace the prestyloid PPS fat anteriorly. The most common primary lesions in this compartment are neurogenic tumors (17%–25% of all PPS neoplasms) and paragangliomas (10%–15%).

Schwannomas more frequently arise from the vagal nerve or from the cervical sympathetic chain. Malignant degeneration has seldom been reported (Al Otieshan et al. 1998). The typical MR appearance of a schwannoma is that of an ovoid mass with a slightly hyperintense signal on T2-weighted images; the lesion can be inhomogeneous because of areas of hemorrhage or cystic degeneration (Fig. 9.8). After the administration of a contrast agent, marked enhancement may lead to a misdiagnosis of a hypervascular tumor. Actually, a schwannoma is a relatively hypovascular lesion and the enhancement is due to extravascular leakage through abnormally permeable vessels with poor venous drainage (Fig. 9.9).

Less frequent are neurofibromas, in 10% of cases associated to von Recklinghausen syndrome (Tandon et al. 1992). These lesions may undergo marked fatty replacement.

Paragangliomas arise from chemoreceptor cells, basically present at three different anatomical sites: at the level of the nodose ganglion of vagal nerve, just below the skull base (vagal paraganglioma), at the carotid bifurcation (carotid paraganglioma) and at the level of the jugular foramen (jugular paraganglioma). A marked enhancement and, at MR, a 'salt and pepper' pattern are quite typical: this is due to the presence of tortuous large caliber vessels (detected as flow voids) within the mass (Fig. 9.10). Nevertheless, this pattern can be difficult to see or even absent, particularly in small lesions with predominantly small caliber feeding vessels (Fig. 9.11) (Som and Curtin 1995). Carotid body tumors typically splay the internal and external carotid artery and may extend superiorly in the PPS. A vagal glomus tumor has a prevalent extracranial growth and only rarely reaches the carotid bifurcation. A jugular paraganglioma is centered in the jugular foramen, often eroding the surrounding bone and extending into the middle ear (Swartz et al. 1998). CT and MR allow an accurate diagnosis of glomus tumors in most cases; the role of angiography is restricted to accurate assessment of the arterial feeders and to preoperative embolization.

Several vascular anomalies may be encountered in the retrostyloid compartment. Sometimes the ICA shows a tortuous course, running behind the posterior pharyngeal wall: correct assessment avoids a disastrous biopsy of a misinterpreted submucosal pharyngeal lesion. An occlusion of ICA, or a IJV thrombosis, are uncommonly encountered: MR shows a complex pattern of signal intensities of the intraluminal clot reflecting the different phases of hemoglobin degradation. MR is an accurate technique to diagnose dissection of the ICA. Aneurysms of the extracranial part of the ICA occur; rarely these aneurysms cause

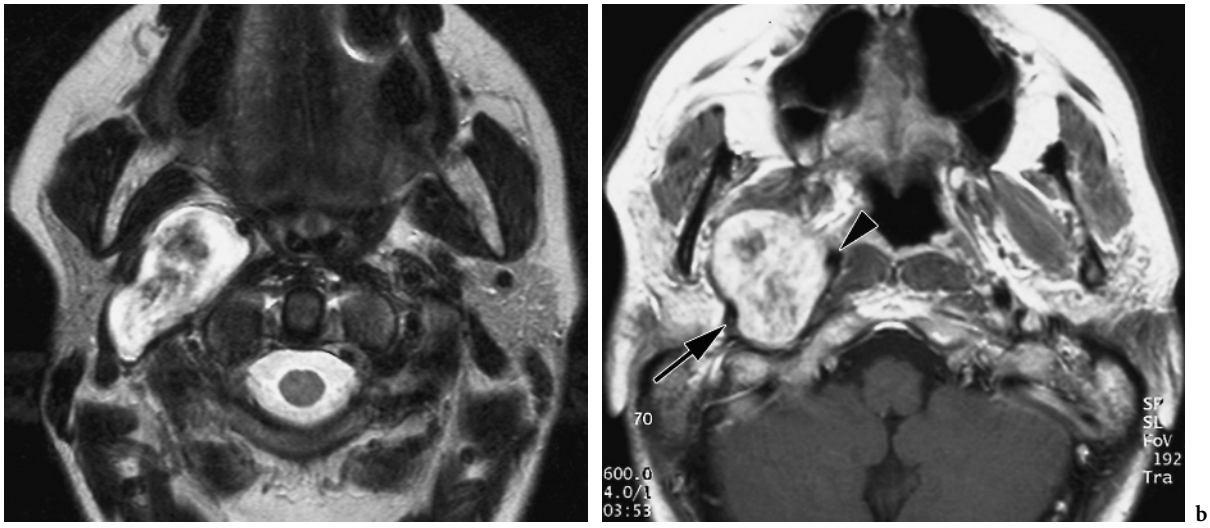

a b

Fig. 9.8a,b. T2-weighted (**a**) and gadolinium-enhanced T1-weighted (**b**) spin-echo images, showing a inhomogeneous mass in the retrostyloid compartment of the PPS, displacing the internal carotid artery (*arrowhead*) anteromedially, and the internal jugular vein (*arrow*) posterolaterally. Vagal schwannoma

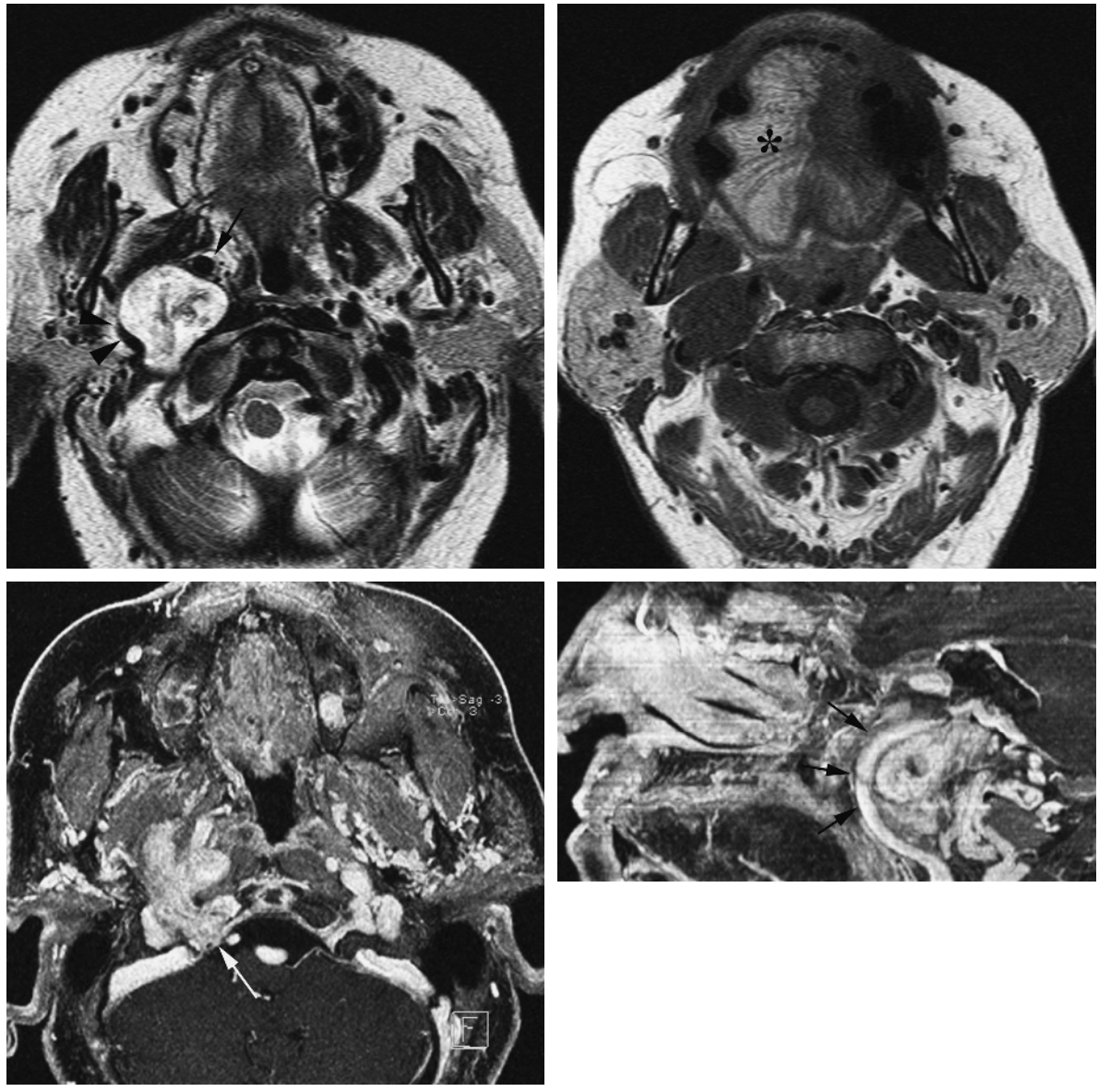

Fig. 9.9a–d. Axial T2-weighted (**a**), axial plain T1-weighted spin-echo image (**b**), gadolinium-enhanced 3D-gradient echo T1-weighted sequence, reformatted in oblique axial (**c**) and sagittal (**d**) plane. Solid mass lesion in the right PPS: anterior displacement of the internal carotid artery (*black arrows*) and stylopharyngeal muscle (*arrowheads*) indicates the retrostyloid compartment as the site of origin. T2 hyperintensity and bright enhancement (in the absence of vascular flow voids) are consistent with neurogenic tumor. Tumor extension within the condylar canal (*white arrow*) along with denervation atrophy of the right hemitongue (*asterisk*) suggests schwannoma of the XIIth cranial nerve (hypoglossal nerve). The diagnosis was confirmed at surgery

cranial nerve palsy. The diagnosis of such an aneurysm is usually straightforward (Fig. 9.12).

9.3.2 Secondary Lesions of the Parapharyngeal Space

The key to correctly identify the site of origin of a lesion arising from a space neighbouring the PPS, is to carefully assess its relationships with the PPS fat and large vessels. A neoplasm of the masticator space displaces this fat plane posteromedially (Fig. 9.13), while a tumor of the pharyngeal mucosal space will usually infiltrate the retrostyloid compartment (Fig. 9.14), displacing the fat tissue laterally. A retropharyngeal lesion (most often a retropharyngeal adenopathy) displaces the fat of the PPS anterolaterally (Fig. 9.15).

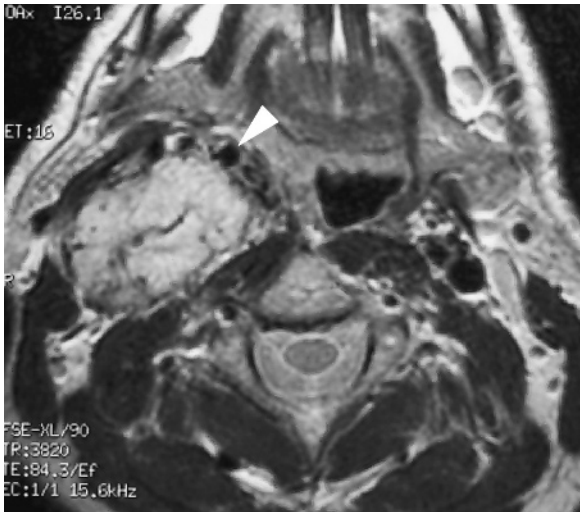

Fig. 9.10. Axial gadolinium-enhanced T1-weighted spin-echo image. A strongly enhancing mass, showing intratumoral signal voids, is present in the retrostyloid compartment of the PPS. The internal carotid artery is displaced anteromedially (*arrowhead*); the internal jugular vein is compressed and displaced posteromedially, not clearly identifiable on this image. (Image courtesy of Bert De Foer, MD, Antwerp, Belgium)

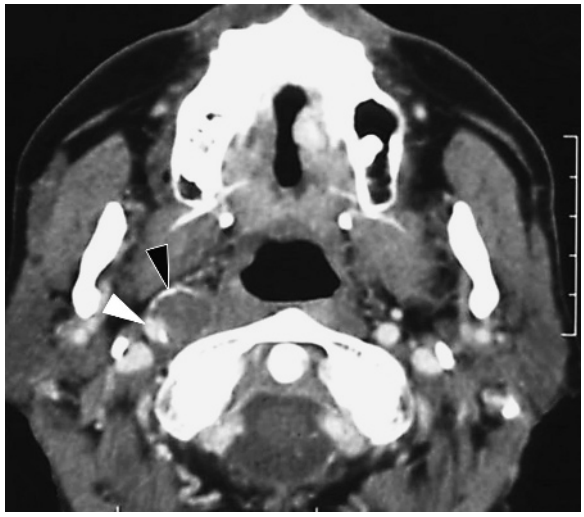

Fig. 9.12. Axial contrast-enhanced CT image shows nodular lesion in the retrostyloid compartment of the PPS. At first sight one may think about retropharyngeal adenopathy. However, the narrowed lumen of the internal carotid artery (*white arrowhead*) is within the peripheral part of the mass, which also shows some peripheral calcifications (*black arrowhead*): these findings are compatible with an internal carotid artery aneurysm

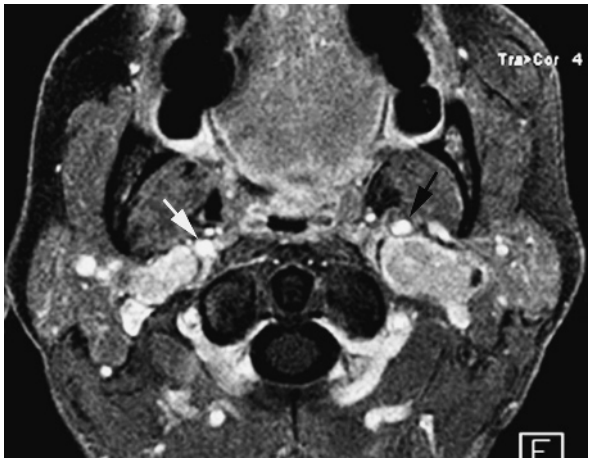

a

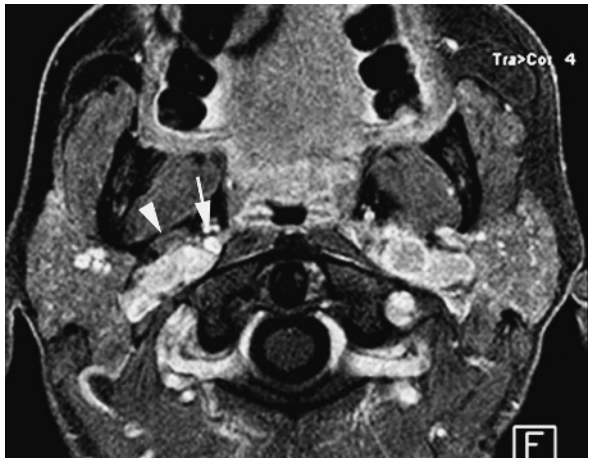

b

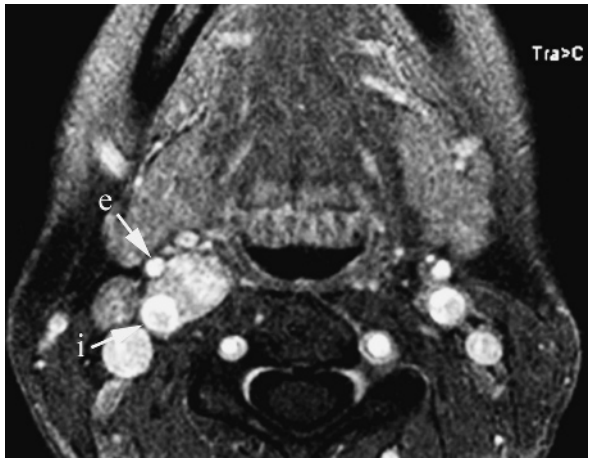

c

Fig. 9.11a–c. Gadolinium-enhanced 3D gradient-echo T1-weighted sequence in axial plane. Bilateral retrostyloid PPS mass (**a,b**): on the right side the internal carotid artery is anteromedially displaced (*white arrows*), and the stylopharyngeal muscle is anteriorly displaced (*white arrowhead*); on the left, anterior displacement of internal carotid artery is more evident (*black arrow*). Serpiginous flow voids are more clearly demonstrated at the periphery of the left lesion, probably due to its larger size. More caudally (**c**), a third lesion is demonstrated just medial to internal (*i*) and external (*e*) carotid artery, few millimetres above carotid bifurcation. MR findings are consistent with bilateral vagal paraganglioma and right carotid body tumor; this diagnosis is also strongly supported by a familial history for paraganglioma

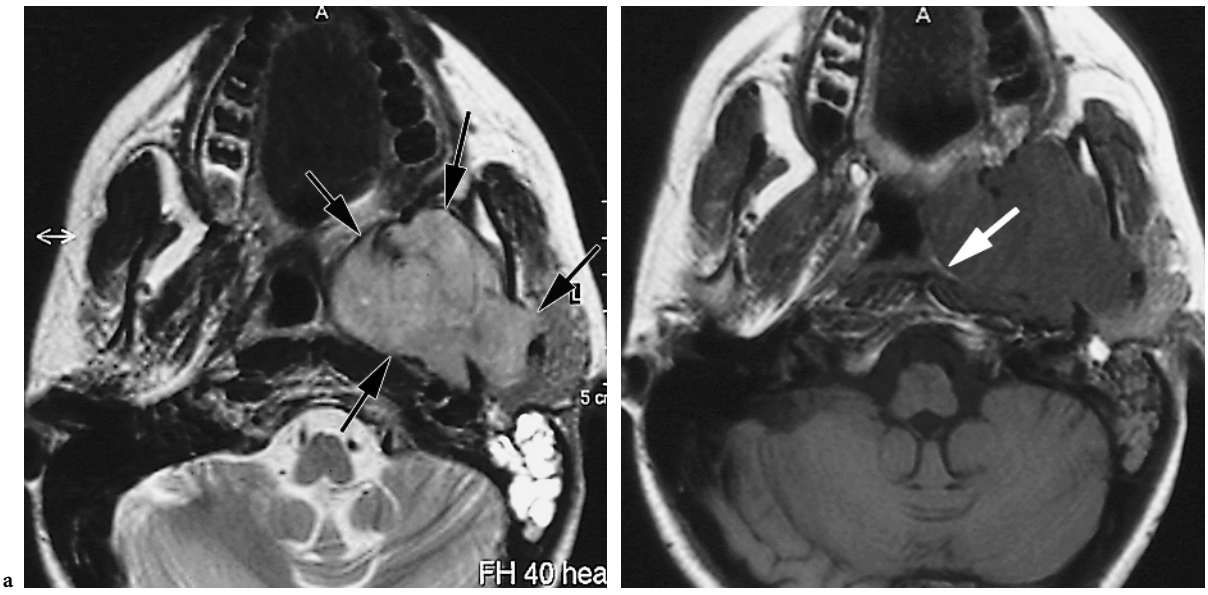

a b

Fig. 9.13a,b. Axial T2-weighted (**a**) and plain T1-weighted spin-echo image (**b**) in a 22-year old patient presenting with hearing loss on left side and increasing difficulties with mastication. A soft tissue mass (*black arrows*) is seen on the deep side of the mandible, extending into the PPS; a thin layer of fat can be recognized on the posteromedial side of the mass (*white arrow*). The lesion involves the deep lobe of the parotid gland. Contrary to the patient shown in Fig. 9.4, the pterygoid musculature can not be recognized anymore, suggesting that the point of origin is within the masticator space. Fluid is present in the mastoid, secondary to dysfunction of the eustachian tube. Biopsy revealed rhabdomyosarcoma

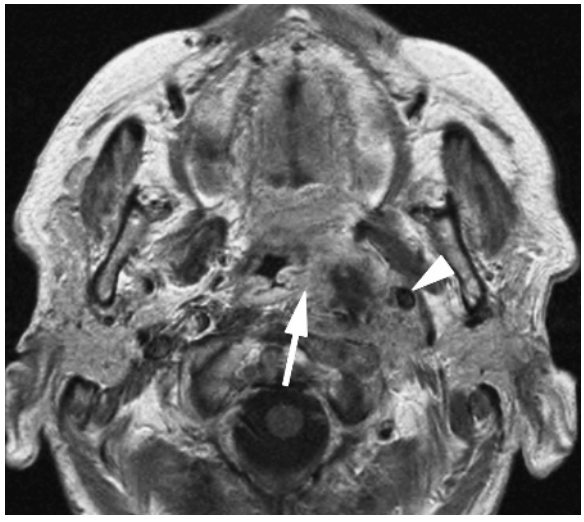

Fig. 9.14. Patient presenting with increasing left-sided neck and facial pain. Axial gadolinium-enhanced T1-weighted spin-echo image shows poorly defined, partially liquefied mass in the left PPS, mainly within the retrostyloid compartment. The adjacent pharyngeal wall (*arrow*) appears inhomogeneous, with disruption of the constrictor muscle. Anterolateral displacement of the internal carotid artery (*arrowhead*), as well as of the prestyloid fat plane. Involvement of the prevertebral and paraspinal compartment is seen. Pharyngeal biopsy showed squamous cell cancer

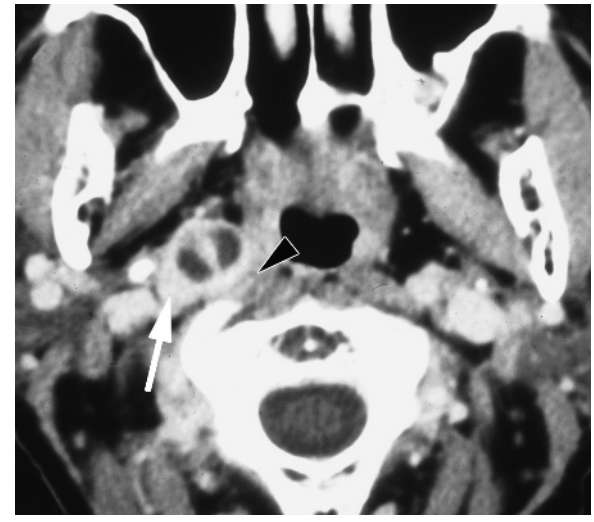

Fig. 9.15. Axial contrast-enhanced CT image at level of nasopharynx. Centrally necrotic retropharyngeal adenopathy (lymphatic metastasis of recurrent laryngeal cancer). A retropharyngeal adenopathy is typically situated between the prevertebral muscle (*arrowhead*) and the internal carotid artery (*arrow*); large adenopathies, such as in this case, displace the prestyloid fat anterolaterally

Large and aggressive neoplasms, such as sometimes seen with sarcoma, nasopharyngeal cancer or lymphoma, may show a transspatial growth pattern; in such circumstances, a precise diagnosis on imaging studies is not possible.

Secondary involvement of the parapharyngeal space may also be observed in benign multicompartmental lesions, i.e. lesions characterized by the aptitude to grow across the boundaries that separate the deep spaces of the head and neck, thus invading simultaneously more than two compartments. Among these, hemangioma and lymphangioma exhibit a rather peculiar imaging pattern consisting of hypodensity on plain CT and hyperintensity on T2-weighted MR sequences. Dotted calcifications – better demonstrated on CT – may be seen in hemangiomas; MR may reveal serpiginous flow voids representing dilated vascular channels. On the other hand, lymphangioma may exhibit spontaneous T1 hyperintensity, due to highly hyperproteinaceous or fatty content. Contrast agent application better differentiates the two entities: hemangioma shows bright (though frequently non-homogeneous) enhancement; lymphangioma, on the other hand, shows no contrast uptake, though enhancement of the multiple subtle septa crossing the lesion is occasionally observed (Figs. 9.16 and 9.17) (Sigal 1998).

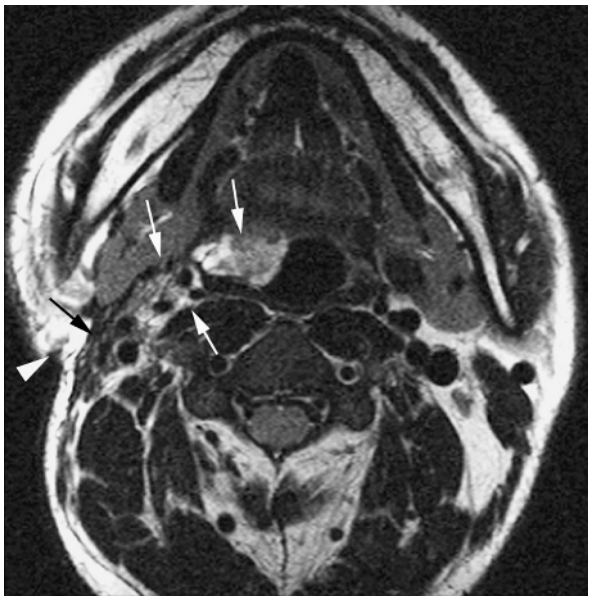

a

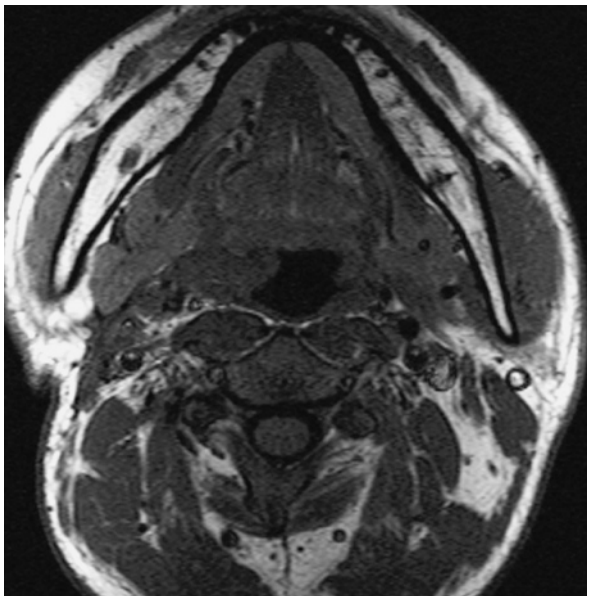

b

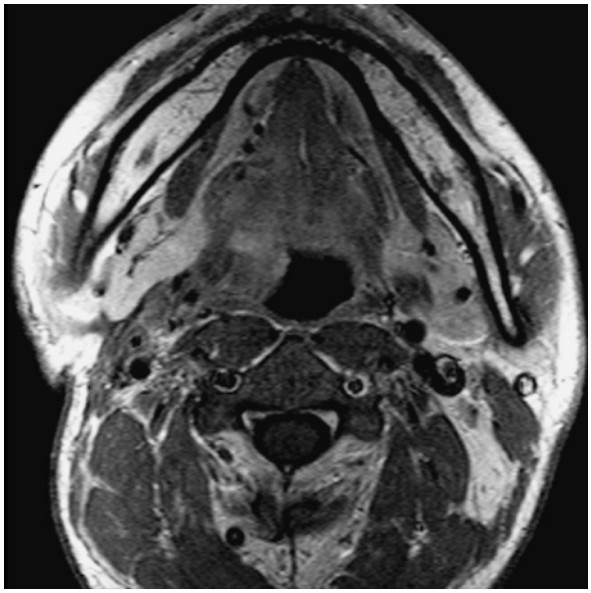

c

Fig. 9.16a–c. T2-weighted spin-echo (**a**), plain (**b**) and gadolinium-enhanced T1-weighted spin-echo (**c**) images in the axial plane. Recurrent lymphangioma. The patient had received surgery 1 year before, as demonstrated by skin retraction (*white arrowhead*) and deep scar tissue in the proximity of external and internal carotid artery (*black arrow*). Residual lymphangioma is demonstrated in the PPS medially extending to the pharyngeal mucosal space (tonsillar fossa, base of tongue) (*white arrows*). The lesion shows bright T2 signal, no significant enhancement is observed after contrast application. The diagnosis was confirmed with fine needle aspiration under ultrasound guidance

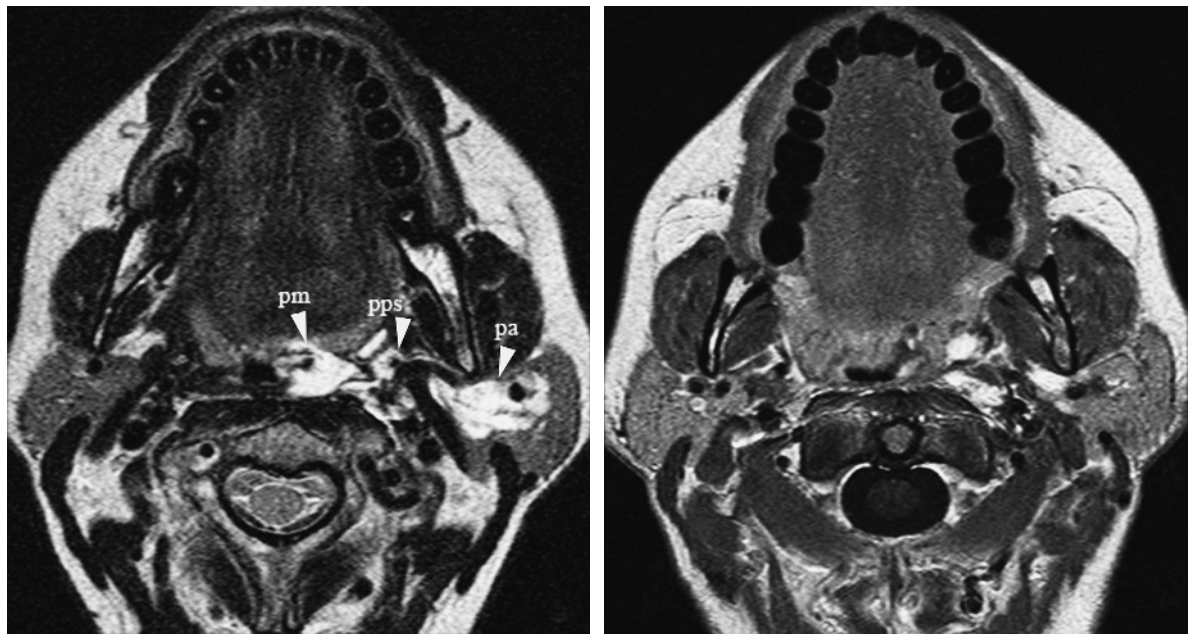

Fig. 9.17a,b. A T2-weighted spin-echo (**a**) and gadolinium-enhanced T1-weighted spin-echo image (**b**), axial plane. Multicompartmental lesion invading the left parotid (*pa*), parapharyngeal (*pps*) and pharyngeal mucosal (*pm*) space. The lesion exhibits T2 hyperintense signal, the slightly more caudal T1 section demonstrates enhancement of the parapharyngeal component. Findings are consistent with hemangioma

Parapharyngeal abscess is a rare event in the era of broad spectrum antibiotics, generally secondary to head and neck infections (odontogenic, pharyngeal, tonsillar, otomastoideal, or of salivary origin). On CT and MR, the detection of a fluid filled cavity lined by an enhancing peripheral rim rather safely indicates the presence of an abscess, whereas a soft tissue swelling associated with non-homogeneity and effacement of fat planes suggests cellulitis. Actually, the discrimination between the two entities, potentially critical for treatment planning, may be hampered by a significant number of false positives, particularly when cellulitis must be differentiated from an early abscess (Elden et al. 2001). Imaging also plays a key role in detecting major complications, more commonly occurring when the infectious process involves the retrostyloid compartment, such as IJV thrombosis, skull base osteomyelitis or extension in the retropharyngeal space (Nicolai et al. 2005).

References

Al Otieschan AA, Saleem M, Manohar MB, Larson S, Atallah A (1998) Malignant schwannoma of the parapharyngeal space. J Laryngol Otol, 112:883–887

Elden LM, Grundfast KM, Vezina G (2001) Accuracy and usefulness of radiographic assessment of cervical neck infections in children. J Otolaryngol 30:82–89

Farina D, Hermans R, Lemmerling M, Op de beeck K (1999) Imaging of the parapharyngeal space. J Belge Radiol 82:234–240

Grégoire V, Levendag P, Ang KK, et al (2003) CT-based delineation of lymph node levels and related CTVs in the node-negative neck: DAHANCA, EORTC, GORTEC, NCIC,RTOG consensus guidelines. Radiother Oncol 69:227–236

Kakani RS, Bahadur S, Kumar S, Tandon DA (1992) Parapharyngeal lipoma. J Laryngol Otol 106:279–281

Lombardi D, Nicolai P, Antonelli AR, Maroldi R, Farina D, Shaha AR (2004) Parapharyngeal lymph node metastasis: an unusual presentation of papillary thyroid carcinoma. Head Neck 26:190–196

Luna-Ortiz K, Navarrete-Alemán JE, Granados-García M, Herrera-Gómez A (2005) Primary parapharyngeal space tumors in a Mexican cancer center. Otolaryngol Head Neck Surg 132:587–591

Maroldi R, Battaglia G, Maculotti P, Bondioni MP, Gheza G, Chiesa A (1994) Diagnostica per immagini delle lesioni dello spazio parafaringeo. In: Mosciaro O (ed) I Tumori parafaringei. Printed by Studio Forma, Verona, pp 69–103

Miller FR, Wanamaker J., Lavertu P, Wood BG (1996) Magnetic resonance imaging and the management of parapharyngeal space tumors. Head Neck 18:67–77

Mukherji SK, Castillo M (1998) A simplified approach to the spaces of the suprahyoid neck. Radiol Clin North Am 36:761–780

Nasser JG, Attia EL (1990) A conceptual approach to learning

and organizing the surgical anatomy of the skull base. J Otolaryngol 19:114–121
Nicolai P, Lombardi D, Berlucchi M, Farina D, Zanetti D (2005) Drainage of retro-parapharyngeal abscess: an additional indication for endoscopic sinus surgery. Eur Arch Otorhinolaryngol Jan 25; [Epub ahead of print]
Olsen KD (1994) Tumors and surgery of the parapharyngeal space. Laryngoscope 104:1–28
Pang KP, Goh CH, Tan HM (2002) Parapharyngeal space tumours: an 18 year review. J Laryngol Otol 116:170–175
Sigal R (1998) Infrahyoid neck. Radiol Clin North Am 36:781–799
Som PM, Curtin HD (1995) Lesions of the parapharyngeal space. Role of MR imaging. Otolaryngol Clin North Am 28:515–542
Stell PM, Mansfield AO, Stoney PJ (1985) Surgical approaches to tumors of the parapharyngeal space. Am J Otolaryngol 6:92–97
Swartz JD, Harnsberger HR, Mukherji SK (1998) The temporal bone: contemporary diagnostic dilemmas. Radiol Clin North Am 36:819–854
Tandon DA, Bahadur S, Misra NK, Deka RC, Kapila K (1992) Parapharyngeal neurofibromas. J Laryngol Otol 106:243–246

10 Masticator Space Neoplasms

Thierry P. Duprez and Emmanuel E. Coche

CONTENTS

10.1 Masticator Space Anatomy

The masticator space (MS) is a deep facial space delineated by a splitting of the deep cervical fascia which encloses the four muscles of mastication: the medial and the lateral pterygoid, the masseter, and the temporalis muscles – hence the denomination of "masticator space" (Harnsberger 1995; Mukherji and Chong 2004). The MS also contains the ramus and posterior body of the mandible and the third division of the fifth cranial nerve (mandibular trigeminal branch or V3). The V3 nerve gives motor innervation to the mastication muscles and relays sensory information from the inferior teeth, gums and lower lip/chin region through the inferior alveolar nerve. The nerve emerges from the endocranium to the MS through the foramen ovale. The space is easy to identify on both CT and MR images (Figs. 10.1, 10.2) because of easily recognizable shape and location of the mastication muscles (Harnsberger and Osborn 1991; Mukherji and Castillo 1998). The inferior limit of the MS is the attachment of the medial pterygoid muscle to the mandible. The space has two distinct superior margins. The base of the skull is the superior limit of the "infratemporal fossa" or "nasopharyngeal masticator space" which encompasses all soft tissue below the foramen ovale. The second superior margin is the attachment of the temporalis muscle to the outer table of the skull; this part is called the "temporal fossa", or the "suprazygomatic masticator space" because it is above the zygomatic arch (Fig. 10.2). The MS is separated from the parapharyngeal space by a fascial layer extending from the medial pterygoid muscle to the skull (Curtin 1987). The fascia is also attached to the anterior aspect of the mandibular ramus, has an interface with the oral cavity, and reaches the posterior margin of the ramus, where the masticator space constitutes the anterior border of the parotid space.

10.2 Introduction to Masticator Space Malignancies

Tumors in the MS may arise from each major component of the space (muscles, bone, V3), or may be the extension of a tumor arising from adjacent spaces. Muscular malignancies are of mesenchymal origin in the vast majority of the cases. Imaging features of the different sarcomas are poorly specific. Metastases must be included in the differential diagnosis of MS

T. P. Duprez, MD; E. E. Coche, MD, PhD
Department of Radiology and Medical Imaging, Université Catholique de Louvain, Cliniques Universitaires Saint-Luc, Avenue Hippocrate, 10, 1200 Brussels, Belgium

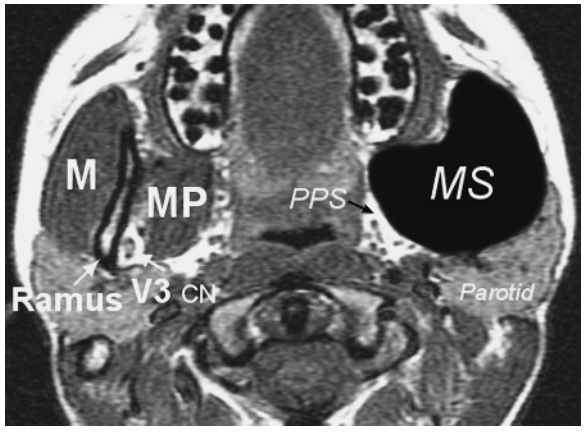

Fig. 10.1. Masticator space anatomy. Transverse T1-weighted image: masticator space (*MS*) has been highlighted on the left side, excluding the parotid gland posteriorly and the buccinator muscle anteriorly. Critical contents of MS are (right side): *M*, masseter muscle; *MP*, medial pterygoid muscle; *V3*, mandibular branch of the fifth cranial nerve, and ramus of the mandible. Observe close relation to the fatty parapharyngeal space (*PPS*)

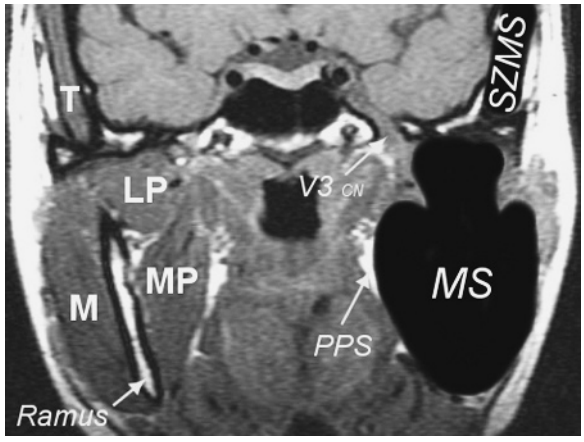

Fig. 10.2. Masticator space anatomy. Coronal T1-weighted image: similar to Fig. 10.1, the masticator space (*MS*) has been highlighted on the left side. Observe the presence of a second more cranial compartment containing the belly of the temporalis muscle (*T*), i.e. the suprazygomatic masticator space (*SZMS*). Other critical contents of the MS include: *LP*, lateral pterygoid muscle; *MP*, medial pterygoid muscle; *M*, masseter muscle; *V3*, mandibular branch of the fifth cranial nerve. The fatty parapharyngeal space and bone marrow of the ramus disclose hypersignal intensity

masses, but primitive osteosarcoma is the most frequent malignancy arising from the mandibular bone component of the space (Chong and Fan 1996). The V3 cranial nerve which courses medial to the lateral pterygoid muscle before penetrating the base of the skull through the foramen ovale constitutes a "highway" for tumoral spreading of malignant neoplasms from the MS to the base of the skull and the endocranium. The MS may be invaded by infiltrative malignancies arising from adjacent anatomical spaces, the most frequent one being primary squamous cell carcinoma (SCC) of the pharynx or of the retromolar trigone. Infectious mass-occupying processes are the main alternative hypothesis to benign/malignant neoplastic diseases of the MS. Since the imaging findings of MS neoplasms have low specificity, the diagnosis requires the knowledge of clinical/biological data and ultimately relies on the anatomopathological examination of biopsy or surgical specimens (Eskey et al. 2000).

10.3 Practical Issues for Masticator Space Imaging

- *Changes in muscle volumes.* The four mastication muscles account for the majority of the MS volume. Many processes involving the space may have a dramatic – direct or indirect – impact on muscular trophicity, thereby affecting the total MS volume (Hardin et al. 1985):
  a) Space-occupying processes lead to MS enlargement.
  b) Infiltration along the V3 nerve may lead to MS volume shrinkage by denervation atrophy of the muscles.
  Comparison between both sides on MR images is therefore warranted regarding intrinsic signal intensity characteristics of muscles on both T2- and post-contrast T1-weighted images, and regarding muscles' volumes. Benign masseteric muscle hypertrophy is a common benign condition in which muscles are symmetrically or asymmetrically enlarged, with normal signal intensities when compared to unenlarged muscles (see also Sect. 10.4.5) (Waldhart and Lynch 1971). Denervation atrophy with increased contrast-enhancement of the masticator muscles at early phase may be seen when the V3 nerve has been infiltrated by a malignant process without true neoplastic infiltration of the muscles (Davis et al. 1995; Russo et al. 1997).
  It may be difficult to distinguish tumoral muscle infiltration from the early phase of muscle denervation related to the neoplastic invasion of the V3 nerve. Long-standing denervation leads to delayed muscle fatty atrophy which is

easily distinguishable from radiation-induced muscular fibrosis (Parsons 1994).

- *Pathways of tumor spread to the skull base.* Because of the attachment of the MS muscles to the base of the skull and the presence of the V3 nerve, infiltrative processes may readily reach and destroy the base of the skull. Careful assessment of the skull base must be regarded as a part of comprehensive radiological work-up for MS abnormalities (Harnsberger 1995).

- *Preferential spreading of MS processes to the oral cavity.* Infections or malignancies involving the MS may spread early to the oral cavity (OC) because of the close contiguity of the two areas and because of the absence of a firm fascial layer which could act as a barrier against tumor progression. Anatomical structures of the OC being adjacent to the MS are the distal portion of the parotid duct, and the buccinator muscle and space, an assessment of which must be included in the checklist of radiological MS work-up (Harnsberger 1995).

- *Clinical symptoms of MS involvement with malignancies.* Pain or numbness of the ipsilateral chin and jaw are the main 'neurologic' symptoms of infiltration of the third branch of the trigeminal nerve (V3).
  Trismus, a reactive spasm of masticator muscles resulting in mouth opening impairment, is the typical symptom for muscular involvement by malignancies or infections (Schellhas 1989; Russo et al. 1997).
  The clinical tripod of MS muscles atrophy, mandibular dental pain, and serous otitis media secondary to dysfunction of the tensor muscle of the soft palate has been regarded almost pathognomonic for malignant infiltration of the V3 nerve (Caldemeyer et al. 1998).

→ Empirical rules for radiological examination of the masticator space:
  a) Cover the *entire course of the cranial nerve V3* from the root entry zone in lateral pons to the mental foramen of the mandible, especially when symptoms suggesting involvement of the nerve are present.
  b) Cover the *full extent of all masticator muscles*, including the suprazygomatic area (temporalis muscle) since infiltrative processes rapidly involve the whole muscular corpus and dystrophic processes are often diffuse.
  c) Image *both mandible and skull base* which are osseous boundaries of the MS from/to which many processes either originate or infiltrate

10.4 Radiological Patterns of Neoplastic Masticator Space Involvement

The first step for accurately proposing diagnostic hypotheses for MS masses is to determine whether the lesion appears 'extrinsic' (originating from outside) or 'intrinsic' (originating from inside) to the MS. Four criteria can be used to assess the MS origin of a space-occupying process (Harnsberger 1995):
- The epicentre of the mass is located within the masticator muscles or the mandible.
- The mass is anterior to the fatty parapharyngeal space.
- The mass invades the parapharyngeal space from anterior to posterior.
- The fat of the parapharyngeal space is displaced posteriorly.

The displacement pattern of a mass arising from the MS is anterior to posterior with slight internal obliquity (Fig. 10.3). Posterior bowing of the anterior margin of the parapharyngeal space is often seen. The benign or malignant nature of a neoplasm often remains speculative until histopathological analysis is performed on biopsy or surgical specimens. Usually, malignancy is suspected in the presence of a heterogeneous and infiltrative process, and benignity is hypothesized in the presence of a sharply and well delineated process. But these criteria have low accuracy in MS examination since malignancies may have sharply defined margins (such as seen in many sarcomas originating either from bone or soft tissues), and benign neoplasms may have a poorly vascularized or fibrous core resulting in a heterogeneous texture of the lesion. Clinical data including the history of the growth rate of the tumor and the associated signs of pain, trismus and visible inflammatory changes, together with white blood cell count and inflammatory markers at routine blood analysis are crucial. The presence of mandibular or skull base bone destruction in a space-occupying process without inflammatory signs is strongly suggestive for malignancy. Perineural spreading is almost pathognomonic for a malignant neoplasm and is frequently associated with pain or dysaesthesias. Extrinsic/intrinsic and presumptively malignant/benign features of the le-

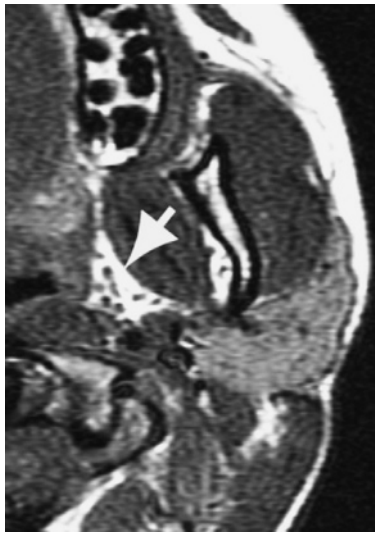

Fig. 10.3. Direction of mass effect from masticator space (MS). Transverse T1-weighted close-up on MS: the *arrow* shows the direction of the mass effect from within the MS. Impingement on the fatty parapharyngeal space with posterior bowing of its anterior margin is frequently seen

sion may result in the semiological categorization of the following five patterns of neoplasms involving the MS.

10.4.1 Extrinsic Impingement on the MS by Benign Neoplasm

A benign mass-occupying process originating from adjacent area(s) displaces the MS muscles without infiltrating them. The impingement on the MS is often asymptomatic or causes few symptoms. Complaints of mechanical impairment of mastication due to the mass effect of the lesion on muscle and/or mandibula, or both, are rarely present, as the displaced muscles are not involved by secondary inflammatory or tumoral change, and the V3 nerve is not invaded. Similarly, mandibular/dental pain is absent since the integrity of the V3 nerve is not compromised (Fig. 10.4).

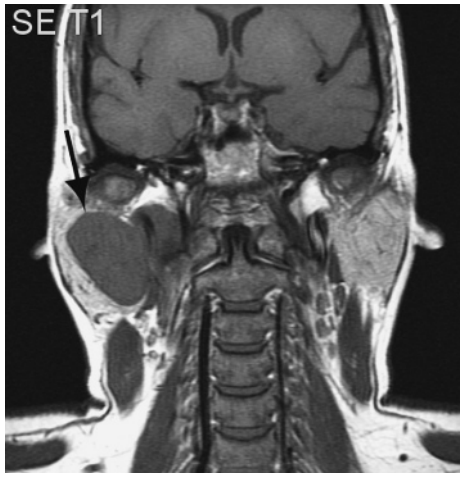

a

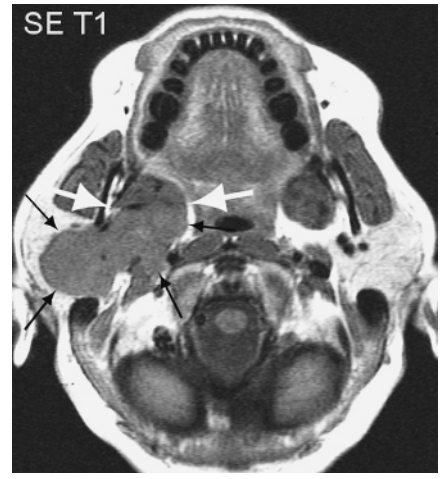

b

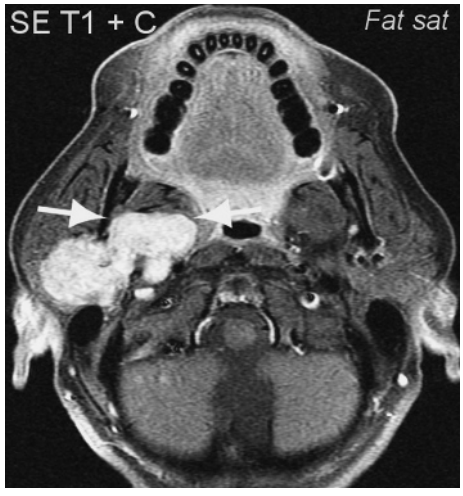

c

Fig. 10.4a–c. Pattern of extrinsic impingement on the masticator space by benign neoplasm. A 34-year-old woman with surgically-proven pleomorphic adenoma of the parotid gland. **a** Coronal unenhanced T1-weighted spin-echo (*SE*) MR image showing large, well-delineated, hypointense lesion in both the superficial and deep lobe of the right parotid gland (*arrows*). **b** Transverse unenhanced T1-weighted SE MR image showing the same lesion as a 'diabolo-like' well delineated and homogeneous mass (*thin black arrows*). The medial pterygoid muscle is pushed forward but does not show infiltration. A demarcation between tumor and muscle is present (*between thick white arrows*). Observe internal displacement of the fatty parapharyngeal space. **c** Transverse post-contrast T1-weighted SE MR image with fat saturation (*FS*) showing intense and homogeneous enhancement by abnormal tissue. Lesion is clearly delineated from surrounding structures and impinges on pterygoid muscle which does not display intrinsic changes. Clear-cut interface is more obvious than on previous illustration (*between arrows*)

10.4.2
Extrinsic Infiltration of the MS by a Malignant Neoplasm

Extrinsic malignancies arising from areas adjacent to the MS often have infiltrative potentialities which may result in functional impairment such as dental/mandibular pain due to V3 nerve invasion, and trismus due to mastication muscle invasion and V3 invasion. The invasion of bone, muscles and nerve may occur concomitantly or not.

Nasopharyngeal carcinoma is a common cause of malignant infiltration of mastication muscles (Chong 1997) (Fig. 10.5). The retromolar trigone also constitutes a common site of origin of squamous cell cancer invading the MS; mandibular bone invasion is commonly present (Rosai 1996) (Fig. 10.6).

10.4.3
Intrinsic Benign Neoplasm of the MS

Only a few benign neoplasms may arise from within the MS. The paradigmatic one is the schwannoma of the V3 nerve which mainly occurs in cases of type 2 neurofibromatosis (NFB type 2) (Smirniotopoulos and Murphy 1996; Weber et al. 2000). The VIIIth cranial nerve is the most frequently involved in this condition, but the Vth nerve is the second preferentially involved pair. Clinical background (autosomal dominant inheritance) and imaging work-up showing multiple masses arising from cranial nerves together with multiples meningiomas and ependymomas are strongly suggestive of NFB type 2, which is ten times less frequent than NFB type 1 and can be confirmed by genetic analysis

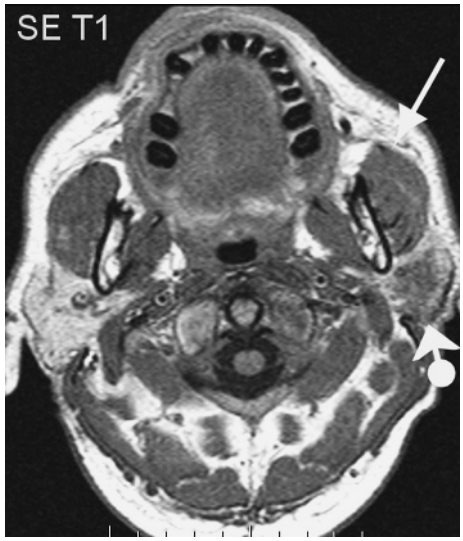

a

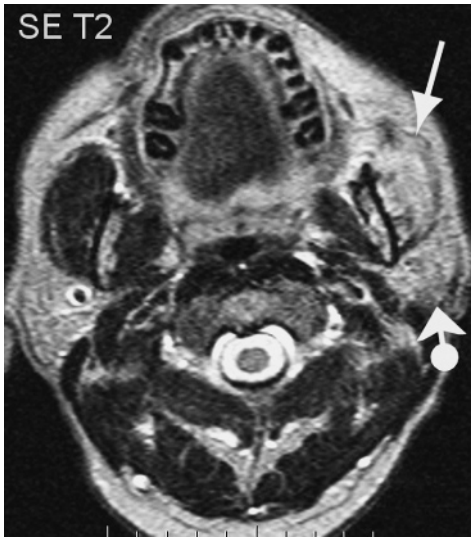

b

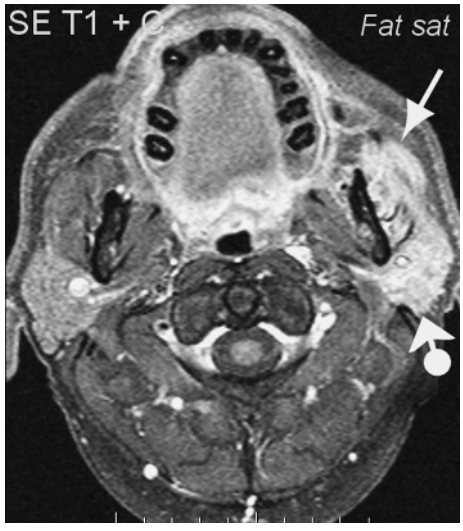

c

Fig. 10.5a–c. Pattern of masticator space muscle infiltration by extrinsic malignant neoplasm. A 58-year-old man with adenoid cystic carcinoma of the parotid gland. **a** Unenhanced transverse T1-weighted SE image showing hypointense area within the left parotid gland, resulting from fat replacement by the tumoral process (*ball-arrowhead*). Apparently normal masseter (*arrowhead*). **b** Transverse T2-weighted SE image demonstrating diffuse abnormal hyperintensity within left masseter (*arrow*), together with shrinkage and hypointense areas within left parotid (*ball-arrowhead*). **c** Transverse contrast-enhanced T1-weighted SE image with fat saturation demonstrating strong enhancement within both left parotid (*ball-arrowhead*) and masseter muscle (*arrow*). Anatomopathological examination of biopsy specimens demonstrated malignant infiltration of both the V3 nerve and the masseter muscle

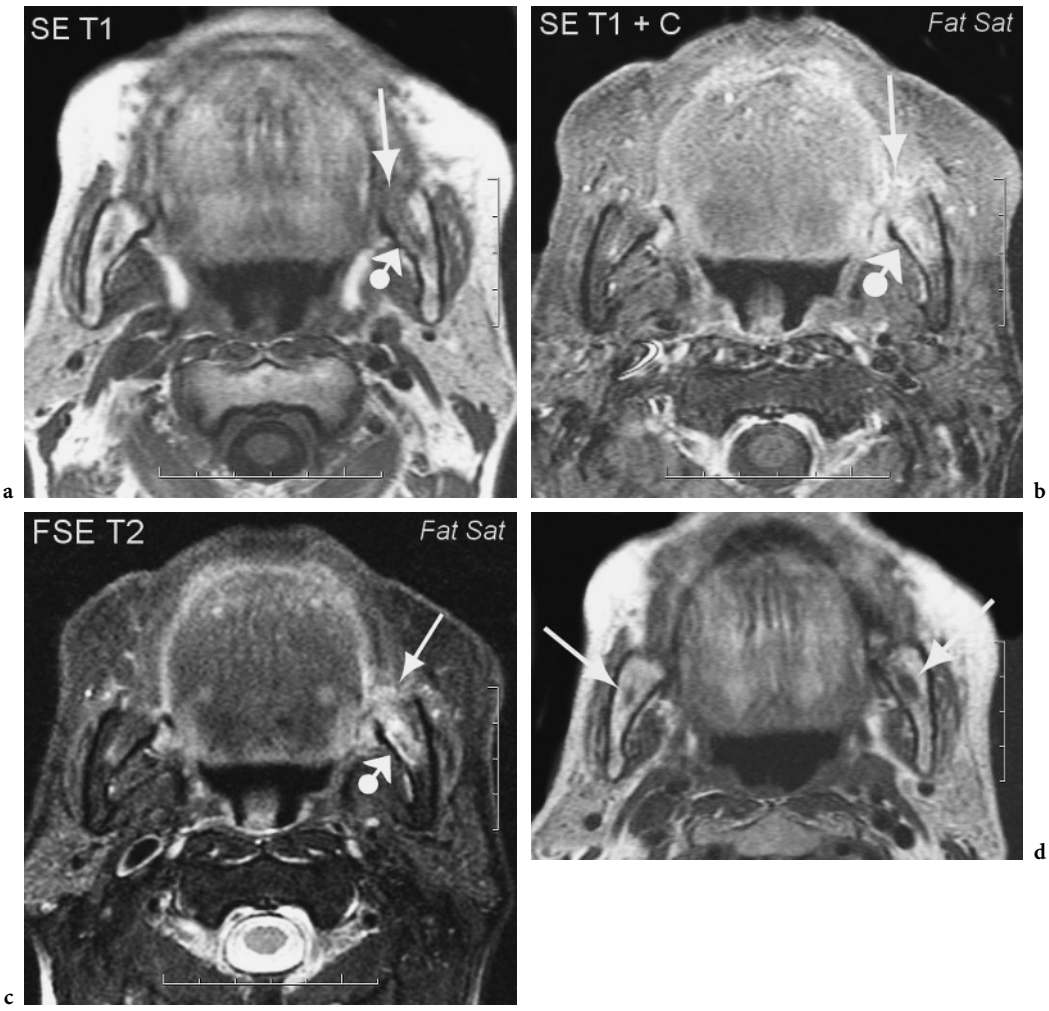

Fig. 10.6a–d. Pattern of masticator space (MS) muscle infiltration by extrinsic malignant neoplasm. A 48-year-old man with squamous cell carcinoma (*SCC*) of the retromolar trigone (*RMT*) invading MS. **a** Unenhanced transverse T1-weighted MR image showing tumoral epicentre in RMT (*arrow*) and tumoral spreading into the mandibular ramus (*ball-arrowhead*). **b** Post-contrast transverse T1-weighted MR image with fat suppression showing enhancement of both extra- (*arrow*) and intra- (*ball-arrowhead*) osseous components of the tumor. **c** Transverse T2-weighted FSE MR image with fat suppression option showing hypersignal intensity within both components of the diseased area. **d** Unenhanced transverse T1-weighted image shows enlargement of the left mandibular canal on left side, compatible with perineural tumor spread

(Kyriakos and El-Mofty 1999) (Fig. 10.7). Other benign MS neoplasms are rare; they include synovial chondromatosis and benign minor salivary gland tumors.

10.4.4 Intrinsic Malignancies of the MS

Malignancies which may arise from the MS are:

- Osteosarcoma (OS)
- Rhabdomyosarcoma (RMS)
- Malignant fibrous histiocytoma
- Non-Hodgkin's lymphoma
- Fibrosarcoma
- Hemangiosarcoma
- Malignant minor salivary gland (adenoid cystic, mucoepidermoid, adenocarcinoma, low-grade polymorphous adenocarcinoma)

OS and RMS are the most frequently observed intrinsic tumors of the MS.

Mandibular ameloblastoma and desmoid fibromatosis are usually benign conditions but may exhibit local aggressiveness in a small subset of patients (Cole and Guiss 1969; Delbaso 1998).

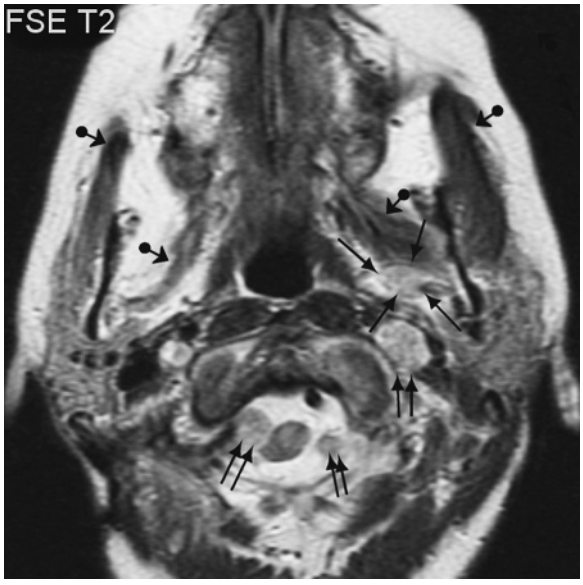

Fig. 10.7. Pattern of intrinsic benign neoplasm of the masticator space. A 26-year-old woman with genetically-proven neurofibromatosis type 2 presenting with multiple schwannomas of the endocranium, the base of the skull and the spinal canal. Transverse FSE T2-weighted image showing neurofibroma within the left masticator space (*between black arrows*). Numerous similar lesions are observed within spinal canal and left carotid space (*paired black arrows*). Observe severe atrophy of the right masseter and right lateral pterygoid when compared to the left side (*ball-arrowheads*)

Osteosarcoma (OS) of the mandible. In contrast to long bone OS, which are most commonly diagnosed during childhood, mandibular OS are found in adults and constitute the majority of head and neck OS (Marcus et al. 1994; Chong and Fan 1996). Known risk factors for developing OS are Paget's disease, fibrous dysplasia, and irradiation. CT may significantly underestimate the true extraosseous and bone marrow extension and MRI, therefore, is mandatory for a comprehensive work-up of the tumoral extension (see Sect. 10.5.1) (Fig. 10.8).

Rhabdomyosarcoma (RMS) of mastication muscles. RMS is most often seen in the paediatric age where it accounts for 50%–70% of all childhood sarcomas (Cunningham et al. 1996). Half of the patients are diagnosed before the age of 5 years. Multimodal therapeutic strategies, including surgery, chemotherapy and radiation therapy, provide the best survival rate. Prognosis has significantly improved over the past decade with a current 5-year disease-free rate of about 75%. RMS should always be considered in the presence of a primary tumor from the MS arising in childhood, showing bone destruction (Fig. 10.9).

10.4.5 Pseudo-neoplastic Benign Hypertrophy of MS Muscles

In its typical form, the muscles are symmetrically increased in size in an adolescent or young adult, without further complaints (Waldhart and Lynch 1971). Bruxism or excessive chewing tendency has been described in association with the condition. Enlarged muscles display normal tissue features on both CT and MR images, except for their increase in size. The bilateralism of the megaly is strongly suggestive for benign hypertrophy; however, hypertrophy of the masseter muscle may also occur unilaterally. Unilateral enlargement of the masseter muscle can also be due to the presence of a vascular malformation (Fig. 10.10).

10.5 Special Concerns

10.5.1 Synergy Between CT and MRI in Radiological Work-Up of MS Neoplasms

The superiority of CT in depicting subtle bone changes is evident. Since the MS contains mandibular bone, CT is useful for detecting, delineating and characterizing cortical bone involvement. But the true extent of the infiltrative process within the trabecular bone network is poorly assessed by the technique. For this purpose, MRI is clearly superior. The replacement of the normal fatty marrow (displaying bright T1 signal intensity) by the neoplastic proliferation (displaying low signal) allows precise delineation of the full extent of the tumoral process within the bone marrow space. Moreover, the exquisite soft tissue contrast obtained by MRI also enables precise and accurate delineation of the lesion into the adjacent extra-osseous soft tissues.

Isotopic bone scanning still remains a valuable additional technique by screening the whole skeleton in a one-step procedure, which is of major value in malignancies with a high tendency to spread to the bones, such as OS (Fig. 10.11). Nowadays, positron emission tomography using fluoro-deoxy-glucose as tracer (FDG-PET) is routinely performed in cases of MS malignant neoplasms because of the precise and sensitive delineation of the primary tumor and the high sensitivity for detection of distant metastatic foci and possibly a second concomitant synchronous malignant neoplasm.

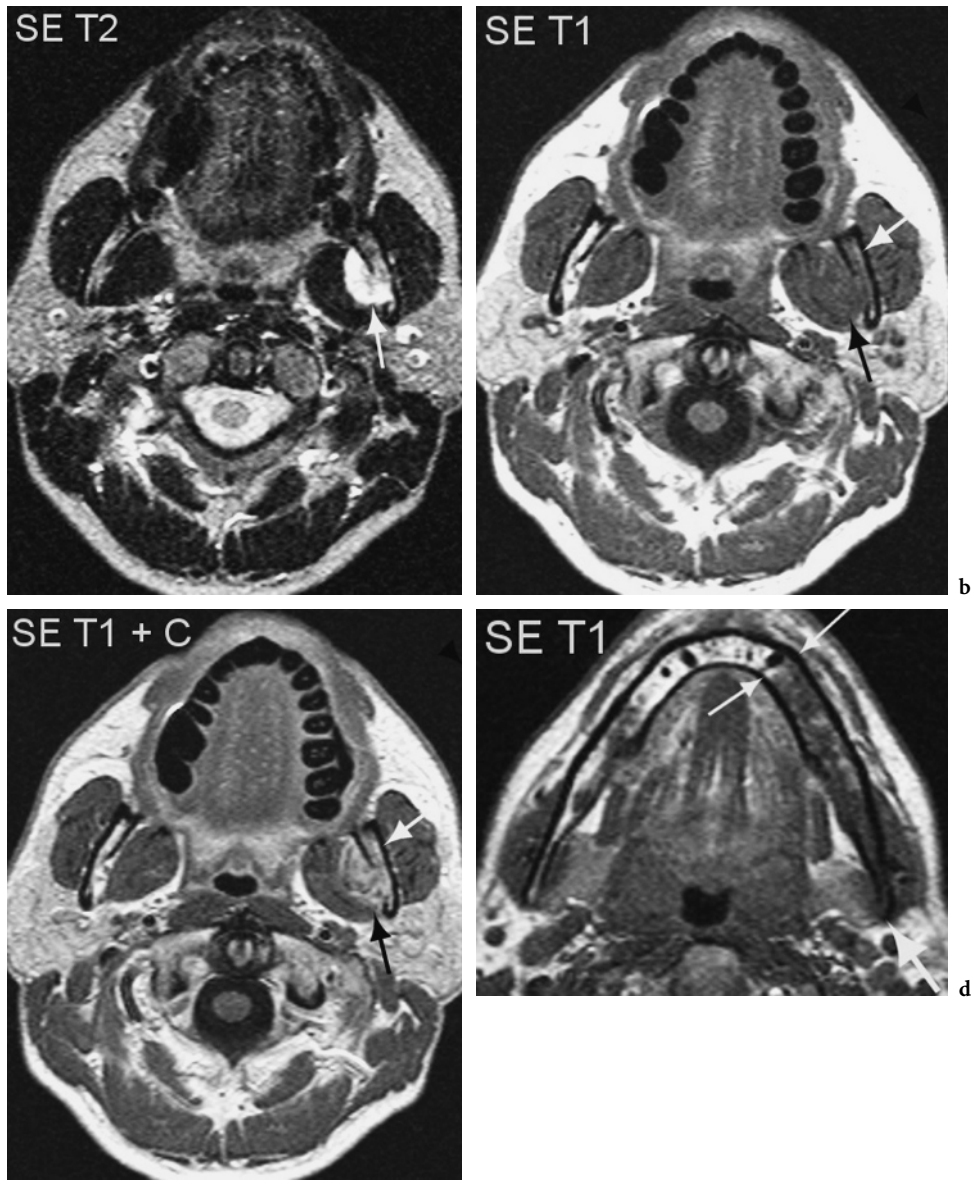

Fig. 10.8a–d. Pattern of intrinsic malignancies arising within the masticator space. A 44-year-old man presenting with isolated dysaethesias of the left V3 territory, suffering osteosarcoma. **a** Transverse T2-weighted SE image showing strongly hyperintense tumoral mass arising from the medial aspect of the ascending ramus of the mandible and impinging on the lateral pterygoid muscle (*arrow*). **b** Transverse unenhanced T1-weighted SE image showing disappearance of the normal brightness of the fatty bone marrow of the ascending ramus of the mandible (*white arrow*). Tumoral mass (*black arrow*) is isointense to muscle. **c** Transverse contrast-enhanced T1-weighted SE image in a similar plane to Fig. 10.7 showing enhancement of the tumoral mass (*black arrow*), clearly delineating enhanced tumor from adjacent pterygoid muscle. The bone marrow of the ascending ramus also enhances (*white arrow*). **d** Axial unenhanced T1-weighted SE image shows extensive infiltration of the mandibular bone marrow: the normal bright fatty marrow has been replaced by material displaying low signal intensity; the anterior border of the bone marrow infiltration is indicated by *white arrows*

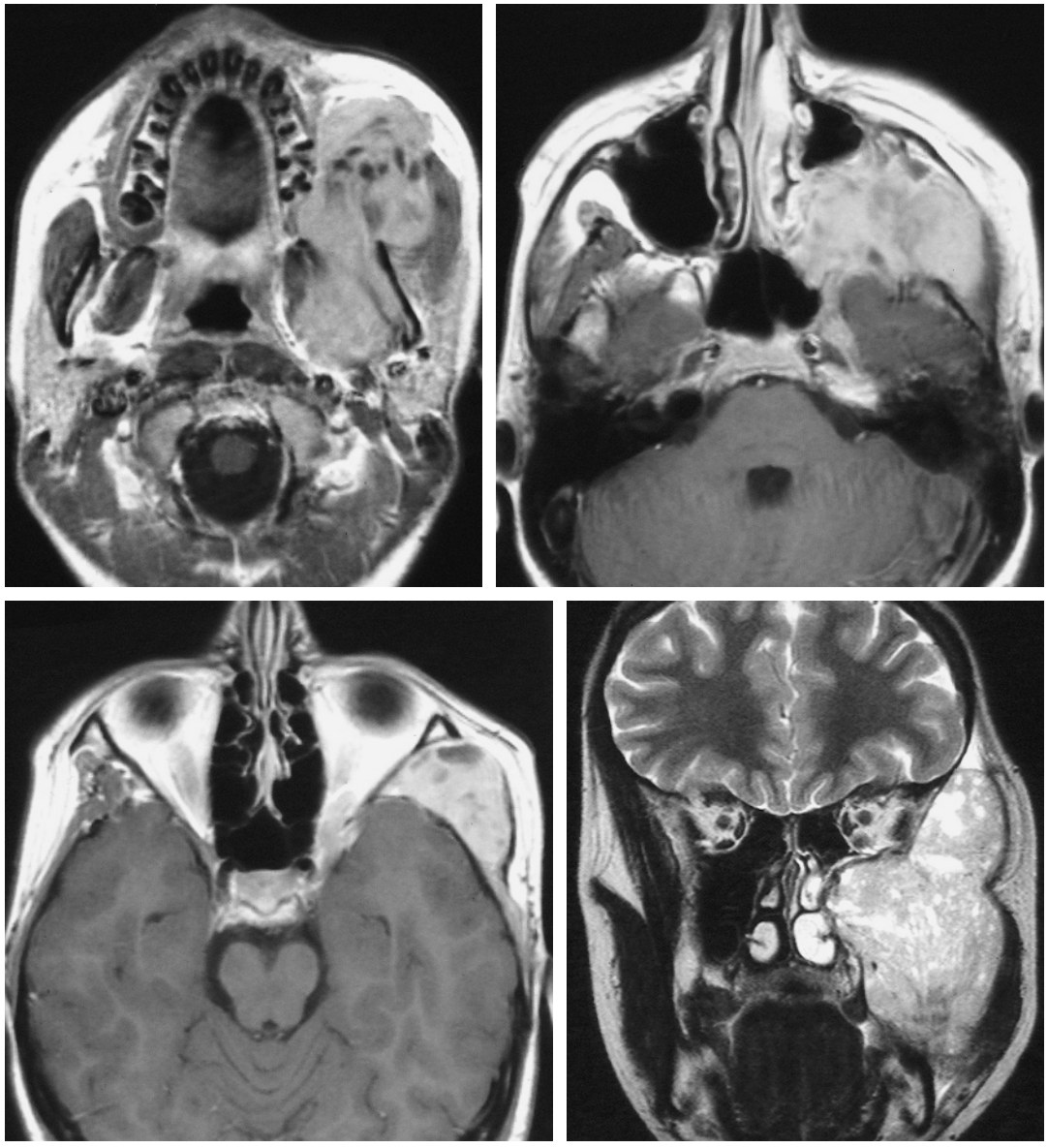

Fig. 10.9a–d. Pattern of intrinsic malignancies arising within the MS. Axial contrast-enhanced T1-weighted SE images (**a–c**), and coronal T2-weighted SE image (**d**). Rhabdomyosarcoma (courtesy of Robert Hermans, MD, PhD, Leuven, Belgium). A 20-year-old woman presenting with progressive swelling of the left cheek. A large contrast-enhanced soft tissue mass is present within the left infratemporal fossa. Lesion involves the mandibular ramus and masticatory muscles with anterior extension into the cheek. Superiorly the mass grows behind the maxillary sinus with pterygopalatine fossa involvement. Perineural tumoral spread along the V2 and V3 cranial nerve reaching the cavernous sinus can be recognized. More cranially, involvement of the superior orbital fissure and extension into the extracranial temporal fossa is seen

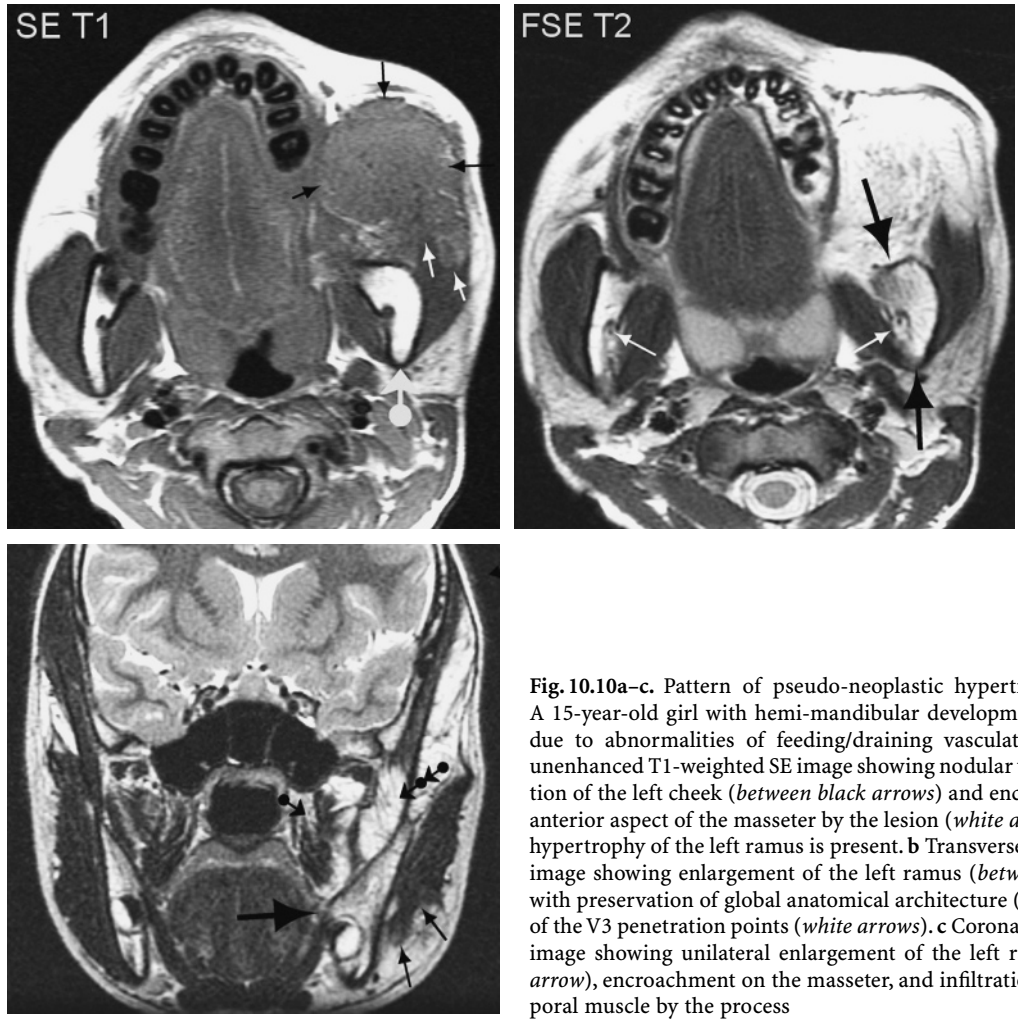

Fig. 10.10a–c. Pattern of pseudo-neoplastic hypertrophy of the MS. A 15-year-old girl with hemi-mandibular developmental hypertrophy due to abnormalities of feeding/draining vasculature. **a** Transverse unenhanced T1-weighted SE image showing nodular venous malformation of the left cheek (*between black arrows*) and encroachment on the anterior aspect of the masseter by the lesion (*white arrows*). Secondary hypertrophy of the left ramus is present. **b** Transverse T2-weighted FSE image showing enlargement of the left ramus (*between black arrows*) with preservation of global anatomical architecture (e.g. the symmetry of the V3 penetration points (*white arrows*). **c** Coronal T2-weighted FSE image showing unilateral enlargement of the left ramus (*thick black arrow*), encroachment on the masseter, and infiltration of the left temporal muscle by the process

10.5.2 Imaging of the Tumoral Spread Along the V3 Cranial Nerve

Assessment of tumoral invasion of the mandibular branch of the trigeminal nerve (V3) is crucial because all head and neck tumors with tumoral nerve involvement carry a bad prognosis, and because nerve infiltration requires appropriate local treatment (including excision of the diseased nerve if possible, and the inclusion of its entire course into radiation therapy portals). Perineural spread is most often seen in adenoid cystic and squamous cell carcinoma which are the most 'neurophilic' malignant neoplasms of the head and neck. V3 perineural infiltration symptoms and signs are usually overshadowed by the primary disease. Denervation atrophy is the common consequence of malignant nerve involvement. Atrophy of the temporalis and masseter muscles may be visible at clinical examination. Facial neuralgia may be the prominent symptom. Inclusion of the full course of the V3 nerve into the field of view of the MR examination is mandatory when imaging suprahyoid head and neck neoplasms, especially in those arising from the MS (Fig. 10.12).

10.5.3 Treatment and Post-treatment Issues

10.5.3.1 Role of Initial Imaging Findings in Optimizing Treatment Strategy

Imaging findings have a crucial impact on the therapeutic strategy by precisely defining the size of the lesion and the involvement of the adjacent non-mucosal structures such as bones, muscles, nerves and

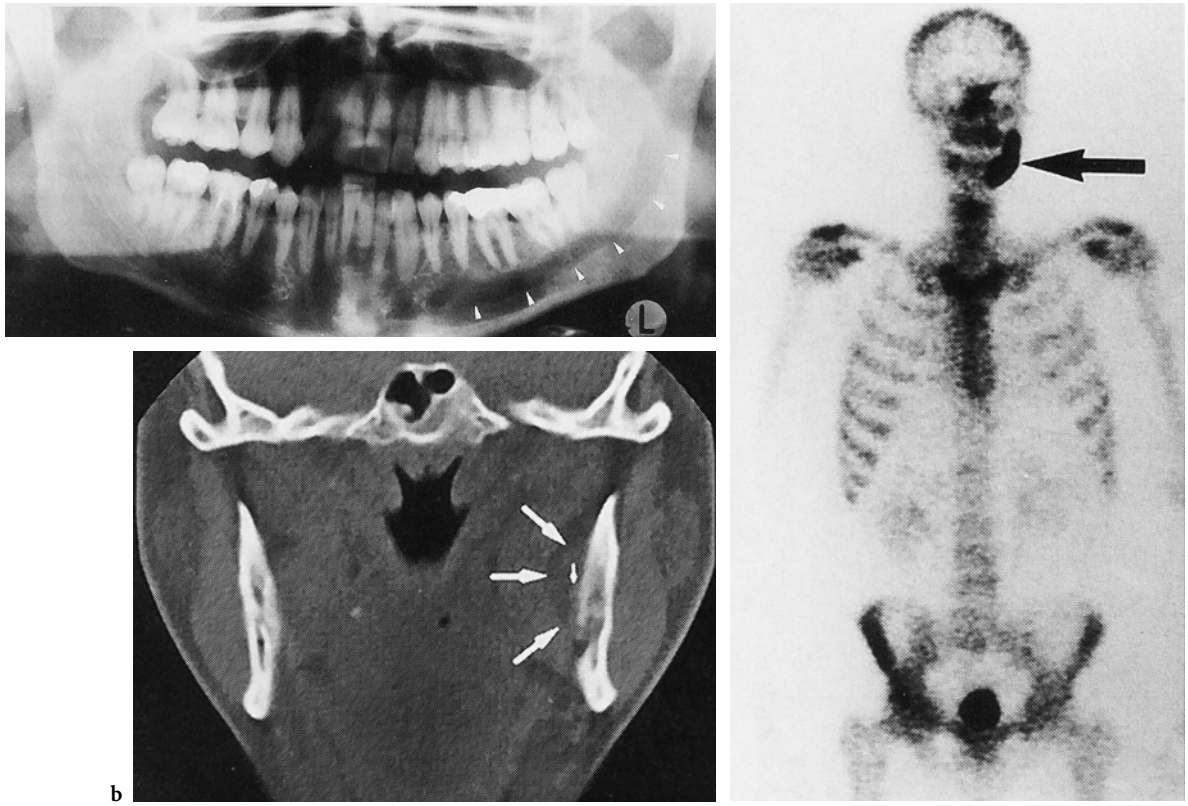

Fig. 10.11a–c. Synergy of OPG, CT scan, MRI and isotopic bone scanning in OS. Osteosarcoma of the mandible: same case as in Fig. 10.8. **a.** Panoramic radiography showed regular enlargement of the left mandibular canal (*arrowheads*) but without adjacent bone destruction. **b** CT confirmed enlargement of the mandibular canal (not shown) and the presence of soft tissue mass interposed between masseter and pterygoid muscles *(large white arrows*). Limited periosteal reaction is seen (*little white arrow*). **c** Bone scan using 99 mTc-medronate as tracer fails to reveal distant bone metastases. Tracer uptake in the primitive site is dramatically increased, showing the osteoblastic activity. [Reprinted with permission from De Batselier et al. (1997)]

skin. The histological nature of the lesion is the second major determinant for the therapeutic strategy.

Other factors determining the therapeutic options are the general and psycho-social status of the patient. Figure 10.13 summarizes the available therapeutic options in HN cancers, also applying to those of the MS. Key points are the curability and the complete surgical resectability of the neoplasm.

Basic principles of therapeutics in HN malignancies (including those of the MS) are:

- Avoidance of 'partial' surgery, except for the purpose of palliative care.
- Avoidance of systematic multiple therapies if unnecessary, e.g. if surgery alone is curative, chemotherapy and radiation therapy are 'reserved' therapeutic options for salvaging possible recurrence.
- Imaging guidance for both surgery and radiation therapy volume delineation.

Regarding MS structures:

- Tumoral spread along the V3 course requires complete excision and/or irradiation of the nerve.
- Muscle infiltration requires the resection and/or irradiation of all involved muscles.
- Mandibular invasion requires the resection of diseased bone segments.
- Skull base invasion almost precludes any surgical curative option.

10.5.3.2 Potential Roles for Imaging Monitoring During and After Treatment

Three main goals are potentially achieved by post-treatment imaging follow-up examinations: the assessment of the response to the treatment, the visualisation of treatment complications, and the early detection of tumoral recurrence. Frequency and interval of imag-

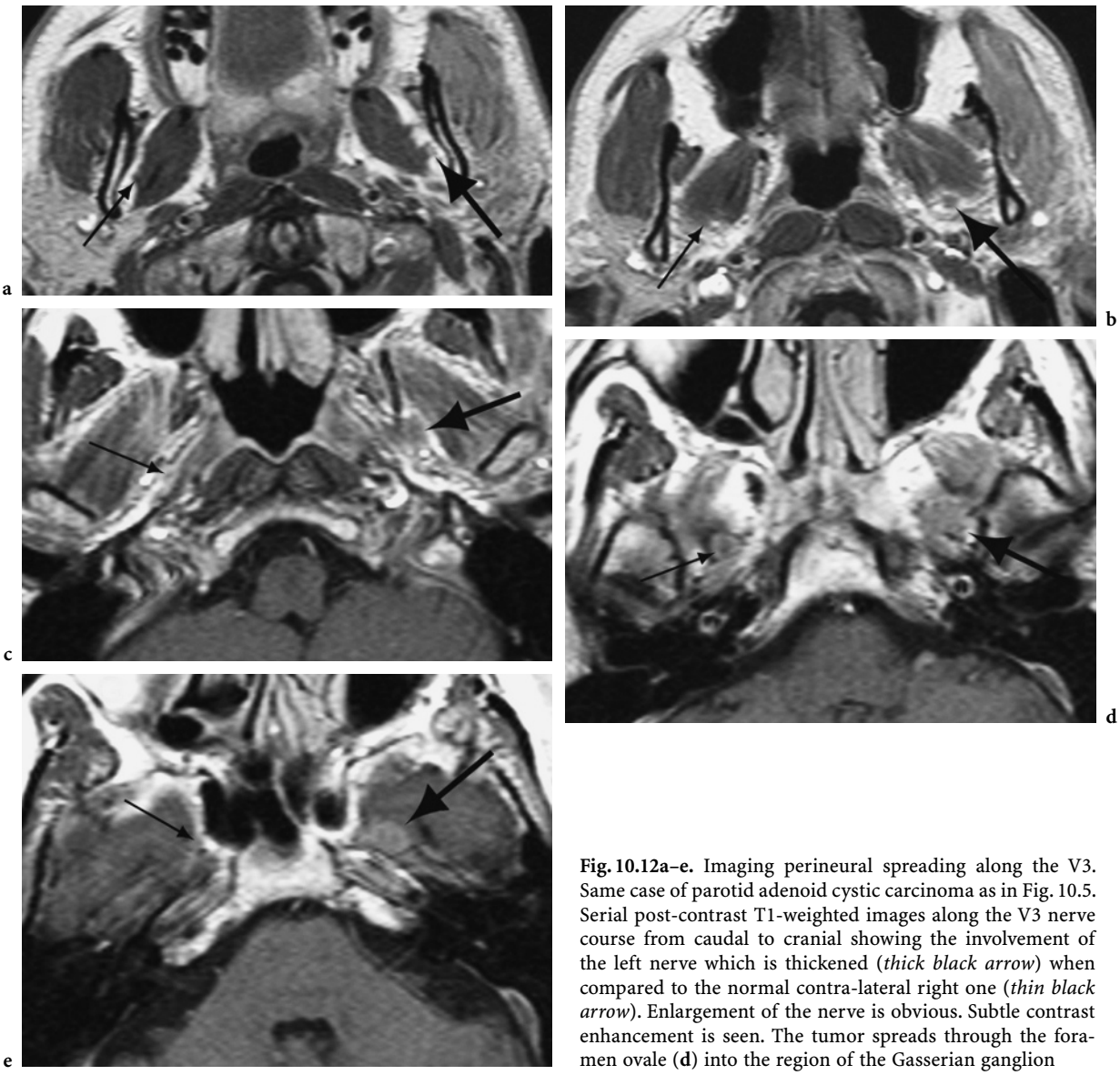

Fig. 10.12a–e. Imaging perineural spreading along the V3. Same case of parotid adenoid cystic carcinoma as in Fig. 10.5. Serial post-contrast T1-weighted images along the V3 nerve course from caudal to cranial showing the involvement of the left nerve which is thickened (*thick black arrow*) when compared to the normal contra-lateral right one (*thin black arrow*). Enlargement of the nerve is obvious. Subtle contrast enhancement is seen. The tumor spreads through the foramen ovale (**d**) into the region of the Gasserian ganglion

ing follow-up examinations are usually defined by local institutional guidelines (ours at http://www.md.ucl.ac.be/ccmf/guidelines). The response to the treatment is primarily assessed by clinical examination. In our institution, a follow-up examination is routinely performed within 1–3 months after treatment completion in patients treated by radiation therapy and/or chemotherapy. In operated cases, early imaging follow-up has lower interest and is usually not performed. Neither treatment complications nor tumoral recurrence are systematically investigated using imaging modalities in asymptomatic patients. Basic principles of post-therapeutic imaging are the clinical guidance for triggering follow-up imaging and the clinical relevance of imaging findings. Only patients in whom clinical signs like reappearance of pain, abnormal swelling, newly appeared mucosal changes, or reappearance of masticator spasm (trismus) or V3 dysaesthesias, suggest a treatment complication or tumor recurrence have follow-up imaging in an "*à la carte*" mode.

The second basic principle is to perform follow-up imaging only when imaging findings may subsequently alter the therapeutic strategy. If no more curative option exists then follow-up imaging loses clinical relevance and has only scientific relevance in the peculiar frame of prospective therapeutic trials.

Clinical triggering and relevance aside, a limitation of post-treatment imaging is that CT and/or MR images may be inconclusive because of the difficulty to distinguish post-therapeutic benign changes from

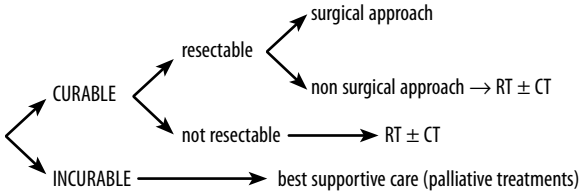

Fig. 10.13. Algorithm of therapeutic options for HN malignancies. *CT*, chemotherapy; *RT*, radiation therapy

active disease. In such cases PET or PET-CT studies may be helpful.

10.5.3.3 Imaging of Treatment Complications

Main complications of surgical treatment are functional impairment of mastication function and VIIth/Vth cranial nerve dysfunction. Reconstructive surgery efficiently corrects the unsightly effects of radical surgery on physical appearance. However, the compensation for functional impairment may be less satisfactory.

The main complications of radiation therapy include damage to normal tissues such as spinal cord or brainstem injury and optic neuritis leading to chronic neurological impairment. Xerostomia due to radiation-induced involution of major salivary glands is reduced by sparing unaffected glands in anatomical irradiation planning. Finally, mucosal and bone necrosis may occur within a variable delay after irradiation. Mandibular osteoradionecrosis (ORN) is an uncommon 'collateral' tissue damage after radiation therapy due to radiation-induced vasculitis reducing the arterial blood supply to bone which results in decreased capabilities for repairing micro-/macroscopic bone injuries. CT shows variable degrees of loss of trabeculae within spongious bone, permeative disruptions in cortical bone margins, bone fragmentation and sequestrations, and even gas within damaged bone tissues. Fracture, osteomyelitis, and fistulas are seen (Hermans 2003). Prominent but benign soft tissue swelling may mimick tumor recurrence in this condition (Chong et al. 2000).

References

Caldemeyer KS, Mathews VP, Righi PD, Smith RR (1998) Imaging features and clinical significance of perineural spread or extensions of head and neck tumors. Radiographics 18:97–110

Chong VFH (1997) The masticator space in nasopharyngeal carcinoma. Ann Oto Rhinol Laryngol 106:979–982

Chong VFH, Fan YF (1996) Radiology of the masticator space. Clin Radiol 51:457–465

Chong J, Hinckley LK, Ginsberg LE (2000) Masticator space abnormalities associated with mandibular osteoradionecrosis: MR and CT findings in five patients. AJNR Am J Neuroradiol 21:175–178

Cole NM, Guiss LW (1969) Extra-abdominal desmoid tumors. Arch Surg 98:530–533

Cunningham MJ, McGuirt WF, Meyers EN (1996) Cancer of head and neck in pediatric population. In: Myers EN, Suen JY (eds) Cancer of head and neck, 3rd edn. WB Saunders, Philadelphia, pp 598–624

Curtin HD (1987) Separation of the masticator space from the parapharyngeal space. Radiology 163:195–204

Davis SB, Mathews VP, Willians DW III (1995) Masticator muscle enhancement in subacute denervation atrophy AJNR Am J Neuroradiol 16:1292–1294

De Batselier P, Reychler H, Youssefpour A, Noël H, de Barsy C, Duprez T (1997) Ostéosarcome de la mandibule. J Radiol 78:461–463

Delbaso AM (1998) An approach to the diagnostic imaging of jaw lesions, dental implants, and temporomandibular joints. Radiol Clin North Am 36:855–890

Eskey CJ, Robson CD, Weber AL (2000) Imaging of benign and malignant soft tissue tumors of the neck. Radiol Clin North Am 38:1091–1104

Hardin CW, Harnsberger HR, Osborn AG, Doxey GP, Davis RK, Nyberg DA (1985) Infection and tumor of the masticator space: CT evaluation. Radiology 157:413–417

Harnsberger HR (1995) Handbook of head and neck imaging, 2nd edn. Mosby-Year Book, St Louis

Harnsberger HR, Osborn AG (1991) Differential diagnosis of head and neck lesions based on their space of origin: the suprahyoid part of the neck. AJR Am J Roentgenol 157:147–154

Hermans R (2003) Imaging of mandibular osteoradionecrosis. Neuroimag Clin North Am 13:597–604

Kyriakos M, El-Mofty S (1999) Pathology of selected soft tissue of head and neck. In: Thawley SE, Panje WR, Batsakis JG, Lindbergg RD (eds) Comprehensive management of head and neck tumors, 2nd edn. WB Saunders, Philadelphia, pp 1322–1394

Marcus RB, Post C, Mancuso AA (1994) Pediatric tumor of the head and neck. In: Million RR, Cassini NJ (eds) Management of head and neck cancer. Lippincott, Philadelphia, pp 811–839

Mukherji SK, Castillo M (1998) A simplified approach to the spaces of the extracranial head and neck. Radiol Clin North Am 36:761–780

Mukherji SK, Chong V (2004) Masticator space. In: Mukherji SK, Chong V (eds) Atlas of head and neck imaging. The extracranial head and neck, 1st edn. Thieme, New York, pp 3–67

Parsons T (1994) The effect of radiation on normal tissues of the head and neck. In: Million RR, Cassini NJ (eds) Management of head and neck cancer. Lippincott, Philadelphia, pp 245–289

Rosai J (1996) Oral cavity and oropharynx. In: Rosai J (ed) Ackerman's surgical pathology, 8th edn. Mosby, St. Louis, pp 223–255

Russo CP, Smoker WRK, Weismann JL (1997) MR appearance of trigeminal and hypoglossal motor denervation. AJNR Am J Neuroradiol 18:1375–1383

Schellhas KP (1989) MR imaging of muscles of mastication. AJR Am J Roentgenol 153:847–55

Smirniotopoulos JG, Murphy FM (1996) Central nervous system manifestations of the phakomatoses and other inherited syndrome. In: Atlas SW (ed) Magnetic resonance imaging of the brain and of the spine, 2nd edn. Raven Press, Philadelphia, pp 773–802

Waldhart E, Lynch JB (1971) Benign hypertrophy of the masseter muscles and mandibular angles. Arch Surg 102:115–118

Weber AL, Montandon C, Robson CD (2000) Neurogenic tumors of the neck. Radiol Clin North Am 38:1077-1090

11 Neoplasms of the Sinonasal Cavities

Robert Hermans

CONTENTS

11.1 Introduction

Many different types of malignant tumors arise within the sinonasal cavities. These tumors constitute less than 1% of all malignant neoplasms. The incidence of these tumors shows geographical differences, being clearly higher in parts of Africa and Japan than in the US. Sinonasal carcinoma is a disease mainly occurring in the age range of 50–70 years, although some tumor types (such as lymphoma, minor salivary gland tumors or esthesioneuroblastoma) also occur in younger patients.

The risk for developing certain types of sinonasal carcinoma is associated with exposure to certain exogenous factors: woodworkers have a much higher risk for developing an adenocarcinoma; exposure to nickel correlates with a higher risk for squamous cell carcinoma.

Tumors arising in the paranasal sinuses have abundant place to grow without causing many symptoms. The symptoms themselves are usually aspecific; sometimes associated inflammatory disease overshadows the tumor. For these reasons, sinonasal neoplasms are usually diagnosed in an advanced stage, except for occasional nasal cavity lesions presenting early because of nasal obstruction (Parsons et al. 1994). Deformation of or extension into the hard palate or maxillary alveolar process may cause pain or mal fitting of a denture. Extension through the ventral maxillary wall causes swelling of the face; trismus may develop with extension through the posterior maxillary wall and infiltration of the masticatory muscles. Orbital symptoms occur by interference with the lacrimal apparatus or neoplastic infiltration of the orbit. Different neurologic symptoms, mainly pain and cranial nerve paralysis, may be encountered when the skull base is invaded; especially the pterygopalatine fossa and neighbouring fissures and foramina, as well the floor of the anterior cranial fossa are at risk for tumor invasion.

The nasal vestibule is covered with skin, and malignant tumors arising at this site are often squamous cell carcinomas, with a natural history resembling skin cancer. Early lesions present as a small ill-healing ulcer or crust. Tumors at this site may already show a more extensive spread as thought after initial clinical evaluation; they grow toward the upper lip and nasal septum, and in a later stage also towards the maxilla, nasal and oral cavity.

R. Hermans, MD, PhD
Professor, Department of Radiology, University Hospitals Leuven, Herestraat 49, 3000 Leuven, Belgium

11.2 Normal Radiological Anatomy

Anatomical structures, relevant to the radiological description of sinonasal tumor extent, are shown in Figs. 11.1 and 11.2.

11.3 Indications for Imaging Studies

Imaging is necessary for evaluating paranasal extension and possible intracranial spread, orbital involvement, infratemporal extension, spread to the nasopharynx, oropharynx or oral cavity and spread along neurovascular bundles (Table 11.1).

The neck and facial lymph nodes (Tart et al. 1993) are not routinely studied in cases of sinonasal cancer. When there is extension into the skin, oral cavity or pharynx, or when a recurrent tumor is present, the facial lymph nodes and the upper neck nodes are at risk, and should be included in the imaging study. The presence of metastatic lymph nodes is a sign of poor prognosis.

Often CT will adequately show the tumor extension. Involvement of the delicate bony structures in this region is better seen with CT than with MRI. CT

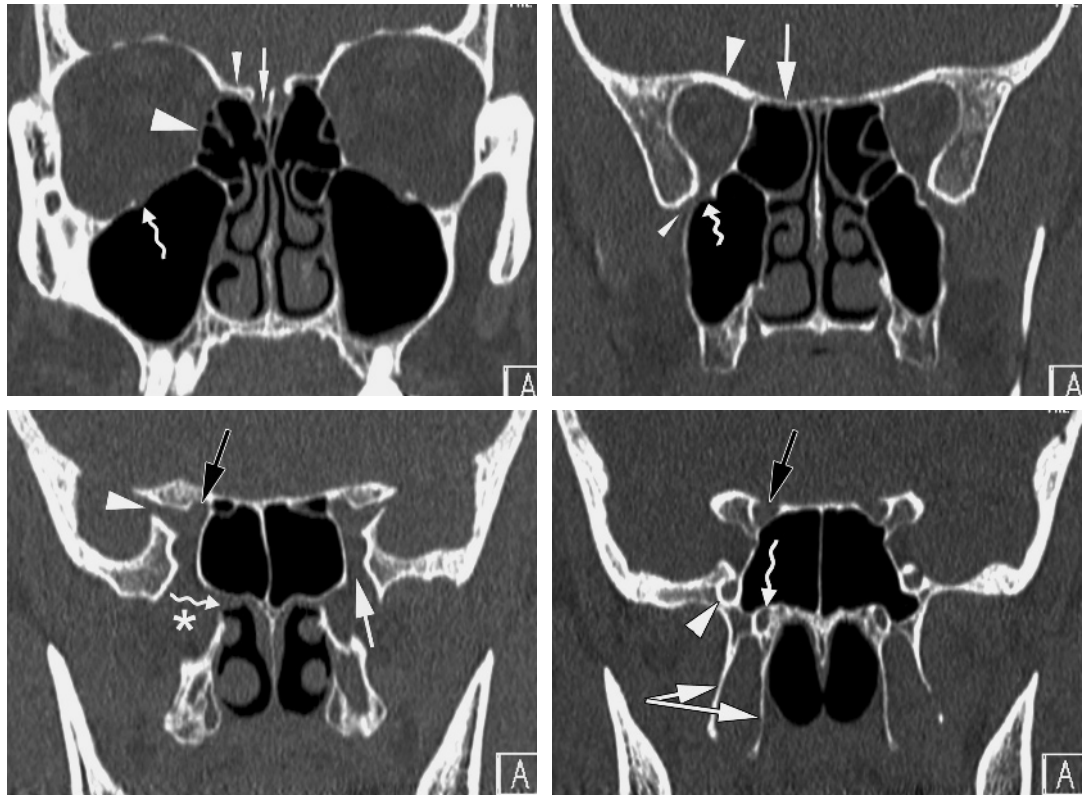

Fig. 11.1a–d. Coronal 1-mm thick CT images. **a** The roof of the nasal cavity is called the lamina cribrosa (*arrow*), and that of the ethmoidal cells is the fovea ethmoidalis (*thin arrowhead*). The orbit is separated from the ethmoidal cells by the thin lamina papyracea (*thick arrowhead*). The infraorbital canal can be seen within the floor of the orbit, containing the infraorbital nerve (*curved arrow*). **b** Section through the apex of the orbitae, covered by the ala minor of the sphenoid (*thick arrowhead*); both alae minores are connected by the planum sphenoidale (*arrow*), forming the roof of the sphenoid sinuses. The opening between the ala major of the sphenoid and the maxilla corresponds to the inferior orbital fissure (*thin arrowhead*). The infraorbital canal is seen in its most proximal part (*curved arrow*). **c** Section posterior to the maxilla and through the apex of the orbitae. The inferior orbital fissure (*white arrow*) is connecting the pterygopalatine fossa (*asterisk*) to the orbital apex. The pterygopalatine fossa communicates at this level with the nasal cavity through the sphenopalatine foramen (*curved arrow*). The superior orbital fissure (*arrowhead*) is located between the ala minor and ala major of the sphenoid. Entrance to the optic canal (*black arrow*). **d** Section through the pterygoid processes (medial and lateral plate, *white arrows*), somewhat posterior to (**c**)**.** The optic canal (*black arrow*) runs through the base of the ala minor. The foramen rotundum (*arrowhead*) is running through the junction of the ala major and the body of the sphenoid bone. Entrance to pterygoid (*vidian*) canal (*curved arrow*)

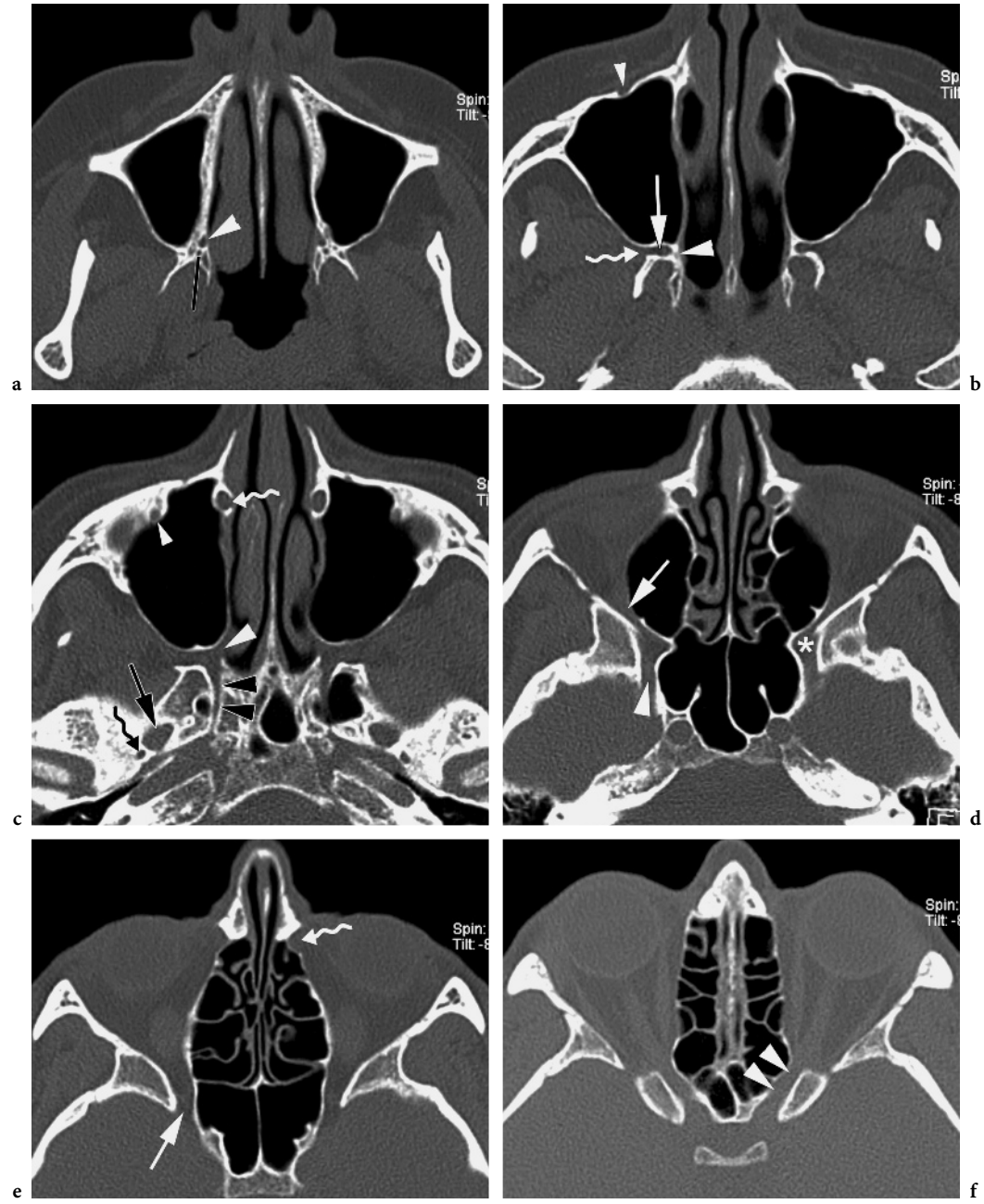

Fig. 11.2a–f. Axial 1-mm thick CT images. **a** Section at the junction of the pterygoid process and maxillary tuber. Greater palatine canal (*arrowhead*) and lesser palatine canal (*black line*), connecting the oral cavity to the pterygopalatine fossa, are indicated. **b** Section, cranial to (**a**), at the level of the pterygopalatine fossa (*arrow*). Medially, this fossa is closed by the perpendicular plate of the palatine bone (*large arrowhead*). Anteriorly, it is bordered by the posterior wall of the maxillary sinus and posteriorly by the pterygoid process of the sphenoid bone. Laterally, it communicates with the infratemporal fossa through the pterygomaxillary fissure (*curved arrow*). Entrance to infraorbital canal (*small arrowhead*). **c** Section cranial to (**b**). Near its junction with the sphenoid bone, the perpendicular plate of the palatine bone shows a notch; this forms the sphenopalatine foramen, allowing communication between the pterygopalatine fossa and nasal cavity (*large white arrowhead*). Posterior to the pterygopalatine fossa, the pterygoid (Vidian) canal is seen (*black arrowheads*). Infraorbital canal (*small white arrowhead*). Nasolacrimal duct (*white curved arrow*). Foramen ovale (*black arrow*). Foramen spinosum (*black curved arrow*). **d** Section cranial to (**c**). The pterygopalatine fossa (*asterisk*) is seen to communicate with the orbit through the inferior orbital fissure (*arrow*) and with the middle cranial fossa through the foramen rotundum (*arrowhead*). **e** Section through the orbits, cranial to (**d**). The superior orbital fissure (*arrow*) allows communication between the orbital content and the cavernous sinus. Entrance to nasolacrimal duct (*curved arrow*). **f** Section through the orbits, slightly cranial to (**e**). The optic nerve runs through the optic canal (*arrowheads*) in the base of the ala minor

Table 11.1. Issues to be addressed during imaging of nasosinusal cancer. CT and MRI are often complementary methods in the evaluation of sinonasal cancer; imaging method best suited for a particular issue is between parentheses

Tumor Mass
Tissue characteristics, such as vascularity (MR)
Presence of intratumoral calcifications (CT)
Subtle bone expansion or erosion at tumor border (CT)
Differentiation from surrounding inflammation (MR)
Tumor Extension in neighboring structures
Skull base (CT/MRI)
Intracranial compartment (MRI)
Orbit (MRI)
Perineural spread (MRI)
Neck (when extension into skin, oral cavity or pharynx, or in case of recurrent tumor)
Lymph nodes (CT)

demonstrates the presence of intratumoral calcifications, which is helpful in the differential diagnosis. MRI is indicated as complementary study when the tumor is growing closely to the intracranial compartment (usually at the roof of the nose and ethmoidal sinuses, sometimes along the posterior wall of the frontal sinus or posterolateral walls of the sphenoid sinus), to evaluate possible dural involvement or transdural extension. MRI is also best to evaluate subtle orbital involvement. The precise borders of a cancer growing into the extrasinusal soft tissues can be more precisely determined with MRI. Subtle perineural spread may also be detected more easily with MRI. A major advantage of MRI over CT is the better differentiation of tumor tissue from accompanying inflammatory changes in the paranasal sinuses (Som et al. 1988).

In patients who had only a limited CT study of the paranasal sinuses (usually unenhanced coronal sections), because the symptoms of the patient were initially attributed to inflammatory disease, a complementary MRI study is indicated to evaluate more comprehensively the tumor extent.

11.4 Imaging Appearance and Extension Patterns of Sinonasal Neoplasms

11.4.1 Appearance of the Tumor Mass on CT and MRI

Most lesions appear as a solid, moderately enhancing mass lesion on CT studies. Local bone destruction is characteristic of malignant tumors, as opposed to the expansion of the sinus cavity seen with benign tumors and mucocoeles (Lloyd 1988).

Such imaging findings are highly suggestive for a malignant tumor, but no specific histological diagnosis can be made based on these findings. Punctate intralesional calcifications are occasionally seen in squamous cell carcinoma (Lloyd 1988); intratumoral calcifications may be seen in some other epithelial tumors, such as inverted papilloma or adenocarcinoma; calcifications may also be present in esthesioneuroblastoma, a tumor from neurogenic origin (see below). A calcified or ossified matrix is often present in the rare chondro- and osteosarcomas, but these lesions rather affect the bone structures and invade secondarily the nose and/or sinuses (see below).

On MRI sinonasal neoplasms usually show an intermediate signal intensity, both on T2- and T1-weighted sequences. The intermediate T2 signal intensity allows separation of the tumor mass from high intensity inflammatory changes (Fig. 11.3). Only some sinonasal tumors show a high T2 signal intensity: this is mainly seen with tumors from salivary gland origin or neuromas, and in these cases differentiation from surrounding inflammatory changes may be more difficult on T2-weighted images (Som et al. 1988). Also some carcinomas may show hyperintense areas on T2-weighed images, presumably due to necrosis (Fig. 11.4). In such cases the gadolinium-enhanced T1-weighted images will help to differentiate the enhancing mass lesion from non-enhanced edema or fluid within the sinonasal cavities.

Tissue characterisation is not possible using MRI: the observed signal intensities in different tumors show substantial overlap (Yousem et al. 1992). Sinonasal melanoma may show spontaneous hyperintensity on T1-weighted images and low signal intensity on T2-weighted images, attributed to the presence of melanin, which is a paramagnetic substance (Loevner and Sonners 2002). However, not all melanomas contain melanin.

11.4.2 Extension Towards Neighbouring Structures

11.4.2.1 Anterior Cranial Fossa

When the tumor extends to the nasoethmoidal roof, intracranial spread through the floor of the anterior cranial fossa may occur. Coronal and sagittal sections are best suited for demonstration of such spread.

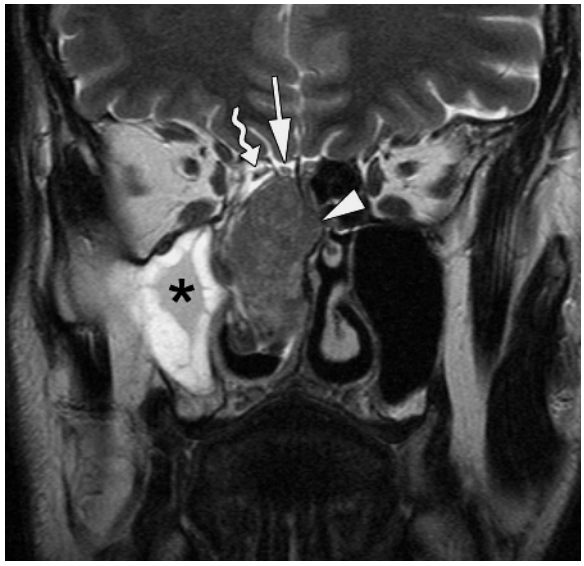

The first sign of anterior cranial fossa involvement is erosion of the delicate bone interface between the sinonasal cavity and the anterior cranial fossa; such early bone invasion is best detected on coronal CT images.

Tumor spread beyond the bony nasoethmoidal roof is best seen using MRI. Linear dural enhancement as seen on coronal or sagittal T1-weighted images is not specific for dural invasion; it often represents reactive (inflammatory) changes. Dural enhancement with focal nodularity, dural thickening of more than 5 mm, and pial enhancement are highly suggestive for neoplastic dural invasion (Eisen et al. 1996) (Fig. 11.5).

Brain invasion is seen as enhancement of the brain parenchyma; this is better visualized on MR studies than on CT studies, as is the often associated localized brain edema surrounding the area of brain parenchyma invasion (Kraus et al. 1992) (Fig. 11.6).

11.4.2.2 Orbit

Involvement of the orbit usually occurs through the medial or inferior wall; coronal sections are therefore best suited to detect such spread. Just as with the floor of the anterior cranial fossa, the earliest sign of orbital involvement is erosion of the delicate bony orbital borders (lamina papyracea and/or floor of the orbit). With further tumor growth, the extraconal fat will get displaced without direct invasion. This occurs because the strong periorbita (the orbital 'periost') acts as a barrier to tumor spread, walling off the tumor from the orbital fat (Fig. 11.4).

CT can quite accurately show erosion of the bony orbital walls, a condition which occurs frequently in

Fig. 11.3a–c. Coronal T2-weighted spin echo image (**a**), plain (**b**) and gadolinium-enhanced (**c**) T1-weighed spin echo images. Soft tissue mass in the right nasal cavity, adherent to the nasal septum, focally growing through this structure (*arrowhead*). The lesion reaches the lamina cribrosa, but the anterior cranial fossa structures (including the olfactory bulb) appear normal (*arrow*). Retro-obstructive inflammatory changes are seen in the ipsilateral maxillary sinus; compared to the peripheral part, the central part of the maxillary sinus shows lower intensity on the T2-weighted image and higher intensity on the plain T1-weighted image due to thickening of intraluminal secretions. Also in the posterior ethmoid cells (*curved arrow*) inflammatory changes are seen, separating the tumor from the lamina papyracea. The tumor mass shows moderate enhancement. In the anterior cranial fossa, no dural enhancement is seen. The tumor was successfully removed by endoscopic surgery; postoperative radiotherapy was administered. The lesion corresponded to an intestinal-type adenocarcinoma

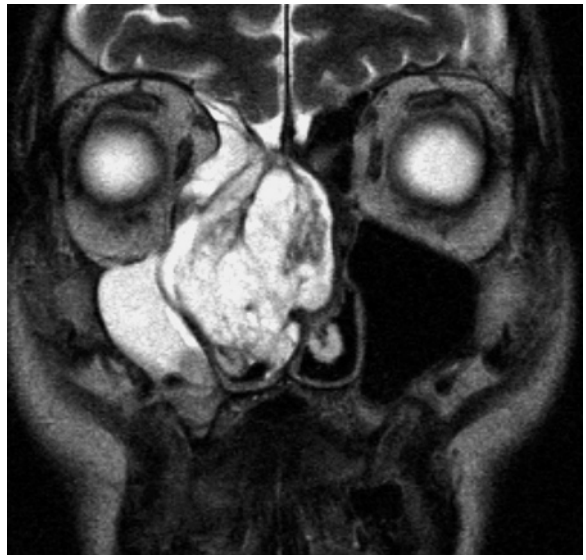

a

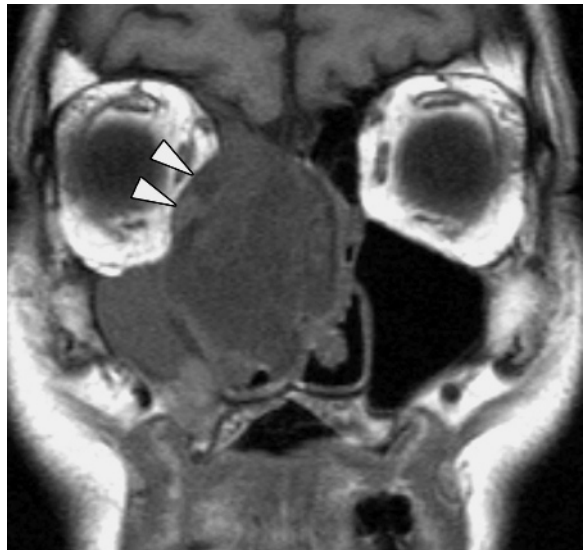

b

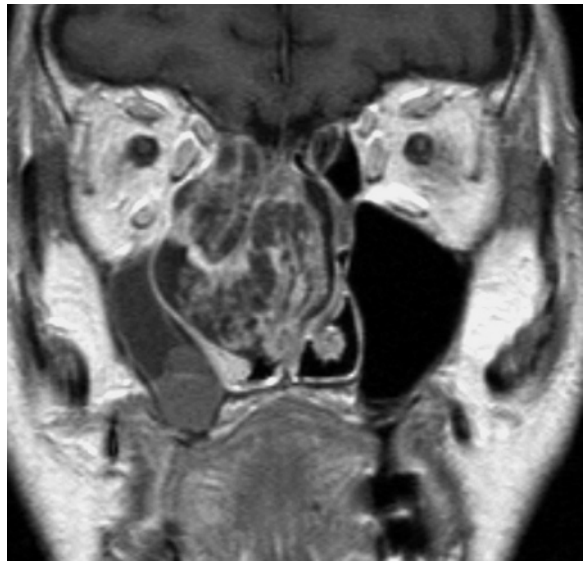

c

ethmoidal cancer. However, erosion of the lamina papyracea is not a crucial finding, as this bone is partially or completely resected at surgery (Maroldi et al. 1997). More important is the assessment of the periorbita, as the degree of involvement of this structure determines largely the surgical management of the orbital structures.

At present, there are no absolutely reliable imaging findings for invasion of the periorbita. Both on CT and MRI, displacement of the periorbita can not be distinguished from neoplastic invasion of the periorbita (Graamans and Slootweg 1989). A nodular interface with the orbit is a slightly more specific, but less sensitive sign of orbital invasion (Eisen et al. 2000).

When the tumor has crossed the periorbit, direct tumoral invasion of the different intra-orbital structures becomes possible. Enlargement, abnormal signal and/or enhancement of the extra-ocular muscles, when present, are very specific signs of orbital invasion (Fig. 11.7). Also infiltration of the orbital fat is a sign with high specificity for orbital invasion (Eisen et al. 2000).

Tumor extension may occur by invasion and tracking of the nasolacrimal canal. Invasion of the nasolacrimal duct and sac can be diagnosed by CT or MRI with high accuracy (Eisen et al. 2000).

11.4.2.3 Infratemporal Fossa and Middle Cranial Fossa

Extension towards the infratemporal fossa occurs through the posterolateral wall of the maxillary sinus, and is therefore best detected on axial slices. The earliest sign is cortical erosion of the maxillary wall, best seen on CT images (Fig. 11.8). After infiltration of the retromaxillary fat, the tumor will reach the masticatory muscles, causing mass effect and eventually infiltration of these structures.

Fig. 11.4a–c. Coronal T2-weighted spin echo image (**a**), coronal plain (**b**) and gadolinium-enhanced (**c**) T1-weighted spin echo images. Large nasoethmoidal soft tissue mass on the right side, displacing (possibly invading) the nasal septum. The lesion largely appears very intense on the T2-weighted image, isointense to the retro-obstructive inflammation in the right maxillary sinus. Better differentiation between the tumor mass and retro-obstructive secretions is possible by integrating the information from the T1-weighted images. Slight lateral displacement of the medial orbital wall is seen, without infiltration of the orbital fat. During surgery, the lesion was contained by the (non-involved) periorbita. Pathologic examination revealed an intestinal-type adenocarcinoma, showing a very myxoid stroma

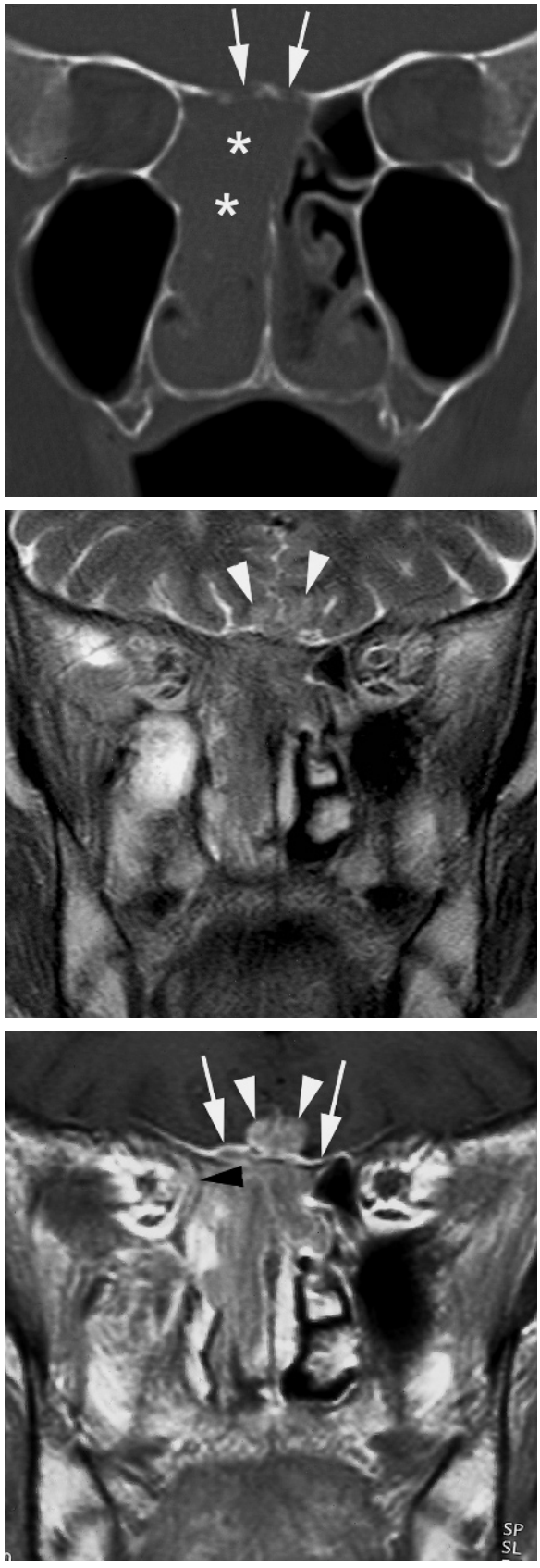

The pterygopalatine fossa may become involved by tumor growth through the posterior wall of the maxillary sinus, or via perineural tumor spread.

Perineural tumor spread usually occurs along the nerve sheath, not within the nerve itself. Such perineural spread may be discontinuous, with skip areas. Although adenoid cystic carcinoma is notorious for its tendency towards perineural spread, such extension pattern is also seen in other tumor types, such as squamous cell carcinoma. Perineural tumor spread occurs more frequently in case of tumor recurrence. Perineural tumor spread is associated with a decreased survival rate. Symptoms include pain, paresthesias and muscle weakness and atrophy, but about 40% of patients do not show particular symptoms. Imaging diagnosis is important to avoid tumor 'recurrence' from unrecognized perineural spread; however, microscopic perineural tumor spread cannot be recognized by CT and MRI (Nemzek et al. 1998).

Imaging findings in perineural tumor spread include (Fig. 11.9):

- Thickening and/or enhancement of one or more nerve branches
- (Often small) tumoral lesions at some distance from the primary site, in a neural 'crossroad' such as the pterygopalatine fossa or Meckel's cave
- Widening, destruction or enhancement of a skull base neural foramen or canal (e.g. foramen ovale, vidian canal)
- Denervation atrophy of muscles supplied by the affected nerve

Fig. 11.5a–c. a Coronal unenhanced CT image (bone window) in a patient complaining of frontal headache and a single episode of epistaxis. A large right-sided nasoethmoidal mass (*asterisks*) is seen, growing through the superior part of the nasal septum and destroying the bony ethmoidal walls and middle turbinate. Erosions in the roof of the nasal cavity and ethmoidal cells are noted (*arrowheads*). Biopsy revealed squamous cell carcinoma. **b** Coronal T2-weighted spin echo image. The tumor mass appears with intermediate signal intensity, and is clearly growing through the nasal septum. Subtle brain hyperintensity is seen in the anterior cranial fossa (*arrowheads*). At this moment, the patient has retro-obstructive inflammation in the right maxillary sinus. **c** Coronal gadolinium-enhanced T1-weighted spin echo image. The enhancing tumor mass is seen to extend into the anterior cranial fossa (*white arrowheads*), and can not be delineated from the overlying brain parenchyma. Neighbouring enhancing dural thickening (*arrows*), probably due to reactive inflammation; some extradural tumor extension is suspected at the right side. Note the subtle enhancement against the orbital side of the lamina papyracea (*black arrowhead*), representing early orbital invasion. The brain invasion, the reactive dural changes and the intraorbital extension were pathologically proven in this patient

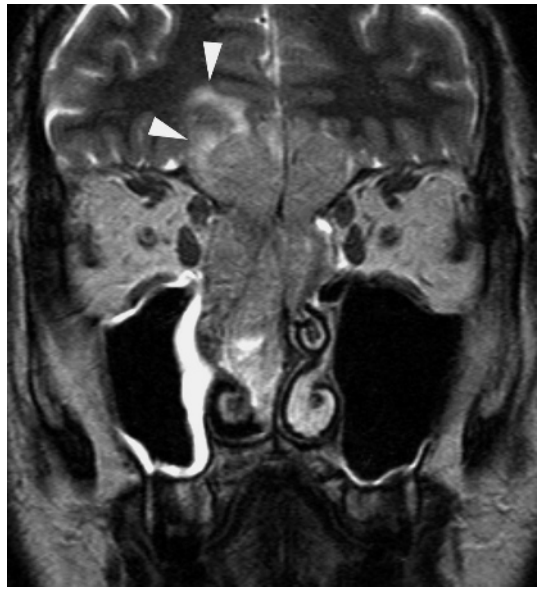

a

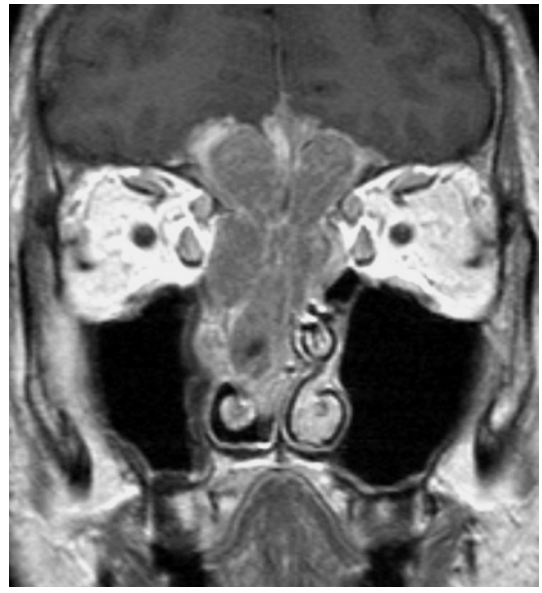

b

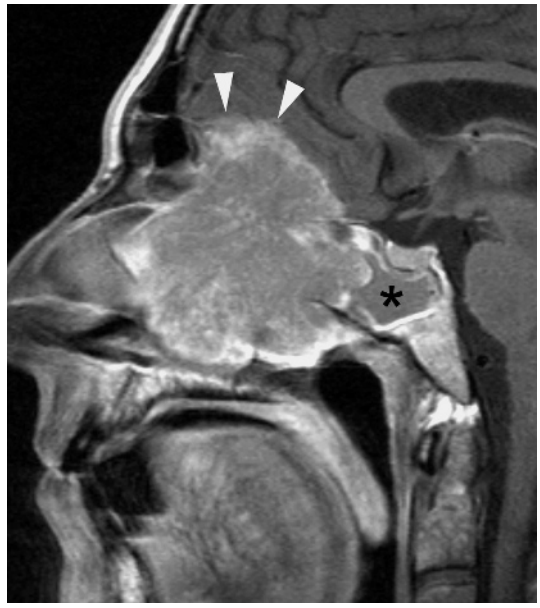

c

Fig. 11.6a–c. a Coronal T2-weighted spin echo image. Large, bilateral nasoethmoidal soft tissue mass, involving the anterior cranial fossa. The lesion can not be clearly delineated from the brain parenchyma. Perilesional edema (*arrowheads*) is seen in the right frontal lobe. No orbital involvement. **b** Coronal gadolinium-enhanced T1-weighted spin echo image. Moderate enhancement of the mass lesion is seen. **c** Sagittal gadolinium-enhanced T1-weighted spin echo image. Poor delineation between the intracranial tumor component and the surrounding brain tissue (*arrowhead*). Posteriorly, the lesion invades the anterior portion of the sphenoid sinus; retroobstructive inflammation (*asterisk*). Biopsy revealed undifferentiated carcinoma. The lesion was considered to be inoperable due to the extensive intracranial involvement. The mass completely disappeared during radiation therapy. At present, the patient is followed-up for 3 years, without evidence of tumor recurrence

Several neural pathways exist towards the pterygopalatine fossa, such as the infraorbital nerve, the posterior superior alveolar neurovascular bundle in the posterolateral wall of the maxillary sinus, and the neurovascular bundle in the greater and lesser palatine foramina (Ginsberg and DeMonte 1998; Mancuso et al. 1988).

From the pterygopalatine fossa, the tumor may grow superiorly into the inferior orbital fissure and infiltrate the orbital apex. Further superior extension will lead to infiltration of the superior orbital fissure, from where the tumor has easy access to the cavernous sinus. The tumor may grow posteriorly along the maxillary nerve in the foramen rotundum, eventually also leading to the cavernous sinus.

11.5 Tumor Types

The focus of this section is on malignant neoplasms of the sinonasal region. However, a number of histologically benign lesions are included, as they may mimick the radiological appearance of a malignant lesion, and/or because they may show clinically an aggressive behaviour.

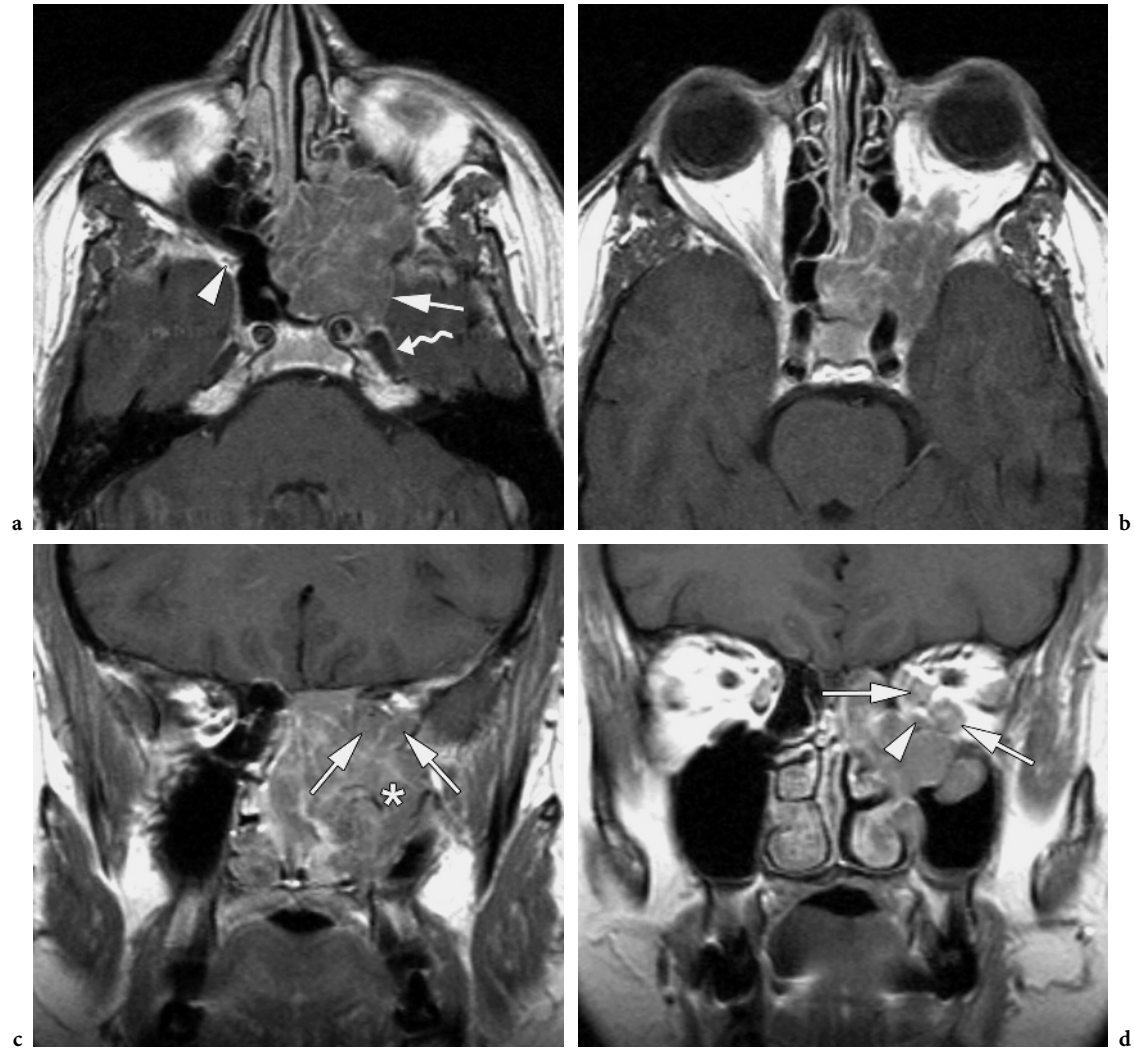

Fig. 11.7a–d. Patient presenting with nasal obstruction and progressive loss of vision on left side. **a,b** Axial gadolinium-enhanced T1-weighted spin echo images (**a** caudal to **b**). Moderately enhancing soft tissue mass in the left nasal cavity, growing into the posterior ethmoidal cells and sphenoid sinus. Extension into the pterygopalatine fossa (indicated by *arrowhead* on opposite side) and into the cavernous sinus (*arrow*), encasing the internal carotid artery, and reaching the anterior margin of Meckel's cave (*curved arrow*). At the level of the superior orbital fissure (**b**), the tumor grows into the orbital apex. **c,d** Coronal gadolinium-enhanced T1-weighted spin echo images (**c** posterior to **d**). Extension into the maxillary sinus (*asterisk*). Thickening and increased enhancement of the medial and inferior rectus muscle (*arrows*), corresponding to neoplastic involvement. On the more anterior image (**d**), apart from the muscular thickening, some infiltration of the peri-orbital fat is also noticed (*arrowhead*). Biopsy revealed undifferentiated carcinoma. The patient was treated by a combination of irradiation and chemotherapy. No evidence of tumor recurrence 3 years after treatment

11.5.1 Epithelial Tumors

11.5.1.1 Inverted Papilloma

Inverted papilloma is an uncommon epithelial tumor of the nose and paranasal sinuses. Essentially, this is a benign tumor, but recurrence after resection is fairly common, and in 7%–15% of patients an associated squamous cell carcinoma is found in the resection specimen. Even in the absence of frank malignancy, an inverted papilloma may behave aggressively, with rapid recurrences and invasion of surrounding structures (Pasquini et al. 2004).

The name refers to the characteristic invagination of the proliferating epithelium beneath the surface. Inverted papillomas typically arise from the lateral nasal wall, in the region of the middle turbinate. At presentation, they often involve both the nasal cavity and the adjacent maxillary cavity; the ethmoids may also be involved, but extension to the frontal and sphenoid sinus is not often seen. A polypoid mass is seen during clinical examination, sometimes resembling an antrochoanal polyp.

Apart from showing the location of the tumor mass at the junction of the nose and maxillary antrum, usually with a well defined bone defect at the maxillary ostium, CT may demonstrate the presence of intratumoral calcifications (Fig. 11.10). Sometimes the bony walls adjacent to the tumor appear sclerotic.

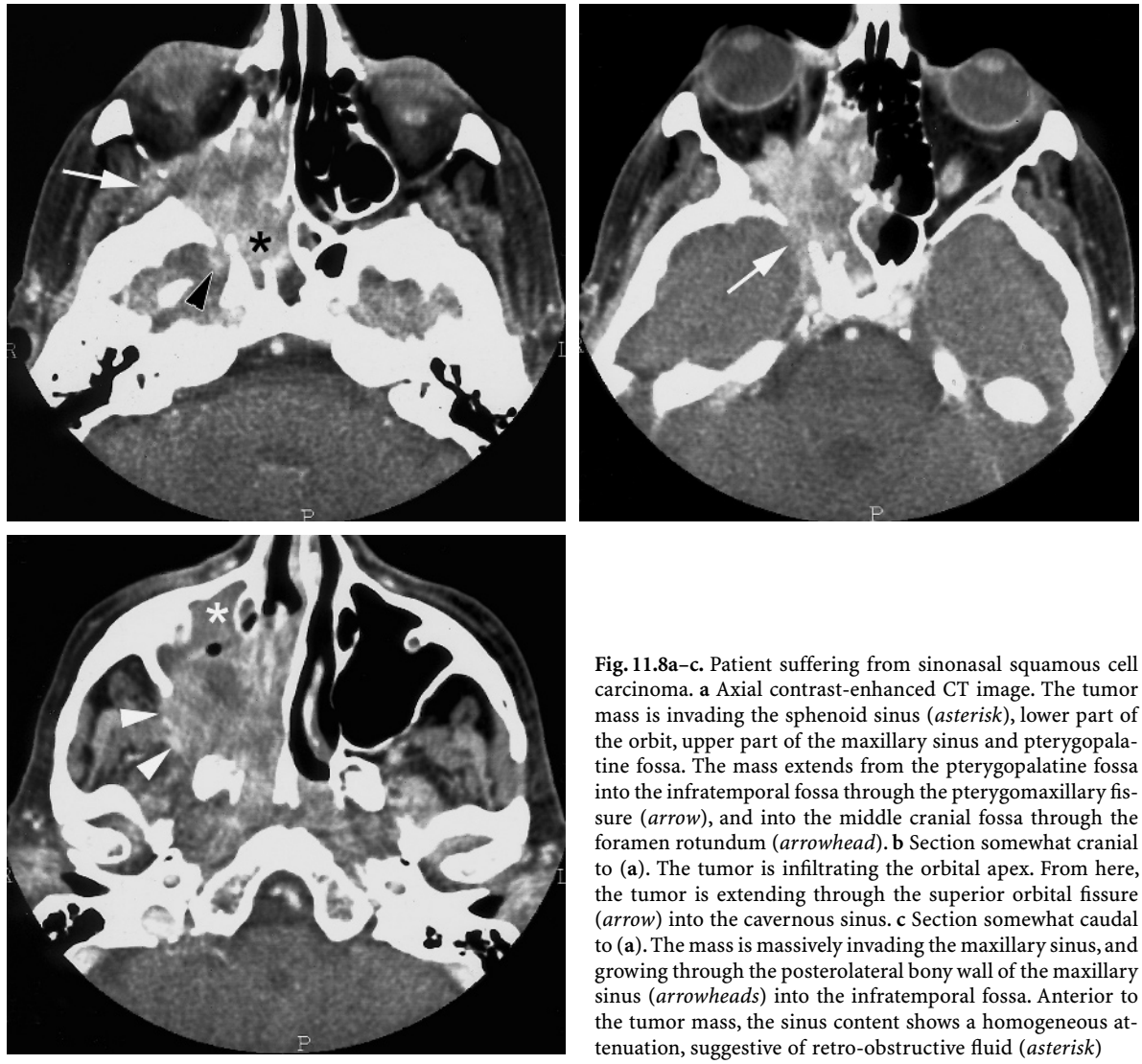

Fig. 11.8a–c. Patient suffering from sinonasal squamous cell carcinoma. **a** Axial contrast-enhanced CT image. The tumor mass is invading the sphenoid sinus (*asterisk*), lower part of the orbit, upper part of the maxillary sinus and pterygopalatine fossa. The mass extends from the pterygopalatine fossa into the infratemporal fossa through the pterygomaxillary fissure (*arrow*), and into the middle cranial fossa through the foramen rotundum (*arrowhead*). **b** Section somewhat cranial to (**a**). The tumor is infiltrating the orbital apex. From here, the tumor is extending through the superior orbital fissure (*arrow*) into the cavernous sinus. **c** Section somewhat caudal to (**a**). The mass is massively invading the maxillary sinus, and growing through the posterolateral bony wall of the maxillary sinus (*arrowheads*) into the infratemporal fossa. Anterior to the tumor mass, the sinus content shows a homogeneous attenuation, suggestive of retro-obstructive fluid (*asterisk*)

Fig. 11.9a–f. Patient with history of recurrent upper lip skin cancer, treated at another institution, now presenting with left-sided facial pain. **a-c** Axial gadolinium-enhanced T1-weighted spin echo images. Soft tissue swelling is seen in the upper lip (*arrow*, **a** and **b**), reaching the infra-orbital foramen (*curved arrow*, **b**). At a level slightly more cranial, enhancement of the infra-orbital nerve (*white arrowheads*, **c**) and the maxillary nerve, passing through the pterygopalatine fossa and foramen rotundum (*black arrowhead*, **c**) is seen. Thickening and increased enhancement of the cavernous sinus (*curved arrow*, **c**). **d-f** Coronal gadolinium-enhanced T1-weighted spin echo images. Enhancement of left infra-orbital nerve (compare to opposite side, *arrows*), maxillary nerve in foramen rotundum (*arrowheads*) and cavernous sinus (*curved arrows*). These findings are consistent with recurrent cancer in the upper lip, spreading perineurally along the left infra-orbital and maxillary nerve, into the cavernous sinus

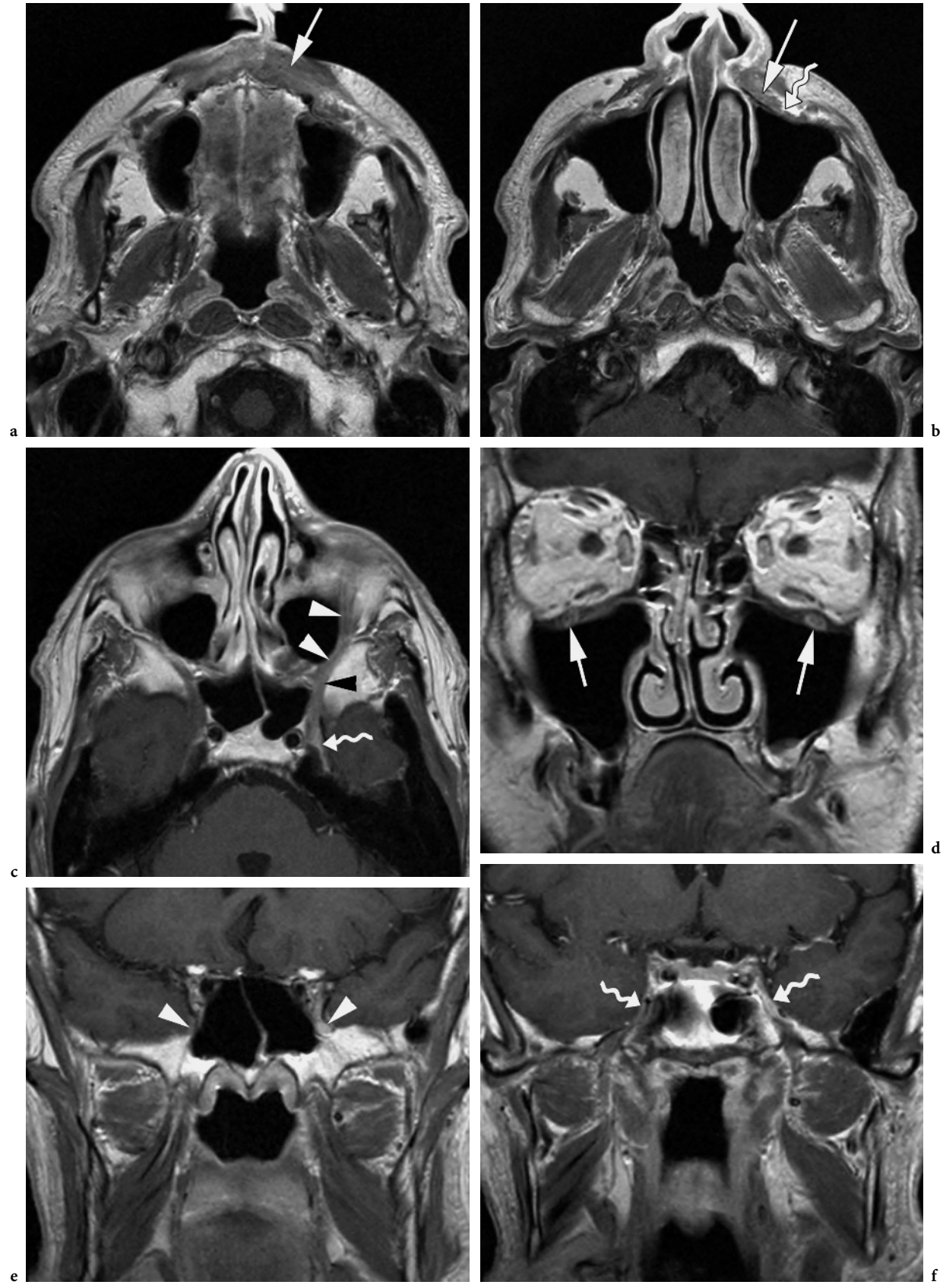
a
b
c
d
e
f

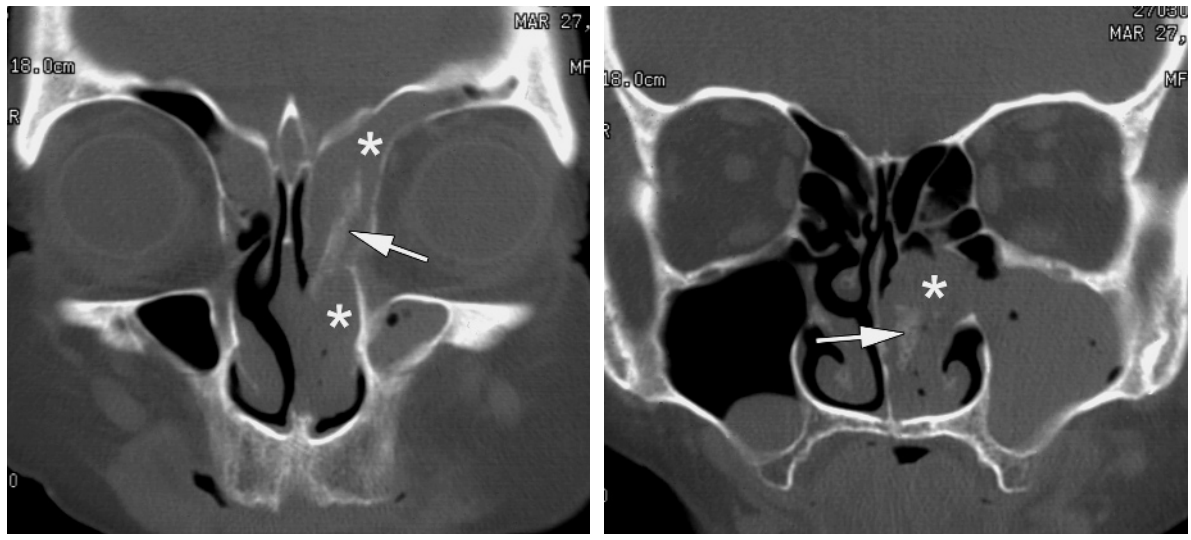

a b

Fig. 11.10a,b. Coronal CT images (**a** anterior to **b**) showing expansile mass lesion in left nasal cavity, frontal sinus and ethmoidal cells (*asterisks*). The lesion contains rough calcifications (*arrows*). Inverted papilloma; the soft tissue thickening in the left maxillary sinus corresponded to inflammatory secretions

Some inverted papillomas are radiologically indistinguishable from an antrochoanal polyp. Because of the sclerosis of the sinus wall, it may also mimic chronic sinus infection. The MR characteristics of the soft tissue mass are nonspecific, not allowing differentiation from other tumor types.

11.5.1.2 Squamous Cell Carcinoma

Squamous cell carcinoma is the most common type of sinonasal carcinoma, constituting about 60% of all cases. Most sinonasal squamous cell carcinomas arise in the nose or the maxillary sinus, but when first seen the tumor usually is already involving the nose, ethmoidal cells and maxillary antrum. Primary frontal or sphenoidal squamous cell carcinoma is rare.

Sinonasal squamous cell carcinoma does not show specific CT or MR characteristics. The main goal of imaging is to determine the submucosal extent of sinonasal neoplasms. Both surgical and radiotherapeutic management require an accurate mapping of tumor extent (Maroldi et al. 1997; Hermans et al. 1999). The prognosis is affected by involvement of critical anatomical areas (Suarez et al. 2004).

11.5.1.3 Adenocarcinoma

Adenocarcinoma is a malignant neoplasm of epithelial cells, arranged in a glandular or gland-like pattern. About 10% of all sinonasal neoplasms have a glandular origin. Adenocarcinomas have a pronounced predilection for the ethmoid sinuses and the superior part of the nasal cavity.

The term 'adenocarcinoma' is used for those glandular malignancies that cannot be placed within another more definable class of tumor, such as adenoid cystic carcinoma, acinic cell carcinoma or mucoepidermoid carcinoma. Some sinonasal adenocarcinoma may present with a histological pattern closely resembling adenocarcinoma of the colon, villous adenoma or even normal intestinal mucosa; the term 'intestinal-type adenocarcinoma (ITAC)' is used for these tumors. The risk to develop ITAC is related to exposure to wood dust. As the inhaled wood particles concentrate on the anterior part of the nasal septum and turbinates, the high incidence of a nasoethmoidal localisation in occupational adenocarcinoma can be explained (Barnes et al. 2001). Non-occupational ITAC has a predilection for the maxillary sinus, and this localisation is associated with a worse prognosis.

The imaging findings in sinonasal adenocarcinoma are similar to those in sinonasal squamous cell carcinoma.

11.5.1.4 Adenoid Cystic Carcinoma

Adenoid cystic carcinoma is a malignant epithelial tumor which develops in the major and minor salivary glands. Of all malignant paranasal sinus tumors, 5%–15% are adenoid cystic carcinomas (Kim et al. 1999).

Adenoid cystic carcinoma of the sinonasal cavity is a slowly progressive, aggressive neoplasm that has a high incidence of both local recurrence and distant metastasis, regardless of treatment modality. Cervical lymph node metastasis of adenoid cystic carcinoma is rarely seen.

Recurrence and metastasis can occur decades after treatment of the primary tumor. This behaviour can be partially explained by its tendency to extend submucosally and perineurally along major and minor nerves. The complexity of the local anatomy can make treatment difficult. The proximity of the tumors to the skull base and the major nerves combined with the tumor's tendency to spread perineurally contributes to the difficulty to obtain surgical margins free of disease (Wiseman et al. 2002). Therefore, accurate pre-operative imaging is required to select patients for surgery and to determine surgical borders. MRI is a sensitive method to detect perineural tumor spread; however, sensitivity for mapping the entire perineural tumor extent is only about 63% (Nemzek et al. 1998).

Most cases are ultimately fatal, although long disease-free intervals are observed. Therefore, the presence of distant metastatic disease is considered not to be a contraindication to surgical treatment of the primary tumor in order to achieve local control. A combination of surgery and radiotherapy offers these patients the best chance for disease control (Wiseman et al. 2002).

11.5.1.5 Staging of Sinonasal Carcinomas

The staging of sinonasal carcinomas is based on the clinical examination and imaging findings. The anatomic subsites distinguished for staging are reported in Table 11.2. There is a different T-staging system for maxillary sinus carcinomas (Table 11.3) and ethmoidal carcinoma (Table 11.4). The N staging is similar to that of laryngeal and oro-hypopharyngeal cancer.

Table 11.2. Anatomical sites and subsites in the nasal cavity and paranasal sinuses (UICC 2002)

Nasal cavity
Septum
Floor
Lateral wall
Vestibule
Maxillary sinus
Ethmoid sinus
Left
Right

Table 11.3. T staging of maxillary sinus cancer (UICC 2002)

T1	Tumor limited to the sinus mucosa, with no erosion or destruction of bone
T2	Tumor causing bone erosion or destruction, including extension into the hard palate and/or middle nasal meatus, but not to posterior maxillary sinus wall and pterygoid plates
T3	Tumor invades any of the following: posterior bony wall of maxillary sinus, subcutaneous tissues, floor or medial wall of orbit, pterygoid fossa, ethmoid sinuses
T4a	Tumor invades any of the following: anterior orbital contents, cheek skin, pterygoid plates, infratemporal fossa, cribriform plate, sphenoid or frontal sinuses
T4b	Tumor invades any of the following: orbital apex, dura, brain, middle cranial fossa, cranial nerves other than maxillary nerve, nasopharynx, clivus

Table 11.4. T staging of nasal cavity and ethmoid sinus cancer (UICC 2002)

T1	Tumor restricted to one subsite of nasal cavity or ethmoid sinus, with or without bony invasion
T2	Tumor involves two subsites in a single site or extends to involve an adjacent site within the nasoethmoidal complex, with or without bone invasion
T3	Tumor extends to invade the floor or medial wall of the orbit, maxillary sinus, palate, or cribriform plate
T4a	Tumor invades any of the following: anterior orbital contents, skin of nose or cheek, minimal extension to anterior cranial fossa, pterygoid plates, sphenoid or frontal sinuses
T4b	Tumor invades any of the following: orbital apex, dura, brain, middle cranial fossa, cranial nerves other than maxillary nerve, nasopharynx, clivus

11.5.1.6 Other Tumors From Epithelial Origin

11.5.1.6.1 Dental Tumors (Ameloblastoma)

Ameloblastoma is a benign odontogenic epithelial neoplasm that histologically mimics the embryonic enamel organ but does not differentiate to the point of forming dental hard tissue; it behaves as a slowly growing expansile radiolucent tumor. This tumor occurs most commonly in the mandible (80%). Two basic histological forms are distinguished: the simple follicular form, and the plexiform form.

Distant metastasis may occur without cytologic evidence of malignancy, but this is rarely seen; such lesions are called 'malignant ameloblastomas'. The term 'ameloblastic carcinoma' is used for ameloblastoma showing cytological evidence of malignancy in

the primary or recurrent tumor, regardless of whether it has metastasized.

There are no specific radiological signs for an ameloblastoma; it appears as a multilocular, osteolytic lesion, sometimes with bone trabeculas running through it. An ameloblastoma may also appear as a unilocular lesion. In about 10% of cases a tooth is retained within the lesion. The lesion is usually well demarcated and may thin the surrounding cortical bone. Cortical bone disruption occurs late in the disease; extension in neighbouring soft tissue is uncommon (Fig. 11.11).

Although slowly growing and nearly painless, maxillary ameloblastoma can reach a considerable size within the mid-facial structures, involving the orbit, skull base and even brain. Despite wide resection, recurrence is commonly seen due to invasion of the adjacent bone (Zwahlen and Grätz 2002). Some cases of recurrent ameloblastoma respond readily to radiotherapy (Miyamoto et al. 1991). Due to local progressive disease, maxillary ameloblastoma is a potential lethal disease.

Malignant variants of other odontogenic epithelial tumors exist, but are very rare. Malignant transformation may rarely occur in odontogenic cysts. About half of the cases of central mucoepidermoid carcinoma are associated with dental cysts; such tumors usually occur in the mandible (Simon et al. 2003). Several types of odontogenic sarcomas have been described (Verbin and Appel 2001).

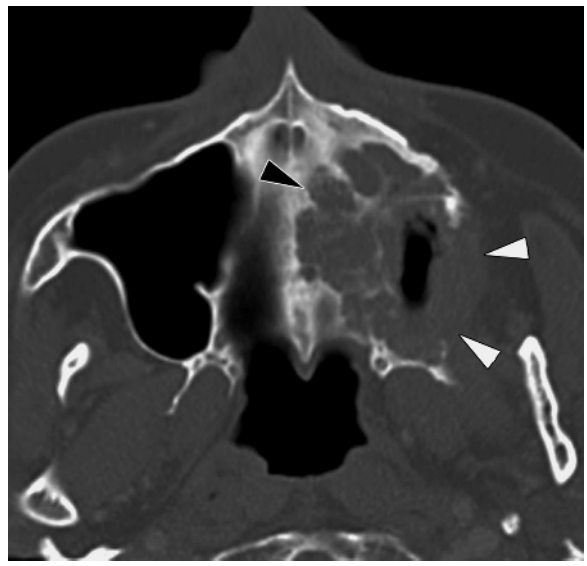

Fig. 11.11. Axial CT image (*bone window*) shows multicystic lesion in the left maxillary sinus invading the hard palate (*black arrowhead*). More laterally, the lesion appears less compartmentalized, and causes destruction of the lateral maxillary wall (*white arrowheads*). Plexiform ameloblastoma

11.5.1.6.2 Malignant Melanoma

Sinonasal malignant melanoma (MM) is uncommon, representing <7% of all malignant sinonasal neoplasms (Matias et al. 1988). Contrary to the increasing incidence of skin MM, the incidence of mucosal MM has remained stable over the last decades.

Sinonasal MM is presumed to originate from melanocytic precursors normally present in the mucosa. There are more often located within the nose (anterior part of nasal septum, lower and middle turbinate) than in the paranasal sinuses.

The tumor mass usually shows no specific findings, although sometimes it may show spontaneous hyperintensity on T1-weighted images, due to the presence of hemorrhage; melanin, a paramagnetic substance, is frequently lacking (Prasad et al. 2003). Bone destruction may or may not be present.

On light microscopy, mucosal MM may be confused with other malignancies, including sarcomas, plasmacytomas, and carcinomas. This diagnosis is confirmed by ancillary immunohistochemical studies (Medina et al. 2003). A metastasis from skin MM to the sinonasal tract should also be considered in the differential diagnosis.

Treatment is usually by a combination of surgery and irradiation (Patel et al. 2002).

Skin and also mucosal MM may, similarly to other neoplasms in this area, show perineural tumor spread along cranial nerve branches; this may occur after a long latent period following primary diagnosis (Chang et al. 2004).

11.5.1.6.3 Metastasis

Metastatic lesions in the sinonasal cavities are uncommon. The most common tumor causing sinonasal metastasis is renal cell carcinoma (Fig. 11.12). Other tumors causing sinonasal metastasis are lung and breast cancer. Also tumor originating from other organs have been reported to metastasize to the nose and paranasal sinuses, but this is very rare (Fig. 11.13).

These metastases cause aspecific symptoms, such as nasal obstruction. Renal cell cancer may cause epistaxis. Renal cell carcinomas are known for their tendency to early metastasis, and symptoms due to the metastatic sinonasal lesion may be the initial manifestation (Lee et al. 2005).

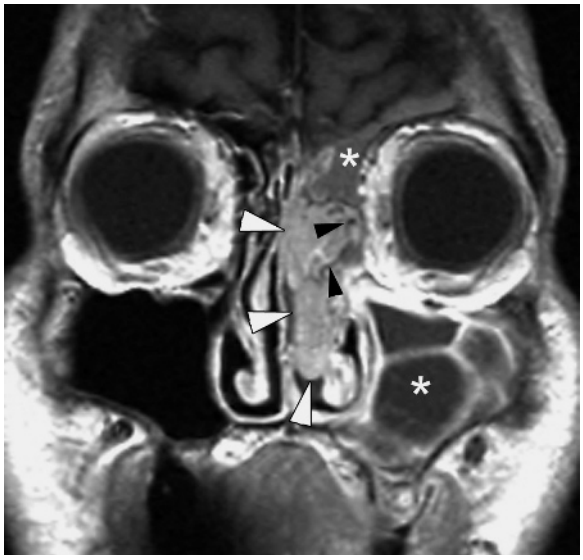

Fig. 11.12. Coronal gadolinium enhanced T1-weighted spin echo image in a patient with a history of renal cell cancer and bone metastases, now presenting with sinusitis. An enhancing soft tissue mass is seen in the left nasoethmoidal cavity (*white arrowheads*); possibly some signal voids are seen within the lesion (*black arrowheads*). Retro-obstructive secretions/inflammation in the left frontal and maxillary sinus (*asterisks*). Biopsy showed metastatic renal cell cancer

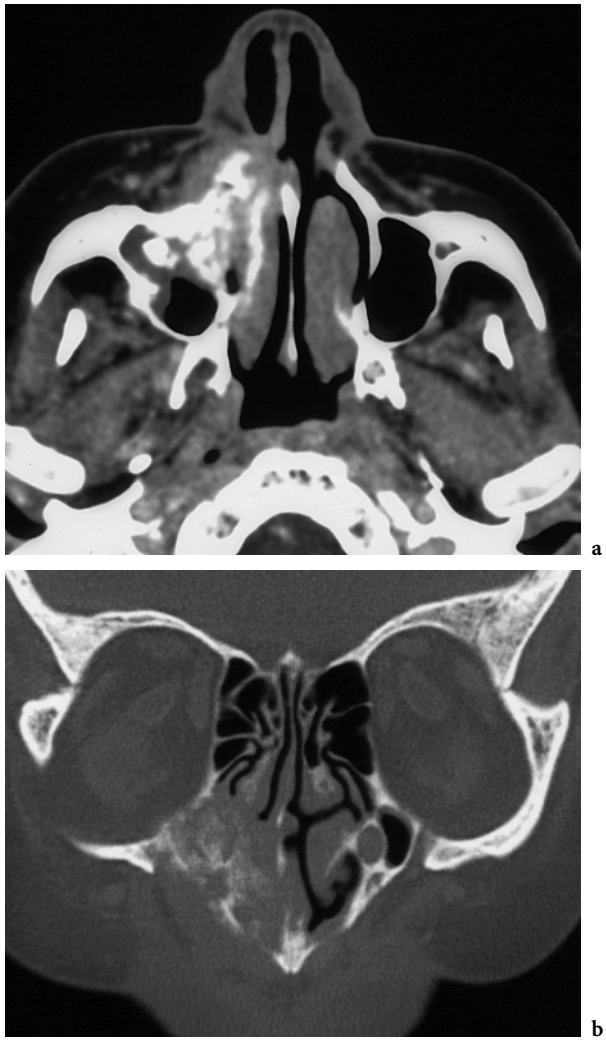

Fig. 11.13a,b. Contrast-enhanced axial (**a**, soft tissue algorithm) and coronal (**b**, bone algorithm) CT images showing soft tissue mass centered on the anteromedial part of the right maxilla, causing osteolysis. Biopsy findings were compatible with metastatic prostatic cancer

11.5.2 Non-epithelial Tumors

11.5.2.1 Neuro-ectodermal and Nervous System Tumors

11.5.2.1.1 Nasal Glioma

Nasal glioma is an uncommon lesion, consisting of a mass of heterotopic glial tissue at the root of the nose, either intra- or extranasally, not communicating with the intracranial fluid spaces. The absence of such a communication differentiates it from a nasal encephalocele. Nasal glioma is not a neoplasm but a congenital malformation.

11.5.2.1.2 Olfactory Neuroblastoma

Olfactory neuroblastoma is a rare malignant tumor, occurring in all age groups, but with a peak incidence between the second and fourth decades. It is also called esthesioneuroblastoma. It arises from olfactory epithelium, a structure of neural crest origin. It accounts for about 3% of all tumors of the nasal cavity and paranasal sinuses.

Radiologically, this tumor most often presents as an enhancing soft tissue mass with or without bony bowing and destruction, depending on the stage of the disease. In the initial stage, a small unilateral mass in the nasal vault with or without unilateral ethmoid involvement may be seen. At a later stage extensive nasal fossa involvement and widespread involvement of the paranasal sinuses and bony destruction may be recognized. Further growth leads to expansion of bony margins with orbital or intracranial involvement. Usually, no hyperostosis or new bone forma-

tion is recognized, although punctuate calcifications can occur. However, in rare cases gross calcifications may be seen (Fig. 11.14) (Vanhoenacker et al. 1993). Olfactory neuroblastoma associated with significant hyperostosis has also been reported (Regenbogen et al. 1988).

Histological diagnosis may prove to be difficult. Differentiation from lymphoma, sarcoma, melanoma and undifferentiated sinonasal cancer may be difficult.

Olfactory neuroblastoma is clinically staged according to the Kadish classification (Kadish et al. 1976) (Table 11.5). Like most malignant sinonasal tumors, olfactory neuroblastoma frequently is diagnosed in an advanced stage of disease. Another classification, according to Hyams, is based on histopathologic grading, distinguishing low-grade and high-grade tumors (Miyamoto et al. 2000). Hyams' grading is an important prognostic factor and should be considered in therapeutic planning (Constantinidis et al. 2004).

The natural history of this tumor is variable and difficult to predict; some cases show slow progression, while others display a very aggressive course. Currently there is no recommended standardized therapy. Multimodal therapeutic strategies, combining surgery, radiotherapy and chemotherapy, have been developed in recent years and have lead to improved survival rates.

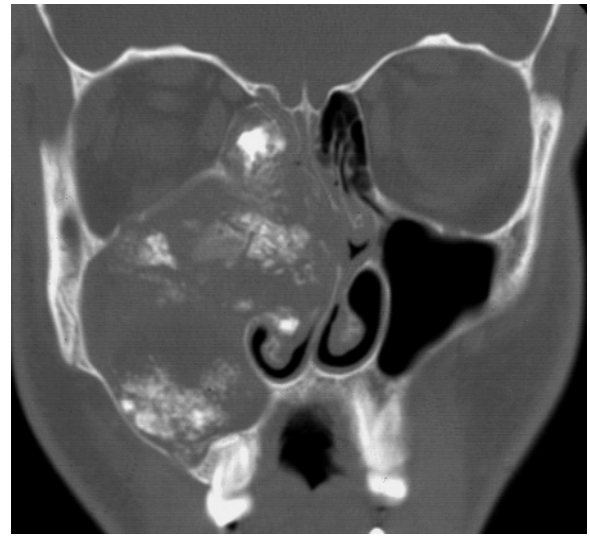

Fig. 11.14. Coronal CT image, bone window, obtained in a 14-year-old boy presenting with epistaxis and unilateral nasal obstruction. Large expansile mass in the right ethmoid, middle nasal meatus and maxillary sinus. Note deformation of the lamina papyracea and orbital floor. Bowing and irregular aspect of the anterolateral wall of the maxillary sinus. The lamina cribrosa and fovea ethmoidalis appear intact. Extensive intralesional calcifications are present. On MRI (not shown), the mass appeared inhomogeneous, without evidence of intracranial extension. The lesion turned out to be an olfactory neuroblastoma. Treatment was by radiotherapy and surgery

Table 11.5. Classification of olfactory neuroblastoma according to Kadish (1976)

Stage A	Disease confined to nasal cavity
Stage B	Disease confined to the nasal cavity and one or more paranasal sinuses
Stage C	Disease extending beyond the nasal cavity or paranasal cavities

11.5.2.1.3 Neuro-endocrine and Undifferentiated Carcinoma

Sinonasal undifferentiated carcinoma (SNUC) is a highly malignant neoplasm, showing no glandular or squamous differentiation. Histologically, the differential diagnosis from other malignant neoplasms occurring within the sinonasal tract may be difficult. Also radiologically, no distinction can be made between SNUC and many other malignant sinonasal neoplasms. The prognosis of SNUC is poor; management is by aggressive multimodality treatment (Kim et al. 2004).

It is a matter of debate whether neuro-endocrine carcinoma is a separate entity. A variety of neoplasms showing neuro-endocrine differentiation may involve the sinonasal cavity, such as olfactory neuroblastoma, invasive pituitary adenoma and others (Barnes et al. 2001). Undifferentiated carcinoma has been described to be at the extreme end of the spectrum of sinonasal neuro-endocrine neoplasms, with olfactory neuroblastoma being on the other, differentiated end of the spectrum.

11.5.2.1.4 Peripheral Nerve Sheath Tumors (PNST)

Benign PNSTs have been divided into neurilemoma (schwannoma) and neurofibroma. Three types of neurofibromas are classically described: localized, diffuse, and plexiform. All three types of neurofibromas can be associated with neurofibromatosis type I. Plexiform neurofibromas are essentially pathognomonic of neurofibromatosis type I (Murphey et al. 1999).

Malignant PNST corresponds to a spindle cell sarcoma arising from nerve or neurofibroma, or dem-

onstrating nerve tissue differentiation; sometimes foci of mature cartilage and bone, skeletal muscle differentiation (called 'malignant Triton tumor'), and glandular or epithelioid components are histologically recognized (Heffner and Gnepp 1992).

PNSTs are rarely encountered in the sinonasal region and present with aspecific symptoms (Buob et al. 2003).

11.5.2.1.5 Ewing Sarcoma and Primitive Neuro-ectodermal Tumor (PNET)

These two neoplasms, which are very rarely seen in the sinonasal cavity, typically occur in childhood and young adults. They appear histologically very similar, and are distinguished based on immunohistochemical and ultrastructural differences.

These are aggressive neoplasms, that rapidly metastasize to distant sites.

11.5.2.1.6 Meningioma

Extracranial meningiomas are rare. The most frequent sites for extracranial meningiomas are the orbit, nose, paranasal sinuses and middle ear, and at the skull base foramina. Sinonasal meningioma most frequently affects the nasal cavity (Thompson and Gyure 2000) (Fig. 11.15). Extracranial meningiomas are formed by direct extension outside the skull of a primary intracranial meningioma, by metastasis from a malignant intracranial meningioma, or originate from extracranial arachnoid cell clusters. These cell clusters accompany certain of the cranial nerves outside the cranium.

The imaging characteristics are similar to those of intracranial meningioma: an enhancing mass lesion, remodelling bone, is seen.

11.5.2.2 Mesenchymal Neoplasms

11.5.2.2.1 Vascular Tumors

11.5.2.2.1.1 Juvenile Angiofibroma

Juvenile angiofibroma is an uncommon, highly vascular, locally invasive benign tumor which originates almost exclusively in the posterior nasal cavity of adolescent males. The tumor has the potential to kill or to cause serious morbidity due to uncontrolled growth, and sometimes also indirectly due to treatment complications. The prefix 'juvenile' is commonly used, but the lesion also occurs in childhood and (rarely) middle age. The tumor has been reported to occur in young females, but these examples are so exceptional that some authors state that sex chromosome studies are indicated if the diagnosis is confirmed in a female patient. The onset of symptoms occurs between 7 and 21 years of age. Symptoms include nasal obstruction, recurrent severe epistaxis, purulent rhinorrhea, facial deformity and nasal speech. The diagnosis can usually be made on the basis of history, physical examination and imaging studies. Clinically, a deep red mass with increased vascularity of the overlying mucosa is seen. Biopsy is seldom required and dangerous to perform.

On CT and MRI, the tumor appears as a strongly contrast-enhancing mass lesion in the posterior nasal cavity and nasopharynx. Intratumoral flow voids are present on MR images. The mass lesion is typically centred on the sphenopalatine foramen and very often extends into the pterygopalatine fossa, resulting in widening of this fossa with anterior bowing of the posterior maxillary wall (Fig. 11.16). As the tumor grows, it tends to extend into the ipsilateral nasal cavity. Invasion of the neighbouring skull base

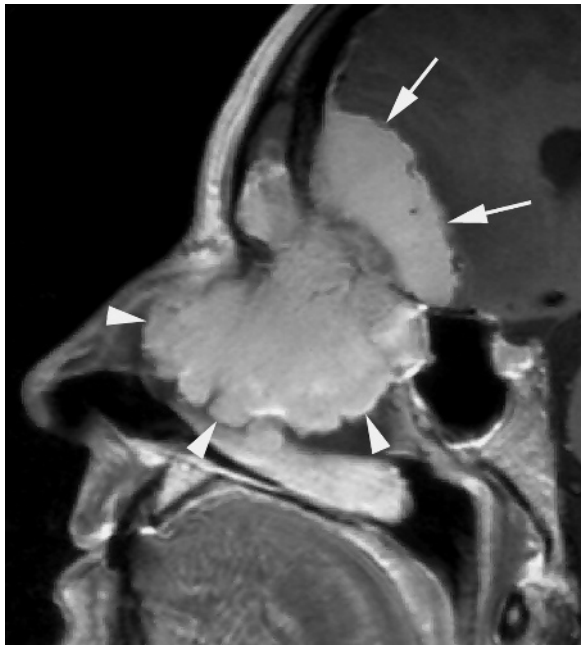

Fig. 11.15. Sagittal T1-weighted spin-echo image in a patient presenting with a nasal soft tissue mass. A large and strongly enhancing lesion is seen in the anterior cranial fossa (*arrows*), extending into the nose (*arrowheads*). Meningioma

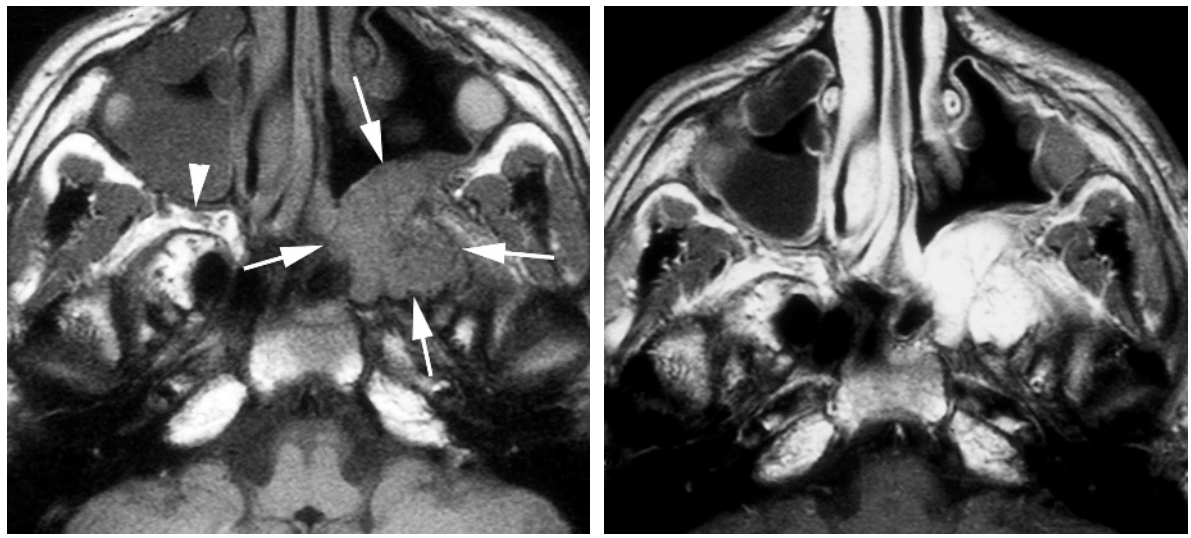

Fig. 11.16a,b. Male adolescent presenting with recurrent epistaxis. Axial T1-weighted image spin echo image (**a**) shows a mass lesion (*white arrows*) centered on the left pterygopalatine fossa, anteriorly displacing the posterior maxillary wall and extending into the skull base. Normal right pterygopalatine fossa (*arrowhead*). The axial T1-weighted image after injection of gadolinium (**b**) demonstrates the dramatic enhancement of the lesion; some subtle flow voids are visible in the lesion

structures is often seen; in more than half of patients the sphenoid sinus is invaded through the roof of the nasopharynx (Fig. 11.17). Orbital and infratemporal spread are not uncommon. In large tumors, even intracranial extension may be seen. Angiography shows a hypervascular tumor, mainly supplied by the internal maxillary artery and ascending pharyngeal artery; this procedure is not usually needed for diagnosis, but is performed for presurgical tumor embolization. Natural regression almost never occurs. The tumor is radiosensitive, but the preferred therapy is complete surgical resection after selective tumor embolization. The prognosis is good, although fatalities due to haemorrhage are possible. Recurrences are probably related to incomplete resection, due to the multilobular nature of the tumor and its ability to invade adjacent spaces.

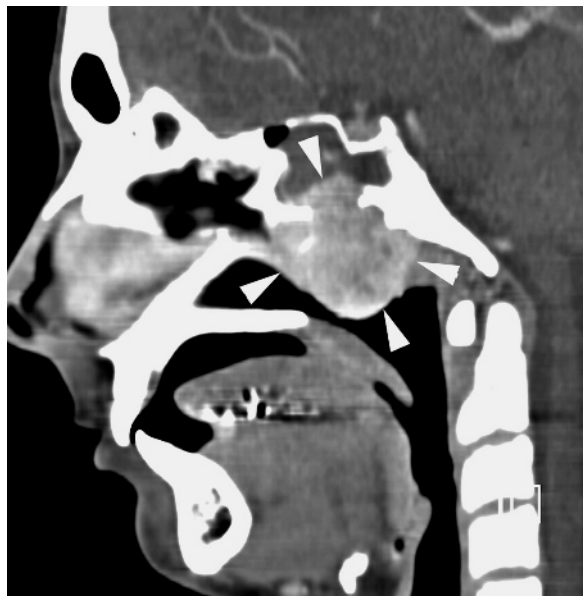

Fig. 11.17 Male adolescent presenting with nasal obstruction; no history of epistaxis. Sagittal reformatting of axial contrast-enhanced CT images. A strongly enhancing soft tissue mass (*arrowheads*) is seen in the choanae and in the nasopharyngeal roof, invading the sphenoid sinus. Juvenile angiofibroma

11.5.2.2.1.2
Angiomatous Polyp

An angiomatous polyp corresponds to a vascular compromised nasochoanal component of an antrochoanal polyp or sphenochoanal polyp. Because of the compression of the feeder vessels in the polyp, a sequence of dilatation and stasis of feeder vessels, oedema, infarction and neovascularization is set up (De Vuysere et al. 2001). This may lead to total necrosis or more often to an angiomatous polyp (Fig. 11.18). The term 'angiomatous polyp' is sometimes also used for a vascularized and fibrosed nasal polyp, presumed to be the response to minor trauma, but little can be found about this in the literature.

11.5.2.2.1.3
Hemangioma

Hemangioma is a benign vascular tumor that is especially common on the skin but may be present in

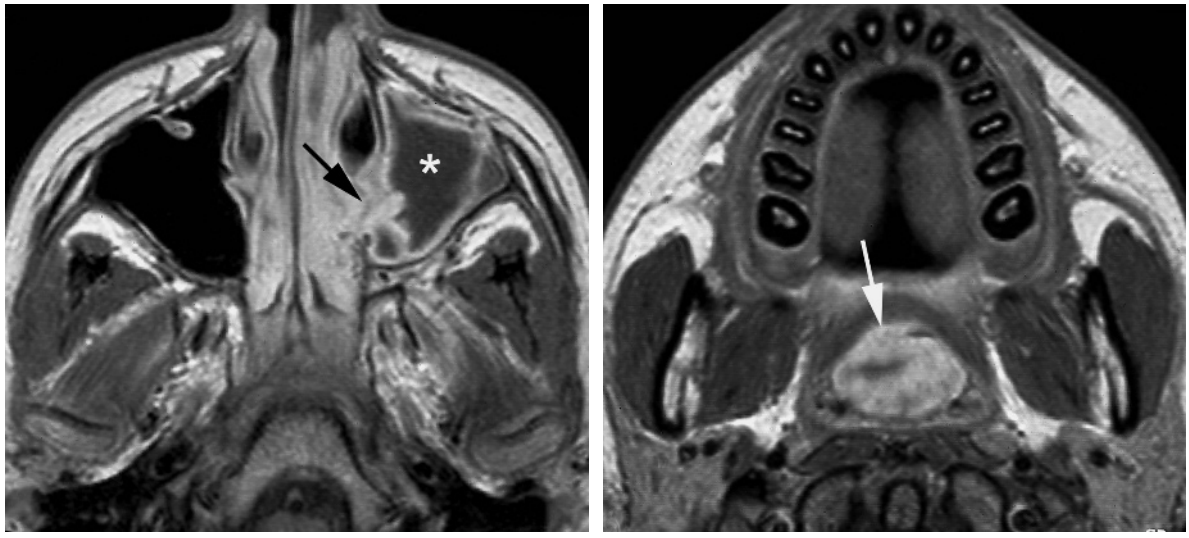

Fig. 11.18a,b. Axial gadolinium-enhanced T1-weighted images show maxillary polyp (*asterisk*) passing through an accessory ostium into the posterior nasal cavity (**a**, *arrow*). The pharyngeal component enhances strongly (**b**, *arrow*): angiomatous polyp. Vascular compromise at the level of the accessory ostium may induce a sequence of dilatation, stasis and occlusion of the feeder vessels, eventually leading to neovascularisation of the extrasinusal polyp component

any tissue, including bone. It is the most common tumor of childhood. Hemangiomas are not usually seen at birth, but show a rapid postnatal proliferation with slow involution afterwards. A hemangioma should not be confused with a vascular malformation, which is present at birth (although not always evidently) and grows with the child into adulthood.

About 60% of haemangiomas occur in the head and neck. Most are cutaneous lesions, but they also occur in the deeper tissues. A non-osseous localisation within the nose and/or paranasal sinuses is very uncommon. They may block the airway when located within the nose (Fig. 11.19). Hemangiomas in the paranasal sinuses are more rare than in the nose. Paranasal hemangioma sometimes causes destruction of adjacent bone, making it difficult to differentiate them from a malignant lesion (Fig. 11.20) (Kim et al. 1995).

Hemangioma within the maxillofacial bony structures is also rare; the mandible is affected most commonly.

11.5.2.2.1.4 Hemangiopericytoma

Hemangiopericytoma is a vascular tumor that can arise wherever capillaries are present. The pericytes surrounding the endothelial cells are believed to be the cells of tumor origin. About 15%–25% of hemangiopericytomas occur in the head and neck region, half of these in the nose or paranasal sinuses. It is a rapidly growing, usually painless tumor, and is seen at all ages. The prognosis after resection is unpredictable; they should be regarded as locally aggressive tumors with a relatively high recurrence rate. On CT and MRI, a hemangiopericytoma appears as an expansile, bone remodelling lesion with variable enhancement of the mass (Fig. 11.21).

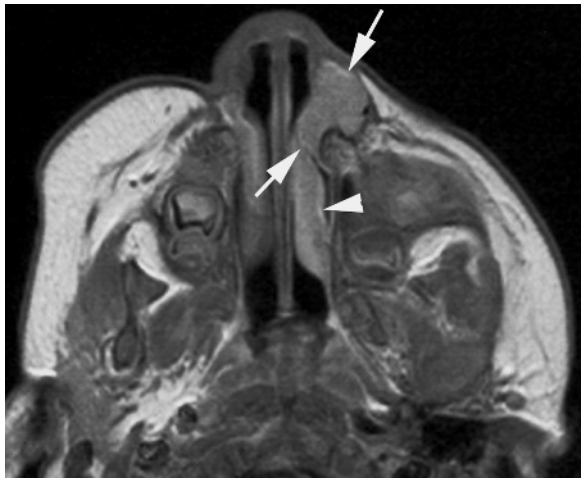

Fig. 11.19. Axial gadolinium-enhanced T1-weighted spin-echo image in a 5-month-old patient. Enhancing soft tissue tumor (*arrows*) in the wall of the left nostril, somewhat extending in the left nasal cavity; inferior nasal concha (*arrowhead*). Hemangioma

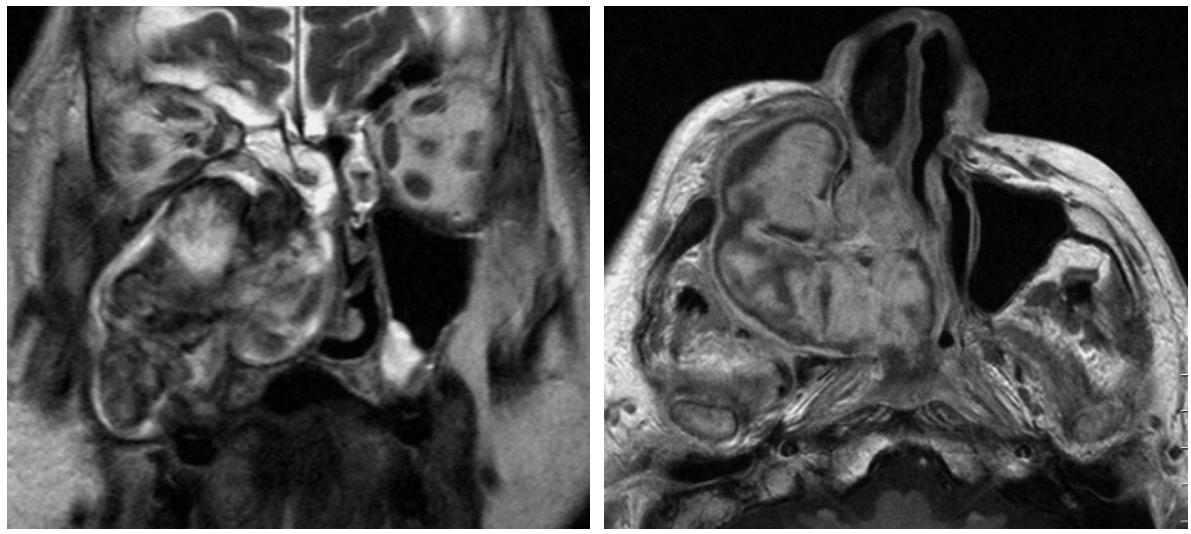

Fig. 11.20a,b. Coronal T2-weighted spin echo image (**a**) and axial gadolinium-enhanced spin echo image (**b**) in a 64-year-old patient, presenting with nasal obstruction, epistaxis and facial deformity; the complaints had been present for years. A large heterogenous soft tissue mass is seen in the nose and maxillary sinus, showing moderate enhancement. Expansion of the right maxillary sinus is evident. The lesion was endoscopically resected. Histologic examination showed hematoma with reparative phenomena; focally, clusters of vessels were recognized, suggesting an underlying vascular malformation or hemangioma

11.5.2.2.2 Osseous and Cartilaginous Tumors

11.5.2.2.2.1 Osteosarcoma

Osteosarcoma is a malignant neoplasm arising from bone forming cells. About 6% of the osteosarcomas originate in the maxillofacial skeleton, the mandible being the most frequent site. There is a wider age distribution in maxillofacial osteosarcoma than in skeletal osteosarcoma which occurs predominantly in the second decade of life. On imaging, these neoplasms appear as mass lesions, causing osteolysis or mixed lytic–sclerotic bone alterations. Within the tumor, new bone formation is commonly seen (Fig. 11.22).

11.5.2.2.2.2 Chondrosarcoma

Chondrosarcoma is a malignant neoplasm derived from cartilage cells. In the head and neck, they are seen originating from the jaw bones, sinonasal region (usually nasoethmoidal), skull base, larynx and trachea. It is difficult to firmly differentiate between benign chondroma and low-grade chondrosarcoma on a small amount of tissue obtained by biopsy; both may show a lobular growth pattern. Compared to chondroma, low-grade chondrosarcoma may display only minimally increased cellularity and nuclear atypia, a pattern overlapping with benign chondromas; there is no appreciable degree of mitotic activity in such lesions.

The distinctive imaging feature of these tumors is a mass containing scattered calcifications, as visible on CT. On MRI they usually display low signal on T1-

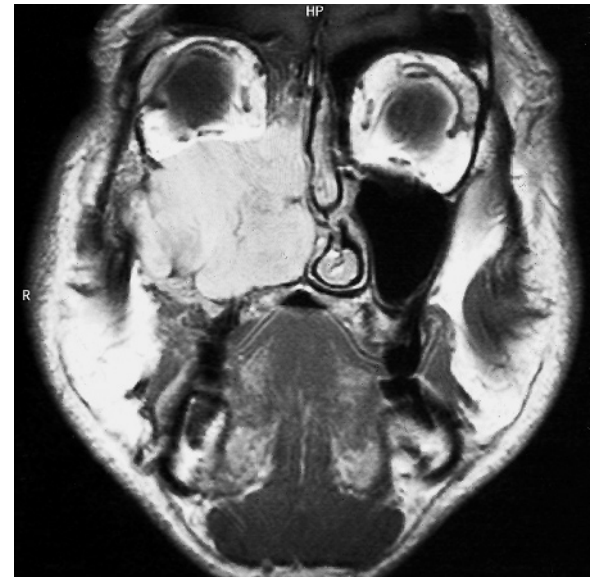

Fig. 11.21. Coronal T1-weighted gadolinium-enhanced spin-echo image. A strongly enhancing expansile mass is seen in the right maxillary sinus, displacing and eroding the orbital floor, extending into the nasal cavity and through the lateral maxillary wall. This patient suffered hemangiopericytoma

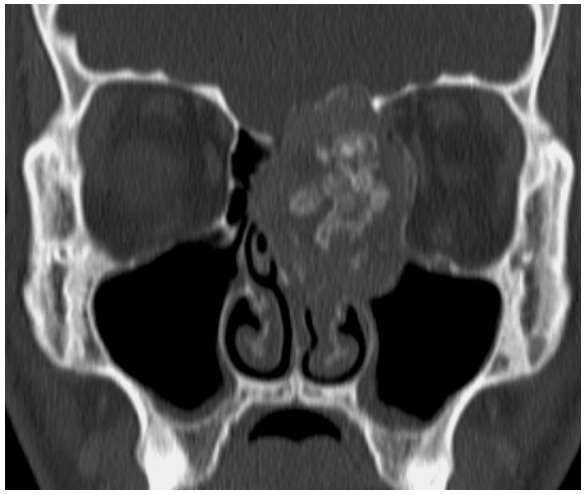

a

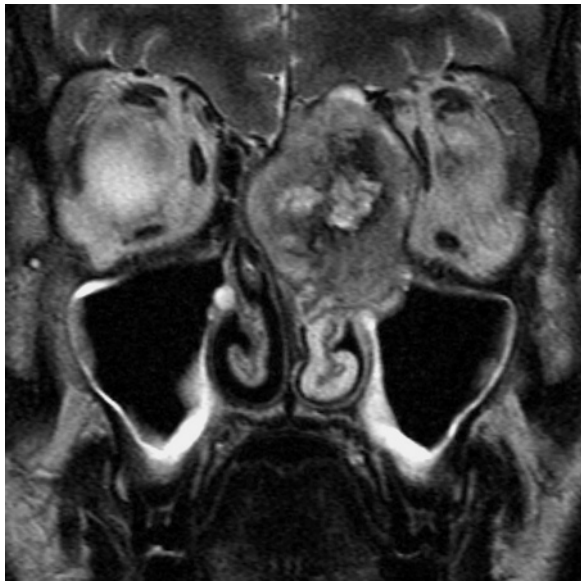

b

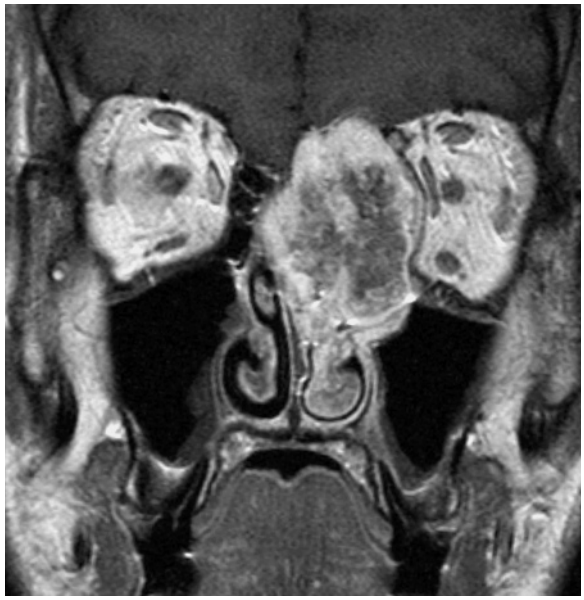

c

weighted and high signal on T2-weighted sequences, as well as presence of low signal intensity septa separating high signal intensity lobules on T2-weighted images (De Beuckeleer et al. 1995). After injection of gadolinium, these tumors typically show enhancement of scalloped margins and curvilinear septa (the so-called 'ring-and-arc pattern'); the enhanced areas correspond to fibrovascular bundles surrounding hyaline cartilage lobules (Fig. 11.23) (Aoki et al. 1991).

Surgery is the only curative modality of cartilaginous tumors. Low-grade chondrosarcomas may locally recur if incompletely resected, but have only limited risk of metastatic disease.

11.5.2.2.3 Soft Tissue Sarcomas

11.5.2.2.3.1 Rhabdomyosarcoma

Rhabdomyosarcoma is a malignant tumor of skeletal muscle. This tumor mainly occurs in children. Apart from lymphoma, it is the most common malignant tumor of the head and neck in childhood. Rhabdomyosarcoma is divided into four histological subtypes: embryonal, botryoid, alveolar and pleomorphic; the embryonal and botryoid subtype account for about 90% of primary head and neck lesions. Head and neck rhabdomyosarcoma has three sites of predilection: the orbit, the nasopharynx and paranasal cavities, and the temporal bone.

These tumors are usually large at presentation and nearly always invade neighbouring structures (Fig. 11.24).

Rhabdomyosarcoma may show early metastases, sometimes before significant local invasion occurs. The lung is the most frequent site of distant metastasis (Herrmann et al. 2003). As the treatment is determined by the local tumor extent and the possible presence of distant disease, imaging should include a CT and/or MRI scan of the primary tumor site and a CT scan of the chest. In patients at risk of developing meningeal extension, a gadolinium-enhanced MR study of the brain should be performed.

Fig. 11.22a–c. A 26-year-old patient presenting with severe headache and proptosis on the left side. **a** Coronal CT image (*bone window*). Expansile nasoethmoidal mass lesion on the left, growing through the nasal septum, displacing the medial orbital wall and causing destruction of the nasoethmoidal roof. The lesion contains areas of gross calcification and/or ossification. **b,c** Corresponding coronal T2-weighted (**b**) and gadolinium-enhanced T1-weighted spin echo image (**c**). Biopsy showed osteosarcoma

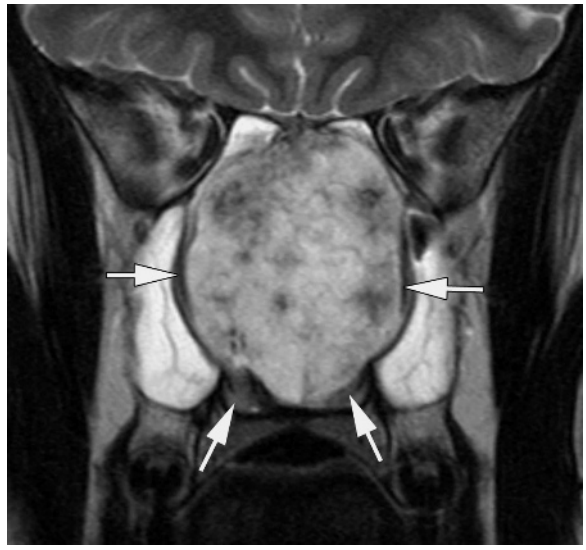

a

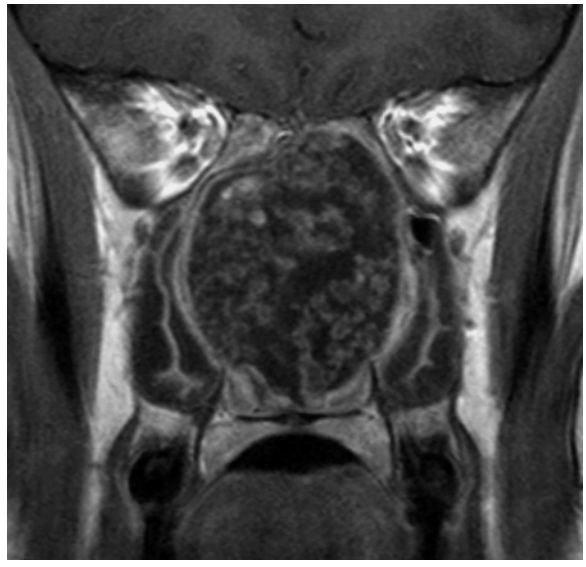

b

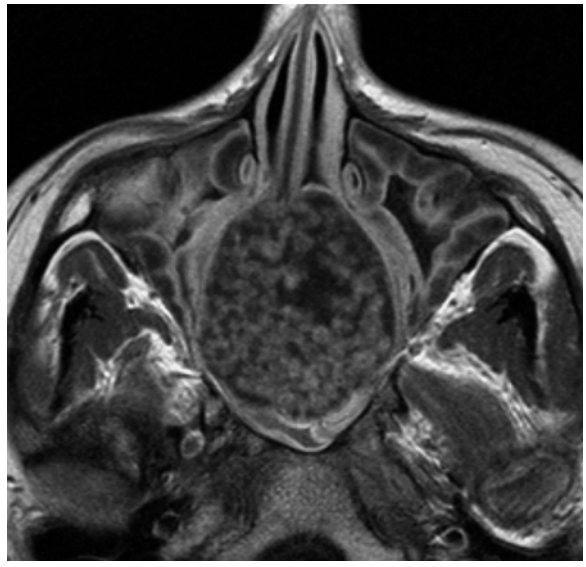

c

11.5.2.2.3.2
Other Soft Tissue Sarcomas

Other soft tissue sarcomas, such as leiomyosarcoma, fibrosarcoma and malignant fibrous histiocytoma have been reported to occur in the sinonasal area, but they are all very rare.

11.5.2.3
Lymphoreticular Tumors

11.5.2.3.1
Lymphoma

For a more general discussion on lymphoma, see Chap. 16.

In non-Hodgkin lymphoma (NHL), two distinct extranodal sites are recognized: extranodal lymphatic spread or involvement of Waldeyer's ring, and extranodal extralymphatic spread. Extranodal extralymphatic NHL occurs most commonly in the sinonasal cavities and orbits. In a series of 55 cases of extranodal NHL of the head and neck, 11 patients (34%) had involvement of the sinonasal cavities and/or palatum (Fig. 11.25). In most of these cases, bone alterations were present and appeared always lytic; tumor traversing bone without clear lysis was not observed (Hermans et al. 1994). The radiological appearance of such a tumor mass is aspecific, but the association with pathological neck lymph nodes (especially when appearing large and non-necrotic on imaging studies) and/or involvement of Waldeyer's ring, suggests the diagnosis of NHL (Hermans et al. 1994).

11.5.2.3.2
Plasmocytoma

Plasmocytoma is usually a polyostotic neoplasm (multiple myeloma), but solitary lesions may occur. The maxillofacial skeleton is affected in about 30%

Fig. 11.23a–c. A 15-year-old patient presenting with progressive nasal obstruction. **a** Coronal T2-weighted spin echo image. Large midline nasal mass, showing overall high intensity but transversed by low-intensity bands. The nasal septum can not be recognized. The lesion reaches the left lamina cribrosa, but there is no evidence of erosion of this structure. The inferior and middle nasal conchae (*arrows*) are pushed against the lateral nasal wall. Inflammatory changes in the surrounding paranasal sinuses. **b** Coronal gadolinium-enhanced T1-weighted spin echo image shows a 'ring and arc' enhancement pattern. **c** Axial gadolinium-enhanced T1-weighted spin echo image. The lesion is centered on the nasal septum. The tumor was surgically removed. Histology showed low grade chondrosarcoma

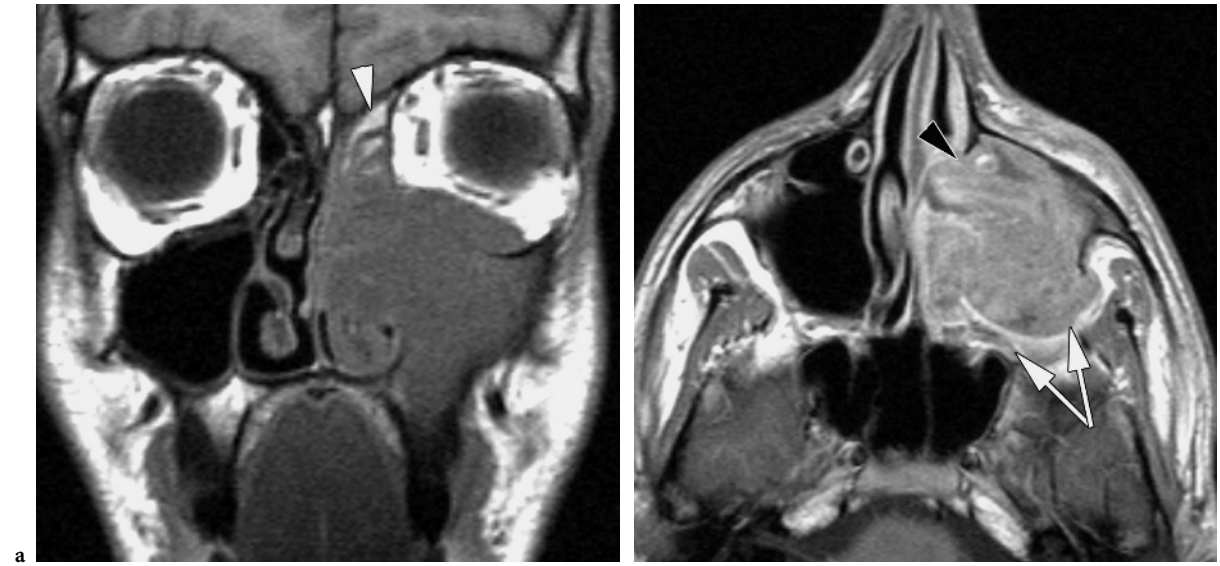

Fig. 11.24a,b. Coronal T1-weighted spin echo image (**a**) shows large mass in the left maxillary sinus, growing through the orbital floor, and into the nasal cavity and adjacent ethmoidal cells; high signal intensity just below the fovea ethmoidalis probably corresponds to thickened secretions (*white arrowhead*). Axial gadolinium-enhanced T1-weighted spin (**b**) also reveals posterior extension into the pterygopalatine fossa and retromaxillary fat (*arrows*); invasion of the nasolacrimal canal (*black arrowhead*). Rhabdomyosarcoma

of the cases, the mandible more frequently than the maxilla. Radiologically, multiple sharply demarcated osteolytic lesions are seen, usually with a diameter smaller than 2 cm; sometimes it may appear as confluent osteolytic lesions with poorly defined borders or as generalized osteoporosis. Solitary lesions may be difficult to differentiate from odontogenic tumors or odontogenic cysts.

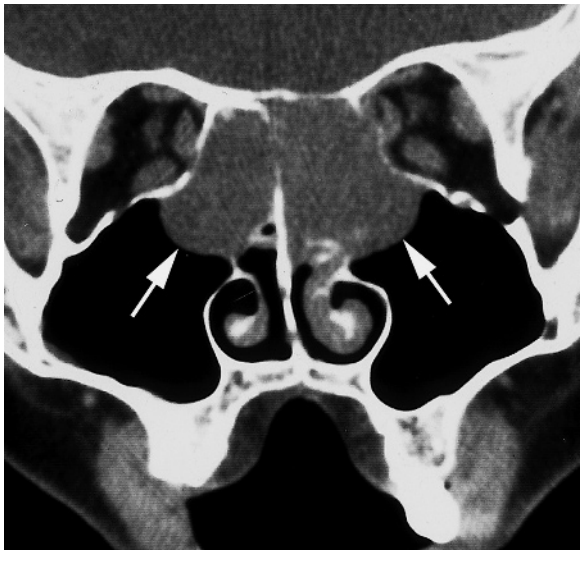

Fig. 11.25. Coronal CT image (soft tissue window). Polypoid nasoethmoidal soft tissue mass (*arrows*), bulging into the maxillary sinuses; destruction of ethmoidal septae and erosion of surrounding bone structures is seen. Non-Hodgkin lymphoma

Extramedullary plasmocytoma is an uncommon plasma cell neoplasm, arising most frequently from the soft tissues of the head and neck region, without evidence of systemic disease. The most common sites are the nose and the paranasal sinuses. The gross appearance is nonspecific (Fig. 11.26). It may spread to surrounding soft tissues and invade bone, and may show lymphatic metastasis. There is controversy as to whether extramedullary plasmacytoma is a separate clinicopathological entity, or a stage in the development of multiple myeloma. Intramedullary lesions often evolve to multiple myeloma after a few years whereas extramedullary lesions, commonly involving sinonasal structures, typically remain solitary (Bourjat et al. 1999).

11.5.2.4 Fibro-osseous Disease

The most important entities belonging to the heading fibro-osseous disease are fibrous dysplasia and ossifying fibroma.

Fibrous dysplasia is a condition in which normal medullary bone is replaced by an abnormal proliferation of fibrous tissue, resulting in asymmetrical distortion and expansion of bone; it may be con-

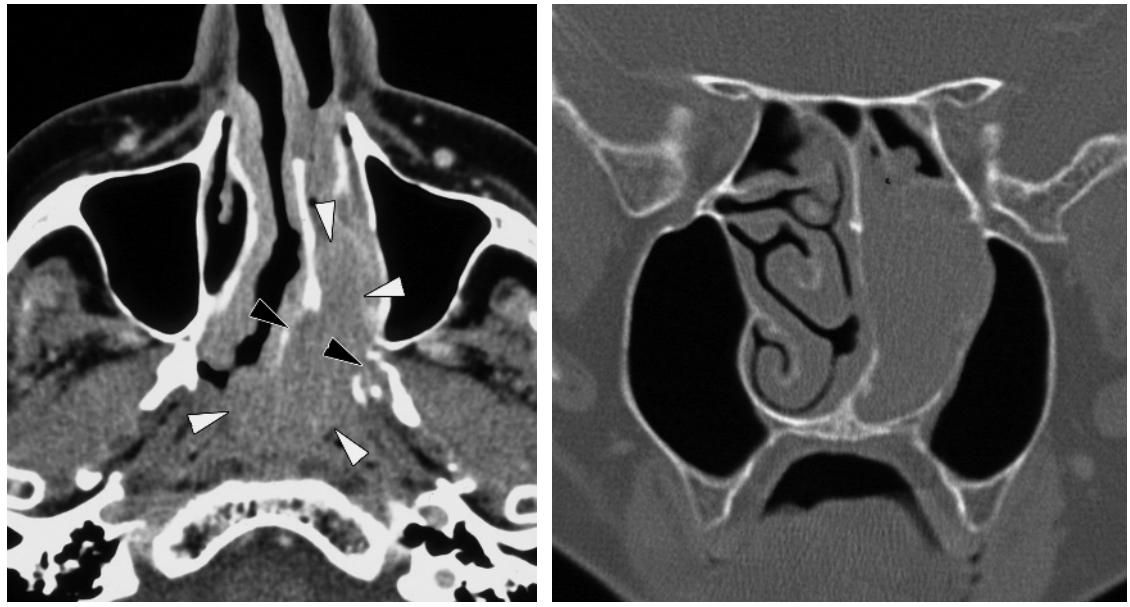

Fig. 11.26a,b. Axial contrast-enhanced (**a**) and coronal (bone window) CT image (**b**) in a 72-year-old patient. Soft tissue mass in left nasal cavity (*white arrowheads*), growing into the nasopharynx. Erosion of the posterior side of the nasal septum and pterygoid process (*black arrowheads*). On the coronal image, lysis is apparent of all three nasal turbinates, as well as bulging of the medial maxillary wall. Extramedullary plasmocytoma

fined to a single bone (monostotic fibrous dysplasia) or involve multiple bones (polyostotic fibrous dysplasia).

The monostotic form may involve any of the facial bones, but is most commonly seen in the maxilla. The association of the polyostotic form with sexual precocity and cutaneous pigmentation in a female patient is known as McCune-Albright syndrome.

Fibrous dysplasia is a disease of young patients. It may be an incidental finding. In the maxilla it usually presents with swelling and deformity of the cheek, but sometimes it causes nasal obstruction and/or orbital symptoms. Fibrous dysplasia may give rise to a mucocele. Involvement of the skull base may cause neurovascular compression. Extensive involvement of the face is referred to as leontiasis ossea.

Usually no new lesions appear after the cessation of skeletal growth. The lesions become more sclerotic with time but may continue to grow slowly into adulthood. Occasionally, reactivation of the lesions occurs during pregnancy.

Aggressive clinical behaviour of maxillary fibrous dysplasia has been described, causing pain and rapid development of a mass, although histopathological examination shows typical findings of fibrous dysplasia without evidence of malignancy. However, secondary malignant degeneration into a sarcoma (0.5% of cases) should be considered when stable or recurrent fibrous dysplasia produces pain or soft tissue extension.

Radiologically, fibrous dysplasia appears as enlarged bone with a dense ground-glass appearance; sometimes the lesions have a more osteolytic appearance, with regions of more dense calcification within them (Fig. 11.27). On MRI, the lesions usually have a low to intermediate signal intensity on all sequences, with marked contrast enhancement; incidentally found fibrous dysplasia may be confused with a neoplastic lesion on an MR study (Fig. 11.28).

Ossifying fibroma is a benign tumor composed of fibrous tissue and containing bone or osteoid. Ossifying fibroma of the craniofacial skeletal mainly, but not exclusively, occurs in children, hence the name juvenile ossifying fibroma (JOF). Two histopathological variants are distinguished: psammomatoid JOF and trabecular JOF (El-Mofty 2002). The imaging findings in JOF overlap with those in fibrous dysplasia (Commins et al. 1998). An aneurysmal bone cyst may develop in psammomatoid JOF; in such case, fluid levels are apparent on imaging studies. Both types may show a fast and aggressive growth pattern, eroding and invading the surrounding bone.

The term ossifying fibroma has also been used to describe odontogenic neoplasms in adults, which are also known as cemento-ossifying fibroma and cementifying fibroma.

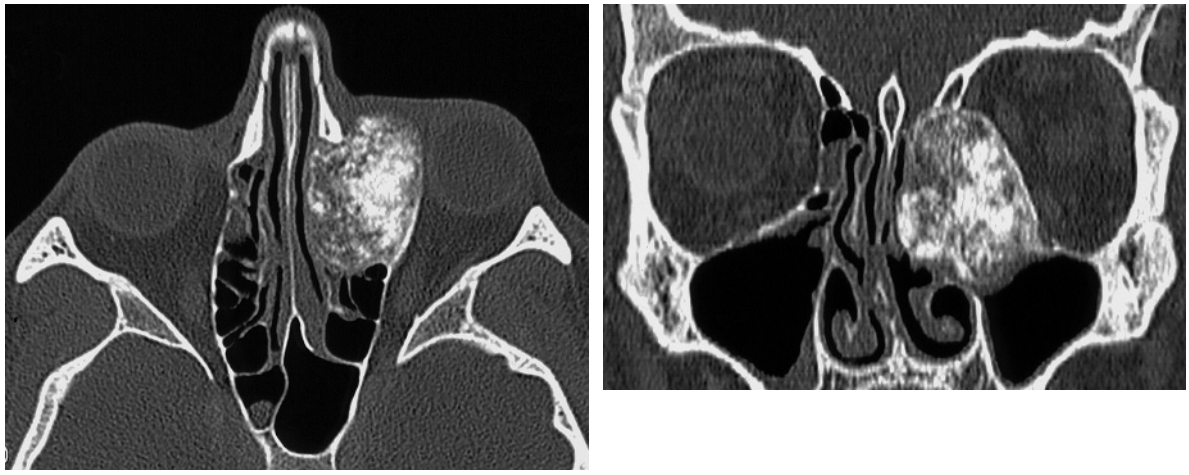

Fig. 11.27a,b. Axial (**a**) and coronal (**b**) CT images (bone window) in a 20-year-old patient with progressive naso-orbital swelling on the left. A largely calcified, well-delimited lesion is seen centered on the left ethmoid, involving the fovea ethmoidalis and lamina papyracea, and displacing the medial orbital wall and extending into the naso-orbital corner. The lesion was resected, and histologic examination showed fibrous dysplasia

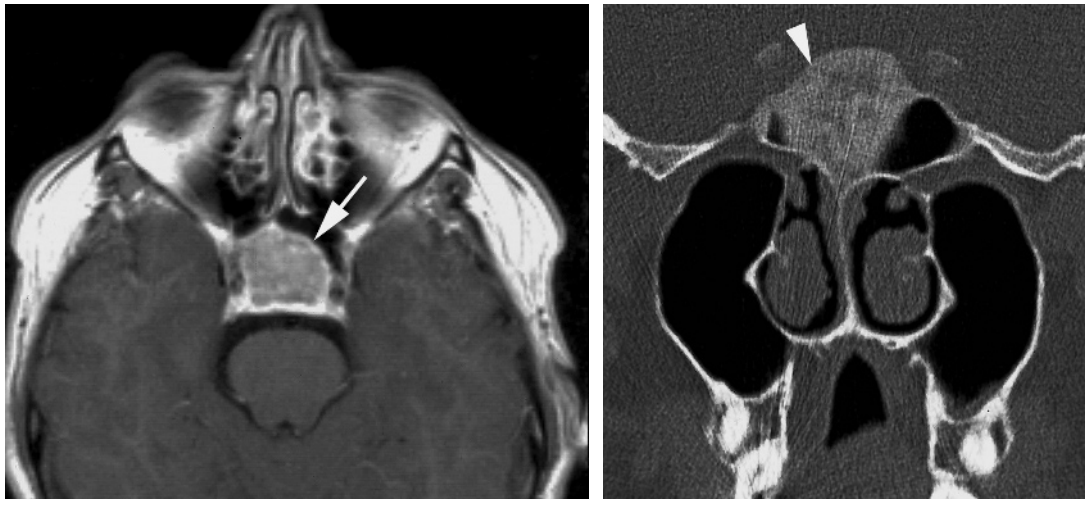

Fig. 11.28a,b. Patient presenting with episodes of visual disturbances. On an axial gadolinium-enhanced T1-weighted brain spin-echo image, an enhancing mass lesion is seen in the sphenoid sinus (**a**, *arrow*), initially suspected to correspond to a neoplastic lesion. Coronal CT image shows the typical ground-glass appearance of fibrous dysplasia (**b**, *arrowhead*)

11.6 Therapeutic Relevance of Imaging Findings

Many patients with malignant sinonasal neoplasms are managed surgically. Most cancers will require some form of transfacial surgical approach, with more or less extensive resection of sinonasal structures.

Preoperative imaging may influence the composition and approach of the surgical team treating a patient with sinonasal cancer (Ahmadi et al. 1993). Surgical resection of sinonasal neoplasms involving the anterior skull base requires a combined transfacial and transcranial approach to allow an en bloc resection of the tumor. This means that a neurosurgical team and a head and neck surgical team will work in close cooperation during such an anterior fossa craniofacial resection. This procedure is indicated for lesions involving or transgressing the anterior skull base, and should be considered when a tumor comes close to the skull base and is unlikely to be resected completely using a standard transfacial technique (Kraus and Andersen 1997). Dural invasion can usually be handled safely during a craniofacial resec-

tion, but cure (often at the expense of neurological sequelae) can hardly ever be obtained if brain invasion is present.

The surgical management of orbital involvement is controversial. In general, if the tumor has not grown through the periorbita, the eye may be surgically preserved (Eisen et al. 2000). Involved periorbita can be resected, but the functional results of patch reconstruction are not very good; furthermore, all these patients will need postoperative radiotherapy, including the orbit. Invasion of the orbital fat precludes complete resection of the tumor without orbital exenteration. In a number of cases, the final decision regarding orbital exenteration will have to made depending on the intra-operative findings (Maroldi et al. 1997).

Perineural extension towards the foramen rotundum and cavernous sinus makes surgical clearance of the tumor highly unlikely; it also suggests a low probability of cure with radiation therapy.

Nasal endoscopy has an important role in the diagnostic work-up of these patients, enhancing the traditional speculum and mirror examination of the nose, and being complementary to CT and/or MRI; endoscopy is also an excellent way to follow-up patients and look for early recurrences. In few cases endoscopic resection of a tumoral mass might be feasible. Imaging is essential in the selection of patients for such a limited intervention. The patients are to be advised of the possibility of proceeding with a traditional procedure because of tumor extent. Experience with this approach is relatively limited (Jorissen 1995; Levine et al. 1997; Goffart et al. 2000).

Surgery can be the sole treatment modality or part of a multimodality treatment plan, depending on tumor extent; often a combined treatment will be necessary. In advanced sinonasal cancer, surgery is often combined with radiation therapy to improve outcome. The radiation fields are individualized based on disease extent; the radiation dose to critical structures as the eye and brain should be as low as possible to avoid added morbidity. CT and/or MRI findings play an important role in this regard; in a postoperative situation the surgical and pathological findings also influence the radiation portal set-up.

11.7 Imaging After Therapy

Residual or recurrent cancer after therapy displays similar tissue characteristics on CT or MR studies, as the primary tumor before treatment. A focal, rounded, contrast-enhancing soft tissue mass within the previous tumor bed is suggestive for tumor recurrence (Fig. 11.29). However, after surgery and radiotherapy, scar, granulation tissue and/or

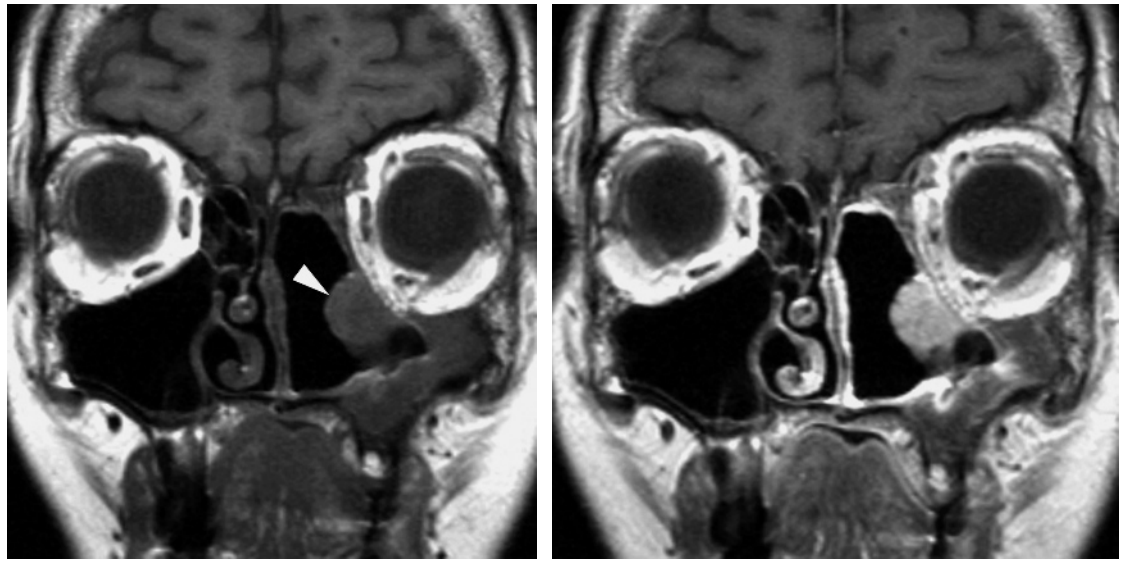

Fig. 11.29a,b. Patient treated by endoscopic surgery and radiotherapy for left-sided maxillary squamous cell carcinoma. At 2 years later, endoscopic examination was suspicious for tumor recurrence. Coronal T1-weighted spin-echo images, before (**a**) and after (**b**) injection of gadolinium, show nodular, enhancing mass lesion (*arrowhead*) abutting the floor of the left orbit. Some inflammatory changes are present in the left maxillary sinus. The lesion was resected and corresponded to recurrent cancer

inflammation is frequently present within the sinonasal cavity. Differentiating by imaging between a small focus of cancer and such non-neoplastic tissue changes may be very difficult. On MRI, the signal characteristics displayed by these various tissues may overlap with those of cancer (Loevner and Sonners 2002).

Currently, no clear guidelines concerning the use of imaging methods in the posttreatment surveillance of sinonasal cancer patients are available. In a study on 51 patients treated by radical surgery for malignant sinonasal neoplasms, subclinical tumor recurrence was detected with higher sensitivity by imaging (CT or MRI) than by clinical-endoscopic evaluation (89.7% versus 68.7%); the false positive rate with imaging was higher (4.7% versus 1.4%). The accuracy of imaging was slightly higher, but not significantly different from that of clinical-endoscopic examination (92.1% versus 88.8%) (Farina et al. 2001).

While interpreting a follow-up study, attention should be paid not only to the original tumor bed, but also to neural crossroads, such as the pterygopalatine fossa; tumor recurrence may become manifest as a soft tissue mass at some distance from the primary localisation by perineural spread (see Fig. 11.9)

References

Ahmadi J, Hinton DR, Segall HD, et al. (1993) Dural invasion by craniofacial and calvarial neoplasms: MR imaging and histopathologic evaluation. Radiology 188:747–749

Aoki J, Sone S, Fujioka F, Terayama K, Ishii K, Karakida O, Imai S, Sakai F, Imai Y (1991) MR of enchondroma and chondrosarcoma: rings and arcs of Gd-DTPA enhancement. J Comput Assist Tomogr 15:1011–1016

Barnes L, Brandwein M, Som PM (2001) Diseases of the nasal cavity, paranasal sinuses, and nasopharynx. In: Barnes L (ed) Surgical pathology of the head and neck, 2nd edn. Marcel Dekker, New York, pp 509-513, 516–517

Bourjat P, Kahn JL, Braun JJ (1999) Imagerie des plasmocytomes solitaires maxillo-mandibulaires. J Radiol 80:859–862

Buob D, Wacrenier A, Chevalier D, Aubert S, Quinchon JF, Gosselin B, Leroy X (2003) Schwannoma of the sinonasal tract: a clinicopathologic and immunohistochemical study of 5 cases. Arch Pathol Lab Med 127:1196–1199

Chang PC, Fischbein NJ, McCalmont TH, Kashani-Sabet M, Zettersten EM, Liu AY, Weissman JL (2004) Perineural spread of malignant melanoma of the head and neck: clinical and imaging features. AJNR Am J Neuroradiol 25:5–11

Commins DJ, Tolley NS, Milford CA (1998) Fibrous dysplasia and ossifying fibroma of the paranasal sinuses. J Laryngol Otol 112:964–968

Constantinidis J, Steinhart H, Koch M, Buchfelder M, Schaenzer A, Weidenbecher M, Iro H (2004) Olfactory neuroblastoma: the University of Erlangen-Nuremberg experience 1975–2000. Otolaryngol Head Neck 130:567–574

De Beuckeleer LH, De Schepper AM, Ramon F, Somville J (1995) Magnetic resonance imaging of cartilaginous tumors: a retrospective study of 79 patients. Eur J Radiol 21:34–40

De Vuysere S, Hermans R, Marchal G (2001) Sinochoanal polyp and its variant, the angiomatous polyp: MRI findings. Eur Radiol 11:55–58

Eisen MD, Yousem DM, Montone KT, et al. (1996) Use of preoperative MR to predict dural, perineural, and venous sinus invasion of skull base tumors. AJNR Am J Neurorad 17:1937–1945

Eisen MD, Yousem DM, Loevner LA, Thaler ER, Bilker WB, Goldberg AN (2000) Preoperative imaging to predict orbital invasion by tumor. Head Neck 22:456–462

El-Mofty S (2002) Psammomatoid and trabecular juvenile ossifying fibroma of the craniofacial skeleton: two distinct clinicopathologic entities. Oral Surg Oral Med Oral Pathol Oral Radiol Endod 93:296–304

Farina D, Battaglia G, Maculotti P, Marconi A, Maroldi R (2001) Effectiveness of imaging in detecting subclinical recurrence in the follow-up of 51 treated nasosinusal malignancies. Eur Radiol 11 (S1):199 (abstract)

Ginsberg LE, DeMonte F (1998) Imaging of perineural tumor spread from palatal carcinoma. AJNR Am J Neuroradiol 19:1417–1422

Goffart Y, Jorissen M, Daele J, Vander Poorten V, Born J, Deneufbourg JM, Zicot AF, Remacle JM (2000) Minimally invasive endoscopic management of malignant sinonasal tumours. Acta Otorhinolaryngol Belg 54:221–232

Graamans K, Slootweg PJ (1989) Orbital exenteration in surgery of malignant neoplasms of the paranasal sinuses. Arch Otolaryngol Head Neck Surg 115:977–980

Heffner DK, Gnepp DR (1992) Sinonasal fibrosarcomas, malignant schwannomas, and "Triton" tumors. A clinicopathologic study of 67 cases. Cancer 70:1089–1101

Hermans R, Horvath M, De Schrijver T, Lemahieu SF, Baert AL (1994) Extranodal non-Hodgkin lymphoma of the head and neck. J Belge Radiol 77:72–77

Hermans R, De Vuysere S, Marchal G (1999) Squamous cell carcinoma of the sinonasal cavities. Semin Ultrasound CT MR 20:150–161

Herrmann BW, Sotelo-Avila C, Eisenbeis JF (2003) Pediatric sinonasal rhabdomyosarcoma: three cases and a review of the literature. Am J Otolaryngol 24:174–180

Jorissen M (1995) The role of endoscopy in the management of paranasal sinus tumours. Acta Otorhinolaryngol Belg 49:225–228

Kadish S, Goodman M, Wang CC (1976) Olfactory neuroblastoma: a clinical analysis of 17 cases. Cancer 37:1571–1576

Kim HJ, Kim JH, Kim JH, Hwang EG (1995) Bone erosion caused by sinonasal cavernous hemangioma: CT findings in two patients. AJNR Am J Neuroradiol 16:1176–1178

Kim GE, Park HC, Keum KC, et al. (1999) Adenoid cystic carcinoma of the maxillary antrum. Am J Otolaryngol 20:77–84

Kim BS, Vongtama R, Juillard G (2004) Sinonasal undifferentiated carcinoma: case series and literature review. Am J Otolaryngol 25:162–166

Kraus DH, Lanzieri CF, Wanamaker JR, Little JR, Lavertu P (1992) Complementary use of computed tomography and

magnetic resonance imaging in assessing skull base lesions. Laryngoscope 102:623–629
Kraus DH, Andersen PE (1997) Anterior fossa craniofacial resection: techniques. In: Kraus DH, Levine HL (eds) Nasal neoplasia. Thieme, New York, pp 119–139
Lee HM, Kang HJ, Lee SH (2005) Metastatic renal cell carcinoma presenting as epistaxis. Eur Arch Otorhinolaryngol 262:69–71
Levine HL, Timen SM, Papsidero MJ (1997) Endoscopic management of nasal and sinus neoplasms. In: Kraus DH, Levine HL (eds) Nasal neoplasia, Thieme, New York, pp 175–181
Loevner LA, Sonners AI (2002) Imaging of neoplasms of the paranasal sinuses. Magn Reson Imaging Clin N Am 10:467–493
Lloyd GAS (1988) Epithelial tumours. In: Diagnostic imaging of the nose and paranasal sinuses. Springer Verlag, London, pp 95–110
Mancuso AA, Harnsberger HR, Dillon WP (1988) Paranasal sinuses, nasal cavity, and facial bones. In: Workbook for MRI and CT of the head and neck, 2nd edn. Williams & Wilkins, Baltimore, pp 56–76
Maroldi R, Farina D, Battaglia G, Maculotti P, Nicolai P, Chiesa A (1997) MR of malignant nasosinusal neoplasms. Frequently asked questions. Eur J Radiol 24:181–190
Matias C, Corde J, Soares J (1988) Primary malignant melanoma of the nasal cavity. J Surg Oncol 39:29–32
Medina JE, Ferlito A, Pellitteri PK, Shaha AR, Khafif A, Devaney KO, Fisher SR, O'Brien CJ, Byers RM, Robbins KT, Pitman KT, Rinaldo A (2003) Current management of mucosal melanoma of the head and neck. J Surg Oncol 83:116–122
Miyamoto CT, Brady LW, Markoe A, Salinger D (1991) Ameloblastoma of the jaw. Treatment with radiation therapy and a case report. Am J Clin Oncol 14:225–230
Miyamoto RC, Gleich LL, Biddinger PW, Gluckman JL (2000) Esthesioneuroblastoma and sinonasal undifferentiated carcinoma: impact of histological grading and clinical staging on survival and prognosis. Laryngoscope 110:1262–1265
Murphey MD, Smith WS, Smith SE, Kransdorf MJ, Temple HT (1999) (From the archives of the AFIP 1999) Imaging of musculoskeletal neurogenic tumors: radiologic-pathologic correlation. Radiographics 19:1253–1280
Nemzek WR, Hecht S, Gandour-Edwards R, et al. (1998) Perineural spread of head and neck tumors: how accurate is MR imaging? AJNR Am J Neuroradiol 19:701–706
Pasquini E, Sciarretta V, Farneti G, Modugno GC, Ceroni AR (2004) Inverted papilloma: report of 89 cases. Am J Otolaryngol 25:178–185
Parsons JT, Stringer SP, Mancuso AA, Million RR (1994) Nasal vestibule, nasal cavity, and paranasal sinuses. In: Million RR, Cassisi NJ (eds) Management of head and neck cancer: a multidisciplinary approach. J.B. Lippincott Company, Philadelphia, pp 551–598
Prasad ML, Busam KJ, Patel SG, Hoshaw-Woodard S, Shah JP, Huvos AG (2003) Clinicopathologic differences in malignant melanoma arising in oral squamous and sinonasal respiratory mucosa of the upper aerodigestive tract. Arch Pathol Lab Med 127:997–1002
Patel SG, Prasad ML, Escrig M, Singh B, Shaha AR, Kraus DH, Boyle JO, Huvos AG, Busam K, Shah JP (2002) Primary mucosal malignant melanoma of the head and neck. Head Neck 24:247–257
Regenbogen VS, Zinreich SJ, Kim KS, Kuhajda FP, Applebaum BI, Price JC, Rosenbaum AE (1988) Hyperostotic esthesioneuroblastoma: CT and MR findings. J Comput Assist Tomogr 12:52–56
Simon D, Somanathan T, Ramdas K, Pandey M (2003) Central mucoepidermoid carcinoma of mandible – a case report and review of the literature. World J Surg Oncol 1:1. doi:10.1186/1477–7819–1–1
Som PM, Shapiro MD, Biller HF, Sasaki C, Lawson, W (1988) Sinonasal tumors and inflammatory tissues: differentiation with MR imaging. Radiology 167:803-808
Suarez C, Llorente JL, Fernandez De Leon R, Maseda E, Lopez A (2004) Prognostic factors in sinonasal tumors involving the anterior skull base. Head Neck 26:136–144
Tart RP, Mukherji SK, Avino AJ, et al. (1993) Facial lymph nodes: normal and abnormal CT appearance. Radiology 188:695–700
Thompson LD, Gyure KA (2000) Extracranial sinonasal tract meningiomas: a clinicopathologic study of 30 cases with a review of the literature. Am J Surg Pathol 24:640–650
UICC, International Union Against Cancer (2002) TNM classification of malignant tumours, 6th edn. Wiley-Liss, New York, p 43–45
Vanhoenacker P, Hermans R, Sneyers W, Vanderperre H, Clarysse J, Loncke R, Baert AL (1993) Atypical aesthesioneuroblastoma: CT and MRI findings. Neuroradiology 35:466–467
Verbin RS, Appel BN (2001) Odontogenic tumors. In: Barnes L (ed) Surgical pathology of the head and neck, 2nd edn. Marcel Dekker, New York, pp 1557–1648
Wiseman SM, Popat SR, Rigual NR, Hicks WL Jr, Orner JB, Wein RO, McGary CT, Loree TR (2002) Adenoid cystic carcinoma of the paranasal sinuses or nasal cavity: a 40-year review of 35 cases. Ear Nose Throat J 81:510–517
Yousem DM, Fellows DW, Kennedy DW, Bolger WE, Kashima H, Zinreich SJ (1992) Inverted papilloma: evaluation with MR imaging. Radiology 185:501–505
Zwahlen RA, Grätz KW (2002) Maxillary ameloblastomas: a review of the literature and of a 15-year database. J Craniomaxillofac Surg 30:273–279

12 Parotid Gland and Other Salivary Gland Tumors

Frédérique Dubrulle and Raphaëlle Souillard

CONTENTS

F. Dubrulle, MD; R. Souillard, MD
Plateau Technique d'Imagerie, Hôpital Huriez Sud, CHU Lille, 59000 Lille, France

12.1 Introduction

The parotid gland is the largest salivary gland. It is located in the parotid space. The parotid gland can be affected by a variety of pathologic processes, especially neoplastic. Parotid tumors represent less than 3% of all head and neck tumors and are most frequently benign. These tumors require surgery in most cases and imaging is essential in the work-up of these lesions.

12.2 Anatomy

The parotid space is a paired lateral suprahyoid neck space surrounded by the superficial layer of the deep cervical fascia. This space extends from the external auditory canal and the mastoid tip superiorly to the angle of the mandible below. It contains the parotid gland, intra- and extra-parotid lymph nodes. The gland contains about 20 intraglandular lymph nodes which are considered normal if their transverse diameter is less than 8 mm. The gland also contains extracranial branches of the facial nerve, and vessels: the external carotid artery and the retromandibular vein just behind the mandibular ramus (Fig. 12.1).

The facial nerve exits the skull base via the stylomastoid foramen and continues within the parotid gland from its posterior and superior part to its anterior and inferior part, lateral to the retromandibular vein. It then divides into superior temporofacial branches and inferior cervical branches. By convention, the facial nerve is used as a reference plane within the gland to separate the external superficial lobe and the internal deep lobe, but actually there is no true anatomic division. The facial nerve is not seen with imaging and its course can only be estimated (Fig. 12.1) (Harnsberger 2004).

The parotid space is directly lateral to the anterior part of the parapharyngeal space (prestyloid space),

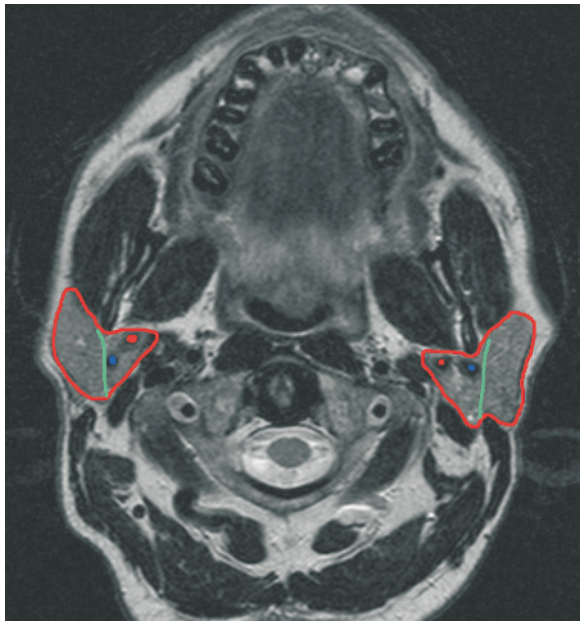

Fig. 12.1. Anatomy of the parotid space. The parotid space (outlined in *red*) is made of the parotid gland, the retromandibular vein (*blue circle*), the external carotid artery (*red circle*) and intra- and extra-parotid lymph nodes. It also contains the facial nerve, which is not directly seen on imaging; it is used as a reference plane (*green line*) to separate the parotid gland into an external superficial lobe and an internal deep lobe

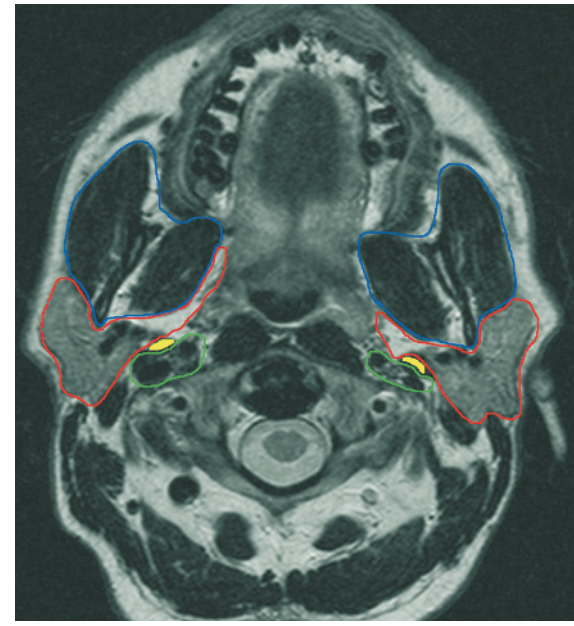

Fig. 12.2. Lateral and internal to the parotid space is the anterior part of the parapharyngeal space (or prestyloid compartment) (both outlined in *red*); there is no real anatomic division between these two spaces. The most internal part of the deep parotid lobe bulges in the prestyloid compartment. Posterior (retrostyloid) part of the parapharyngeal space, also called the carotid space (outlined in *green*), separated from the anterior parapharyngeal space by the styloid process (indicated in *yellow*), as well as muscles and a fascial layer originating from it (see also Chap. 9). Masticator space (outlined in *blue*)

without real anatomic division between these two spaces. The deep portion of the parotid gland bulges in the prestyloid compartment in which deep lobe tumors can extend (Fig. 12.2). The prestyloid compartment also contains fat tissue, accessory salivary glands and a prestyloid branch of the mandibular nerve (V3).

Anterior to the parotid space is the masticator space or infratemporal fossa, which contains the pterygoid muscles.

Posterior to the prestyloid parapharyngeal space is the carotid space or retrostyloid parapharyngeal space (Fig. 12.2).

There is an anatomic division between these different spaces (the masticator space, the carotid space and the anterior parapharyngeal space). Benign tumors will respect these anatomic limits whereas they will be infiltrated by malignant tumors.

The parotid gland also contains salivary ducts. The main parotid duct, or Stensen's duct, emerges from the anterior part of the parotid gland, runs over the masseter muscle and in the superficial cervical fascia and then abruptly courses medially to pierce the buccinator muscle, forming a nearly 90° angle with this muscle, terminating in the buccal mucosa at the level of the second upper molar (Fig. 12.3).

12.3 Imaging Issues

When a patient presents with a palpable mass of the parotid space, the radiologist has to answer several key questions, which are essential to the head and neck surgeon in order to determine the best therapy (Harnsberger 2004; Shah 2002; Vogl et al. 1999):

- *Is the mass intra- or extraparotid?* Small, intraparotid masses are easy to identify. For large and deep lobe masses, the knowledge of the different cervical spaces is essential. The pattern of displacement of the prestyloid parapharyngeal space has to be analyzed.
- *Is the parotid space mass single or multiple? Unilateral or bilateral?* Multiple lesions are suggestive

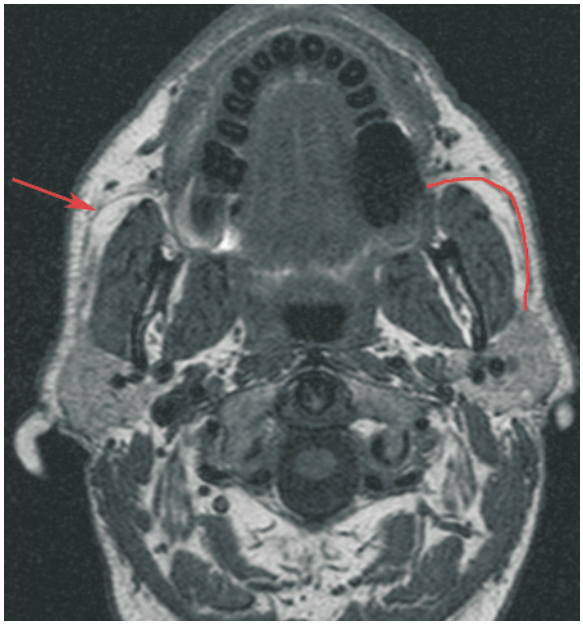

Fig. 12.3. The main parotid salivary duct canal or Stensen's duct (*red*) emerges from the anterior part of the parotid gland, runs over the masseter muscle and in the superficial cervical fascia, then forms a 90° angle (*arrow*), pierces the buccinator muscle to terminate in the oral cavity at level of the second upper molar

for specific tumors: for example, bilateral tumors are suggestive of Warthin's tumor, multiple cystic formations suggest Sjögren's syndrome or benign lymphoepithelial lesions possibly related to HIV.

- *Does the tumor show benign or malignant characteristics?* The surgical approach will depend on these characteristics. If malignancy is suspected, is there evidence of perineural spread along the facial nerve or branches of the trigeminal nerve? In that case, the therapeutic attitude will be different.
- *Is the tumor limited to the superficial lobe of the parotid?* A superficial parotidectomy is sufficient for a benign, well-circumscribed, superficial lobe lesion. On the other hand, a superficial lesion extending in the deep lobe requires a total parotidectomy (O'Brien 2003).
- *What is the relationship of the mass to the facial nerve?* The facial nerve is not seen on imaging but its intraparotid course can be estimated (plane between the stylomastoid foramen and the lateral border of the retromandibular vein).
- *Is it possible to determine the histologic type of a benign tumor?* A pleomorphic adenoma of the parotid gland will require surgery, whereas Warthin's tumor in elderly patients may be followed up clinically and by imaging.

In order to answer all these key questions, MR imaging is the primary modality of choice for parotid gland tumors (Joe and Westesson 1994; Shah 2004).

The classical sequences used are: axial and coronal turbo spin-echo T2-weighted and spin-echo T1-weighted sequences with a slice thickness of 2–3 mm and a spin-echo T1-weighted sequence after contrast administration. A sequence with fat saturation after contrast administration is useful to better visualise potential perineural extension along the facial nerve or intracranial extension. This sequence is also useful to analyze correctly the tumoral enhancement.

A sequence to analyze the cervical lymph nodes is necessary if a malignant tumor is suspected. MR sialography can be useful if a pseudo-tumoral pathology such as Sjögren syndrome is suspected.

Diffusion-weighted sequence with calculation of an ADC map may be interesting to better characterize non specific tumors (Ikeda et al. 2004).

12.4 Benign Parotid Tumors

Benign tumors of the parotid gland represent about 85% of all parotid tumors (Okahara et al. 2003).

12.4.1 Benign Mixed Tumor or Pleomorphic Adenoma

12.4.1.1 General Description

This is the most common parotid gland tumor and it represents 70%–80% of all tumors of the parotid gland. The lesion is usually solitary. Of all pleomorphic adenomas, 90% occur in the superficial lobe. If the lesion originates from the deep lobe, it can become large, extending in the anterior parapharyngeal space without causing symptoms.

There is a female predominance (sex ratio: 2/1). Facial nerve paralysis is uncommon.

12.4.1.2 Histological Findings

Pleomorphic adenoma is encased in a capsule that may be incomplete. It contains epithelial, myoepithelial and stromal (mucoid, myxoid, chondroid) cellular components. Calcifications are rare. Sites of cystic

changes and hemorrhage may be present, especially if the tumor is large.

The lesion may show multicentric outgrowths through its capsule. For this reason, partial parotidectomy is recommended whenever a pleomorphic adenoma is suspected, provided the tumor can be removed with a safe margin. The risk of recurrence is very high when only an enucleation of the tumor is performed. In some centers, even total parotidectomy is routinely performed for pleomorphic adenoma, in order to limit the risk of recurrence as much as possible.

12.4.1.3 Imaging Findings

- Typically, pleomorphic adenoma is a solitary, well-circumscribed mass. It may be lobulated. This tumor has low T1-weighted and high T2-weighted signal intensities. It may demonstrate a low T2-weighted signal intensity capsule. It shows homogeneous enhancement on T1 contrast-enhanced images, well illustrated on delayed contrast-enhanced T1-weighted images with fat saturation (Figs. 12.4, 12.5) (Ikeda et al. 1996). Imaging findings may be less typical in the case of larger tumors, but the lesion remains lobulated and well-circumscribed. Areas of hemorrhage appear as regions of high signal intensity on both T1- and T2-weighted images (Fig. 12.6). Myxoid degeneration appears as heterogeneous and intermediate T2-weighted signal intensity (Fig. 12.7). In these large tumors, signal intensity can be heterogeneous on early contrast-enhanced images but it can appear more homogeneous on delayed contrast-enhanced, fat-suppressed T1-weighted images (Fig. 12.4). An extension to the deep lobe of the parotid gland must be looked for and reported. Large tumors of the deep lobe are usually mixed tumors (Figs. 12.8, 12.9).
- Non-typical forms of pleomorphic adenoma are rare. These lesions have a low T2-weighted signal intensity which corresponds to fibrous tissue (Fig. 12.10). The correct diagnosis may be difficult but a solitary, well-circumscribed, encapsulated lesion is suggestive of benign tumor (Harnsberger 2004).
- Calcified lesions are uncommon; these calcifications occur after a long evolution.
- Recurrent pleomorphic adenoma tends to be multifocal and more aggressive (Fig. 12.11).
- Malignant degeneration within a pleomorphic adenoma is rare but exists. The most common type of malignancy associated with pleomorphic adenoma is a carcinoma ex pleomorphic adenoma, or sometimes an adenocarcinoma. Malignant characteristics are then present on imaging studies (see below).

12.4.1.4 Differential Diagnosis

- *Warthin's tumor or papillary cystadenoma lymphomatosum.* Especially in the case of non-typical imaging findings of pleomorphic adenoma (see Sect. 12.6 below).
- *Malignant tumor.* Features suggesting malignancy are heterogeneous enhancement, an infiltrating mass with irregular margins, perineural tumor spread or infiltration of adjacent fat tissue.
- *Non-Hodgkin lymphoma of the parotid gland.* The clinical presentation may be suggestive (see below and Chap. 16).
- Parotid nodal metastasis (often from skin carcinoma or melanoma, sometimes systemic metastasis).

12.4.2 Warthin's Tumor or Papillary Cystadenoma Lymphomatosum

12.4.2.1 General Description

This is the second most frequent benign tumor arising in the parotid gland and it represents 10%–25% of all parotid tumors.

It is more common in males than in females (sex ratio: 3/1). The mean age at presentation is 60 years old. About 90% of patients with this tumor are cigarette smokers. This diagnosis should not be suggested before the age of 40 years old (Harnsberger 2004).

It arises almost exclusively in the lower portion of the superficial lobe of the parotid gland. There is a bilateral involvement in 15%–20% of patients, which presents simultaneously or metachronously, the contralateral location may be discovered on imaging only.

These are slow-growing tumors and malignant transformation is uncommon, occurring in less than 1% of Warthin's tumors.

The recommended treatment is superficial parotidectomy, sparing the intraparotid facial nerve. Considering the slow-growing nature of this tumor and its very low risk of degeneration, a clinical and radiological follow-up can be proposed especially in elderly people in whom the diagnosis of Warthin's tumor is suspected on imaging.

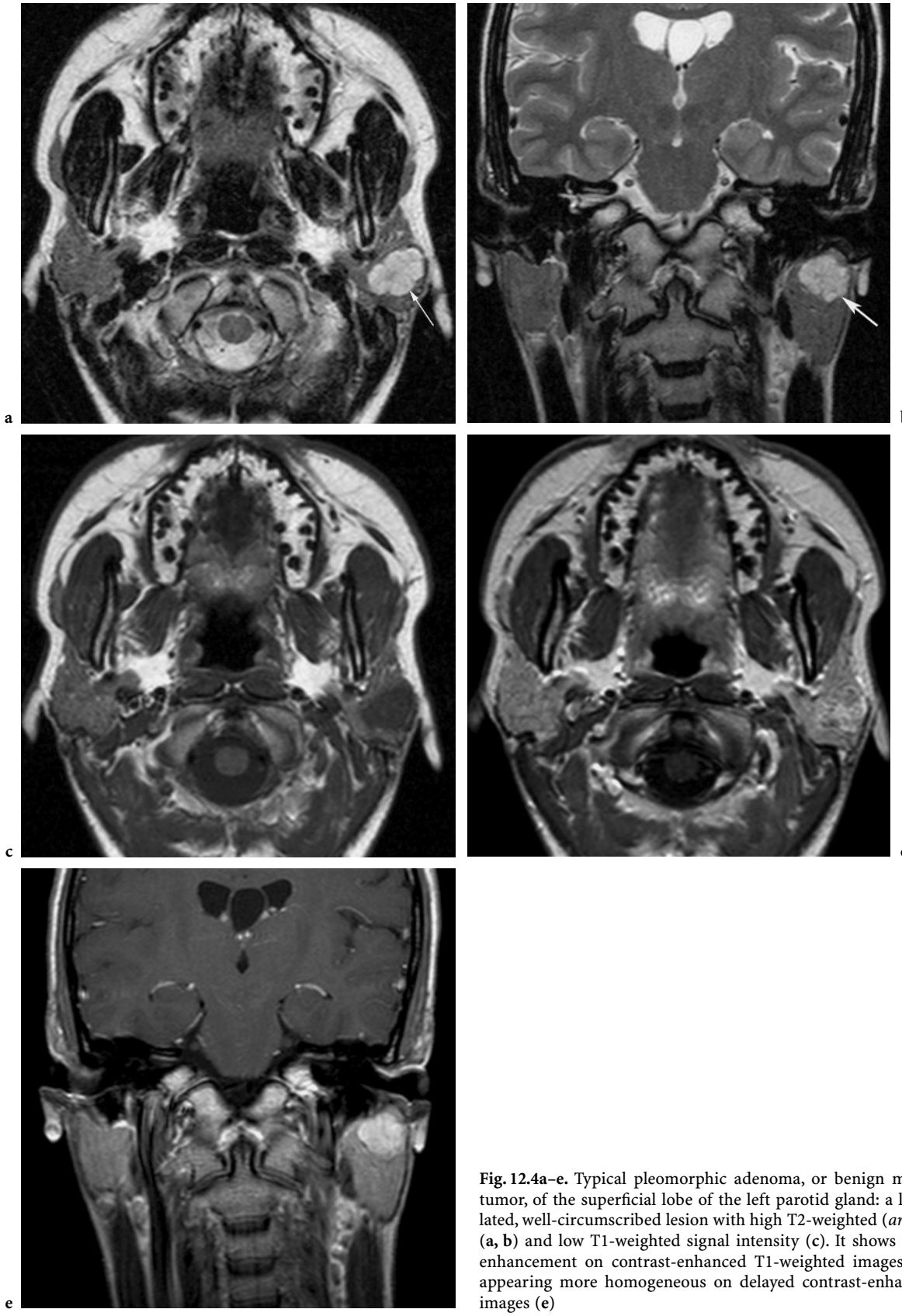

Fig. 12.4a–e. Typical pleomorphic adenoma, or benign mixed tumor, of the superficial lobe of the left parotid gland: a lobulated, well-circumscribed lesion with high T2-weighted (*arrow*) (**a, b**) and low T1-weighted signal intensity (**c**). It shows clear enhancement on contrast-enhanced T1-weighted images (**d**), appearing more homogeneous on delayed contrast-enhanced images (**e**)

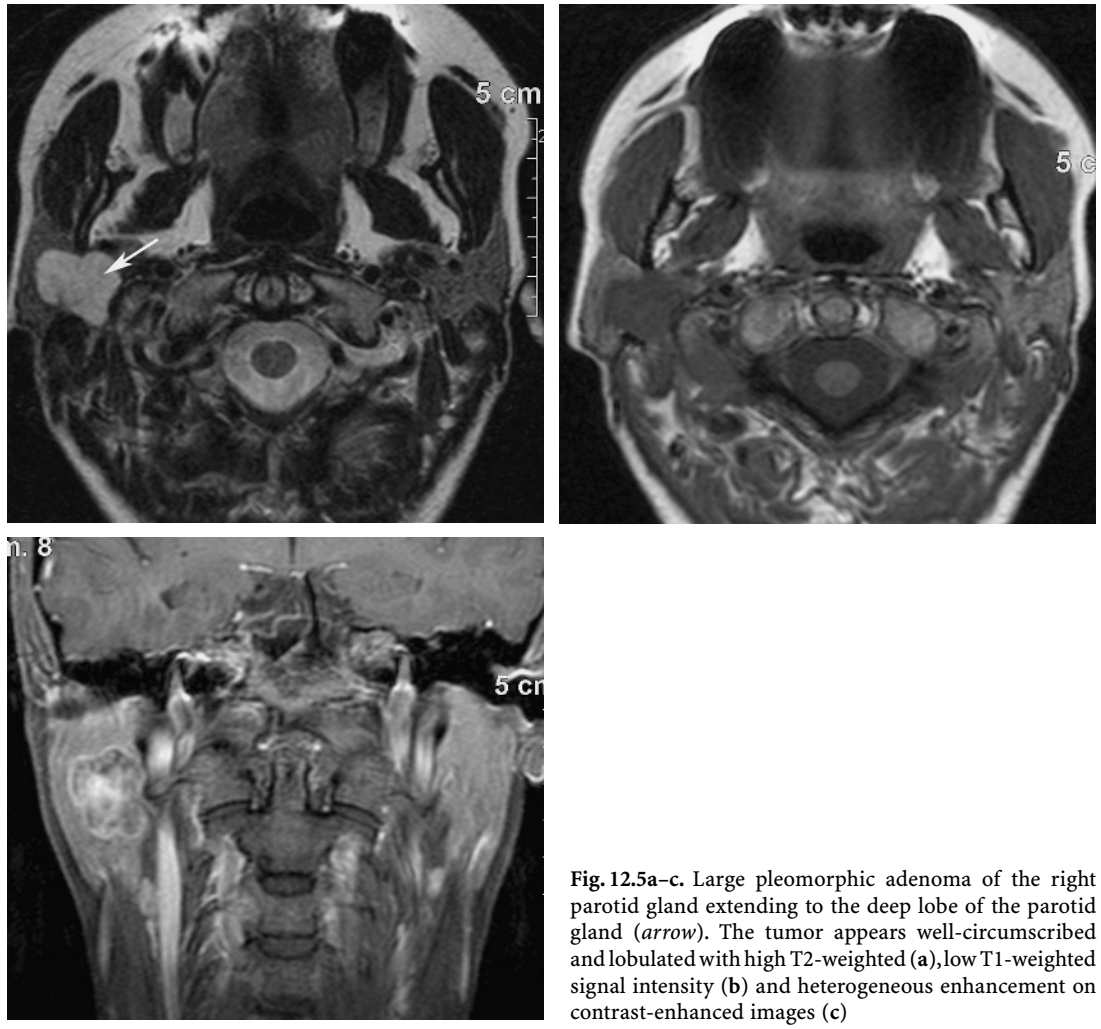

a b c

Fig. 12.5a–c. Large pleomorphic adenoma of the right parotid gland extending to the deep lobe of the parotid gland (*arrow*). The tumor appears well-circumscribed and lobulated with high T2-weighted (**a**), low T1-weighted signal intensity (**b**) and heterogeneous enhancement on contrast-enhanced images (**c**)

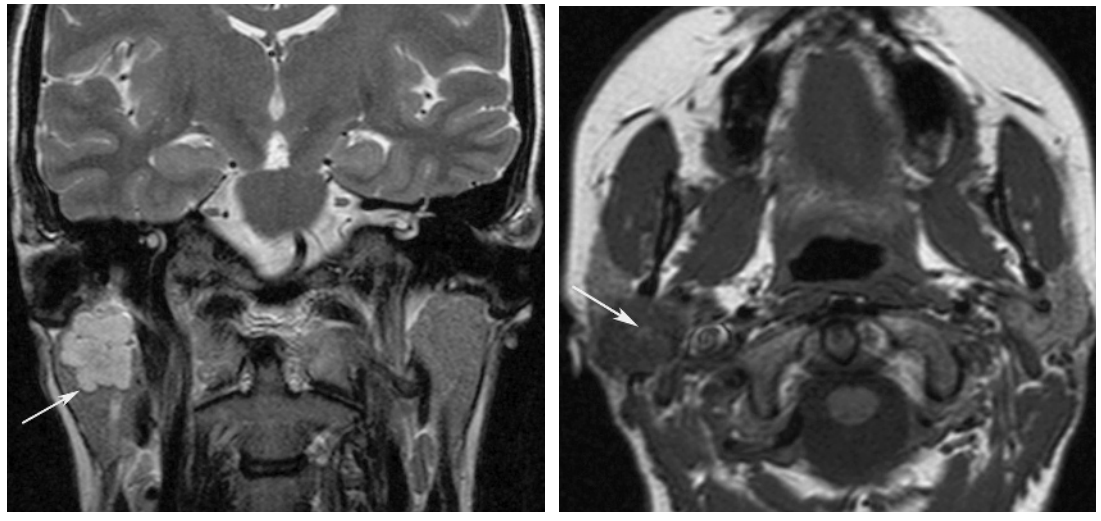

a b

Fig. 12.6a,b. Pleomorphic adenoma of the right parotid gland: a well-delineated, lobulated tumor showing a typically high T2-weighted signal intensity and a low signal intensity "capsule" (*arrow*) (**a**). On the plain T1-weighted images (**b**), the tumor has a low signal intensity with small regions of high T1-weighted signal intensity, corresponding to hemorrhagic areas (*arrow*)

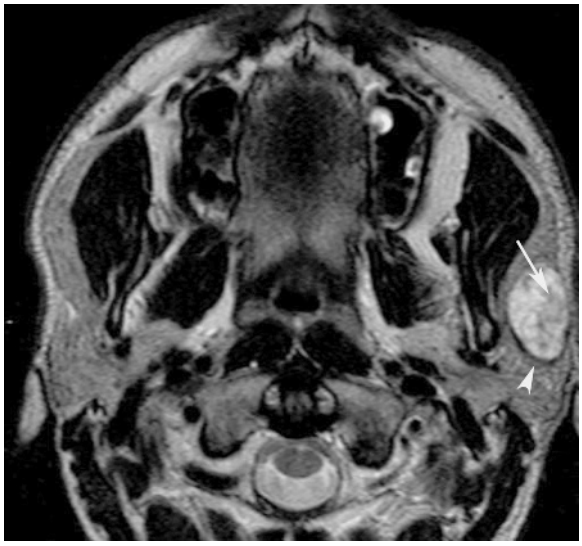

Fig. 12.7. Pleomorphic adenoma of the left parotid gland with a high T2-weighted signal intensity and small heterogeneous areas of lower signal intensity, related to myxoid degeneration (*arrow*). The capsule is well identified (*arrowhead*)

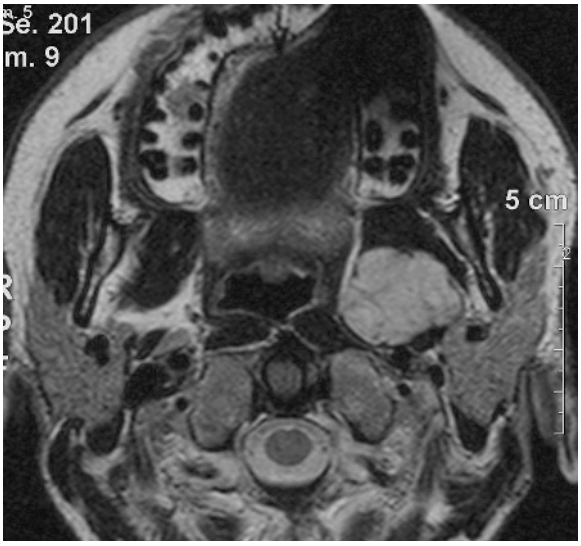

Fig. 12.8. Pleomorphic adenoma extending to the left anterior parapharyngeal space with typical high signal on T2-weighted images

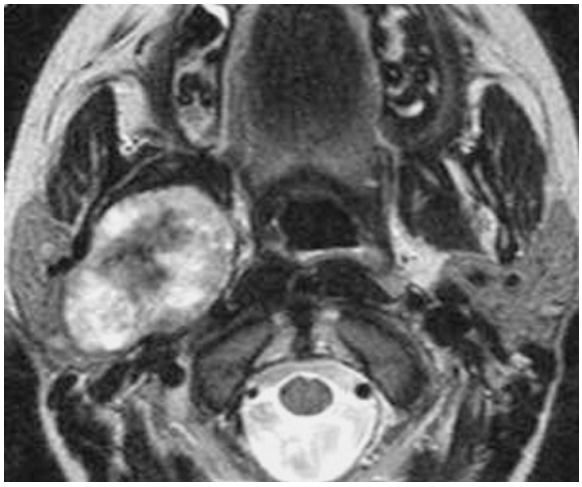

Fig. 12.9. Large pleomorphic adenoma of the deep lobe of the right parotid gland with non-homogeneous, high signal intensity on this T2-weighted image. Larger tumors typically show slightly heterogeneous signal intensity

12.4.2.2 Histological Findings

The papillary cystadenoma lymphomatosum is encapsulated. It arises within the lymphoid tissue of the parotid gland and is composed of lymphoid stroma and epithelium. The epithelial component is characterized by cystic spaces; it can show hemorrhagic areas. For these reasons, Warthin's tumors tend to be nonhomogeneous on imaging.

12.4.2.3 Imaging Findings

Warthin's tumor has typically a heterogeneous appearance on imaging, due to cystic and hemorrhagic changes, with overall benign characteristics: a well-circumscribed lesion measuring 2–4 cm in diameter.

The tumor has low T1-weighted signal intensity, with small areas of high signal intensities due to accumulation of proteinous fluid, cholesterol crystals or hemorrhagic changes. Such areas are seen in about 60% of the cases and are typical of the diagnosis of Warthin's tumor (Figs. 12.12, 12.13) (Ikeda et al. 2004).

The tumor has intermediate and high T2-weighted signal intensities. The high signal intensities areas correspond to cystic foci.

It shows a mild enhancement on contrast-enhanced T1-weighted images. Cystic spaces show no enhancement. A typical aspect of the tumor is a ring enhancement (Fig. 12.12). Fat-suppressed, contrast-enhanced T1-weighted images illustrate better the heterogeneous enhancement of the tumor.

Multiple lesions in one parotid gland or bilaterally have to be looked for. Bilateral lesions in the lower parts of the parotid glands are virtually pathognomonic (Figs. 12.13, 12.14).

Warthin's tumor may extend to the deep lobe of the parotid gland (Fig. 12.13). On the other hand, a primary location in the deep lobe is very rare.

On diffusion-weighted imaging, Warthin's tumors present a low ADC value (Ikeda et al. 2004).

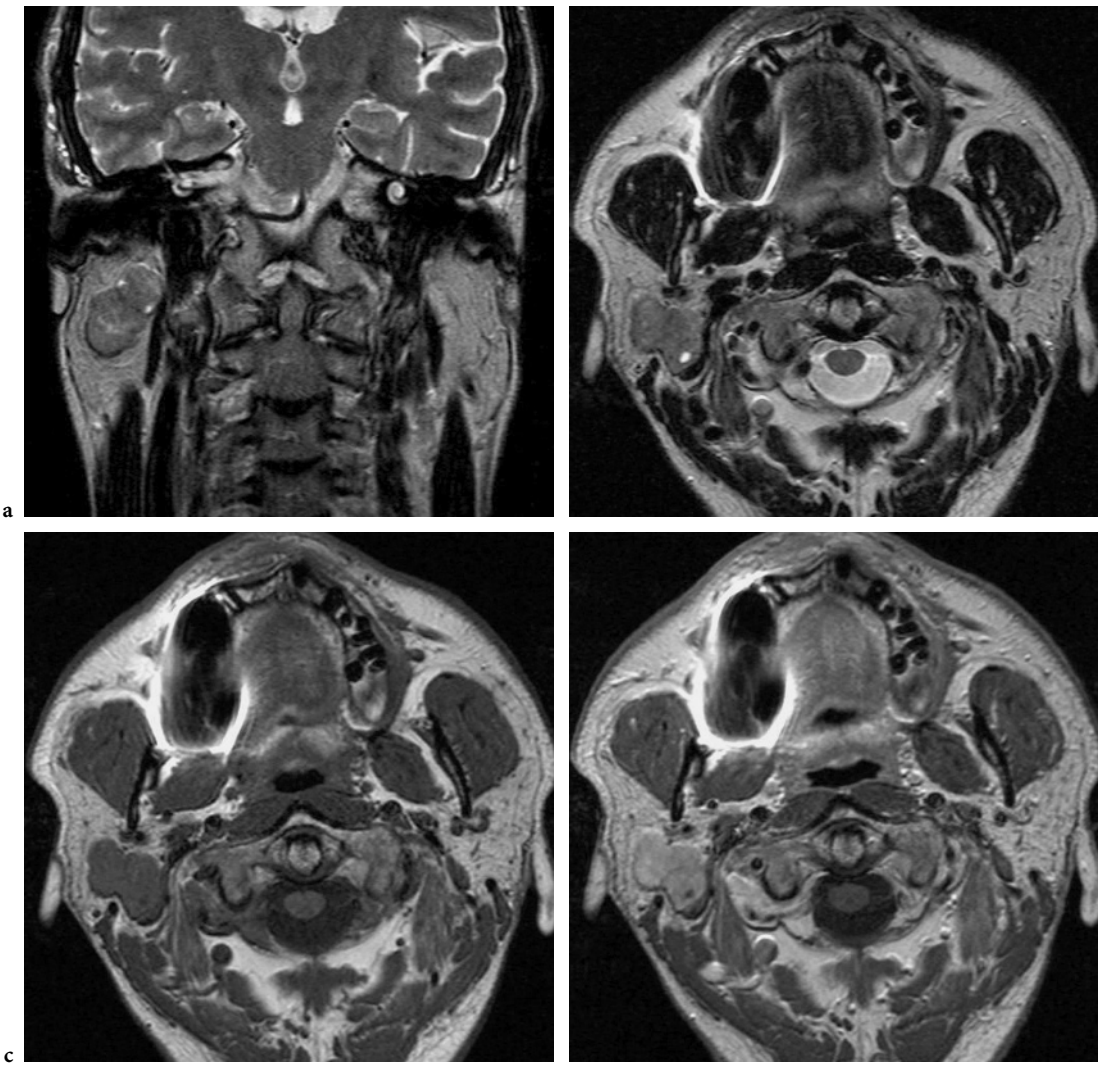

Fig. 12.10a–d. Atypical pleomorphic adenoma of the left parotid gland, with a low T2-weighted signal intensity (**a,b**), and low T1-weighted signal intensity (**c**). This tumor, however, shows benign characteristics: a well-delineated, sharply outlined mass with homogeneous enhancement (**d**)

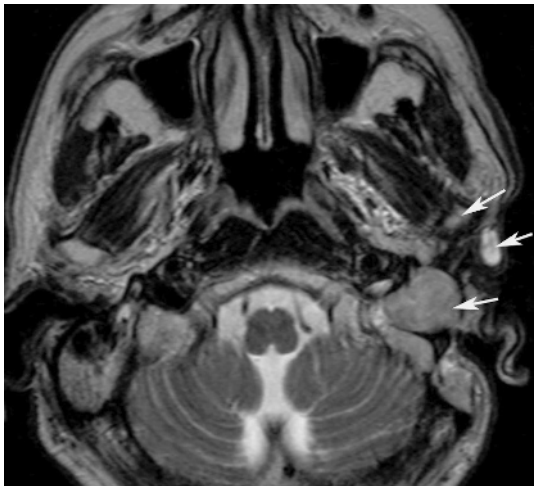

Fig. 12.11. Multifocal recurrent pleomorphic adenoma after partial parotidectomy (*arrows*)

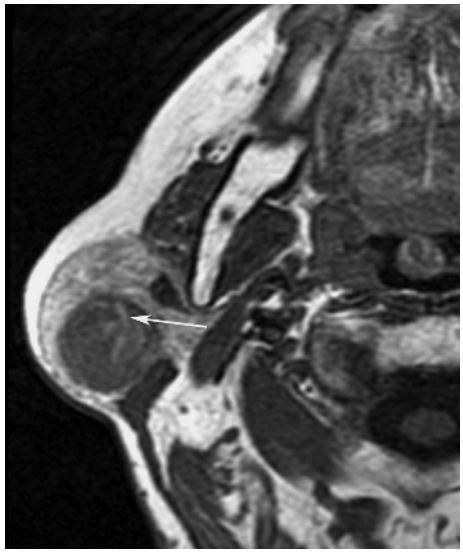

a

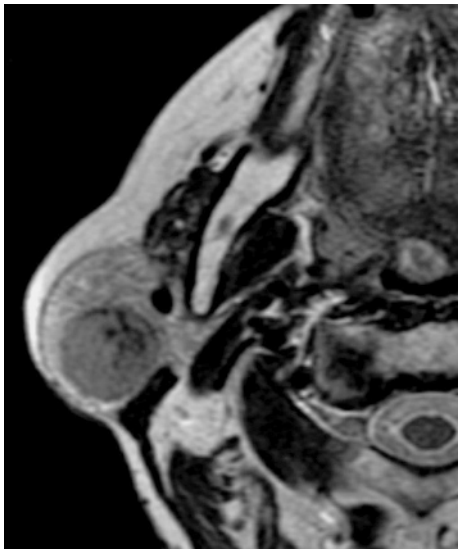

b

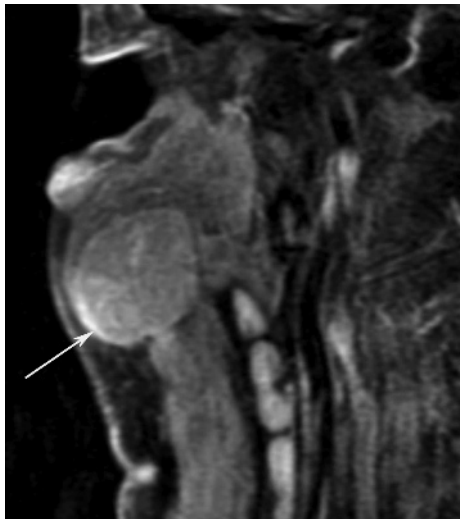

c

Fig. 12.12a–c. Typical Warthin's tumor in the superficial lobe of the right parotid gland showing a low T1-weighted signal intensity with small high signal intensity areas (*arrow*, **a**), a low T2-weighted signal intensity (**b**), and a mild enhancement most pronounced in the periphery of the mass (*arrow*, **c**)

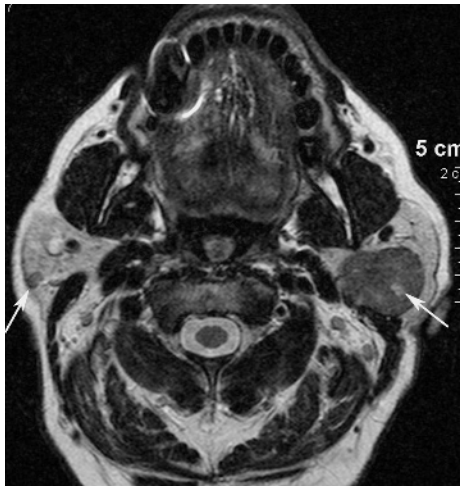

Fig. 12.13. Typical Warthin's tumor involving both the superficial and deep lobe of the left parotid gland. The tumor shows a low T1-weighted signal intensity (*arrow*) with small spontaneously hyperintense areas (due to hemorrhagic changes and cholesterol crystals). Note the small contralateral Warthin's tumor (*arrow*)

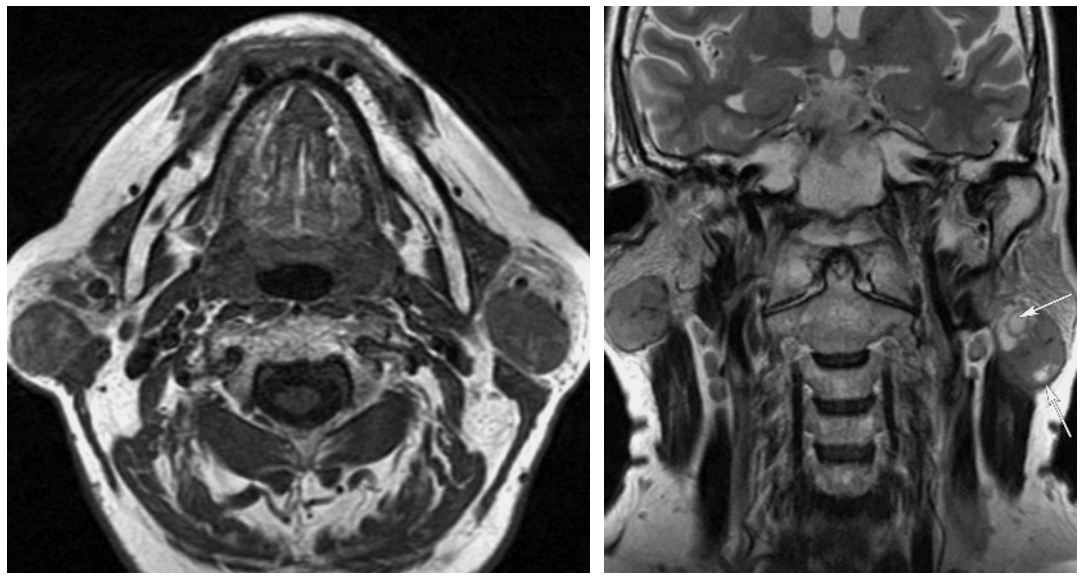

a b

Fig. 12.14a,b. Typical bilateral Warthin's tumor with a low T1-weighted (**a**) and a low T2-weighted signal intensity. Areas of cystic changes show a high T2-weighted signal intensity within the left lesion (**b**)

12.4.2.4 Differential Diagnosis

- Atypical pleomorphic adenoma
- Benign lymphoepithelial lesions in HIV-positive patients
- Malignant tumor with few malignant characteristics on imaging

12.4.3 Other Benign Tumors

12.4.3.1 Lipoma

It represents 1% of all parotid gland tumors. CT and MR findings are characteristic: well-circumscribed lesion with negative HU values on CT, showing high T1-weighted and high T2-weighted signal intensities, without enhancement on contrast-enhanced T1-weighted images. The high T1-weighted signal intensity disappears on fat-suppressed sequences (Fig. 12.15).

12.4.3.2 Neurogenic Tumor

A schwannoma of the intraparotid portion of the facial nerve may occur but remains exceptional in this localization. It can be solitary or multiple.

Imaging findings are non-specific but show characteristics of a benign tumor, centred on the facial nerve plane, with low T1-weighted, high T2-weighted signal intensities and homogeneous enhancement. When large in size, cystic changes may occur, making the diagnosis on imaging more difficult.

12.4.4 Congenital Tumors

12.4.4.1 Lymphangioma

Lymphangioma presents as lobulated, multiloculated, cystic mass with septations. Some of the cystic areas can show spontaneous high signal intensity. Sometimes fluid–fluid levels are seen. Cystic foci do not enhance. Cystic lymphangioma often occurs in the lower portion of the parotid gland (Fig. 12.16).

Mixed vascular malformations exist, such as the cavernous lymphangioma, composed of (enhancing) solid areas and dilated lymphatic spaces.

12.4.4.2 Infantile Hemangioma

This is the most frequent tumor of the parotid space in infants and young children. This tumor shows a three-phase evolution: rapid growth until the age of

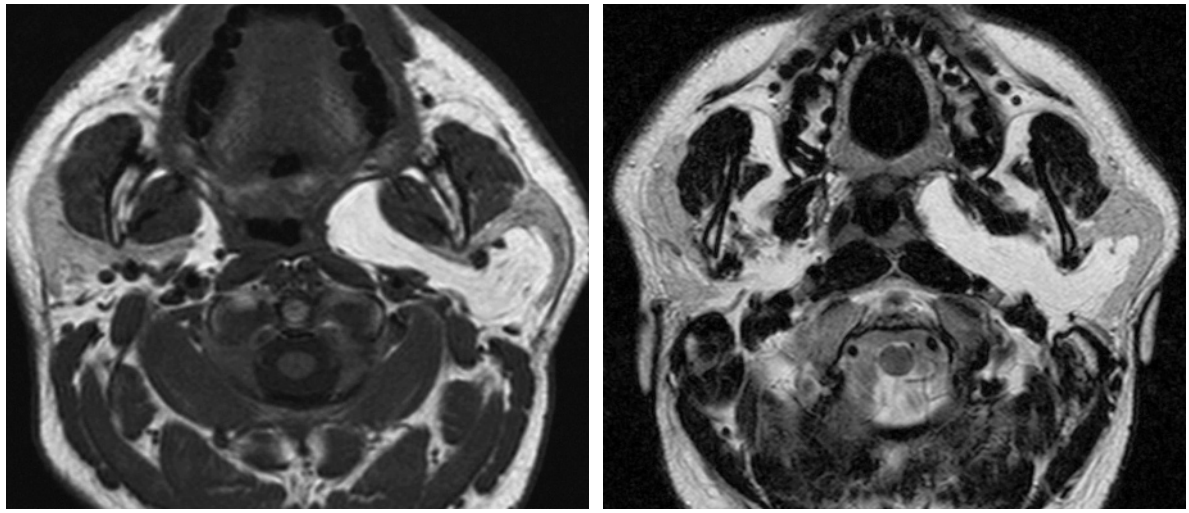

Fig. 12.15a,b. Lipoma of the left parotid gland extending to the deep lobe and the anterior parapharyngeal space, showing a spontaneous high T1-weighted signal intensity (**a**) and a high T2-weighted signal intensity (**b**)

about 10 months, then stabilization and finally regression with sometimes an incomplete involution with residual calcifications.

Imaging findings are a large solid mass which shows intermediate T1-weighted, high T2-weighted signal intensities, and intense and fast enhancement with multiple enlarged vascular signal voids (Fig. 12.17).

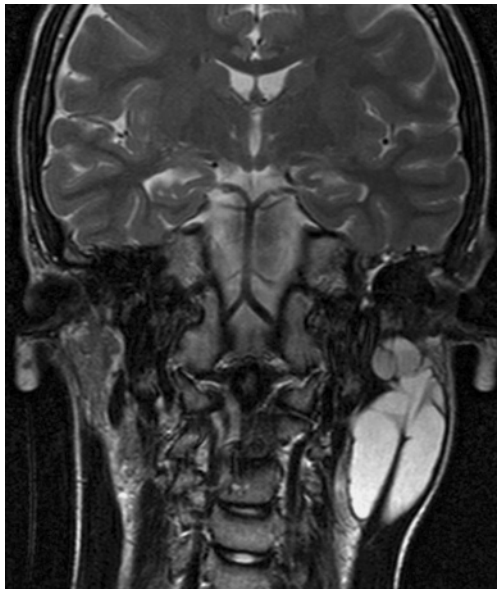

Fig. 12.16. Cystic lymphangioma of the inferior pole of the left parotid gland. Typical aspect of a lobulated, septated, cystic mass showing a high T2-weighted signal intensity

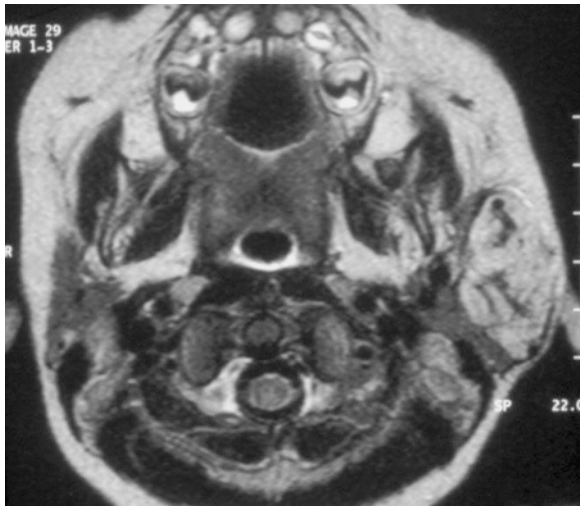

Fig. 12.17. Infantile capillary hemangioma: a large solid mass of the left parotid space showing intense enhancement and containing multiple enlarged vascular signal voids

12.4.5 Cystic Tumors

12.4.5.1 Solitary Cystic Lesion

A solitary cystic lesion of the parotid gland is rare (Som et al. 1995). The cystic nature of the lesion has to be confirmed on imaging using specific sequences. Actually, most parotid gland tumors have a high T2-weighted

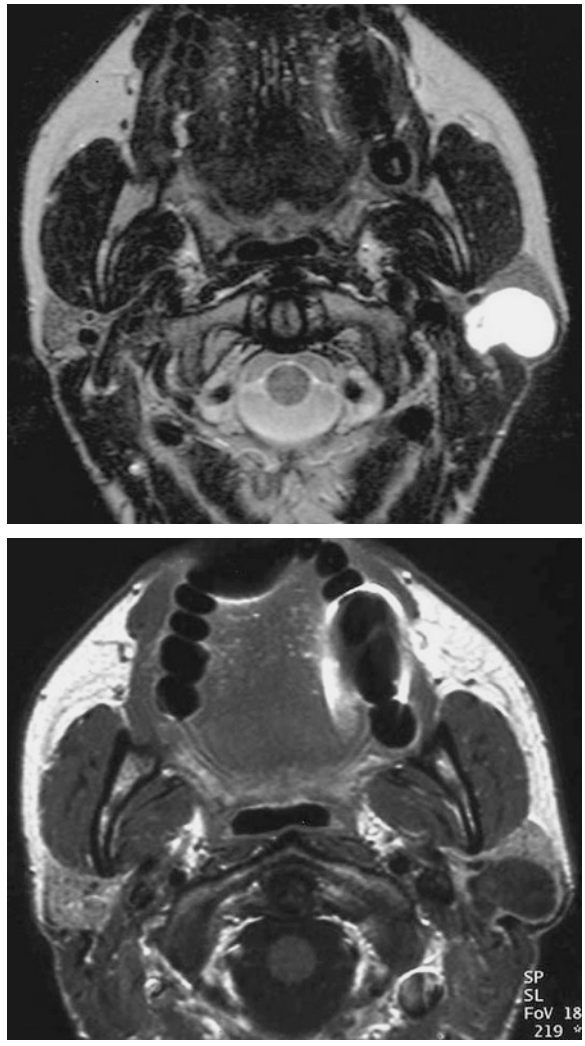

Fig. 12.18a,b. Solitary simple cystic lesion of the left parotid gland with a high T2-weighted (**a**) and a low T1-weighted signal intensity without any contrast enhancement (**b**)

signal intensity, so this finding does not systematically correspond to a cystic lesion. A cystic formation shows a low T1-weighted signal intensity without any enhancement on contrast-enhanced T1-weighted sequence. It has a high T2-weighted signal intensity including T2-weighted sequence with long echo time (Fig. 12.18). Cystic lesion appears hypointense on diffusion-weighted sequence at b factor of 800 or 1000 s/mm².

A cystic lesion of the parotid gland is suggestive of first branchial cleft abnormality, and a fistulous connection in or around the external auditory canal must be looked for (Van der Goten et al. 1997). If the cyst appears to be unilocular and non-communicating, the differential diagnosis is between a non-communicating branchial cleft cyst and a simple cyst of the parotid gland.

12.4.5.2 Dermoid Cysts

Dermoid cysts may occur in the parotid space. Their heterogeneous structure (fat, bone, skin adnexa) is highly suggestive of this diagnosis.

12.4.5.3 Epidermoid Cysts

Rarely epidermoid cysts occur in the parotid gland. They show typical signal intensities on MRI: a low T1-weighted, a high T2-weighted signal intensity and no enhancement on contrast-enhanced T1-weighted images. A diffusion-weighted sequence is very helpful because epidermoid cysts show high signal intensity at b factor of 800 or 1000 s/mm^2, with a very small apparent diffusion coefficient (ADC) value (around 0.5×10^{-3} mm^2/s).

These are slow-growing tumors and a single follow-up imaging study can be proposed.

12.4.5.4 Multiple Intraparotid Cystic Lesions

Multiple intraparotid cystic lesions must evoke the possibility of benign lymphoepithelial lesions, as may be seen in HIV positive patients (Holliday et al. 1998).

The etiology remains unknown; they are probably of inflammatory nature.

Imaging findings are multiple, bilateral cystic and solid masses, enlarging both parotid glands, associated with tonsillar hyperplasia and bilateral cervical adenopathy.

These lesions are well-circumscribed, sometimes heterogeneous, with low T1-weighted and high T2-weighted signal intensities (Fig. 12.19).

The clinical profile should help in the diagnosis.

12.5 Malignant Parotid Tumors

Malignant tumors represent 15% of all parotid tumors. Clinical symptoms suggestive for malignancy are: facial nerve paralysis, pain, skin infiltration, a rapidly-enlarging lesion and cervical adenopathy. Prognosis depends on histologic grade.

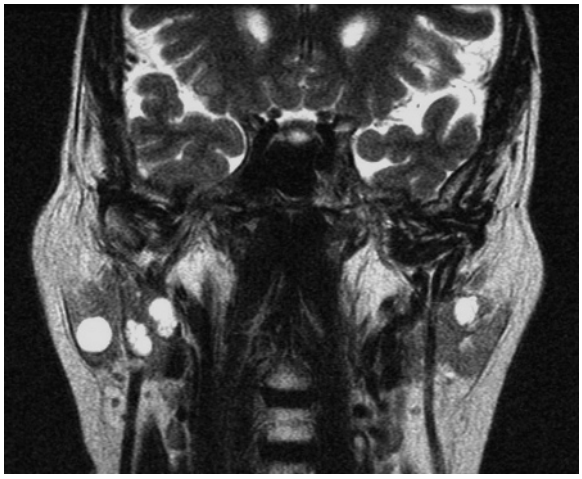

Fig. 12.19. Multiple bilateral cystic lesions in a HIV-positive patient, corresponding to benign lymphoepithelial lesions

12.5.1 Histologic Classification

- *Adenocarcinoma, squamous cell carcinoma and undifferentiated carcinoma.* These malignant tumors have a predilection for men and most cases occur over the age of 60 years. They are most frequently rapidly-growing tumors, presenting with facial nerve paralysis and early infiltration of the infratemporal fossa. The prognosis of these cancers is very bad.
- *Adenoid cystic carcinoma.* This malignant tumor occurs more commonly in the submandibular gland and the minor salivary glands. Adenoid cystic carcinoma is a slow-growing, widely infiltrative tumor with a tendency for perineural spread along the facial nerve and trigeminal nerve (auriculotemporal nerve and mandibular nerve). A significant number of patients develop late intracranial recurrence due to perineural infiltration. Distant metastases develop in 40%–50%.
- *Mucoepidermoid carcinoma.* This has a female predominance and is most frequently seen in the 40- to 60-year age group. Prognosis depends on the histologic grade. Low-grade mucoepidermoid carcinoma may have a clinical and radiological presentation of a benign tumor. High grade tumors have a high risk of local recurrence and distant metastases.
- *Non-Hodgkin lymphoma.* This develops from intraparotid lymph nodes and is frequently associated to a systemic lymphoma with cervical lymphadenopathy and other lymphoma localizations. Patients suffering Sjögren's syndrome have an increased risk of developing parotid lymphoma.
- *Intraparotid metastases.* The vast majority of parotid metastases of known primary tumors originate from the skin in the head and neck region.
- *Liposarcoma and rhabdomyosarcoma.* These are rare parotid neoplasms.

12.5.2 Imaging Findings

12.5.2.1 Parotid Cancer

The aim of imaging is to identify the malignant features of a tumor in order to initiate the best therapy as soon as possible. Subtle signs of malignancy (Figs. 12.20–12.23) (Freling et al. 1992) that have to be scrutinized include the following:

- Poorly-defined margins, indicating an invasive mass, including infiltration of the adjacent fat tissue, which can be an early and only sign suggesting malignancy, best depicted on precontrast T1-weighted images.
- Cervical lymphadenopathy.
- Extension to the adjacent deep facial spaces (Fig. 12.24) such as the masticator and parapharyngeal space.
- Perineural spread along the facial nerve or trigeminal nerve, better depicted on contrast-enhanced images with fat saturation, is typically seen in adenoid cystic carcinoma (Fig. 12.25) (Harnsberger 2004; Som and Brandwein 1996).
- Low T2-weighted signal intensity may indicate malignancy (Som and Biller 1989), but may also be seen in some benign tumors.

Histologic diagnosis is not possible on imaging.

If a malignant tumor is suspected on imaging, a fine needle aspiration may be performed. This allows differential diagnosis with a benign tumor in 85%–90% of cases (Zbaren et al. 2001).

The typical treatment of these malignant tumors is wide surgical resection, lymph node dissection and radiation therapy.

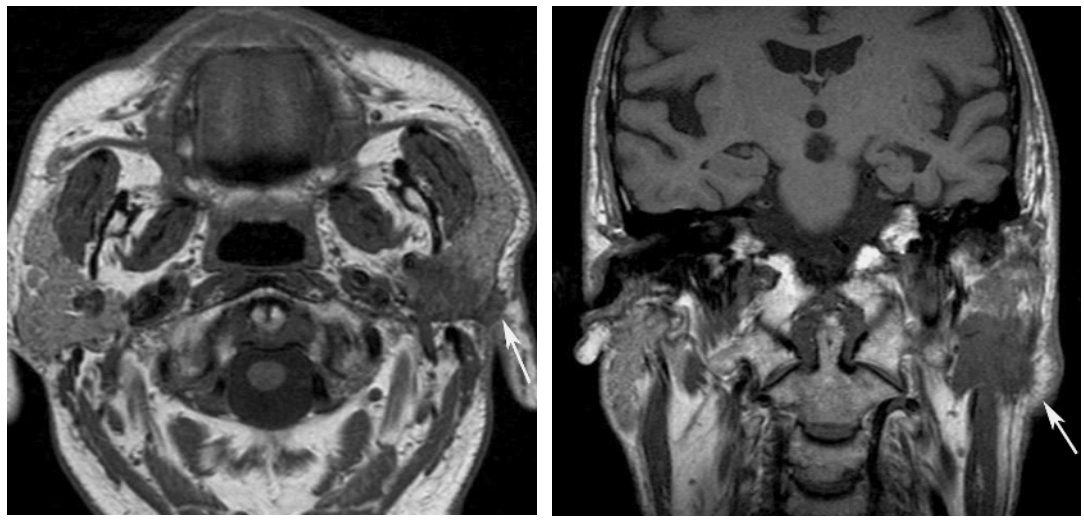

Fig. 12.20a,b. Malignant tumor of the left parotid gland, with ill-defined margins, infiltrating the adjacent subcutaneous fat tissue (*arrow*), well appreciated on pre-contrast T1-weighted images (**a, b**). Adenocarcinoma

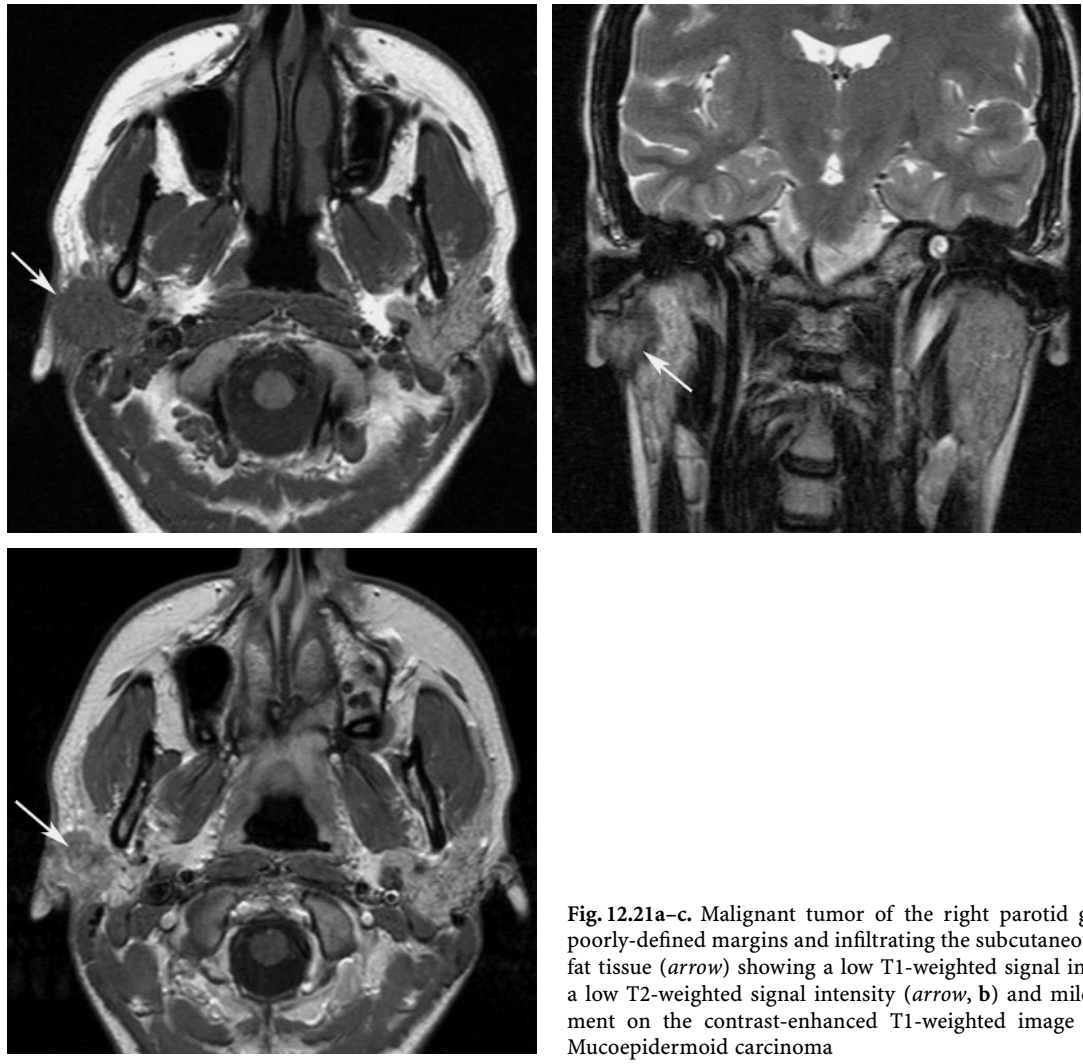

Fig. 12.21a–c. Malignant tumor of the right parotid gland, with poorly-defined margins and infiltrating the subcutaneous adjacent fat tissue (*arrow*) showing a low T1-weighted signal intensity (**a**), a low T2-weighted signal intensity (*arrow*, **b**) and mild enhancement on the contrast-enhanced T1-weighted image (*arrow*, **c**). Mucoepidermoid carcinoma

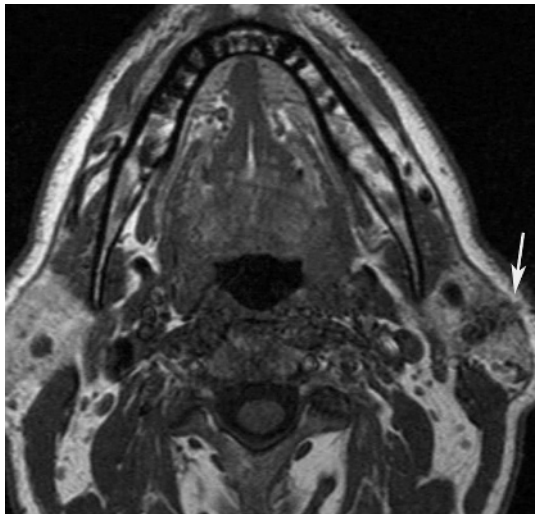

a

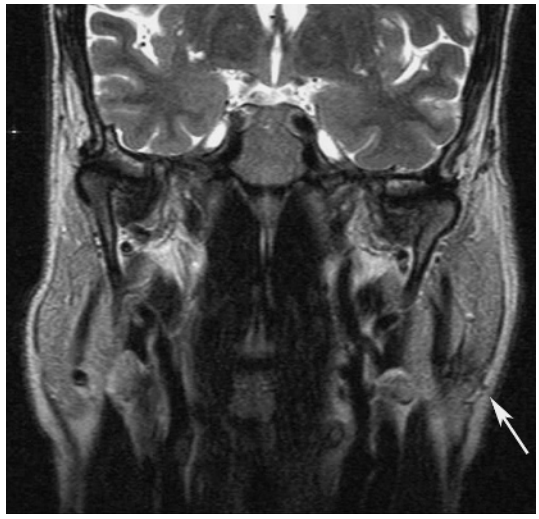

b

Fig. 12.22a,b. Small malignant tumor of the inferior pole of the left parotid gland (**a**). The ill-defined margins, low T2-weighted signal intensity (**b**), and infiltration of the adjacent fat tissue suggest malignancy (*arrow*). Mucoepidermoid carcinoma

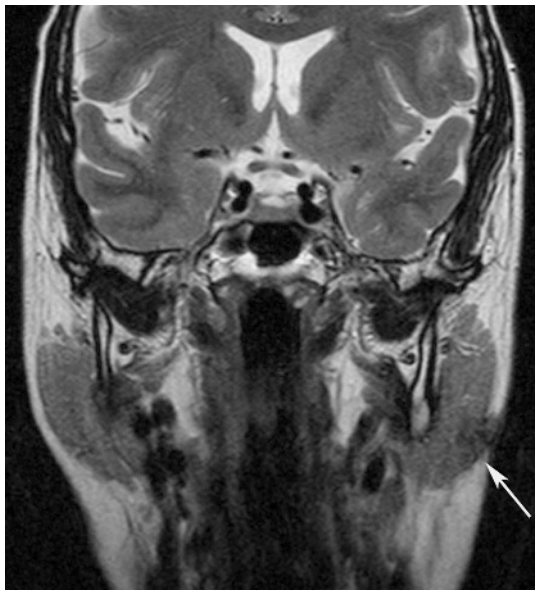

a

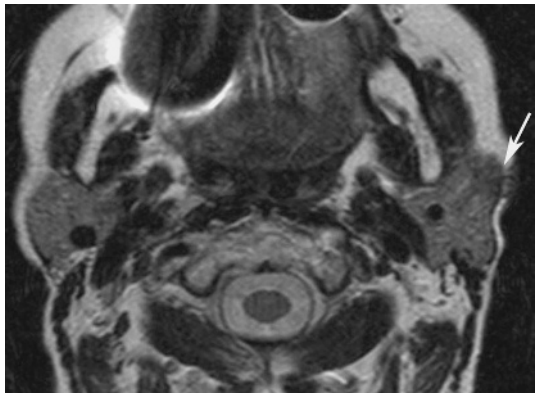

b

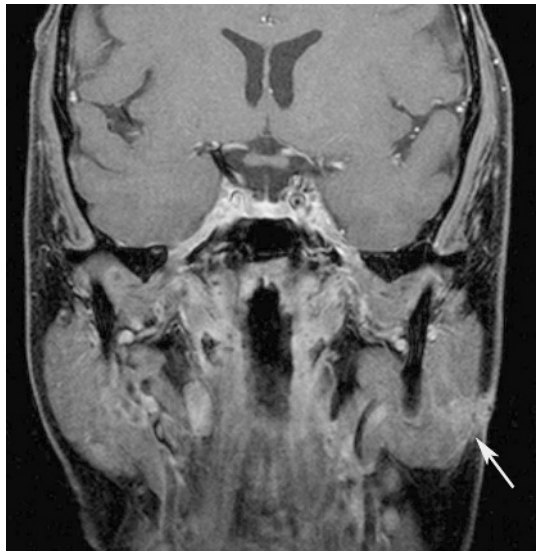

c

Fig. 12.23a–c. Malignant tumor in the superficial lobe of the left parotid gland, with a low T2-weighted signal intensity (*arrow*, **a**). The infiltration of the adjacent fat tissue is well identified on pre-contrast T1-weighted image (*arrow*, **b**), as well as on the contrast-enhanced T1-weighted images with fat saturation (*arrow*, **c**). Adenocarcinoma

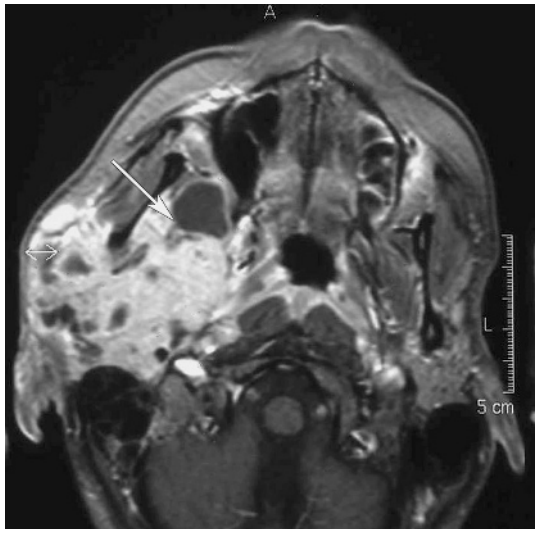

Fig. 12.24. Adenoid cystic carcinoma of the right parotid gland extending to the parapharyngeal space and the infratemporal fossa (*arrow*)

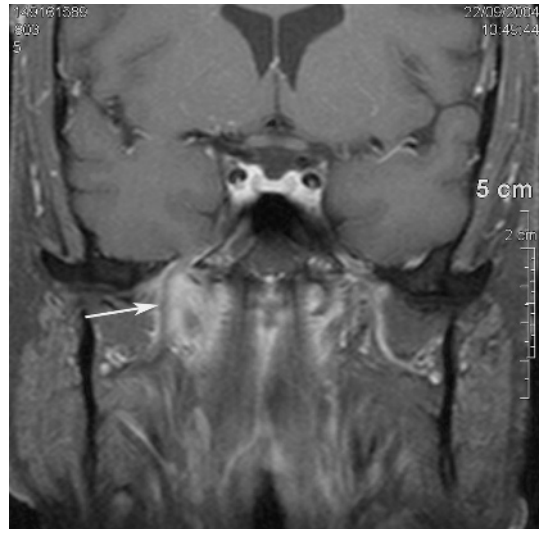

Fig. 12.25. Adenoid cystic carcinoma of the deep lobe of the right parotid gland, showing perineural spread along the mandibular branch of the trigeminal nerve (*arrow*) towards the foramen ovale

12.5.2.2 Non-Hodgkin Lymphoma

Non-Hodgkin lymphoma often has more specific imaging features: multiple homogeneous nodal lesions with intermediate T1-weighted and T2-weighted signal intensities and moderate enhancement, rarely necrotic. Usually, there is also cervical lymphadenopathy showing the same signal intensity on all MR sequences (Fig. 12.26). The submandibular gland as well as the lacrimal glands may also be involved. Fine needle aspiration may confirm the diagnosis. However, the histologic diagnosis has to be confirmed by a larger tissue sample (such as an adenopathy). The treatment consists of chemotherapy, possibly associated with radiotherapy.

12.6 Difficult Cases

- Really difficult cases in imaging parotid gland tumors are rare and represent less than 10% of all cases. However, it can be impossible to differentiate an atypical parotid benign tumor, such as atypical pleomorphic adenoma, from a malignant tumor showing few typical malignant characteristics. Diffusion-weighted sequences are helpful in such situations. The lesion's signal intensity at b factor of 1000 s/mm² and 0 s/mm², and the ADC value need to be evaluated. Pleomorphic adenoma appears hypointense on diffusion-weighted sequence at b factor of 1000 s/mm², with an ADC value > 1.2 (Fig. 12.27). On the other hand, malignant tumors, including lymphoma, show a much lower ADC value, < 1.2. If the ADC value is > 1.2, suggestive of a pleomorphic adenoma, surgery of the lesion can be proposed. If the ADC value is < 1.2, fine needle aspiration can be done in order to first exclude malignancy. However, there is no consensus whether to perform fine needle aspiration or not. As already mentioned, this procedure allows differentiation of benign tumors from malignant tumors in 85%–90% of all cases (Zbaren et al. 2001; Lim et al. 2003). On the contrary, a specific histologic diagnosis for benign tumors is possible only in 40% of cases (Hamilton et al. 2003), except for cystadenolymphoma for which a diagnosis is possible in 74% of cases (Parwani and Ali 2003).
- It can also be very hard to differentiate an atypical pleomorphic adenoma showing a low T2-weighted signal intensity from a Warthin's tumor. In such situations, MR diffusion-weighted imaging is very helpful: a pleomorphic adenoma appears hypointense on diffusion-weighted sequence at b factor of 1000 s/mm², with a ADC value > 1.2, whereas a Warthin's tumor presents a high signal intensity at b factor of 1000 s/mm² with a low ADC value, lower than the one observed in case of malignant tumor (Ikeda et al. 2004).

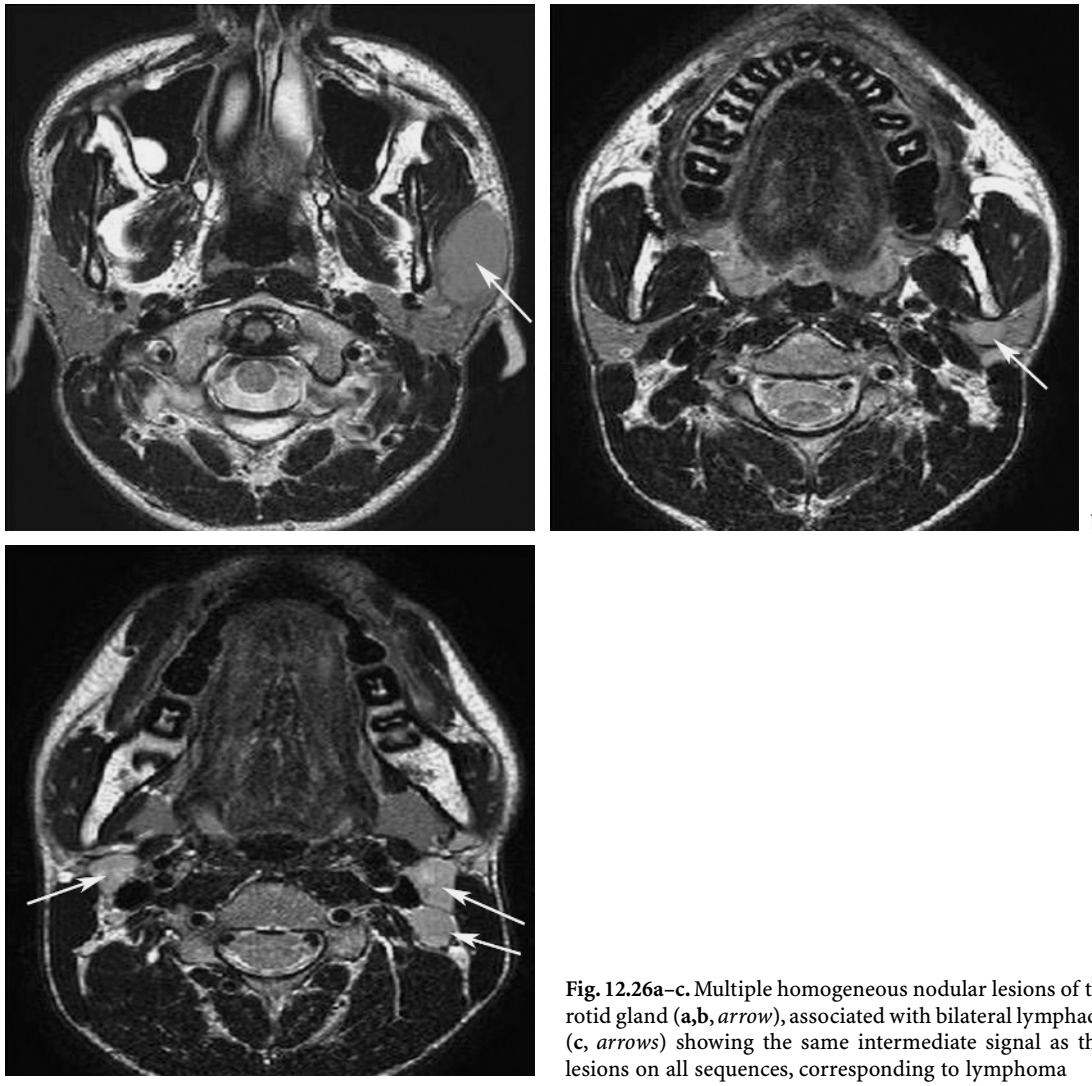

Fig. 12.26a–c. Multiple homogeneous nodular lesions of the left parotid gland (**a,b**, *arrow*), associated with bilateral lymphadenopathy (**c**, *arrows*) showing the same intermediate signal as the parotid lesions on all sequences, corresponding to lymphoma

- Diffusion-weighted imaging also allows making the difference between a simple intraparotid cyst and an epidermoid cyst. An epidermoid cyst shows a high signal on diffusion-weighted images at b factor of 1000 s/mm² with a very small ADC value (around 0.5), favouring this diagnosis (see above).

12.7 Pseudotumors of the Parotid Gland

12.7.1 Sjögren's Syndrome

This is a chronic systemic autoimmune disease that affects salivary and lacrimal glands.

The best diagnostic clue on imaging is bilateral enlargement of both parotid glands, usually asymmetric, with multiple small cystic and solid lesions; sometimes calcifications are present.

On MR imaging, a miliary pattern of small cysts throughout both parotids is diagnostic of Sjogren's syndrome. The small collections show low T1-weighted, high T2-weighted signal intensities; the small cysts do not enhance, while the surrounding parenchyma shows mild enhancement. MR sialography suggest the diagnosis of Sjögren's syndrome by showing multiple cystic lesions while the salivary ducts appear normal (Fig. 12.28) (Ohbayashi et al. 1998; Izumi et al. 1996).

The differential diagnosis includes benign lymphoepithelial cystic lesions in HIV positive

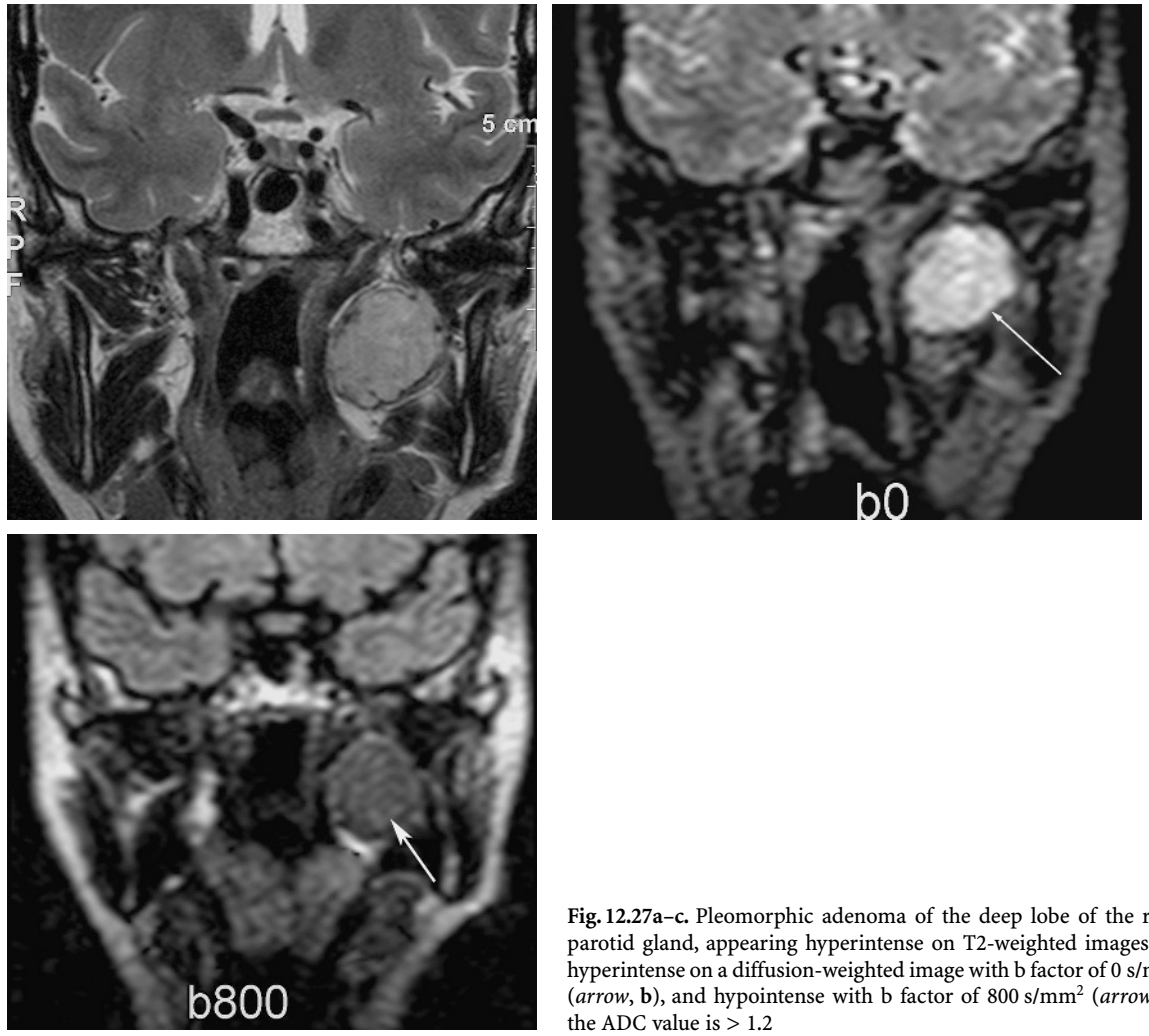

a b c

Fig. 12.27a–c. Pleomorphic adenoma of the deep lobe of the right parotid gland, appearing hyperintense on T2-weighted images (**a**), hyperintense on a diffusion-weighted image with b factor of 0 s/mm^2 (*arrow*, **b**), and hypointense with b factor of 800 s/mm^2 (*arrow*, **c**); the ADC value is > 1.2

patients; cystic areas are usually larger in this pathology.

A solid tumoral mass, developing in the parotid gland in a patient with Sjögren's syndrome, is suspect for lymphoma.

12.7.2 Sarcoidosis

Sarcoidosis is a systemic disease. The parotid glands are affected in 10%–30% of patients. It can present with solid and cystic lesions involving both parotid glands, often associated with cervical adenopathy.

Differential diagnosis must be made with non-Hodgkin lymphoma, in which the imaging pattern commonly consists of bilateral, solid, nodal-appearing intraparotid masses. The clinical presentation is usually suggestive of the diagnosis.

12.8 Tumors of the Other Salivary Glands

The paired submandibular and sublingual glands are referred to as major salivary glands, such as the parotid glands. The minor salivary glands are submucosal clusters of salivary tissue present in the oral cavity, particularly at the junction of hard palate and soft palate, pharynx, upper respiratory tract, as well as in the anterior parapharyngeal space. Whereas parotid tumors are frequently benign, other salivary glands tumors are often malignant.

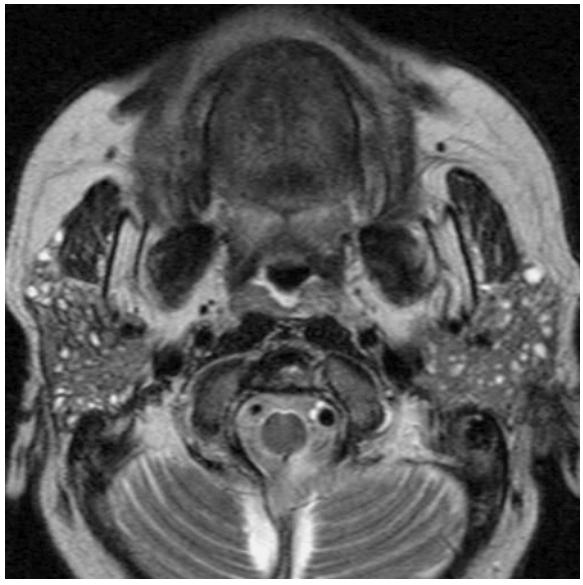

a

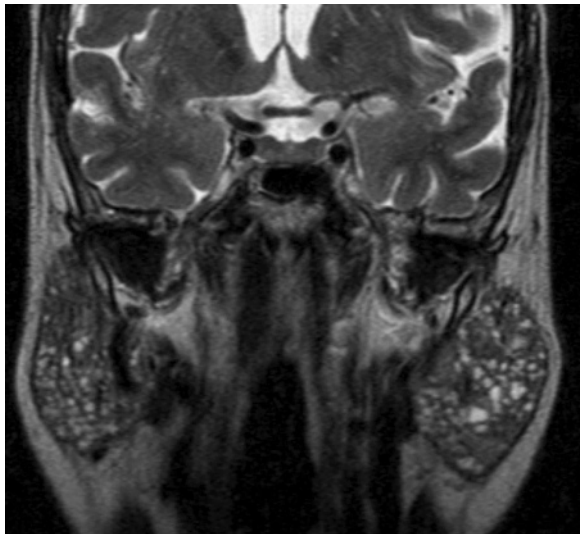

b

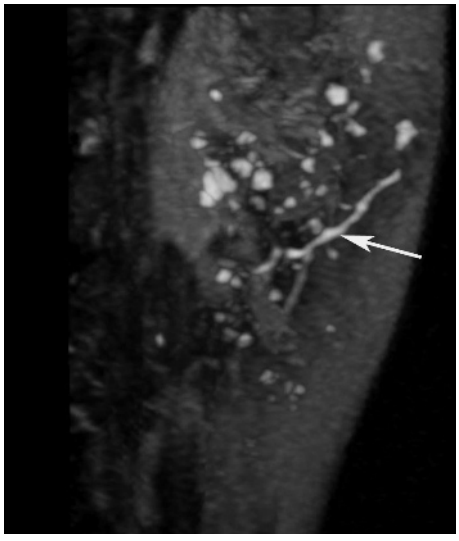

c

Fig. 12.28a–c. Miliary pattern appearance of multiple cystic lesions throughout both enlarged parotid glands, showing high T2-weighted signal intensity, in a patient affected by Sjögren's syndrome (**a,b**). These cystic lesions and the normal salivary ducts (*arrow*) are well seen on MR sialography (**c**)

12.8.1 Minor Salivary Glands Tumors

- Adenoid cystic carcinoma and mucoepidermoid carcinoma are the most frequent malignancies. A tumor of the palate is suspicious of a minor salivary gland tumor. Perineural spread toward the maxillary branch of the trigeminal nerve (V2) is suggestive of adenoid cystic carcinoma. Cervical lymphadenopathy may be present. Treatment consists of wide surgical resection, often associated with radiotherapy. Mucoepidermoid carcinoma often mimics a benign tumor (a well-defined, non infiltrative tumor) and has a better prognosis than adenoid cystic carcinoma (Fig. 12.29).
- Pleomorphic adenoma of minor salivary gland origin in the anterior parapharyngeal space is rare (see Chap. 9). These are usually slow-growing, large tumors without much clinical symptoms, presenting with the MR characteristics of a pleomorphic adenoma: a well-defined, lobulated mass with low T1-weighted, high T2-weighted signal intensities and important enhancement. These lesions often appear heterogeneous (Fig. 12.8). The differential diagnosis is a pleomorphic adenoma arising in the deep lobe of the parotid gland (Fig. 12.9).

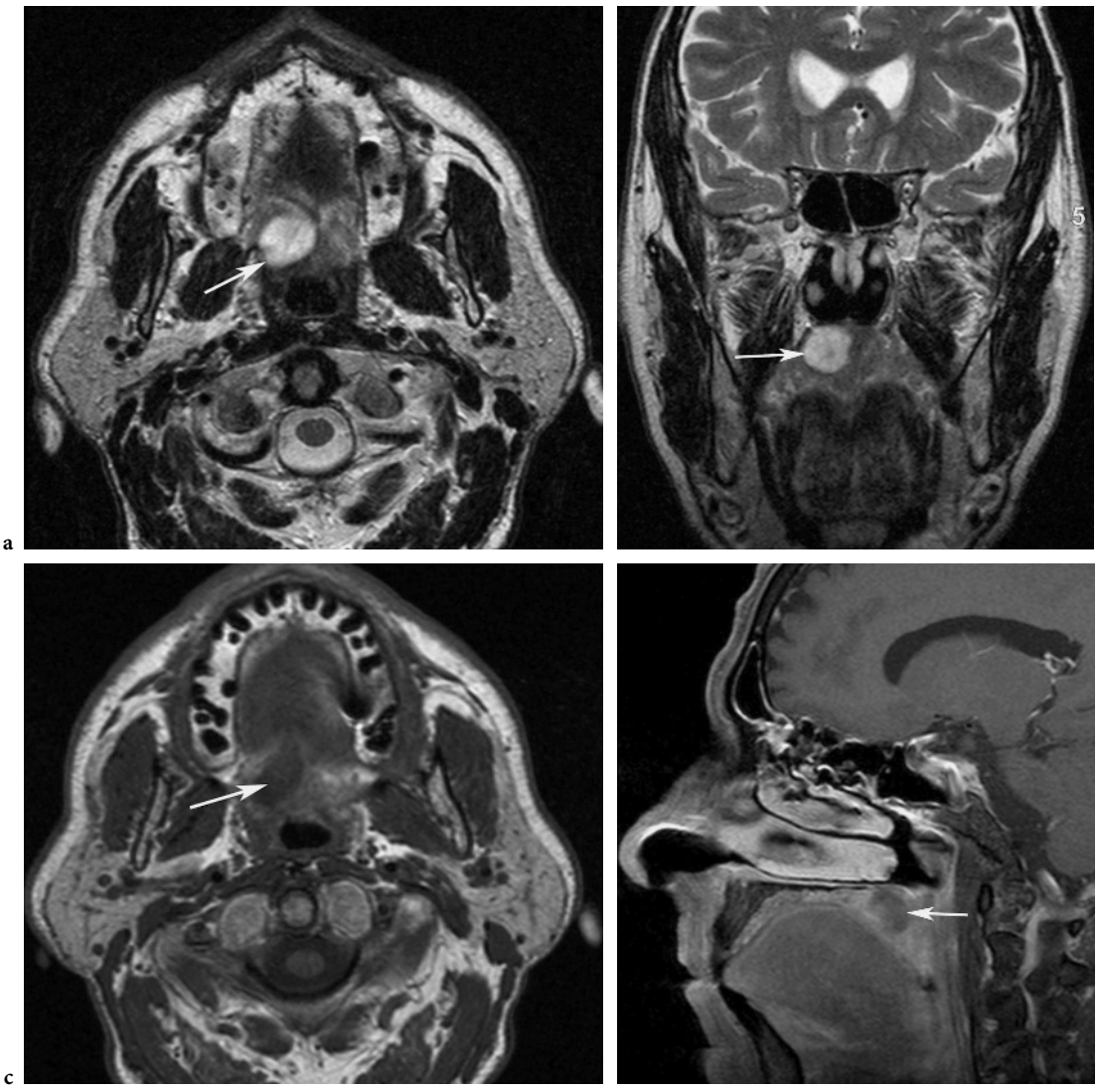

Fig. 12.29a–d. Mucoepidermoid tumor of a minor salivary gland at the junction of hard palate and soft palate: an ovoid, well-demarcated lesion showing high, heterogeneous T2-weighted (**a,b**), and low T1-weighted signal intensity (**c**), with mild contrast enhancement (**d**)

12.8.2 Submandibular Gland Tumors

- The role of imaging is to determine whether a submandibular lesion is either a salivary gland tumor or an adenopathy. In case of a salivary localization, the lesion appears to be malignant in 55% of patients (Kaneda et al. 1996).
- Adenoid cystic carcinoma and mucoepidermoid carcinoma are the most frequent submandibular gland tumors. On MR imaging, these tumors are usually poorly defined, with low T1-weighted, intermediate T2-weighted signal intensities and heterogeneous enhancement. The surrounding structures, such as the adjacent cervical deep spaces, muscles, mandible and cervical lymph nodes, have to be analyzed in order to rule out tumoral involvement. Treatment consists of a wide resection with neck dissection, and frequently adjuvant radiotherapy. Imaging follow-up must last a very long time because of the possibility of late recurrence.
- Benign mixed tumor is the most frequent benign tumor arising in the submandibular gland. MR imaging characteristics are similar to those of intraparotid pleomorphic adenoma. Typical appearance on CT is a hypodense, lobulated mass with heterogeneous enhancement related to cystic

and hemorrhagic changes. Fine needle aspiration of submandibular gland tumors has poor sensitivity and specificity. Surgical resection of the submandibular gland may be proposed if the lesion is small, homogeneous, well-defined, showing MR characteristics of a benign mixed tumor. Wide surgical resection associated with neck dissection has to be performed if the lesion is larger, heterogeneous, ill-defined, suggestive of a malignant tumor.

- Chronic sialadenitis due to obstruction of the ductal system can clinically simulate a tumoral lesion of the submandibular space. Imaging is very useful to look for the obstructive calculus in Wharton's duct and the inflammatory modifications of the submandibular gland. On imaging, the involved gland is usually enlarged, diffusely and densely enhancing, associated with dilatation of the main salivary duct, often containing a calculus at its distal part. Lithiasis is well depicted on CT (Fig. 12.30).

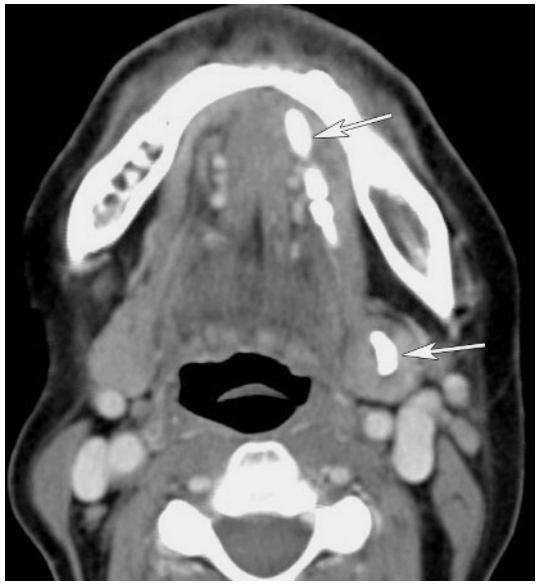

Fig. 12.30. Chronic sialadenitis: multiple calcified lithiasis (*arrows*) within the left submandibular gland and Wharton's duct

12.8.3 Sublingual Gland Tumors

- About 80% of the sublingual gland tumors are malignant. Again, the two main etiologies are adenoid cystic carcinoma and mucoepidermoid carcinoma (Sumi et al. 1999). On MR imaging, these tumors are more or less well-circumscribed and have a low T1-weighted, an intermediate T2-weighted signal intensity and a heterogeneous enhancement (Fig. 12.31). Extension outside the sublingual space has to be looked for, such as extension to the mandible or to the cervical lymph nodes. These lesions are usually well-circumscribed in case of mucoepidermoid tumor (Fig. 12.32). Treatment consists of a wide resection with neck dissection, most often associated with radiation therapy. Because of the risk of recurrence, a long term follow-up is recommended.
- A ranula is a mucous retention cyst that originates from the sublingual gland. It most commonly results from trauma or inflammation (Macdonald et al. 2003). A ranula occurs in two forms. The first one, the simple ranula, is a retention cyst that remains located in the sublingual space (Fig. 12.33). The second type is the plunging ranula, which is a mucocele extending through the mylohyoid muscle, to the submandibular space. On MR imaging, the simple ranula is a cystic formation with a low T1-weighted, a high T2-weighted signal intensity and a thin enhancement ring on contrast-enhanced images. The plunging ranula appears as a multi-lobulated cystic formation; it sometimes shows a spontaneous high T1-weighted signal intensity because of its protein concentration, a high T2-weighted signal intensity with much more important enhancement of the cyst wall. On CT, a ranula usually has a low attenuation because of its high water content; the cyst wall may enhance after contrast administration. The differential diagnosis includes epidermoid cysts and cystic hygromas of the sublingual space.

12.9 Conclusion

Most of parotid gland lesions are benign tumors. The best imaging approach to analyze parotid gland tumors is MR imaging. In many cases, the MRI findings are indicative of a benign or malignant nature. In case of benign tumors, an etiologic diagnosis can sometimes be suggested on MRI. MR diffusion-weighted sequence appears to be helpful in improving the diagnostic yield in case of atypical or difficult cases.

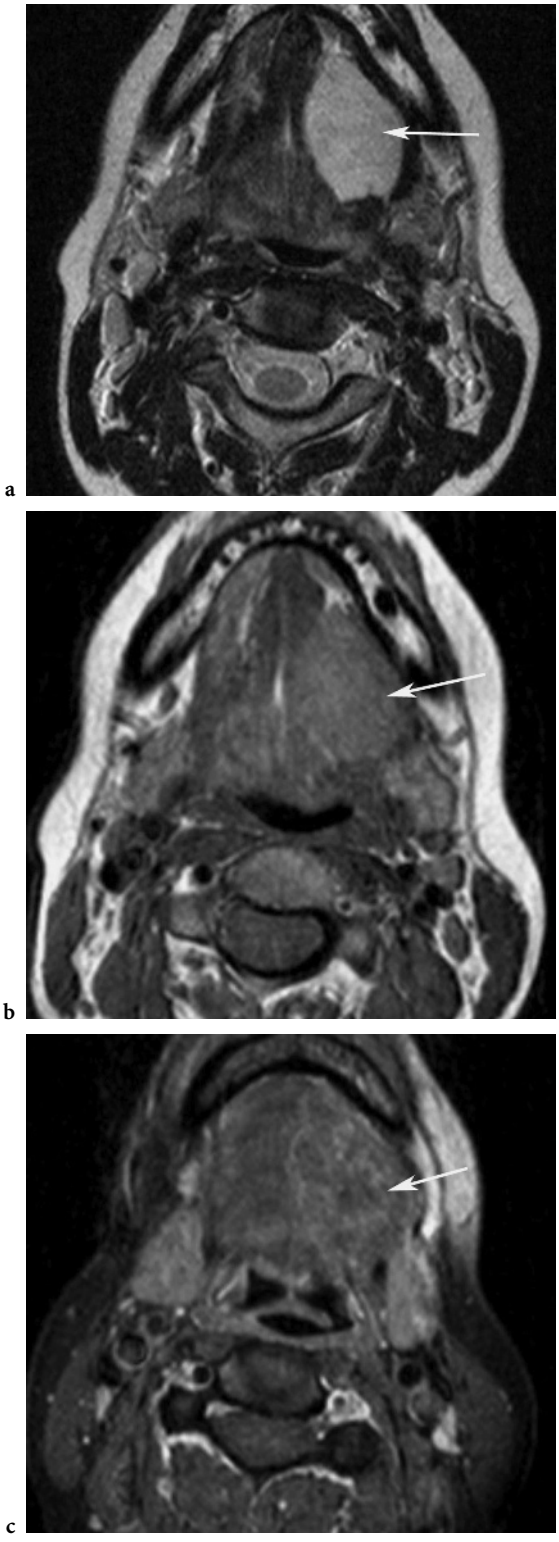

Fig. 12.31a–c. Adenoid cystic carcinoma of the left sublingual gland: huge mass appearing hyperintense on a T2-weighted image (*arrow*, **a**), hypointense on a T1-weighted image (*arrow*, **b**), showing a moderate and heterogeneous enhancement on a contrast-enhanced T1-weighted image (*arrow*, **c**)

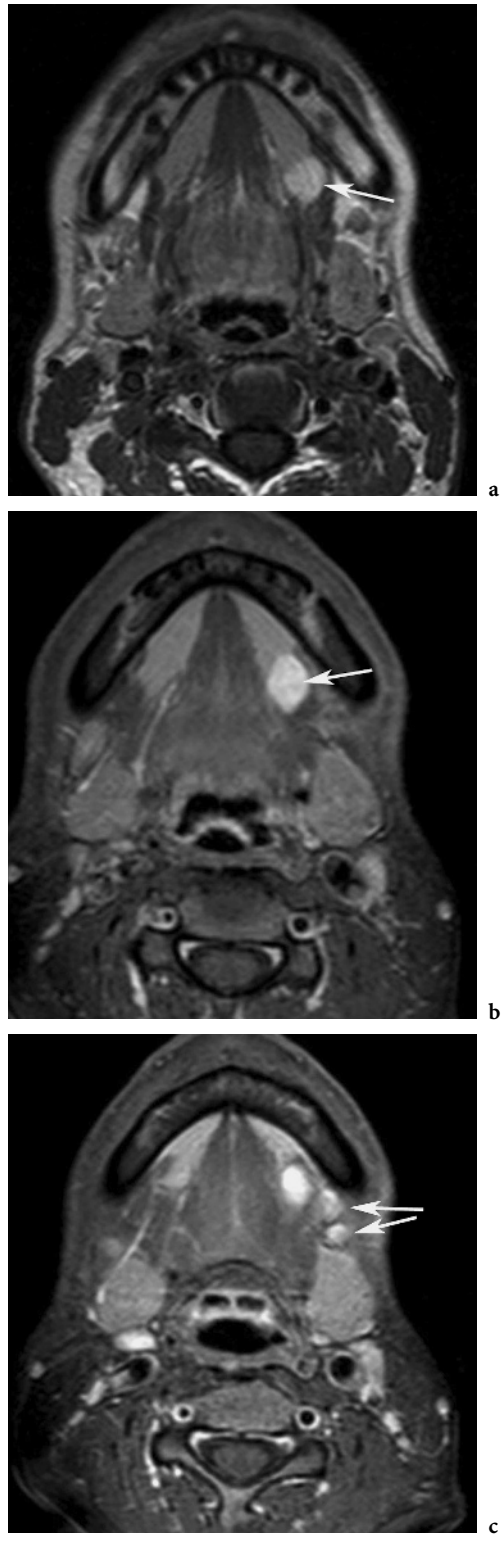

Fig. 12.32a–c. Small mucoepidermoid tumor of the left sublingual gland showing a high T2-weighted signal intensity (*arrow*, **a**) and an important enhancement on contrast-enhanced T1-weighted images (*arrow*, **b**), associated with two small adjacent submandibular adenopathies (*arrow*, **c**)

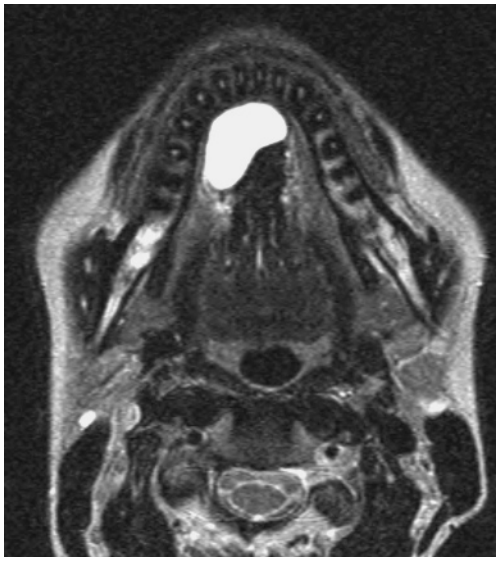

Fig. 12.33. Cystic formation in the anterior part of the right sublingual space, compressing the genioglossal muscles and extending over the midline. Confirmed simple ranula. (Courtesy of Robert Hermans, MD, PhD, Leuven, Belgium)

References

Freling NJM, Molenaar WM, Vermey A, Mooyaart EL, Panders AK, Annyas AA, Thijn CJP (1992) Malignant parotids tumors: clinical use of MR imaging and histologic correlation. Radiology 185:691–696

Hamilton BE, Salzman KL, Wiggins RH, Harnsberger HR (2003) Earring lesions of the parotid tail. AJNR Am J Neuroradiol 24:1757–1764

Harnsberger HR (2004) Diagnostic imaging head and neck, 1st edn Amirsys Inc, Salt Lake City Utah, Part III, section 7:2–36 and part III, section 4:26–48

Holliday RA, Cohen WA, Schinella RA, Rothstein SG, Persky MS, Jacobs JM, Som PM (1998) Benign lymphoepithelial parotid cyst and hyperplastic cervical adenopathy in AIDS-risk patients: a new CT appearance. Radiology 168:439–441

Ikeda K, Katoh T, Ha-Kawa SK, Iwai H, Yamashita T, Tanaka Y (1996) The usefulness of MR in establishing the diagnosis of parotid pleiomorphic adenoma. AJNR Am J Neuroradiol 17:55–59

Ikeda M, Motoori K, Hanazawa T, Nagai Y, Yamamoto S, Ueda T, Funatsu H, Ito H (2004) Warthin tumor of the parotid gland: diagnostic value of MR imaging with histopathologic correlation. AJNR Am J Neuroradiol 25:1256–1262

Izumi M, Eguchi K, Ohki M, Uetani M, Hayashi K, Kita M, Nagataki S, Nakamura T (1996) MR imaging of parotid gland in Sjogren's symdrome: a proposal for new criteria. AJR Am J Roentgenol 166:1483–1487

Joe VQ, Westesson PL (1994) Tumors of the parotid gland: MR imaging characteristics of various histologic types. AJR Am J Roentgenol 163:433–438

Kaneda T, Minami M, Ozawa K, Akimoto Y, Kawana T, Okada H, Yamamoto H, Suzuki H, Sasaki Y (1996) MR of submandibular gland: normal and pathologic states. AJNR 17:1575–1581

Lim LH, Chao SS, Goh CH, Ng CY, Goh YH, Khin LW (2003) Parotid gland surgery: a review of 118 cases in an Asian population. Head Neck 25:543–548

O'Brien CJ (2003) Current management of benign parotid tumors: the role of limited superficial parotidectomy. Head Neck 25:946–952

Ohbayashi N, Yamada I, Yoshino N, Sasaki T (1998) Sjogren syndrome: comparison of assessments with MR sialography and conventional sialography. Radiology 209:683–688

Okahara M, Kiyosue H, Hori Y, Matsumoto A, Mori H, Yokoyama S (2003) Parotid tumors: MR imaging with pathological correlation .Eur Radiol 13[Suppl 4]:L25–33

Parwani AV, Ali SZ (2003) Diagnostic accuracy and pitfalls in fine-needle aspiration interpretation of Whartin tumor. Cancer 99:166–171

Shah GV (2002) MR imaging of salivary glands. Magn Reson Imaging Clin N Am 10:631–662

Shah GV (2004) MR imaging of salivary glands. Neuroimaging Clin N Am 14:777–808

Som PM, Biller HF (1989) High-grade malignancies of the parotid glands: identification with MR imaging. Radiology 173: 823–826

Som PM, Brandwein M (1996) Salivary glands. In: Som PM, Curtin HD (eds) Head and neck imaging, 3rd edn. Mosby, St. Louis, pp 823–914

Som PM, Brandwein MS, Silvers A (1995) Nodal inclusion cysts of the parotid gland and parapharyngeal space: a discussion of lymphoepithelial, AIDS-related parotid, branchial cyst, cystic Whartin's tumors and cysts in Sjogren's syndrome. Laryngoscope 105:1122–1128

Sumi M, Izumi M, Yonetsu K, Nakamura T (1999) Sublingual gland: MR features of normal and diseased states. AJR Am J Roentgenol 172:717–722

Van der Goten A, Hermans R, Van Hover P, Crevits I, Baert AL (1997) First branchial complex anomalies: report of 3 cases. Eur Radiol 7:102–105

Vogl TJ, Balzer J, Mack M, Steger W (1999) Salivary glands. In: Differential diagnosis in head and neck imaging. Thieme, Stuttgart New York, pp 237–253

Zbaren P, Schar C, Hotz MA, Loosli H (2001) Value of fine needle aspiration cytology of parotid gland masses. Laryngoscope 111:1989–1992

13 Malignant Lesions of the Central and Posterior Skull Base

Ilona M. Schmalfuss

CONTENTS

13.1 Introduction

Evaluation of skull base lesions is challenging. On the one hand, the skull base is not directly accessible for clinical evaluation, and an underlying lesion is suspected or can be only roughly outlined based on neurological deficits. On the other, cross-sectional radiological studies are excellent in demonstrating a skull base lesion and its extent, but their evaluation is intimidating to the majority of the radiologists. There are three main reasons for the intimidation of the radiologists: The anatomical complexity of the skull base, the ability of normal anatomical structures to mimic pathology and the rarity of skull base lesions preventing dedicated training throughout residency and even during fellowship. In addition, inappropriate choice of an imaging study, imaging parameters and or sequences may amplify the insecurity of the radiologist.

Recognition of anatomical mimics and of medically treatable conditions is essential as the majority of skull base lesions are inaccessible for biopsy. The biopsy route may extend through normal pertinent anatomical structures such as inner ear in case of a petrous apex lesion, or may need to be performed via an intracranial route. Differentiation of malignant from benign lesions is critical as different surgical intervention may apply, the lesion might be vascular in nature preventing a biopsy, or occasionally treatment might be conducted without a tissue diagnosis, e.g. radiation therapy in case of paragangliomas. In addition, determination of the exact origin and extent of a lesion is crucial for radiation therapy and even more for surgical planning purposes. All these points will be addressed in this chapter.

13.2 Anatomy

The anatomy of the skull base is very complex; not only the bony structures play an important role but also the cranial nerves and vasculature coursing through it. Knowledge of the location of the different neural and vascular foramina and channels, as well as of the different neuronal connections, can therefore explain the wide range of clinical symptoms and facilitate the detection of extracranial tumor spread.

The skull base is formed by the ethmoid, sphenoid, and paired occipital, frontal and temporal bones. It is divided into three regions: anterior, central and posterior skull base. Only the central and the posterior skull base will be discussed in this chapter as the an-

I. M. Schmalfuss, MD
Department of Radiology, Malcolm Randall VA Medical Center and University of Florida College of Medicine, 1601 SW Archer Road, Gainesville, Florida 32608, USA

terior skull base is included in Chap. 11. The distinction of the central to posterior skull base is ambiguous as the roof of the petrous apex represents part of the central skull base while the posterior margin borders the posterior skull base. Since the majority of the malignant petrous apex lesions are surgically approached from the posterior fossa, the petrous apex will be included in the posterior skull base in the subsequent discussion.

13.2.1 Central Skull Base

The sphenoid bone forms the middle portion of the central skull base. It is subdivided into the central sphenoid body housing the sella and the sphenoid sinuses, the greater sphenoid wings forming the boundary to the anterior skull base, the lesser sphenoid wings and the pterygoid processes that are protruding below the skull base and serve as attachments for the medial and lateral pterygoid muscles. Parts of the temporal bones compose the lateral portions of the central skull base and are formed by the mastoid, tympanic, petrous and squamous bones. The greater sphenoid wing is connected via the sphenosquamous suture and the petrosphenoidal fissure with the squamous and petrous portion of the temporal bone, respectively. The anterior portion of the squamous bone creates the lateral border of the central skull base while the petrous bone together with the clivus form the boundary towards the posterior skull base. The petrous bone and the clivus are separated by the petrooccipital fissure.

The central skull base represents the floor of the middle cranial fossa which is primarily filled with the temporal lobes laterally and the cavernous sinuses medially. The cavernous sinuses are located between the dura and the periosteum of the body of the sphenoid bone, and between the superior orbital fissure anteriorly and the petrous apex posteriorly. Each cavernous sinus contains a complex venous plexus that surrounds the internal carotid artery and the cranial nerve VI. The cranial nerve VI enters the cavernous sinus through a small bony channel within the medial petrous apex called Dorello's canal. The cranial nerves III through V are actually located within the dural flap that forms the lateral boundary of the cavernous sinus rather than within the cavernous sinus itself. These cranial nerves and the internal carotid artery exit the intracranium through different foramina located within the central skull base.

The superior orbital fissure and the optic canal are the most anterior openings of the central skull base. The optic nerve, optic nerve sheath and the ophthalmic artery course through the optic canal while the cranial nerves III, IV and VI as well as the lacrimal, frontal and nasociliary branches of the first division of the trigeminal nerve (V1) exit the cavernous sinus into the orbital apex through the superior orbital fissure. The foramen rotundum is located just posterior to the superior orbital fissure and houses the second division of the trigeminal nerve (V2) (Fig. 13.1). The foramen rotundum communicates anteriorly with the pterygopalatine fossa where a few ganglionic branches leave V2 to travel to the pterygopalatine ganglion (Fig. 13.2) (Moore et al. 1999). V2 gives off the zygomatic and the posterior superior alveolar nerves and then continues anteriorly as the infraorbital nerve within the infraorbital canal. The third division of the trigeminal nerve (V3) courses through the central skull base within the foramen ovale that is situated posteromedially to the foramen rotundum (Fig. 13.3). V3 courses inferiorly to enter the masticator space. Just medial and posterior to the foramen ovale is a groove within the central skull base, located immediately posterior to the cavernous sinus, containing the Meckel's cave. The Meckel's cave houses the trigeminal ganglion anteroinferiorly where the three divisions of the trigeminal nerve are merging together (Kaufman and Bellon 1973; Williams et al. 2003). The trigeminal ganglion gives rise to multiple individual rootlets that course superiorly into

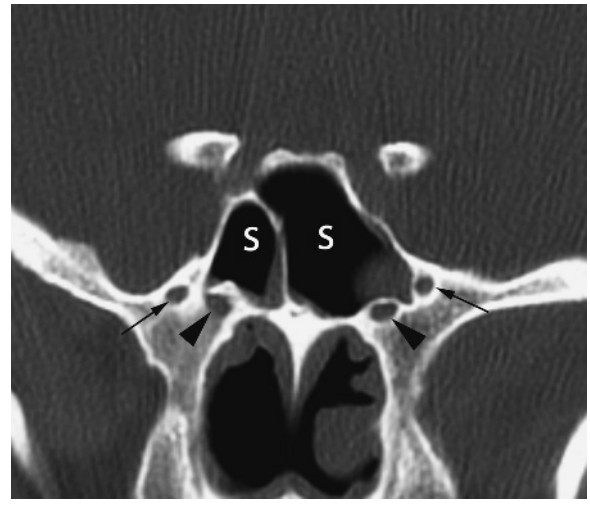

Fig. 13.1. Coronal CT image displayed in bone window demonstrating the relationship of the foramen rotundum (*arrows*) and vidian canal (*arrowheads*) to each other and the sphenoid sinus (*s*) within the central skull base

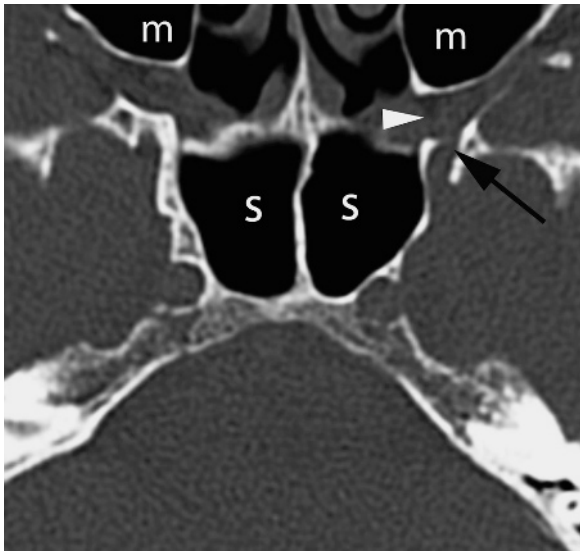

Fig. 13.2. Axial CT image displayed in bone window illustrates the communication of the foramen rotundum (*arrow*) with the pterygopalatine fossa (*arrowhead*) that is located immediately posterior to the maxillary sinus (*m*). *s,* Sphenoid sinus

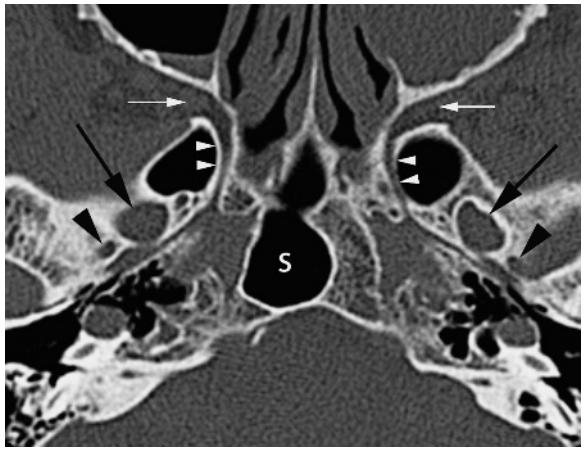

Fig. 13.3. Axial CT image of the central skull base displayed in bone window shows the larger foramen ovale (*black arrows*) on each side and the smaller foramen spinosum (*black arrowheads*) posterior lateral to it. Both assume an oval shape. The *white arrowheads* demarcate the vidian canal that extends from the inferior portion of the pterygopalatine fossa (*white arrows*) to the foramen lacerum within the petrous apex (not demonstrated at this level). *s*, Sphenoid sinus

the trigeminal cistern. The individual rootlets merge together to form the main trunk of the trigeminal nerve just posterior to the trigeminal cistern.

The foramen spinosum and the lacerum portion of the carotid canal are the most posterior foramina of the central skull base (Fig. 13.3). The foramen spinosum is located just posterolateral to the foramen ovale and contains the middle meningeal artery, a distal branch of the external carotid artery, and the meningeal branch of the facial nerve (Fig. 13.3). The middle meningeal artery branches off into multiple small vessels intracranially that form grooves within the superior surface of the central skull base and along the inner table of the frontal and anterior parietal skull. The lacerum portion of the carotid canal is located more medially within the body of the sphenoid bone, at the junction of the petrous apex and clivus (Tauber et al. 1999). It represents the exit site of the internal carotid artery from the carotid canal within the petrous portion of the temporal bone (Fig. 13.4). The internal carotid artery continues superiorly as the carotid siphon to lie within a sigmoid shaped groove along the sphenoid bone within the cavernous sinus. The internal carotid artery exits the cavernous sinus medial to the anterior clinoid process. The vidian canal courses inferior to the carotid siphon within the sphenoid bone forming a direct communication between lacerum portion of the carotid canal and the pterygopalatine fossa (Fig. 13.3) (Chong and Fan 1998). It contains the vidian nerve that is composed of preganglionic parasympathetic fibers of the greater superficial petrosal nerve, the postganglionic sympathetic fibers of the deep petrosal nerve and sensory fibers from the cranial nerve VII.

13.2.2 Posterior Skull Base

The posterior skull base is shaped like a cup. The clivus and the petrous apex create the anterior boundary while the occipital bone forms the posterior and inferior border of the posterior skull base. The lateral boundary of the posterior skull base is established by the occipital bone posteriorly and the mastoid and petrous portions of the temporal bone superoanteriorly and inferoanteriorly, respectively. The occipitomastoid suture connects the occipital bone with the mastoid portion of the temporal bone. The different anatomical structures of the posterior fossa create numerous grooves, crests and foramina within the posterior skull base.

The cerebellar hemispheres cause two indentations along the posterior surface of the posterior skull base with a midline internal occipital crest in between. The occipital crest provides the attachment for the falx cerebelli and extends from the foramen of magnum to the internal occipital protuberance. One vertical and two horizontal grooves extend superiorly

and laterally from the internal occipital protuberance housing the superior sagittal sinus and the transverse sinuses, respectively. The horizontal grooves extend anteroinferiorly to continue as the sigmoid sulci that contain the sigmoid sinus on each side. The sigmoid sinus subsequently enters the jugular foramen and continues through the skull base into the neck as the internal jugular vein.

The jugular foramen and the foramen magnum are the largest openings of the posterior skull base. The jugular foramen lies at the posterior end of the petro-occipital fissure and is bordered by the petrous bone of the temporal bone anteriorly and the occipital bone posteriorly. It is partially subdivided by the jugular spine into two compartments: the pars venosa and the pars nervosa (Fig. 13.5) (Inserra et al. 2004; Sen et al. 2001). Only occasionally the bony jugular spine continues as a fibrous or osseous septum posteriorly to completely separate these two compartments. The pars venosa lies posterolateral and contains the internal jugular bulb laterally and the cranial nerves X and XI medially (Fig. 13.5). The pars nervosa is located anterior medially and contains the cranial nerve IX medially and often the inferior petrosal sinus laterally (Fig. 13.5). The internal carotid artery enters the skull base anterior to the jugular foramen (Fig. 13.5). Therefore, all three of these cranial nerves lie between the internal jugular vein and the internal carotid artery below the skull base, with the cranial nerve IX being the most anterior lateral and the cranial nerve XI the most posterior medial in position.

The cranial nerve XI is very unique as it extends through the posterior skull base twice: Once to exit the skull base through the jugular foramen as mentioned above and once to enter the posterior cranial fossa through the foramen magnum as parts of its fibers originate from the cervical spinal cord. The remaining spinal accessory nerve fibers originate from the medulla oblongata that merges with the cervical spinal cord fibers at the foramen of magnum. The cranial nerves XI lie posterior to the vertebral arteries that ascend from cervical to intracranial through the foramen of magnum. The vertebral arteries give rise to the posterior cerebellar arteries that course posteroinferiorly to supply the inferior cerebellar hemispheres. In turn, the paired posterior spinal arteries arise either from the intracranial portion of the vertebral arteries or occasionally from the posterior cerebellar arteries and continue inferiorly to descend through the foramen of magnum to supply the spinal cord.

The posterior skull base has few additional, smaller openings. The porus acusticus is the medial opening of the internal auditory canal along the posterior surface of the petrous bone. It contains the cranial nerve VII and VIII as well as branches of the anterior inferior cerebellar artery that supply the inner ear. Inferior and posterior to it are the openings of the cochlear and vestibular aqueducts, respectively. The vestibular aqueduct courses almost parallel to the posterior margin of the petrous bone between the vestibule and the intracranium and contains the endolymphatic duct. In contrast, the cochlear aqueduct runs almost parallel to the internal auditory canal between the basal turn of the cochlea and the intracranium within the inferior aspect of the petrous portion of the temporal bone and transmits the perilymphatic duct (Mukherji et al. 1998). Even more inferiorly within the petrous bone is the hypoglossal foramen located just inferomedial to the jugular foramen (Fig. 13.6). It contains the cranial nerve XII, the hypoglossal venous plexus and a meningeal branch of the ascending pharyngeal artery. Below the skull base, the cranial nerve XII continues inferiorly

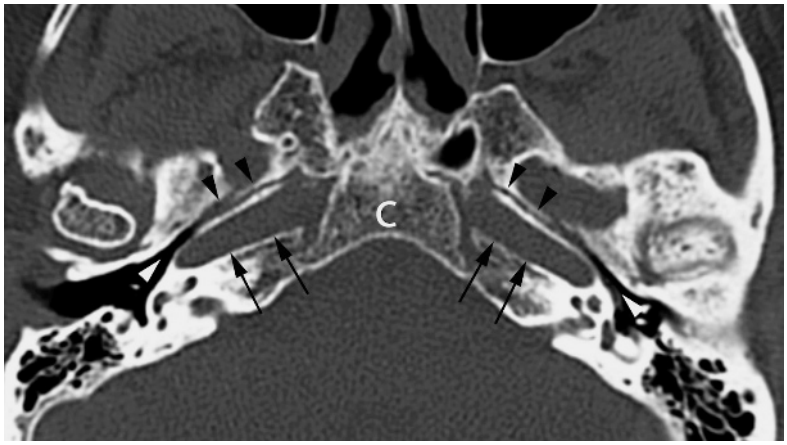

Fig. 13.4. Axial CT image displayed in bone window illustrates the close relationship of the clivus (*c*) centrally and the internal carotid artery canal within the petrous apex laterally (*arrows*). The Eustachian tube courses parallel to the internal carotid artery canal through the petrous bone (*black arrowheads*). The *white arrowheads* demarcate the Eustachian tube openings within the middle ear cavities

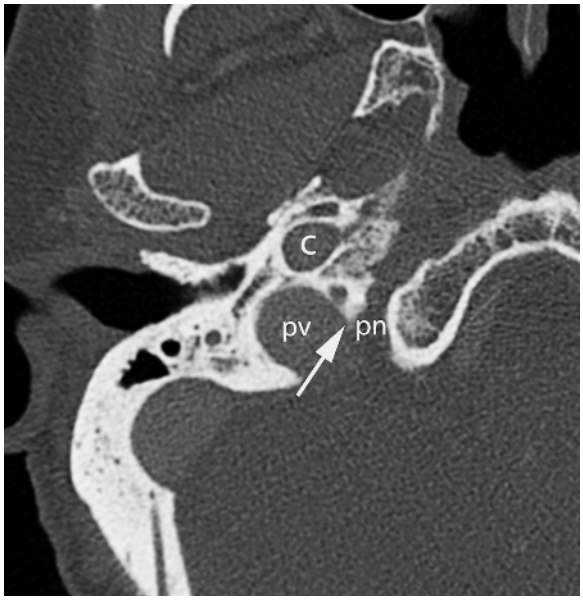

Fig. 13.5. Axial CT image of the right jugular fossa displayed in bone window shows the jugular spine (*arrow*) dividing the jugular foramen into the pars venosa (*pv*) laterally and pars nervosa (*pn*) medially. The internal carotid artery (*c*) lies anterior to the pars venosa (*pv*)

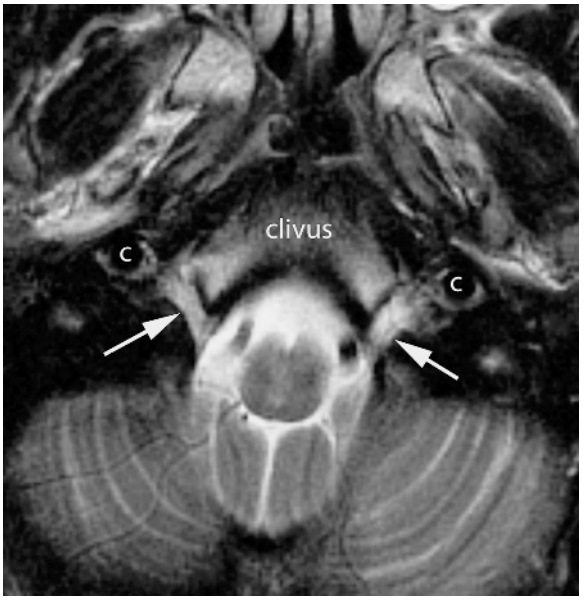

Fig. 13.6. Axial T2-weighted image through the lower clivus demonstrates the oblique course of the hypoglossal canal (*arrows*) along the lateral edge of the clivus on each side. The exit of the hypoglossal canal (*arrows*) is in close proximity to the internal carotid artery (*c*)

between the internal carotid artery and the internal jugular vein.

13.3 Clinical Presentation

Only few skull base lesions present with specific, disease related symptoms that significantly help to narrow the differential diagnosis. The Gradenigo's triad represents one of them and is characterized by ipsilateral cranial nerve VI paralysis, severe facial pain in V1 distribution and inflammatory disease of the inner ear and/or mastoid air cells (Gradenigo 1904). As the triad indicates, this symptom complex has been associated with acute inflammatory disease of the ear. However, less than 50% of the patients present with all three of these symptoms. In particular, cranial nerve VI palsy has been described as the least reliable clinical sign of the triad making distinction to other skull base entities more difficult (Price and Fayad 2002). Hence, the majority of patients with skull base pathology present with non-specific neurological symptoms related to the mass effect caused by the lesion. These symptoms can be related to cranial nerve dysfunction, vascular compromise or direct compression of the brain or orbital structures. The clinical symptoms of cranial nerve palsies are summarized in Table 13.1.

13.4 Normal Anatomical Variations

Normal anatomical variations are asymptomatic and typically discovered incidentally in patients that seek medical attention for an unrelated reason. Asymmetric aeration of the petrous apex is most likely the most common entity that is mistaken for a petrous apex mass, in particular on MR imaging (Fig. 13.7). CT certainly is easier to interpret in this regard; however, close attention to the imaging characteristics can facilitate the correct diagnosis on MR images as well. In particular, lack of mass effect and increased T1 signal intensity of the fatty bone marrow within the unaerated petrous apex is characteristic (Fig. 13.7a). Asymmetric accumulation of fluid within the petrous apex air cells will show intermediate T1 and high T2 signal intensity and may be mistaken for a chondrosarcoma; however, the lack of mass effect and of contrast enhancement as well as often accompanied fluid within the middle ear cavity

Table 13.1. Clinical symptoms of cranial nerve palsies

Cranial nerve	Symptoms
Cranial nerve III (Oculomotor nerve)	Diplopia due to inability to move the ipsilateral eye superiorly, inferiorly and medially Ptosis Fixed and dilated pupil
Cranial nerve IV (Trochlear nerve)	Diplopia due to inability to move the ipsilateral eye inferomedially
Cranial nerve V (Trigeminal nerve)	Loss of sensation or dysaesthesia in the ipsilateral face Ipsilateral loss of jaw clenching and side to side movement
Cranial nerve VI (Abducens nerve)	Diplopia due to inability to move the ipsilateral eye laterally
Cranial nerve VII (Facial nerve)	Loss of taste in the anterior 2/3 of the tongue Ipsilateral facial drop
Cranial nerve VIII (Vestibulocochlear nerve)	Ipsilateral sensorineural hearing loss Dizziness
Cranial nerve IX (Glossopharyngeal nerve)	Loss of oropharyngeal sensation Loss of taste and sensation to the posterior 1/3 of tongue
Cranial nerve X (Vagus nerve)	Nasal speech due to ipsilateral palatal weakness Hoarseness due to ipsilateral vocal cord paralysis
Cranial nerve XI (Spinal accessory nerve)	Weakness and wasting of the ipsilateral sternocleidomastoid and trapezius muscles
Cranial nerve XII (Hypoglossal nerve)	Wasting and fasciculation of the tongue Tongue tip deviation to paralyzed side on protrusion

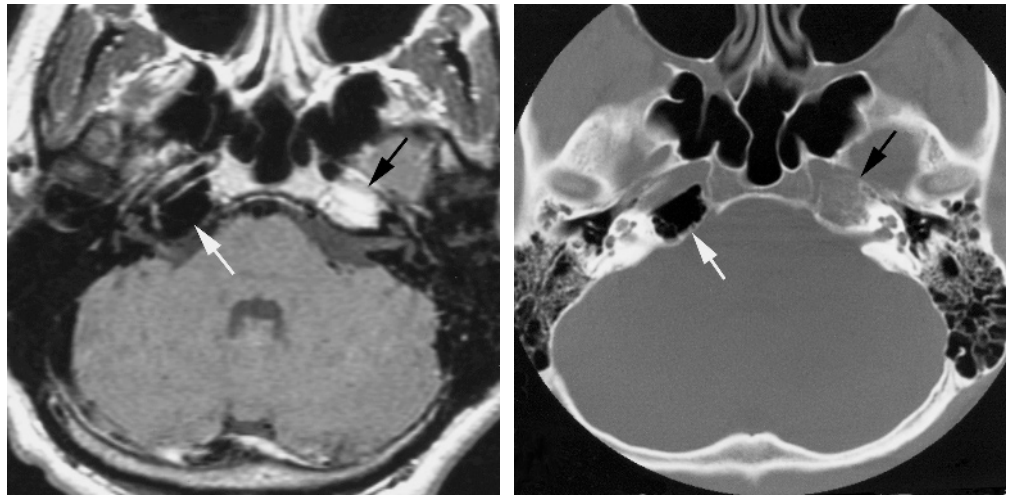

a **b**

Fig. 13.7a,b. Axial non-contrast enhanced T1-weighted (**a**) and CT image displayed in bone window (**b**) illustrate the appearance of an aerated petrous apex on the right (*white arrows*) and of non-aerated petrous apex on the left (*black arrows*). The non-aerated petrous apex is increased in T1 signal intensity (*black arrow* in **a**) in this patient due to fatty bone marrow but may also assume lower attenuation when red bone marrow is present in this location, e.g. in young patients

and/or mastoid air cells should call such a diagnosis into question.

A high riding jugular bulb or a jugular bulb diverticulum might be mistaken for a mass within the jugular foramen. Close evaluation of all images in the different planes and on the various sequences typically reveals inconsistency of the flow pattern with the classic flow void seen in at least one plane or on one sequence in such cases.

Mottled fatty replacement of the bone marrow may mimic a diffuse infiltrative process of the skull base that might be impossible to distinguish from lymphoma, leukemia, multiple myeloma or diffuse metastatic disease. Correlation to clinical symptoms, age, gender and history of an underlying malignancy might help to develop a risk profile that does or does not warrant further evaluation with bone scan, bone marrow biopsy or cross-sectional imaging follow-up.

13.5 Pathology

The skull base is composed of different tissue components and houses a variety of structures that can serve as the origin of skull base masses. Therefore, the spectrum of possible skull base abnormalities is very broad. Skull base lesions overall are rare, with metastatic disease and lymphoma accounting for most of the lesions. Primary malignancies of the skull base are even more scarce but can be often mistaken for benign lesions, and vice versa, creating a diagnostic dilemma. In addition, some of the benign entities show an aggressive growth pattern that might require more aggressive treatment. Therefore, the discussion of pathology of the skull base will also include benign entities that can be mistaken for or that need to be treated more like a malignant lesion.

Skull base lesions can be divided into two broad categories: diffuse or localized abnormalities. Diffuse involvement of the skull base may manifest as diffuse replacement of the bone marrow or as multi-focal lesions. Localized lesions in turn can be subdivided into region-specific and region-non-specific entities. This approach in the evaluation of skull base abnormalities is an important starting point. The exact location of the lesion together with its imaging characteristics, patient's demographics and clinical presentation might then further narrow the differential diagnostic considerations.

13.5.1 Malignant Lesions Causing Diffuse or Multi-focal Skull Base Involvement

Multiple myeloma, lymphoma, leukemia and metastatic disease are the main malignant entities able to cause diffuse replacement of the bone marrow or multi-focal involvement of the skull base (Figs. 13.8 and 13.9). Often, the skull and the visualized portions of the cervical spine are also affected (Fig. 13.8a). Although any primary cancer can metastasize to the skull base, prostate, lung and breast cancer outnumber the other malignancies (Laigle-Donadey et al. 2005; Layer et al. 1999).

13.5.2 Mimics of Malignant Lesions Causing Diffuse or Multi-focal Skull Base Involvement

Diffuse replacement of the fatty by red bone marrow due to chronic anemia may mimic diffuse infiltration of the skull base by an underlying malignant entity. MR imaging findings are often not helpful as both

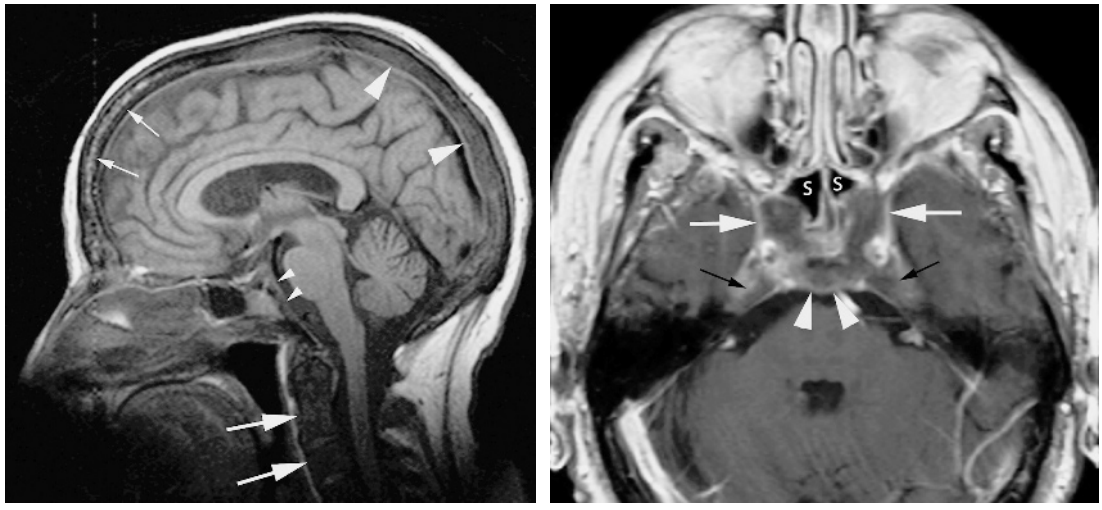

a b

Fig. 13.8a,b. Sagittal non-contrast enhanced T1-weighted image (**a**) demonstrates completely replaced fatty bone marrow by diffuse metastatic disease in the majority of the skull (*large arrowheads* in **a**) and cervical spine (*large arrows* in **a**) while the bone marrow of the frontal skull is more mottled in appearance (*small arrows* in **a**) that is consistent with less extensive involvement. In addition, there is lack of fatty bone marrow within the clivus (*small arrowheads* in **a**) due to involvement by metastatic disease. The extent of the skull base metastasis is markedly better seen on the axial contrast enhanced T1-weighted image (**b**) showing posterior bulging of the clivus (*arrowheads* in **b**), extension into the petrous apex bilaterally (*black arrows* in **b**), into the cavernous sinuses (*white arrows* in **b**) and into the sphenoid sinuses (*s* in **b**)

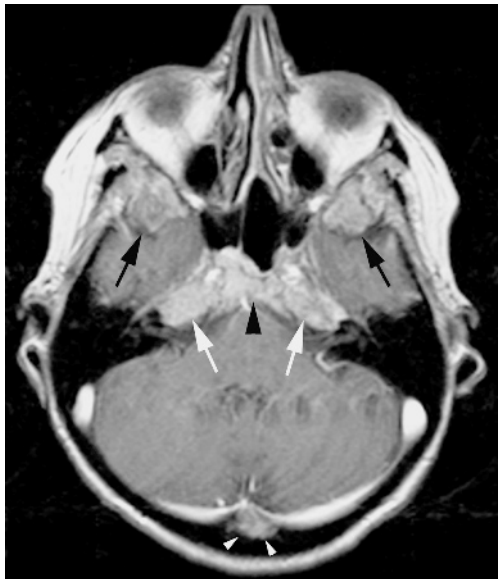

Fig. 13.9. Axial contrast enhanced T1-weighted image through the upper orbit level shows replacement of the fatty bone marrow with associated bony expansion of the greater sphenoid wings bilaterally (*black arrows*), clivus (*black arrowhead*), petrous apexes (*white arrows*) and in the occipital skull (*white arrowheads*) related to multiple myeloma

entities result in decreased attenuation of the bone marrow on T1- and fast spin-echo T2-weighted images and show enhancement following intravenous contrast administration (Laigle-Dondey et al. 2005; Yildrim et al. 2005; Loevner et al. 2002). CT may or may not provide additional clues as not all patients with multiple myeloma, lymphoma, leukemia or metastatic disease show bony destruction within the diploic space or early erosions of the inner and or outer table. Therefore, clinical history and laboratory results might provide the most helpful information in some patients. Bone marrow expansion can also occur and mimic diffuse malignant involvement of the skull base and skull. It is usually seen with severe anemia such as hemolytic anemia or thalassemia (Yildrim et al. 2005; Tunaci et al. 1999). MR might deliver ambiguous results but CT usually solves the dilemma as the bone thickening caused by the bone marrow expansion is in disproportion to the preserved diploic trabecula and the intactness of the inner and outer tables of the skull (Fig. 13.10). Sites of extrapoetic bone marrow, such as within the paranasal sinuses, might occasionally also be seen, supporting the benign nature of the bone marrow expansion (Tunaci et al. 1999; Joseph et al. 2004).

Gorham, or vanishing bone disease, is an extremely rare bone disorder that can occur at any age and affects both genders equally. This disease is characterized by osteolysis of unknown etiology that is associated with angiomatous proliferation within the bone or adjacent soft tissues (Gorham et al. 1954). It can manifest as single or multiple lytic lesions involving any bone, but the calvarium and the mandible are most commonly affected (Fig. 13.11). Since it is such a rare entity, metastatic disease or multiple myeloma will be by far the most common cause of multiple lytic bony lesions.

13.5.3 Non-region Specific, Localized Malignant Skull Base Lesions

All malignancies that can cause diffuse or multi-focal involvement of the skull base (metastatic disease, lymphoma, leukemia and plasmocytoma) as well as different sarcomas can present as localized lesions anywhere in the skull base. These might be difficult to distinguish from each other without further clinical information. In general, metastatic disease is more aggressive in appearance and causes frank bone destruction even in early stages, while localized lymphoma and leukemia (often referred to as chloroma) show more permeative growth pattern with preservation of the diploic trabecula and of the cortical bony margins even with large tumors (Figs. 13.12 and 13.13). In addition, it has been reported that highly cellular tumors with small extracellular compartments, such as lymphoma, leukemia and Ewing' sarcoma, often demonstrate re-

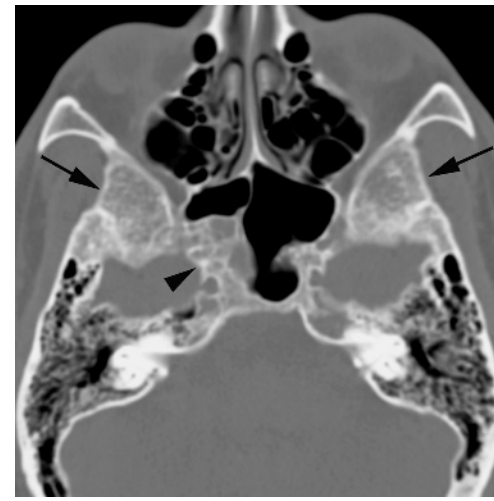

Fig. 13.10. Axial CT displayed in bone windows demonstrates marked expansion of the greater sphenoid wings (*arrows*) that is also more cystic in appearance within the body of the sphenoid bone on the right (*arrowhead*). Thalassemia is the underlying cause of bony expansion in this patient

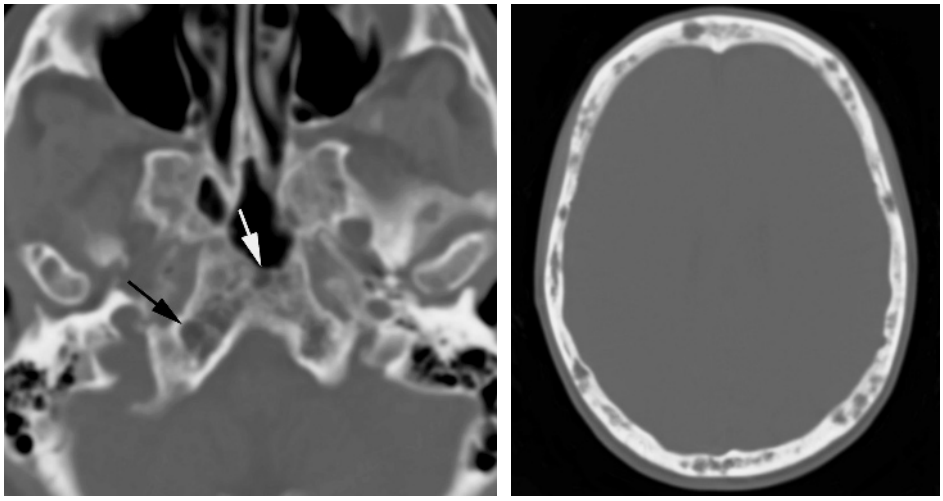

a b

Fig. 13.11a,b. Axial CT images displayed in bone window through the central skull base (**a**) and skull (**b**) show multiple small punched out skull base (*arrows*) and numerous lytic skull lesions caused by Gorham's disease

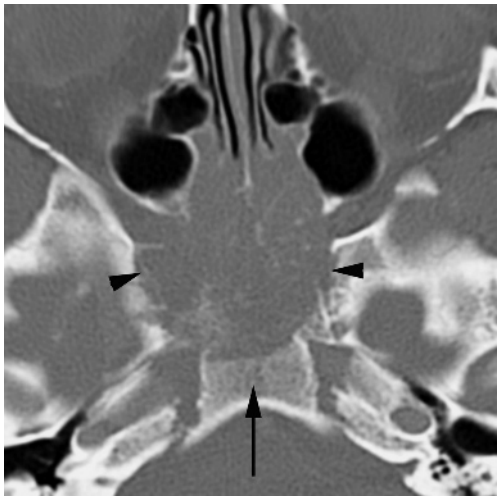

Fig. 13.12. Axial CT image displayed in bone window shows destruction of the sphenoid body (*arrowheads*) and clivus (*arrow*) caused by an aggressive skull base metastasis

stricted diffusion on the diffusion weighted images (DWI), with increased signal intensity on the DWI and reduced signal intensity on the apparent diffusion coefficient (ADC) maps (Guo et al. 2002; Mascalchi et al. 2005). In contrast, metastatic disease typically does not show restricted diffusion. Therefore, DWI might be a useful tool in narrowing the differential diagnostic possibilities in patients with inconclusive conventional MR and clinical findings.

Ewing's sarcoma is a rare and highly malignant neoplasm of the bone arising from the primitive neuroectoderm (Rueda-Franco and Lopez-Correla 1995; Kozlowski et al. 1991). It most commonly involves the long bones, pelvis, ribs and only very rarely the skull base and vault. It typically occurs in children between 5 and 13 years of age. Neurological deficits are the leading clinical symptoms caused by the mass effect from the tumor. Aggressive chemotherapy is the primary and usually successful treatment choice for Ewing's sarcoma, while surgery is reserved for cranial nerve decompression and radiation therapy for tumors unresponsive to chemotherapy (Carlotti et al. 1999). On imaging, Ewing's sarcoma presents as an osteolytic lesion causing erosions of the inner and/or outer table in association with an extracranial soft tissue mass of variable size and a significant epidural component causing local mass effect upon the adjacent brain parenchyma. The epidural component of the tumor rarely invades the dura or the brain parenchyma. On CT, the tumor itself is usually iso- to hyperdense and shows heterogeneous enhancement following intravenous contrast administration. MR is superior in delineation of the epidural component to adjacent dura and brain parenchyma. In addition, the restricted diffusion seen on the DWI part of the study might provide useful hints to the nature of the mass (Guo et al. 2002; Mascalchi et al. 2005). In recent years, spectral karyotyping has been introduced as an additional diagnostic tool as it has been shown that Ewing's sarcomas have a characteristic 11;22 chromosomal translocation and/or EWS/FLI1 fusion transcript (Carlotti et al. 1999).

Osteosarcoma is the second most common primary bone tumor after multiple myeloma of the skeleton. It typically arises from the metaphysis of the long bones, especially of the femur and proximal tibia. It only very rarely involves the skull and skull base.

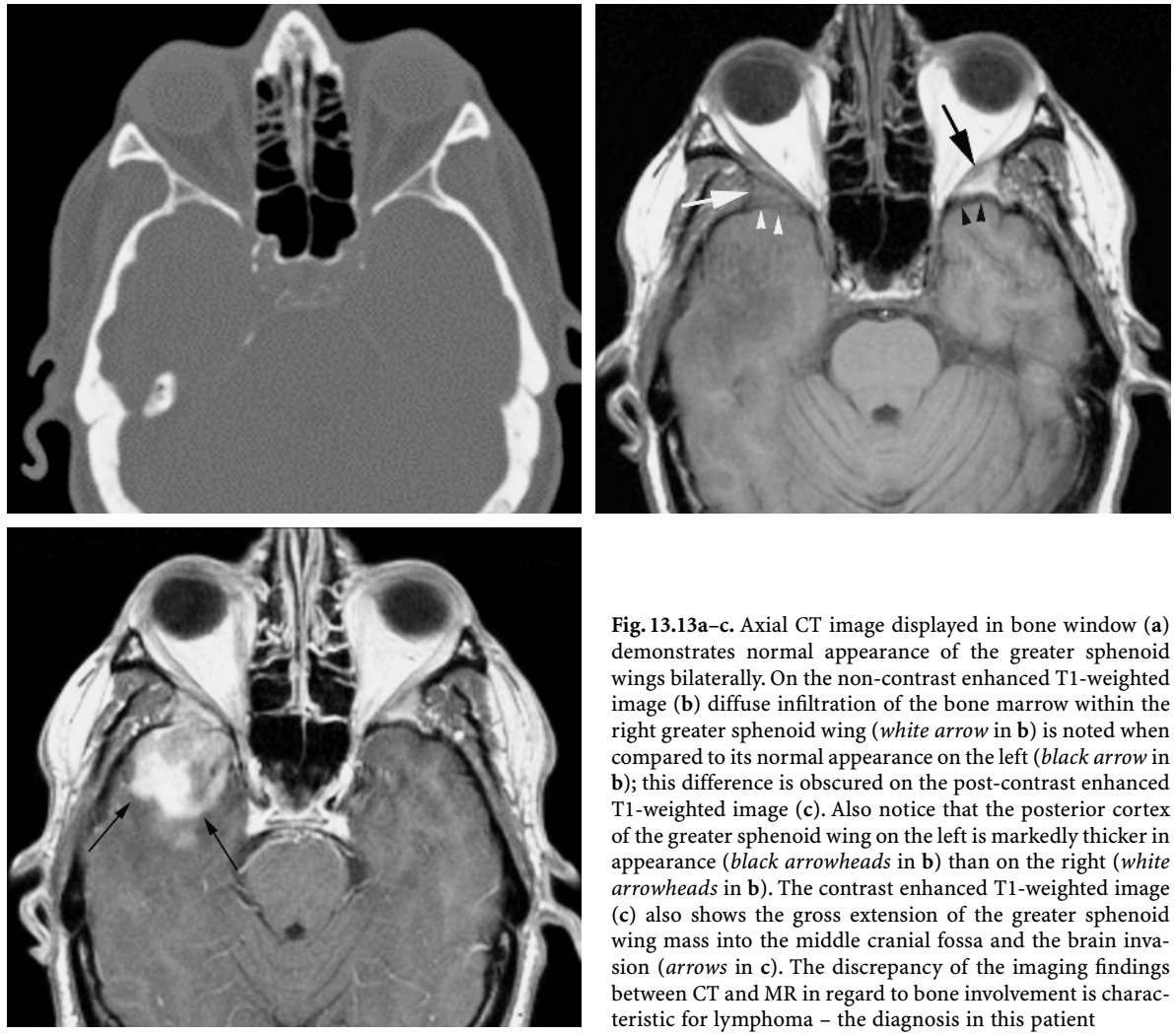

Fig. 13.13a–c. Axial CT image displayed in bone window (**a**) demonstrates normal appearance of the greater sphenoid wings bilaterally. On the non-contrast enhanced T1-weighted image (**b**) diffuse infiltration of the bone marrow within the right greater sphenoid wing (*white arrow* in **b**) is noted when compared to its normal appearance on the left (*black arrow* in **b**); this difference is obscured on the post-contrast enhanced T1-weighted image (**c**). Also notice that the posterior cortex of the greater sphenoid wing on the left is markedly thicker in appearance (*black arrowheads* in **b**) than on the right (*white arrowheads* in **b**). The contrast enhanced T1-weighted image (**c**) also shows the gross extension of the greater sphenoid wing mass into the middle cranial fossa and the brain invasion (*arrows* in **c**). The discrepancy of the imaging findings between CT and MR in regard to bone involvement is characteristic for lymphoma – the diagnosis in this patient

Secondary osteosarcomas are also rare and usually occur in the setting of previous radiation therapy or arising from benign lesions with malignant potential such as Paget's disease, multiple osteochondromatosis and chronic osteomyelitis (Salvati et al. 1993; Shinoda et al. 1993). The imaging characteristics depend on the type of the osteosarcoma. While parosteal osteosarcoma is limited to the outer table, the other types of osteosarcomas show inner and outer table involvement with associated involvement of the subdural space and brain parenchyma in approximately 40% of cases (Garland 1945). The degree of intracranial involvement is inversely related to patient's prognosis (Whitehead et al. 1998). Small fluid–fluid levels may be seen in cases of telangiectatic osteosarcoma. Radical surgical excision is the treatment of choice which is usually not feasible in the skull base. Therefore, patients with skull base osteosarcomas are carrying a worse prognosis than patients with osteosarcomas of other parts of the skeleton.

13.5.4 Mimics of Non-region Specific, Localized Malignant Skull Base Lesions

Fibrous dysplasia of the skull base is relatively common and is a developmental anomaly of the bone forming mesenchyma in which the transformation of woven to lamellar bone is disturbed. This causes an arbitrary arrangement of the bony trabeculae that are embedded in an overgrowth of a well-vascularized fibrous stroma. It represents a benign lesion, with extremely low potential for malignant transformation that usually occurs secondary to radiation therapy (Utz et al. 1989). Fibrous dysplasia is often

mistaken for a skull base tumor as it can assume any appearance on MR imaging (Fig. 13.14) (Chong and Fan 1998; Utz et al. 1989). It may show low attenuation on all sequences reflecting the high degree of mineralization but can also demonstrate any other combination of signal intensities on the various sequences without or with mild to extensive enhancement reflecting the different degrees of fibrous and cystic components. In contrast, plain radiographs and CT show characteristic imaging features with bone marrow expansion, "ground glass" appearance and preservation of the adjacent cortex (Fig. 13.14b). Only rarely, fibrous dysplasia presents as a lytic lesion. It is usually unilateral and monostotic in nature. It can occur anywhere in the skull but prefers the anterior and central skull base. It spares the membranous labyrinth, facial nerve canal and the internal auditory canal. Clinically, it is silent in the majority of cases and is usually incidentally found on imaging. The symptomatic patients seek medical attention because of cosmetically undesirable skull and/or facial deformities, or neurological symptoms caused by narrowing of the skull base neural foramina and subsequent cranial nerve compression that may benefit from decompressive surgery.

Langerhans cell histiocytosis is a group of idiopathic neoplasms that are characterized by proliferation of mature eosinophilic and specialized bone marrow-derived Langerhans cells. Three major types have been described: infantile form (Letterer-Siwe disease), Hand-Schüller-Christian disease and eosinophilic granuloma (Howarth et al. 1999). Eosinophilic granuloma represents the localized form of Langerhans cell histocytosis and represents the variety most commonly seen by radiologists. It typically occurs in children between 5 and 15 years of age. The lesions are usually asymptomatic but may manifest with bone pain, palpable soft tissue mass or symptoms related to mass effect such as proptosis or cranial nerve neuropathies (Miller et al. 1978). Usually eosinophilic granuloma presents as unifocal bony lesions, typically involving the frontal and temporal bones (DiNardo and Wetmore 1989). On imaging, eosinophilic granuloma presents as a radiolucent, round to oval punch-out bony defect without sclerosis of its margins, with an enhancing soft tissue mass within the bony defect. Hand-Schüller-Christian disease is a chronic, systemic and multi-focal variant of Langerhans cell histiocytosis with peak onset between 2 and 10 years of age. These patients typically present with diabetes insipidus, exophthalmos, chronic otorrhea and hearing loss related to multi-focal and/or bilateral skull and skull base involvement. Other organs (lymph nodes in 50%, liver in 20%, spleen in 30%) and skin might also be involved (Howarth et al. 1999). Letterer-Siwe disease is a diffuse, systemic and the most severe form of Langerhans cell histocytosis. It presents in children

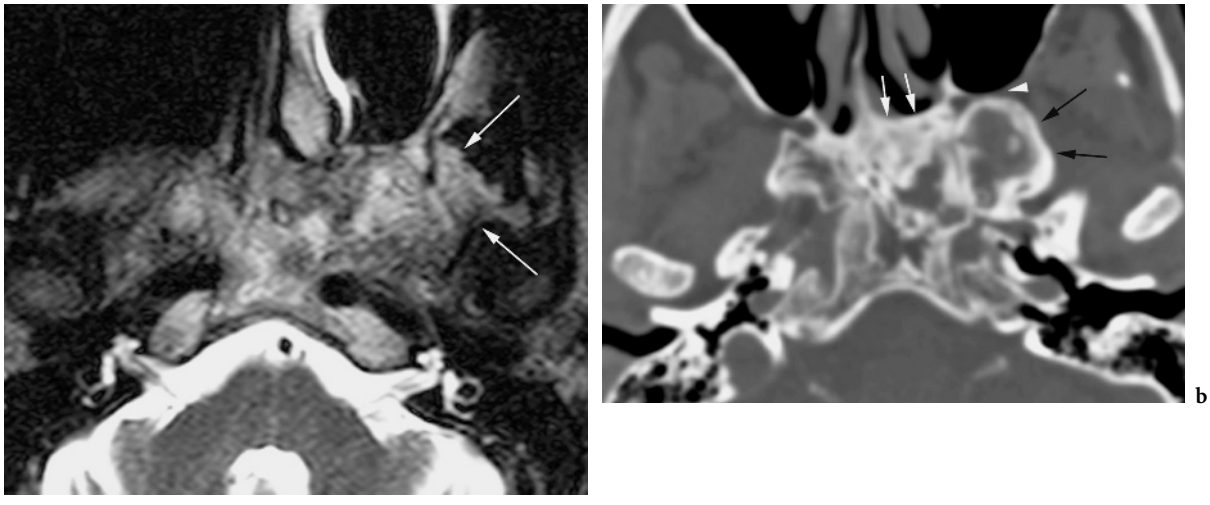

Fig. 13.14a,b. Axial T2-weighted image through the central skull base (**a**) demonstrates marked enlargement of the sphenoid body and even more of the left pterygoid process (*arrows* in **a**). The differential diagnosis for such an appearance is broad with benign and malignant entities. The axial CT image (**b**) displayed in bone window clearly shows that this is fibrous dysplasia as focal areas of ground-glass appearance (*white arrows* in **b**) are seen but more importantly there is preservation of the bony cortex even in the significantly enlarged pterygoid process on the left (*black arrows* in **b**) – a characteristic feature of fibrous dysplasia. Notice the severe narrowing of the pterygopalatine fossa (*arrowhead* in **b**) that could result in cranial nerve or vascular dysfunction

less than 2 years of age with skin eruption, anemia and hepatosplenomegaly. It is universally fatal within a few years. While solitary bone lesions are treated locally with curettage or excision, systemic chemotherapy and or bone marrow transplantation is indicated in the systemic forms of the disease (Howarth et al. 1999).

Dermoid tumors are uncommon lesions and represent inclusion cysts rather than true neoplasms. They derive from misplaced ectodermal elements during the process of neural tube closure. The tumors are usually well-defined and multi-lobulated in appearance. They have an outer connective tissue capsule that is lined with stratified squamous epithelium and contains hair follicles, different glands, desquamated epithelial keratin and most importantly some lipid material. This composition influences the heterogeneous appearance of these tumors on imaging. Nevertheless, these tumors typically contain various amounts of lipid material that is visible on imaging as very low density on CT images and high signal intensity on T1-weighted images, facilitating the correct diagnosis (Smirniotopoulos and Chiechi 1995; Gormley et al. 1994). Contrast enhancement is uncommon. Dermoid tumors involving the central nervous system typically present as a midline intracranial mass. Skull, skull base and orbit represent the most common extracranial location in the head and neck region (Cummings et al. 2004). Complete surgical excision is the standard treatment. Resectability, however, depends upon the location of the tumor, e.g. encroachment upon vasculature and nerves.

13.5.5 Malignant Central Skull Base Lesions

Invasive and malignant pituitary gland tumors are rare and represent a continuum of disease, as pituitary carcinomas usually occur in the setting of pre-existing invasive pituitary gland tumors (Ragel and Couldwell 2004). Both show locally aggressive growth pattern with tendency for early skull base invasion in contrast to the slowly growing benign pituitary gland tumors that like to decompress into the suprasellar cistern (Fig. 13.15). Distinct immunohistochemical markers (interleukin 6 and heat shock protein 27) that have been found to be elevated in invasive types but not in the benign variants of pituitary gland tumors are felt to be responsible for this biological aggressiveness of the invasive tumor variants (Gandour-Edwards et al. 1995). Often these tumors are large at presentation or fast growing on serial follow-up. Otherwise, they show similar imaging characteristics to their benign variants. Their large size and local aggressive growth pattern sometimes make them difficult to distinguish from other malignant central skull base lesions (Figs. 13.15 and 13.16). The majority of invasive variants of pituitary gland tumors are endocrinologically active with 42% secreting adrenocorticotrophic hormone (ACTH) and 33% prolactin. Presence of metastatic disease distinguishes the invasive pituitary gland tumor from the carcinoma form (Ragel and Couldwell 2004). Metastatic disease primarily occurs to the central nervous system (cerebrum, cerebellum, spinal cord, leptomeninges and subarachnoid space) and search for it needs to be conducted in suspected invasive pituitary gland tumor as metastatic lesions might be already present on the initial imaging study. Systemic metastases most commonly involve the lymph nodes, bone, liver and ovaries. Overall, pituitary carcinomas have a very poor prognosis with a reported 1-year survival rate of 34%. For the patient it is critical that the radiologist recognizes the invasive nature of a pituitary gland tumor, as an aggressive treatment plan is critical prior to development of metastatic disease.

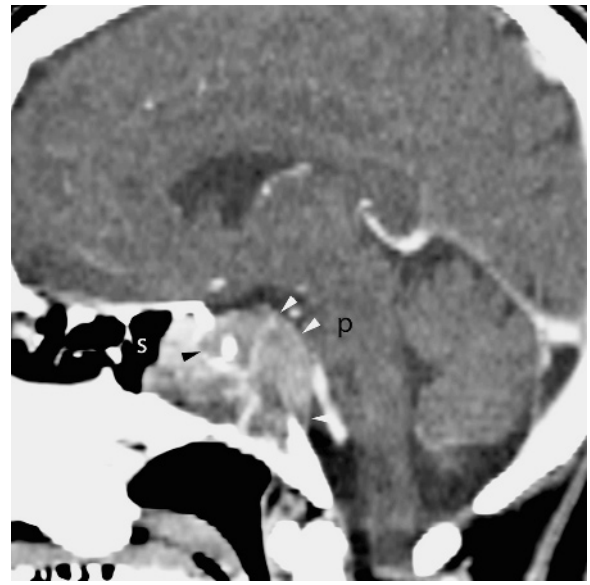

Fig. 13.15. Contrast enhanced, sagittal multiplanar CT reformation displayed in soft tissue window illustrates a large central skull base mass with gross invasion of the sphenoid sinus (*s*). In addition, the clivus (*c*) is almost completely involved by this mass that also bulges posteriorly into the prepontine cistern (*white arrowheads*) where it flattens the pons (*p*). The sella (*black arrowhead*) is also involved without significant suprasellar component. This represented an invasive pituitary gland adenoma. Please notice the discrepancy between the suprasellar and the intraclival component that is more characteristic for aggressive pituitary gland tumor variants

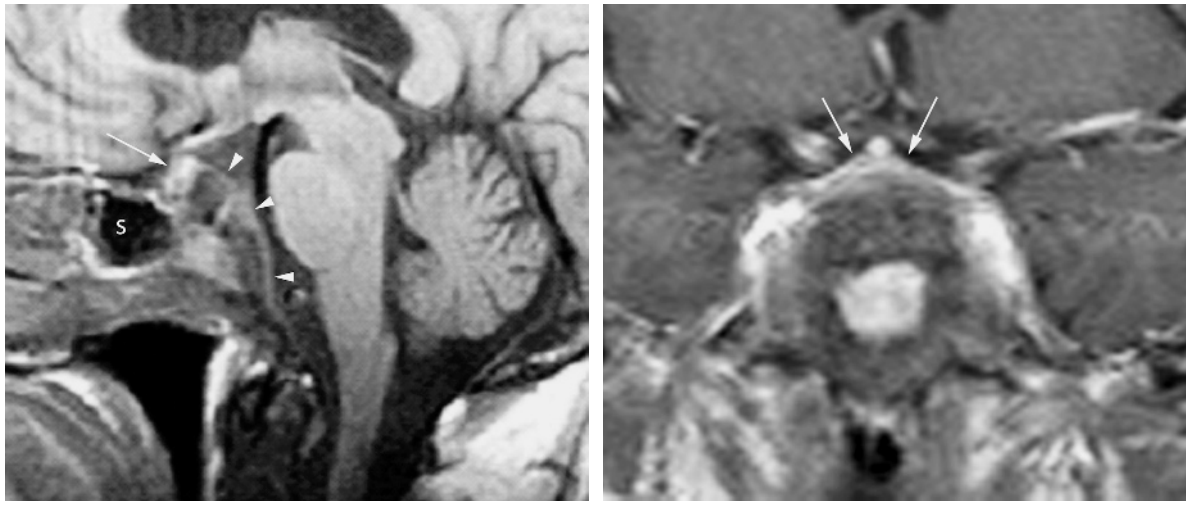

a b

Fig. 13.16a,b. Sagittal (**a**) and coronal (**b**) contrast enhanced T1-weighted images demonstrate a large central skull base mass completely involving the clivus. The extent of the mass is similar to Fig. 13.15 although the sphenoid sinus (*s* in **a**) is not involved and the posterior bulging into the prepontine cistern (*arrowheads* in **a**) is not as extensive. More importantly, however, is that the pituitary gland can be seen as it is displaced anterior and superior on the sagittal view (*arrow* in **a**) and is markedly flattened on the coronal view (*arrows* in **b**) obviating an invasive pituitary tumor as the etiology of this skull base mass. This represented a metastatic lesion

Neuroblastoma is an embryonal malignancy arising from neuroblasts of the sympathetic nervous system (Brodeur and Castleberry 2001). They can occur as primary or secondary neuroblastomas of the skull base. The primary neuroblastomas arise from the olfactory bulb and are therefore discussed in Chap. 11. Secondary neuroblastomas represent metastatic disease to the skull base with a tendency for orbital wall involvement including the portions formed by the greater sphenoid wings (Fig. 13.17). Little has been reported in regard to imaging findings of metastatic neuroblastoma to the skull base; however, since neuroblastoma is a small cell tumor with high cellularity and little extracellular space it is not surprising that it shows restricted diffusion on DWI (Fig. 13.17c). Patients with orbital involvement may present with proptosis, periorbital ecchymosis, diplopia or vision loss. Otherwise, the symptoms are related to the primary lesions, "blueberry muffin" resembling skin disease or a paraneoplastic systemic syndrome with myoclonic jerking and random eye movements (=opsoclonus) (Brodeur and Castleberry 2001). The treatment and prognosis of neuroblastoma depends upon tumor stage, age of the patient, histological and molecular features.

In the central skull base region, schwannomas may arise from cranial nerve III through VI. Benign trigeminal nerve (cranial nerve V) schwannomas are the most common cranial nerve tumors with a reported incidence of up to 0.4% of all intracranial tumors. Malignant schwannomas are even more rare. All but trigeminal nerve malignant schwannomas have been linked to neurofibromatosis type 1 (Stone et al. 2001). Malignant schwannomas of the trigeminal nerve are rather sporadic in occurrence with no known risk factors. The clinical presentation of the benign and malignant variants of central skull base schwannomas is similar and related to dysfunction of the cranial nerve primarily involved and subsequent mass effect related dysfunction of the remaining cranial nerves within the cavernous sinuses. There are no characteristic distinguishing imaging features between benign and malignant types of schwannomas. The more aggressive nature of the schwannoma may be suggested when rapid tumor growth or extensive nerve involvement is seen. In addition, presence of early erosions of the skull base foramina that are in disproportion to the size of the schwannoma might provide important clues (Stone et al. 2001). Due to the rarity of malignant schwannomas little is known in regard to most optimal treatment. Complete surgical resection is certainly the main goal but usually not feasible. In addition, it has been reported that malignant schwannomas have 50% local recurrence rate despite negative surgical margins and adjuvant radiotherapy. Therefore, the overall prognosis is poor with a reported 5-year survival between 38% and 65% (Stone et al. 2001).

Primary extradural meningioma of the skull base is rare with its malignant variant being extraordinarily

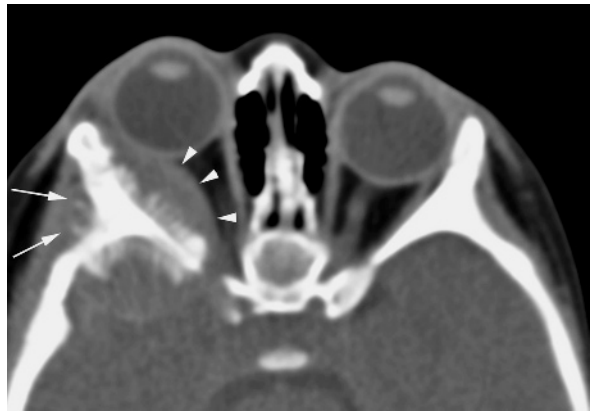

a

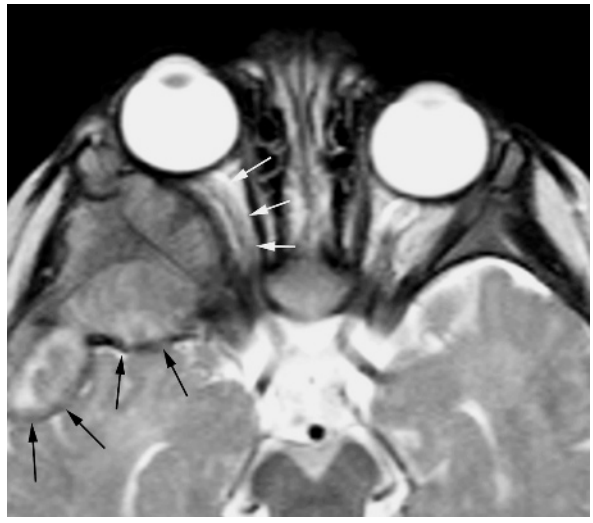

b

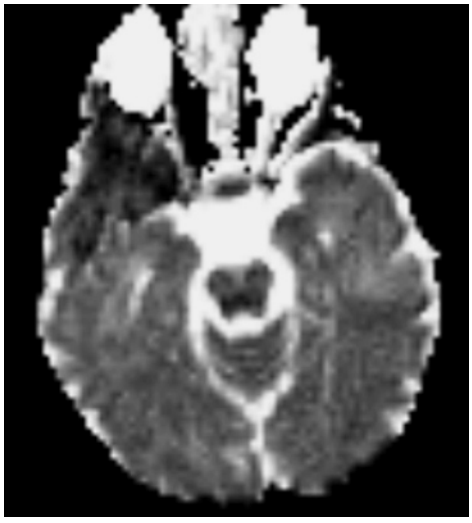

c

Fig. 13.17a–c. Axial CT image displayed in soft tissue window (**a**) shows a large mass centered in the greater sphenoid wing on the right side (*arrows* in **a**) with extensive periosteal reaction and an orbital component (*arrowheads* in **a**). The intracranial component (*black arrows* in **b**) is markedly better seen on the axial T2-weighted image (**b**) that also displays the displacement of the optic nerve sheath complex medially (*white arrows* in **b**). The ADC map (**c**) shows lower attenuation than the adjacent brain parenchyma, consistent with restricted diffusion, characteristic of small blue cell tumors such as neuroblastoma metastasis in this case

uncommon (Van Tassel et al. 1991). Both entities will be discussed in this section together as their imaging findings overlap and the benign form may mimic malignant central skull base lesions. Primary extradural meningiomas are thought to arise from ectopic meningocytes or arachnoid cap cells that are trapped in a fracture line or suture during trauma or molding of the head at birth, respectively (Turner and Laird 1966; Azar-Kian et al. 1974). Most commonly extradural meningiomas are therefore intra-osseous in nature and often involve the greater sphenoid wing which is in part related to the high number of sutures in this location (Fig. 13.18). In contrast to the intradural variant, there is no gender preference and the extradural type shows a bimodal peak with manifestation at older age as well as in the second decade of life (Lang et al. 2000). More than half of these lesions are hyperostotic on plain films and CT studies potentially mimicking prostatic cancer metastasis or fibrous dysplasia (Fig. 13.18a). Only approximately 35% present as osteolytic and 6% as mixed lesions (Crawford et al. 1996; Tokgoz et al. 2005). Spiculated appearing periosteal reaction might be present (Fig. 13.18a). Often a soft tissue component of variable size is seen which might be difficult to distinguish from adjacent musculature and/or dura on CT images (Fig. 13.18b,c). MR is superior in this regard due to its increased soft tissue detail. As on CT, extradural meningiomas may show variable internal signal characteristics and different degrees of contrast enhancement primarily reflecting the degree of hyperostosis. Interestingly, it has been shown that the extradural type of meningiomas has a higher incidence for malignant degeneration than the intradural variant with a reported risk of 11% and 2%, respectively (Tokgoz et al. 2005). It has been described that meningiomas presenting with osteolysis and an extracranial soft-tissue component are more likely aggressive and, therefore, more often malignant in nature (Fig. 13.18). In addition, it has been shown that malignant meningiomas have the tendency to show restricted diffusion on DWI (Filippi et al. 2001). Complete surgical resection is the treatment of first choice which is not always possible in cases of skull base meningiomas.

13.5.6 Malignant Lesion at the Junction of Central to Posterior Skull Base

Chordomas represent rare, locally invasive and slow growing tumors. Histologically, they resemble benign tumors; however, the majority of authors consider these low grade malignancies due to their aggressive local growth pattern and their low risk for metastatic disease (Erdem et al. 2003). They originate from embryonic remnants of primitive notochord at the spheno-occipital synchondrosis. The skull base is the second most common location. The majority of chondromas occur at the distal end of the notochord in the sacral region. Different histological subtypes have been reported such as chondroid and myxoid variants. Chordomas may present at any age but show a predilection for the 4th decade and for males. The onset of symptoms is insidious, reflecting the slow growth pattern of these tumors. However, at some point these patients become symptomatic and most commonly present with headaches and diplopia secondary to cranial nerve VI palsy. This is not unexpected as the cranial nerve VI courses through the medial portion of the petrous apex within the Dorello's canal, in close proximity to the spheno-occipital fissure. The vast majority of chordomas are midline in position with relatively symmetric bilateral tumor growth. Only less than 15% of chordomas have been reported to originate from the petrous apex simulating a chondrosarcoma. On CT, chordomas classically present as large, relatively well-circumscribed, lytic bone lesions arising from the clivus (Fig. 13.19a). Often intratumoral calcifications are seen representing small bony sequestra left behind from bone destruction or true calcifications in case of the chondroid variant. The associated soft tissue mass is usually slightly hyperdense in appearance demonstrating moderate to marked enhancement following intravenous contrast administration (Fig. 13.19b). Although it is easy to de-

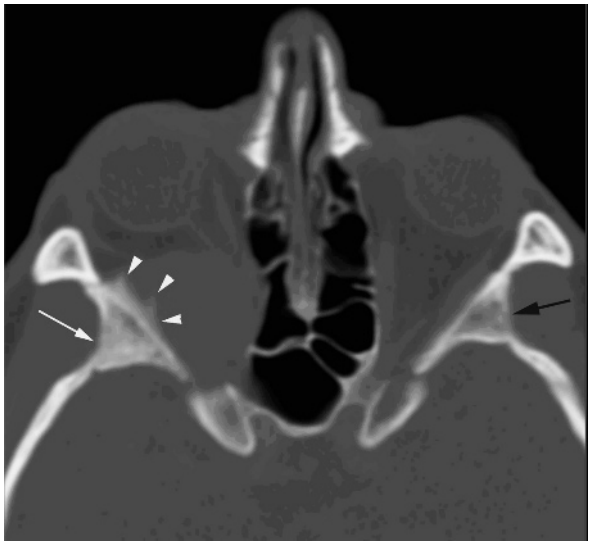

a

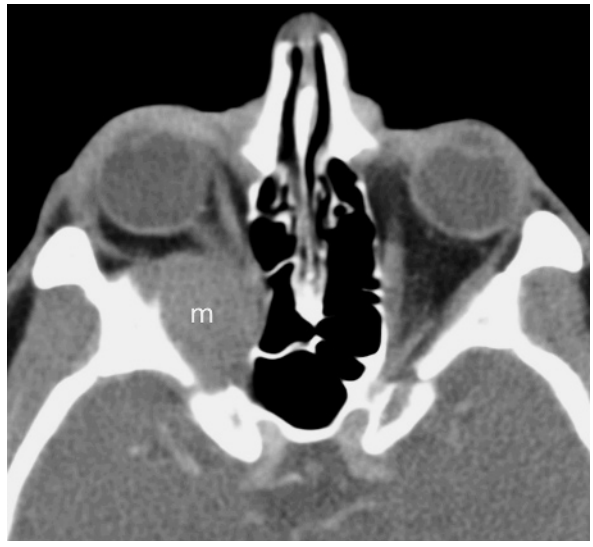

b

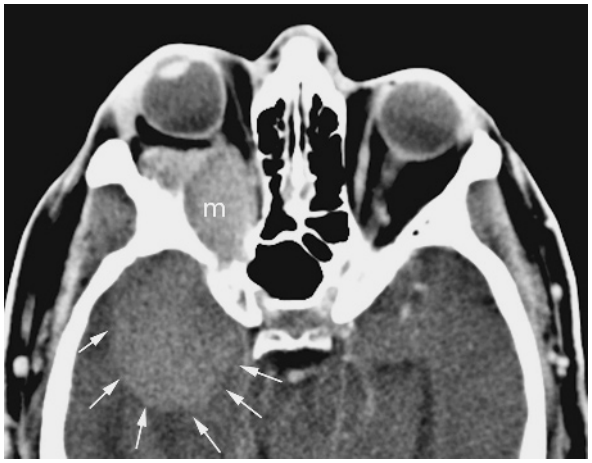

c

Fig. 13.18a–c. Axial CT images displayed in bone (**a**) and soft tissue (**b**) windows show slight sclerosis of the greater sphenoid wing on the right (*white arrow* in **a**) when compared to the left (*black arrow* in **a**) with marked periosteal region (*arrowheads* in **a**) and a large orbital component (*m* in **b**) causing mild proptosis. These CT findings and mass location are typical of an extra-dural, intra-osseous meningioma. Axial contrast enhanced CT image of the same patients performed 6 months later (**c**) shows moderate enlargement of the orbital component (*m* in **b**) with more pronounced proptosis and a new large intracranial component (*arrows* in **b**) that extended superiorly to involve the lower half of the frontal lobe (not demonstrated). The rapid growth pattern of this mass is consistent with a malignant meningioma that was confirmed surgically and on pathological evaluation

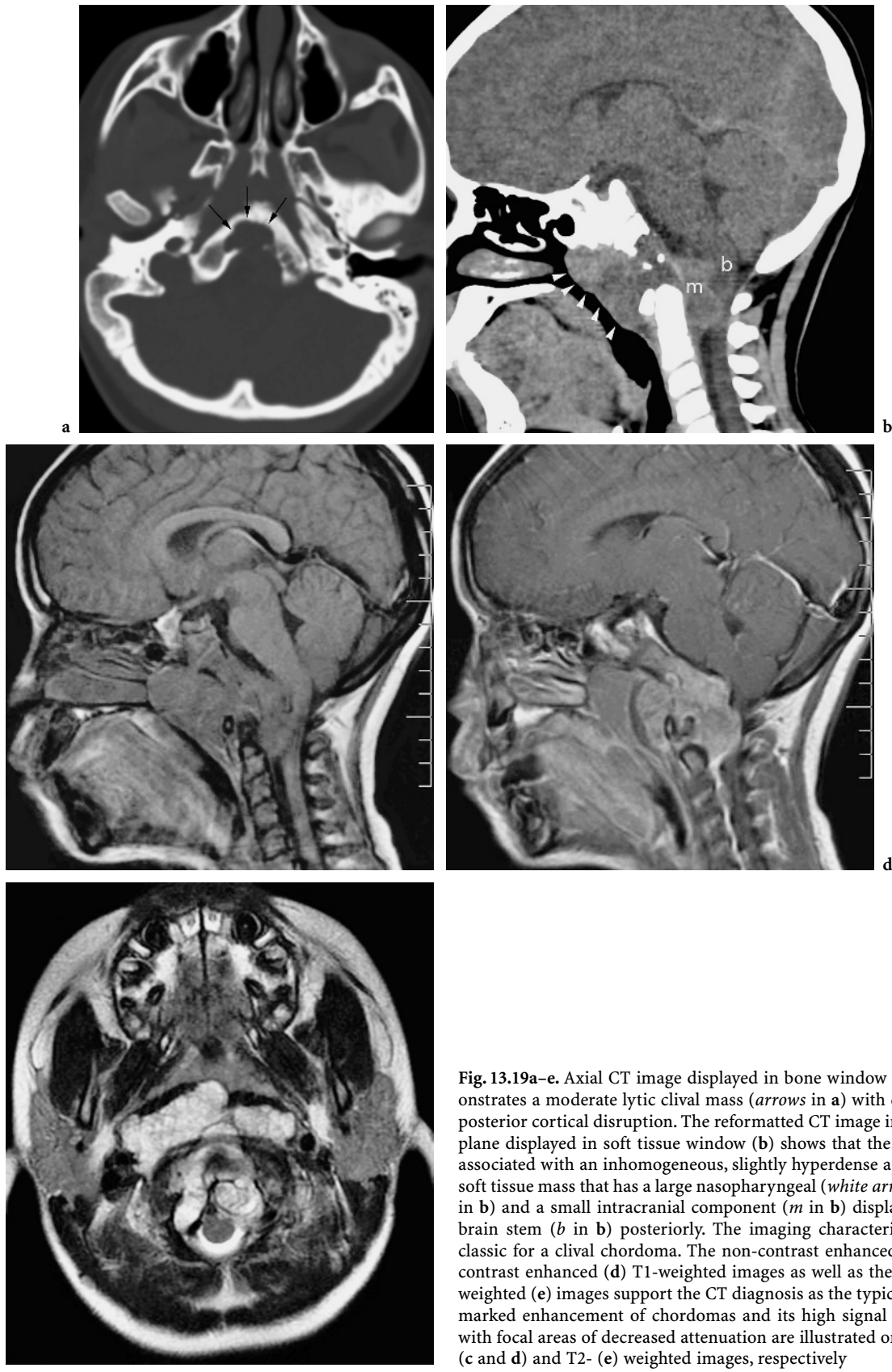

Fig. 13.19a–e. Axial CT image displayed in bone window (**a**) demonstrates a moderate lytic clival mass (*arrows* in **a**) with complete posterior cortical disruption. The reformatted CT image in sagittal plane displayed in soft tissue window (**b**) shows that the lesion is associated with an inhomogeneous, slightly hyperdense appearing soft tissue mass that has a large nasopharyngeal (*white arrowheads* in **b**) and a small intracranial component (*m* in **b**) displacing the brain stem (*b* in **b**) posteriorly. The imaging characteristics are classic for a clival chordoma. The non-contrast enhanced (**c**) and contrast enhanced (**d**) T1-weighted images as well as the axial T2 weighted (**e**) images support the CT diagnosis as the typically seen marked enhancement of chordomas and its high signal intensity with focal areas of decreased attenuation are illustrated on the T1- (**c** and **d**) and T2- (**e**) weighted images, respectively

tect a chordoma with CT, MR has been proven to be considerably superior, in particular the T2-weighted sequence, in the delineation of the tumor extent, and is therefore the most pertinent study for treatment planning purposes. On MR imaging, chordomas show a low to intermediate T1 and high T2 signal intensity with small focal areas of decreased T2 attenuation caused by tumoral calcifications or small foci of intratumoral hemorrhage (Fig. 13.19c,e). Moderate to marked heterogeneous contrast enhancement is typically seen (Fig. 13.19c,d). Total surgical resection is the optimal treatment but is usually not feasible in the skull base region. Therefore, post-surgical radiation therapy is usually utilized to improve patient's prognosis, which is primarily affected by the amount of tumor tissue left behind within the surgical bed (Erdem et al. 2003). Overall, the reported survival rate is poor with a 5-year survival rate of approximately 50% (Forsyth et al. 1993).

13.5.7 Mimics of Malignant Central Skull Base Lesions

Cephalocele is a rare entity in which brain tissue and or meninges protrude through a bony defect from intracranial to extracranial. In the central skull base region, intra-sphenoidal and trans-sphenoidal cephaloceles have been encountered (Jabre et al. 2000). Trans-sphenoidal cephaloceles are usually congenital in nature. They are typically midline in position and therefore may present on imaging as a midline bony gap associated with a cystic nasopharyngeal mass. This type of cephalocele is usually complex in nature containing optic nerves, hypothalamus or other adjacent midline structures. These patients might present with pituitary gland dysfunction due to protrusion of the pituitary gland into the meningoencephalocele or more commonly because of associated maldevelopment of the sella and pituitary gland. The intra-sphenoidal cephaloceles are typically lateral in location and most commonly post-traumatic in nature. These usually contain a variable amount of temporal lobe tissue and may present with seizures or rhinorrhea, bearing increased risk of meningitis. Therefore, they are often treated with surgery. On CT, a bony gap in the sphenoid body and partial or complete opacification of one or both sphenoid sinuses is seen (Bolger and Reger 2003). On CT, they can be mistaken for mucoceles or aggressive skull base masses when associated with mass effect within the sphenoid sinus. On MR the diagnosis is easier as the extracranial brain tissue and/or meninges are directly demonstrated, in particular on T2-weighted images (Fig. 13.20). On

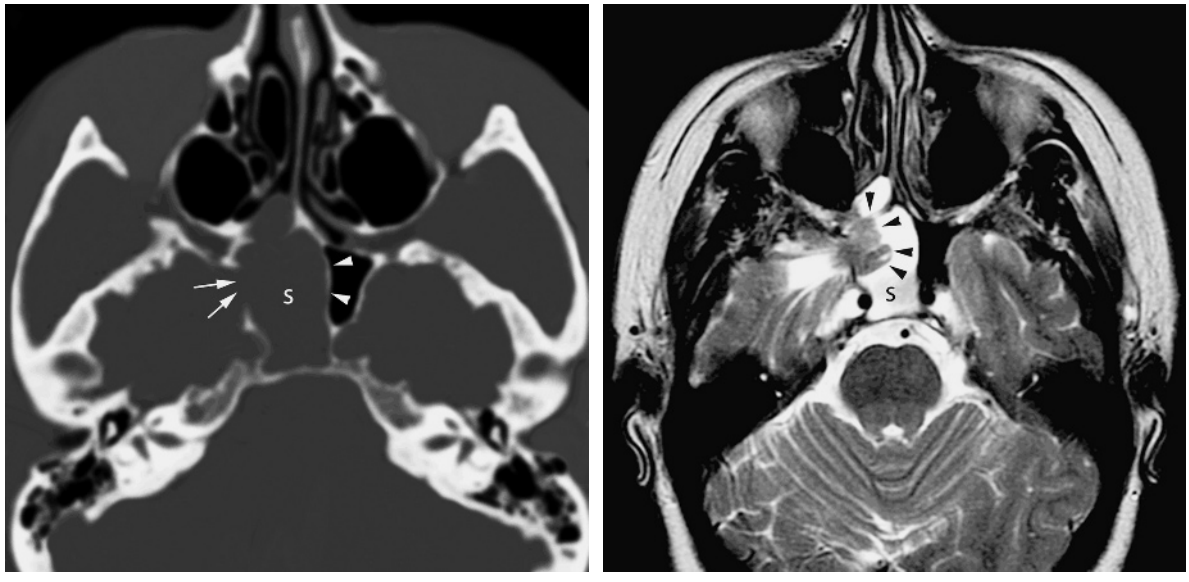

a b

Fig. 13.20a,b. Axial CT image displayed in bone window (**a**) demonstrates complete opacification of the sphenoid sinus on the right (*s*) with an approximately 1-cm bony gap in the lateral wall of the sphenoid sinus (*arrows* in **a**) and mild bowing of the sphenoid septum to the left (*arrowheads* in **a**). Although these imaging findings might be mistaken for a sphenoidal mucocele and less likely for an aggressive sphenoid sinus tumor, the direction of bowing of the edges of the bony gap suggests that this is an intracranial process secondarily involving the sphenoid sinus. This is confirmed on the axial T2-weighted image (**b**) that clearly shows protrusion of brain tissue (*arrowheads* in **b**) into the sphenoid sinus (*s* in **b**) through the bony defect. These imaging findings are therefore consistent with a lateral sphenoid myeloencephalocele

CT, however, the location of the bony gap, the pattern of bone remodeling rather than destruction and potentially associated mild bowing of the involved bone towards the sphenoid sinus provide important diagnostic clues that warrant further evaluation with MRI, or CT with intrathecal contrast injection.

13.5.8 Malignant Posterior Skull Base Lesions

Chondrosarcomas are rare malignant cartilaginous tumors of variable aggressiveness (Evans et al. 1977). Their aggressiveness depends upon the tumor subtype and grade. The dedifferentiated and mesenchymal variants are more aggressive than the classic variant. The classic variant is the most common and represents a low grade chondrosarcoma. This type of chondrosarcoma shows the least aggressive growth pattern, minimal risk of metastatic disease and is often difficult to distinguish from chordomas histologically and clinically (Bourgouin et al. 1992). As with chordomas, headaches and diplopia related to cranial nerve VI palsy are the most common symptoms at presentation. However, chondrosarcomas usually occur in younger patients with a peak incidence in the 2nd and 3rd decade, and even more importantly they are off midline (petroclival) in location (Hassounah et al. 1985). Their paramedian location also predisposes these patients for lower cranial nerve deficits, in particular hearing loss. CT images typically demonstrate a destructive mass centered in the petrous apex with ring and arcs in it reflecting the chondroid nature of this tumor (Fig. 13.21). Variable amount of soft tissue component is seen, typically isodense to the adjacent brain parenchyma before, and showing some but variable enhancement following intravenous contrast administration. Chondrosarcomas have low to intermediate signal intensity on T1, and high signal intensity on T2-weighted sequences, with a variable enhancement pattern (Fig. 13.22). As with chordomas, total surgical resection is the most desirable treatment in combination with radiation therapy if positive resection margins are present. Despite the histological and clinical similarities, the classic type of chondrosarcoma has been reported to have a better prognosis than chordomas with a 5-year survival rate of approximately 90%. This, however, is not true for the other chondrosarcoma variants (Forsyth et al. 1993; Evans et al. 1977).

Endolymphatic sac tumors are also very rare. They may occur sporadically or in association with von Hippel-Lindau disease (Luff et al. 2002). The patients typically present with hearing loss, tinnitus, vertigo and or facial nerve dysfunction (Choyke et al. 1995). Bilateral involvement has been reported in von Hippel-Lindau disease patients. The majority of these tumors are low grade adenocarcinomas or papillary cystadenomas that are indistinguishable from each other based on imaging (Mukherji and

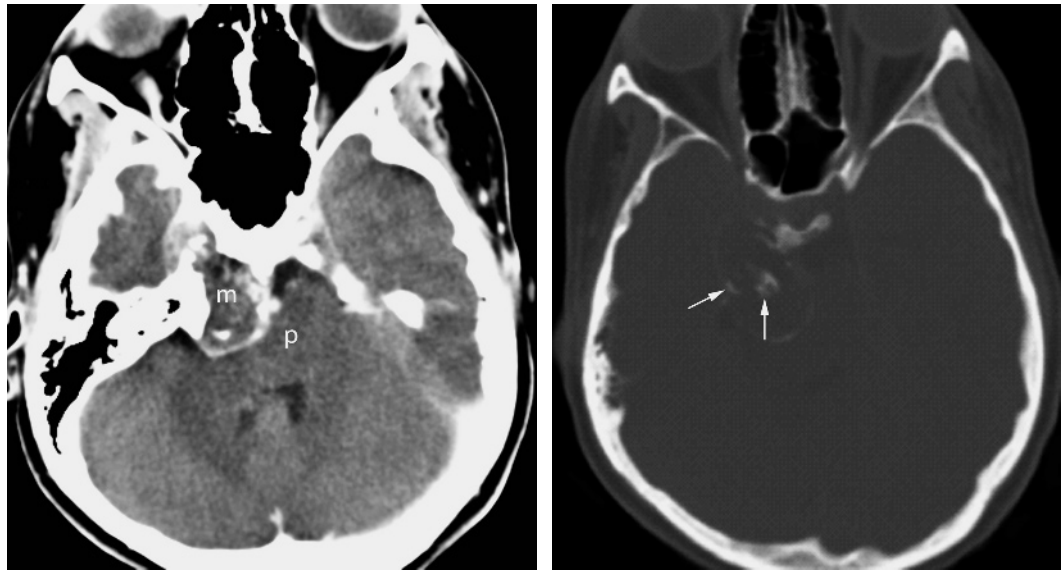

a b

Fig. 13.21a,b. Axial CT image displayed in soft tissue window (**a**) shows a large, heterogeneous mass (*m* in **a**) centered in the petrous apex on the right with marked mass effect upon the adjacent pons (*p* in **a**). The axial CT image in bone window (**b**) shows the characteristic ring and arcs (*arrows* in **b**) appearance of chondrosarcomas that has been confirmed surgically and histologically in this patient.

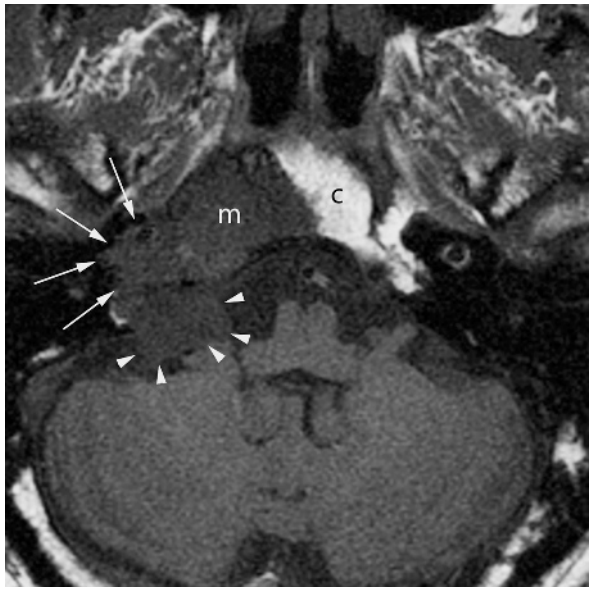

a

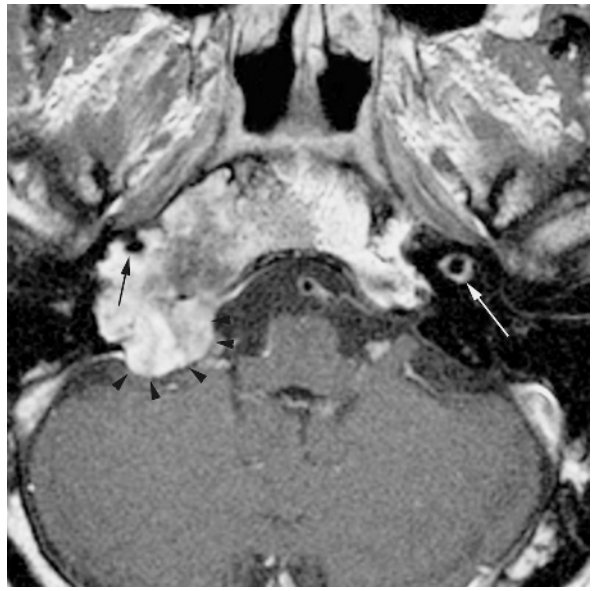

b

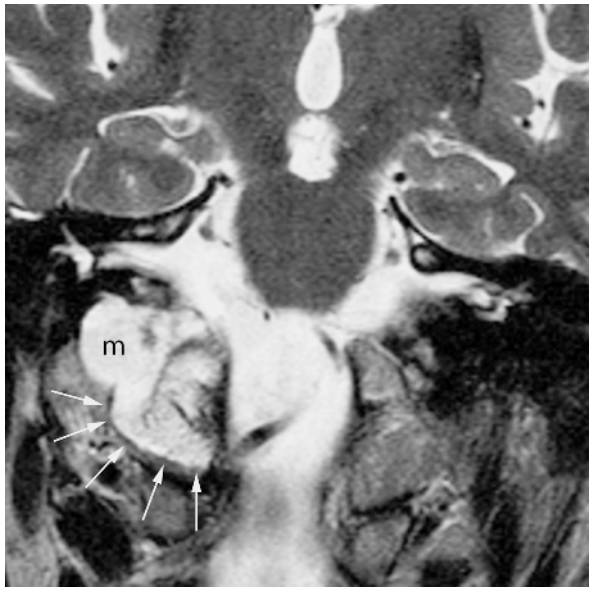

c

Fig. 13.22a–c. Axial non-contrast enhanced T1-weighted image (**a**) shows a large mass (*m*) involving the right lateral portion of the clivus (*c*) and the medial petrous apex, where involvement of the jugular foramen (*arrows* in **a**) and a small intracranial component (*arrowheads* in **a**) are seen. The bony extent of the mass is less clearly appreciated on the contrast enhanced T1-weighted image (**b**) while the intracranial component (*arrowheads* in **b**), as well as the jugular foraminal component that is almost completely surrounding the internal carotid artery on the right (*black arrow* in **b**) are much better seen. The internal carotid artery is also markedly decreased in diameter when compared to the normal internal carotid artery on the left (*white arrow* in **b**). The coronal T2-weighted image (**c**) displays the typical high signal intensity of chondrosarcomas (*m* in **c**) and better illustrates the inferior extension of the tumor below the skull base (*arrows* in **c**)

Castillo 1996). On CT, local destruction is seen in the retrolabyrinthine petrous bone, at the aperture of the vestibular aqueduct, with characteristic intratumoral bone spicules that might be associated with an enlarged vestibular aqueduct. The T1-weighted images demonstrate characteristic hyperintense foci within the tumor substance with extensive enhancement following intravenous contrast administration. Endovascular embolization prior to surgical resection may be required.

Paragangliomas are rare tumors of neural crest origin (Rao et al. 1999). In the posterior skull base, they are most commonly seen in the jugular fossa and are called glomus jugulare tumors. They arise from the paraganglion cells of the Jacobson or Arnold nerve which are branches of the cranial nerve IX and X, respectively (Rao et al. 1999). The majority of the paragangliomas are benign in nature. Up to 13% of glomus jugulare tumors have been reported to be malignant. Both types will be discussed in this section together as they both demonstrate a locally aggressive growth pattern making them indistinguishable from each other (Figs. 13.23 and 13.24). Demographic data are not helpful either as both forms most commonly occur in middle aged females that typically present with tinnitus (Brewis et al. 2000). It has been suggested that the incidence of pain is higher and the occurrence of hearing loss lower with the malignant

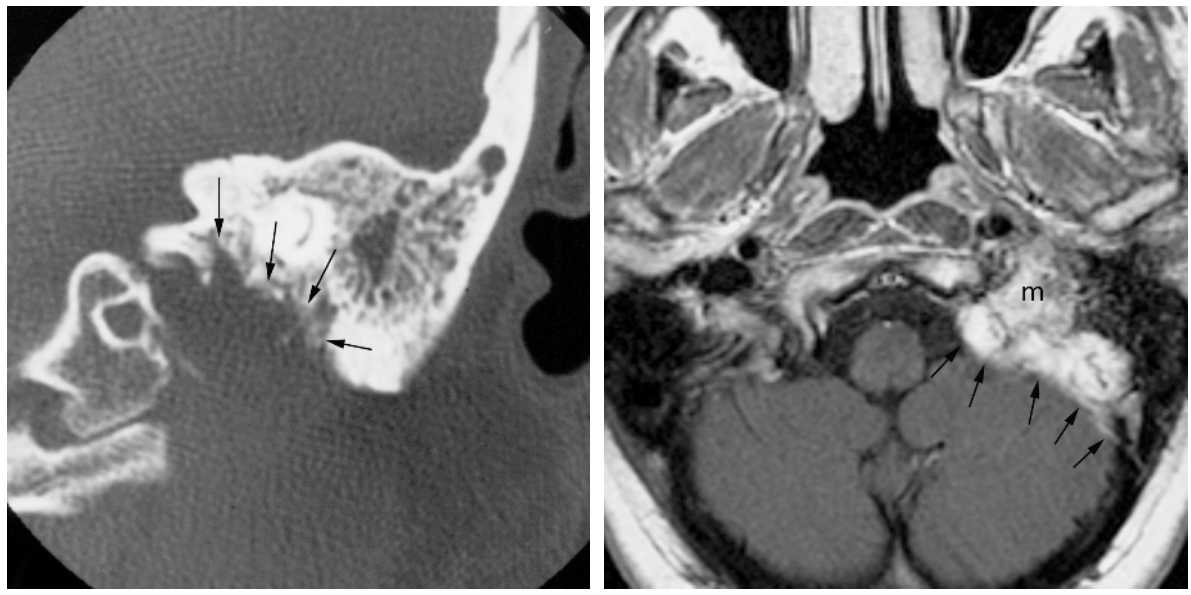

a b

Fig. 13.23a,b. Coronal CT image displayed in bone window (**a**) shows the marked erosions along the lateral and superior jugular foramen (*arrows* in **a**) that are caused by a large inhomogeneously enhancing mass (*m* in **b**) as seen on this contrast enhanced axial T1-weighted image (**b**). The mass is also extending into the posterior fossa (*arrows* in **b**) where it results in mild impression upon the left cerebellar hemisphere. The location and imaging findings are classic for a jugular foramen paraganglioma

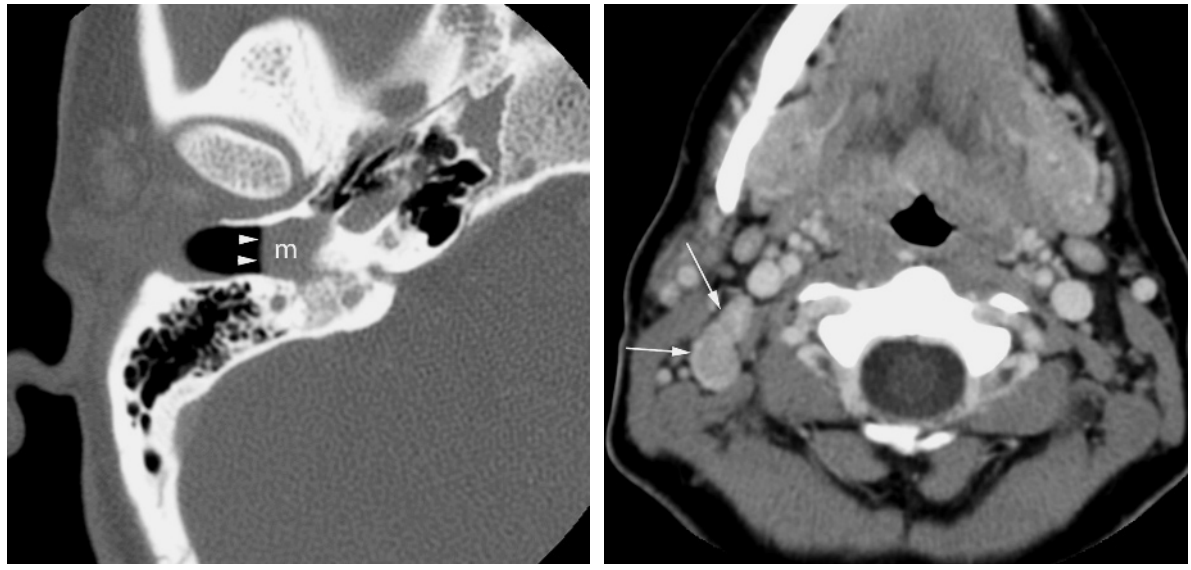

a b

Fig. 13.24a,b. Axial contrast enhanced CT images through the middle ear displayed in bone window (**a**) and through the upper neck displayed in soft tissue window (**b**) from a 35-year-old female with tinnitus and hearing loss and with classic imaging findings of paraganglioma originating within the jugular foramen on other images. **a** Image illustrating the tendency of the jugular paragangliomas to grow into the middle ear cavity (*m* in **a**). The tympanic membrane is markedly displaced laterally (*arrowheads* in **a**). The image through the neck demonstrates abnormal group 2A lymph nodes on the right (*arrows* in **b**) allowing the diagnosis of malignant paraganglioma. This patient underwent right modified lymph node dissection confirming the nodal metastatic disease that was not suspected on clinical examination

variants. The main differentiating feature, however, is the existence of metastatic lesions in the malignant form (Fig. 13.24b). Metastatic disease most commonly spreads to the bone, lung and cervical lymph nodes and might present even years after the initial diagnosis and treatment (Fig. 13.24b). While nuclear medicine examination with Indium 111 labeled somatostatin analogues is an excellent way to evaluate

for metastatic disease, CT and or MR are primarily utilized to evaluate the primary tumor within the jugular fossa. On CT, a glomus jugulare tumor causes destruction of the walls of the jugular foramen and adjacent petrous bone giving the so-called mouth eaten appearance (Figs. 13.23 and 13.24). On MR, a hypervascular mass with flow voids and extensive enhancement is seen in the jugular fossa region. On both studies, the tendency of the glomus jugulare to grow into the middle ear cavity and posterior fossa are seen, although the intracranial involvement is better demonstrated with MR (Figs. 13.23 and 13.24). In approximately 10% of patients, multi-focal and/or bilateral involvement is seen. The benign forms of glomus jugulare can be treated with surgical resection following intraarterial embolization, radiation therapy or both as the tumor is known to be radiosensitive and total surgical resection is often difficult. Since radiation therapy is known to leave a residual mass of variable activity behind, treatment of the malignant forms with radiation therapy alone is currently not recommended but rather surgical resection with post-operative radiation therapy. Utilization of Iodine 131 labeled MIBG for treatment of the metastatic lesions has been reported with mixed preliminary results (Bomanji et al. 2001).

Malignant schwannomas of the cranial nerve VII through XII demonstrate the same rarity, behavior and imaging findings as the malignant schwannomas of the cranial nerve III through IV (see Sect. 13.5.5 for details).

13.5.9 Mimics of Malignant Posterior Skull Base Lesions

Congenital cholesteatoma is a rare disease arising from aberrant ectoderm that is trapped during embryogenesis within the temporal bone (Robert et al. 1995). Histologically, the lesion is lined with stratified squamous epithelium and filled with debris. It typically presents in children and young adults. It can occur anywhere within the temporal bone; when located in the petrous apex it might simulate a malignant lesion of the skull base. Petrous apex congenital cholesteatomas present with facial nerve palsy, sensorineural hearing loss and/or vertigo. On CT, a hypodense, non-enhancing, expansile mass is seen with variable degrees of bony destruction. Congenital cholesteatoma is usually low to intermediate in signal intensity on T1- and high signal intensity on T2-weighted images. Presence of restricted diffusion on DWI has also been reported which is not surprising as cholesteatomas histologically resemble epidermoid tumors (Aikele et al. 2003). Surgical excision is the treatment of choice and recurrent disease is common

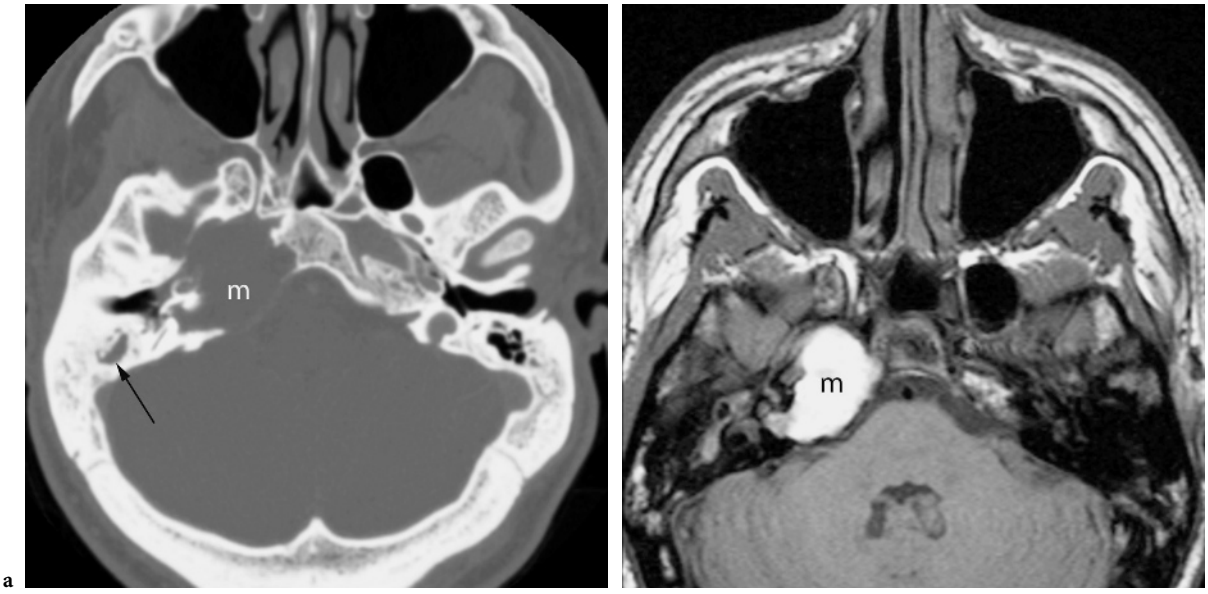

a b

Fig. 13.25a,b. Axial CT displayed in bone window (**a**) shows a large lytic lesion (*m* in **a**) centered within the petrous apex without signs of cartilaginous matrix to suggest a chondrosarcoma. The non-contrast enhanced T1-weighted image in axial plane (**b**) shows spontaneous very high signal intensity of the mass (*m* in **b**) that is characteristic for cholesterol granulomas in contrast to the low to intermediate signal intensity seen in chondrosarcomas that occur in the same location. In addition, there is a small amount of fluid (*arrow* in **a**) present in the mastoid air cells on the right supporting the diagnosis of cholesterol granuloma

with subtotal resection. In such patients, DWI might be a helpful tool for evaluation of residual or recurrent disease if the lesion is at least 5 mm in size.

Cholesterol granuloma represents an accumulation of granulation tissue intermixed with blood products and cholesterol crystals within the middle ear or petrous apex (Farrior et al. 1981). Patients with cholesterol granuloma classically have a long standing history of chronic otitis media. Lesions in the petrous apex are often quiet large at the time of diagnosis and may therefore present with hearing loss, tinnitus and/or cranial neuropathies (Goldofsky et al. 1991). On CT, cholesterol granulomas present as expansile, well-defined masses (Fig. 13.25a) (Greenberg et al. 1988). When large, the site of origin might be difficult to determine making distinction from other types of

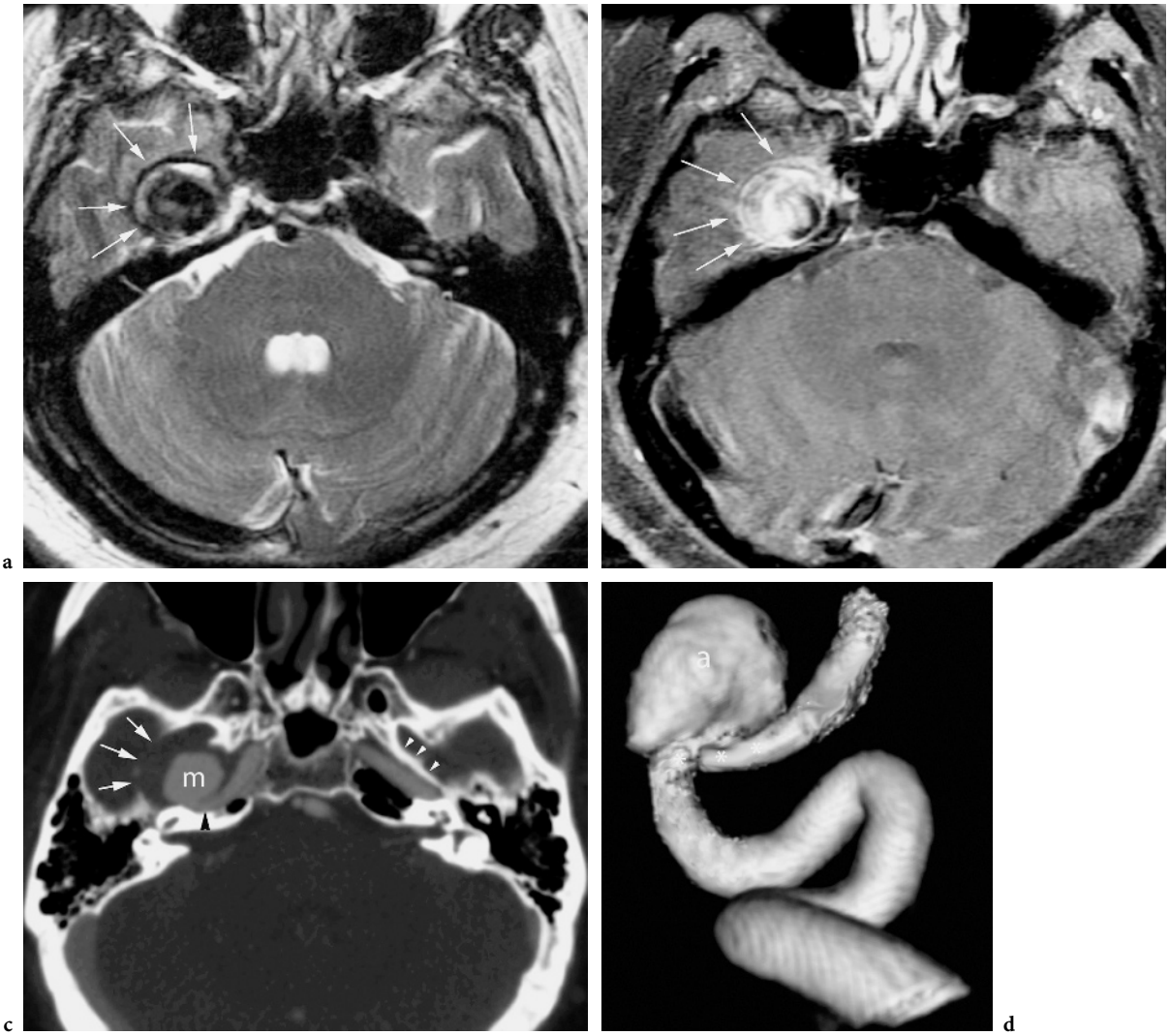

Fig. 13.26a–d. These images are from a 76-year-old male patient who underwent MR examination for dementia. Axial T2-weighted image (**a**) shows a round and well defined mass (*arrows* in **a**) of mixed signal intensity centered within the petrous apex. The mass (*arrows* in **b**) shows marked inhomogeneous enhancement on the contrast enhanced fat suppressed T1-weighted image (**b**). The imaging findings were therefore suspicious for an aneurysm of the petrous segment of the internal carotid artery and the patient underwent CT angiography for further evaluation. The contrast enhanced source image displayed in an intermediate window (**c**) shows extensive lateral bowing of the lateral wall of the internal carotid canal on the right (*white arrows*) when compared to the left (*white arrowheads*) caused by a centrally markedly enhancing mass (*m* in **c**) that is contiguous with the internal carotid artery (*black arrowheads* in **c**). The gap between the enhancing central component (*m* in **c**) and the bony bowing (*white arrows* in **c**) reflects the degree of mural thrombus. The maximal intensity projection (*MIP*) image (**d**) nicely displays the patent portion of the saccular aneurysm (*a* in **d**) arising from the petrous segment of the internal carotid artery (*asterisks* in **d**)

petrous apex lesions, in particular petrous apex aneurysm, difficult. As cholesterol granulomas are often large at the time of initial scanning, CT images often show bony gaps that may be mistaken for bone destruction or erosions suggesting an aggressive or malignant lesion. On MRI, cholesterol granulomas are classically of increased signal intensity on T1- and T2-weighted images, with no or minimal peripheral enhancement following contrast administration (Fig. 13.25b). Cholesterol cysts are essentially identical to cholesterol granulomas but occur in the absence of chronic middle ear disease. Mucoceles of the petrous apex share the same imaging characteristics as cholesterol granulomas on CT, but usually demonstrate decreased signal intensity on T1-weighted images. Mucoceles of the petrous apex are very rare and are felt to be related to post-inflammatory obstruction. All of these lesions are usually treated with surgical drainage.

Internal carotid artery aneurysms can occur within the cavernous sinuses, causing remodeling of the adjacent sphenoid bone, or within the petrous bone. The cavernous sinus aneurysms are more common and usually do not demonstrate a diagnostic dilemma. Petrous segment internal carotid aneurysms, in contrast, are rare. They can be congenital, post-traumatic or post-infectious in etiology (Liu et al. 2004). Aneurysms in this location are usually asymptomatic and are incidentally found on CT or MR studies performed for other indications. In symptomatic patients, symptoms are primarily non-specific in nature (headaches) or related to local mass effect (cranial neuropathies, Horner's syndrome or tinnitus). Embolic events have not been associated with petrous segment aneurysm even with larger mural thrombus formation (Liu et al. 2004). On CT, they usually present as an expansile mass with marked enhancement following intravenous contrast administration. The degree and homogeneity of enhancement depends upon the amount of mural thrombus and the size of patent lumen (Fig. 13.26). If no intravenous contrast is given, they may mimic a cholesterol granuloma, cholesterol cyst or a petrous apex mucocele. Close search for the internal carotid canal within the petrous bone and evaluation of the vector of the associated bone remodeling usually results in the correct diagnosis. Contrast enhanced CT and/or CT angiography might then be performed to confirm the diagnosis and to classify the type of the aneurysm (Fig. 13.26). On MR, petrous apex aneurysms usually present with mixed signal intensity and enhancement pattern, related to the turbulent flow within the aneurysmal segment (Fig. 13.26). Even MR angiography is usually difficult to interpret as the turbulent flow causes signal drop out due to reentry phenomenon or thrombus formation that underestimates the size or makes the aneurysm difficult to appreciate at all. This constellation of imaging findings may result in misdiagnosis of the aneurysm as a non-vascular benign and or malignant skull base lesion. In the instance of present flow voids within the aneurysm, the aneurysm might be completely missed as the difference in signal intensity to adjacent petrous apex, in particular when the petrous apex is aerated, might be very small and therefore not appreciable to the radiologist's eye. The bottom line is that internal carotid artery aneurysms in this location might pose a diagnostic dilemma and the radiologist should consider it every time a petrous apex lesion is observed on CT or MRI to prevent a potential biopsy with usually fatal outcome. The treatment of petrous segment aneurysm remains challenging, in particular when the patient has no or minimal symptoms. Currently, a "wait and see" approach is applied to this latter patient group as these type of aneurysms do not suffer life-threatening bleeding episodes. Endovascular intervention (balloon or coil occlusion of the internal carotid artery and/or stent placement) or surgical trapping with revascularization bypass is currently reserved for symptomatic patients (Liu et al. 2004).

Petrous apicitis is usually caused by otitis media that extended anteromedially into the aerated petrous apex cells without or with progression to osteomyelitis in the early and delayed stages, respectively. Usually, the patients present with fever reflecting the acute nature of the infection in combination with some or all of the symptoms of the Gradenigo's triad (see Sect. 13.3) (Gradenigo 1904). In the early stages, obliteration of the petrous apex air cells with fluid in association with otomastoid disease is seen. In the later stages, additional bony destruction with trabecular breakdown and cortical erosions is present, reflecting the degree of underlying osteomyelitis (Fig. 13.27a). All these changes are readily visible on CT. Petrous apicitis is prone to intracranial complications such as epidural or brain abscess formation, subdural empyema, meningitis and sinus thrombosis or thrombophlebitis (Fig. 13.27b). These possible complications are usually better delineated with MR imaging. Petrous apicitis, in particular when associated with osteomyelitis or intracranial complications, represents a surgical emergency requiring debridement of the petrous apex and drainage of possible abscesses or empyemas. However, recently, successful conservative treatment of uncomplicated petrous apicitis has been reported (Burston et al. 2005).

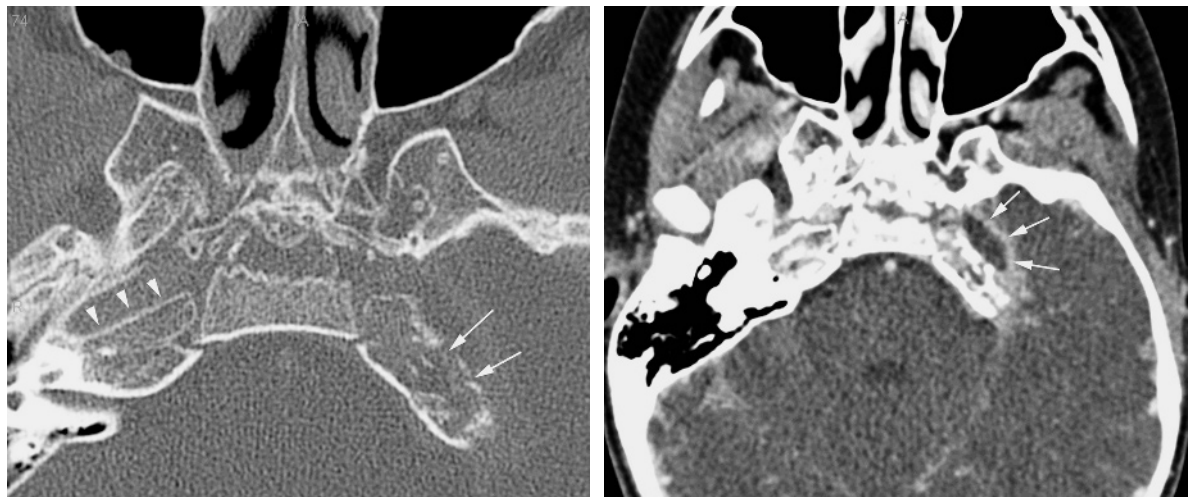

Fig. 13.27a,b. Axial CT image displayed in bone window (**a**) demonstrates marked dehiscence of the bony cortex (*arrows* in **a**) and fragmented appearance of the petrous apex on the left when compared to the right (*arrowheads* in **a**). The contrast enhanced axial CT image displayed in soft tissue window shows an extradural fluid accumulation with marked ring enhancement (*arrows* in **b**). The constellation of the imaging findings together with fever and signs of otitis media on clinical examination are consistent with petrous apicitis, complicated by an epidural abscess that was surgically proven

13.6 Imaging Protocol

In view of the broad variety of lesions that can involve the skull base, it is not surprising that there is no single imaging protocol that fits all these entities. The imaging protocol will primarily depend upon availability, presenting symptoms, patient's history, and extent of tumor. Overall, CT is usually the study of first choice as it is widely available and easily accessible. Based on symptoms, MR should be the initial diagnostic study for patients with cranial neuropathies, while CT is primarily reserved as a screening tool for more non-specific symptoms such as headaches and dizziness. Presence of risk factors for a certain disease process (e.g. chronic otomastoiditis or neurofibromatosis), or a history of underlying malignancy in combination with the clinical presentation, might raise the suspicion for a specific entity that it is better evaluated with one or the other imaging tool. The extent of the tumor is usually unpredictable based on clinical examination alone and therefore, review of the images while the patient is still on the scanner with immediate modification of the imaging protocol represents the most optimal work-up of patients with skull base lesions. Despite most optimal image quality, a significant number of patients will end up with both – CT and MR – studies for narrowing of the differential diagnostic considerations and better delineation of the tumor margins (Figs. 13.13, 13.17, 13.19 and 13.20).

Although no specific protocol is given here, the following issues need to be considered or followed to facilitate the most optimal quality of a cross-sectional study: CT and MRI should be obtained as a high resolution study with a small field of view (8–14 cm) that is coned down to the area of interest, such as the central skull base or temporal bone. The images should be performed with contiguous slices. It is recommended that CT images are acquired with a slice thickness of 1 mm or less for optimal display of the bony details of the skull base in bone algorithm. In the era of interactive capabilities of the picture archive communication system (PACS), such thin sections are also desirable in soft tissue algorithms to allow high quality multi-planar reformations that facilitate better delineation of the lesion from adjacent anatomical structures. In contrast, such thin slices are not feasible nor desirable with MR, as the signal to noise would be too low and/or the imaging time too long. Therefore, MR images should be obtained with a slice thickness of 3 mm (Casselman 2005). When a large lesion is present, the slice thickness might need to be increased to 4 mm to be able to cover the entire tumor in a reasonable time frame.

High resolution fast spin-echo T2- and standard T1-weighted sequences, without and with intravenous contrast administration, should be performed in axial and coronal planes (Casselman 2005). Some tumors also benefit from sagittal imaging such as chordomas. The standard T1-weighted images

are most sensitive for bony invasion while the T2-weighted images are very helpful in delineation of the outer tumor margins (Figs. 13.13a,b and 13.22a,b). Post-contrast enhancement T1-weighted images are most useful for evaluation of involvement of adjacent soft tissues (Fig. 13.22a,b). Utilization of fat suppression techniques in the skull base is controversial as it is hampered by loss of most of the anatomical landmarks, and is predisposed for susceptibility artifacts. In addition, the suppression of fat makes the typically high signal difference between tumor and adjacent fatty bone marrow disappear, and the detectability of a lesion on the contrast enhanced, fat suppressed images will depend upon the degree of intra-lesional contrast accumulation (Casselman 2005). Therefore, it is advisable to obtain standard non-contrasted T1-weighted images without fat suppression in at least one imaging plane (preferentially the axial plane) that would supplement the fat suppressed images. Additional imaging sequences such as heavily T2-weighted high resolution volumetric acquisitions or MR angiography/venography might also be considered for further evaluation of the cisternal portions of the cranial nerves or of the intracranial vasculature, respectively. It is also recommended to perform larger field of view images (20–22 cm) that cover the entire head in non-enhanced T1 and fluid attenuation inversion recovery (FLAIR) weighing that could serve as an overview for optimal positioning of the subsequently acquired high resolution images; these would allow the detection of additional lesions as well as possible complications related to the skull base mass such as infarction at the same time. Additional DWI through the entire head might not only further characterize the age of potential infarction, but also narrow the differential diagnosis in some instances.

13.7 Radiologist's Role

Pre-treatment, the radiologist's main role is the delineation of the extent of the skull base lesion, including delineation of possible involvement of the neurovascular structures (Casselman 2005). Narrowing of the differential diagnostic considerations is certainly desirable but not as critical as the tumor extent. In addition, the radiologist might offer biopsy of a lesion when a soft tissue component is present below the skull base and accessible for biopsy with CT guidance. CT guided biopsy of the bony skull base itself is difficult due to the high frequency of traversing nerves and vessels. Central skull base lesions can often be reached by placement of a guiding needle through the mandibular notch or through the buccal space along the anterior margin of the mandibular ramus.

During the treatment phase, the interventional radiologist might perform intra-arterial embolization of a vascular tumor prior to surgical resection or treat a petrous segment internal carotid aneurysm with balloon/coil occlusion.

Post-treatment imaging is critical as surgical resections are often subtotal in extent and radiation therapy may leave residual masses of unknown activity. To facilitate the radiologist's ability to detect recurrent tumor as soon as possible, it is advisable to obtain a baseline CT and/or MR study approximately 6 weeks following treatment, and to perform the subsequent follow-up examinations with the same imaging protocol and technique.

References

Aikele P, Kittner T, Offergeld C, Kaftan H, Huttenbrink KB, Laniado M (2003) Diffusion-weighted MR imaging of cholesteatoma in pediatric and adult patients who have undergone middle ear surgery. AJR Am J Roentgenol 181:261–265

Azar-Kian B, Sarwar M, Marc JA, Schlechter MM (1974) Intraosseous meningioma. Neuroradiology 246–253

Bolger WE, Reger C (2003) Temporal lobe encephalocele appearing as a lytic lesion of the skull base and pterygoid process. Ear Nose Throat J 82:268–272

Bomanji JB, Hyder SW, Gaze MN, Gacinovic S, Costa DC, Coulter C, Ell PJ (2001) Functional imaging as an aid to decision-making in metastatic paraganglioma. Br J Radiol 74:266–269

Bourgouin PM, Tampieri D, Robitaille Y, Robert F, Bergeron D, del Carpio R, Melancon D, Ethier R (1992) Low-grade myxoid chondrosarcoma of the base of the skull: CT, MRI, and histopathology. J Comput Assist Tomogr 16:268–273

Brewis C, Bottrill ID, Wharton SB, Moffat DA (2000) Metastases from glomus jugulare tumours. J Laryngol Otol 114:17–23

Brodeur GM, Castleberry RP (2001) Neuroblastoma. In: Pizzo PA and Poplack DG (eds) Principles and practice of pediatric oncology. Lippincott Williams & Wilkins, Philadelphia, pp 796

Burston BJ, Pretorius PM, Ramsden JD (2005) Gradenigo's syndrome: successful conservative treatment in adult and pediatric patients. J Laryngol Otol 119:325–329

Carlotti CG Jr, Drake JM, Hladky JP, Teshima I, Becker LE, Ruthka JT (1999) Primary Ewing's sarcoma of the skull in children. Utility of molecular diagnostics, surgery and adjuvant therapies. Pediatr Neurosurg 31:307–315.

Casselman JW (2005) The skull base: tumoral lesions. Eur Radiol 15:534–542

Chong VFH, Fan YF (1998) Radiology of the sphenoid bone. Clin Radiol 53:882–893

Choyke PL, Glenn GM, Walther MM, Patronas NJ, Linehan WM,

Zbar B (1995) Von Hippel Lindau disease: genetic, clinical and imaging features. Radiology 146:629–642
Crawford TS, Kleinschmidt-DeMasters BK, Lillehei KO (1995) Primary intraosseous meningioma. Case report. J Neurosurg 83:912–915
Cummings TJ, George TM, Fuchs HE, McLendon RE (2004) The pathology of extracranial scalp and skull masses in young children. Clin Neuropathol 23:34–43
DiNardo LJ, Wetmore RF (1989) Head and neck manifestations of histocytosis-X in children. Laryngoscope 99:721–724
Erdem E, Angtuaco EC, Van Hemert R, Park JS, Al-Mefty O (2003) Comprehensive review of intracranial chordomas. Radiographics 23:995–1009
Evans HL, Ayala AG, Romsdahl MM (1977) Prognostic factors in chondrosarcoma of bone. A clinicopathologic analysis with emphasis on histologic grading. Cancer 40:818–831
Farrior B, Kampsen E, Farrior JB (1981) The positive pressure of cholesterol granuloma idiopathic blue eardrum. Differential diagnosis. The Laryngoscope 91:1286–1296
Filippi CG, Edgar MA, Ulug AM, Prowda JC, Heier LA, Zimmerman RD (2001) Appearance of meningiomas on diffusion-weighted images: correlating diffusion constants with histopathologic findings. AJNR Am J Neuroradiol 22:65–72
Forsyth PA, Cascino TL, Shaw EG, Scheithauer BW, O'Fallon JR, Dozier JC, Piepgras DG (1993) Intracranial chordomas: a clinicopathological and prognostic study of 51 cases. J Neurosurg 78:741–747
Gandour-Edwards R, Kapadia SB, Janecka IP, Martinez AJ, Barnes L (1995) Biologic markers of invasive pituitary adenomas involving the sphenoid sinus. Mod Pathol 8:160–164
Garland LH (1945) Osteogenic sarcoma of the skull. Radiology 45:45–48
Goldofsky E, Hoffman RA, Holliday RA, Cohen NL (1991) Cholestrol cyst of the temporal bone: diagnosis and treatment. Ann Otol Rinol Laryngol 100:181–186
Gorham LW, Wrighte AW, Schulz HH, Maxon FC (1954) Disappearing bones: a rare form of massive osteolysis, report of two cases, one with autopsy findings. Am J Medicine 17:674–681
Gormley WB, Tomecek FJ, Qureshi N, Malic GM (1994) Craniocerebral epidermoid and dermoid tumours: a review of 32 cases. Acta Neurochir (Wien) 128:115–121
Gradenigo G (1904) Sulla leptomeningite circonscritta e sulla paralisi dell' abducenta di origine otitica. Giornale dell'Accademia di medicina di Torino 10:59–84
Greenberg JJ, Oot RF, Wismer GL, Davis KR, Goodman ML, Weber AE, Montgomery WW (1988) Cholesterol granuloma of the petrous apex: MR and CT evaluation. AJNR Am J Neuroradiol 6:1205–1214
Guo AC, Cummings TJ, Dash RC, Provenzale JM (2002) Lymphomas and high-grade astrocytomas: comparison of water diffusibility and histological characteristics. Radiology 224:177–183
Hassounah M, Al-Mefty O, Akhtar M, Jenkins JR, Fox JL (1985) Primary cranial and intracranial chondrosarcoma. A survey. Acta Neurosurgica 78:123–132
Howarth DM, Gilchrist GS, Mullan BP, Wiseman GA, Edmonson JH, Schomber PJ (1999) Langerhans cell histocytosis: diagnosis, natural history, management, and outcome. Cancer 85:2278–2290
Inserra MM, Pfeister M, Jackler RK (2004) Anatomy involved in the jugular foramen approach for jugulotympanic paraganglioma resection. Neurosurg Focus 17:41–44
Jabre A, Tabaddor R, Samaraweera R (2000) Transphenoidal meningoencephalocele in adults. Surg Neurol 54:183–187
Joseph M, Rajshekhar V, Chandy MJ (2004) Haematopoietic tissue presenting as a sphenoid sinus mass: case report. Neuroradiology 42:153–154
Kaufman B, Bellon EM (1973) The trigeminal nerve cistern. Radiology 108:597–602
Kozlowski K, Cambell J, Mc Alister W, Babyn P, Cama A, Masel J, Pelizza A, Taccone A (1991) Rare primary cranial vault and base of skull tumours in children: report of 30 cases and short literature review. Radiol Med 81:213–213
Laigle-Donadey F, Tailliber S, Martin-Duverneuil N, Hildebrand J, Delattre JY (2005) Skull-base metastases. J Neurooncol 75:63–69
Lang FF, Macdonald OK, Fuller GN, DeMonte F (2000) Primary extradural meningiomas: a report of nine cases and review of literature from the era of computerized tomography scanning. J Neurosurg 93:940–950
Layer G, Steudal A, Schuller H, van Kaick G, Grunwald F, Riser M, Schild HH (1999) Magnetic resonance imaging to detect bone marrow metastases in the initial staging of small cell lung carcinoma and breast carcinoma. Cancer 85:1004–1009
Liu JK, Gottfried ON, Amini A, Couldwell WT (2004) Aneurysms of the petrous internal carotid artery: anatomy, origins, and treatment. Neursurg Focus 17:1–9
Loevner LA, Tobey JD, Yousem DM, Sonners AI, Hsu WC (2002) MR imaging characteristic of cranial bone marrow in adult patients with underlying systemic disorder compared with healthy control subjects. AJNR Am J Neuroradiol 23:248–254
Luff DA, Simmons M, Malik T, Ramsden RT, Reid H (2002) Endolymphatic sac tumours. J Laryngol Otol 116:398–401
Mascalchi M, Filippi M, Floris R, Fonda C, Gasparotti R, Villari N (2005) Diffusion-weighted MR of the brain: methodology and clinical application. Radiol Med (Torino) 109:155–197
Miller C, Lloyd TV, Johnson JC, Hunt WE (1978) Eosinophilic granuloma of the base of the skull. Case report. J Neurosurg 49:464–466
Moore KL, Dalley AF (1999) Head and neck. In Moore KL, Dalley AF (eds) Clinically oriented anatomy, 4th edn. Lippincott Williams & Wilkins, Philadelphia, pp 1093–1096
Mukherji SK, Castillo M (1996) Adenocarcinoma of the endolymphatic sac: imaging features and preoperative embolization. Neuroradiology 38:179–180
Mukherji SK, Baggett HC, Alley J, Carrasco VH (1998) Enlarged cochlear aqueduct. AJNR Am J Neuroradiol 19:330–332
Price T, Fayad G (2002) Abducens nerve palsy as the sole presenting symptom of petrous apicitis. J Laryngol Otol 116:726–729
Ragel BT, Couldwell WT (2004) Pituitary carcinoma: review of the literature. Neurosurg Focus 16:1–9
Rao AB, Koeller KK, Adair CF (1999) From the archives of the AFIP. Paragangliomas of the head and neck: radiologic-pathologic correlation. Radiographics 19:1605–1632
Robert Y, Carcasset S, Rocourt N, Hennequin C, Dubrulle F, Lamaitre L (1995) Congenital cholesteatoma of the temporal bone: MR findings and comparison with CT. AJNR Am J Neuroradiol 16:755–761

Rueda-Franco F, Lopez-Correla E (1995) Sarcomas in the central nervous system of children. Pediatric Neurosurg 22:49–56

Salvati M, Ciappetta P, Capone R, Santoro R, Raguso M, Raco A (1993) Osteosarcoma of the skull in a child: a case report and review of the literature. Childs Nerv Syst 9:437–439

Sen C, Hague K, Kacchara R, Jenkins A, Das S, Catalano P (2001) Jugular foramen: microscopic anatomic features and implications for neural preservation with reference to glomus tumors involving the temporal bone. Neurosurg 48:838–847

Shinoda J, Kimura T, Funakoshi T, Iwata H, Tange K, Kasai C, Miyata Y (1993) Primary osteosarcoma of the skull. J Neurooncol 17:81–88

Smirniotopoulos JG, Chiechi MV (1995) Teratomas, dermoid, and epidermoids of the head and neck. Radiographics 15:1437–1455

Stone JA, Cooper H, Castillo M, Mukherji SK (2001) Malignant schwannoma of the trigeminal nerve. AJNR Am J Neuroradiol 22:505–507

Tauber M, van Loveren HR, Jallo G, Romano A, Keller JT (1999) The enigmatic foramen lacerum. Neurosurgery 44:386–391

Tokgoz N, Oner YA, Kaymaz M, Ucar M, Yilmaz G, Tali TE (2005) Primary intraosseous meningioma: CT and MRI appearance. AJNR Am J Neuroradiol 26:2053–2056

Tunaci M, Tunaci A, Engin G, Ozkorkmaz B, Dincol G, Acunas G, Acunas B (1999) Imaging features of thalassemia. Eur Radiolol 9:1804–1809

Turner OA, Laird AT (1966) Meningioma with traumatic etiology. J Neurosurg 24:96–98

Utz JA, Krandorf MJ, Jelinek JS, Moser RP Jr, Berrey BH (1989) MR appearance of fibrous dysplasia. J Comput Assist Tomogr 13:845–851

Van Tassel P, Lee YY, Ayala A, Carrasco CH, Klima T (1991) Case report 680. Intraosseous meningioma of the sphenoid bone. Skeletal Radiol 20:383–386

Whitehead RE, Melhem ER, Kasznica J, Eustace S (1998) Telangiectatic osteosarcoma of the skull base. AJNR Am J Neuroradiol 19:754–757

Williams LS, Schmalfuss IM, Sistrom CL, Inoue T, Tanaka R, Seoane ER, Mancuso AA (2003) MR imaging of the trigeminal ganglion, nerve and the perineural vascular plexus: normal appearance and variants with correlation to cadaver specimens. AJNR Am J Neuroradiol 24:1317–1323

Yildirim T, Agildere AM, Oguzkurt L, Barutcu O, Kizilkilic O, Kocak R, Alp Niron E (2005) MRI evaluation of cranial bone marrow signal intensity and thickness in chronic anemia. Eur J Radiol 53:125–130

14 Thyroid and Parathyroid Neoplasms

Soraya Robinson

CONTENTS

14.1 Imaging Modalities

14.1.1 Plain X-Ray

X-rays of the neck, the chest or barium swallows can give hints mainly regarding thyroid disease, such as narrowing of tracheal, hypopharyngeal or oesophageal lumen, their shifting away from the midline, and coarse calcifications (Fig. 14.1). Their importance has remarkably decreased since the development and refinement of modern cross-sectional techniques. Reports on radiographically visible calcified parathyroid adenomas are anecdotal (Polga and Balikian 1971; Warter et al. 1975; Randel et al. 1987).

Despite its much lower sensitivity to detect pulmonary metastases than CT, chest X-ray is still part of the routine follow-up program after removal of primary tumours (Lorenzen et al. 1998) (Fig. 14.2).

Bony changes of hyperparathyroidism can be easily visible on plain X-rays.

14.1.2 Ultrasound

High-resolution ultrasound is performed with frequencies between 7.5–12.5 MHz. Its role in the pre- and postoperative management of thyroid and parathyroid lesions is regarded controversial in the literature. There is agreement that it can prove the presence or absence of thyroid nodules and assess their texture (solid versus cystic), number and location, which eases the interpretation of nuclear medicine studies for both organs.

Apart from gaining information about the morphology of a lesion, ultrasound is also used for guidance of fine needle aspiration biopsy (see Sect. 14.1.2.3), percutaneous laser thermal ablation and ethanol injection (Baskin 2004). While the latter seeps into the surrounding tissue and can cause excessive scarring, which makes subsequent surgery difficult, US-guided percutaneous laser ablation has been used successfully in patients at poor surgical risk for debulking of hypofunctioning masses for amelioration of local compression symptoms, where radioablation does not work (Pacella et al. 2004). Although it has been used for palliation in anaplastic carcinoma, caution is needed because of the friability of neoplastic tissue, where the extent of therapy is difficult to predict and the proximity of the big cervical vessels a danger.

S. Robinson, MD
Department of Radiology, Helsinki University Central Hospital, Haartmaninkatu 4, POB 340, 00029 HUS Helsinki, Finland

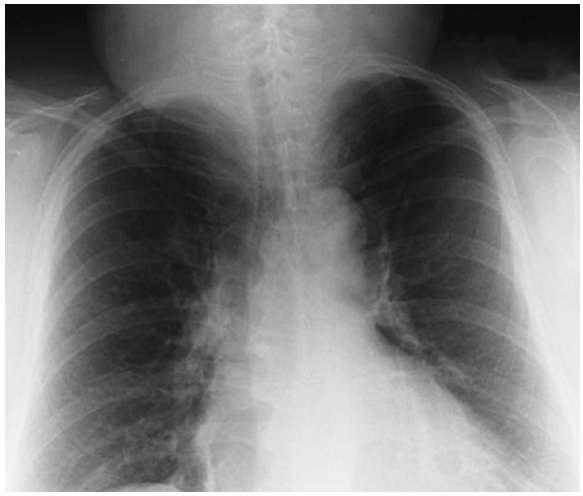

Fig. 14.1. Chest X-ray: huge struma shifting the trachea to the right and narrowing its transverse diameter by half

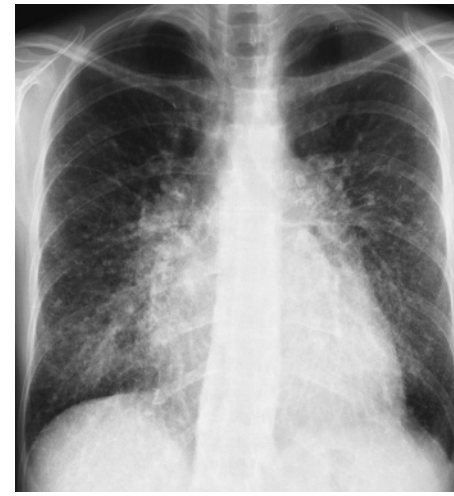

Fig. 14.2. Chest X-ray: disseminated pulmonary metastases from medullary carcinoma

14.1.2.1 Thyroid Gland

The thyroid lobes lie fairly symmetric on either side of the trachea, connected by the isthmus of variable width and display homogenous, glandular structures with interspersed branches from the upper and lower thyroid vessels. Neck ultrasound performed for other indications yields 40%–50% of thyroid incidentalomas: non-palpable thyroid nodules, which were hitherto clinically silent (Iannuccilli et al. 2004). But only 5%–6.5% of those will be malignant. To reduce morbidity and costs of unnecessary thyroid surgery, many authors have tried to establish criteria for benign, indeterminate, and malignant looking nodules.

Coarse calcifications are typical for colloid cysts, which do not require further management in the absence of other manifestations.

Microcalcifications (too numerous to count), extracapsular invasion or lymphadenopathy are considered to be definite signs of malignancy (Iannuccilli et al. 2004) (Fig. 14.3).

Size criteria for metastatic thyroid nodes have not yet been established. They tend to loose their spindle shape and become rounder and inhomogeneous (Figs. 14.4, 14.5). More lymph nodes than normal are visible, especially in the lower jugular and accessory group (level 4, 5). Internal calcifications are frequently seen with or without posterior shadowing (Fig. 14.6). Adenopathies, as well as local tumour recurrences may be partly or purely cystic (Fig. 14.7).

Although some groups have published additional suspicious criteria, such as marked hypoechogenicity, irregular, or microlobulated borders, a shape that is more tall than wide, and penetrating vessels in colour flow mapping and a pulsatility index of ≥ 1, most agree that including indeterminate signs in the malignant group increases the sensitivity at the cost of losing specificity and does not avoid overlap of benign and malignant disease (Iannuccilli et al. 2004; Fukunari et al. 2004).

Indeterminate findings are indistinct borders, dense nodules and incomplete hypoechoic halos (Figs. 14.8, 14.9).

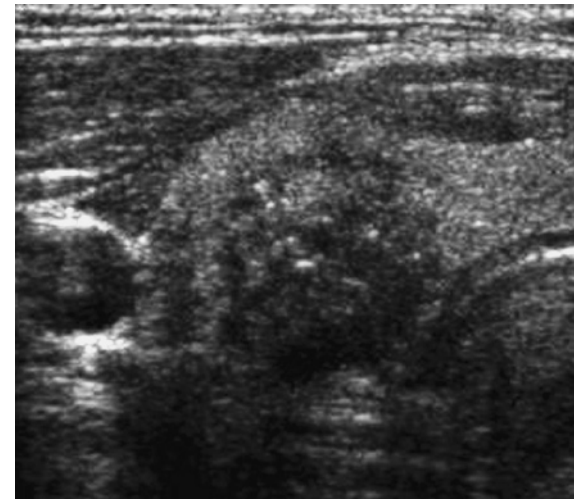

Fig. 14.3. Ultrasound: ill-defined, hypoechoic mass in the right thyroid lobe with microcalcifications and slight posterior shadowing from papillary carcinoma

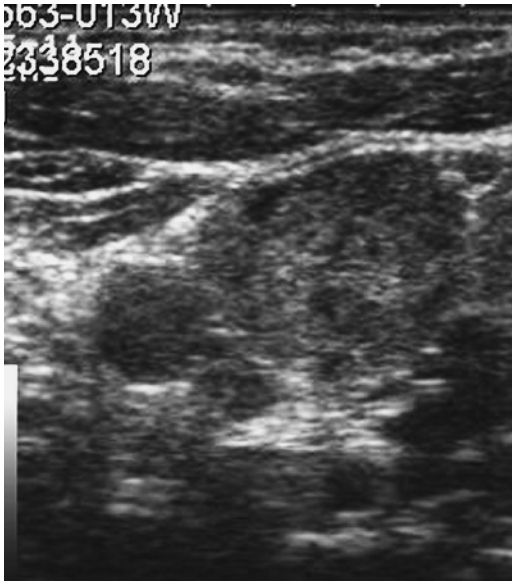

Fig. 14.4. Ultrasound: round, heterogeneously hyperechoic lymph node metastasis from papillary carcinoma

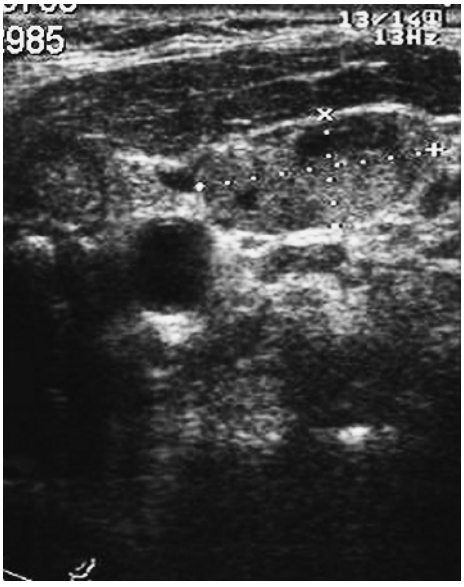

Fig. 14.5. Ultrasound: ovoid, but inhomogeneous lymph node metastasis from papillary carcinoma

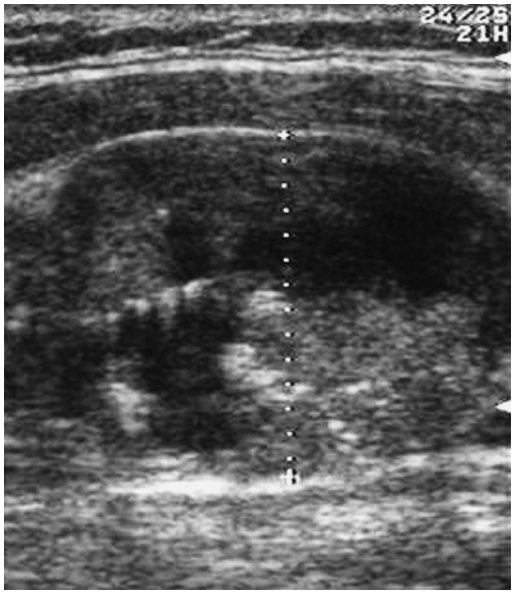

Fig. 14.6. Ultrasound: enlarged, heterogeneous, partly calcified lymph node metastasis from papillary carcinoma

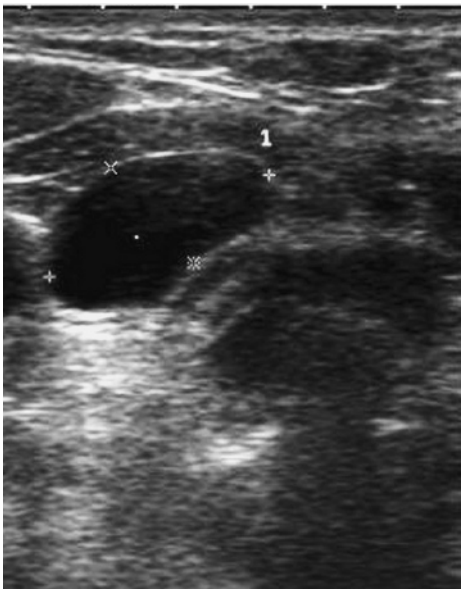

Fig. 14.7. Ultrasound: purely cystic local recurrence after radioablation of papillary carcinoma

Most carcinomas are hypoechoic, which do not accumulate radioiodine (cold nodule).

14.1.2.2 Parathyroid Gland

Normal parathyroid glands are only exceptionally visualized. Enlarged glands can be found behind the lower and upper pole of the thyroid glands. Delineating the cleavage plane between the two organs is noteworthy. At times, depiction is eased, when the patient is swallowing (Simeone et al. 1981).

Abnormal parathyroid glands are typically round to ovoid, hypoechoic and show increased vascularity (Prager et al. 1999) (Fig. 14.10). Cystic degeneration and completely anechoic avascular findings are rare

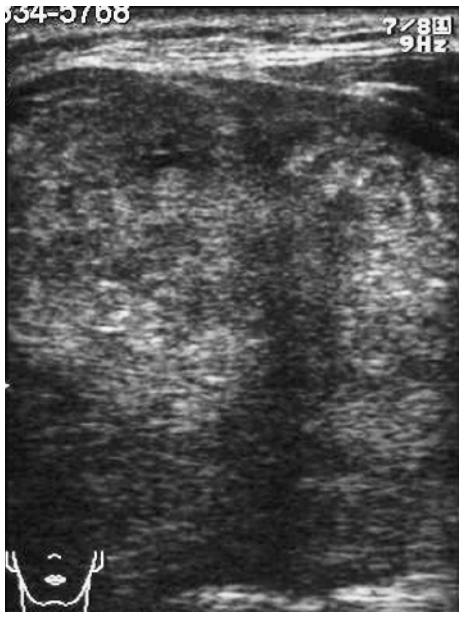

Fig. 14.8. Ultrasound: enlarged thyroid lobe containing ill-defined papillary carcinoma with microcalcifications

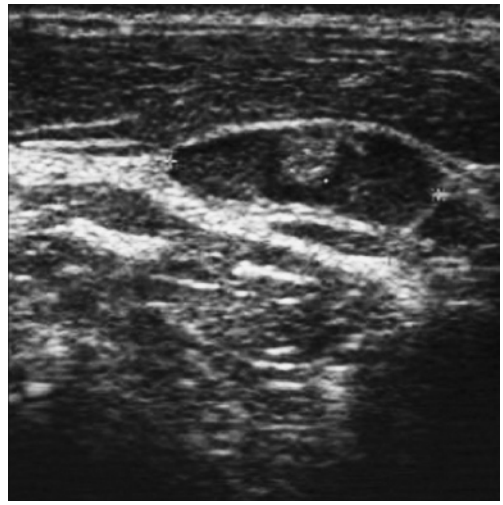

Fig. 14.9. Ultrasound: spindle shaped lymph node metastasis with inhomogeneous and dense centre from papillary carcinoma

(Randel et al. 1987). It can be impossible to establish the diagnosis of parathyroid carcinoma preoperatively in the absence of capsular rupture or lymphadenopathy (Fig. 14.11).

The report should include information on the presence or absence of enlarged glands, the affected side, whether the lesion is near the lower or upper thyroid pole or in an ectopic position, whether there is a single gland involved, or multiglandular disease. Precise description of the thyroid lobes helps correct interpretation of scintigraphic studies. Intraoperative ultrasound is also successfully used in some centres (Prager et al. 1999).

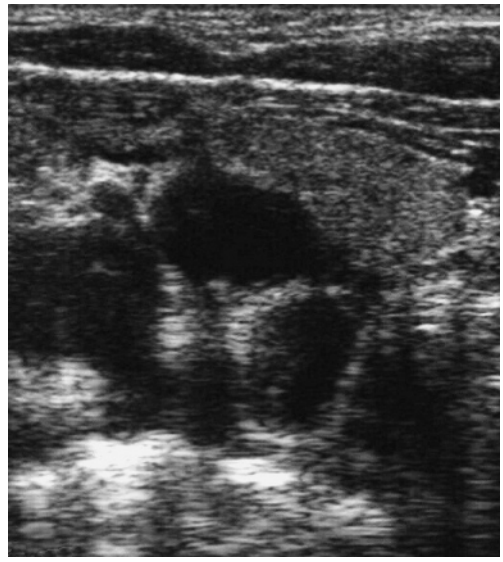

Fig. 14.10. Ultrasound: partly cystic parathyroid adenoma

14.1.2.3 Fine Needle Aspiration Biopsy

M. Taavitsainen, MD
Medivire Aleksi, Kluuvikatu 4a, FIN-00100 Helsinki, Finland

The abundant cellularity of thyroid neoplastic lesions makes them ideal targets for aspiration biopsy. With appropriate US guidance of the needle tip the risk of missing a neoplastic lesion is low.

Fine needle aspiration biopsy (FNAB) is performed with fine needles (0.4–0.7 mm outer diameter) using needle movements in the lesion for detachment and suction for retrieval. The amplitude of the needle movement should be at least 0.5 cm (Kreula 1990a). The suction force is produced with vacuum in a syringe that is attached to the needle either directly or with a connecting tube. A vacuum of 2 ml is enough to produce maximal suction force (Kreula 1990b).

The material can be prepared either as air dried smears or fixed, for example, in 50% ethanol for later centrifugation and staining. The choice of the technique is dependent on the training of the pathologist.

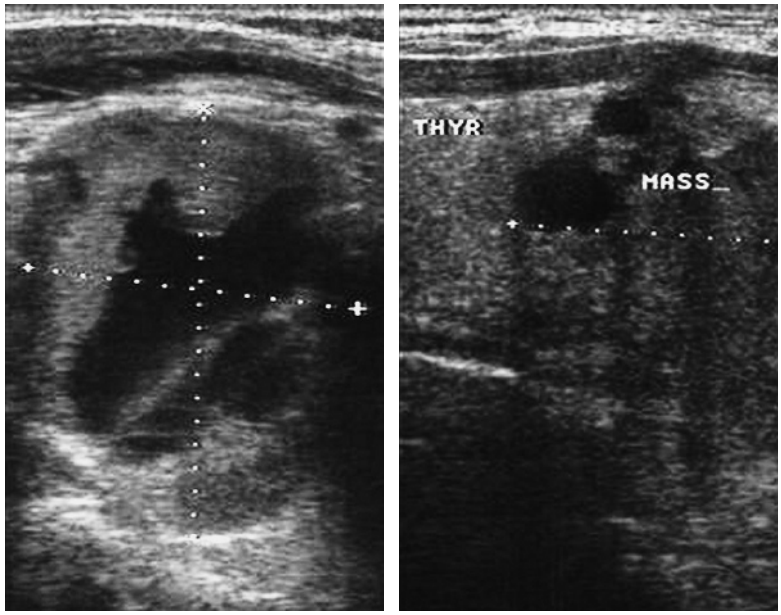

a b

Fig. 14.11a,b. Ultrasound: extremely enlarged parathyroid gland with central necrosis in parathyroid carcinoma; transverse (**a**); longitudinal section (**b**)

Histology from material obtained by core-needle biopsy (0.9- to 1.4-mm thick needles are attached to a spring-loaded device) has also been applied for the diagnosis of thyroid lesions, especially for lymphomas (Quinn et al. 1994; Screaton et al. 2003).

The technique is a safe outpatient procedure, where occasional minimal intrathyroidal bleeding causing slight discomfort is mentioned as a rare complication. Bleeding may worsen the sample quality. The needle thickness should therefore be kept as small as possible. In fibrotic goitre nodules it may be difficult to aspirate diagnostic material.

Unfortunately, cytology cannot differentiate between follicular adenoma and follicular carcinoma.

In patients with hyperparathyroidism biopsies do not play a central role.

It is also appropriate to confirm the character of the target cytologically before ablation of the gland with ethanol injection. In addition, fluid aspiration of a lower neck cyst and laboratory assessment of its parathormone content can establish the diagnosis of a rare parathyroid cyst, which occurs more often on the left side (Ginsberg et al. 1978).

14.1.3 Computed Tomography

Computed tomography (CT) of the neck is nowadays usually performed in multi-slice mode, which provides higher spatial resolution than conventional CT scanners (Ishigaki et al. 2004).

Many contrast enhanced CT examinations performed for other indications will reveal incidental thyroid pathology (Fig. 14.12). If a patient has thyroid disease of unknown origin, one should rather perform MRI. On average, a dose of 100 ml of iodine containing contrast agent will deliver a dose of 20–30 g iodine and will block the thyroid gland for subsequent scintigraphy or radioablation for 6–8 weeks (Laurie et al. 1992). Rarely, it may provoke a thyrotoxic crisis, which may be prevented by premedication with 500 mg oral perchlorate 2–4 h before and after iodine application and 3×300 mg perchlorate over the next week (Hehrmann et al. 1996).

Otherwise, the examination should be done from the skull base to the mediastinum down to the carina to exclude lymphadenopathy or ectopic parathyroid adenomas (Harnsberger 2004). At 30 s after intravenous administration of 100 ml non-ionic contrast medium the scan is performed in thin sections (e.g. slice thickness 1 mm, pitch 3, reconstruction increment 1 mm).

Evaluation includes size of thyroid lobes and isthmus, their density, homogeneity, and calcifications (Figs. 14.13, 14.14). In case of masses their borders and effect on larynx/trachea, hypopharynx/oesophagus, prevertebral fascia, big vessels and their relationship to the sternum, as well as possible lymphadenopathy, are assessed (Fig. 14.15).

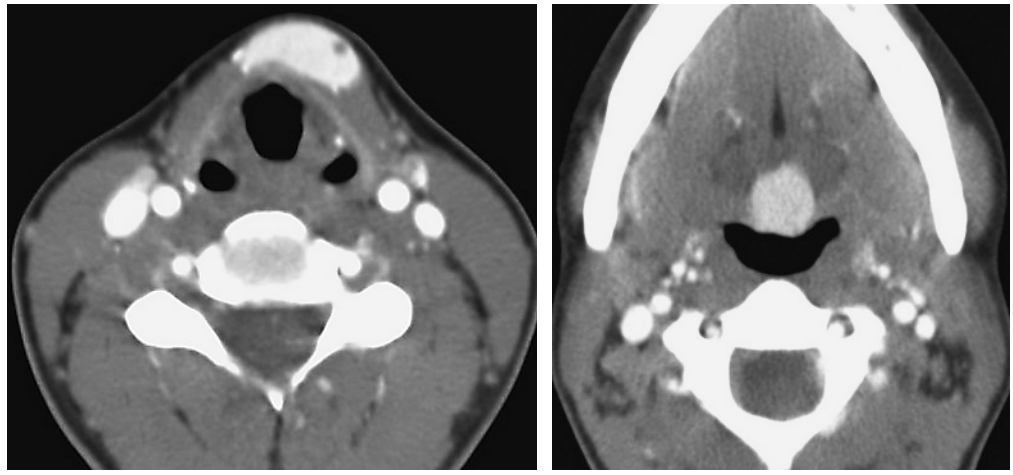

a b

Fig. 14.12a,b. CT: lingual thyroid

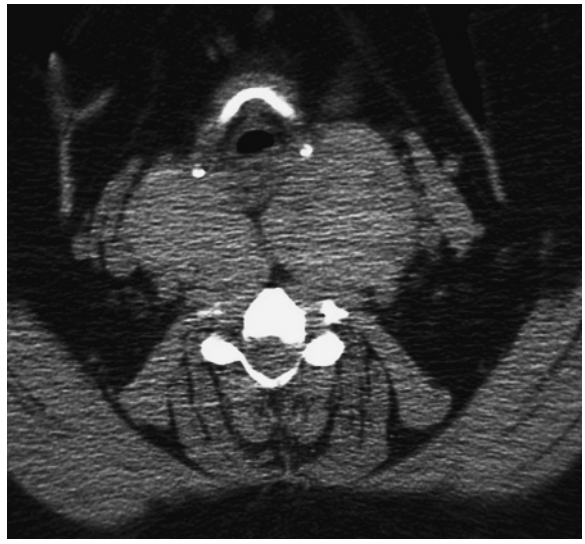

Fig. 14.13. CT: large, retropharyngeal struma

In hyperparathyroidism, enhancing round or ovoid lesions behind the thyroid gland or in ectopic position anywhere from the carotid bifurcation to the mediastinum are sough.

CT can be applied in malignant thyroid tumors, for example to rule out associated disease in multiple endocrine neoplasia (MEN) syndromes, or metastatic disease (Figs. 14.16, Fig. 14.17).

14.1.4 Magnetic Resonance Imaging

MRI is performed with a circular-polarized neck coil for the neck and a phased-array body coil for the mediastinum (Czerny et al. 2003). The latter profits from cardiac gating. A matrix of 512×512, FOV of 20–25 cm and slice thickness of 2–3 mm have proven to be most useful. Commonly applied section planes are axial and coronal. Precontrast SE-T1, fat-suppressed T2-weighted (turbo)SE and postcontrast T1-weighted fat-suppressed SE sequences help delineation of disease.

Evaluation criteria are similar to the ones applied for CT. It is worth mentioning that haemorrhage into thyroid nodules, a high protein content of colloid, but also malignant primary tumour and lymph nodes may appear hyperintense on T1 before contrast administration (Figs. 14.18, 14.19). Partly or purely cystic recurrences or lymph node metastases are not uncommon (Figs. 14.20, 14.21). Coarse calcifications are hypointense on all sequences, microcalifications may go undetected.

Enlarged parathyroid glands are slightly hypointense to muscle, hyperintense on T2 and strongly enhance with contrast agent. While ^{99m}Tc-SestaMIBI with or without SPECT is more sensitive in the detection of (mediastinal) parathyroid disease, MRI is superior in evaluating the topographic relations on which the therapeutic decision (e.g. transsternal versus transthoracic approach) is based.

Furthermore, MRI has proven superior in the evaluation of distant metastases, especially of brain and bone marrow (Mirallié et al. 2005) (Fig. 14.22).

14.1.5 Nuclear Medicine

Nuclear medicine is indispensable in the management of thyroid and parathyroid neoplasms.

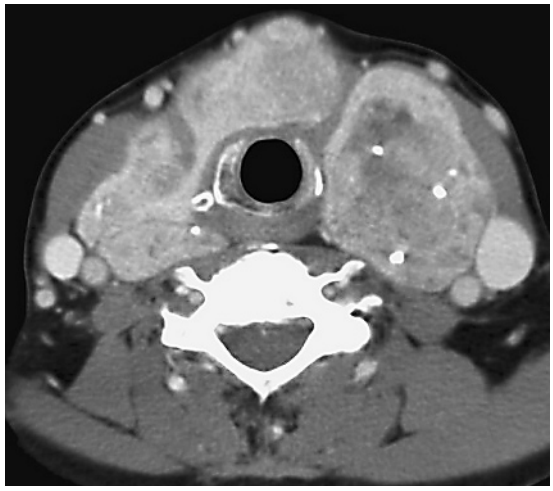

a

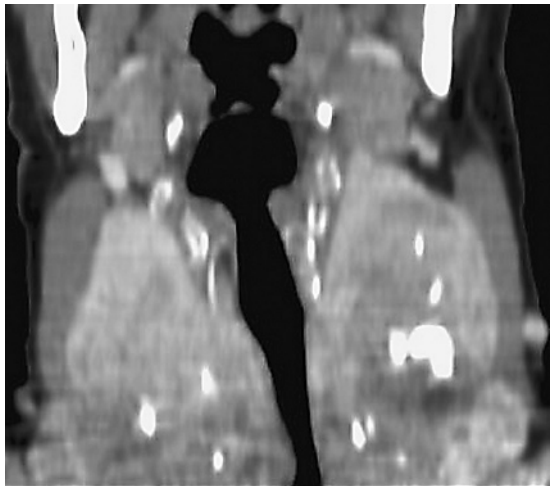

b

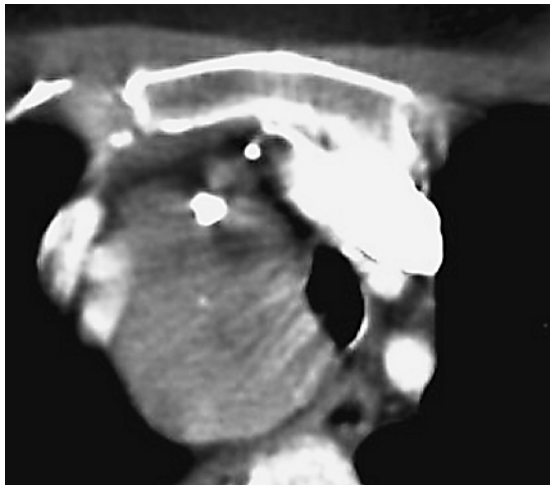

c

Fig. 14.14a–c. CT: huge struma involving both lobes and the isthmus with cystic parts and coarse calcifications; transverse (**a**); coronal (**b**); sagittal: extension into posterior mediastinum (**c**)

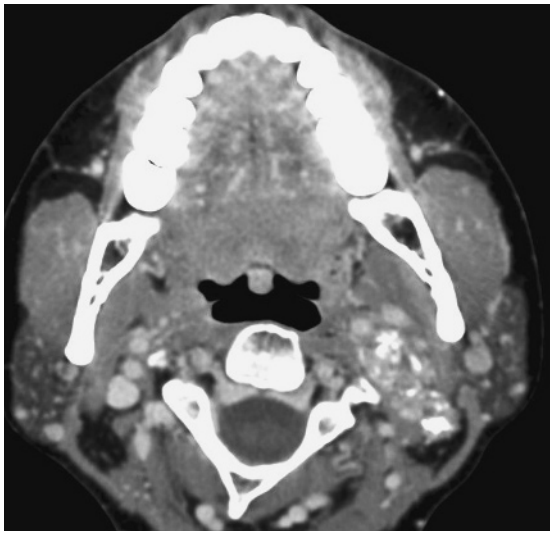

Fig. 14.15. CT: calcified lymph node metastasis in the left upper jugular group (level II) from medullary carcinoma

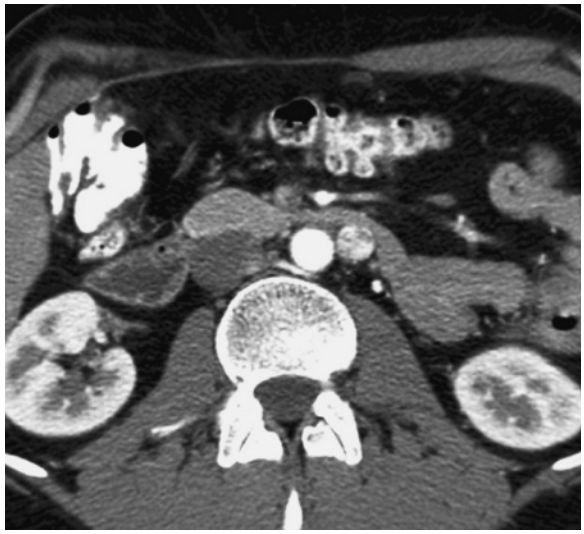

Fig. 14.16. CT: left paraaortal paraganglioma in patient with medullary thyroid carcinoma

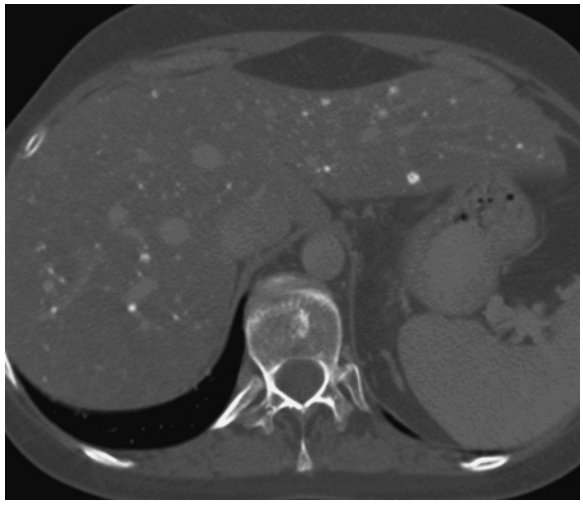

Fig. 14.17. CT: calcified liver metastases from medullary carcinoma

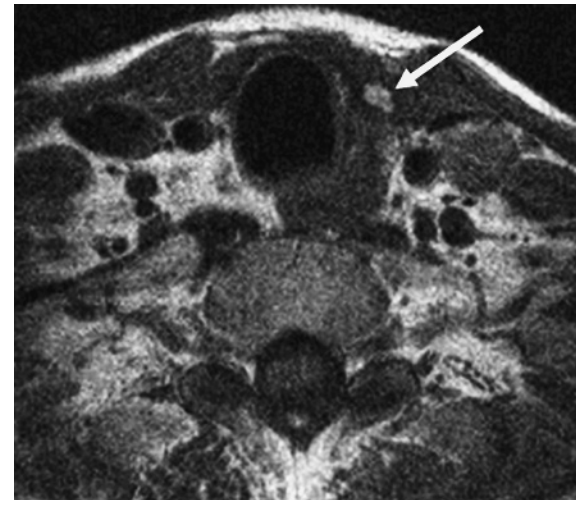

Fig. 14.18. Precontrast T1-weighted MR image: hyperintense recurrence from papillary carcinoma in left thyroid bed (*arrow*)

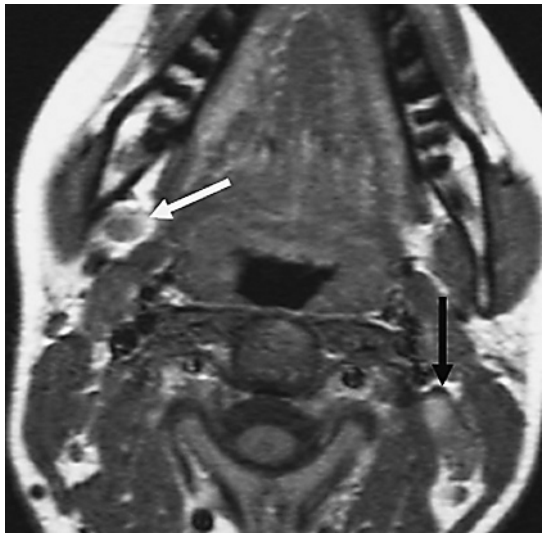

Fig. 14.19. Precontrast T1-weighted MR image: slightly hyperintense lymph node metastases from papillary carcinoma in the right submandibular (level I, *white arrow*) and in the left upper jugular group (level II, *black arrow*) behind the vessels

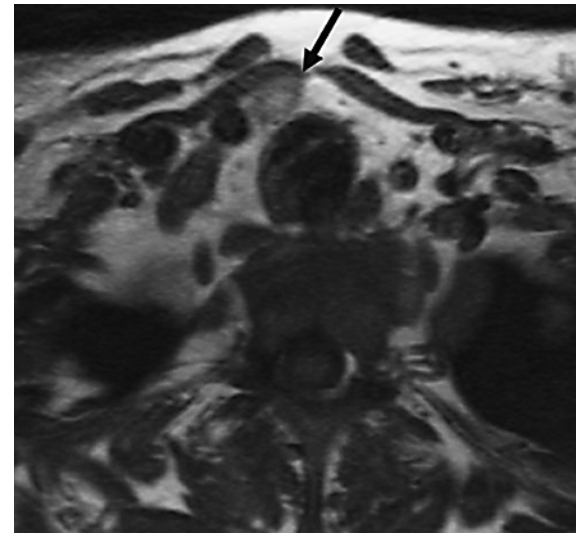

Fig. 14.20. Precontrast T1-weighted MR image: slightly hyperintense recurrence in right thyroid bed 2 months after radioablation (*arrow*)

If tracer accumulation in the thyroid gland is not homogenous, it can either be "hot", if an area is increased compared to the surrounding gland, or "cold", if it accumulates less than the gland. The latter is associated with an up to 20% risk of malignancy. After thyroidectomy tumour cell remnants can be ablated with internal radiotherapy. In the follow-up, tracer accumulation can highlight recurrent and metastatic disease, especially, if thyroglobulin is elevated over 10 ng/ml.

^{99m}Tc pertechnetate, ^{123}I and ^{131}I scintigraphy are used for diagnosis of thyroid disorders. Technetium is applied intravenously and imaging performed 20 min later, or iodine is given orally and the patient scanned after 4–24 h. Diagnostic ^{131}I scans can be performed post thyroidectomy to detect local and metastatic disease. If positive, therapeutic ablation with ^{131}I follows. In other centres, in all differentiated T2 tumours, in cases with extension beyond the thyroid capsule or with lymph node metastases, radio-

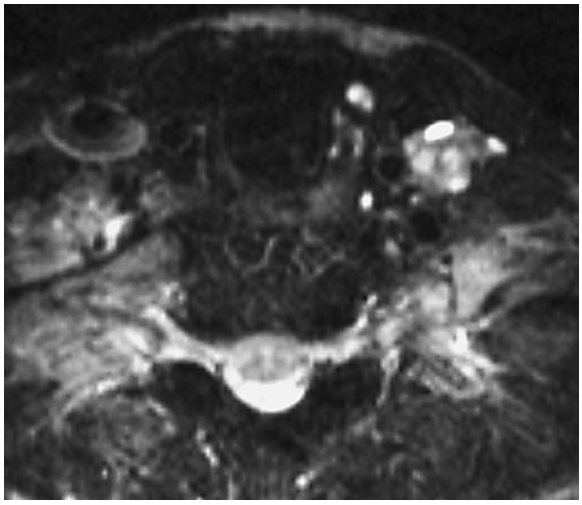

Fig. 14.21. T2-weighted MR image: heterogeneous, partly cystic lymph node metastasis in left middle jugular group (level III) from papillary carcinoma

iodine ablation is performed (Schlumberger et al. 2004).

Diagnostic ^{131}I dose detects less medullary thyroid bone involvement than the therapeutic dose. The same applies for pulmonary micrometastases and ^{131}I therapy, which detects more than the low dose diagnostic scan (Mirallié et al. 2005).

Precise localization of the foci of ^{131}I uptake can be difficult because of lack of anatomic landmarks (Yamamoto et al. 2003). Physiologic uptake from salivary glands, urinary bladder, gastrointestinal tract and liver can be misleading. While making it possible to assess the third dimension of uptake extension, SPECT ^{131}I scintigraphy improves the sensitivity, even more so with CT image fusion, thus influencing further patient management (Ruf et al. 2004). Dedicated SPECT/CT are available in specialized centres only. Comparable results have been achieved with external markers and manual landmark selection.

^{99m}Tc methoxyisobutylisonitrile (Sesta-MIBI) is highly effective in detecting deposits of metastatic differentiated thyroid cancer and useful in medullary thyroid carcinoma. It is superior to all other modalities in delineating parathyroid tumours, especially in mediastinal location (Adams et al. 2004).

Metaiodobenzylguanidine (MIBG) is the modality of choice for pheochromocytoma and paraganglioma in MEN 2 (Bombardieri et al. 2004). ^{111}In-pentetreotide has high accuracy for paragangliomas, even when they are not detected by conventional imaging methods (Bombardieri et al. 2004).

Parathyroid scintigraphy can be impeded by superimposing thyroid masses or multinodular goitre. This difficulty may be overcome by subtraction techniques (while ^{201}thallium/^{99m}Tc pertechnetate, ^{99m}Tc Sesta-MIBI/^{123}In subtraction have been standart methods up till recently, ^{99m}Tc Sesta-MIBI/^{99m}Tc pertechnetate is now considered to be more reliable). Thallium and sestamibi are taken up both by thyroid and parathyroid glands. ^{99m}Tc pertechnetate and ^{123}I are only taken up by the thyroid gland. Hypermetabolic thyroid disease including multinodular goitre, thyroiditis, thyroid

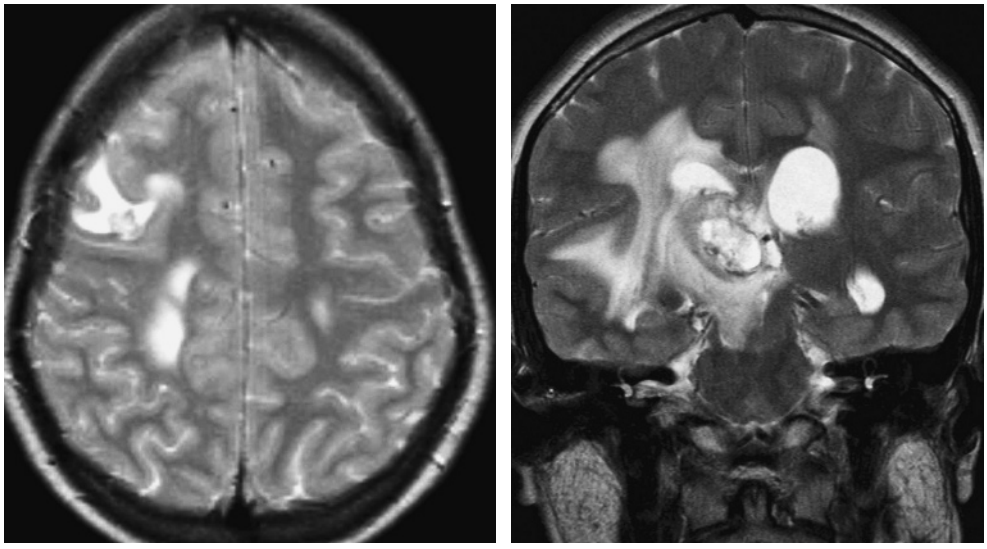

a **b**

Fig. 14.22.a,b. MRI: brain metastases with surrounding edema from papillary thyroid carcinoma; in right frontal and temporal lobe (**a**); in right basal ganglia with compression of ipsilateral lateral ventricle and blockage of contralateral foramen of Monro (**b**)

adenoma and thyroid carcinoma may retain ^{99m}Tc sestamibi leading to false positive parathyroid adenoma results (Macdonald 2004c).

Images of the neck and chest are obtained 5 min after intravenous administration of ^{99m}Tc- sesta-MIBI and again after intravenous application of ^{99m}Tc pertechnetate and evaluated after subtraction. Since its sensitivity for the detection of parathyroid tumours is supposed to be around 86%, it should be the initial test in patients with hyperparathyroidism (Lumachi et al. 2004; Prager et al. 1999) (Fig. 14.23). If ultrasound and scintigraphic findings are not consistent, SPECT can be obtained (Rubello et al. 2004).

Somatostatin receptor scintigraphy is performed with ^{111}In-octreotide and reported to be moderately sensitive in the detection of metastases from differentiated thyroid carcinoma unable to concentrate iodine. The sensitivity is higher when thyroglobulin levels are higher than 50 ng/ml or when mediastinal lesions are involved (Giammarile et al. 2004). Its usefulness has also been demonstrated for medullary carcinoma (Loevner 2003; Fiore et al. 2004; Bombardieri et al. 2004).

Thyroid lymphoma is the only malignancy in which intense uptake of ^{67}Gallium is reported.

Recently, many publications have focused on FDG-PET(/CT): ^{18}Fluorine fluorodeoxyglucose visualizes increased glucose metabolism of cancer (Heron et al. 2004). Hybrid imaging combines emission and transmission tomography with the advantage of both anatomic and metabolic information (Kainberger et al. 2003). Several authors have shown its superiority in the follow-up of patients with differentiated thyroid carcinoma, when their thyroglobulin level is elevated over 10 ng/ml, but their ^{131}I whole body scan negative (Nahas et al. 2005; Menzel et al. 2004; Ruiz Franco-Baux et al. 2005). While its specificity reaches 100%, a negative scan cannot rule out recurrent disease.

FDG-PET(/CT) can also be helpful for suspected recurrence of medullary carcinoma with elevated tumour marker but negative imaging findings ("minimal" disease) (De Groot et al. 2004).

Radiolabeled methylenediphosphonate (^{99m}Tc MDP) is in successful use for evaluation of bone metastases in anaplastic carcinoma.

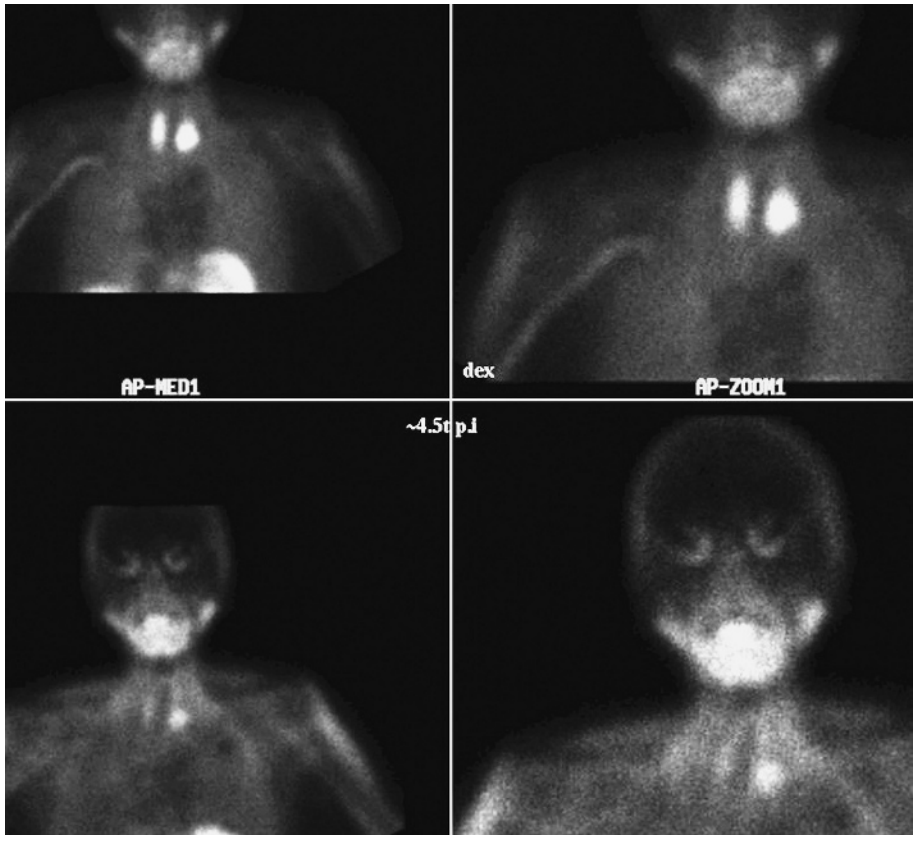

Fig. 14.23. ^{99m}Tc Sesta-MIBI/^{99m}Tc pertechnetate subtraction scintigraphy: uptake in both enlarged thyroid lobes is subtracted, only accumulation in left parathyroid adenoma and physiologically in salivary glands stays

14.2 Thyroid Gland

14.2.1 Embryology

The thyroid gland develops median at the base of the tongue between the first and second pharyngeal pouch from endodermal epithelial cells. It subsequently descends through the tongue, anterior to the hyoid bone along the thyroglossal duct and then assumes a paramedian position. If the duct fails to obliterate, it can persist at any position, and form a median or paramedian neck cyst. Ectopic thyroid tissue is most commonly found at the base of the tongue, more rarely further down.

Before its removal, one has to make sure that the patient has thyroid tissue in its regular position (Fig. 14.12a,b). It may harbour any thyroid disease. The incidence of thyroid carcinoma in a median neck cyst is as low as 1% (Kurzen et al. 1999).

The ultimobranchial body derives from the fifth branchial pouch, is infiltrated by migrating cells from the neural crest and is then incorporated into the thyroid gland, giving rise to the parafollicular C-cells (Loevner 2003).

14.2.2 Anatomy

The thyroid bed is enclosed in the visceral space formed by the middle layer of the deep cervical fascia (Harnsberger 2004). The shield-shaped thyroid gland lies in front of the larynx and upper trachea with its superior margin near the oblique line of the thyroid cartilage and its inferior margin at the level of the fourth or fifth tracheal ring (Loevner 2003). The adult gland weighs between 15 and 35 grams and comprises a volume of about 18 ml. It can be enlarged during pregnancy and menstruation. The thyroid lobes measure around 4×3×2 cm each and are connected by the isthmus, which can be of variable width. Approximately 50%–70% of people have an accessory lobe stretching from the isthmus upwards in a median or paramedian position, called the pyramidal lobe as a remnant from the thyroglossal duct.

Since the cervical fascia attaches to larynx and trachea, the thyroid gland also shows intradeglutitive elevation.

The normal thyroid gland interposes between the trachea and hypopharynx, thus forming a slight, smooth indentation on the distended hypopharynx as shown on a barium swallow (Roddie and Kreel 1997).

The thyroid gland drains into paratracheal, jugular and superior mediastinal lymph nodes. In one fifth of patients, a direct lymphatic connection of the posterior part of the thyroid gland to the parapharyngeal and retropharyngeal space was found and therefore, a solitary lymph node metastasis from thyroid malignancies to the parapharyngeal space is not necessarily associated with an increased risk of level II–VI metastases (Lombardi et al. 2003).

14.2.3 Physiology and Implications for Follow-Up

The thyroid is a multilobular gland consisting of many small epithelial lined follicles containing colloid. The wall consists of follicular and papillary cells and is the site of hormone production.

Under the influence of hypothalamic thyrotropic releasing hormone, the pituitary gland releases thyroid stimulating hormone (TSH), which triggers thyroid hormone production. The thyroid gland needs a sufficient amount of iodine supply to trap iodide from the plasma and store it within the follicular cells, bound to thyroglobulin. After oxidation and organic iodination, hormonally inactive precursors (mono- and diiodotyrosine) are found, which are then recombined to the active hormones triiodothyronine (T3, the most active form) and thyroxin (T4, the most abundant form). Only minute amounts of thyroglobulin are detectable in the blood of normal persons. In thyroidectomized patients (as treatment for differentiated cancer), the level of thyroglobulin after withdrawal of thyroid hormone replacement therapy, or nowadays after application of recombinant human thyroid stimulating hormone (rhTSH), should decrease (Bombardieri et al. 2003). There is no detectable thyroglobulin level below which the risk of persistent or recurrent disease can be totally excluded (Schlumberger et al. 2004). Persistent elevated levels over 10 ng/ml, depending on the local laboratory, or subsequent rise may be a sign of tumour remnant or recurrent disease. In some centres, patients then immediately proceed to radioablation to treat disseminated foci (de Rosario 2005). Others first perform whole body scintigraphy to confirm the presence of recurrent disease. Unfortunately, dedifferentiation of tumour cells in the course of the disease may go along with a loss of the ability to produce thyroglobulin (Schlumberger et al. 2004).

The thyroid gland also contains parafollicular C cells or medullary cells of ultimobranchial origin. Their production of calcitonin is remarkably increased by calcium or pentagastrin, and the calcitonin level can be used as a screening test for medullary thyroid carcinoma. They also express a high density of carcinoembryonic antigen (CEA), which can both serve as a tumour marker and be used in radioimmunotherapy with radiolabeled anti-CEA monoclonal antibodies or dendritic cell vaccination (Mirallié et al. 2005; Juweid et al. 2000; Stift et al. 2004).

14.2.4 Pathology

14.2.4.1 Benign Disease

Some non-neoplastic entities will also be discussed as they are relevant for subsequent understanding the imaging features of malignant disease.

14.2.4.1.1 Struma (Multinodular Goitre)

If the oral iodine supply does not suffice for normal hormone production (for children 90–120 micrograms/day, for adults 200 micrograms/day and for pregnant women 250 micrograms/day), the thyroid gland tries to compensate by initially hypertrophic and later hyperplastic growth, which may be diffuse or nodular (Hehrmann et al. 1996). In successful compensation, the patient has normal thyroid function (euthyroid). Eventually, follicles may coalesce, forming macroscopic colloid cysts, where haemorrhage, calcification and scarring may occur. In rare cases, one single area of the gland is responsible for hormone production and may even produce excess hormone without responding to the lack of TSH stimulation (autonomous adenoma = hot nodule).

Enlargement of the thyroid gland commonly occurs in the pretracheal space. Further growth is then directed downwards into the anterior mediastinum, where the gland takes a retrosternal position anterior to the common carotid arteries and the internal jugular veins (Macdonald 2004c). There, it cannot be assessed anymore by ultrasound. It can be reached surgically via a cervical approach.
Posterior enlargement of the gland can be directed downwards into the posterior mediastinum (10%) (Fig. 14.14c). The thyroid then assumes a location behind the big vessels and is preferably reached via sternotomy. Cranial extension behind the hypopharynx occurs in 7.4% and is resected via a cervical approach (Fig. 14.13).

In iodine deficient areas, goitre is endemic (with moderate deficiency: 20%–30% prevalence) (Macdonald 2004a). Iodine prophylaxis of house animals raises the iodine contents of milk and dairy products and eggs (Lamberg 1986). More commonly, salt iodination is performed to reduce the goitre prevalence to about 5% (Lind et al. 2002).

The role of imaging is to assess displacement, narrowing and length of the stenotic segment of trachea, hypopharynx and oesophagus, and report retrosternal extent.

14.2.4.1.2 Thyroid Adenoma

These can either be true benign neoplasms of thyroid glandular epithelium with fibrous encapsulation or just focal adenomatous hyperplasia with incomplete capsule. Their size is usually below 4 cm and they are palpable, when over 1 cm (Glastonbury 2004a). In people aged over 60 years, nodules can be palpated with a prevalence of 5%–6%. In CT and MRI performed for other indications, incidental thyroid nodules are found in 14.5% of patients. Ultrasound and autopsy find nodules with an incidence of 50% in the same age group.

Although ultrasound features, such as hyperechogenicity, coarse calcifications, complete halo and regular margins have been associated with benign nodules, imaging findings are non-specific and cannot exclude thyroid cancer. Most suspicious are hypoechoic nodules, which do not accumulate tracer (cold nodules), because they have a 20% risk of malignancy.

Rapid enlargement can be alarming for the patient, but is usually due to haemorrhage.

Some clinicians have only palpable nodules biopsied, others take a diameter of 1 cm as a threshold and ultrasound may be used for guidance.

Clinical factors favouring malignancy are age below 20 or above 60 years, prior neck irradiation, family history of familial endocrine neoplasia (MEN 2A or B), a hard, immobile nodule or neck adenopathy.

14.2.4.1.3 Hashimoto's Thyroiditis (Chronic Lymphocytic Thyroiditis)

This autoimmune disorder occurs predominantly in women in the fourth and fifth decade with famil-

ial predisposition, rarely also in children (Loevner 2003; Glastonbury 2004b). Autoantibodies have been identified against thyroglobulin, thyroperoxidase and TSH receptors, leading to lymphocytic and plasma cell infiltration, follicular atrophy and fibrosis. In the acute phase, the gland may be enlarged and the patient hyperthyroid. Later on, the gland is atrophic and the function reduced. Imaging findings are non-specific, mostly patchy and inhomogeneous. Ultrasound follow-up is mandatory, because these patients have a 70–80 times increased risk of developing thyroid non-Hodgkin's lymphoma.

14.2.4.2 Malignant Neoplasms

14.2.4.2.1 Differentiated Thyroid Carcinoma

14.2.4.2.1.1 Papillary Carcinoma

It comprises 40%–60% of all malignant thyroid tumours and affects three times more women than men, especially in their third to fourth decade (Czerny et al. 2003). It is the most common endocrine tumour and represents 2% of all human cancers (Passler et al. 2003). Previous low-dose irradiation for cervical childhood haemangiomas, Hashimoto's thyroiditis and Graves' disease are seen to be predisposing factors.

Disease can be multifocal straight from the beginning in 20% of cases. This is seen by some authors as intraglandular lymphatic spread (Loevner 2003). If a papillary tumour has follicular components, it biologically behaves like a papillary tumour. An uncommon subtype is the columnar cell variant, which has a much more aggressive course with frequently extrathyroidal spread and vascular invasion at the time of manifestation (Zagar et al. 2003). In goitre deficient areas in the world, iodine prophylaxis has brought a decrease in the incidence of anaplastic carcinoma, but a slight increase in the incidence of papillary carcinoma (Passler et al. 2003).

Imaging studies may be normal, show a dominant nodule or multifocal nodules, but may also show a diffusely infiltrative tumour. In 30% of patients, psammoma bodies (= tiny calcifications) can be found. On imaging studies the lesions are indistinguishable from adenomas in the absence of extracapsular spread or lymphadenopathy. A total of 50% of patients have lymph node metastases; while their size may be within normal limits, they may be calcified, partly or completely cystic or haemorrhagic (Fig. 14.24). Unlike necrotic squamous cell lymph node metastases, their wall may be so thin that they can easily be mistaken for benign neck cysts. Not uncommonly they appear hyperintense on unenhanced T1-weighted images.

Haematogenous spread to lungs, bones, and central nervous system occur less commonly (5%), especially in the absence of nodal manifestations (Fig. 14.22b).

Although the pathological tumour node metastasis (pTNM) classification of the sixth edition (2002) of the Union Internationale Contre la Cancer (UICC)/American Joint Committee on Cancer (AJCC) recommends including all thyroid tumours of up to 20 mm as pT1, this does not appear to be justified for Passler et al. (2005). They showed that there was a statistically significant difference in survival between tumours smaller and bigger than 10 mm. In a follow-up period of 10 years, none of the patients with lesions smaller than 10 mm died as compared to nine patients with bigger tumours out of a series of 319 patients. Therefore, they recommend limited surgery (hemithyroidectomy) only in tumours smaller than 10 mm in the absence of multifocality; all other patients should undergo total thyroidectomy, central neck dissection (bilateral resection of lymphatic tissue along both recurrent laryngeal nerves in the paratracheal groove), and diagnostic lymph node dissection (removal of the central jugular lymph nodes). If positive lymph nodes are detected by intra-operative frozen section analysis, complete lateral dissection of the lymphatic tissue should follow with the aim of sparing the big vessels, all nerves and muscles. If metastases are fixed along the internal jugular vein,

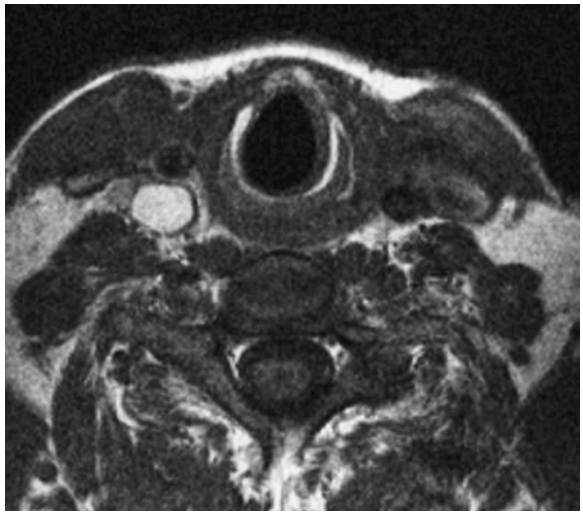

Fig. 14.24. Precontrast T1-weighted MR image: hyperintense lymph node metastasis in right lower jugular group (level IV) from papillary carcinoma

en bloc resection together with the vein, with preservation of the carotid artery and the vagal nerve, is performed (modified radical neck dissection).

All patients with positive lymph nodes are postoperatively treated with radioiodine ablation. Hormone substitution is given in differentiated cancer to reduce the TSH level, as TSH stimulates the growth of thyroid cells.

Annual follow-up includes clinical examination, biochemical measurements including thyroglobulin levels, ultrasound of the neck, and chest X-ray.

The 20-year survival rate reaches 90%–95%, but recurrences after decades do occur in less than 10% (Fig. 14.25).

Differentiated thyroid carcinomas in childhood and adolescence are rare and belong mainly to the papillary group. Despite frequent multifocality, extracapsular spread, lymph node involvement in up to 90% and distant metastases in up to 20% at the time of manifestation, a curative therapeutic approach is often still possible, because of their high differentiation (Meller et al. 1998).

It should be noted that small occult thyroid cancers are commonly found post mortem (Arem et al. 1999).

14.2.4.2.1.2
Follicular Carcinoma

This accounts for 15%–20% of thyroid malignancies and also affects women three times as often as men. It shows many similarities to papillary tumours, but is slightly more aggressive. The minimally invasive form has a 20-year survival of 95%, the highly invasive form of 53%. Tumour findings are also unspecific and the lesions are less often calcified. Haematogenous metastases and local recurrences are more common than lymph node metastases (Fig. 14.26). The latter occur only in around 8% (Loevner 2003). Tumours are also avid for iodine.

14.2.4.2.2
Medullary Thyroid Carcinoma

About 5%–10% of all thyroid malignant tumours originate from the parafollicular C-cells; 70%–80% of those occur sporadically, 20%–30% in familial form. The latter comprises multiple endocrine neoplasia type 2A and B (MEN 2A,B) and familial medullary thyroid cancer without multiple endocrine neoplasia. Male and females are affected equally. MEN 2A includes patients with medullary thyroid carcinoma in early adulthood, pheochromocytoma, and parathyroid hyperplasia or adenomas. Patients with MEN 2B suffer from medullary thyroid carcinoma in childhood, mucosal neuroma, often bilateral and malignant pheochromocytoma, occasionally cafe-au-lait spots, and possibly Gardner's syndrome (mucocutaneous pigmented nevi, intestinal polyps). Thyroidectomy is advised to be performed in childhood with frequent tumour marker evaluation.

Some patients without MEN have mutations, which make them prone to multiple paragangliomas, pheochromocytoma, and thyroid and kidney malignancies (Neumann et al. 2004) (Fig. 14.16).

Medullary cancers are solid with irregular margins and cannot be differentiated from other thyroid

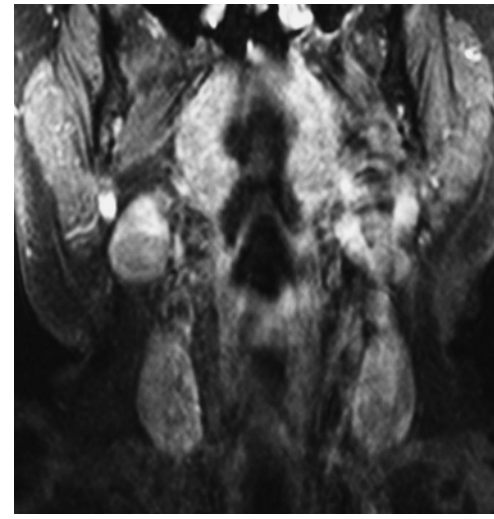

Fig. 14.25. Postcontrast coronal T1-weighted MR image shows irregularly enhancing lymph node metastasis in right upper jugular group (level II) 25 years after papillary carcinoma

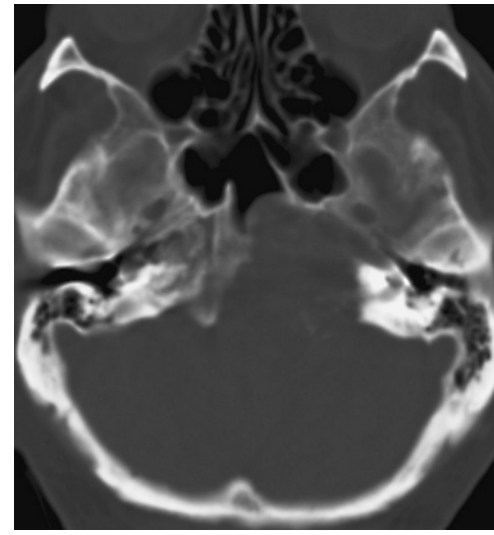

Fig. 14.26. CT: osteolytic skull base metastasis from follicular thyroid carcinoma

nodules, unless there is extrathyroidal involvement. They may be multifocal and can calcify in snowstorm appearance (Fig. 14.27). Lymph node metastases can occur at the time of manifestation of the primary tumour with a frequency as high as 80%, bilateral in 28%–49% and with involvement of the mediastinum in 36% of patients (Hamy et al. 2003; Szakáll et al. 2002). It is for this reason that initial bilateral neck dissection and removal of superior mediastinal nodes seems justified (Glastonbury 2004c).

Radical resection is the treatment goal, since palliative treatment options (external beam radiotherapy, radionuclide therapy, chemotherapy) have less value (Stift et al. 2004).

Medullary carcinoma secretes calcitonin (giving rise to diarrhea), opening the possibility of postoperative follow-up and screening for hitherto unaffected family members.

Until recently, it has been assumed that less than one third of patients suffers from bone metastases at the time of primary tumour diagnosis. Mirallié et al. (2005) reported in advanced medullary cancer suspected initial bone involvement by MRI in 94.2% and confirmed it in 74.3% with bone marrow biopsy. This has important clinical implications for patients receiving radioimmunotherapy with radiolabeled anti-carcinoembryonic antigen monoclonal antibodies. Haematological toxicity of internal radiotherapy (acute aplasia 4–6 weeks after injection of radioactivity or long-term myelodysplasia) is higher when the bone marrow is involved with tumour. Looking for bone metastases with pre-treatment (whole-body) MRI enables the patient to receive internal radiotherapy at a lower dose and avoid treatment side effects (Ghanem et al. 2005).

Medullary thyroid carcinoma also seems to be suited for dendritic cell based immunotherapy (Stift et al. 2004). Decreased tumour marker levels, clinical and radiological reduction in tumour size and stabilization of disease have been reported.

Medullary carcinoma does not concentrate iodine and can therefore safely be examined with iodine containing contrast agent. However, radionuclides specific for neuroendocrine tissue such as ^{131}I metaiodobenzylguanidine (MIBG) and the somatostatin analogue ^{111}In octreotide have been successfully used for primary tumour and metastatic disease (Loevner 2003). CT/^{111}In-octreotide SPECT digital fusion seems to improve visualization of tumour (Fiore et al. 2004). At present, ^{18}F-FDG PET has the highest reported sensitivity for delineation of occult medullary cancer (De Groot et al. 2004).

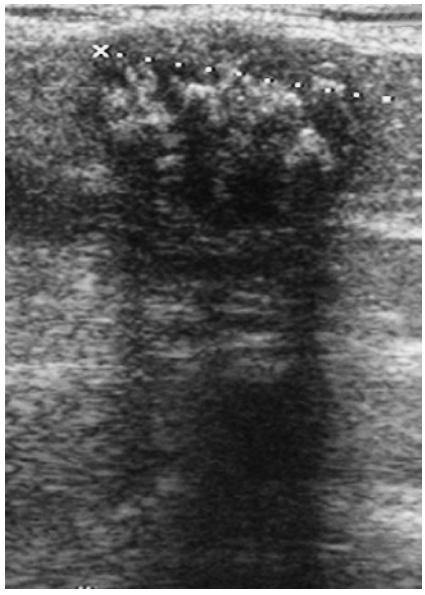

Fig. 14.27. Ultrasound: lymph node metastasis with numerous tiny calcifications from medullary carcinoma

14.2.4.2.3 Anaplastic Thyroid Carcinoma

Approximately 10% of all thyroid malignancies are anaplastic carcinomas and affect most often elderly women with a long-standing history of multinodular goitre (Macdonald 2004b). At presentation the lesion's diameter typically exceeds 5 cm. They range amongst the most malignant tumours. Due to their aggressive growth, life expectancy rarely exceeds several months from the time of diagnosis. Primary tumour and lymph node metastases (occurring in 40%) are heterogeneous with calcifications, haemorrhage and necrosis, both reflecting the underlying goitre and their dedifferentiated nature (Fig. 14.28). Patients suffer from compression and local invasion of the upper aerodigestive tract with vocal cord paralysis in 30% of cases (Fig. 14.29). About 50% of patients develop metastases in lungs, bones and brain. The tumour does not accumulate radioiodine or express thyroglobulin. Usually, only palliative treatment by radiotherapy, surgery and laser thermal ablation is possible (Loevner 2003; Pacella et al. 2004).

14.2.4.2.4 Thyroid Non-Hodgkin Lymphoma

Extranodal, extralymphatic lymphoma exclusively arising in the thyroid gland is rare. It comprises less

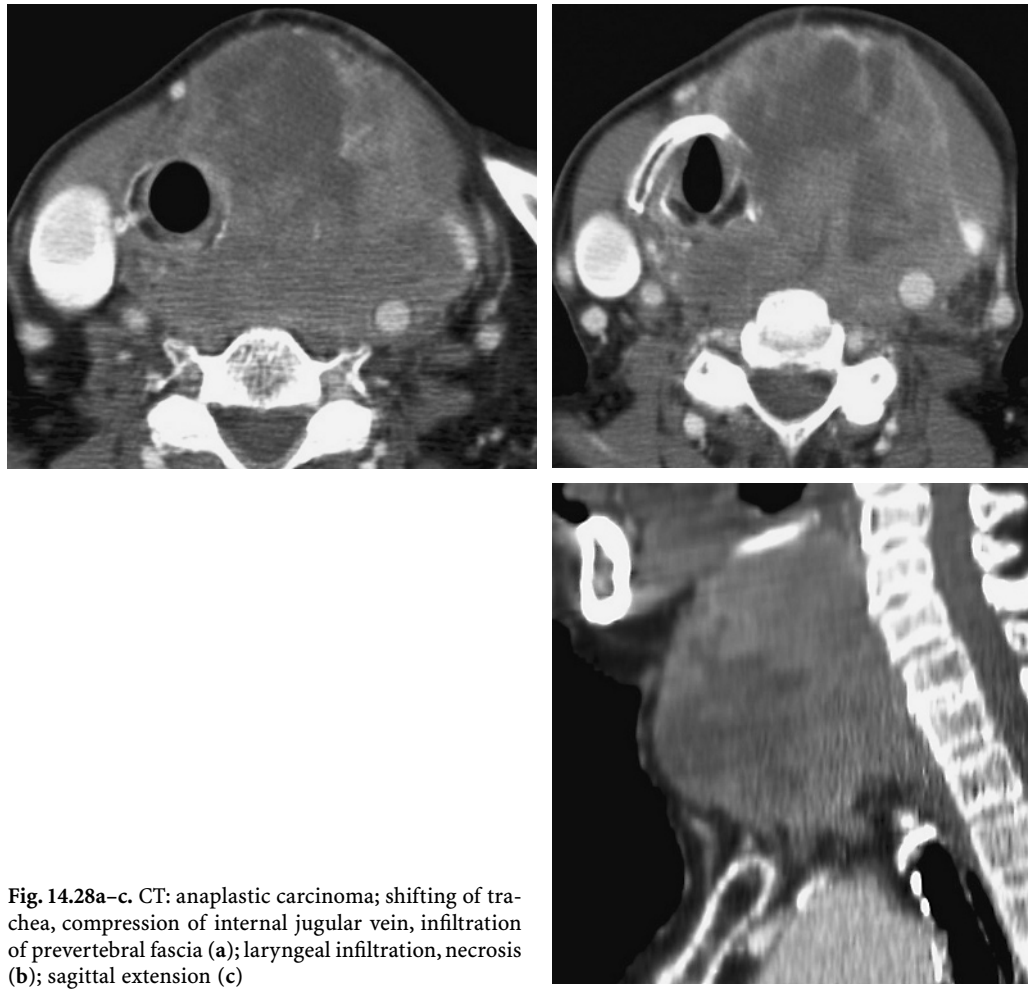

Fig. 14.28a–c. CT: anaplastic carcinoma; shifting of trachea, compression of internal jugular vein, infiltration of prevertebral fascia (**a**); laryngeal infiltration, necrosis (**b**); sagittal extension (**c**)

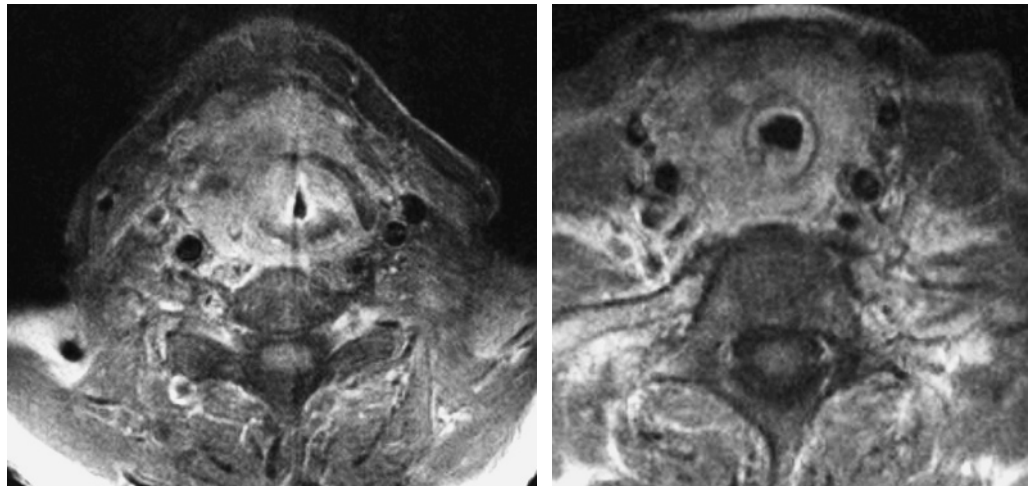

Fig. 14.29a,b. Postcontrast T1-weighted MR image: anaplastic carcinoma 35 years after irradiation of Hodgkin's lymphoma; laryngeal invasion at glottic level, with thyroid cartilage destruction (**a**); infiltration of tracheal wall and prevertebral fascia (**b**)

than 5% of all extranodal lymphomas and approximately 1%–3% of all thyroid malignancies. Elderly women with a long-standing history of goitre are most commonly affected. About 85% suffer from Hashimoto thyroiditis. Any rapid thyroid enlargement in a Hashimoto patient is suspicious of a lymphoma until proven otherwise. While a single mass occurs most commonly (80%), multiple nodules or diffuse infiltration are also possible. The lesion is typically homogeneously hypodense on CT, slightly hyperintense on T2-weighted MR images, and enhances very little with contrast agent. Necrosis or calcifications are atypical. When cervical lymph nodes are involved, they are usually multiple, bilateral and solid.

Tumours are usually poorly differentiated non-Hodgkin B-cell lymphoma, less commonly low grade malignant lymphoma of mucosa-associated lymphoid tissue (MALT). Thick needle biopsy might be needed to establish the diagnosis.

Lymphomas do not accumulate iodine and technetium, but are avid for gallium. 67Gallium scintigraphy is used to differentiate residual tumour from scar after radiochemotherapy. FDG-PET allows whole-body staging.

Patients with a thyroid lymphoma restricted to the gland itself have a 5-year survival rate of 85%. Lymph node involvement reduces it to 35%.

14.3 Parathyroid Gland

14.3.1 Embryology, Anatomy and Physiology

The inferior parathyroid glands arise together with the thymus from the third branchial pouch and eventually migrate downwards to stop at the dorsal inferior surface of the thyroid gland (Loevner 2003). If the traction of the thymus is strong, they may descend as far down into the mediastinum as the aortopulmonary window. An ectopic localisation in the anterior, posterior mediastinum, retrooesophageal or prevertebral space, or an intrathyroidal or intrathymic localisation are also possible; this occurs in 15%–20% of patients.

The superior parathyroid glands originate from the fourth branchial pouch, migrate downwards far less and have a more constant position more medial and posterior behind the upper pole of the thyroid.

Tissue fragmentation during migration results in accessory parathyroid glands, and this is found in up to 13% of cases at autopsy.

The parathyroid glands are typically found in pairs behind the upper and lower thyroid gland poles. Approximately 80% of people have four glands, but numbers between one and 12 have been reported (Loevner 2003).

The average parathyroid gland is smaller than 5 mm, weighs approximately 30–40 mg, and consists mainly of chief cells (Simeone et al. 1981).

The parathyroid glands drain into jugular, retropharyngeal and mediastinal lymph nodes (Rufener and Cohen 2003).

The parathyroid glands produce parathormone, which increases osteoclast activity, intestinal calcium absorption and reduces renal calcium excretion, thereby increasing blood calcium level.

Hypercalcaemia decreases parathormone level.

14.3.2 Pathology

14.3.2.1 Hyperparathyroidism

Hyperparathyroidism is the most common endocrine disorder, occurring in one out of 700 adults (Rubello et al. 2004; Loevner 2003). In primary hyperparathyroidism, the parathyroid glands do not respond to hypercalcaemia with a decrease of parathormone. This can be caused by parathyroid adenoma (single in 75%–85% or multiple in 2%–3%), parathyroid hyperplasia (10%–15%), parathyroid carcinoma (1%–5%) or rarely in paraneoplastic syndromes, in which adenosquamous carcinoma of the colon, hepatocellular carcinoma, squamous cell carcinoma of the head and neck or melanomas produce a parathormone related protein (Thompson et al. 2001; Loevner 2003). Laboratory findings are hypercalcaemia and hypophosphataemia. Patients suffer from characteristic peptic gastrointestinal ulcers, pancreatitis, renal calculi and bony changes. The latter consist of subchondral and subperiostal resorption with osteolytic destruction in more advanced stages, a sclerotic component in the spine ("rugger-jersey spine"), chondrocalcinosis and brown tumours (Figs. 14.30–14.32) (Youssefzadeh 2001a).

In long-standing disease with disturbances of phosphate metabolism or chronic hypocalcaemia, such as in chronic renal failure or malabsorption, the parathyroid glands try to compensate by hyperpla-

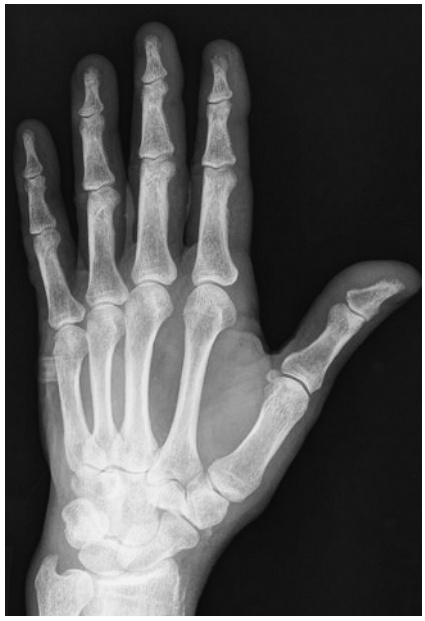

Fig. 14.30. X-ray of the left hand: subperiostal resorption on the radial side of the middle phalanx II and III, acroosteolysis (especially digits 1,2,4) in hyperparathyroidism

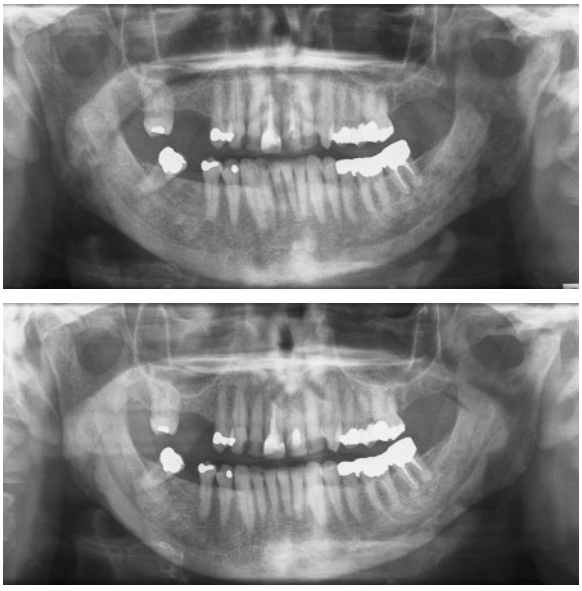

Fig. 14.31a,b. Panoramic radiography in hyperparathyroidism: loss of spongiosa, fibrous replacement, subchondral resorption, especially in left temporomandibular joint (**a**); severe progression within 1 year, collapse of left condyle (**b**)

sia, leading to secondary hyperparathyroidism with hypocalcaemia and hyperphosphataemia. Patients suffer from renal osteodystrophy, which is a combination of hyperparathyroid bony changes with an osteomalacic component, characterized by osteopenia, Looser zones and bowing deformities of the bones (Youssefzadeh 2001b).

Tertiary hyperparathyroidism develops, if an autonomous adenoma is superimposed on secondary hyperparathyroidism.

14.3.2.2 Patient Management in Hyperparathyroidism

Bilateral neck exploration is the standard procedure in primary hyperparathyroidism and many surgeons operate without preoperative localization, since none of the present examination modalities have satisfactory sensitivity and specificity for detecting pathological parathyroid glands (Prager et al. 1999; MacDonald 2003c; Loevner 2003). The thyroid lobes are mobilized and macroscopically altered parathyroid glands removed. If no enlarged gland is found, an extended cervical exploration with revision of thyme apex, paratracheal, paraoesophageal and paralaryngeal tissue, as well as the area around the carotid sheath, is carried out. Rarely, hemithyroidectomy has to be performed to exclude intrathyroidal

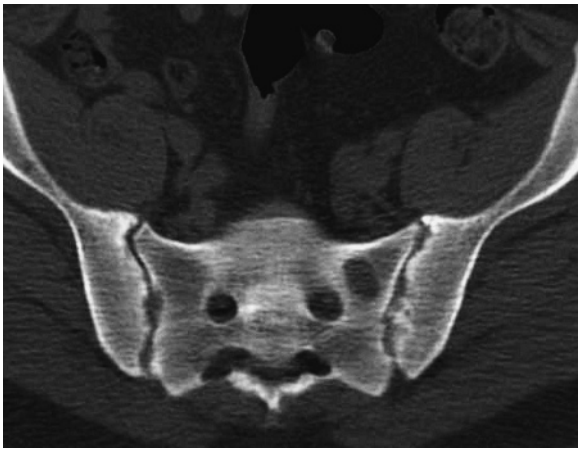

Fig. 14.32. CT, bone window: subchondral resorption in sacroiliac joints, brown tumour in left side of sacrum due to hyperparathyroidism, caused by parathyroid carcinoma

parathyroid adenoma. If there is a suspicion of an adenoma in mediastinal fatty tissue, transcervical thymectomy follows. Sternotomy for mediastinal exploration is only done after an attempt of radiological localization. If the tumour is adherent to surrounding tissue and a carcinoma cannot be excluded, en bloc resection including the ipsilateral thyroid gland is performed. Lymph nodes are handled as in thyroid carcinomas (see above).

Experienced surgeons have a success rate of 97% with less than 1% of patients with permanent hypoparathyroidism (Niederle et al. 2003).

Recently, minimally invasive procedures have been introduced in endocrine surgery and require precise radiological examination after biochemical testing. If scintigraphy and ultrasound favour single gland disease, a unilateral minimally invasive procedure can be performed to reduce surgical trauma and improve the cosmetic result. Patients with concomitant thyroid nodules, familial hyperparathyroidism, multiple endocrine neoplasia or history of previous neck irradiation are excluded.

Especially elderly patients or those with an increased anaesthesiological risk profit from minimally invasive radio-guided parathyroidectomy (Rubello et al. 2004).

The value of cross-sectional imaging techniques differs in the literature. For ultrasound, sensitivities of 50%–70% and specificities of 90%–95% for glands heavier than 1 g have been reported (Figs. 14.10, 14.11). Contrast-enhanced CT is considered to be slightly superior with sensitivity and specificity of 70% and 90%, respectively, but impedes scintigraphy with iodinated tracers for the next 6–8 weeks (Loevner 2003). The accuracy of MRI is more or less similar to that of CT (Roddie and Kreel 1997). Tc-99m Sesta-MIBI scintigraphy has the highest sensitivity and specificity (over 90%). When a combination of MIBI scintigraphy and ultrasound is used, a sensitivity of 98% can be reached in single gland disease (Prager et al. 2003). Ultrasound is also important to rule out concomitant thyroid nodules.

CT or MRI are usually only performed for persistent disease in the search for ectopic lesions.

Parathyroid angiography and venous sampling are only considered when non-invasive imaging modalities are not diagnostic (MacDonald 2004c).

References

Adams BK, Devi RT, Al-Haider ZY (2004) Tc-^{99m} Sestamibi localization of an ectopic mediastinal parathyroid tumour in a patient with primary hyperparathyroidism. Clin Nucl Med 29:149–152

Arem R, Padayatty SJ, Saliby AH, Sherman SI (1999) Thyroid microcarcinoma: prevalence, prognosis, and management. Endocr Pract 5:148–156

Baskin HJ (2004) New applications of thyroid and parathyroid ultrasound. Minerva Endocrinol 29:195–206

Bombardieri E, Seregni E, Villano C, Aliberti G, Mattavelli F (2003) Recombinant human thyrotropin (rhTSH) in the follow-up and treatment of patients with thyroid cancer. Tumori 89:533–536

Bombardieri E, Seregni E, Villano C, Chiti A, Bajetta E (2004) Position of nuclear medicine techniques in the diagnostic work-up of neuroendocrine tumours. Q J Nucl Med Mol Imaging 48:150–163

Czerny C, Hörmann M, Kurtaran A, Niederle B (2003) Imaging of diseases of the thyroid gland in Austria. Wien Klin Wochenschr 115:71–74

De Groot JW, Links TP, Jager PL, Kahraman T, Plukker JT (2004) Impact of ^{18}F-fluoro-2-deoxy-D-glucose positron emission tomography (FDG-PET) in patients with biochemical evidence of recurrent or residual medullary thyroid cancer. Ann Surg Oncol 11:786–794

de Rosario PW, Guimaraes V, Ribeiro Maia FF, Fagundes TA, Purisch S, Padrao EL, Rezende LL, Barroso AL (2005) Thyroglobulin before ablation and correlation with posttreatment scanning. Laryngoscope 115:264-267

Fiore D, Rubello D, Casara D, Pelizzo MR, Franchi A, Muzzio PC (2004) Role of CT/111 In-octreotide SPECT digital fusion imaging in the localization of loco-regional recurrence of medullary thyroid carcinoma. Minerva Chir 59:295–299

Fukunari N, Nagahama M, Sugino K, Mimura T, Ito K, Ito K (2004) Clinical evaluation of color Doppler imaging for the differential diagnosis of thyroid follicular lesions. World J Surg 28:1261–1265

Ghanem N, Uhl M, Brink I, Schafer O, Kelly T, Moser E, Langer M (2005) Diagnostic value of MRI in comparison to scintigraphy, PET. MS-CT and PET/CT for the detection of metastases of bone. Eur J Radiolog 55:41–55

Giammarile F, Houzard C, Bournaud C, Hafdi Z, Sassolas G, Borson-Chazot F (2004) Diagnostic management of suspected metastatic thyroid carcinoma: clinical value of octreotide scintigraphy in patients with negative high-dose radioiodine scans. Eur J Endocrinol 150:277–283

Ginsberg J, Young JEM, Walfish PG (1978) Parathyroid cysts-medical diagnosis and management. JAMA 240:1506–1507

Glastonbury CM (2004a) Thyroid adenoma. In: Harnsberger R (ed) Diagnostic imaging. Head and neck. Amirsys Inc., Salt Lake City, pp III-11–16

Glastonbury CM (2004b) Hashimoto thyroiditis. In: Harnsberger R (ed) Diagnostic imaging. Head and neck. Amirsys Inc., Salt Lake City, pp III-11-(4–7)

Glastonbury CM (2004c) Medullary thyroid carcinoma. In: Harnsberger R (ed) Diagnostic imaging. Head and neck. Amirsys Inc., Salt Lake City, pp III-11-(28–31)

Hamy A, Raffaitin P, Floch I, Paineau J, Mirallie E, Visset J (2003) The importance of lymph node dissection in medullary thyroid macrocarcinomas. Ann Chir 128:447–451

Harnsberger R (2004) Visceral space anatomy-Imaging Issues. In: Harnsberger R (ed) Diagnostic imaging. Head and neck. Amirsys Inc., Salt Lake City, pp III-11(2–3)

Hehrmann R, Klein D, Mayer D, Ploner O (1996) Risk of hyperthyroidism from X-ray contrast media. Akt Radiol 6:243–248

Heron DE, Andrade RS, Flickinger J, Johnson J, Agarwala SS, Wu A, Kalnicki S, Avril N (2004) Hybrid PET-CT simulation for radiation treatment planning in head-and-neck cancers: a brief technical report. Int J Radiation Oncology Biol Phys 60:1419–1424

Iannuccilli JD, Cronan JJ, Monchik JM (2004) Risk for malig-

nancy of thyroid nodules as assesses by sonographic criteria. J Ultrasound Med 23:1455–1464
Ishigaki S, Shimamoto K, Satake H, Sawaki A, Itoh S, Ikeda M, Ishigaki T, Imai T (2004) Multi-slice CT of thyroid nodules: comparison with ultrasonography. Radiation Medicine 22:346–353
Juweid ME, Hajjar G, Stein R, Sharkey RM, Herskovic T, Swayne LC, Suleiman S, Pereira M, Rubin AD, Goldenberg DM (2000) Initial experience with high-dose radioimmunotherapy of metastatic medullary thyroid cancer using ^{131}I-MN-14 F(ab)2 anticarcinoembryonic antigen MAb and AHSCR. J Nucl Med 41:93–103
Kainberger F, Kurtaran A, Kienast O, Dobrozemsky G, Czerny C, Kletter K (2003) Hybrid imaging for endocrine diseases: new perspectives. Wien Klin Wochenschr 115:87–90
Kim MK, Mandel SH, Baloch Z, Livolsi VA, Langer JE, Didonato L, Fish S, Weber RS (2004) Morbidity following central compartment reoperation for recurrent or persistent thyroid cancer. Arch Otolaryngol Head Neck Surg 130:1214–1216
Kreula J (1990a) Effect of sampling technique on specimen size in fine needle aspiration biopsy. Invest Radiol 25:1294–1299
Kreula J (1990b) Suction and cell yield in fine needle aspiration biopsy. J Interv Radiol 5:131–135
Kurzen FS, Flügel W, Brauer C-F, Schneider W, Adler D (1999) Metastasiertes dystopes papilläres Schilddrüsenkarzinom in einer medianen Halszyste. HNO 47:741–744
Lamberg BA (1986) Endemic goitre in Finland and changes during 30 years of iodine prophylaxis. Endocrinol Exp 20:35–47
Laurie AJ, Lyons SG, Lassen EC (1992) Contrast material iodides: potential effect on radioactive thyroid uptake. J Nucl Med 33:237–238
Lind P, Kumnig G, Heinisch M, Igerc I, Mikosch P, Gallowitsch HJ, Kresnik E, Gomez I, Unterweger O, Aigner H (2002) Iodine supplementation in Austria: methods and results. Thyroid 12:903–907
Loevner L (2003) Thyroid and parathyroid glands. In: Som PM, Curtin HD (eds) Head and neck imaging. Mosby, St. Louis, pp 2134–2172
Lombardi D, Nicolai P, Antonelli AR, Maroldi R, Farina D, Shaha AR (2003) Parapharyngeal lymph node metastasis: an unusual presentation of papillary thyroid carcinoma. Head Neck 26:190–193
Lorenzen J, Beese M, Mester J, Brumma K, Beyer W, Clausen M (1998) Chest X ray: routine indication in the follow-up of differentiated thyroid cancer? Nuklearmedizin 37:208–212
Lumachi F, Tregnaghi A, Zucchetta P, Marzola MC, Cecchin C, Marchesi P, Fallo F, Bui F (2004) Technetium-^{99m} sestamibi scintigraphy and helical CT together in patients with primary hyperparathyroidism: a prospective clinical study. Br J Radiol 77:100–103
Macdonald AJ (2004a) Multinodular goiter. In: Harnsberger R (ed) Diagnostic imaging. Head and neck. Amirsys Inc., Salt Lake City, pp III-11(8–11)
Macdonald AJ (2004b) Anaplastic carcinoma. In: Harnsberger R (ed) Diagnostic imaging. Head and neck. Amirsys Inc., Salt Lake City, pp III-11(32–35)
Macdonald AJ (2004c) Parathyroid adenoma. In: Harnsberger R (ed) Diagnostic imaging. Head and neck. Amirsys Inc., Salt Lake City, pp III-11(20–22)
Meller J, Conrad M, Behr T, Gratz S, Becker W (1998) Differentiated thyroid gland carcinoma in children and adolescents. Klin Padiatr 210:373–378
Menzel C, Zaplatnikow K, Diehl M, Dobert N, Hamscho N, Grunwald F (2004) The influence of thyroglobuline on functional imaging in differentiated thyroid cancer. Nucl Med Commun 25:239–243
Mirallié E, Vuillez JP, Bardet S, Frampas E, Dupas B, Ferrer L, Faivre-Chauvet A, Murat A, Charbonnel B, Barbet J, Goldenberg DM, Chatal JF, Kraeber-Bodere F (2005) High frequency of bone/bone marrow involvement in advanced medullary thyroid cancer. Clin Endocrinol Metab 90:779–788
Nahas Z, Goldenberg D, Fakhry C, Ewertz M, Zeiger M, Ladenson PW, Wahl R, Tufano RP (2005) The role of positron emission tomography/computed tomography in the management of recurrent papillary thyroid cancer. Laryngoscope 115:237–243
Nasir A, Chaudhry AZ, Gillespie J, Kaiser HE (2000) Papillary microcarcicoma of the thyroid: a clinico-pathologic and prognostic review. In Vivo 14:367–376
Neuhold N, Kaiser H, Kaserer K (2001) Latent Carcinoma of the thyroid in Austria: a systematic autopsy study. Endocr Pathol 12:23–32
Neumann HPH, Pawlu C, Peczkowska M, Bausch B, McWhinney SR, Muresan M, Buchta M, Franke G, Klisch J, Bley TA, Hoegerle S, Boedeker CC, Opocher G, Schipper J, Januszewicz A, Eng C (2004) Distinct clinical features of paraganglioma syndromes associated with SDHB and SDHD gene mutations. JAMA 292:943–951
Niederle B, Prager G, Kaczirek K, Scheuba C, Passler C, Asari R (2003) Minimally invasive endocrine surgery: aspects of diagnostic imaging. Wien Klin Wochenschr 115:10–18
Pacella CM, Bizzarri G, Spiezia S, Bianchini A, Guglielmi R, Crescenzi A, Pacella S, Toscano V, Papini E (2004) Thyroid tissue: US-guided percutaneous Laser thermal ablation. Radiology 232:272–280
Passler C, Prager G, Scheuba C, Asari R, Kaserer K, Zettnig G, Niederle B (2003) Application of staging systems for differentiated thyroid carcinoma in an endemic goiter region with iodine substitution. Ann Surg 237:227–234
Passler C, Scheuba C, Asari R, Kaczirek K, Kaserer K, Niederle B (2005) Importance of tumour size in papillary and follicular thyroid cancer. Br J Surgery 92:184–189
Polga JP, Balikian JP (1971) Partially calcified functioning parathyroid adenoma. Case demonstrated roentgenographically. Radiology 99:55–56
Prager G, Czerny C, Kurtaran A, Passler C, Scheuba C, Niederle B (1999) The value of preoperative localization studies in primary hyperparathyroidism. Chirurg 70:1082–1088
Prager G, Czerny C, Ofkuoglu S, Kurtaran A, Passler C, Kaczirek K, Scheuba C, Niederle B (2003) Impact of localization studies on feasibility of minimally invasive parathyroidectomy in an endemic goiter region. J Am Coll Surg 196:541–548
Quinn S, Nelson H, Demlow T (1994) Thyroid biopsies: fine needle aspiration biopsy versus spring activated core biopsy needle in 102 patients. J Vasc Interv Radiol 5:619–623
Randel SB, Gooding GAW, Clark OH, Stein RM, Winkler B (1987) Parathyroid variants: US evaluation. Radiology 165:191–194
Roddie ME, Kreel L (1997) Endocrine disease. In: Grainger RG, Allison D (eds) Diagnostic radiology. Churchill Livingstone, New York, pp 1302–1323
Rubello D, Casara D, Giannini S, Piotto A, Carbonare LD, Pagetta C, Boni G, Mariani G, Pier C, Pelizzo MR (2004) Minimally

invasive radioguided parathyroidectomy: an attractive therapeutic option for elderly patients with primary hyperparathyroidism. Nucl Med Commun 25:901–908

Ruf J, Lehmkuhl L, Bertram H, Sandrock D, Amthauer H, Humplik B, Ludwig Munz D, Felix R (2004) Impact of SPECT and integrated low-dose CT after radioiodine therapy on the management of patients with thyroid carcinoma. Nucl Med Commun 25:1177–1182

Rufener JB, Cohen JI (2003) Metachronous spread of parathyroid carcinoma to a retropharyngeal lymph node. Head Neck 25:968–971

Ruiz Franco-Baux JV, Borrego Dorado I, Gomez Camarero P, Rodriguez JR, Vazquez Albertino RJ, Navarro Gonzalez E, Astorga Jimenez R (2005) F-18-fluordeoxyglucose positron emission tomography on patients with differentiated thyroid cancer who present elevated human serum thyroglobulin levels and negative I-131 whole body scan. Rev Esp Med Nucl 24:5–13 (Spanish)

Schlumberger M, Pacini F, Wiersinga WM, Toft A, Smit JWA, Franco FS, Lind P, Limbert E, Jarzab B, Jamar F, Duntas L, Cohen O, Berg G (2004) Follow-up and management of differentiated thyroid carcinoma: a European perspective in clinical practice. Eur J Endocrinol 151:539–548

Screaton N, Berman L, Grant W (2003) US-guided core-needle biopsy of the thyroid gland. Radiology 226:827–832

Simeone JF, Mueller PR, Ferrucci JT, vanSonnenberg E, Wang C-A, Hall DA, Wittenberg J (1981) High-Resolution real-time sonography of the parathyroid. Radiology 141:745–751

Stift A, Sachet M, Yagubian R, Bittermann C, Dubsky P, Brostjan C, Pfragner R, Niederle B, Jakesz R, Gnant M, Friedl J (2004) Dendritic cell vaccination in medullary thyroid carcinoma. Clinical Cancer Research 10:2944–2953

Szakáll S, Ésik O, Bajzik G, Repa I, Dabasi G, Sinkovics I, Ágoston P, Trón L (2002) ^{18}F-FDG PET detection of lymph node metastases in medullary thyroid carcinoma. J Nucl Med 43:66–71

Thompson JT, Paschold EH, Levine EA (2001) Paraneoplastic hypercalcaemia in a patient with adenosquamous cancer of the colon. Am Surg 67:585–588

Warter J, Sibilly A, Hertz S, Geisler F, Jeanmaire H (1975) Primary hyperparathyroidism. Round calcification as a sign of cervico-mediastinal localization of a parathyroid adenoma. Ann Med Interne 126:429–435

Yamamoto Y, Nishiyama Y, Monden T, Matsumara Y, Satoh K, Ohkawa M (2003) Clinical usefulness of fusion of ^{131}I Spect and CT images in patients with differentiated thyroid carcinoma. J Nucl Med 44:1905–1910

Youssefzadeh S (2001a) Hyperparathyroidism. In: Bohndorf K, Imhof H, Pope TL (eds) Musculoskeletal imaging. Thieme, Stuttgart, pp 244–247

Youssefzadeh S (2001b) Renal osteodystrophy. In: Bohndorf K, Imhof H, Pope TL (eds) Musculoskeletal imaging. Thieme, Stuttgart, pp 248–249

Zagar I, Vidergar-Kralj B, Schwarzbartl-Pevec AA, Pompe F (2003) Columnar cell thyroid carcinoma-diagnostic dilemmas and pitfalls. Nucl Med Rev Cent East Eur 6:155–158

15 Neck Nodal Disease

Jonas A. Castelijns and M. W. M. van den Brekel

CONTENTS

15.1 Introduction

In the assessment of cervical lymph nodes imaging plays a major role. It is used mainly for N staging in known malignancies, but can also play a role in differential diagnosis of lymphadenopathy. Imaging plays an increasing role in evaluating the degree of extension and spread of the disease in the neck to serve as a prognosticator and determine optimal treatment. Most metastases originate from carcinomas of the mucous membranes, skin, thyroid and salivary glands, and in these cases, apart from staging the neck, the primary tumor is optimally assessed by the imaging modality as well.

J. A. Castelijns, MD, PhD
Professor, VU University Medical Center, Department of Radiology, De Boelelaan 1117, 1081 HV Amsterdam, The Netherlands
M. W. M. van den Brekel, MD, PhD
Department of Otolaryngology – Head & Neck Surgery, The Netherlands Cancer Institute, Antoni van Leeuwenhoek Hospital, Plesmanlaan 121, 1066 CX Amsterdam, The Netherlands

Lymphatic metastasis is the most important mechanism in the spread of most head and neck carcinomas. The rate of metastasis probably reflects the aggressiveness of the primary tumor and, except for thyroid cancer in young patients, is an important prognosticator for head and neck carcinoma. Not only presence, but also number of nodal metastases, the level in the neck, the size of the nodes and presence of extranodal spread are important prognostic features. In most institutions throughout the world, the neck is staged mainly by palpation. Although palpation has the advantage of being both easy and inexpensive to perform and repeat, it is generally accepted to be inaccurate. Both the sensitivity and specificity are in the range of 60%–70% depending on the tumor site studied. The risk of palpably occult metastases is to a large extent dependent on the size and site and other characteristics of the primary tumor (Martinez Gimeno et al. 1995). Because of the risk of occult metastasis, it is common practice to treat the neck electively. The "acceptable" risk to perform elective treatment is hard to define. In a meta-analysis, a risk of occult metastases higher than 20% was calculated to be optimal for deciding to perform an elective treatment (Weiss et al. 1994).

This chapter on imaging of neck node metastases reviews neck anatomy and the patterns of lymphatic tumor spread. Radiological features of lymph node involvement caused by infectious disease and metastases are discussed. The focus will be on CT, US, US-guided fine-needle aspiration (FNAC) cytology and MRI. Lymphomas will be discussed in Chap. 16, and PET will be discussed in Chap. 17.

15.2 Neck Anatomy and Patterns of Metastasis

Of the estimated 800 lymph nodes in the human body, 300 lymph nodes are situated in the neck. In the recent past the regional categorization of lymph

nodes as described by Rouvière (1932) was the most widely used for lymphadenopathy.

Presently, most clinicians use the recently revised classification into seven levels as recently changed and adapted by the American Academy of Otolaryngology (Fig. 15.1) (Robbins et al. 2002). One of the major reasons for adapting the classification was that the majority of patients with head and neck malignancies presently undergo sectional imaging prior to treatment.

Som et al. (2000) integrated anatomical imaging criteria with the clinically used classification. According to this classification, level 1A includes all submental nodes that are between the medial margins of the anterior bellies of the digastric muscles below the mylohyoid muscle. Level 1B are the submandibular nodes. These are above the hyoid bone, below the mylohyoid muscle, in front of the posterior belly of the digastric muscles and around the submandibular glands.

Level 2 includes the upper internal jugular nodes. This level extends from the skull base to the level of the bottom of the body of the hyoid bone. Lymph nodes in this level are posterior to the back of the submandibular gland and anterior to the back of the sternocleidomastoid muscle. Level 2 nodes can be subclassified into levels 2A and 2B. Level 2A nodes are situated around the internal jugular vein; level 2B nodes are posterior to the internal jugular vein, separated from the vein by a fat plane. Nodes medial to the internal carotid artery are called retropharyngeal lymph nodes.

Level 3 nodes include the mid-jugular nodes. They extend from the level of the bottom of the hyoid bone to the level of the bottom of the cricoid cartilage. They lie anterior to the back of the sternocleidomastoid muscle. They are also lateral to the carotid arteries.

Level 4 nodes include the low-jugular nodes. They extend from the level of the bottom of the cricoid bone to the level of the clavicle. They lie anterior to a line connecting the back of the sternocleidomastoid muscle and the posterolateral margin of the anterior scalene muscle. They are also lateral to the carotid arteries.

Level 5 nodes are nodes in the posterior triangle. They are posterior to the back of the sternocleidomastoid muscle from the skull base to the clavicle. Level 5 is also divided into level 5A and 5B. Level 5A extends inferiorly toward the bottom of the cricoid bone whereas 5B extends from the bottom of the cricoid cartilage to the clavicle. They also are anterior to the anterior edge of the trapezius muscle.

Level 6 includes the visceral nodes which are inferior to the lower body of the hyoid bone, superior to the top of the manubrium sterni, and between the left and right common carotid arteries or the internal carotid arteries.

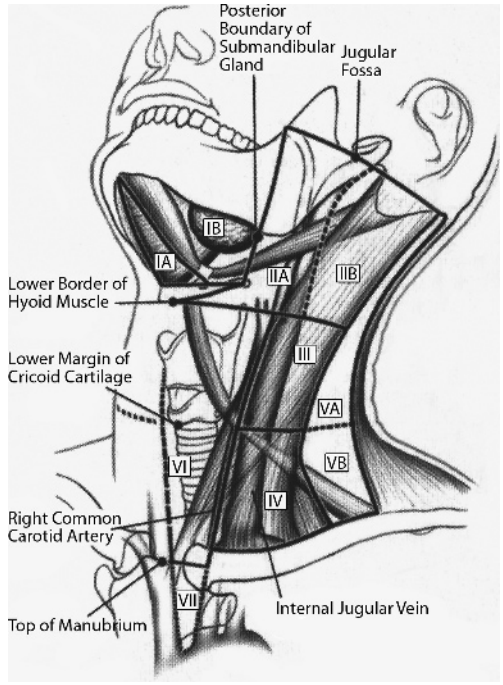

Fig. 15.1. Diagram of the neck as seen from the left anterior view. This figure gives an outline of the levels of the classification. Note that the line of separation between levels I and II is the posterior margin of the submandibular gland. The separation between levels II and III and level V is the posterior edge of the sternocleidomastoid muscle. However, the line of separation between levels IV and V is an oblique line extending from the posterior edge of the sternocleidomastoid muscle to the posterior edge of the anterior scalene muscle. The posterior edge of the internal jugular vein separates level IIA and IIB nodes. The top of the manubrium separates levels VI and VII. [From Som PM et al. (1999), with permission]

Level 7 nodes are superior mediastinal nodes. They are between the carotid arteries below the level of the top of the manubrium and above the level of the innominate vein. For consistency with the prior classifications, the following nodal groups, as well as the other superficial nodes, are referred to by their anatomical names, e.g., retropharyngeal, parotid, facial, occipital, and postauricular.

Most tumors originating from the mucosal lining of the upper aerodigestive tract have a well-defined and more predictable pattern of metastasis to the neck than melanomas (Shah 1990; Byers et al. 1997; King et al. 2000; Pathak et al. 2001; de Wilt et al. 2004; Ross et al. 2004). Although skip metastases do occur, the incidence is low (around 5%).

Knowledge of these patterns of metastases is important for radiologists, as the search for metastases

on axial scans is made easier. Furthermore, it is essential if US-guided aspiration is used to aspirate from the most suspicious (sentinel) lymph node (van den Brekel et al. 1998a; Nieuwenhuis et al. 2000). Level 1 is the drainage region for anterior oral carcinomas, lip, facial and sinonasal carcinomas. Lymph node metastases are mostly localized in front and lateral to the submandibular gland, and never inside it. Level 2 is the most frequently involved level of the neck. Most tumors originating from the (oro)pharynx, posterior oral cavity, supraglottic larynx, and parotid gland metastasize primarily to this level; however, frequently even anterior oral cavity carcinomas as well as glottic, naso- and hypopharyngeal carcinomas, metastasize to this level. Lymph nodes in level 3 are the first echelon for glottic, subglottic and hypopharyngeal carcinomas. Level 4 is very rarely the only involved level in head and neck primaries. In case of lymph node metastases at this level, the primary tumor can be localized subglottically, in the thyroid gland, or in the proximal oesophagus. Occasionally, anterior tongue, mid-, or lower-esophageal carcinomas, breast, lung, or gastric carcinomas present initially with level 4 metastases. Level 5 is only rarely involved in non-advanced head and neck cancer patients. Only in nasopharyngeal carcinomas and skin carcinomas of the neck or occipital skull is this level frequently involved. Paratracheal metastases are often the first metastases in thyroid and subglottic cancer, but also occur in hypopharyngeal and esophageal cancers (King et al. 2000; Morrissey et al. 2000; Plaat et al. 2005).

Skin carcinomas and melanoma have a less predictable pattern of metastasis but often metastasize to superficial lymph nodes, i.e., nuchal, peri-auricular, parotid, occipital, facial, superficial cervical, and posterior triangle (level 5) lymph nodes (van den Brekel et al. 1998b; Pathak et al. 2001; Wagner et al. 2000).

15.3 Benign Lymphadenopathy in the Neck

Reactively enlarged lymph nodes are very common and are most often caused by viral or bacterial infections. The history, serology, cytology, and bacterial examination, together with intracutaneous testing (e.g., mycobacteria), can in general establish the diagnosis. At least in some cases imaging can be important in guiding the differential diagnosis. A single mass with irregular peripheral enhancement is most often caused by a lymph node abscess, an atypical mycobacterial infection, or cat scratch disease. In suppurative bacterial lymphadenitis, contrast-enhanced CT can be of value in assessing whether abscess formation has occurred, which necessitates drainage (Lazor et al. 1994). In case of single or multiple nodal enlargements with homogeneous enhancement on both CT and MR imaging, Castleman's disease should be in the differential diagnosis (Yamashita et al. 1993). Multiple conglomerates of lymph nodes with and without central hypodensity and irregular enhancement can be caused by tuberculosis (Robson 2000; Moon et al. 1997). Ultrasound can also be helpful in differentiating different kinds of nodal enlargements (Ahuja and Ying 2002).

Bilateral diffuse lymph node enlargement without necrosis is frequently caused by viral infections, such as mononucleosis, herpes, cytomegalovirus, rubella, or seldom HIV. The HIV infections can also be present with cystic lesions in the parotid glands or associated malignancies. Infections, such as toxoplasmosis, are rarely the cause of diffuse nodal enlargement, whereas in some patients no diagnosis can be made. Sarcoidosis is also a rare cause of multiple cervical nodal enlargement. In these cases the salivary glands can be swollen as well and radiographs of the thorax may reveal mediastinal lymph node enlargement.

Differential diagnosis between lymphadenopathy and other swellings of the neck can often be facilitated by CT, MR imaging, or US. Clinically, carotid body paragangliomas can mimic lymphadenopathy. Imaging is helpful in these cases by showing the vascular nature and exact location of the lesion; however, flow voids may be absent if the glomus tumor is small (Rao et al. 1999). Median (thyroglossal) or lateral (brachial) cervical cysts have a typical low-density center and sometimes rim enhancement appearance on enhanced CT. T2-weighted MR imaging shows the typical cystic appearance. It should be realized that squamous cell metastases can rarely present as cystic lesions as well. Apart from the use in differential diagnosis, the assessment of the exact localization and extent of a lesion can be of value if surgical treatment is considered. In tumors, cysts, and infections, imaging can help in assessing infiltration in surrounding tissue and in assessing the relation with vital structures such as the carotid artery, the prevertebral fascia, the skull base, or the brachial plexus.

15.4 Metastatic Lymphadenopathy

Metastases to lymph nodes in the neck originate most frequently from squamous cell carcinomas of the mu-

cosal lining of the upper aerodigestive tract. Tumor metastases more seldom originate from the salivary gland, thyroid gland, or skin neoplasms.

15.4.1 Thyroid Carcinoma

Neck node metastases from well-differentiated thyroid carcinomas occur frequently and are often clinically occult. In some studies, the rate of occult metastases from papillary thyroid carcinoma is as high as 60%–80% (Frazell and Foote 1955; Ahuja et al. 1991; Balazs et al. 1998; Mirallie et al. 1999; Chow et al. 2002), whereas follicular carcinomas less frequently develop lymph node metastases. The most important echelons are the level 4 and 6 lymph nodes. There is little literature available on the accuracy of imaging in the detection of paratracheal metastases. Because radioactive iodine can cure small metastases after thyroidectomy, imaging has relatively few implications in papillary carcinomas without palpable neck nodes. However, to detect metastases early, US with guided FNAC is the most reliable technique, that is routinely used for follow-up (Amar et al. 1999; Frasoldati et al. 2003; Kouvaraki et al. 2003).On CT or MR imaging every depicted and slightly enlarged node is suspicious, and sometimes discrete calcifications are seen on CT. As no iodine contrast agents should be used, CT is less useful than US with guided FNAC. Hypo- or hyperintensity may reflect cyst formation or haemorrhage on MRI. On T2-weighted MR imaging, signal intensity of lymph nodes is high.

In medullary carcinomas, the rate of metastases to the neck is high as well. Regional lymph nodes metastases are present in over 75% of cases at the time of diagnosis (Moley and DeBenedetti 1999; Scollo et al. 2003). Because of the prognostic significance, in medullary carcinomas elective neck dissection is often recommended but still controversial and imaging can play a pivotal role in decision making. As imaging of the paratracheal nodes is not very reliable, a routine paratracheal dissection is recommended.

15.4.2 Salivary Gland Carcinomas

The great majority of salivary gland carcinomas occur in the parotid glands, followed by the submandibular glands, and mucosal salivary glands in the head and neck (see Chap. 12). According to the 1991 WHO classification system, 19 subtypes of salivary gland carcinomas exist. The most frequent histologies are mucoepidermoid cancer, adenoid cystic cancer, adenocarcinoma, acinic cell carcinoma and carcinoma ex pleiomorphic adenoma. Lymph node metastases are an important prognostic factor in salivary gland cancer (Vander Poorten et al. 1999; Vander Poorten et al. 2000; Terhaard et al. 2004). The incidence of lymph node metastases from salivary gland cancer is dependent on the size of the primary tumor and the histologic subtype. Overall, some 20% of all parotid carcinomas are pN+, whereas lymph node metastases are rare in low grade acinic cell carcinomas and relatively common in high grade mucoepidermoid cancer (Vander Poorten et al. 1999). However, in a recent study from Stennert et al. (2003), the reported incidence of (occult) metastases was much higher. If neck node metastases are present, a modified radical neck dissection is in general advocated. Because the incidence of neck node metastases is in general reported to be below 20%, elective neck dissection is controversial (Armstrong et al. 1992; Korkmaz et al. 2002; Stennert et al. 2003). A common policy is to perform frozen section of the first echelon nodes in level 2. If these are positive, the parotidectomy will be followed by a neck dissection. However, this policy has the disadvantage that surgery time is difficult to plan. Therefore, preoperative assessment of the neck, using either MRI or US-FNAC is a logical approach (McIvor et al. 1994). There is a tendency to treat the primary with surgery and postoperative radiotherapy and the neck with elective radiotherapy if staged N0 preoperatively and at frozen section of level 2 nodes.

15.4.3 Skin Neoplasms

Metastatic patterns from skin carcinomas and melanomas differ and are more variable than metastases from mucosal carcinomas.

Whereas basal cell carcinomas very rarely give rise to neck metastases, squamous cell carcinomas, especially when infiltrating deeply, do so in up to 2%–15% of cases (Tavin and Persky 1996; O'Brien et al. 2001). The parotid gland is a major nodal echelon for all tumors anterior to a vertical plane cranial to the ear. Tumors behind this line mainly spread to the posterior neck nodes and occipital nodes.

Melanomas give rise to lymph node metastases more often, although the patterns of metastases are less predictable (de Wilt et al. 2004). The incidence

of lymph node metastases is in the range of 20% for intermediate thickness melanomas. Because of that, the sentinel node procedure has gained widespread acceptance although it has not been clarified whether early detection of lymph node metastases (and early treatment) has prognostic importance in skin melanoma. For the head and neck area, the accuracy of the sentinel node procedure is less than for other parts of the body, and in up to 10% of the patients, the sentinel node cannot be identified or renders false negative results (Jansen et al. 2000; Maffioli et al. 2000; Stadelmann et al. 2004). To assess the neck non-invasively, several authors have shown that US and US-FNAC is the modality of first choice, more reliable than palpation or CT (Tregnaghi et al. 1997; van den Brekel et al. 1998b; Rossi et al. 2000; Blum et al. 2000; Voit et al. 2000; Ross et al. 2004). Because of that, US-FNAC can be used to select patients for a sentinel node procedure (negative US-FNAC) or during follow-up.

15.4.4 Mucosal Squamous Cell Carcinoma

With the use of imaging techniques, such as CT, MRI, and US, better accuracy than with palpation can be achieved. The accuracy of imaging techniques for the neck is to a far extent determined by the employed diagnostic criteria (Som 1992; van den Brekel et al. 1990b). In general, none of the currently available imaging techniques are able to depict small tumor deposits inside lymph nodes. As the incidence of exclusively micrometastases in clinically N0 necks with occult metastases is 25%, no imaging technique can ever reach a sensitivity over 75% without losing a high specificity (van den Brekel et al. 1996).

The characteristics of metastatic lymph nodes that can be depicted are increased size, a rounder shape, and presence of non-contrast-enhancing parts or irregular contrast enhancement, caused by tumor necrosis, tumor keratinization, or cystic areas inside the tumor.

Nodal shape is used by several authors (van den Brekel et al. 1990b). In general, a round shape is considered more suspicious than an oval or flat shape (Steinkamp et al. 1994a). In reactive nodes, the ratio of the longest diameter over the shortest diameter is 2 or higher in 86% of cases (Bruneton et al. 1994). Grouping of lymph nodes is used as a criterion by several authors as well. Whereas necrosis is a very reliable criterion for lymph node metastases, it is unfortunately quite rare or not often visible in small lymph nodes. Yousem et al. (1992) and Curtin et al. (1998) found that CT is more sensitive and accurate than MRI in depicting nodal necrosis. Contrast-enhanced MRI is certainly more sensitive in detecting necrosis than unenhanced MRI (van den Brekel et al. 1990a; Chong et al. 1996).

Because irregular contrast enhancement is often not present in small lymph node metastasis, as present in palpably N0 sides of the neck, the size (and shape) of lymph nodes plays an important role in assessing their nature (Umeda et al. 1998). However, size, shape, and grouping criteria are not very accurate for the clinically N0 neck. As the size of lymph nodes varies according to the level in the neck and because small metastatic deposits inside lymph do not always cause enlargement of a lymph node, it is very difficult to define the optimal size criteria (van den Brekel et al. 1998c). The size criteria in the literature may vary between 5 and 30 mm (van den Brekel et al. 1990b; Som 1992; Vassallo et al. 1992; Friedman et al. 1993; Bruneton et al. 1994; Hudgins 1994; Steinkamp et al. 1994a). Several studies have tried to calculate criteria by evaluating nodal size and the histopathological outcome in neck dissection specimens (FRIEDMAN et al. 1990; van den Brekel et al. 1990b; Don et al. 1995; Curtin et al. 1998). Friedman et al. (1990) studied the maximal axial diameter and found a cut-off point of 1 cm. By comparing three lymph node diameters we previously found that the minimal axial diameter is a better criterion than the more widely used maximal axial diameter or the longitudinal diameter (van den Brekel et al. 1990b). Don et al. (1995) found that 68 of 102 (67%) metastatic nodes had a longitudinal diameter smaller than 1 cm, whereas in our study this was 48 of 144 (33%). For the minimal axial diameter we even found that 102 of 144 (71%) were smaller than 1 cm. As a consequence, the current size criterion of 1 cm or larger misinterprets the majority of all metastases.

Although the most important question for the clinician concerns the clinically negative neck, radiologists currently base the criteria on studies encompassing all head and neck cancer patients. In a previous US study, the sensitivity and specificity of different size criteria for different levels in the neck in patients with positive and negative clinical findings was compared (van den Brekel et al. 1998a). In this study we concluded that size criteria of 1 cm have a low sensitivity in the palpably N0 neck and that it is justified to use different criteria for different levels of the neck. In the palpably N0 neck, for level 2 a criterion of 7 mm for the minimal diameter renders the best compromise, whereas for the rest of the

neck, lymph nodes with a minimal diameter of 6 mm should be considered suspicious. In another study, it was shown that using a surface area of 45 mm^2 correlated better with histopathology than using a minimal or maximal axial diameter (Umeda et al. 1998). Morphological criteria, such as focal cortical widening or depiction of small tumor areas inside a lymph node, will become more important as the contrast and spatial resolution of imaging techniques increases (Vassallo et al. 1992). Using newer contrast agents in MRI or power duplex Doppler has revealed new radiological criteria (Bellin et al. 1998; Di Martino et al. 2000; Moritz et al. 2000; Fischbein et al. 2003). Thus far, however, these are not shown to be reliable in lymph nodes measuring less than 1 cm. As morphologic criteria are unreliable in small lymph nodes, it is our opinion that lymph nodes should be aspirated to obtain cells for cytological assessment if management consequences are attached to these radiological findings.

15.5 Imaging Techniques

15.5.1 CT and MR Imaging

Using spiral CT, axial images are obtained from skull base to clavicle. Intravenous contrast as an initial bolus followed by a drip infusion is necessary to obtain enough contrast. Slice thickness should preferably be 3 mm without an interslice gap to obtain a high resolution and depict small nodes with central necrosis.

Our protocol for MRI of the extracranial head and neck uses a neck coil for the neck area. Firstly, a sagittal T1-weighted localizer scan is obtained. At least one pre-contrast examination of T1-weighted images is obtained in the axial plane from skull base to clavicle. The MR images are obtained with 7-mm slice thickness and 1.4-mm interslice gap. T1-weighted images offer the best anatomical resolution because of the high signal-to-noise ratio per unit time and their relative freedom from motion artifacts. Additionally, for most primary tumors axial T2-weighted images and sometimes sagittal or coronal T2-weighted examinations are performed. Vessels are more easily differentiated from lymph nodes on T2-weighted spin-echo images. Depending on the primary tumor, other techniques might be necessary. We find short TI inversion recovery sequences very helpful in detecting even small lymph nodes (Fig. 15.2a,b). Gadolinium-DTPA with or without fat-suppressed MR imaging techniques are necessary to reliably depict tumor necrosis inside lymph nodes and is often helpful in delineating the primary tumor as well. T2-weighted MR images may also be helpful demonstrate central necrosis (Fig. 15.3a,b). Resolution of detailed head and neck region requires thin sections. The image slice thickness should be 3–5 mm, with an interslice gap of 1–2 mm, on a 192×256 matrix. The field of view should be kept as small as possible.

For the depiction and characterization of neck nodes there are proponents for CT as well as for MRI. Most studies that have compared the accuracy of CT to MRI for the assessment of the neck have found no significant difference between these two modalities (Hillsamer et al. 1990; Lenz et al. 1993; van den Brekel et al. 1993; Friedman et al. 1993; Curtin et al. 1998). In general, the technique employed for imaging of the primary tumor is used to stage the neck as well. In patients who are dyspnoeic or cannot lie still, CT is less hampered by motion artefacts than MRI. Furthermore, CT is indicated in patients with claustrophobia or with contraindications for MRI. Generally, CT and MRI have a higher accuracy than palpation in detecting metastatic disease. As necrosis is the most reliable radiological criterion, it is of utmost importance to use MRI and CT techniques that are optimal for the depiction of necrosis. Routine CT and MRI can not distinguish reactively enlarged lymph nodes from enlarged metastatic lymph nodes without necrosis. Recent developments of superparamagnetic MRI contrast agents have been proposed to improve the ability of MRI in differentiating metastatic from benign cervical lymph nodes. The initial results have been encouraging; however, the costs associated with multiple MRI studies and the logistical problems associated with the need for delayed imaging may prevent this technique from gaining wide acceptance (Anzai et al. 1994; Bellin et al. 1998; Sigal et al. 2002). Furthermore, the need for strongly T2-weighted gradient-echo images, with low spatial resolution, hampered the visibility of small metastases. Our initial experience was not very good. Other techniques, such as magnetization transfer imaging and spin lock imaging, have been shown to give some clues in differentiating different parotid tumors (Markkola et al. 1996); however, thus far no tissue characterization has been reported inside small lymph nodes. Currently, diffusion-weighted MRI is being investigated as a non-invasive tool for differentiating benign from malignant lymph nodes (van de Caveye et al. 2005).

Some authors have reported their results on the important issue of accuracy of CT or MRI for the assessment of the N0 neck (Stern et al. 1990; Feinmesser et al. 1990; Hillsamer et al. 1990; Friedman et al. 1990; Ishii et al. 1991; van den Brekel et al. 1993; Yucel et al. 1997; Atula et al. 1997; Righi et al. 1997). In these studies on the N0 neck the specificities and sensitivities of CT, MRI, US, and US fine-needle aspiration cytology vary considerably. As a rule, between 40% and 60% of all occult metastases are found using either CT or MRI, at the cost of some false positives. An important reason for false-negative interpretations is the fact that in 25% of the tumor-positive neck dissections only (undetectable) micrometastases smaller than 3 mm are present (van den Brekel et al. 1996).

15.5.2 Ultrasound

A linear transducer with a frequency of at least 7.5 MHz should be used in US. The optimal technique involves coronal and/or sagittal imaging of the sub-

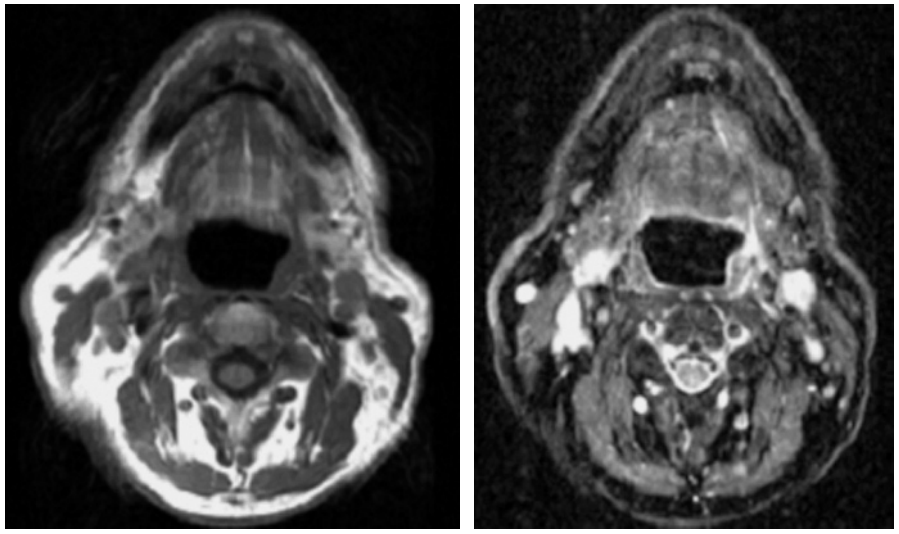

Fig. 15.2a,b. Patient with a large supraglottic carcinoma. **a** Axial T1 SE MR images shows slightly enlarged lymph nodes in both subdigastric areas. **b** Axial STIR image at the corresponding level shows high signal lymph nodes in high contrast with surrounding low signal fat

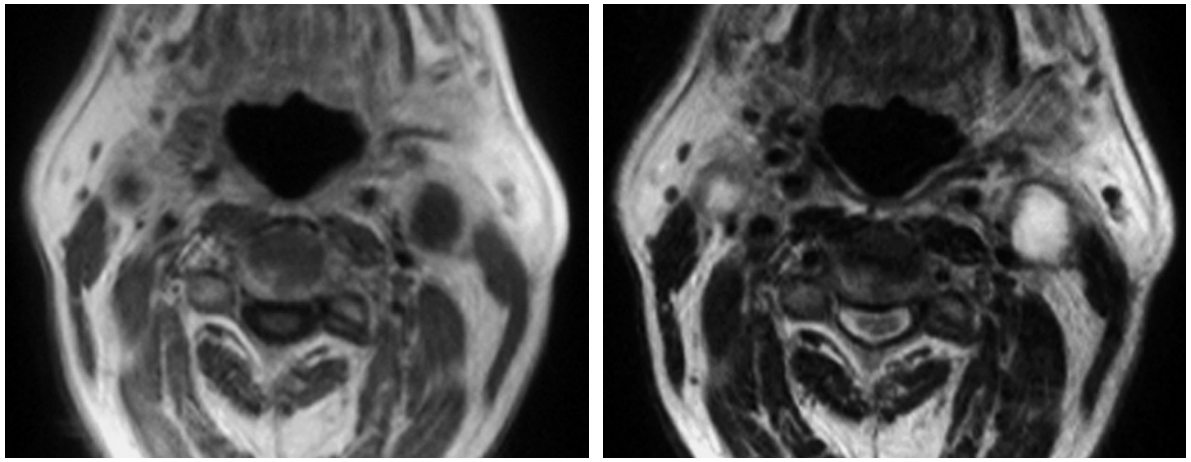

Fig. 15.3a,b. Patient with right-sided oropharyngeal carcinoma. **a** Axial post-gadolinium T1 SE MR image shows bilateral large lymph node in the subdigastric region, and with peripheral enhancement, suspicious for metastatic spread. **b** Axial T2 SE MR image shows a central area of high signal intensity within these adenopathies

mandibular lymph nodes and involves axial imaging of the lymph nodes around the jugular vein. On US lymph nodes are in general depicted as low echogenic oval or round structures. Small lymph nodes are visualized in almost all persons and patients. A hilus, containing vessels and fat, is visualized in almost 90% of all reactively enlarged lymph nodes and is seen as a central area of higher echogenicity (Figs. 15.4 and 15.5). Lymph node metastases at the submandibular level are most often located in front of the submandibular gland and around the facial artery adjacent to the mandible. The subdigastric lymph nodes (level 2) are in general the largest and have to be distinguished from the many vascular branches and suprahyoid muscles at this level. Especially when nodes in this area are high against the skull base or deep and almost parapharyngeal they are difficult to visualize.

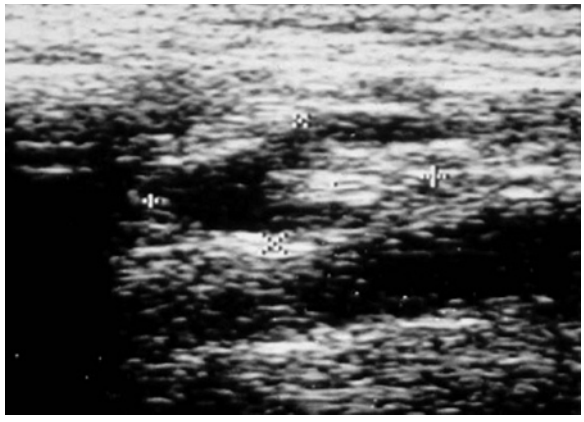

Fig. 15.4. US examination perpendicular to the mandible shows a small lymph node with an echogenic hilus

In general, US is reported to be superior to palpation in detecting lymph node metastases (Prayer et al. 1990; Ishii et al. 1991). Whereas some authors report it to be superior to contrast-enhanced CT and MRI (Vassallo et al. 1993), others have found similar accuracies (van den Brekel et al. 1993; Giancarlo et al. 1998). Advantages of US over other imaging techniques are its price and low patient burden. Furthermore, US is the only available imaging technique that can be used for frequent routine follow-up. Because gray-scale criteria are not very accurate, there is a great need for additional criteria in small lymph nodes. The potential value of Doppler US criteria (avascular pattern, scattered pattern (Fig. 15.6), peripheral vascularity (Fig. 15.7a,b)) as an adjunct to differentiate between benign and metastatic lymph nodes has been the topic of several studies. This technique enables the visualization of small irregularities in vascularization (Sato et al. 1998; Moritz et al. 2000; Ahuja et al. 2001); however, these irregularities are seldom visible in lymph nodes smaller than 1 cm.

In general, more nodes can be detected with higher-frequency transducers and more details can be visualized inside the lymph nodes. US is applicable during follow-up and an increase in size is a strong argument for metastasis (Yuasa et al. 2000).

15.5.3 Ultrasound-Guided Aspiration Cytology

Because many authors have found that borderline lymph nodes cannot be reliably scored on US, CT, and MRI, and because radiological criteria are not as reliable as cytological, US-FNAC is gaining popularity (Fig. 15.8a,b). In the United States this technique

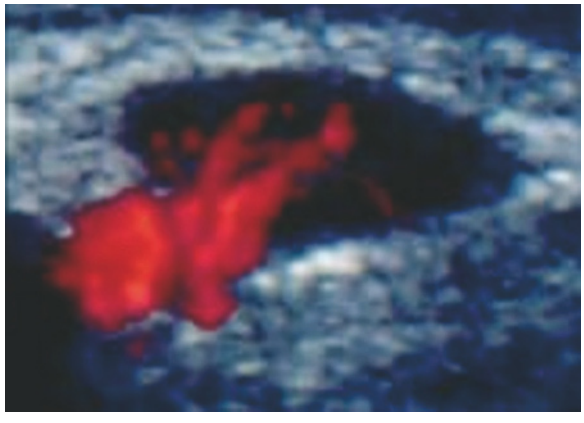

Fig. 15.5. US color examination shows the vascular hilus of a small lymph node

Fig. 15.6. US color examination shows a scattered vascular pattern within a lymph node. This may indicate a benign inflammatory node, but may also correspond to malignant spread

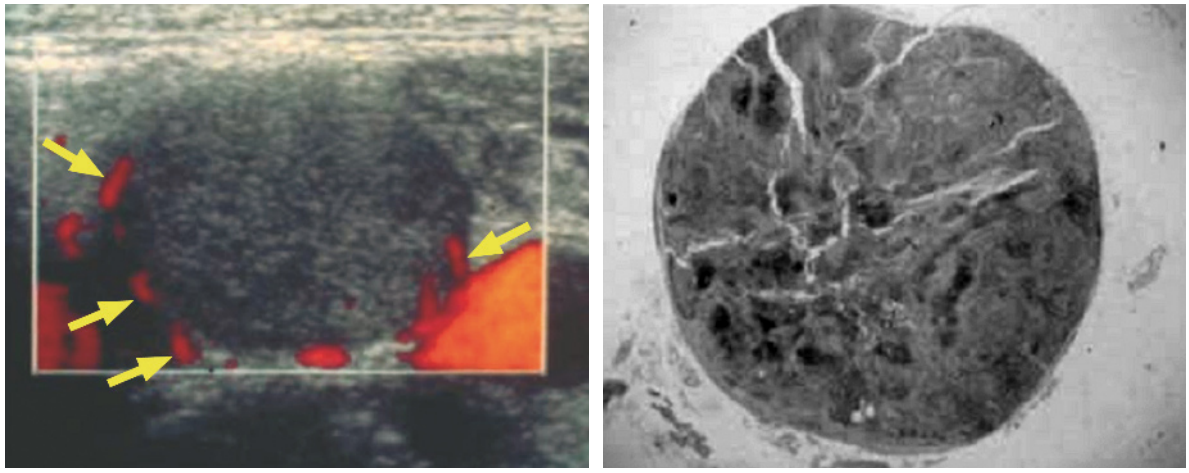

Fig. 15.7. a US color examination shows a subcapsular or peripheral pattern with minor flow signals in the periphery of the lymph node (*arrows*). **b** Microscopic specimen of the same lymph node shows a large avascular area, which corresponds to metastatic tumor spread in the lymph node. Minor vessels are observed in peripheral tissue

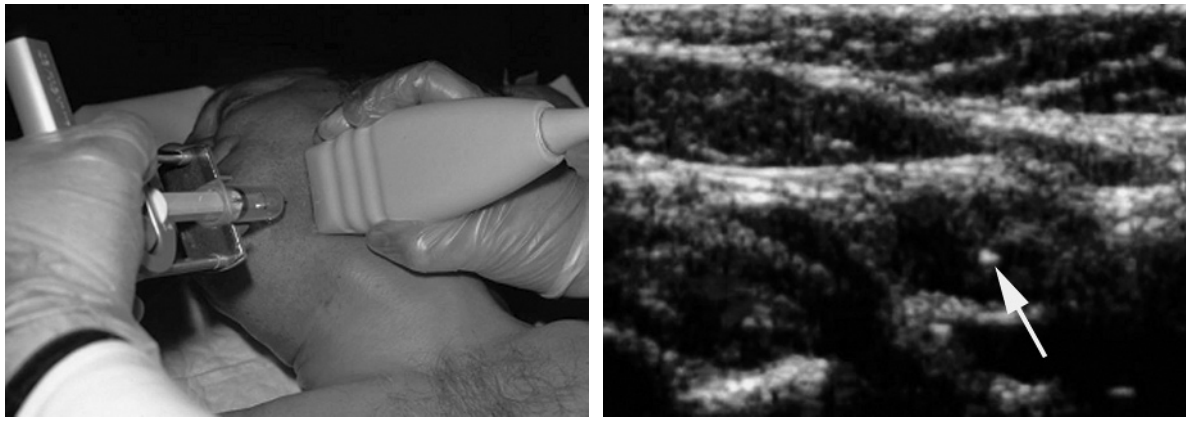

Fig. 15.8. a US guided aspirations should be performed by using a syringe holder and a 0.6×25-mm needle. The needle is introduced into the skin about 1 cm from the middle of the long axis of the transducer. **b** After visualization of the needle point, as a hyper-echogenic dot (*arrow*) inside the hypo-echogenic lymph node, aspiration is started and continued by moving the needle gently up and down

has received less acceptance because it is operator dependent. Although the technique is not difficult, considerable training is required to aspirate from lymph nodes as small as 4–5 mm and still obtain sufficient cells (van den Brekel et al. 1991a; McIvor et al. 1994), and to select the most suspicious lymph nodes from which to aspirate. For this it is necessary to have clinical information on the primary tumor and knowledge about the patterns of lymphatic spread from this tumor.

It has been shown that US-FNAC has a very high specificity, approaching 100% as epithelial cells in lymph nodes are seldom diagnosed falsely. To obtain a high enough sensitivity, lymph nodes as small as 4–5 mm in the first two echelons should be aspirated. Although aspirating smaller nodes will probably increase the sensitivity, it is difficult to obtain a diagnostic aspirate from nodes of 3 mm or smaller. In a previous report, we found that with use of this US-guided aspiration cytology we obtained a sensitivity of 73% with a specificity of 100% in N0 necks (van den Brekel et al. 1991a; van den Brekel et al. 1993). This was significantly better than CT or MRI. Only two other studies compared US-FNAC to CT and MRI and found it to also be superior (Atula et al. 1997; Hodder et al. 2000). In addition, for melanoma metastasis it was found to be the most accurate technique. Recently, however, in a multicenter study using US-guided aspiration, Takes et al. (1998) reported a sensitivity of only 42% for the N0 neck. Righi et al. (1997) found a sensitivity of 50%, which was inferior to 60% for CT; however, in Righi et al.'s study,

most false negatives were found in the beginning of the study and some of the patients were irradiated or suffering non-squamous cell carcinoma.

Generally, false-negative results may be the result of aspirating the wrong node or the wrong part of the correct node (sampling error). Furthermore, the cytopathologist may overlook single tumor cells. A technique which was supposed to increase the accuracy of US-guided aspiration is better selection of the node to aspirate by the sentinel node procedure. The concept of the sentinel node approach is based on the knowledge that nodal metastases progress in an orderly manner with the first site of metastases occurring in the sentinel node.

Techniques similar to the sentinel node procedures as used in melanoma and breast cancer can be employed, and initial reports in oral cancer are encouraging (Rossi et al. 2000; Ross et al. 2004). However, it remains an invasive diagnostic technique that has not yet shown its exact indications and limitations in head and neck cancer. The technique involves injecting Tc-99m-labeled sulfur colloid around the primary tumor site. The localization of the sentinel node is then performed by planar scintigraphy and the use of a hand-held gamma camera. We have tried to combine the non-invasive US-FNAC procedure with lymphoscintigraphic detection of the most appropriate node to aspirate (i.e. the sentinel node) (Colnot et al. 2001).Unfortunately, this combination of the sentinel node procedure and US-guided FNAC has not improved our results obtained without SN scintigraphy (Nieuwenhuis et al. 2000; Nieuwenhuis et al. 2002). In these studies we could also show that the sensitivity of US-FNAC for the palpably N0 varied widely in relation to the patient population studied. In patients treated with elective neck dissection, the sensitivity was 71%, similar to our previous studies (van den Brekel et al. 1991b). However, in the group of patients treated with transoral excision only and follow-up of the neck, the sensitivity was only 25%. The reasons for this lower sensitivity might be the unreliability of histopathological examination in the electively treated group. Probably more important is the fact that in the transoral excision group, the primary tumours and thus the metastases were smaller.

15.6 Clinical Impact of Diagnostic Evaluation

Regional metastasis is one of the most important factors in prognosis and treatment of patients with mucosal head and neck squamous cell cancer. In addition, since lymphatic metastasis is a frequent event, a decision to treat the lymph nodes in the neck has to be made in almost all patients, even if metastases are not apparent clinically. It is therefore important to assess as reliably as possible whether a patient has regional lymph node metastases. We discuss the clinical impact of diagnostic evaluation of the neck for the clinically negative neck, the clinically positive neck, and for detection of recurrent disease after treatment of the neck with irradiation.

15.6.1 Clinically Negative (N0) Neck

As a consequence of the low sensitivity of palpation, a neck side without palpable metastases is at risk of harbouring occult metastasis. This risk is to a large extent dependent on the size, site, and other characteristics of the primary tumor. For example, for T1 oral cavity cancer, it is in the range of 30%–40% whereas for T3 oropharyngeal carcinomas, it is in the range of 50%–60% (van den Brekel et al. 1999a; Nieuwenhuis et al. 2002). In glottic tumours the risk is quite low, whereas supraglottic tumours have a risk comparable to oral carcinomas (Levendag et al. 1988). There are significant differences in metastatic rates reported in the literature, probably caused by differences in patient populations, follow-up and scrutiny of histopathological examination (Ghouri et al. 1994; van den Brekel et al. 1996; Enepekides et al. 1999; Hamakawa et al. 2000).

In many head and neck primaries not only the ipsilateral site is at risk, but the contralateral site has a significant risk to harbour metastases as well, especially when the primary has grown close to or extends over the midline. In a neck without palpable nodes, imaging can help in detecting occult metastases or in increasing the confidence that the neck is really tumor negative and can be observed. Depiction of suspicious, non-palpable lymph nodes can convert selective neck treatment or a wait-and-see policy to more secure comprehensive treatment of all levels of the neck. Negative imaging results, on the other hand, can be used as an argument to refrain from elective treatment of the neck if the risk of radiologically occult metastases is considered to be low enough (Weiss et al. 1994; van den Brekel et al. 1999b; Nieuwenhuis et al. 2002). In many studies, a risk below 20% is considered to be low enough for a wait-and-see policy, although this cut-off point is very arbitrary. In practice, most patients with non-glottic,

infiltrating tumours undergo some form of elective neck treatment. So, even when no metastases can be detected, the neck will be treated in the majority of the patients. Disadvantages of this policy are costs, overtreatment and morbidity for the majority of the patients. Modern imaging techniques may be helpful by decreasing the initial risk of occult metastasis. If the risk of occult metastasis is below 20%, the clinician may refrain from a neck dissection and adapt a wait-and-see policy with careful follow-up to detect a neck metastasis as early as possible. So far, several authors have shown the applicability of this approach (Westhofen 1987; Quetz et al. 1998; Schipper et al. 1999; van den Brekel et al. 1999b; Szmeja et al. 1999; Nieuwenhuis et al. 2002). As a risk of 20% of occult metastases is considered acceptable to observe the neck, and because most T2 oral carcinomas carry a risk of approximately 40% for palpably occult metastases, the sensitivity of any imaging technique should be at least around 50% for non-palpable neck disease so as to detect half of the occult metastases.

As previously observed, US-guided FNAC in experienced hands is a highly specific and relatively sensitive technique in detecting palpably occult metastases, and the authors have adapted their policy of elective neck treatment in selected patients (Quetz et al. 1998; van den Brekel et al. 1999b; Nieuwenhuis et al. 2002). In selected patients who can be treated with transoral excision for T1 and T2 oral, oropharyngeal, and supraglottic carcinomas, or selected patients who undergo laryngectomy for laryngeal carcinomas, the authors rely on the US-guided FNAC findings and do not routinely treat the neck electively. These patients are followed very meticulously, using US-guided FNAC at 12-week intervals. Our experience with this wait-and-see policy has been encouraging. About 20% of the patients with oral cancer treated with transoral excision only do develop a neck node metastasis during follow-up, but over 80% of these can be salvaged by timely treatment. This high salvage rate is certainly related to the short delay of diagnosis due to follow-up by US-guided FNAC.

15.6.2 Clinically Positive (N+) Neck

The relevance of depiction of extranodal spread or the exact number and levels of metastases is not important if a patient is treated surgically as the final histopathology report will guide further therapy and most surgeons treat all levels of the neck once a positive lymph node is detected; however, accurate depiction of these features becomes more important if selective neck dissections are considered for limited disease or when radiotherapy is the primary treatment and no histopathology will become available (van den Brekel, et al. 1994; Hermans et al. 2001).

CT, US, and MRI are not very accurate in the assessment of the exact number of metastases in the neck or the number of levels involved, as relatively large detectable metastases are very often accompanied by small undetectable micrometastases (van den Brekel et al. 1990b; van den Brekel et al. 1992). Extranodal spread is radiologically characterized by ablation of fat planes and irregular nodal borders. It was reported that CT could only identify extranodal spread in large nodes (Close et al. 1989), while Som (1992) reported a sensitivity of 100%. Yousem et al. (1992) reported an accuracy of CT of 90%, whereas in their study MRI had an accuracy of 78%. On the other hand, Carvalho (1991) studied the value of CT in detecting extranodal spread and found a sensitivity of 63% and a specificity of 60%. In a study of Woolgar (1994), in 16% of the cases N0 at CT, extranodal tumor spread was present. In our opinion, only major macroscopic extranodal spread (infiltration) can be detected with acceptable accuracy by preoperative staging techniques. As even pathologists do not always agree on the presence of microscopic extranodal spread, and because it is very often a discrete histopathological sign, radiological assessment is unreliable.

Assessment of tumor volume has been shown to be an important prognosticator in laryngeal, and to a lesser extent pharyngeal carcinoma (Castelijns et al. 1995; Nathu et al. 2000; van den Broek et al. 2004). Assessment of nodal volume (Jakobsen et al. 1998) is studied less, but has clinical importance in predicting outcome as well. Necrosis in lymph nodes, as depicted at CT or MRI, can also be important to predict response to radiotherapy or chemoradiation. As nodal necrosis is a sign of tumor hypoxia, it can be anticipated that these lymph nodes respond less to radiotherapy (Kaanders et al. 1998; Hermans et al. 2003). Indeed, Dietz (2000) has shown that diminished vascularity in lymph nodes as shown with duplex Doppler, as well as high tumor volume measured at CT, is a poor predictive sign for patients treated with chemoradiation. In another study, it was shown that if the lymph node necrosis area at CT encompasses more than 1/3 of the total volume or if nodal volume exceeds 110 ml, survival drops dramatically (Grabenbauer et al. 1998; Wang et al. 1996). Recently, it has been shown that with use

of functional MRI, tumor hypoxia can be measured and predicts chemoresistance (Bhattacharya et al. 2004). Another method of assessing tumor hypoxia is Tc-imidazole scintigraphy (Hoebers et al. 2002). Also, the standardized uptake value of FDG-PET was shown to be a predictive marker for patients treated with radiotherapy (Allal et al. 2002).

Other important prognostic parameters are the number of lymph node metastases and the level of the lymph nodes. Although lymph node level is used only in N staging of nasopharyngeal carcinomas, several studies have shown its importance in other sites of the head and neck (O'Brien et al. 1986; Jones et al. 1994). Although imaging can detect lymph node metastases more accurately than palpation, no studies have been performed to establish the accuracy in assessing the number of levels or the number of nodes involved. As larger (depicted) metastases are frequently accompanied by multiple smaller metastases (van den Brekel et al. 1990b; van den Brekel et al. 1992), not visible at imaging, it can be anticipated that the assessment of the number nodes and levels involved will be quite inaccurate.

CT and MRI may be helpful for the detection of retropharyngeal paratracheal and mediastinal lymph nodes. This may lead to a more expanded surgical treatment of the neck or extension of the radiotherapy fields. Furthermore, the presence of these lymph nodes is important for prognostication (Sham et al. 1993; Olmi et al. 1995; Chandawarkar et al. 1996; Plaat et al. 2005). Unfortunately, paratracheal node metastases are often very small and difficult to detect at CT or US (Yang et al. 1998). For this reason elective paratracheal dissection is recommended in aggressive thyroid cancer, laryngeal cancer with subglottic extension and hypopharyngeal cancer.

Assessment of invasion of vital structures can be both prognostically and therapeutically relevant, as the resectability becomes uncertain and prognosis very bad once vital structures are invaded. In this respect, invasion of the common or internal carotid artery is probably most important (Freeman et al. 2004), although invasion of both internal jugular veins, the skull base, or thoracic inlet pose similar therapeutic challenges. The reported accuracy of CT, MRI, and US in detecting tumor invasion into the carotid artery varies widely (Langman et al. 1989; Pradeep et al. 1991; Mann et al. 1994; Yousem et al. 1995). Palpation simultaneous with real-time US can be helpful to detect carotid wall invasion (Gritzmann et al. 1990). In general, a tumor encircling the vessel over 270° on CT or MRI at a distance of above 4 cm, or a tumor that is immobile from the vessel using sono-palpation, indicates involvement of the vessel wall and often non-resectability (Fig. 15.9).

15.6.3 Recurrent Disease in the Neck

Detection of recurrences is clinically most relevant if therapeutic options are still present. As many patients have had initial treatment of the neck with neck dissection and postoperative radiotherapy, neck recurrences can rarely be treated effectively. However, even for these patients the establishment of a diagnosis is important. Only in patients treated for the primary tumor only (wait-and-see for the neck) or those treated on the neck with exclusively radiotherapy, chemoradiation or limited surgery, routine follow-up imaging examinations of the neck to detect early recurrences seem warranted. Thus far, CT and also MRI have disappointed in the early detection of recurrent or residual disease in the neck. Radiation therapy and surgery can lead to changes that may mask the detection of disease by physical examination.

There is growing evidence that imaging is important in detecting recurrent or residual disease after radiation therapy in an early clinical stage. Especially CT and MRI have been studied in this regard (Mukherji et al. 1994; Pameijer et al. 1999; Hermans et al. 2000). In patients who have a high likelihood of loco-regional recurrence, a baseline MRI or CT can be obtained 2–4 months after the initial treatment. Using the baseline scan, abnormalities that develop later can then be easier detected.

The use of US, US-FNAC or duplex Doppler for the follow-up of the treated neck has been studied by several authors (Westhofen 1987; Hessling et al. 1991; Steinkamp et al. 1994b; Ahuja et al. 1999). Westhofen (1987) showed that US-FNAC was superior to CT in detecting neck recurrences after previous treatment. To our opinion, routine US-FNAC follow-up for at least 1 year is warranted if the neck was not treated electively (except for T1–2 glottic carcinomas, small skin carcinomas or non-infiltrating carcinomas). We also use it to assess the radiotherapeutically treated N+ neck, 6–8 weeks post treatment. In these cases, however, the cytology is much more difficult to interpret. Recently, several authors have shown the high negative predictive value and accuracy of PET for the follow-up after radiotherapy of head and neck tumors (Anzai et al. 1996; Slevin et al. 1999; Li et al. 2001; Kitagawa et al. 2003; Kubota et al. 2004). In case the PET scan is negative, further investigations are not needed according to most authors.

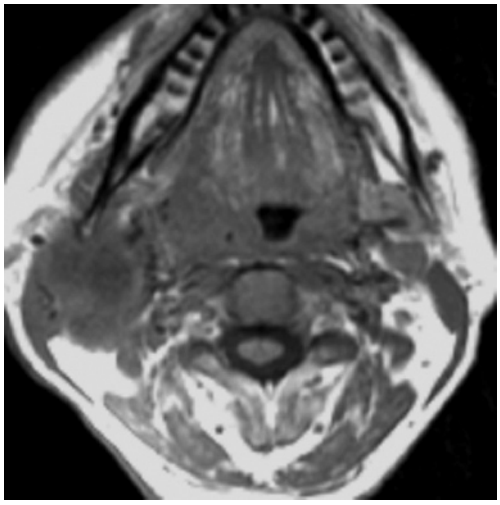

Fig. 15.9. Axial plain T1-weighted MR image shows a lymph node at right subdigastric level with intermediate signal intensity; the irregular border suggests extranodular spread. Also, a small lymph node is seen on the left side at same level

References

Ahuja A, Ying M (2002) An overview of neck node sonography. Invest Radiol 37:333–342

Ahuja S, Ernst H, Lenz K (1991) Papillary thyroid carcinoma: occurrence and types of lymph node metastases. J Endocrinol Invest 14:543–549

Ahuja AT, Ho SS, Leung SF, Kew J, Metreweli C (1999) Metastatic adenopathy from nasopharyngeal carcinoma: successful response to radiation therapy assessed by color duplex sonography. AJNR Am J Neuroradiol 20:151–156

Ahuja A, Ying M, Yuen YH, Metreweli C (2001) Power Doppler sonography to differentiate tuberculous cervical lymphadenopathy from nasopharyngeal carcinoma. AJNR Am J Neuroradiol 22:735–740

Allal AS, Dulguerov P, Allaoua M, et al (2002) Standardized uptake value of 2-[(18)F] fluoro-2-deoxy-D-glucose in predicting outcome in head and neck carcinomas treated by radiotherapy with or without chemotherapy. J Clin Oncol 20:1398–1404

Amar A, Rapoport A, Rosas MP (1999) Evaluation of lymph node reactivity in differentiated thyroid carcinoma. Sao Paulo Med J 117:125–128

Anzai Y, McLachlan S, Morris M, Saxton R, Lufkin RB (1994) Dextran-coated superparamagnetic iron oxide, an MR contrast agent for assessing lymph nodes in the head and neck. AJNR Am J Neuroradiol 15:87–94

Anzai Y, Carroll WR, Quint DJ, Bradford CR, Minoshima S, Wolf GT, Wahl RL (1996) Recurrence of head and neck cancer after surgery or irradiation: prospective comparison of 2-deoxy-2-[F-18]fluoro-D-glucose PET and MR imaging diagnoses. Radiology 200:135–141

Armstrong JG, Harrison LB, Thaler HT, Friedlander-Klar H, Fass DE, Zelefsky MJ, Shah JP, Strong EW, Spiro RH (1992) The indications for elective treatment of the neck in cancer of the major salivary glands. Cancer 69:615–619

Atula TS, Varpula MJ, Kurki TJ, Klemi PJ, Grenman R (1997) Assessment of cervical lymph node status in head and neck cancer patients -- palpation, computed tomography and low field magnetic resonance imaging compared with ultrasound-guided fine-needle aspiration cytology. Eur J Radiol 25:152–161

Balazs G, Gyory F, Lukacs G, Szakall S (1998) Long-term follow-up of node-positive papillary thyroid carcinomas. Langenbecks Arch.Surg. 383:180–182

Bellin MF, Roy C, Kinkel K, Thoumas D, Zaim S, Vanel D, Tuchmann C, Richard F, Jacqmin D, Delcourt A, Challier E, Lebret T, Cluzel P (1998) Lymph node metastases: safety and effectiveness of MR imaging with ultrasmall superparamagnetic iron oxide particles--initial clinical experience. Radiology 207:799–808

Bellin MF, Lebleu L, Meric JB (2003) Evaluation of retroperitoneal and pelvic lymph node metastases with MRI and MR lymphangiography. Abdom Imaging 28:155–163

Bhattacharya A, Toth K, Mazurchuk R, Spernyak JA, Slocum HK, Pendyala L, Azrak R, Cao S, Durrani FA, Rustum YM (2004) Lack of microvessels in well-differentiated regions of human head and neck squamous cell carcinoma A253 associated with functional magnetic resonance imaging detectable hypoxia, limited drug delivery, and resistance to irinotecan therapy. Clin Cancer Res 10:8005–8017

Blum A, Schlagenhauff B, Stroebel W, Breuninger H, Rassner G, Garbe C (2000) Ultrasound examination of regional lymph nodes significantly improves early detection of locoregional metastases during the follow-up of patients with cutaneous melanoma: results of a prospective study of 1288 patients. Cancer 88:2534–2539

Bruneton JN, Balu-Maestro C, Marcy PY, Melia P, Mourou MY (1994) Very high frequency (13 MHz) ultrasonographic examination of the normal neck: detection of normal lymph nodes and thyroid nodules. J Ultrasound Med 13:87–90

Byers RM, Weber RS, Andrews T, McGill D, Kare R, Wolf P (1997) Frequency and therapeutic implications of "skip metastases" in the neck from squamous carcinoma of the oral tongue. Head Neck 19:14–19

Carvalho P, Baldwin D, Carter R, Parsons C (1991) Accuracy of CT in detecting squamous carcinoma metastases in cervical lymph nodes. Clin Radiol 44:79–81

Castelijns JA, van den Brekel MW, Smit EM, Tobi H, van Wagtendonk FW, Golding RP, Venema HW, van Schaik C, Snow GB (1995) Predictive value of MR imaging-dependent and non-MR imaging-dependent parameters for recurrence of laryngeal cancer after radiation therapy. Radiology 196:735–739

Chandawarkar RY, Kakegawa T, Fujita H, Yamana H, Hayabuthi N (1996) Comparative analysis of imaging modalities in the preoperative assessment of nodal metastasis in esophageal cancer. J Surg Oncol 61:214–217

Chong VF, Fan YF, Khoo JB (1996) MRI features of cervical nodal necrosis in metastatic disease. Clin Radiol 51:103–109

Chow SM, Law SC, Au SK, Leung TW, Chan PT, Mendenhall WM, Lau WH (2002) Differentiated thyroid carcinoma: comparison between papillary and follicular carcinoma in a single institute. Head Neck 24:670–677

Close LG, Merkel M, Vuitch MF, Reisch J, Schaefer SD (1989) Computed tomographic evaluation of regional lymph node involvement in cancer of the oral cavity and oropharynx. Head Neck 11:309–317

Colnot DR, Nieuwenhuis EJ, van den Brekel, et al (2001) Head

and neck squamous cell carcinoma: US-guided fine-needle aspiration of sentinel lymph nodes for improved staging -- initial experience. Radiology 218:289–293

Curtin HD, Ishwaran H, Mancuso AA, Dalley RW, Caudry DJ, McNeil BJ (1998) Comparison of CT and MR imaging in staging of neck metastases. Radiology 207:123–130

de Wilt JH, Thompson JF, Uren RF, Ka VS, Scolyer RA, McCarthy WH, O'Brien CJ, Quinn MJ, Shannon KF (2004) Correlation between preoperative lymphoscintigraphy and metastatic nodal disease sites in 362 patients with cutaneous melanomas of the head and neck. Ann Surg 239:544–552

Di Martino E, Nowak B, Hassan HA, Hausmann R, Adam G, Buell U, Westhofen M (2000) Diagnosis and staging of head and neck cancer: a comparison of modern imaging modalities (positron emission tomography, computed tomography, color-coded duplex sonography) with panendoscopic and histopathologic findings. Arch Otolaryngol Head Neck Surg 126:1457–1461

Dietz A, Delorme S, Rudat V, Zuna I, Conradt C, Vanselow B, Weidauer H (2000) Prognostic assessment of sonography and tumor volumetry in advanced cancer of the head and neck by use of doppler ultrasonography. Otolaryngol Head Neck Surg 122:596–601

Don DM, Anzai Y, Lufkin RB, Fu YS, Calcaterra TC (1995) Evaluation of cervical lymph node metastases in squamous cell carcinoma of the head and neck. Laryngoscope 105:669–674

Enepekides DJ, Sultanem K, Nguyen C, Shenouda G, Black MJ, Rochon L (1999) Occult cervical metastases: immunoperoxidase analysis of the pathologically negative neck. Otolaryngol Head Neck Surg 120:713–717

Feinmesser R, Freeman JL, Noyek AM, Birt D, Gullane P, Mullen JB (1990) MRI and neck metastases: a clinical, radiological, pathological correlative study. J Otolaryngol 19:136–140

Fischbein NJ, Noworolski SM, Henry RG, Kaplan MJ, Dillon WP, Nelson SJ (2003) Assessment of metastatic cervical adenopathy using dynamic contrast-enhanced MR imaging. AJNR Am J Neuroradiol 24:301–311

Frasoldati A, Pesenti M, Gallo M, et al (2003) Diagnosis of neck recurrences in patients with differentiated thyroid carcinoma. Cancer 97:90–96

Frazell EL, Foote FW (1955) Papillary thyroid carcinoma: pathological findings in cases with and without clinical evidence of cervical node involvement. Cancer 8:1164–1166

Freeman SB, Hamaker RC, Borrowdale RB, Huntley TC (2004) Management of neck metastasis with carotid artery involvement. Laryngoscope 114:20–24

Friedman M, Mafee MF, Pacella BL, Strorigl TL, Dew LL, Toriumi DM (1990) Rationale for elective neck dissection in 1990. Laryngoscope 100:54–59

Friedman M, Roberts N, Kirshenbaum GL, Colombo J (1993) Nodal size of metastatic squamous cell carcinoma of the neck. Laryngoscope 103:854–856

Ghouri AF, Zamora RL, Sessions DG, Spitznagel EL, Harvey JE (1994) Prediction of occult neck disease in laryngeal cancer by means of a logistic regression statistical model. Laryngoscope 104:1280–1284

Giancarlo T, Palmieri A, Giacomarra V, Russolo M (1998) Preoperative evaluation of cervical adenopathies in tumours of the upper aerodigestive tract. Anticancer Res 18:2805–2809

Grabenbauer GG, Steininger H, Meyer M, Fietkau R, Brunner T, Heinkelmann P, Hornung J, Iro H, Spitzer W, Kirchner T, Sauer R, Distel L (1998) Nodal CT density and total tumor volume as prognostic factors after radiation therapy of stage III/IV head and neck cancer. Radiother Oncol 47:175–183

Gritzmann N, Grasl MC, Helmer M, Steiner E (1990) Invasion of the carotid artery and jugular vein by lymph node metastases: detection with sonography. AJR Am J Roentgenol 154:411–414

Hamakawa H, Takemura K, Sumida T, Kayahara H, Tanioka H, Sogawa K (2000) Histological study on pN upgrading of oral cancer. Virchows Arch 437:116–121

Hermans R, Pameijer FA, Mancuso AA, Parsons JT, Mendenhall WM (2000) Laryngeal or hypopharyngeal squamous cell carcinoma: can follow-up CT after definitive radiation therapy be used to detect local failure earlier than clinical examination alone? Radiology 214:683–687

Hermans R, Op de beeck K, Van den Bogaert W, Rijnders A, Staelens L, Feron M, Bellon E (2001) The relation of CT-determined tumor parameters and local and regional outcome of tonsillar cancer after definitive radiation treatment. Int J Radiat Oncol Biol Phys 50:37–45

Hermans R, Meijerink M, Van den Bogaert W, Rijnders A, Weltens C, Lambin P (2003) Tumor perfusion rate determined noninvasively by dynamic computed tomography predicts outcome in head-and-neck cancer after radiotherapy. Int J Radiat Oncol Biol Phys 57:1351–1356

Hessling KH, Schmelzeisen R, Reimer P, Milbradt H, Unverfehrt D (1991) Use of sonography in the follow-up of preoperatively irradiated efferent lymphatics of the neck in oropharyngeal tumours. J Craniomaxillofac Surg 19:128–130

Hillsamer PJ, Schuller DE, McGhee RB, Chakeres D, Young DC (1990) Improving diagnostic accuracy of cervical metastases with computed tomography and magnetic resonance imaging. Arch Otolaryngol Head Neck Surg 116:1297–1301

Hodder SC, Evans RM, Patton DW, Silvester KC (2000) Ultrasound and fine needle aspiration cytology in the staging of neck lymph nodes in oral squamous cell carcinoma. Br J Oral Maxillofac Surg 38:430–436

Hoebers FJ, Janssen HL, Olmos AV, et al (2002) Phase 1 study to identify tumour hypoxia in patients with head and neck cancer using technetium-99m BRU 59-21. Eur J Nucl Med Mol Imaging 29:1206–1211

Hudgins PA (1994) Contrast enhancement in head and neck imaging. Neuroimaging Clin N Am:101–115

Ishii J, Amagasa T, Tachibana T, Shinozuka K, Shioda S (1991) US and CT evaluation of cervical lymph node metastasis from oral cancer. J Craniomaxillofac Surg 19:123–127

Jakobsen J, Hansen O, Jørgensen KE, Bastholt L (1998) Lymph node metastases from laryngeal and pharyngeal carcinomas--calculation of burden of metastasis and its impact on prognosis. Acta Oncol 37:489–493

Jansen L, Kroop HS, Nieweg OE, et al (2000) Sentinel node biopsy for melanoma in the head and neck region. Head Neck 22:27–33

Jones AS, Roland NJ, Field JK, Phillips DE (1994) The level of cervical lymph node metastases: their prognostic relevance and relationship with head and neck squamous carcinoma primary sites. Clin Otolaryngol Allied Sci 19:63–69

Kaanders JH, Pop LA, Marres HA, Liefers J, van den Hoogen FJ, van Daal WA, van der Kogel AJ (1998) Accelerated radiotherapy with carbogen and nicotinamide (ARCON) for laryngeal cancer. Radiother Oncol 48:115–122

King AD, Ahuja AT, Leung SF, Lam WW, Teo P, Chan YL, Metreweli C (2000) Neck node metastases from nasopharyngeal carcinoma: MR imaging of patterns of disease. Head Neck 22:275–281

Kitagawa Y, Nishizawa S, Sano K, et al (2003) Prospective comparison of 18F-FDG PET with conventional imaging modalities (MRI, CT, and 67Ga scintigraphy) in assessment of combined intraarterial chemotherapy and radiotherapy for head and neck carcinoma. J Nucl Med 44:198–206

Korkmaz H, Yoo GH, Du W, Hocwald E, Otero-Garcia JE, Volkan Adsay N, Shibuya T, Jacobs JR (2002) Predictors of nodal metastasis in salivary gland cancer. J Surg Oncol 80:186–189

Kouvaraki MA, Shapiro SE, Fornage BD, Edeiken-Monro BS, Sherman SI, Vassilopoulou-Sellin R, Lee JE, Evans DB (2003) Role of preoperative ultrasonography in the surgical management of patients with thyroid cancer. Surgery 134:946-54; discussion 954-5

Kubota K, Yokoyama J, Yamaguchi K, et al (2004) FDG-PET delayed imaging for the detection of head and neck cancer recurrence after radio-chemotherapy: comparison with MRI/CT. Eur J Nucl Med Mol Imaging 31:590–595

Langman AW, Kaplan MJ, Dillon WP, Gooding GA (1989) Radiologic assessment of tumor and the carotid artery: correlation of magnetic resonance imaging, ultrasound, and computed tomography with surgical findings. Head Neck 11:443–449

Lazor JB, Cunningham MJ, Eavey RD, Weber AL (1994) Comparison of computed tomography and surgical findings in deep neck infections. Otolaryngol Head Neck Surg 111:746–750

Lenz M, Kersting-Sommerhoff B, Gross M (1993) Diagnosis and treatment of the N0 neck in carcinomas of the upper aerodigestive tract: current status of diagnostic procedures. Eur Arch Otorhinolaryngol 250:432–438

Levendag PC, Hoekstra CJ, Eijkenboom WM, Reichgelt BA, Van Putten WL (1988) Supraglottic larynx cancer, T1-4 N0, treated by radical radiation therapy. Problem of neck relapse. Acta Oncol 27:253–260

Li P, Zhuang H, Mozley PD, Denittis A, Yeh D, Machtay M, Smith R, Alavi A (2001) Evaluation of recurrent squamous cell carcinoma of the head and neck with FDG positron emission tomography. Clin Nucl Med 26:131–135

Maffioli L, Belli F, Gallino G, Ditto A, Castellani MR, Testoni M, Sturm E, Bombardieri E, Cascinelli N (2000) Sentinel node biopsy in patients with cutaneous melanoma of the head and neck. Tumori 86:341–342

Mann WJ, Beck A, Schreiber J, Maurer J, Amedee RG, Gluckmann JL (1994) Ultrasonography for evaluation of the carotid artery in head and neck cancer. Laryngoscope 104:885–888

Markkola AT, Aronen HJ, Paavonen T, Hopsu E, Sipilä LM, Tanttu JI, Sepponen RE (1996) Spin lock and magnetization transfer imaging of head and neck tumors. Radiology 200:369–375

Martinez Gimeno C, Rodriguez EM, Vila CN, Varela CL (1995) Squamous cell carcinoma of the oral cavity: a clinicopathologic scoring system for evaluating risk of cervical lymph node metastasis. Laryngoscope 105:728–733

McIvor NP, Freeman JL, Salem S, Elden L, et al (1994) Ultrasonography and ultrasound-guided fine-needle aspiration biopsy of head and neck lesions: a surgical perspective. Laryngoscope 104:669–674

Mirallie E, Sagan C, Hamy A, et al (1999) Predictive factors for node involvement in papillary thyroid carcinoma. Univariate and multivariate analyses. Eur J Cancer 35:420–423

Moley JF, DeBenedetti MK (1999) Patterns of nodal metastases in palpable medullary thyroid carcinoma: recommendations for extent of node dissection. Ann Surg 229:880-7; discussion 887-8

Moon WK, Han MH, Chang KH, Im JG, Kim HJ, Sung KJ, Lee HK (1997) CT and MR imaging of head and neck tuberculosis. Radiographics 17:391–402

Moritz JD, Ludwig A, Oestmann JW, et al (2000) Contrast-enhanced color Doppler sonography for evaluation of enlarged cervical lymph nodes in head and neck tumors. AJR Am J Roentgenol 174:1279–1284

Morrissey DD, Talbot JM, Cohen JI, Wax MK, Andersen PE (2000) Accuracy of computed tomography in determining the presence or absence of metastatic retropharyngeal adenopathy. Arch Otolaryngol Head Neck Surg 126:1478–1481

Mukherji SK, Mancuso AA, Kotzur IM, Mendenhall WM, Kubilis PS, Tart RP, Lee WR, Freeman D (1994) Radiologic appearance of the irradiated larynx. Part I. Expected changes. Radiology 193:141–148

Nathu RM, Mancuso AA, Zhu TC, Mendenhall WM (2000) The impact of primary tumor volume on local control for oropharyngeal squamous cell carcinoma treated with radiotherapy. Head Neck 22:1–5

Nieuwenhuis EJ, Colnot DR, Pijpers HJ, Castelijns JA, van Diest PJ, Brakenhoff RH, Snow GB, van den Brekel MW (2000) Lymphoscintigraphy and ultrasound-guided fine needle aspiration cytology of sentinel lymph nodes in head and neck cancer patients. Recent Results Cancer Res 157:206–217

Nieuwenhuis EJ, Castelijns JA, Pijpers R, van den Brekel MW, Brakenhoff RH, van der Waal I, Snow GB, Leemans CR (2002) Wait-and-see policy for the N0 neck in early-stage oral and oropharyngeal squamous cell carcinoma using ultrasonography-guided cytology: is there a role for identification of the sentinel node? Head Neck 24:282–289

O'Brien CJ, Smith JW, Soong SJ, Urist MM, Maddox WA (1986) Neck dissection with and without radiotherapy: prognostic factors, patterns of recurrence, and survival. Am J Surg 152:456–463

O'Brien CJ, McNeil EB, McMahon JD, Pathak I, Lauer CS (2001) Incidence of cervical node involvement in metastatic cutaneous malignancy involving the parotid gland. Head Neck 23:744–748

Olmi P, Fallai C, Colagrande S, Giannardi G (1995) Staging and follow-up of nasopharyngeal carcinoma: magnetic resonance imaging versus computerized tomography. Int J Radiat Oncol Biol Phys 32:795–800

Pameijer FA, Hermans R, Mancuso AA, Mendenhall WM, Parsons JT, Stringer SP, Kubilis PS, van Tinteren H (1999) Pre- and post-radiotherapy computed tomography in laryngeal cancer: imaging-based prediction of local failure. Int J Radiat Oncol Biol Phys 45:359–366

Pathak I, O'Brien CJ, Petersen-Schaeffer K, McNeil EB, McMahon J, Quinn MJ, Thompson JF, McCarthy WH (2001) Do nodal metastases from cutaneous melanoma of the head and neck follow a clinically predictable pattern? Head Neck 23:785–790

Plaat RE, de Bree R, Kuik DJ, van den Brekel MW, van Hattum AH, Snow GB, Leemans CR (2005) Prognostic importance

of paratracheal lymph node metastases. Laryngoscope 115:894–898
Pradeep VM, Padmanabhan V, Sen P, Ramachandran K, Sasidharan K, Krishnamoorthy S, Nair MK (1991) Sonographic evaluation of operability of malignant cervical lymph nodes. Am J Clin Oncol 14:438–441
Prayer L, Winkelbauer H, Gritzmann N, Winkelbauer F, Helmer M, Pehamberger H (1990) Sonography versus palpation in the detection of regional lymph-node metastases in patients with malignant melanoma. Eur J Cancer 26:827–830
Quetz JU et al (1998) Sonography for detection of late lymph node metastases in the head and neck region: an effective method of follow-up screening? Br J Cancer 77[Suppl 1]:15.
Rao AB, Koeller KK, Adair CF (1999) From the archives of the AFIP. Paragangliomas of the head and neck: radiologic-pathologic correlation. Armed Forces Institute of Pathology. Radiographics 19:1605–1632
Righi PD, Kopecky KK, Caldemeyer KS, Ball VA, Weisberger EC, Radpour S (1997) Comparison of ultrasound-fine needle aspiration and computed tomography in patients undergoing elective neck dissection. Head Neck 19:604–610
Robbins KT, Clayman G, Levine PA, Medina J, Sessions R, Shaha A, Som P, Wolf GT (2002) Neck dissection classification update: revisions proposed by the American Head and Neck Society and the American Academy of Otolaryngology-Head and Neck Surgery. Arch Otolaryngol Head Neck Surg 128:751–758
Robson CD (2000) Imaging of granulomatous lesions of the neck in children. Radiol Clin North Am 38:969–977
Ross GL, Soutar DS, Gordon MacDonald D, Shoaib T, Camilleri I, Roberton AG, Sorensen JA, Thomsen J, Grupe P, Alvarez J, Barbier L, Santamaria J, Poli T, Massarelli O, Sesenna E, Kovács AF, Grünwald F, Barzan L, Sulfaro S, Alberti F (2004) Sentinel node biopsy in head and neck cancer: preliminary results of a multicenter trial. Ann Surg Oncol 11:690–696
Rossi CR, Scagnet B, Vecchiato A, Mocellin S, Pilati P, Foletto M, Zavagno G, Casara D, Montesco MC, Tregnaghi A, Rubaltelli L, Lise M (2000) Sentinel node biopsy and ultrasound scanning in cutaneous melanoma: clinical and technical considerations. Eur J Cancer 36:895–900
Rouvière H (1932) Anatomie des lymphatiques de l'homme. Masson et Cie, Paris
Sato N, Kawabe R, Fujita K, Omura S (1998) Differential diagnosis of cervical lymphadenopathy with intranodal color Doppler flow signals in patients with oral squamous cell carcinoma. Oral Surg Oral Med Oral Pathol Oral Radiol Endod 86:482–488
Schipper J, Gellrich NC, Marangos N, Maier W (1999) Value of B-image ultrasound in patients with carcinomas of the upper aerodigestive tract and N0 lymph node stage. Laryngorhinootologie 78:561–565
Scollo C, Baudin E, Travagli JP, Caillou B, Bellon N, Leboulleux S, Schlumberger M (2003) Rationale for central and bilateral lymph node dissection in sporadic and hereditary medullary thyroid cancer. J Clin Endocrinol Metab 88:2070–2075
Shah JP (1990) Patterns of cervical lymph node metastasis from squamous carcinomas of the upper aerodigestive tract. Am J Surg 160:405–409
Sham JS, Cheung YK, Choy D, Chan FL, Leong L (1993) Computed tomography evaluation of neck node metastases from nasopharyngeal carcinoma. Int J Radiat Oncol Biol Phys 26:787–792
Sigal R, Vogl T, Casselman J, et al (2002) Lymph node metastases from head and neck squamous cell carcinoma: MR imaging with ultrasmall superparamagnetic iron oxide particles (Sinerem MR) -- results of a phase-III multicenter clinical trial. Eur Radiol 12:1104–1113
Slevin NJ, Collins CD, Hastings DL, Waller ML, Johnson RJ, Cowan RA, Birzgalis AR, Farrington WT, Swindell R (1999) The diagnostic value of positron emission tomography (PET) with radiolabelled fluorodeoxyglucose (18F-FDG) in head and neck cancer. J Laryngol Otol 113:548–554
Som PM (1992) Detection of metastasis in cervical lymph nodes: CT and MR criteria and differential diagnosis. AJR Am J Roentgenol 158:961–969
Som PM, Curtin HD, Mancuso AA (1999) An imaging-based classification for the cervical nodes designed as an adjunct to recent clinically based nodal classifications. Arch Otolaryngol Head Neck Surg 125:388–396
Som PM, Curtin HD, Mancuso AA (2000) The new imaging-based classification for describing the location of lymph nodes in the neck with particular regard to cervical lymph nodes in relation to cancer of the larynx. ORL J Otorhinolaryngol Relat Spec 62:186–198
Stadelmann WK, Cobbins L, Lentsch EJ (2004) Incidence of nonlocalization of sentinel lymph nodes using preoperative lymphoscintigraphy in 74 consecutive head and neck melanoma and Merkel cell carcinoma patients. Ann Plast Surg 52:546-9; discussion 550
Steinkamp HJ, Hosten N, Richter C, Schedel H, Felix R (1994a) Enlarged cervical lymph nodes at helical CT. Radiology 191:795–798
Steinkamp HJ, Mäurer J, Cornehl M, Knöbber D, Hettwer H, Felix R (1994b) Recurrent cervical lymphadenopathy: differential diagnosis with color-duplex sonography. Eur Arch Otorhinolaryngol 251:404–409
Stennert E, Kisner D, Jungehuelsing M, Guntinas-Lichius O, Schröder U, Eckel HE, Klussmann JP (2003) High incidence of lymph node metastasis in major salivary gland cancer. Arch Otolaryngol Head Neck Surg 129:720–723
Stern WB, Silver CE, Zeifer BA, Persky MS, Heller KS (1990) Computed tomography of the clinically negative neck. Head Neck 12:109–113
Szmeja Z, Wierzbicka M, Kordylewska M (1999) The value of ultrasound examination in preoperative neck assessment and in early diagnosis of nodal recurrences in the follow-up of patients operated for laryngeal cancer. Eur Arch Otorhinolaryngol 256:415–417
Takes RP, Righi P, Meeuwis CA, et al (1998) The value of ultrasound with ultrasound-guided fine-needle aspiration biopsy compared to computed tomography in the detection of regional metastases in the clinically negative neck. Int J Radiat Oncol Biol Phys 40:1027–1032
Tavin E, Persky M (1996) Metastatic cutaneous squamous cell carcinoma of the head and neck region. Laryngoscope 106:156–158
Terhaard CH, Lubsen H, Van der Tweel I, Hilgers FJ, Eijkenboom WM, Marres HA, Tjho-Heslinga RE, de Jong JM, Roodenburg JL (2004) Salivary gland carcinoma: independent prognostic factors for locoregional control, distant metastases, and overall survival: results of the Dutch head and neck oncology cooperative group. Head Neck 26:681-92; discussion 692-3
Tregnaghi A, De Candia A, Calderone M, Cellini L, Rossi CR, Talenti E, Blandamura S, Borsato S, Muzzio PC, Rubaltelli

L (1997) Ultrasonographic evaluation of superficial lymph node metastases in melanoma. Eur J Radiol 24:216–221

Umeda M, Nishimatsu N, Teranobu O, Shimada K (1998) Criteria for diagnosing lymph node metastasis from squamous cell carcinoma of the oral cavity: a study of the relationship between computed tomographic and histologic findings and outcome. J Oral Maxillofac Surg 56:585-93; discussion 593-5

van den Brekel MW, Castelijns JA, Stel HV, Valk J, Croll GA, Golding RP, Luth WJ, Meyer CJ, Snow GB (1990a) Detection and characterization of metastatic cervical adenopathy by MR imaging: comparison of different MR techniques. J Comput Assist Tomogr 14:581–589

van den Brekel MW, Stel HV, Castelijns JA, Nauta JJ, van der Waal I, Valk J, Meyer CJ, Snow GB (1990b) Cervical lymph node metastasis: assessment of radiologic criteria. Radiology 177:379–384

van den Brekel MW, Castelijns JA, Stel HV, Luth WJ, Valk J, van der Waal I, Snow GB (1991a) Occult metastatic neck disease: detection with US and US-guided fine-needle aspiration cytology. Radiology 180:457–461

van den Brekel MW, Stel HV, Castelijns JA, Croll GJ, Snow GB (1991b) Lymph node staging in patients with clinically negative neck examinations by ultrasound and ultrasound-guided aspiration cytology. Am J Surg 162:362–366

van den Brekel MW, Stel HV, van der Valk P, van der Waal I, Meyer CJ, Snow GB (1992) Micrometastases from squamous cell carcinoma in neck dissection specimens. Eur Arch Otorhinolaryngol 249:349–353

van den Brekel MW, Castelijns JA, Stel HV, Golding RP, Meyer CJ, Snow GB (1993) Modern imaging techniques and ultrasound-guided aspiration cytology for the assessment of neck node metastases: a prospective comparative study. Eur Arch Otorhinolaryngol 250:11–17

van den Brekel MW, Bartelink H, Snow GB (1994) The value of staging of neck nodes in patients treated with radiotherapy. Radiother Oncol 32:193–196

van den Brekel MW, van der Waal I, Meijer CJ, Freeman JL, Castelijns JA, Snow GB (1996) The incidence of micrometastases in neck dissection specimens obtained from elective neck dissections. Laryngoscope 106:987–991

van den Brekel MW, Castelijns JA, Snow GB (1998a) The size of lymph nodes in the neck on sonograms as a radiologic criterion for metastasis: how reliable is it? AJNR Am J Neuroradiol 19:695–700

van den Brekel MW, Pameijer FA, Koops W, Hilgers FJ, Kroon BB, Balm AJ (1998b) Computed tomography for the detection of neck node metastases in melanoma patients. Eur J Surg Oncol 24:51–54

van den Brekel MW, Castelijns JA, Reitsma LC, Leemans CR, van der Waal I, Snow GB (1999a) Outcome of observing the N0 neck using ultrasonographic-guided cytology for follow-up. Arch Otolaryngol Head Neck Surg 125:153–156

van den Brekel MW, Reitsma LC, Quak JJ, Smeele LE, van der Linden JC, Snow GB, Castelijns JA (1999b) Sonographically guided aspiration cytology of neck nodes for selection of treatment and follow-up in patients with N0 head and neck cancer. AJNR Am J Neuroradiol 20:1727–1731

van den Broek GB, Rasch CR, Pameijer FA, Peter E, van den Brekel MW, Tan IB, Schornagel JH, de Bois JA, Zijp LJ, Balm AJ (2004) Pretreatment probability model for predicting outcome after intraarterial chemoradiation for advanced head and neck carcinoma. Cancer 101:1809–1817

Vander Poorten VL, Balm AJ, Hilgers FJ, Tan IB, Loftus-Coll BM, Keus RB, van Leeuwen FE, Hart AA (1999) The development of a prognostic score for patients with parotid carcinoma. Cancer 85:2057–2067

Vander Poorten VL, Balm AJ, Hilgers FJ, Tan IB, Keus RB, Hart AA (2000) Stage as major long term outcome predictor in minor salivary gland carcinoma. Cancer 89:1195–1204

Vassallo P, Wernecke K, Roos N, Peters PE (1992) Differentiation of benign from malignant superficial lymphadenopathy: the role of high-resolution US. Radiology 183:215–220

Vassallo P, Edel G, Roos N, et al (1993) In-vitro high-resolution ultrasonography of benign and malignant lymph nodes: a sonographic-pathologic correlation. Invest Radiol 28:698–705

Voit C, Mayer T, Proebstle TM, et al (2000) Ultrasound-guided fine-needle aspiration cytology in the early detection of melanoma metastases. Cancer 90:186–193

Wagner JD, Park HM, Coleman JJ, Love C, Hayes JT (2000) Cervical sentinel lymph node biopsy for melanomas of the head and neck and upper thorax. Arch Otolaryngol Head Neck Surg 126:313–321

Wang HM, Ng SH, Wang CH, et al (1996) Correlation between computed tomographic density of lymph node metastases and response to cisplatin-based chemotherapy in patients with head and neck squamous cell carcinoma in an area in which betel quid chewing is prevalent. Cancer 78:1972–1979

Weiss MH, Harrison LB, Isaacs RS (1994) Use of decision analysis in planning a management strategy for the stage N0 neck. Arch Otolaryngol Head Neck Surg 120:699–702

Westhofen M (1987) Ultrasound B-scans in the follow-up of head and neck tumors. Head Neck Surg 9:272–278

Woolgar JA, Vaughan ED, Scott J, et al (1994) Pathological findings in clinically false-negative and false-positive neck dissections for oral carcinoma. Ann R Coll Surg Engl 76:237–244

Yamashita Y, Hirai T, Matsukawa T, Ogata I, Takahashi M (1993) Radiological presentations of Castleman's disease. Comput Med Imaging Graph 17:107–117

Yang CY, Andersen PE, Everts EC, Cohen JI (1998) Nodal disease in purely glottic carcinoma: is elective neck treatment worthwhile? Laryngoscope 108:1006–1008

Yousem DM, Som PM, Hackney DB, Schwaibold F, Hendrix RA (1992) Central nodal necrosis and extracapsular neoplastic spread in cervical lymph nodes: MR imaging versus CT. Radiology 182:753–759

Yousem DM, Hatabu H, Hurst RW, Seigerman HM, Montone KT, Weinstein GS, Hayden RE, Goldberg AN, Bigelow DC, Kotapka MJ (1995) Carotid artery invasion by head and neck masses: prediction with MR imaging. Radiology 195:715–720

Yuasa K, Kawazu T, Kunitake N, Uehara S, Omagari J, Yoshiura K, Nakayama E, Kanda S (2000) Sonography for the detection of cervical lymph node metastases among patients with tongue cancer: criteria for early detection and assessment of follow-up examination intervals. AJNR Am J Neuroradiol 21:1127–1132

Yucel T, Saatci I, Sennaroglu L, Cekirge S, Aydingoz U, Kaya S (1997) MR imaging in squamous cell carcinoma of the head and neck with no palpable lymph nodes. Acta Radiol 38:810–814

16 Neck Lymphoma

Frank A. Pameijer and Rick L. M. Haas

CONTENTS

F. A. Pameijer, MD, PhD
Department of Radiology, The Netherlands Cancer Institute-Antoni van Leeuwenhoek Hospital, Plesmanlaan 121, 1066 CX Amsterdam, The Netherlands
and
Department of Radiology, University Medical Center Utrecht, Heidelberglaan 100, 3584 CX Utrecht, The Netherlands
R. L. M. Haas, MD
Department of Radiotherapy, The Netherlands Cancer Institute-Antoni van Leeuwenhoek Hospital, Plesmanlaan 121, 1066 CX Amsterdam, The Netherlands

16.1 Introduction

The most frequent group of neoplasms in the neck is the carcinomas, followed by the lymphomas. Only 5% of all neoplasms in the neck are malignant lymphomas. Lymphomas are neoplasms of the lymphoreticular system. They arise from lymphocytes and their derivates. Hodgkin's lymphoma (HL) and non-Hodgkin's lymphoma (NHL) are the most common malignancies of the hematopoietic system observed in the head and neck. Frequently, lymphoma is not limited to the head and neck region but also involves other parts of the body. This chapter approaches lymphoma as a systemic disease that can manifest itself in many forms in the head and neck. In many instances, the imaging findings are non-specific and tissue sampling remains the mainstay of making the diagnosis. However, some imaging patterns can (strongly) suggest the diagnosis of lymphoma.

16.1.1 Epidemiology

During the period of 1995–1999, the annual incidence rate of lymphomas in the US was 19 cases per 100,000 persons. Rates of lymphomas historically have been about 40% higher in urban counties than in rural counties. The incidence rates of lymphomas in the US tend to exceed those of most other countries. The rapid increase (1%–5% annually) in lymphoma incidence in the 1970s and 1980s has been exceeded

only by the increase in lung cancer in women and malignant melanomas in both sexes. The increase has been seen for males and females, for whites and blacks, and in all age groups (especially over 65 years of age), except for children (Cartwright et al. 1999; Vose et al. 2002).

16.1.2 Aetiology

The majority of lymphomas arise in lymph nodes, but primary extranodal disease now accounts for 20%–30% of all cases. The most frequent primary extranodal sites are the stomach, small intestine, skin, and brain. The incidence of extranodal disease has increased more rapidly than nodal disease.

Immunodeficiency, including both congenital and acquired conditions (especially in patients on immunosuppressive drugs after organ transplantation), is strongly associated with an increased lymphoma risk. Viruses like the Epstein-Barr virus appear to be important co-factors. A history of lymphatic malignancies in close relatives has been repeatedly shown to increase the risk of NHL by two- to three-fold. Lymphomas may also cluster within families, not by an inherited genetic susceptibility, but because of shared environmental determinants (Cartwright et al. 1999; Vose et al. 2002).

16.1.3 Pathology and Classifications

In 1832, Thomas Hodgkin described a disease, "lymphogranulomatosis maligna", that nowadays bears his name. From that moment on new lymphoma subtypes were recognised that closely resembled but were not exactly the disease discovered by Thomas Hodgkin, and were therefore epiphrased as non-Hodgkin's lymphomas (NHL). Since the early 1960s, several pathologists have attempted to produce classification systems in order to clarify the growing group of NHLs. Each new system was a revision of its predecessor adding new concepts and providing new names to the same entities. In 1982 a consensus system called the "Working Formulation" (WF) was produced combining several previous systems; the British National Lymphoma Investigation's Classification, the Rappaport Classification, the Lukes and Collins Classification, the Kiel Classification, the Dorfman Classification and the first World Health Organization (WHO) Classification. The WF lumped all diseases into three groups depending on their clinical behaviour; the low, intermediate and high-grade lymphomas abbreviated as LG-NHL, IG-NHL and HG-NHL.

The combination of several subtypes in just three groups was intended to help the clinician to distinguish lymphomas with more or less the same clinical course and comparable patient management. Soon, this lumping of different diseases into three groups without any biological basis was found to be artificial. In 1994, the WF was replaced by the Revised European-American Classification of Lymphoid Neoplasms, abbreviated as the REAL Classification (Harris et al. 1994). The basis of this system was a better understanding of the putative normal counterparts and their functions within specific sites of a normal lymph node, like the follicles, the germinal centers, and the mantle and marginal zones. The REAL Classification is based on a subdivision in three groups; B-cell neoplasms, T-cell/natural killer (NK)-cell neoplasms and Hodgkin's disease. The WHO Classification (2001) is a further refinement of the REAL system.

Clinicians still tend to communicate in terminology, which is a mixture derived from the WF, the REAL and the WHO systems. Table 16.1 simplifies the four most important lymphoma entities, their nomenclature and their prevalence among the lymphomas (Harris et al. 1994; WHO 2001). The indolent lymphomas are the former LG-NHL, the aggressive lymphomas used to be called IG-NHL or HG-NHL.

16.2 Hodgkin's Lymphoma

Originally, Thomas Hodgkin described in 1832 a disease "lymphogranulomatosis maligna" that afterwards was called Hodgkin's disease. Since the WHO Classification of 2001, this entity is called Hodgkin's lymphoma (HL). Historically, HL is further divided into four subtypes (see also Sect. 16.3; WHO classification 3.2.1–3.2.4):

1. Nodular sclerosis (NS-HL; 40%–60% of all HL)
2. Lymphocyte predominant (LP-HL; ~2% of all HL)
3. Mixed cellularity (MC-HL; 30%–40% of all HL)
4. Lymphocyte depleted (LD-HL; ~5% of all HL)

Most HL patients present in early stages predominantly with lymphadenopathy in the neck and upper mediastinum (see also Sect. 16.7). Extranodal spread in HL is very rare, splenic involvement being the most prevalent. Usually, only patients in advanced stage

disease show organ involvement by HL. In those cases bone marrow infiltration, intrapulmonary spread (either as deposits or as a direct extension from hilar nodes into the lung parenchyma), liver and other organ involvement can be seen. From an imaging point of view, the following aspects should be emphasised:

- Neck nodes involved by HL usually have the same appearance as other lymphadenopathies. Sometimes, the imaging presentation is more characteristic and the diagnosis of lymphoma can be suggested by the radiologist (see Table 16.5).
- NS-HL poses a problem in terms of response assessment after therapy. Histologically, the malignant component of HL is embedded in a large amount of fibrous tissues (hence the name "sclerosis"). Frequently, residual masses are seen on imaging studies of the neck (and mediastinum) after successful treatment of NS-HL. These masses, though diagnosed as "partial response" on imaging do not necessarily contain viable lymphoma. For those cases the term CRu (complete response unconfirmed, see also Sect. 16.6) is designated (Cheson et al. 1999). Both gallium-67-citrate scintigraphy and 18-fluoro-deoxy-glucose positron emission tomography (FDG-PET) may help to decide on further treatment or not. However, the clinician will try to rebiopsy these CRu nodes, which may pose a problem in mediastinal disease.

16.3 Non-Hodgkin's Lymphomas (NHL) and Specific Entities

Worldwide, the incidence of NHL is about 5–10 times higher than the incidence of HL, largely dependent on regional differences. Of all cases of NHL, 80% is of B-cell origin and 20% is T-cell derived (Cartwright et al. 1999; Vose et al. 2002). The WHO Classification (Harris et al. 2000) of lymphoid neoplasms describes the following diseases:

1 **B-Cell neoplasms**
1.1 Precursor B-cell neoplasm
1.1.1 Precursor B-lymphoblastic leukemia/lymphoma (precursor B-cell acute lymphoblastic leukemia)
1.2 Mature (peripheral) B-cell neoplasms
1.2.1 B-cell chronic lymphocytic leukemia/small lymphocytic lymphoma
1.2.2 B-cell prolymphocytic leukemia
1.2.3 Lymphoplasmacytic lymphoma
1.2.4 Splenic marginal zone B-cell lymphoma (+/- villous lymphocytes)
1.2.5 Hairy cell leukemia
1.2.6 Plasma cell myeloma/plasmacytoma
1.2.7 Extranodal marginal zone B-cell lymphoma of mucosa associated lymphoid tissues (MALT) type
1.2.8 Nodal marginal zone B-cell lymphoma (+/- monocytoid B cells)
1.2.9 Follicular lymphoma
1.2.10 Mantle-cell lymphoma
1.2.11 Diffuse large B-cell lymphoma
1.2.12 Mediastinal large B-cell lymphoma
1.2.13 Primary effusion lymphoma
1.2.14 Burkitt's lymphoma/Burkitt cell leukemia

2 **T-cell and NK-cell neoplasms**
2.1 Precursor T-cell neoplasm
2.1.1 Precursor T-lymphoblastic lymphoma/leukemia (precursor T-cell acute lymphoblastic leukemia)
2.2 Mature (peripheral) T-cell neoplasms
2.2.1 T-cell prolymphocytic leukaemia
2.2.2 T-cell granular lymphocytic leukemia
2.2.3 Aggressive NK-cell leukemia
2.2.4 Adult T-cell lymphoma/leukemia (HTLV1+)
2.2.5 Extranodal NK-/T-cell lymphoma, nasal type
2.2.6 Enteropathy-type T-cell lymphoma
2.2.7 Hepatosplenic gamma-delta T-cell lymphoma
2.2.8 Subcutaneous panniculitis-like T-cell lymphoma
2.2.9 Mycosis fungoides/Sezary syndrome
2.2.10 Anaplastic large-cell lymphoma, T-/null-cell, primary cutaneous type
2.2.11 Peripheral T-cell lymphoma, not otherwise characterized
2.2.12 Angioimmunoblastic T-cell lymphoma
2.2.13 Anaplastic large-cell lymphoma, T-/null-cell, primary systemic type

3 **Hodgkin's lymphoma (Hodgkin's disease)**
3.1 Nodular lymphocyte-predominant Hodgkin's lymphoma
3.2 Classical Hodgkin's lymphoma
3.2.1 Nodular sclerosis Hodgkin's lymphoma (grades 1 and 2)
3.2.2 Lymphocyte-rich classical Hodgkin's lymphoma
3.2.3 Mixed cellularity Hodgkin's lymphoma
3.2.4 Lymphocyte depletion Hodgkin's lymphoma

Note: The follicular (1.2.9) and diffuse large B-cell lymphomas (1.2.11) make up more than half of all lymphomas diagnosed (see also Table 16.1).

Table 16.1. Nomenclature and prevalence of the four most important lymphoma entities

Official name from the WHO Classification (abbreviation)	Synonyms	Malignancy grade	Prevalence among the lymphomas
Diffuse large B-cell lymphoma (DLBCL)	DLCL	Intermediate-grade NHL	30%–40%
Follicular lymphoma (FL)	Follicle center cell lymphoma (FCC) Follicular centricity (cc) Follicular centrocytic/centroblastic (cc/cb)	Low-grade NHL	15%–25%
Marginal zone lymphoma of MALT type (MZL)	MALT lymphoma, maltoma	Low-grade NHL	~10%
Mantle cell lymphoma (MCL)	(Relatively newly recognised entity)	Intermediate-grade NHL	~5%

16.4 Work-Up

The work-up of a patient with lymphoma requires a multidisciplinary approach involving close co-operation among the (head and neck) surgeon, the radiation oncologist, the pathologist, the medical oncologist or haematologist-oncologist and the radiologist.

16.4.1 Diagnosis

The diagnostic process to fully document new lymphoma patients, whether or not localized in the neck, comprises the following minimum requirements:

- Full history (including presence of fever, night-sweats and weight-loss; the so-called B-symptoms) and physical examination with emphasis on all peripheral lymph node regions (neck, axilla and groin), examination of Waldeyer's ring, liver, spleen and skin.
- Full blood count including a differential count of the leukocytes.
- Representative excision biopsy of an entire enlarged lymph node (in nodal disease).
- Bone marrow biopsy.
- Imaging of all lymphatic regions.

16.4.2 Initial Imaging

Standard radiological work-up of a newly diagnosed patient with head and neck lymphoma should include:

- Posteroanterior and lateral chest X-ray.
- Contrast-enhanced (CE) computed tomography (CT) of the neck, chest, abdomen and pelvis.
- Ultrasound (US) of the neck may be useful as an adjunct study.
- Magnetic resonance imaging (MRI) may substitute CECT of the neck, especially if Waldeyer's ring is involved or extranodal head and neck disease is present.

This imaging strategy is usually sufficient to stage a lymphoma patient. In addition, physiologic studies can be performed by nuclear medicine techniques such as gallium-67 or thallium-201 scintigraphy and FDG-PET (Front and Israel 1995; Van Amsterdam et al. 1996; Jerusalem et al. 2001; Moog et al. 1997; Haas et al. 2003). The use of these metabolic techniques may be the most accurate way to stage indeterminate nodes. CT and MRI have completely replaced lymphangiography as a diagnostic tool in lymphoma patients.

16.4.3 Staging

Designed for Hodgkin's lymphoma the Ann-Arbor system is now used for staging all lymphomas (Table 16.2). The system was slightly modified after the Cotswold Convention (Smithers 1971; Lister et al. 1989).

16.5 Treatment

Management of lymphomas is very diverse and depends fully on the specific lymphoma subtype, the stage in which the patient is diagnosed, co-morbidity, the performance status and biological age of the patient. As a concept, lymphoma patients can be treated by chemotherapy, radiotherapy and immunotherapy, and usually in a combined modality approach.

Some frequently applied regimens are the following:

Table 16.2. Ann Arbor Staging system for Hodgkin's Lymphoma

Stage	Description
I	Involvement of a single lymph node region
II	II = Involvement of more than one lymphatic region on only one side of the diaphragm IIE = Localized involvement of one extralymphatic organ or site and its regional lymph nodes with or without other nodes on the same side of the diaphragm IIS = Involvement of more than one lymphatic region on only one side of the diaphragm plus involvement of the spleen IIES = Both
III	III = Involvement of lymph node regions on both sides of the diaphragm IIIE = Involvement of lymph node regions on both sides of the diaphragm plus localized involvement of an extralymphatic organ or site IIIS = Involvement of lymph node regions on both sides of the diaphragm plus involvement of the spleen IIIES = Both
IV	Diffuse or disseminated involvement of one or more extralymphatic organs or tissues with or without associated lymph node enlargement. Organs considered distant include liver, bone, bone marrow, lung and/or pleura, and kidney
	Suffices to each stage: A Without symptoms; e.g. stage IA, or stage IIIA B With symptoms (night sweats, unexplained fever >38°C, unexplained weight loss >10%, within last 6 months); e.g. stage IIB, or stage IVB

- Chemotherapy, single agent: Chlorambucil (oral), Cyclophosphamide (oral), Fludarabin (oral and iv.): in case of indolent lymphomas, predominantly follicular lymphoma.
- Chemotherapy, multi- agent: CVP (= COP), Chlorambucil + Vincristine (=Oncovin) + prednisone in case of indolent lymphomas, CHOP (+/– Rituxan; CHOP = COP + Adriamycin), DHAP (Dexamethasone + high dose Ara-C + Cisplatin), VIM [VP-16 (= Etoposide) + Ifosphamide + Mesna] in case of aggressive lymphomas, predominantly DLCL, BEAM (BCNU + Etoposide + Ara-C + Melphalan) as a conditioning regimen before stem cell transplantations for aggressive lymphomas, ABVD (Adriamycin + Bleomycin + Vinblastin + Dacarbazine), MOPP (Mitoxin + Oncovin + Procarbazin + Prednisone), MOPP-ABV for Hodgkin's lymphoma.
- IF-RT (= involved field radiotherapy): all lymphomas; irradiation on the affected site only, no prophylactic irradiation to adjacent areas (Fig. 16.1).
- EF-RT (= extended field radiotherapy): all lymphomas; irradiation on the affected site plus prophylactic irradiation to adjacent areas.
- [S]TNI = [sub]total nodal irradiation: Hodgkin's lymphoma; irradiation of patient with contraindications for chemotherapy.
- Combined modality regimens: 3–4 × CHOP + IF-RT: aggressive lymphomas, predominantly DLCL in stage I or II, 3–4 × ABVD + IF-RT: Hodgkin's lymphoma, stage I or II.

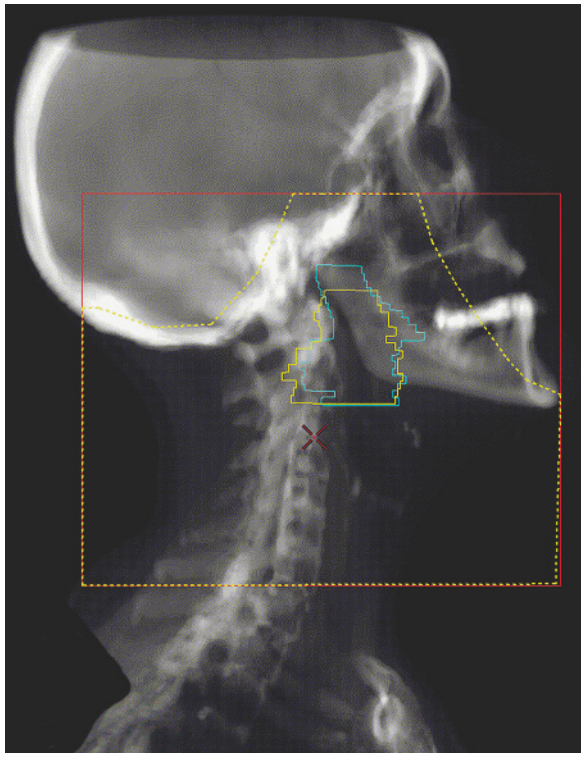

Fig. 16.1. Involved field radiotherapy (IF-RT). IF-RT planning of a patient with grossly enlarged tonsils due to NHL involvement (left tonsil delineated in *blue*, right tonsil in *yellow*). Total radiation volume for this treatment consist of Waldeyer's ring (both tonsils, base of tongue and nasopharyngeal adenoid) together with the occipital lymph nodes and the nodes in level I, II and III (*dashed yellow line*). The *red line* indicates the machine collimator

16.6 Response Assessment

In principle, all imaging studies performed in the initial staging process will be repeated after completion of treatment. Imaging during treatment may also be indicated to decide on further management.

In haematology, response is assessed by the "Cheson criteria" (Cheson et al. 1999). This applies also to response evaluation in head and neck lymphoma. This is in contrast to response assessment in solid tumors, such as carcinomas and sarcomas, for which the RECIST criteria are used (Therasse et al. 2000).

The differences between the Cheson and RECIST criteria, are summarized in Table 16.3 for haematology and Table 16.4 for solid tumors.

16.7 Nodal Disease

Per definition, this is lymphatic malignancy occurring in pre-existing nodal chains (in the head and neck). In hematology, lymph nodes are typically involved by contiguous spread. This is in contrast to solid tumors (i.e. squamous cell carcinoma of the head and neck) where specific lymph node groups are at a higher risk for metastatic involvement based on the preferential lymphatic drainage from the primary tumor site.

16.7.1 The Common Sites

For all imaging modalities depicting nodal disease, including US, CT and MRI, the cervical lymph nodes are described in terms of levels (Som et al. 2000; UICC 1997). In head and neck nodal disease, levels I, II, III, IV and V are most frequently involved (Fig. 16.2).

In clinically suspected neck adenopathy, US may be helpful because it can be used to guide fine needle aspiration cytology (FNAC). An experienced cytopathologist can reliably diagnose lymphoid lesions from FNAC smears, especially in the differential diagnosis from carcinomas. CT and MRI are better equipped for local tumor mapping and staging.

For practical purposes, nodal involvement with HL cannot be exclusively differentiated from nodes with NHL whatever imaging modality is used. In the head and neck, both entities typically present with multiple, uni- or bilateral non-necrotic enlarged lymph nodes involving usual and unusual nodal chains. However, certain imaging features are more characteristic for HL than for NHL.

General features in favour of Hodgkin lymphoma nodes:

- HL presents in lymph nodes in about 98% of cases. When multiple nodes are present, the involved nodal groups are contiguous in about 90% of cases. This suggests a unifocal origin of the disease and subsequent dissemination through lymphatic pathways.

Table 16.4. Overall responses for all possible combinations of tumor responses in target and non-target lesions with or without the appearance of new lesions; the RECIST criteria

Target lesions	Non-target lesions	New lesions	Overall response
CR	CR	No	CR
CR	Incomplete response /SD	No	PR
PR	Non-PD	No	PR
SD	Non-PD	No	SD
PD	Any	Yes or no	PD
Any	PD	Yes or no	PD
Any	Any	Yes	PD

CR, complete response; *PR*, partial response; *SD*, stable disease; *PD*, progressive disease.

Table 16.3. Response criteria for non-Hodgkin's lymphomas; the Cheson criteria

Response category	Physical examination	Lymph nodes	Lymph node masses	Bone marrow
CR	Normal	Normal	Normal	Normal
Cru	Normal	Normal	Normal	Indeterminate
	Normal	Normal	> 75% Decrease	Normal or indeterminate
PR	Normal	Normal	Normal	Positive
	Normal	≥ 50% Decrease	≥ 50% Decrease	Irrelevant
	Decrease in liver/spleen	≥ 50% decrease	≥ 50% decrease	Irrelevant
SD	Does not fulfill any of the criteria above or below			
Relapse/progression (PD)	Enlarging liver/spleen; new sites	New or increased	New or increased	Reappearance

CR, complete response; *Cru*, complete response unconfirmed; *PR*, partial response; *SD*, stable disease; *PD*, progressive disease (or relapse).

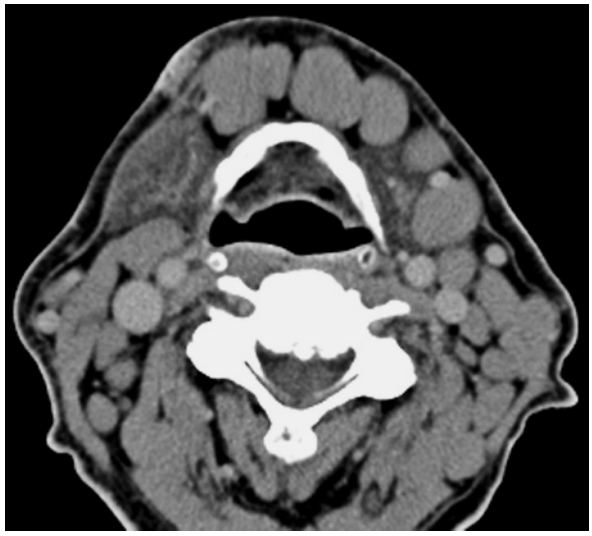

a

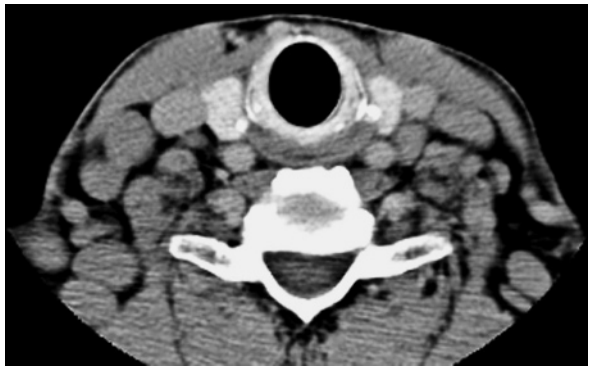

b

Fig. 16.2a,b. Nodal B-NHL. Axial contrast-enhanced CT shows bilateral enlarged level I–V cervical nodes without central necrosis

- Levels III and IV most frequently involved.
- Combination with mediastinal lymphadenopathy is frequent.
- Involvement of extranodal sites such as Waldeyer's ring is uncommon.

General features in favor of non-Hodgkin's lymphoma nodes:

- NHL presents in a generalized fashion (including bone marrow infiltration) much more often than HL.
- Levels II, III and IV often involved.
- NHL often extranodal, both Waldeyer's ring (extranodal lymphatic) as well as extranodal extralymphatic (orbit, salivary glands, sinonasal, etc.).

Specific lymph node imaging features for US, CT and MRI are shown in Table 16.5.

Note: A minority of patients has enlarged lymph nodes with central necrosis on cross-sectional imaging. This imaging pattern is much more frequently seen in patients with head and neck squamous cell cancer. Central necrosis in lymphoma patients usually indicates a higher malignancy grade.

16.7.2 The Uncommon Sites

Manifestations of nodal disease may also be seen in more uncommon sites including pre-tracheal nodes

Table 16.5. Lymph node imaging features on US, CT and MRI for Hodgkin's and non-Hodgkin's lymphoma. For comparison, imaging features for squamous cell carcinoma nodes haven been added. [Adapted from Harnsberger (2004)]

Imaging features	Hodgkin's lymphoma	Non-Hodgkin's lymphoma	Squamous cell carcinoma
US	Well-defined enlarged round nodes with homogeneous appearance	Diffuse homogeneous decreased echogenicity characteristic	Round nodes with loss of hilar echogenicity
CT	Lobulated round nodal masses with variable enhancement. Central necrosis may be present. Calcification (pre-treatment) uncommon	Multiple bilateral ovoid masses in multiple nodal chains. Variable enhancement ranging from isodense to muscle to strong enhancement. Central necrosis may be present. Enhancement pattern may vary within same patient	Diffuse or rim-enhancement of nodes. Central necrosis is typical
MRI	T1WI: enlarged round iso- to hypointense nodes T2WI: Nodes are hyperintense to muscle T1 C+: variable: see CT	T1WI: enlarged nodes isointense to muscle T2WI: Nodes are hyperintense to muscle T1 C+: variable: see CT	T1WI: isointense to muscle; necrosis seen as hypointense focus T2WI: Hyperintense; necrosis shows focal marked hyperintensity T1 C+: inhomogeneous

C+, contrast enhancement

(level VI) and retropharyngeal nodes. Other nodal sites, not included in the UICC nodal classification, include occipital, facial, buccal, peri-parotid, and intraparotid lymph nodes. All these nodes may be sites of origin of lymphoma (Mancuso 1998). There are no differences in imaging appearance between these nodal groups and the level I–V nodes discussed above (Table 16.5).

16.8 Extranodal Disease

Per definition, this is lymphatic malignancy occurring outside pre-existing nodal chains. Extranodal lymphoma can be separated in extranodal lymphatic and extranodal extralymphatic disease (Hermans 2004). Extranodal areas predisposed to develop lymphoma are sites that are normally rich in lymphoid tissue such as Waldeyer's ring (extranodal lymphatic disease). Extranodal extralymphatic sites include the orbit, parotid gland, nasal cavity, paranasal sinuses, as well as the thyroid gland. Although anatomically in close proximity, lymphomas arising in these sites have distinct clinical characteristics. Factors that appear to influence the disease pattern include concurrent conditions, such as Sjögren's syndrome, and geographic factors particularly concerning sinonasal lymphomas (see also Sect. 16.8.4).

Patients with extranodal Hodgkin's lymphoma usually present with a painless mass or complain of systemic symptoms such as night sweats, fever, and weight loss. Whereas the clinical presentation of patients with extranodal NHL in the head and neck often mimic those of patients with squamous cell carcinoma (SCC) arising at the same site. Approximately 10% of patients with NHL present with extranodal primary lesions in the head and neck.

The treatment and prognosis of patients with head and neck lymphoma depends on the pathological subtype of disease and extent of involvement at time of presentation. The most common lymphoma is the diffuse large B-cell lymphoma (65%) in an early stage at presentation. In the parotid gland, however, the indolent histologies (marginal zone lymphoma and follicular lymphoma) prevail. Predominantly patients between 50 and 60 years of age are affected. The male to female ratio is 1.6:1, with the exception of lymphomas of the salivary glands, orbit and thyroid, which occur equally or more frequently in women.

The imaging findings of extranodal head and neck lymphomas are essentially the same as those found in SCC. In 80% of patients with primary extranodal NHL in the head and neck, additional nodal involvement is present. If a primary lesion is associated with large, homogeneously enhancing lymph nodes without central necrosis, the possibility of lymphoma may be suggested. However, this combination of imaging findings may also be encountered in SCC. Therefore, the diagnosis of lymphoma remains based on histologic tissue examination.

16.8.1 Waldeyer's Ring and the Upper Aerodigestive Tract

Waldeyer's ring comprises the lymphoid tissues located superiorly in the nasopharynx, laterally in both tonsillar fossae and inferiorly in the base of tongue. More than half of extranodal head and neck lymphomas occur in Waldeyer's ring, the tonsil being the most prevalent subsite (40%–50% of cases). All subtypes of NHL can be found in Waldeyer's ring, but deposits of Hodgkin's lymphoma are rare (Yuen and Jacobs 1999; Hanna et al. 1997; Aloulou et al. 2002).

16.8.1.1 Nasopharynx

Patients with nasopharyngeal NHL may present with intermittent hearing loss secondary to unilateral or bilateral Eustachian tube obstruction or may have persistent epistaxis or nasal obstruction. Imaging of nasopharyngeal NHL shows two morphological types: a circumscribed, bulky, mucosa-based mass that has not invaded the deep structures around the pharynx (Fig. 16.3), and a mass with a much more

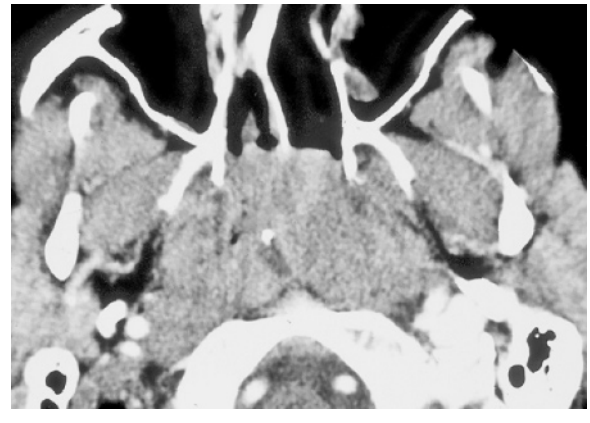

Fig. 16.3. Nasopharyngeal NHL. Axial contrast-enhanced CT shows a bulky mucosal mass filling the nasopharyngeal lumen and extending bilaterally into the choanae. Note: the parapharyngeal fat is intact and there is no bony invasion of the clivus

infiltrative spread pattern. The latter type of primary nasopharyngeal lymphoma may invade the skull base and spread along nerves in a manner similar to that of SCC (King et al. 2003). Both diseases are commonly associated with cervical adenopathy.

In children and adolescents nasopharyngeal lymphoid tissue is prominent. These so-called "adenoids", or nasopharyngeal tonsils are located in the roof of the nasopharynx. Such tissue should not be mistaken as an abnormal mass. Normal lymphoid tissues show uniform enhancement after contrast medium injection and, on MRI, display a typical high signal intensity without invasion of adjacent structures.

16.8.1.2 Tonsillar Fossa

Patients with NHL of the tonsil usually have a unilateral sore throat or obstructive symptoms. Clinically, especially in younger patients, these lesions are difficult to differentiate from reactive hypertrophy. Frequently the diagnosis of NHL is delayed while patients are treated with prolonged courses of antibiotics or even with incision for a suspected tonsillar abscess.

Hermans et al. (1994) described two patterns of tonsillar involvement:

a) Involvement of only the tonsillar fossa. Imaging in these cases shows a unilateral or bilateral enlarged tonsil (Fig. 16.4), without infiltration of surrounding tissues.
b) Tonsillar involvement with extension to the pharyngeal wall. In this subgroup, two types of extension have been described. An infiltrating growth pattern, in which there is extension in the parapharyngeal fat plane and into the extrapharyngeal deep core tissues (masticator space, parotid space etc.). This pattern mimics the growth pattern of carcinomas. The other subtype in this group consists of an exophytic pattern of growth in which the tumor stayed inside the pharyngeal walls but extended outside of the tonsillar margins expanding into the oral cavity (Fig. 16.5). Complete circumferential thickening of the pharyngeal wall without deep infiltration has been reported as quite specific for lymphoma (Hermans et al. 1994).

The signal intensity on T2-weighted, T1-weighted and T1-weighted contrast-enhanced MRI images is as a rule homogeneous and similar to that of normal tonsils. Large tumors can be mildly heterogeneous showing small foci of necrosis. Lymphadenopathy in the ipsilateral upper internal jugular chain can be seen and in those cases, the nodes will be of similar signal intensity to the primary tumor (Fig. 16.4). In 20% of tonsillar NHL gastrointestinal involvement can be diagnosed simultaneously (Hanna et al. 1997).

16.8.1.3 Base of Tongue

Patients with lymphoma in the base of tongue may have obstructive symptoms, sore throat, and occasionally dysphagia or a change in voice. Clinically, these lesions are often submucosal, bulging and soft on palpation. As mentioned, the high concentration of lymphoid tissue in the base of tongue (tonsilla lingualis) predisposes this site to develop lymphoma. The typical imaging appearance on CT (Fig. 16.6) or MRI is a bulky, exophytic mass centered in the tongue base. Enhancement pattern and signal intensities are identical to tonsillar NHL.

16.8.1.4 Larynx

Laryngeal involvement with NHL is very rare. Laryngeal lymphomas tend to have a large submucosal component most frequently centered in the supraglottis. The imaging characteristics are non-specific and comparable to SCC. Multiple lesions strongly suggest the diagnosis of NHL (Hermans et al. 1994). In addition, a laryngeal tumor with a large supraglottic submucosal component (Fig. 16.7) should alert the radiologist to the possibility of NHL (King et al. 2004).

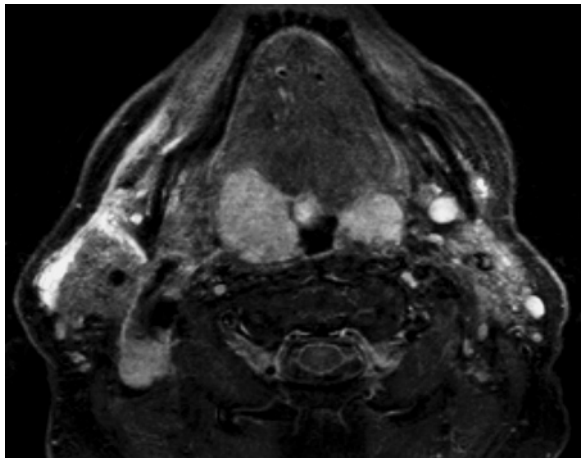

Fig. 16.4. Tonsillar NHL. Axial T2-weighted sequence (TIRM) demonstrates bilateral high signal intensity (SI) soft-tissue masses in the tonsil. Note that there is no invasion of the surrounding deep-tissue planes. There is an associated enlarged level II lymph node on the right with the same high SI appearance

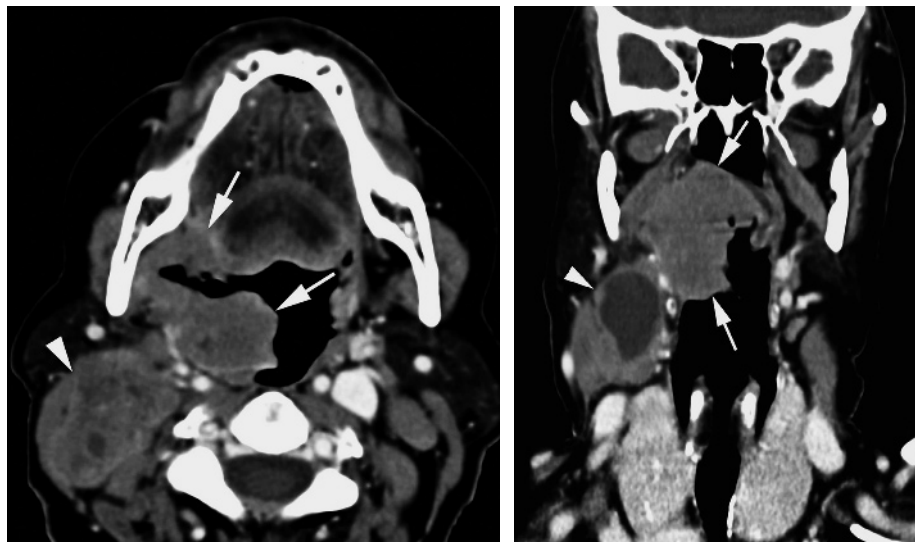

Fig. 16.5a,b. Tonsillar NHL. Contrast-enhanced multislice CT images. (**a**) Axial contrast-enhanced CT shows a soft-tissue mass situated in the right tonsil (*arrows*). There is anterior extension (within the pharyngeal wall) along the glossotonsillar sulcus with slight displacement of the right tongue base. A grossly enlarged lymph node is present in level II (*arrowhead*). (**b**) Coronal reformatting shows the medial extension of the mass (*arrows*) with involvement of the soft palate. The level II lymph node contains a large area of central necrosis (*arrowhead*). (Courtesy of R. Hermans, MD, PhD, Leuven, Belgium)

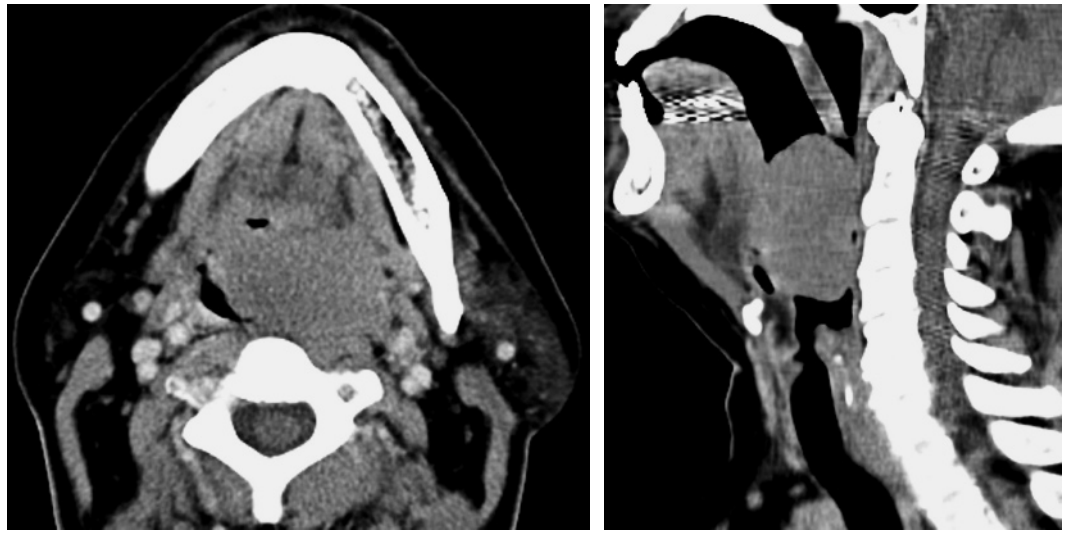

Fig. 16.6a,b. Base of tongue NHL. A female patient with dysphagia. Contrast-enhanced multislice CT images. (**a**) Axial contrast-enhanced CT shows a large homogeneously enhancing mass centered in the left base of tongue. Note that there is no invasion of the surrounding deep-tissue planes. (**b**) Sagittal reformatting demonstrating the exophytic nature of the mass

16.8.2 Orbit

There are a variety of tumors and tumor-like lesions in the orbit, both benign and malignant. In an unselected series of 1264 orbital lesions, 810 (64%) were benign and 454 (36%) were malignant. The percentage of malignant lesions was 20% in children, 27% in young adults and middle-aged patients, and 58% in older patents (age range, 60–92 years). Lymphoma was the most common malignancy in older patients, representing 10% of cases (Shields et al. 2004). Lymphoid tumors of the orbit in children are extremely rare.

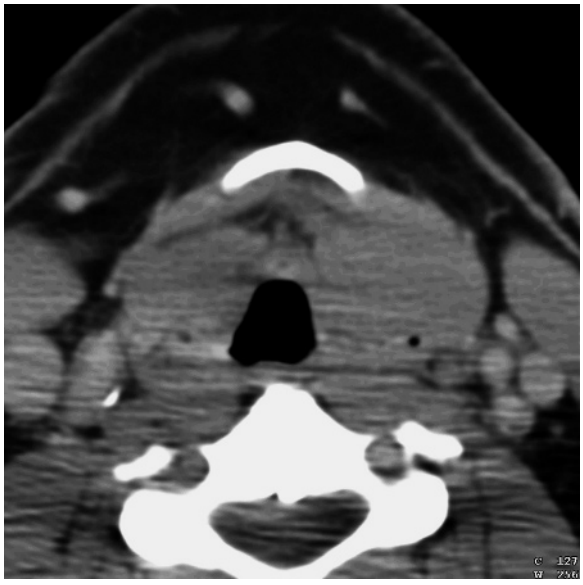

Fig. 16.7. Laryngeal NHL. Axial contrast-enhanced CT image at the lower border of the hyoid bone shows bilateral large submucosal masses. (Courtesy of I.M. Schmalfuss, MD, Gainesville, Florida)

Besides malignant lymphoma, a spectrum of less malignant lymphoid orbital tumors exists ranging from the benign pseudolymphoma or pseudotumor to the reactive and atypical lymphoid hyperplasia. These two latter entities mimic orbital lymphoma, both from an imaging and from a histological point of view. The incidence of idiopathic inflammatory pseudotumor and lymphoid tumors seems to be equal (Yan et al. 2004). Any orbital tissue or combination of tissues may be involved in malignant lymphoma, as well as the less malignant lymphoid orbital tumors.

Anatomically, true lymphoid tissue is found in the subconjunctival and lacrimal glands, predisposing these sites for development of lymphoma. Orbital lymphomas can be subdivided into three groups; conjunctival, lacrimal, and intra-orbital (true intraocular lymphomas are very rare). Orbital lymphomas are mostly indolent, low-grade lesions. Marginal zone lymphoma (MZL), synonym MALT lymphoma, followed by follicular lymphoma is the most prevalent diagnosis (Lee et al. 2005). If MZL is diagnosed, special attention should be focused to the other MZL-prevalent sites like the salivary glands, Waldeyer's ring and the stomach.

Treatment of orbital lymphomas is moderate dose irradiation (25–30 Gy) to the entire orbit with over 90% of local control (Pfeffer et al. 2004; Agulnik et al. 2001).

For imaging of the orbit, both US, CT and MRI can be used.

16.8.2.1 Conjunctiva

Patients with lymphoma arising in the conjunctiva complain of local irritation, itching, ptosis, or the sensation of a mass. Imaging shows unilateral or bilateral symmetrical swelling of the conjunctival tissues. These are smooth, sharply marginated ovoid lesion that show moderate to strong enhancement (Fig. 16.8). In case of conjunctival involvement, differentiation has to be made from preseptal cellulitis, which is usually unilateral, and of sinonasal origin; preseptal pseudotumor is rare (Hermans et al. 1994).

16.8.2.2 Intra-orbital Lymphoma

Painless proptosis, diplopia and visual disturbance are the common presenting symptoms of patients with intraorbital lymphoma. On imaging, orbital lymphomas are homogeneous usually sharply marginated intra- or para-conal masses that occur most often in the anterior portion of the orbit, the retrobulbar area (Fig. 16.9), or in the superior orbital compartment. Mild to moderate enhancement is usually present. Based on the imaging findings alone, there is a differential diagnosis for these types of lesions including malignant lymphoma, pseudotumor, reactive hyperplasia, lacrimal gland tumors, optic nerve tumors and Graves' orbitopathy. This differential can be narrowed when the imaging features are interpreted in conjunction with the clinical signs and symptoms. A somewhat characteristic feature of orbital lymphoid tumors is the tendency to mold themselves around intraorbital structures without (bony) destruction (Fig. 16.9).

16.8.2.3 Lacrimal Gland

Lacrimal gland lymphoma may present with epiphora or as a painless mass noticed for cosmetic reasons. If lymphoma is restricted to the gland itself, the lesion is characteristically located in the superolateral orbital compartment. Cross-sectional imaging shows smooth, unilateral or bilateral (Fig. 16.10), enlargement of the lacrimal gland. If the gland is grossly enlarged, medial and forward displacement of the globe is the clue to the primary location.

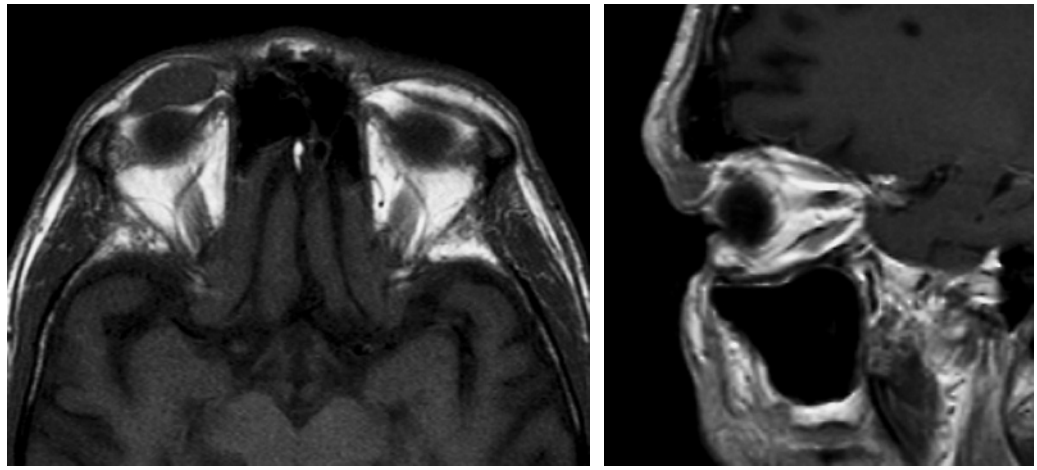

Fig. 16.8a,b. Conjunctival NHL. T1-weighted MR images. (**a**) Axial image at the cranial margin of the orbit shows an ovoid, sharply marginated, lesion located anterior to the right globe. (**b**) Post-contrast sagittal image showing mild homogenous enhancement of the mass located in the upper eyelid

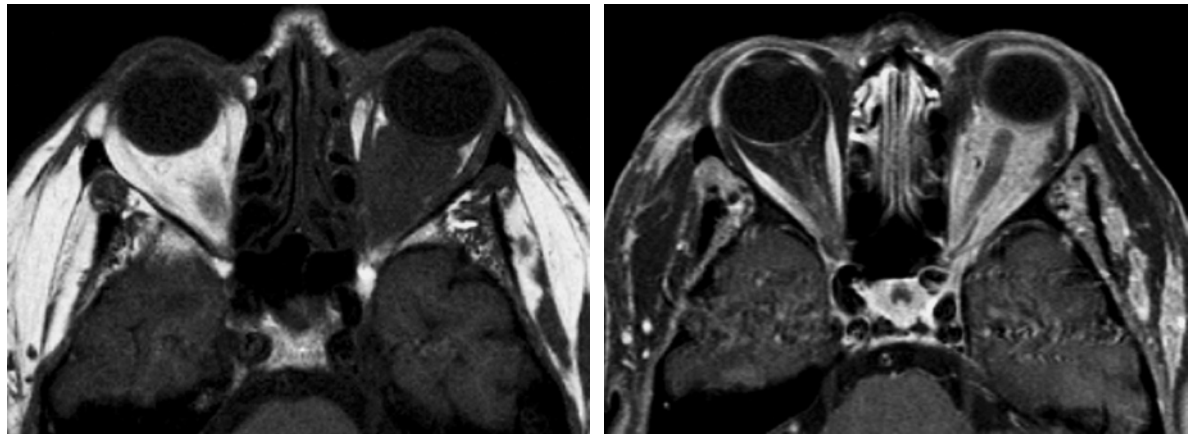

Fig. 16.9a,b. Intra-orbital NHL. T1-weighted axial MR images. (**a**) Non-enhanced image at the level of the optic nerve shows diffuse infiltration of the intraconal space of the left orbit. (**b**) Post-contrast fat-suppressed image showing moderate homogeneous enhancement of the intraconal mass. Note that the lesion is 'molding' around the optic nerve

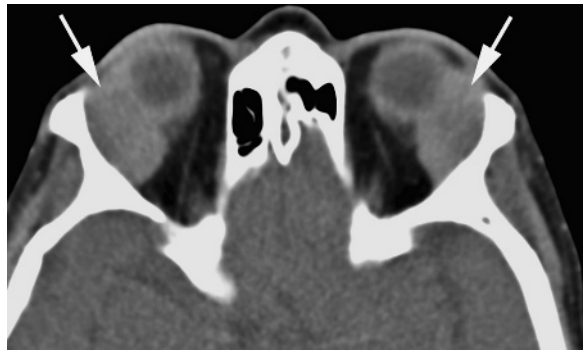

Fig. 16.10. Lacrimal gland NHL. Axial contrast-enhanced CT image through the superior parts of the orbits shows symmetric enlargement of both lacrimal glands (*arrows*). There is mild medial and forward displacement of the globes. (Courtesy of R. Hermans, MD, PhD, Leuven, Belgium)

16.8.3 Salivary Glands

Primary lymphoma of the salivary glands is an uncommon tumor. The parotid gland is affected most often (80% of reported cases) followed by the submandibular gland (20%). There are only isolated reports of primary lymphoma in minor salivary glands; sites most commonly involved include the palate and gingiva.

16.8.3.1 Parotid Gland

Lymphoma of the parotid gland may arise within the parotid parenchyma (primary) or within the intraparotid lymph nodes (secondary).

Primary lymphoma of the parotid gland is rare, accounting for less than 5% of parotid tumors. These lymphomas are classified as MALT lymphomas (see also Table 16.1). These low-grade lymphomas may involve any portion of the gastrointestinal tract where lymphoid tissue is part of the mucosal defence system. Lymphoid tissue is normally present in the parotid gland and absent in the (adult) submandibular and sublingual gland. When MALT lymphoma occurs in the salivary gland, as in other extranodal sites such as the stomach, it is usually an indolent neoplasm that tends to remain localized for long periods of time (Abbondanzo 2001; Palacios et al. 2004; Tonami et al. 2002; Tonami et al. 2003; Yuen and Jacobs 1999). Patients with primary lymphoma of the parotid gland typically present with a painless parotid-region mass or with parotitis with progressive enlargement of the gland. After systemic work-up most patients are found to have early stage localized disease; i.e. Stage IIE (see also Table 16.2).

Patients with Sjögren's syndrome have an increased risk of developing primary parotid lymphoma. Sjögren's syndrome, or sicca syndrome, is an autoimmune disease characterized by keratoconjunctivitis sicca, dryness of mucous membranes, telangiectasias of the face, and bilateral parotid enlargement (Fig. 16.11). The syndrome is often associated with rheumatoid arthritis and Raynaud's phenomenon. The risk of lymphoma in these patients has been estimated to be approximately 44 times the incidence expected in a generally healthy population (Yuen and Jacobs 1999). It may affect any area of the head and neck but may have its first manifestations in the parotid gland. Often these patients are scanned to survey for the possibility of lymphoma.

Lymphoma may also involve the salivary glands (usually parotid) secondary to systemic lymphoma. This secondary involvement is usually not classified as MALT lymphoma, but is more commonly a diffuse large cell lymphoma.

For imaging of (suspected) salivary gland tumors US, CT as well as MRI can be used. Due to their superficial position, the parotid, the submandibular, and the sublingual glands can be imaged with high-resolution US transducers (Gritzmann et al. 2003). This is especially helpful in the diagnostic phase because US can be used to perform fine needle aspiration cytology.

Cross-sectional techniques are better equipped for local tumor mapping and staging purposes. On CT, primary lymphoma is characterized by, partial or total, replacement of the parotid gland by an infiltrating soft tissue mass (Fig. 16.11). Multiple solid, intraparotid masses are suggestive of secondary lymphoma (Fig. 16.12). These enlarged intraparotid lymph nodes are usually sharply marginated round to ovoid lesions with homogeneous attenuation. However, nodal necrosis can occur.

On MRI, primary and secondary lymphoma are characterized by homogeneous intermediate signal intensity (SI) on all imaging sequences. There is also a tendency to 'fade' into the SI of the parotid gland on T2-weighted and contrast-enhanced, fat-suppressed T1-weighted MR images.

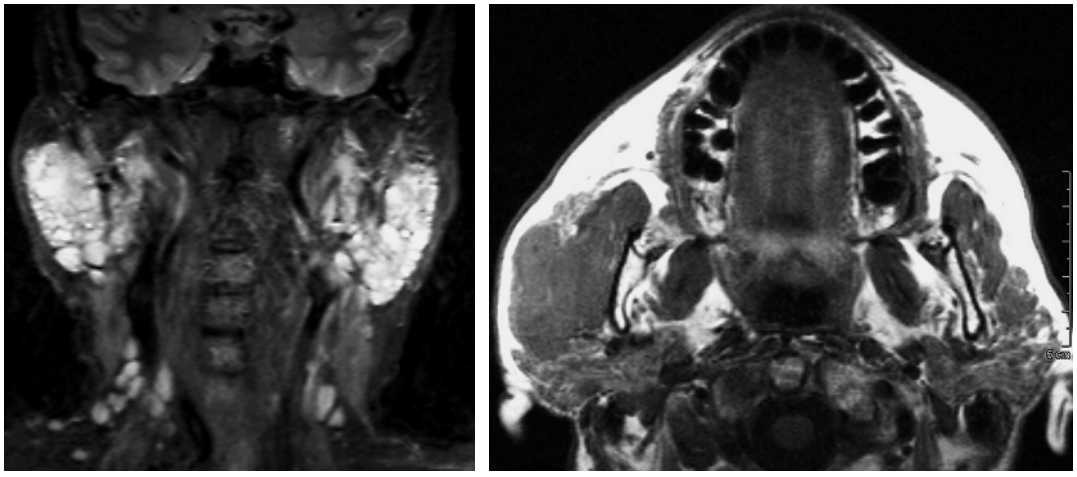

a b

Fig. 16.11a,b. Primary MALT lymphoma of the parotid gland. A female patient with Sjögren's syndrome with progressive parotid enlargement. T2-weighted (TIRM) MR-images. (**a**) Coronal image confirms bilateral parotid swelling. This is caused by innumerable small cysts indicative of chronic sialadenitis with cystic enlargement of terminal salivary ducts. Note multiple non-enlarged level IV nodes bilaterally. (**b**) Axial image shows an additional infiltrative mass located in the superficial lobe of the right parotid gland invading the masseter muscle. Biopsy of this mass revealed MALT lymphoma

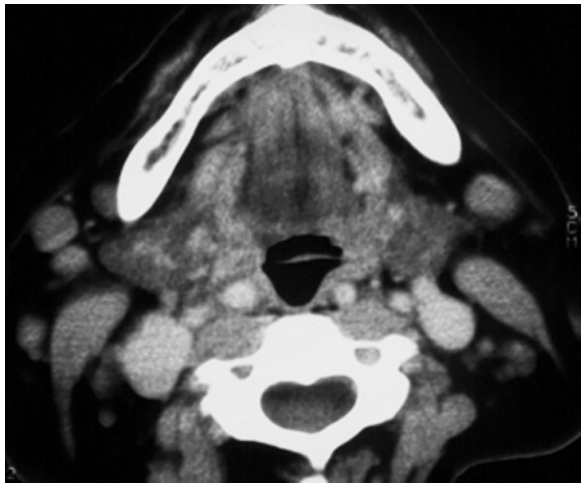

Fig. 16.12. Secondary parotid lymphoma. Axial contrast-enhanced CT-image shows multiple sharply marginated masses within and around both parotid glands representing enlarged intra- en peri-parotid lymph nodes (Courtesy R. Hermans, MD, PhD, Leuven, Belgium)

In the setting of multiple intraparotid and/or periparotid lesions, the age of the patient is important in establishing a differential diagnosis. In younger patients, acute viral or bacterial infections should be considered. Acute otitis media can present with reactive lymphadenopathy of periparotid lymph nodes. Multiple intraparotid cystic lesions should alert the radiologist to the possibility of acquired immunodeficiency syndrome (AIDS). These cystic lesions or 'lymphoepithelial cysts' have been associated with HIV seropositivity. Presence of these abnormalities may be the first indication that the patient has AIDS. Most commonly, with HIV infection there is also a diffuse cervical adenopathy. In about one third of the patients there is hyperplasia of Waldeyer's ring (Kirshenbaum et al. 1991).

The differential diagnosis for elderly patients with multiple intraparotid masses should include lymphoma. Other lesions to be considered include Whartin's tumors and intraparotid metastases from SCC of the skin for unilateral involvement, and Whartin's tumors and melanoma for bilateral involvement.

16.8.4 Sinonasal Cavities

The incidence of nasal and paranasal lymphoma in the US and Europe is low. However, lymphomas of the paranasal sinuses and nasal cavity are relatively prevalent in certain parts of Central and South America, East Asia, including Korea and seem to be associated with Epstein-Barr virus infections (Chisin and Weber 1994; Koom et al. 2004).

Lymphomas arising in the sinonasal cavities are NHL and frequently are observed in patients who have disseminated lymphoma or AIDS. In the nasal cavity the extranodal NK/T-cell lymphoma, nasal type (see also Sect. 16.4; entity 2.2.5) is the most prevalent type which presents usually in Ann Arbor stage I (Table 16.2).

Sinonasal lymphoma most frequently occurs in the nasal cavity and maxillary sinus. Less often, lymphoma is found in the ethmoid sinuses, and only rarely it is found in the sphenoid and frontal sinuses. Patients with maxillary sinus lymphoma present with facial fullness, symptoms of sinusitis or odontogenic pain. Initial symptoms of nasal cavity lymphoma include nasal obstruction and/or epistaxis. Proptosis and epiphora; i.e. orbital and lacrimal gland extension, indicate more widespread disease. Rarely, malignant lymphoma can present as a mass in the canine fossa. If isolated, this most likely represents lymphoma arising in the infraorbital lymph node group; i.e. nodal disease (Tart et al. 1993).

On CT and MRI imaging studies, lymphomas of the sinonasal cavities must be differentiated from the much more common entities of sinusitis, polyposis, as well as granulomatous processes such as Wegener's granulomatosis, and benign and malignant neoplasms (Yuen and Jacobs 1999).

The imaging appearance is non-specific. Lymphomas in the sinonasal cavities tend to be bulky soft tissue masses with moderate enhancement. The growth pattern may be expansile. However, in more advanced cases, aggressive bone erosion may be observed. Based on imaging alone, this more aggressive appearance of lymphoma cannot be differentiated from carcinoma (Fig. 16.13).

16.8.5 Thyroid

Lymphoma of the thyroid gland is an uncommon disease occurring primarily in older women. It may arise primarily from the thyroid or involve the gland as part of a systemic disease.

There is a strong association between thyroid lymphoma and Hashimoto's thyroiditis. Hashimoto's thyroiditis is an autoimmune disease characterized by circulating antithyroglobulin resulting in follicular atrophy, fibrosis, enlargement and firmness of the gland. Surveillance of these patients by yearly physical

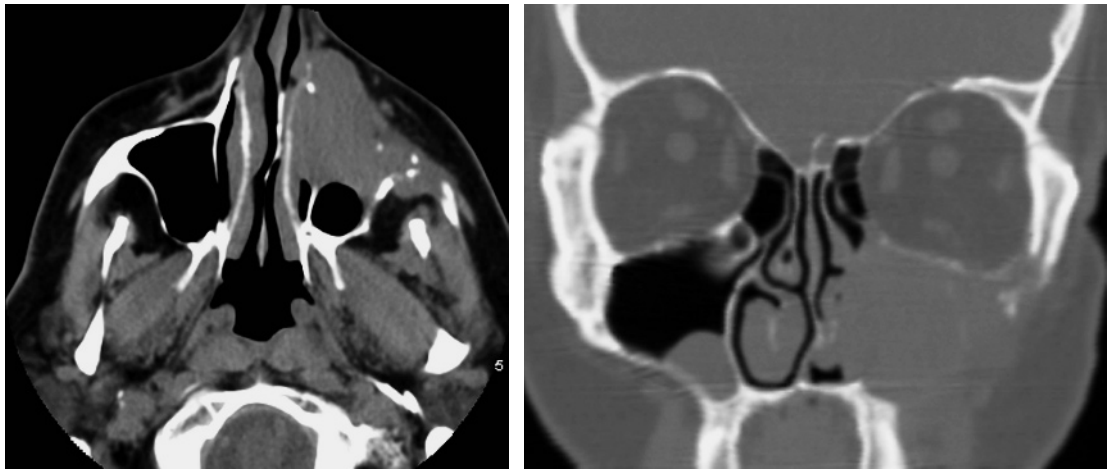

Fig. 16.13a,b. Sinonasal NHL. Contrast-enhanced CT images. (**a**) Axial image shows a soft-tissue mass with homogenous enhancement centered in the left maxillary sinus. Extensive bone destruction. The mass is extending into the nasal cavity and the soft tissues of the cheek. Subtle bony erosion of the posterolateral sinus wall with beginning infiltration of the infratemporal fossa. (**b**) Coronal image (bone window setting) showing the extensive bony destruction. Note retention cyst in the right maxillary antrum

examination and US will facilitate discovery of lymphoma at an early stage. The diagnosis is established by (US-guided) biopsy (Fehr-Merhof 1999). The most common histologies are the diffuse large B-cell lymphomas (up to 70% of cases) and MALT lymphomas (in 6%–27% of cases). Most patients have a short history of an enlarging thyroid or a neck mass causing tracheal compression or swallowing problems. Treatment for MALT lymphomas includes radiation therapy alone. In case of diffuse large B-cell lymphoma, patients will be treated by a combination of radiation with chemotherapy (Widder and Pasieka 2004; Michels et al. 2002; Ansell et al. 1999).

The imaging approach is based on prior clinical evaluation. Small lesions are ideally assessed with US, which is capable of discriminating between solid and cystic nodules. US-guided fine needle aspiration cytology/biopsy provides tissue for pathologic examination of thyroid nodules. On US, thyroid lymphoma may present as a focal mass or diffuse replacement of the thyroid gland. The mass is typically diffusely hypoechoic.

CT and MRI are indicated for larger tumors, especially when extending outside the gland (Weber et al. 2000).

On CT, thyroid lymphoma may be seen as a focal mass, multiple thyroid nodules, or diffuse enlargement of the gland. On non-contrast CT the tumor demonstrates low attenuation. Following contrast administration, these tumors moderately enhance (Fig. 16.14). Associated cervical adenopathy may occur. Calcification and necrosis are unusual (Takashima et al. 1995). These two latter features are much more frequently seen in thyroid goiter.

The MRI appearance of thyroid lymphoma is usually isointense on T1-weighted images with moderate homogeneous enhancement following contrast administration (Fig. 16.15). On T2-weighted sequences, the signal intensity is homogeneously bright (Takashima et al. 1995). Frequently occurring vascular invasion, associated lymphadenopathy and extension into the retropharyngeal area and mediastinum are depicted adequately both by CT and MRI (Fig. 16.15).

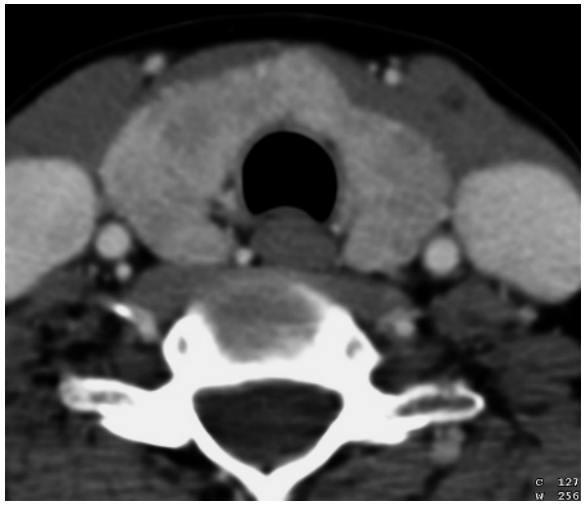

Fig. 16.14. Thyroid lymphoma. Axial contrast-enhanced CT image shows diffuse enlargement of the thyroid gland by a relatively homogenous mass. (Courtesy of I.M. Schmalfuss, MD, Gainesville, Florida)

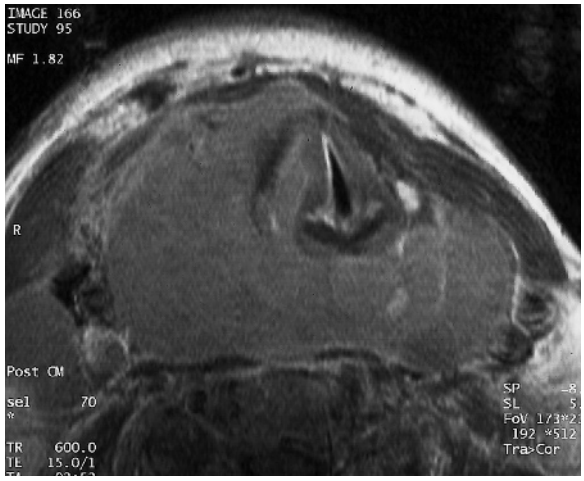

Fig. 16.15. Thyroid lymphoma. Axial contrast-enhanced MR image shows diffuse enlargement of the thyroid gland with homogenous enhancement. Extensive retropharyngeal, as well as intralaryngeal extension. Note enlarged level III lymph node on the right with similar enhancement as the thyroid lymphoma. (Courtesy of R. Hermans, MD, PhD, Leuven, Belgium)

16.8.6 Bone

Bony disease in the setting of head and neck lymphoma is uncommon. Secondary infiltration and/or destruction (mimicking SCC) may occur (Fig. 16.13). However, there are some primary haematological bone disease entities in the head and neck.

16.8.6.1 Primary Lymphoma of Bone

The most common lymphoma affecting bone is the diffuse large B-cell lymphoma. Primary lymphoma of bone occurs most frequently in the mandible followed by the maxilla. In the mandible, most often there are ill-defined lytic destructive areas of variable size. These imaging features are non-specific and the differential diagnosis includes other primary neoplasms of bone, such as osteosarcoma and Ewing's sarcoma.

The jaw is a common site of presentation for the African type of Burkitt's lymphoma. This B-cell lymphoma occurs most frequently in children and young adults with 50% of cases arising in the maxilla or mandible (Fig. 16.16). This disease is found especially in Africa and other underdeveloped countries, much less frequently in the US and Europe. Association with Epstein-Barr virus is postulated (Weber et al. 2003; Muwakkit et al. 2004; Rao et al. 2000).

16.8.6.2 Multiple Myeloma (Kahlers' Disease)

Multiple myeloma (MM) is characterized by a malignant proliferation of plasma cells with monoclonal immunoglobulin or immunoglobulin fragments in the patient's urine. This proliferation of neoplastic cells is associated with bone destruction and involves the bone marrow of the axial skeleton. Although single lesions occasionally occur (solitary plasmacytoma of bone), MM typically shows diffuse involvement of multiple bones. The typical radiographic appearance is that of 'punched-out' round to ovoid, regular radiolucencies in the skull and long bones with no circumferential bone sclerosis (Kesari and Bundock 2004). In the mandible, these lesions show a predilection for the angle, ramus and molar tooth regions. Solitary plasmacytomas of bone usually occur in the vertebra and skull.

16.8.6.3 Extramedullary Plasmocytoma

Extramedullary plasmocytoma (EMP) is a rare soft-tissue malignancy composed of plasma cells. Approximately 80% of EMP's arise in the head and neck, most often occurring in the nasal cavity followed by the paranasal sinuses (Mendenhall et al. 2003; Dimopoulos et al. 1999). On CT, EMPs of the sinonasal cavities are smooth, homogeneous enhancing polypoid masses that remodel surrounding bone (Fig. 16.17). On MR imaging, they have intermedi-

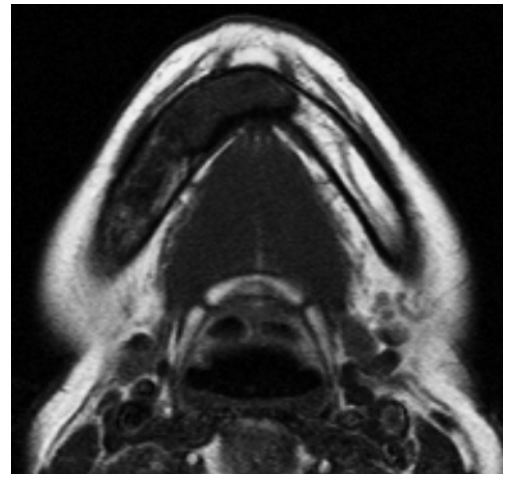

Fig. 16.16. Primary Burkitt's lymphoma of the mandible. Axial T1-weighted non-enhanced MR image shows replacement of the normal fatty marrow by a low signal intensity mass in the median and right part of the mandible, with expansion of the medullary cavity

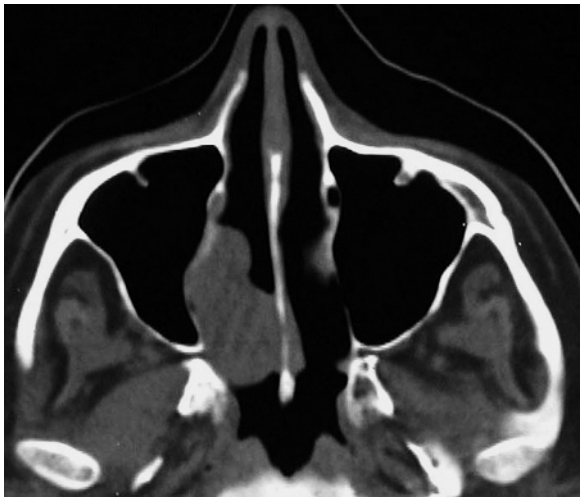

Fig. 16.17. Sinonasal plasmocytoma. Axial non-enhanced CT image (bone window setting) shows a smooth lobulated mass centered in the left nasal cavity. Note subtle remodelling of the medial wall of the left maxillary sinus

ate signal intensity on all imaging sequences. EMPs markedly enhance because they are highly vascular. Spread to the regional lymph nodes is common in EMP; in solitary plasmocytomas of bone this is highly uncommon.

16.8.7 Skin

NHL in the head and neck may also be localized in the skin.

The cutaneous lymphomas can be distinguished in B- and T-cell types. Specific for the cutaneous T-cell lymphomas are the so-called mycosis fungoides and the Sezary syndromes, but they are more likely to be seen on the trunk and extremities than the head and neck (Foss 2004).

Crosti's syndrome should be mentioned. Originally called the reticulohistiocytoma of the dorsum by Crosti in 1951, this disease is nowadays considered a primary cutaneous B-cell lymphoma of follicular center cell origin. This localized skin disease on the back of the head and trunk has a very slowly progressing course, with many patients showing no systemic involvement even after prolonged follow-up (Berti et al. 1988).

When palpation is felt to be insufficient for local staging, CT or MRI can be used for mapping pretherapeutic disease extent and document response post therapy.

16.9 Conclusion

Lymphoma should be approached as a systemic disease that can manifest itself in many forms in the head and neck. Frequently, the imaging findings are non-specific and tissue sampling remains the mainstay of making the diagnosis. Sometimes, involvement of specific sub-sites or specific imaging patterns can (strongly) suggest the diagnosis of lymphoma. However, it should be kept in mind that lymphoma is a possible cause in any infiltrative soft tissue mass in the head and neck, irrespective of the location. In the work-up of a patient with a head and neck lesion, the radiologist may be the first one to suggest this diagnosis.

References

Abbondanzo SL (2001) Extranodal marginal-zone B-cell lymphoma of the salivary gland. Ann Diagn Pathol 5:246–254

Agulnik M, Tsang R, Baker MA, et al. (2001) Malignant lymphoma of mucosa-associated lymphoid tissue of the lacrimal gland: case report and review of literature. Am J Clin Oncol 24:67–70

Aloulou S, Farhat H, Bosq J, et al. (2002) Hodgkin's disease primarily involving the oropharynx: case report and review of the literature. Hematol J 3:164–167

Ansell SM, Grant CS, Habermann TM (1999) Primary thyroid lymphoma. Semin Oncol 26:316–323

Berti E, Alessi E, Caputo R, et al. (1988) Reticulohistiocytoma of the dorsum. J Am Acad Dermatol 19:259–272

Cartwright R, Brincker H, Carli PM, et al. (1999) The rise in incidence of lymphomas in Europe 1985–1992. Eur J Cancer 35:627–633

Cheson BD, Horning SJ, Coiffier B, et al. (1999) Report of an international workshop to standardize response criteria for non-Hodgkin's lymphomas. J Clin Oncol 17:1244–1253

Chisin R, Weber AL (1994) Imaging of lymphoma manifestations in the extracranial head and neck region. Leuk Lymphoma 12:177–189

Dimopoulos MA, Kiamouris C, Moulopoulos LA (1999) Solitary plasmacytoma of bone and extramedullary plasmacytoma. Hematol Oncol Clin North Am 13:1249–1257

Fehr-Merhof A, Flury R, Ruttimann S (1999) From Hashimoto thyroiditis to B-cell lymphoma of the thyroid gland. Schweiz Med Wochenschr 129:883–889

Foss F (2004) Mycosis fungoides and the Sezary syndrome. Curr Opin Oncol 16:421–428

Front D, Israel O (1995) The role of Ga-67 scintigraphy in evaluating the results of therapy of lymphoma patients. Semin Nucl Med 25:60–71

Gritzmann N, Rettenbacher T, Hollerweger A, et al. (2003) Sonography of the salivary glands. Eur Radiol 13:964–975

Haas RL, Valdes-Olmos RA, Hoefnagel CA, et al. (2003) Thal-

lium-201-chloride scintigraphy in staging and monitoring radiotherapy response in follicular lymphoma patients. Radiother Oncol 69:323–328
Hanna E, Wanamaker J, Adelstein D, et al. (1997) Extranodal lymphomas of the head and neck. A 20-year experience. Arch Otolaryngol Head Neck Surg 123:1318–1323
Harnsberger RH (2004) Diagnostic imaging head and neck, 1st edn. Amirsys, Salt lake City, Utah
Harris NL, Jaffe ES, Stein H, et al. (1994) A revised European-American classification of lymphoid neoplasms: a proposal from the International Lymphoma Study Group. Blood 84:1361–1392
Harris NL, Jaffe ES, Diebold J et al. (2000) World Health Organization classification of neoplastic diseases of the hematopoietic and lymphoid tissues: report of the Clinical Advisory Committee meeting – Airlie House, Virginia, November 1997. J Clin Oncol 17:3835–3849
Hermans R (2004) Extranodal lymphoma – neck. Cancer Imaging 4:1–5
Hermans R, Horvath M, De Schrijver T, et al. (1994) Extranodal non-Hodgkin lymphoma of the head and neck. J Belge Radiol 77:72–77
Jerusalem G, Beguin Y, Najjar F, et al. (2001) Positron emission tomography (PET) with 18F-fluorodeoxyglucose (18F-FDG) for the staging of low-grade non-Hodgkin's lymphoma (NHL). Ann Oncol 12:825–830
Kesari S, Bundock EA (2004) Punched-out skull. Arch Neurol 61:958–959
King AD, Lei KI, Richards PS, et al. (2003) Non-Hodgkin's lymphoma of the nasopharynx: CT and MR imaging. Clin Radiol 58:621–625
King AD, Yuen EH, Lei KI, et al. (2004) Non-Hodgkin lymphoma of the larynx: CT and MR imaging findings. AJNR Am J Neuroradiol 25:12–15
Kirshenbaum KJ, Nadimpalli SR, Friedman M, et al. (1991) Benign lymphoepithelial parotid tumors in AIDS patients: CT and MR findings in nine cases. AJNR Am J Neuroradiol 12:271–274
Koom WS, Chung EJ, Yang WI, et al. (2004) Angiocentric T-cell and NK/T-cell lymphomas: radiotherapeutic viewpoints. Int J Radiat Oncol Biol Phys 59:1127–1137
Lee JL, Kim MK, Lee KH, et al. (2005) Extranodal marginal zone B-cell lymphomas of mucosa-associated lymphoid tissue-type of the orbit and ocular adnexa. Ann Hematol 84:13–18
Lister TA, Crowther D, Sutcliffe SB, et al. (1989) Report of a committee convened to discuss the evaluation and staging of patients with Hodgkin's disease: Cotswolds meeting. J Clin Oncol 7:1630–1636
Mancuso AA (1998) Lymphoma: master of chicanery (editorial). AJNR Am J Neuroradiol 19:1808
Mendenhall WM, Mendenhall CM, Mendenhall NP (2003) Solitary plasmacytoma of bone and soft tissues. Am J Otolaryngol 24:395–399
Michels JJ, Delcambre C, Marnay J, et al. (2002) Primary thyroid lymphomas: clinicopathologic study of 30 cases and review of the literature. Ann Pathol 22:10–17
Moog F, Bangerter M, Diederichs CG, et al. (1997) Lymphoma: role of whole-body 2-deoxy-2-[F-18]fluoro-D-glucose (FDG) PET in nodal staging. Radiology 203:795–800
Muwakkit SA, Razzouk BI, Shabb NS, et al. (2004) Clinical presentation and treatment outcome of children with Burkitt lymphoma in Lebanon: a single institution's experience. J Pediatr Hematol Oncol 26:749–753
Palacios E, Larusso G, Rojas R, et al (2004) Lymphoma of the parotid gland in Sjögren's syndrome. Ear Nose Throat J 83:156
Pfeffer MR, Rabin T, Tsvang L, et al. (2004) Orbital lymphoma: is it necessary to treat the entire orbit? Int J Radiat Oncol Biol Phys 60:527–530
Rao CR, Gutierrez MI, Bhatia K, et al. (2000) Association of Burkitt's lymphoma with the Epstein-Barr virus in two developing countries. Leuk Lymphoma 39:329–337
Shields JA, Shields CL, Scartozzi R (2004) Survey of 1264 patients with orbital tumors and simulating lesions. Ophthalmology 111:997–1008
Smithers DW (1971) Summary of papers delivered at the Conference on Staging in Hodgkin's Disease (Ann Arbor). Cancer Res 31:869–870
Som P, Curtin H, Mancuso A (2000) Imaging-based classification for evaluation of neck metastatic adenopathy AJR Am J Roentgenol 174:837–844
Takashima S, Nomura N, Noguchi Y, et al. (1995) Primary thyroid lymphoma: evaluation with US, CT and MRI. J Comput Assist Tomogr 19:282–288
Tart RP, Mukherji SK, Avino AJ, et al. (1993) Facial lymph nodes: normal and abnormal CT appearance. Radiology 188:695–700
Therasse P, Arbuck SG, Eisenhauer EA, et al. (2000) New guidelines to evaluate the response to treatment in solid tumors. European Organization for Research and Treatment of Cancer, National Cancer Institute of the United States, National Cancer Institute of Canada. J Natl Cancer Inst 92:205–216
Tonami H, Matoba M, Yokota H, et al (2002) Mucosa-associated lymphoid tissue lymphoma in Sjögren's syndrome: initial and follow-up imaging features. Am J Roentgenol AJR 179: 485-489
Tonami H, Matoba M, Kuginuki Y, et al (2003) Clinical and imaging findings of lymphoma in patients with Sjögren's syndrome. J Comput Assist Tomogr 27:517-524
UICC (1997) TNM classification of malignant tumours, 5th edn. Springer, Berlin Heidelberg New York
Van Amsterdam JA, Kluin-Nelemans JC, van Eck-Smit BL, et al. (1996) Role of 67Ga scintigraphy in localization of lymphoma. Ann Hematol 72:202–207
Vose JM, Chiu BC, Cheson BD, et al. (2002) Update on epidemiology and therapeutics for non-Hodgkin's lymphoma. Hematology 1:241–262
Weber AL, Randolph G, Aksoy FG (2000) The thyroid and parathyroid glands. CT and MR imaging and correlation with pathology and clinical findings. Radiol Clin North Am 38:1105–1129
Weber AL, Rahemtullah A, Ferry JA (2003) Hodgkin and non-Hodgkin lymphoma of the head and neck: clinical, pathologic, and imaging evaluation. Neuroimaging Clin N Am 13:371–392
Widder S, Pasieka JL (2004) Primary thyroid lymphomas. Curr Treat Options Oncol 5:307–313
World Health Organization Classification of Tumors (2001) Tumors of haematopoietic and lymphoid tissues. Jaffe ES, Harris HL, Stein H, et al. (eds). Oxford University Press, Oxford, pp 162–167
Yan J, Wu Z, Li Y (2004) The differentiation of idiopathic inflammatory pseudotumor from lymphoid tumors of orbit: Analysis of 319 cases. Orbit 23:245–254
Yuen A, Jacobs C (1999) Lymphomas of the head and neck. Semin Oncol 26:338–345

17 Positron Emission Tomography in Head and Neck Cancer

Cathérine Castaigne, Kristoff Muylle, and Patrick Flamen

CONTENTS

C. Castaigne, MD; K. Muylle, MD; P. Flamen, MD, PhD
Nuclear Medicine Bordet, Positron Emission Tomography IRIS, Institut Jules Bordet, 121, Boulevard de Waterloo, 1000 Brussels, Belgium

17.1 Introduction

17.1.1 Metabolic Imaging with Positron Emission Tomography

Positron emission tomography (PET) is the most sensitive and specific technique for in vivo imaging of metabolic pathways and receptor–ligand interactions in the tissues of man (Jones 1996). PET uses positron emitting short living radioisotopes of natural elements, such as oxygen-15, carbon-11, nitrogen-13, and fluorine-18. These radioisotopes allow the synthesis of numerous positron-emitting radiopharmaceuticals targeting specific functional or metabolic expressions (phenotypes) of the disease. Depending on the selected radiopharmaceutical, PET imaging can provide quantitative information regarding blood flow ($H_2{}^{15}O$), hypoxia (^{18}F-misonidazole), DNA metabolism (^{11}C-thymidine; ^{18}F-fluorothymidine), glucose metabolism (^{18}F-2-fluoro-2-deoxy-D-glucose), protein synthesis rate (^{11}C-tyrosine), amino acid metabolism (^{11}C-methionine), and receptor status. A major advance in PET has been the advent of a new generation of imaging tools combining a PET and a CT module in one camera. This allows the simultaneous acquisition of a whole body CT and PET during one single imaging session. The resulting coregistered whole-body PET-CT images allow a perfect integration of the metabolism with the structural and morphologic characteristics of the disease. This new modality has been used increasingly for clinical oncologic imaging since 2001.

17.1.2 Biochemical Foundations of the Use of ^{18}F-FDG as a Marker in Malignancy

The tracer most commonly used worldwide is fluorine-18-labeled 2-fluoro-2-deoxy-D-glucose (FDG). This is a D-glucose molecule in which a hydroxyl

group in the 2-position is replaced by an ^{18}F-label. The use of FDG for in vivo cancer imaging is based upon the higher rate of glucose metabolism in cancer cells, a feature which was first described several decades ago (Warburg 1956).

After malignant transformation, cells demonstrate an increased expression of the epithelial glucose transporter proteins and an increase in the activity of the principal enzymes of the glycolytic pathway. After intravenous administration, FDG competes with plasma glucose for the glucose transporters in the cell membrane. Figure 17.1 illustrates the molecular basis underlying the use of FDG for imaging cancer. Because FDG lacks a hydroxyl group in the 2-position, its first metabolite, FDG-6-phosphate, is not a substrate for the glucosephosphate isomerase, and therefore cannot be converted to the fructose analogue. As most tumors have a low phosphatase activity, the negatively charged FDG-6-phosphate will accumulate intracellularly, resulting in a so-called metabolic trapping (Pauwels et al. 1998). Under steady state conditions, the amount of FDG-6-phosphate accumulated is proportional to the rate of glucose utilisation.

17.1.3 Intratumoral Distribution of FDG at the Cellular Level

Higashi et al. (1993) demonstrated that increased tumoral FDG uptake, although a function of the proliferative activity, is mainly related to the viable tumor cell number. When interpreting data on intensity of FDG accumulation in tumors, it has to be kept in mind that other intratumoral non-malignant cells may significantly contribute to the total radioactivity. It is well known that a variable fraction of a tumor mass consists of non-neoplastic cells, such as stimulated leucocytes, macrophages and proliferating fibroblasts, which appear in association with growth or necrosis of tumor. FDG, as a non cancer-specific tracer, also accumulate in these hypermetabolic cells, to a degree often more marked than neoplastic cells (Kubota et al. 1992). Because the viable non-neoplastic part can constitute a large percentage of the total tumor mass, the total amount of radioactivity measured by PET in the tumor is correspondingly increased. The advantage of this phenomenon is an increase of the overall diagnostic sensitivity of FDG-PET for detecting small neoplastic foci due to the resulting signal amplification. The disadvantage is that specific tumor metabolism cannot be precisely assessed due to this contamination. This is a problem mainly in the field of therapy monitoring. The post-therapeutic FDG signal is then the resultant of several intratumoral changes. On one hand, death of tumor cells leads to a decreased FDG accumulation. On the other hand, however, inflammatory immune and scavenging reactions may be induced by the success of the therapy, and the invasion of the tumor by the inflammatory cells may raise the overall FDG uptake. The latter phenomena may thus cause underestimation of the effectivity of treatment (Haberkorn et al. 1997). To avoid this, the use of more tumor-specific radiotracers (^{11}C-methionine; ^{11}C-thymidine) has been proposed, tracers which should be less sensitive to inflammatory contaminants.

17.1.4 Physical and Technical Aspects of Whole-Body FDG-PET(-CT) Imaging

The biodistribution of the positron-emitting tracers is measured using a dedicated tomographic imag-

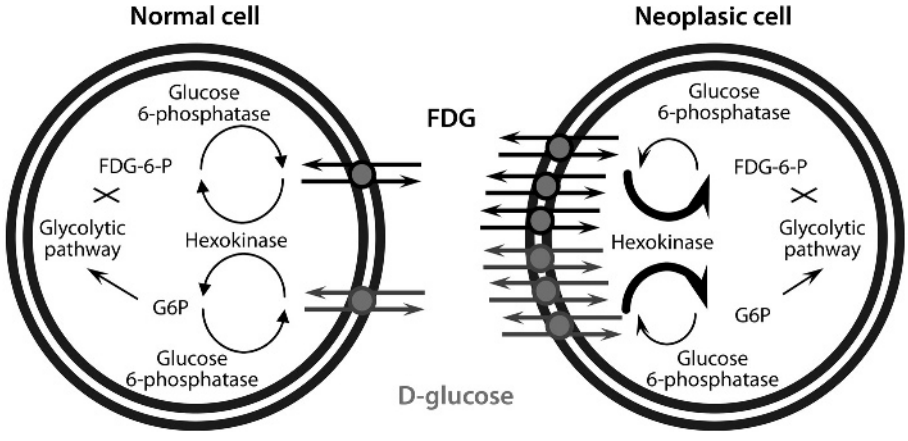

Fig. 17.1. Molecular basis of the use of FDG as a tumour imaging agent

ing device. A positron transverses a few millimetres through the tissue until it combines with an electron in the surrounding media. This generates a pair of photons which travel in nearly opposite directions (180° apart) with an energy of 511 KeV each. These opposed photons can be detected by detector pairs installed in a ring shaped pattern. Photons that simultaneously (i.e. within a predefined time-window) interact with these detectors are registered as decay events. Based on these registrations, tomographic images of the regional radioactivity distribution are reconstructed (emission images).

A typical whole-body FDG-PET scan is started 60–90 min after the intravenous administration of the radiotracer. The axial field of view of the PET system (10–15 cm) is extended by imaging in multiple bed positions, so as to cover the whole body (Dahlbom et al. 1992). An acquisition time of 3–6 min per bed position after a 5–15 mCi (175–550 MBq) injection of FDG produces images of good resolution and contrast, in a total imaging time of 45–60 min. All current PET systems allow for the correction of soft-tissue attenuation of the emitted annihilation photons. The attenuation of a given photon depends on the electron density of the tissues which the photon has to cross before hitting the detectors. Therefore, a density map needs to be created by acquiring a set of corresponding tomographic images with an external positron emitting source of radiation (the transmission scanning) The conventional way of obtaining such a transmission scan is time consuming (about 20 min per patient) and yields images with low counting statistics. Using PET-CT technology, the transmission scanning for attenuation correction can be performed using the CT data (Kinahan et al. 1998). The use of high-speed multislice CT systems reduces the data acquisition time to less than 1 min (reducing total image time to about 30 min) and yields much less noisy attenuation correction maps. However, there are some drawbacks of the use of CT for this purpose. The mean energy of the photons used in CT scan (70 KeV) is much lower than the one of the annihilation photons (511 KeV). By this, CT photons are more attenuated by high density objects within the field of view (metallic prosthesis, dental prosthesis, contrast agents). Goerres et al. (2002) have evaluated for instance the detrimental influence of metallic dental work on the quality of the attenuation corrected PET-CT images of the head and neck region. They concluded that non-attenuation corrected PET images should always be reviewed in these patients in order to avoid misinterpretation due to this artefact.

Another pitfall in attenuation correction using CT is the motion artefact resulting from patient or organ movement between the PET emission scan and the CT transmission scan. This happens more frequently in the head and neck or in the extremities where there is greater freedom of motion. The same phenomenon occurs with the motion of the internal organs just above and below the diaphragm during respiration. This leads to an over-or undercorrection of the PET emission data, thereby creating areas of artifactually increased or decreased FDG activity.

The standard patient preparation employed for PET and CT studies is applied to the PET-CT device. Patients receive 150–550 MBq of FDG 45–60 min prior to the start of the image acquisition. After the patient is positioned on the scanner, an initial topogram is acquired. The topogram is used subsequently to define the examination range for the PET-CT image acquisition. The spiral CT scan is performed next. After completion of the CT portion, the scanner bed is moved to the starting position and the emission scan is started. PET-CT machinery provides the means of performing a CT scan of comparable diagnostic quality to what is performed in the radiology departments. For this, however, optimalisation of the CT imaging protocol used in PET-CT is mandatory. Aspects to consider in this regard are the use of intravenous and digestive contrast. Probably the best option is to add a dedicated (high dose) diagnostic CT after the PET-CT (low dose).

Semi- or fully quantitative assessment of FDG metabolism is often needed, e.g. for the assessment of the metabolic response to an antineoplastic treatment. The most widely used semi-quantitative index of FDG uptake is the standardised uptake value (SUV). For this, the measured tumor radiotracer concentration (Q) is normalised to the injected activity (Q_{inj}) and to the body weight (W) of the patient: $SUV = (Q \times W)/Q_{inj.}$. More complex procedures (not used in daily routine), using kinetic modelling, are necessary to calculate the metabolic rate for glucose (MR_{gluc}; μmoles/min/ml).

17.1.5 General Consideration on the Use of FDG-PET in Head and Neck Cancer

17.1.5.1 Diagnostic Sensitivity

A major limitation of PET is the limited spatial resolution of the imaging tool. For current PET instrumen-

tations it is approximately 5–8 mm. Due to the partial volume effect, tracer activity in all lesions smaller than two times the spatial resolution of the imaging apparatus is underestimated. Below a threshold lesion diameter (depending on the intensity of tracer accumulation), the tracer uptake will therefore no longer be distinguishable from the background activity, leading to false-negative PET results. It is clear that future technological innovations that optimize the spatial resolution of the imaging method, thus reducing the false-negativity of small lesions, will significantly increase the additional diagnostic value of PET imaging in staging head and neck cancer. However, even with the maximal achievable spatial resolution of PET (around 3–4 mm), micrometastases will always remain underdiagnosed.

17.1.5.2 Diagnostic Specificity

FDG is not a very tumor-specific substance, as the leucocytes and macrophages of inflammatory processes also accumulate the tracer. Benign lesion, such as sinusitis, can show variable intensity of FDG uptake. A strong uptake can be visible after dental infection or surgery. Radiation therapy can cause pharyngitis and esophagitis which can be visible as increased uptake in the mucosal membrane. Those are among the major sources of false-positive diagnoses in the application of FDG-PET in oncology (Strauss 1996). Clinical information, before reporting and integration of the PET findings with other data, is absolutely mandatory to reduce the potentially negative impact of occasional false-positive FDG-PET results on patient management.

In addition, the interpretation of FDG-PET images of the head and neck is particularly difficult because of the presence of multiple sites showing a variable degree of physiological FDG accumulation, such as the salivary glands and the lymphoid tissues (see below). Another pitfall in the interpretation of the PET images in the head and neck region is the physiological FDG uptake of the muscles. Muscular uptake can be seen in the masticator muscles, the tip of the tongue and muscles of the face, the neck and the larynx in nervous patients, and in patients who speak during the FDG uptake phase. This can both mimic or hide tumoral activity. PET-CT enhances the confidence of image interpretation by improving the anatomic localization of PET abnormalities, and reduces the number of equivocal PET interpretations. The patient should be instructed not to speak during the FDG uptake phase; muscular uptake can be avoided by using premedication such as diazepam.

The introduction of PET-CT recently led to the identification of another type of PET image artefact sporadically observed bilaterally in the neck and supraclavicular region, often extending into the anterior mediastinum (Fig. 17.2). These irregular hot spots are located in fat planes identifiable on CT and correspond with an increased FDG uptake in brown adipose tissue ("USA-Fat"). This is most often seen in young female patients and seems related to the ambient temperature of the injection room (Cohade et al. 2003).

17.2 Clinical Applications

17.2.1 Physiological FDG Uptake Distribution in the Head and Neck Region

Familiarity with the complex anatomy of the head and neck is essential for an accurate interpretation of FDG-PET images. The normal uptake of FDG in the extracranial head and neck region was first described by Jabour et al. (1993) using correlation with MRI. Marked physiological FDG activity was seen in the lymphoid tissue of the Waldeyer's ring (Fig. 17.3). Moderate activity is seen in the salivary glands, which physiologically secrete low amounts of glucose. Other areas of mild to moderate uptake of FDG was seen in the nasal turbinates, the mucosa of the hard and soft palate, and gingiva.

17.2.2 Staging the Primary Tumour

17.2.2.1 Assessment of the Primary Lesion

Patients with squamous cell carcinoma (SCC) of the head and neck most often have a histologic diagnosis before they are referred for PET examination. Contrast-enhanced CT and MRI are routinely used in order to determine the precise localization, size and anatomic extent of the primary lesion. PET alone is not able to reliably assess organ involvement and invasion of a tumor into adjacent structures. More studies are needed to evaluate the potential role of contrast-enhanced PET-CT for this purpose.

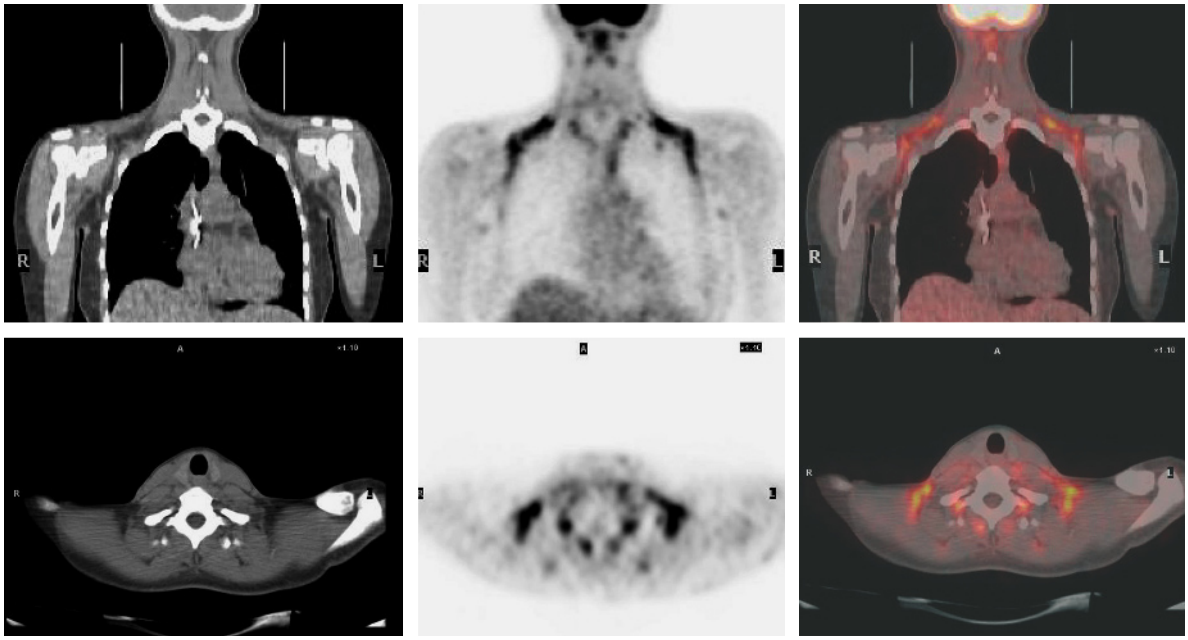

Fig. 17.2. FDG uptake in brown fat tissue. Coronal PET images show multiple symmetric foci of increased FDG uptake in supraclavicular and axillary regions without radiologic evidence of disease in those areas. Bilateral paravertebral muscular uptake is also observed

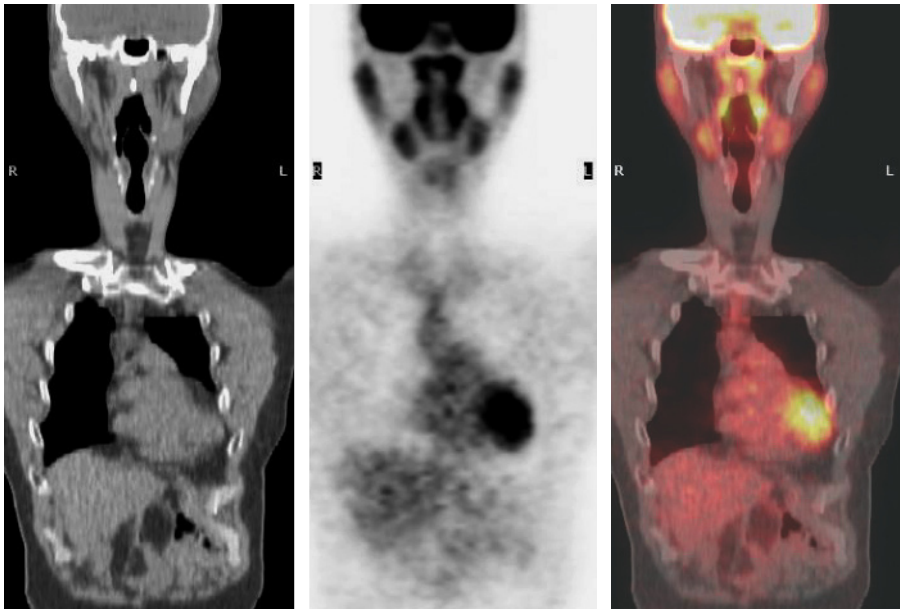

Fig. 17.3. Marked physiological FDG activity in Waldeyer's ring and in the salivary glands

In the few studies that have addressed the ability of PET and CT/MRI to actually visualize a clinically proven primary tumor, PET generally had the highest sensitivity. This is related to the fact that CT/MRI may occasionally fail to delineate a primary tumor that is submucosal or only superficially spreading. For instance, in a prospective controlled study, Di Martino et al. (2000) compared FDG-PET to CT, ultrasound and panendoscopy for the visualisation of the primary tumor in 37 patients with suspected primary head and neck cancers. FDG-PET had a superior sensitivity (95%) and specificity (92%) compared to CT

(68% and 69%, respectively) and color-coded duplex sonography (74% and 75%, respectively, in the accessible regions). While sensitivity of panendoscopy was equal to that of PET (95%), its specificity was lower (85%). The high sensitivity of PET for the detection of small laryngeal tumors has been demonstrated by Lowe et al. (1999) in a prospective study including 12 patients with early stage laryngeal cancer (T1, T2). PET detected 11/12 (92%) primary tumor sites. Nine underwent CT, with normal findings in seven patients.

Of special interest are the often intense lesions found on PET in the parotid gland. McGuirt et al. (1995a) reported on the identification by FDG-PET of benign versus malignant parotid masses. PET identified all malignant lesions (sensitivity, 100%) but made the correct categorization between benign and malignant in only 69% of the 26 cases. Six benign lesions (Warthin's tumors, pleomorphic adenomas and a toxoplasmosis adenopathy) showed false-positive FDG uptake. Therefore, caution is warranted when a positive focal lesion is observed in the parotid salivary gland.

In addition, PET might play a role in patients presenting with a malignant cervical lymph node and an occult primary tumor. PET identifies the unknown primary in 5%–60% of cases, as reported by several authors (Schöder et al. 2004a).

17.2.2.2 Assessment of Lymph Nodes

An important factor in patient assessment, treatment planning, and survival prognostication is accurate staging of the lymph node metastases (Shuller et al. 1984) (Fig. 17.4). Numerous publications have shown that PET has a slightly higher sensitivity and specificity (70%–100% and 82%–94%, respectively) than contrast-enhanced CT of MRI (58%–88% and 41%–96% respectively) (Schöder et al. 2004a). The increased sensitivity of PET indicates that the technique is able to detect lymph node involvement in non-enlarged lymph nodes. This is important as it has been reported that more than 40 % of all lymph node metastases are localized in nodes smaller than 10 mm in diameter, and thus below the diagnostic size criterion of CT/MRI.

Adams et al. (1998) studied 60 patients with histologically proven squamous cell carcinoma by PET imaging before surgery. Pre-operative endoscopy (including biopsy), CT, MRI and sonography of the cervical region were performed in all patients within 2 weeks preceding whole-body FDG-PET. Histopathology of the resected neck specimens revealed a total of 1284 lymph nodes, 117 of which showed metastatic involvement. In that study FDG-PET had a sensitivity of 90% and a specificity of 94% for the detection of lymph node involvement. In contrast, the sensitivity and specificity were 80% and 79% for MR imaging and 82% and 85% for CT, respectively.

Another study reported that the disease probabilities in the lymph nodes were 81.2% for a positive PET and 4.5% for a negative PET result in the initial staging of the disease (Goerres et al. 2003).

Reasons for false-negative PET studies may include a small tumor burden in metastatic nodes, and cystic degeneration or necrosis of metastatic nodes only surrounded by a small rim of viable tumor tissue. In addition, nodal metastases in close proximity to the primary tumor may not be detectable as separate hypermetabolic foci.

False-positive PET findings are usually found in benign lymph nodes containing inflammatory

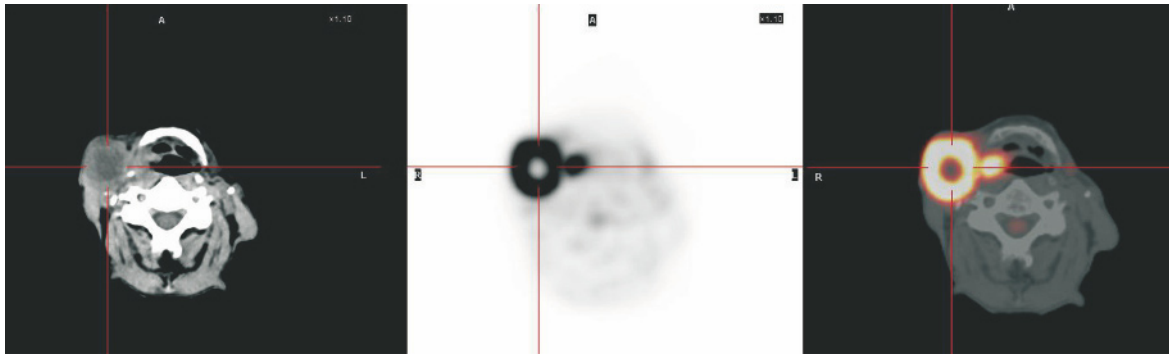

Fig. 17.4. A 58-year-old man with a pharyngeal tumour and a large ipsilateral cervical adenopathy. Transversal PET-CT images show an area with abnormal uptake at the primary tumour site in the pharynx. A large necrotic node in close proximity to the primary tumour is well visualised; only the small rim of viable tumour tissue shows FDG uptake

cells. Reactive changes due to biopsy can also induce sometimes false-positive results. Several authors studied whether quantification techniques could be useful to differentiate true from false-positive lesions. However, quantification of the nodal FDG uptake, expressed as SUV, is not useful for differentiating malignant from reactively inflamed but benign lymph nodes (Kao et al. 2000; Braams et al. 1995). The imperfect specificity, due to false-positive FDG uptake in inflamed lymph nodes has to be corrected by ultrasound guided biopsy or fine needle aspiration. In order to reduce sampling errors the exact anatomical localization of the PET hot spot by means of a correlative PET-CT imaging approach is crucial. The CT information facilitates the correct identification and localization of lymph nodes with increased FDG uptake. The anatomic level can be identified easily, helping in surgical and radiation planning. Using PET-CT, the assessment of loco-regional disease is performed more easily and quickly. Branstetter et al. (2005) recently compared combined PET-CT to PET and CT alone in depicting malignant lesions in the head and neck. A total of 65 consecutive patients known to have or suspected of having head and neck cancer were examined with combined PET-CT. CT was performed with intravenous administration of contrast agent. Each examination was interpreted in three ways: PET images in the absence of CT data, CT images in the absence of PET data, and fused PET-CT images. In this series, PET-CT had a sensitivity of 98%, a specificity of 92%, and an accuracy of 94%; observer confidence was substantially improved with the combined modality.

Other authors (Syed et al. 2005) have compared the interobserver agreement and degree of confidence in anatomical localisation of lesions using PET-CT and PET alone in 24 patients with head and neck cancer. A total of six primary lesions were identified on PET alone and on PET-CT. In all, 15 non-primary tumor sites were identified by PET alone, while 17 by PET-CT. Using PET alone, correct localisation was documented in three of six primary lesions, while PET-CT correctly identified all primary sites. In non-primary tumor sites, PET-CT improved the degree of confidence in anatomical localisation by 51%. They conclude that PET-CT significantly increases inter-observer agreement and confidence in disease localisation in patients with head and neck cancer.

The pre-surgical staging of the clinically N_0 neck is severely hindered by the relatively high false positive and negative rates of currently available conventional imaging techniques. The major problem is a lack of sensitivity for micrometastatic disease. Hamakawa et al. (2000) studied 554 non-metastatic cervical lymph nodes taken from 73 patients with oral cancer by hematoxylin-eosin staining and keratin immunohistochemistry. Occult metastasis was detected in six small lymph nodes < or =5 mm in diameter. The average minor axis of the micrometastasis was 1.36±0.85 mm. This size is far below the technical resolution of the PET scanner, wich is 4–5 mm. PET has therefore probably no place in the staging of cN_0 neck (Stoeckli et al. 2002). The sole reliable analysis for correct staging of a cN_0 neck still is the careful histologic work-up of the neck dissection specimen.

Sentinel node scintigraphy, indicating which loco-regional lymph node to assess microscopically for the presence of malignant cells, has been proposed as a better means for N staging. The technique has evolved as a new standard in breast cancer and melanoma staging. Several preliminary studies in recent years proved sentinel lymph node biopsy to be highly effective also for the detection of occult lymph node metastasis in the field of oral cancer (Balkissoon et al. 2004). In a recent study, Kovacs et al. (2004) proposed a diagnostic ladder, including PET-FDG, as a prerequisite for performing sentinel node scintigraphy (coupled to a probe guided biopsy). They concluded that this staging ladder could considerably reduce the number of extensive neck dissection in oropharyngeal squamous cell carcinoma. These preliminary results should be confirmed by other research groups.

17.2.2.3 Assessment of Distant Metastasis and Synchronous Second Primary Malignancies

One of the advantages of PET imaging is its ability to scan the entire body for disease activity. This allows the detection of a synchronous second primary tumor and distant metastases. Because most secondary cancers observed in head and neck cancer patients, such as bronchogenic cancer and squamous cell carcinoma of the oesophagus, show a high FDG uptake, whole body PET is ideal to identify them (Fig. 17.5). Stokkel et al. (1999) reported that FDG-PET detected a second primary tumor in 12 of 68 patients with primary head and neck cancer. Among the 12 patients, only five were also detected by clinical or radiologic examinations. In a recent prospective study of 33 patients with stage II–IV carcinoma of the oral cavity, oropharynx and larynx, FDG-PET detected distant metastases or synchronous second primary tumors in the aerodigestive tract in almost 30% of cases (seven distant metastases and three syn-

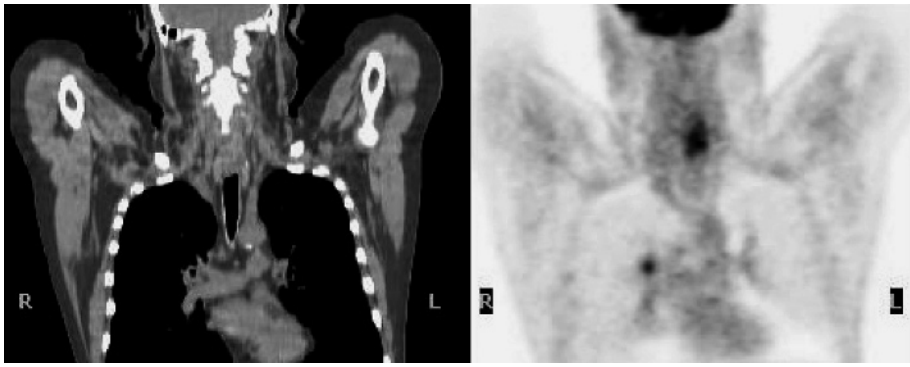

Fig. 17.5. Whole body PET-CT in a 59-year-old man with a SCC of the pharynx also shows an increased FDG uptake at the right pulmonary hilar region, confirmed to be an early stage primary lung cancer

chronous second primary tumors) (Schwartz et al. 2003). Nishiyama et al. (2005) evaluated the presence of simultaneous primary tumors in 53 patients with head and neck cancer. Six patients (11%) had evidence of a simultaneous primary tumor, and five were detected by PET.

17.2.3 Detection and Staging of Recurrent Disease

The basic rationale for the use of PET in the post-therapeutic surveillance of patients with previously treated head and neck SCC is that earlier and more accurate detection of cancer recurrence may improve survival. The specificity of anatomy-based imaging modalities is severely hampered by post-treatment anatomic distortions, tissue thickening, fibrosis and the presence of post-surgical flaps. Indeed, the findings on CT and MRI studies are often equivocal regarding the detection of recurrent or residual tumors in the irradiated or post-surgical head and neck region, and therefore further diagnostic evaluation is required. Deep and multiple biopsy specimens must therefore often be performed for confirmation of cancer. However, doing so can induce necrosis and/or infection in irradiated tissue.

FDG-PET has a high sensitivity and specificity for the detection of recurrent disease, regardless of the primary treatment modality. Results of recent studies indicate a sensitivity between 83% and 100% and a specificity between 61% and 94% for FDG-PET, compared to CT/MRI rates of 38%–75% and 44%–100%, respectively (Schöder et al. 2004a).

The "gold standard" for identifying residual disease in head and neck SCC after therapy is fine-needle biopsy. Collins et al. (1998) demonstrated that if the results from both the fine needle biopsy and FDG-PET were combined, a sensitivity of 94% for detecting recurrent head and neck cancer can be achieved.

Across all studies, the negative predictive value of FDG-PET for detection of recurrent disease is consistently high. Therefore, one could conclude that in a patient with a clinical suspicion of recurrence, a negative FDG-PET scan does not require any further evaluation. In these patients, repeated biopsies should therefore be avoided as these are associated with an increased risk of complication in irradiated tissues, in particular in the larynx.

A probability analysis to assess the clinical utility of FDG-PET in patients with head and neck cancer concluded that the main advantage of PET is the ability to reliably rule out the presence of disease at re-staging (Goerres et al. 2003). In the assessment of recurrence, PET had positive and negative likelihood ratios of 3.96 (2.8–5.6) and 0.16 (0.1–0.25), resulting in probabilities of 49.7% and 3.8%, respectively.

Of special interest is a study by Kunkel et al. (2003) who studied 97 patients with previously resected oral squamous cell carcinoma who were re-staged by FDG-PET. Although 52 of 97 patients had undergone at least one major flap reconstruction, which typically may camouflage regrowth of the tumor, FDG was highly sensitive in revealing tumor recurrence (87%). The specificity of PET varied from 67% for local disease recurrence/second primaries to 99% for lymph node metastasis. Increased FDG uptake predicted an increased hazard of death (hazard ratio, 6.83) and proved to be a highly predictive marker of disease status. A significant association was established for incremental SUVs and 3-year patient survival, indicating that intense glucose metabolism in the tumor is a negative marker of survival in recurrent oral SCC. The authors suggested that a negative

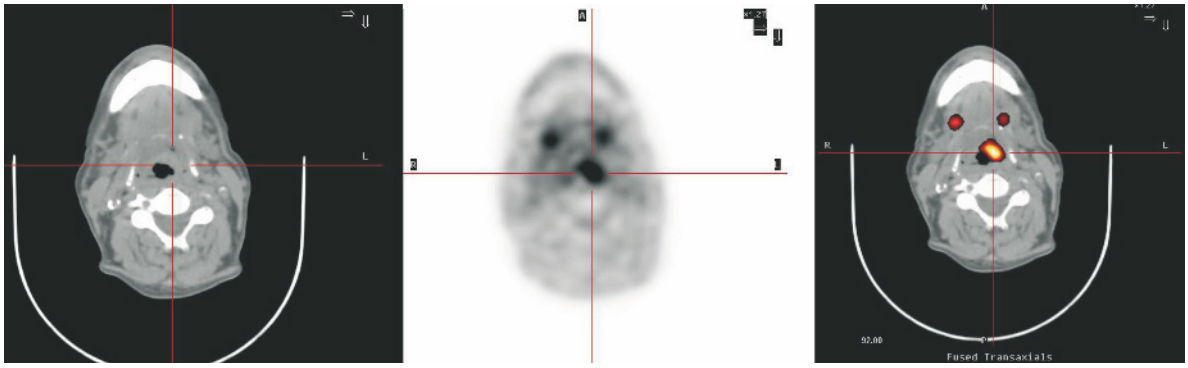

Fig. 17.6. FDG PET-CT images in a 64-year-old man with an history of epiglottic cancer treated by radio-chemotherapy. At 9 months after treatment MRI showed an asymmetry of the epiglottis with no contrast uptake. Transversal PET-CT images show an area of abnormal uptake in the left part of the epiglottis. The PET-CT fusion images allow exact localisation of the lesion. Biopsy confirmed tumor recurrence

PET could justify an early onset of reconstruction measures. If, however, glucose uptake is high, major reconstruction steps should be delayed until further evaluation.

The major challenge of using PET in the setting of recurrent disease is to avoid false-positive diagnosis, particularly at the primary tumor site. Local therapies often induce an inflammatory infiltrate that consists of neutrophils, lymphocytes, and macrophages as well as proliferating fibroblasts. All these cells intensely accumulate FDG. Moreover, most local recurrences are seen in the first 2 years after radiotherapy, coinciding with the period of risk for local inflammation (Terhaard et al. 2001). In that case it is often impossible to discriminate an inflammatory false-positive from a malignant true-positive FDG uptake. Careful correlation of PET and CT/MRI is hereby essential. A positive PET scan without any suspect morphologic correlate requires a biopsy; if the biopsy is negative for recurrent cancer and does not provide reasons for a false-positive PET (inflammation, infection, osteoradionecrosis, etc.), close clinical follow-up and a repeat biopsy may be required. In addition, it is advisable to repeat the PET scanning procedure some weeks later. Terhaard et al. (2001) reported that repeated FDG scanning improved the specificity from 63% to 82% and the positive predictive value from 71% to 84%. If the follow-up FDG-PET shows a decreasing FDG uptake intensity the probability of an underlying recurrence is low and a repeat biopsy can be avoided.

The timing between the PET scan and the end of the local therapy (principally the radiotherapy) is controversial. It may take up to 3 months after radiotherapy for the tumor to disappear completely (Bataini et al. 1990). Some authors reported that early PET after radiotherapy was inaccurate in predicting the presence of cancer; 4 months after radiotherapy was a better predictor of cancer (McGuirt et al. 1995b; Greven et al. 2001). Lonneux et al. (2000) demonstrated that the specificity of PET is drastically reduced in patient scanned early (< 12 weeks) after the end of therapy, related to the high glucose uptake by inflammatory cells that are abundant in irradiated sites. In that study, the accuracy of PET was highest (94%) in the patient subset included more than 12 weeks after the end of the treatment. In contrast, Goerres et al. (2004) support the use of PET performed 6–8 weeks after the completion of a combined radiation and chemotherapy regimen in patients with advanced stage SCC to assess the presence of residual tumor tissue, distant metastases and secondary tumors.

Most studies were conducted in patients who were clinically suspected of having recurrent tumor. The accuracy of FDG-PET for the detection of subclinical recurrence has been studied by Lowe et al. (2000). For this, serial post-therapy FDG-PET imaging was prospectively performed in 44 patients with advanced cancers who had been treated according to a neoadjuvant organ-preservation protocol that included chemotherapy, radiation therapy, and surgical salvage. PET was performed twice during the first post-treatment year (at 2 and 10 months after therapy) and thereafter as needed. PET was studied in comparison to physical examination (including endoscopy) and CT. In all, 16 patients were found to have recurrent disease in the post-operative year. The sensitivities and specificities were calculated to be 44% and 100% for physical examination, 38% and 85% for CT, and 100% and 93% for PET. PET had a statistically significant advantage over the other techniques.

Semiquantitative image analysis using SUV measurements may aid in the interpretation but should not

be the sole criterion on which the study interpretation rests. For instance, Lapela et al. (2000) reported the FDG-PET results obtained in 56 patients with 81 lesions clinically suspect for recurrent carcinoma. The purpose of the study was to compare qualitative image interpretation with quantitative analysis (using SUV). It was found that the visual image analysis was the preferred one, because benign and malignant lesions showed an important overlap in SUV values.

PET-CT could improve the accuracy of detection of a recurrent lesion thanks to the anatomical information provided by the coregistered CT. In a recent study, Schöder et al. (2004b) compared the diagnostic accuracy of attenuation corrected ^{18}FDG-PET with fused ^{18}FDG-PET and CT in patients with head and neck cancer. They also evaluated the effects of PET/CT findings on patient management. A total of 68 patients were reviewed (34 recurrences), presenting a total of 155 foci with abnormal FDG uptake on PET images alone. PET/CT image fusion improved the anatomic localization of 63% of these lesions. The proportion of lesions for which PET/CT image fusion improved the anatomic localization tended to be higher in areas previously treated (surgery or radiotherapy) compared to untreated areas of the head and neck (74% vs. 58% respectively, p=0.06). With PET/CT, the fraction of equivocal lesions decreased by 53% (p<0.01). PET/CT had a higher accuracy of depicting cancer than did PET (96% vs. 90%, p=0.03). Six proven malignancies were missed by PET, while only one was missed by PET/CT. PET/CT findings altered patient management in 18% of patients. The authors concluded that PET/CT is more accurate than PET alone in the detection and anatomic localization of head and neck cancer and has a clear potential to affect patient management.

17.2.4 FDG-PET in Radiation Treatment Planning

Since the introduction of three-dimensional conformal radiation therapy (3DCRT) and intensity-modulated radiation therapy (IMRT), an accurate three-dimensional delineation of target volumes in radiotherapy becomes more and more important. CT has become the reference imaging tool for treatment planning. It provides accurate anatomical definition without geometric distortion. However, the lack of soft tissue contrast between tumors and their surrounding tissues lead to significant intra- and interobserver variations in tumor volume delineation (Hermans et al. 1998).

Only a few reports have studied the potential role of ^{18}FDG-PET for the delineation of gross tumor volume (GTV) in HNSCC (Daisne et al. 2004; Geets et al. 2004).

Daisne et al. (2004) compared CT, MRI and ^{18}FDG-PET for delineation of GTV in 29 patients with pharyngolaryngeal squamous cell carcinoma. They validated the results with the macroscopic surgical specimen when available (nine patients). The average GTV delineated on the surgical specimen was 12.6 cm^3. This volume was smaller than the average GTV assessed by FDG-PET (16.3 cm^3, p=0.06), CT (20.8 cm^3, p=0.003) and MRI (23.8 cm^3, p=0.001). The key finding of this study was that, in comparison with the surgical specimen used as the reference, all the imaging modalities overestimated the tumor extension. Despite this finding, all three imaging modalities failed to depict superficial tumor extension, thereby revealing their insufficient spatial resolution. This warrants the need for adding a security margin that covers the predictable microscopic extension of the tumor to the GTV, which results in the clinical target volume. No significant difference was observed between GTVs delineated at CT and MRI, whereas GTVs assessed at ^{18}FDG-PET were smaller compared to CT and MRI, with a difference ranging from 28% to 37%. The finding that the GTVs delineated at ^{18}FDG-PET were by far the closest to the reference volume assessed from the surgical specimens could have important implications for radiation therapy planning. Another important point made in that study was that PET derived GTVs could be automatically delineated using an automatic algorithm that determined the appropriate iso-activity curve threshold according to the source to background ratio (Daisne et al. 2003). This substantially reduces the duration of the contouring procedure compared to CT or MR imaging and eliminates intra- or interobserver variability. Although the ^{18}FDG-PET-derived GTVs were more accurate than those at CT or MRI, they were still larger than those delineated from the surgical specimens. This overestimation may result from the algorithm used for automatic delineation and/or from the spatial resolution of PET. To date, the question of how the target volume definition would be affected if treatment planning were based only on the area of increased FDG uptake remains to be addressed. Furthermore, it is not known whether such a change of radiation planning would improve local cancer control and outcome for patients. Further work on this interesting topic will undoubtedly be published during the coming years. More information on the use of imaging modalities for radiotherapy planning is found in Chap. 18.

17.2.5 Therapy Monitoring and Planning

It is well known that functional changes, such as tissue metabolism and physiologic functions, often predate structural changes in tissues. Preliminary results from several in vitro and in vivo experiments in different tumor models have recently shown that the change of FDG accumulation early after chemo- or radiotherapy, before any structural effects have occurred, can predict the responsiveness of the tumor to the treatment (Young et al. 1999).

17.2.5.1 Radiotherapy

Histologically similar tumors may respond to irradiation at different rates, and in vitro assays indicate remarkable differences in inherent radiosensitivities of squamous cell cancer of the head and neck (Pekkola-Heino et al. 1992). Since radiosensitivity assays are technically demanding and too slow to be used in routine clinical practice, a reliable and clinically feasible method to predict the outcome of radiotherapy would be of great value. A method capable of early recognition of patients likely to have a poor response to standard radiotherapy would give an opportunity for a more individualized therapy, and save those patients with radiosensitive tumors from mutilating surgery. The use of metabolic imaging techniques in this regard looks very appealing because, by means of these techniques, early metabolic changes induced by the treatment may relate to a final responsiveness of the particular tumor to a particular treatment.

Using conventional diagnostic modalities for identification of residual disease during and after radiation therapy is hampered by radiation-induced facial plane distortion, dense scarring, inflammation and fibrosis. Minn et al. (1988) were the first to indicate the potential of FDG-PET to assess the effects of radiation on head and neck SCC. In that study, 19 patients were studied before and during radiation therapy (at 30 Gy). Of the 19 patients, 14 had decreased FDG uptake in the treated neoplasm. Of these 14 patients, 12 had a marked subjective response to radiotherapy. It was found that among the responders the administered dose of radiotherapy correlated with the decrease in FDG activity. Rege et al. (1993) reported on the effects of radiotherapy on the FDG uptake in normal structures within the radiation port. For this, 11 patients were studied with FDG-PET before, during and 6 weeks after a 6-week course of radiation therapy. FDG uptake in the primary tumor increased early during the course of radiotherapy (< 20 Gy) but decreased near the end of therapy (> 45 Gy), whereas there was no significant change in normal structures of the neck after 6 weeks of radiotherapy. Tumour FDG uptake decreased in all responding cases, but increased after 6 weeks of treatment in those resistant to treatment. They concluded that persistent uptake on FDG-PET 1 month after radiotherapy strongly suggests residual tumor and that tissue changes immediately after the initiation on radiotherapy may lead to false-positive findings. This early 'flare' phenomenon could be explained as a stress reaction of the tumor cells themselves, which has been observed in vitro during chemotherapy, or can be caused by infiltration of the tumor bed by FDG avid inflammatory and scavenging cells. Greven et al. (1994) studied 22 head and neck SCC patients before and 1 and 4 months after high dose irradiation. All patients' tumors showed decreased levels of FDG uptake. Post-radiation PET scans were interpreted as normal in 16/22 patients. Of these, three had histologically documented persistent or recurrent disease. Of the six patients with decreased but persistent FDG uptake, persistent disease has been documented in all. Thus, also this study pointed out that negative findings on scans obtained 1 month after treatment were not an accurate indicator of absence of disease, and that persistent FDG uptake is a bad prognostic sign. In a more recent study, Kunkel et al. (2003) reported that post-radiotherapy FDG uptake predicts survival and local tumor control. The authors analyzed the prognostic significance of glucose metabolism after neoadjuvant radiotherapy (36 Gy) immediately before tumor resection. The 3-year survival rates were 80% in the group with a low SUV (< 4) and 43% in the group with a high SUV (≥ 4). A high FDG uptake was associated with an increased death rate and local progress even when radical resection was performed.

17.2.5.2 Chemotherapy and Combination Therapy

17.2.5.2.1 Early Response

There is a paucity of FDG-PET data obtained during the course of chemotherapy in patients with head and neck SCC and the comparison of the results is difficult because of differences in methods of analyses and the small number of patients studied.

The first report on the use of FDG-PET to assess the metabolic response of head and neck SCC to

chemotherapy was published by Haberkorn et al. (1993). In all, 11 patients underwent FDG-PET imaging before and 1 week after a first chemotherapeutic cycle (5-FU and cisplatinum). The chemotherapy induced change in FDG uptake was correlated with the growth rate as measured by serial CT. It was observed that multiple lymph node in the same patient showed different baseline metabolisms and also different changes following therapy. This was explained by the concept of cell heterogeneity in human tumors; different metastatic clones can lead to metastases with a different biologic behaviour and reactivity to a treatment. Also, in the same study, the primary tumors were more sensitive to therapy than the metastatic lymph nodes.

Lowe et al. (1997) performed serial FDG-PET imaging in 27 patients with stage III/IV head and neck SCC before and after (1–2 weeks) chemotherapy. The sensitivity and specificity of PET for detection of residual disease was 90% (19/21) and 83% (5/6), respectively. Those who achieved complete remission had a mean reduction in FDG uptake of 82%; in comparison, those who had residual disease after therapy had a reduction of 34%.

Dalsaso et al. (2000) prospectively evaluated FDG-PET before and after two or three cycles of chemotherapy in 19 patients with stage III or IV head and neck SCC. A complete pathologic response on biopsy was observed in three patients who had a mean SUV reduction of 82%, the others who had an SUV reduction of only 32% were determined to have residual disease after chemotherapy.

Brun et al. (2002) evaluated FDG-PET for the prediction of radiochemotherapy outcome in locally advanced SCC. A total of 47 patients underwent FDG-PET before and after 1–3 weeks of radical treatment with evaluation of metabolic rate (MR) and SUV. All patients received radiotherapy, and ten also received neoadjuvant chemotherapy. After therapy a high FDG MR (> 16 µmol/min/100 g) was associated with a complete response in 62% of patients while remission occurred in 96% of patients with a low MR (<16 µmol/min/100 g), with 5-year overall survival in 72% and 35%, respectively. Post-treatment SUV showed a poorer association with survival.

17.2.5.2.2 After Completion of Treatment

It is always a challenge to determine the most optimal period for performing FDG-PET imaging during the post-therapy follow-up period.

As already discussed above, FDG-PET performed shortly after a treatment may be associated with high false-positive results because of the tissue healing process, and with false-negative results because of alterations in FDG uptake kinetics. The optimal timing is a balance between a number of competing factors, which include sufficient time for resolution of the therapy induced inflammatory response (to minimize false-positive results) and for residual disease to reach the threshold of resolution by PET (to minimize false-negative results).

In a recent study, Porceddu et al. (2005) evaluated the utility of PET in detecting residual disease in the neck lymph node, at least 8 weeks after (chemo-) radiotherapy in 39 patients who have achieved a complete response at the primary site. In all, 32 patients had a negative PET for residual nodal disease. Only one locoregional failure was observed during the median follow-up of 34 months. The negative predictive value of PET for viable disease in residual neck node was 97%, while the positive predictive value was only 71%. These authors conclude that patients who achieved a complete response at the primary site but have a residual abnormality in the neck which is negative on FDG-PET performed approximately 12 weeks after treatment, do not require neck dissection and can be safely observed. Further studies are needed for confirmation.

Another study on the effects of combined radiochemotherapy was reported by Sakamoto et al. (1998). A total of 22 patients were scanned before treatment, and 1 month after radiotherapy and/or chemotherapy (carboplatin). The mean radiation dose was 57 Gy for the patients undergoing radiation therapy alone, and 42 Gy for those undergoing combination therapy. The post-therapy SUVs were significantly lower than the pre-therapy values (mean 7.0 vs. 3.8). The mean post-therapy SUVs in patients with complete response, partial response and stable disease (no response) were 2.7, 3.6, and 4.5. Histopathological examination revealed that patients with residual viable tumor cells had significantly higher SUVs (range, 2.9–8.3) than those without viable tumor cells (range, 1.9-3.3). These findings were confirmed by Kitagawa et al. (1999). They evaluated the use of FDG-PET to assess the effectiveness of combined intra-arterial chemotherapy and radiotherapy of head and neck SCC. A small group of 14 patients completed the treatment regimen and underwent FDG-PET before and 4 weeks after chemoradiotherapy. In this patient group, pre-treatment FDG uptake was predictive for the response to treatment. Patients with post-treat-

ment tumor SUVs of > 4 were more likely to have persistent disease than those with SUVs < 4.

17.2.6 Prognostic Value

Recent data suggest that FDG uptake may have prognostic value in some tumors, including lung and breast cancer, because patients with high FDG uptake were observed to have a worse outcome. The potential value of FDG in predicting outcome in head and neck cancers, has been suggested in small series of patients.

Pretherapy FDG uptake (expressed as SUV) may be a useful parameter to identify those patients who should require more aggressive treatment.

Some recently published studies on primary tumors suggested that high FDG uptake may be an useful parameter for identifying particularly aggressive tumors. Allal et al. (2002) evaluated pre-therapy FDG uptake as a predictor of local control and disease-free survival (DFS) after radiotherapy with or without chemotherapy in 63 head and neck SCC patients. In a multivariate analysis, SUV was found to be an independent predictor of DFS. Patients with high SUV (> 5.5) had significantly lower 3-year local control (55% vs. 86%) and DFS (42% vs. 79%) rates than patients with low SUV (< 5.5). Another study (Halfpenny et al. 2002) studied 58 patients with newly diagnosed SCC of the head and neck. They underwent FDG-PET before treatment. The median SUV value for all primary tumors was 7.16. Multivariate analysis demonstrated that an SUV > 10 provided prognostic information independent of the tumor stage and diameter. They conclude that high FDG uptake is an important marker for poor outcome in primary head and neck SCC.

Another study from Kitagawa et al. (2003) was prospectively conducted in 20 patients with head and neck cancer who completed the treatment regimen (neoadjuvant chemotherapy and concomitant radiotherapy) and underwent two FDG-PETs (one prior and one after treatment). Tumours with high pre-SUV (> 7) appeared to be more resistant to treatment. This may be because higher FDG uptake indicates greater cell viability or a higher propensity of cells to divide, or both (Haberkorn et al. 1991; Higashi et al. 1993). The data on FDG uptake in association with proliferative activity or with cellularity in malignant tumors are controversial. In clinical studies, cellularity rather than proliferative activity has been suggested to have a significant relationship to FDG.

There is currently no consensus of how the prognostic information derived from PET should influence the patient management. For this purpose, large scale prospective studies are needed in which the value of PET is compared to other molecular prognostic markers (such as p53 mutation, angiogenesis, hypoxia, Ki67, etc.).

17.3 Conclusion

FDG-PET has a good sensitivity and specificity for the detection of primary tumor in the head and neck and for nodal staging. PET-CT will probably be even more powerful than PET alone in the initial staging of head and neck cancer. FDG-PET can detect in a single examination distant metastases and second synchronous tumors. It can help in a significant number of patients to find the primary tumor in cases of neck metastases from an unknown primary.

FDG-PET is highly accurate in suspected tumor recurrence, even in asymptomatic patients. Across all studies, the negative predictive value is consistently high. Therefore, one could conclude that patients with a clinical suspicion of tumor recurrence and a negative FDG-PET scan do not require any further evaluation. A positive PET scan without any suspect morphologic correlate requires a biopsy; if the biopsy is negative for recurrent cancer and does not provide reasons for a false-positive PET, close clinical follow-up and a repeat biopsy may be required.

The treatment response to chemo- and radiation therapy can be monitored with FDG-PET.

New emerging techniques or procedures, such as combining PET with sentinel node scintigraphy for staging the N0 neck, the use of FDG-PET in radiation treatment planning, and the use of PET for early prediction of treatment efficacy look very promising. However, further evaluation and standardization certainly is needed before the implementation in daily clinical practice.

The added value of the recent introduction of PET/CT as multimodality imaging tool in daily practice should not be underestimated in the head and neck region. It permits much better distinction between the different anatomic structures and decreases substantially the fraction of equivocal lesions, providing a higher diagnostic accuracy compared to PET alone, with or without visual comparison with CT images.

References

Adams S, Baum RP, Stuckensen T (1998). Prospective comparison of 18F-FDG-PET with conventional imaging modalities (CT, MRI, US) in lymph node staging of head and neck cancer. Eur J Nucl Med 25:1255–1260

Allal AS, Dulguerov P, Allaoua M, et al. (2002) Standardized uptake value of 2-(18)F fluoro-2-deoxy-D-glucose in predicting outcome in head and neck carcinomas treated by radiotherapy with or without chemotherapy. J Clin Oncol 20:1398–1404

Balkissoon J, Rasgon BM, Schweitzer L (2004) Lymphatic mapping for staging of head and neck cancer. Semin Oncol 31:382–393

Benchaou M, Lehmann W, Slosman D, et al. (1996) The role of FDG-PET in the preoperative assessment of N-staging in head and neck cancer. Acta Otolaryngol 116:332–335

Branstetter BF 4th, Blodgett TM, Zimmer LA, et al. (2005) Head and neck malignancy: is PET/CT more accurate than PET or CT alone? Radiology 235:580–586

Brun E, Kjellen E, Tennvall J, et al. (2002) FDG PET studies during treatment: prediction of therapy outcome in head and neck squamous cell carcinoma. Head Neck 24:127–135

Cohade C, Osman M, Pannu HK, Wahl RL (2003) Uptake in supraclavicular area fat ("USA-Fat"): description on 18F-FDG PET/CT. J Nucl Med 44:170–176

Collins BT, Gardner LJ, Verma Ak, et al. (1998) Correlation of fine needle aspiration biopsy and fluoride-18 fluorodeoxyglucose positron emission tomography in the assessment of locally recurrent and metastatic head and neck neoplasia. Acta Cytol 42:1325–1329

Dahlbom M, Hoffman E, Hoh C, et al. (1992) Whole-body positron emission tomography: part 1. Methods and performance characteristics. J Nucl Med 33:1191–1199

Daisne JF, Sibomana M, Bol A, et al. (2003) Tri-dimensional automatic segmentation of PET volumes based on measured source-to-background ratios: influence of reconstruction algorithms. Radiother Oncol 69:247–250

Daisne JF, Duprez T, Weynand B, et al. (2004) Tumor volume in pharyngolaryngeal squamous cell carcinoma: comparison at CT, MR imaging, and FDG PET and validation with surgical specimen. Radiology 233:93–100

Dalsaso TA, Lowe VJ, Dunphy FR, et al. (2000) FDG PET and CT in evaluation of chemotherapy in advanced head and neck cancer. Clin Positron Imaging 3:1–5

Di Martino E, Nowak B, Hassan H, et al. (2000) Diagnosis and staging of head and neck cancer. Arch Otolaryngol Head Neck Surg 126:1457–1461

Geets X, Daisne JF, Gregoire V, et al. (2004) Role of 11-C-methionine positron emission tomography for the delineation of the tumor volume in pharyngo-laryngeal squamous cell carcinoma: comparison with FDG-PET and CT. Radiother Oncol 71:267–273

Goerres G, Hany TF, Kamel E, et al (2002) Head and neck imaging with PET and PET-CT: artefacts from dental metallic implants. Eur J Nucl Med 29:367–370

Goerres GW, Mosna-Firlejczyk K, Steurer J, et al. (2003) Assessment of clinical utility of F-18-FDG-PET in patients with head and neck cancer: a probability analysis. Eur J Nucl Med Mol Imaging 30:562–571

Goerres GW, Schmid DT, Bandhauer F, et al. (2004) Positron emission tomography in the early follow-up of advanced head and neck cancer. Arch Otolaryngol Head Neck Surg 130:105–109

Greven KE, Williams DW, Keyes JW, et al. (1994) Positron emission tomography of patients with head and neck carcinoma before and after high dose irradiation. Cancer 74:1355–1359

Greven K, Williams DW, McGuirt F, et al. (2001) Serial positron emission tomography scans following radiation therapy of patients with head and neck cancer. Head Neck 263:942–946

Haberkorn U, Strauss LG, Reisser C, et al. (1991) Glucose uptake, perfusion and cell proliferation in head and neck tumors: relation of positron emission tomography to flow cytometry. J Nucl Med 32:1548–1555

Haberkorn U, Strauss LG, Dimitrakopoulou A, et al. (1993) Fluorodeoxyglucose imaging of advanced head and neck cancer after chemotherapy. J Nucl Med 34:12–17

Haberkorn U, Bellemann ME, Altmann A, et al. (1997) PET 2-fluoro-2-deoxy-D-glucose uptake in rat prostate adenocarcinoma during chemotherapy with gemcitabine. J Nucl Med 38:1215–1221

Halfpenny W, Hain SF, Biassoni L, et al. (2002) FDG-PET. A possible prognostic factor in head and neck cancer. Br J Cancer 86:512–516

Hamakawa L, Takemura K, Sumida T et al. (2000) Histological study on pN upgrading of oral cancer. Virchows Arch 437:116–121

Hermans R, Feron M, Bellon E, et al. (1998) Laryngeal tumor volume measurements determined with CT: a study on intra- and interobserver variability. Int J Radiat Oncol Biol Phys 40:553–557

Higashi K, Clavo AC, Wahl RL (1993) In vitro assessment of 2-fluoro-2-deoxy-D-glucose, L-methionine and thymidine as agents to monitor the early response of a human adenocarcinoma cell line to radiotherapy. J Nucl Med 34:773–779

Jones T (1996) The imaging science of positron emission tomography. Eur J Nucl Med 23:807–813

Kao J, Hsieh J, Tsai S, et al. (2000) Comparison of 18-fluoro-2-deoxyglucose positron emission tomography and computed tomography in detection of cervical lymph node metastases of nasopharyngeal carcinoma. Ann Otol Rhinol Laryngol 109:1130–1134

Kinahan PE, Townsend DW, Beyer T, et al. (1998) Attenuation correction for a combined 3D PET/CT scanner. Med Phys 25:2046–2053

Kitagawa Y, Sadato N, Azuma H, et al. (1999) FDG PET to evaluate combined intra-arterial chemotherapy and radiotherapy of head and neck neoplasms. J Nucl Med 40:1132–1137

Kitagawa Y, Sano K, Nishizawa S, et al. (2003) FDG-PET for prediction of tumour aggressiveness and response to intra-arterial chemotherapy and radiotherapy in head and neck cancer. Eur J Nucl Med 30:63–71

Kovács AF, Döbert N, Gaa J, et al. (2004) Positron emission tomography in combination with sentinel node biopsy reduces the rate of elective neck dissections in the treatment of oral and oropharyngeal cancer. J Clin Oncol 22:3973–3980

Kubota R, Yamada S, Kubota K, et al. (1992) Intratumoral distribution of fluorine-18-Fluorodeoxyglucose in vivo: high accumulation in macrophages and granulation tissues studied by microautoradiography. J Nucl Med 33:1972–1980

Kunkel M, Förster GJ, Reichert TE, et al. (2003) Detection of recurrent oral squamous cell carcinoma by 18F-2-fluoro-

deoxyglucose-positron emission tomography. Cancer 98:2257–2265
Lapela M, Eigtved A, Jyrkkio S, et al. (2000) Experience in qualitative and quantitative FDG PET in follow-up of patients with suspected recurrence from head and neck cancer. Eur J Cancer 36:858–867
Lonneux M, Lawson G, Ide C, et al. (2000) Positron emission tomography with fluorodeoxyglucose for suspected head and neck tumor recurrence in symptomatic patient. Laryngoscope 110:1493–1497
Lowe VJ, Dunphy FR, Varvares M, et al. (1997) Evaluation of chemotherapy response in patients with advanced head and neck cancer using (F-18)fluorodeoxyglucose positron emission tomography. Head Neck 19:666–674
Lowe V, Kim H, Boyd JH, et al. (1999) Primary and recurrent early stage laryngeal cancer: preliminary results of 2-(Fluorine 18)fluoro-2-deoxy-D-glucose PET imaging. Radiology 212:799–802
Lowe VJ, Boyd JH, Dunphy FR, et al. (2000) Surveillance for recurrent head and neck cancer using positron emission tomography. J Clin Oncology 18:651–658
McGuirt W, Keyes J, Greven K, et al. (1995a) Preoperative identification of benign versus malignant parotid masses: a comparative study including positron emission tomography. Laryngoscope 105:579–584
McGuirt WF, Williams III DW, Keyes Jr, et al. (1995b) A comparative diagnosis study of head and neck nodal metastasis. Laryngoscope 105:373–375
Minn H, Joensuu H, Ahonen A, et al. (1988) Fluorodexyglucose imaging: a method to assess the proliferative activity of human cancer in vivo comparison with DNA flow cytometry in head and neck tumors. Cancer 61:1776–1781
Minn H, Lapela M, Klemi PJ, et al. (1997) Prediction of survival with fluorine-18-fluorodeoxyglucose and PET in head and neck cancer. J Nucl Med 38:1907–1911
Nishiyama Y, Yamamoto Y, Yokoe K, et al. (2005) FDG PET as a procedure for detecting simultaneous tumours in head and neck cancer patients. Nucl Med Commun 26:239–244.
Pauwels E, McCready VR, Stoot JH, et al. (1998) The mechanism of accumulation of tumour-localising radiopharmaceuticals. Eur J Nucl Med 25:277–305
Pekkola-Heino K, Kulmala J, Grenman R (1992) Sublethal damage repair in squamous cell carcinoma cell lines. Head Neck 14:196–199
Porceddu SV, Jarmolowski E, Hicks RJ, et al. (2005) Utility of positron emission tomography for the detection of disease in residual neck nodes after (chemo)radiotherapy in head and neck cancer. Head Neck 27:175–181
Rege SD, Chaiken L, Hoh CK, et al. (1993) Change induced by radiation therapy in FDG uptake in normal and malignant structures of the head and neck: quantification with PET. Radiology 189:807–812
Sakamoto H, Nakai Y, Ohashi Y, et al. (1998) Monitoring of response to radiotherapy with fluorine-18 deoxyglucose PET of head and neck squamous cell carcinomas. Acta Otolaryngol Suppl 538:254–260
Schwartz DL, Rajendran J, Yueh B, et al. (2003) Staging of the head and neck squamous cell cancer with extended-field FDG-PET. Arch Otolaryngol Head Neck Surg 129:1173–1178
Schöder H, Yeung HWD (2004a) Positron emission imaging of head and neck cancer, including thyroid carcinoma. Semin Nucl Med 34:180–197 (review)
Schöder H, Yeung HWD, Gonen M, et al. (2004b) Head and neck cancer: clinical usefulness and accuracy of PET/CT image fusion. Radiology 231:65–72
Shuller DE, McGuirt WF, McCabe BF, et al. (1984) The prognostic significance of metastatic cervical lymph nodes. Laryngoscope 94:1086–1090
Strauss LG (1996) Fluorine-18 deoxyglucose and false-positive results: a major problem in the diagnostics of oncological patients. Eur J Nucl Med 23:1409–1415
Stoeckli SJ, Steinert H, Pfaltz M, et al. (2002) Is there a role for positron emission tomography with 18F-fluorodeoxyglucose in the initial staging of nodal negative oral and oropharyngeal squamous cell carcinoma. Head Neck 24:345–349
Syed R, Bomanji JB, Nagabhushan N, et al. (2005) Impact of combined (18)F-FDG PET/CT in head and neck tumours. Br J Cancer 92:1046–1050
Terhaard CH, Bongers V, van Rijk PP, et al. (2001) F-18-fluorodeoxy-glucose positron-emission tomography scanning in detection of local recurrence after radiotherapy for laryngeal/pharyngeal cancer. Head Neck 23:933–941
Warburg O. (1956) On the origin of cancer cells. Science 123:309–314
Young H, Baum R, Cremerius U, et al. (1999) Measurement of clinical and subclinical tumour response using 18F-fluorodeoxyglucose and positron emission tomography: review and 1999 EORTC recommendations. Eur J Cancer 35:1773–1782

18 Use of Imaging Data in Radiotherapy Planning of Head and Neck Cancer: Improved Tumour Characterization, Delineation and Treatment Verification

Sandra Nuyts

CONTENTS

S. Nuyts, MD, PhD
Professor, Department of Radiation-Oncology, University Hospital Gasthuisberg, Herestraat 49, 3000 Leuven, Belgium

18.1 Introduction

Radiotherapy is used as part of the treatment in the majority of patients with head and neck cancer (HNC) during the course of their disease. In the last decade there have been important advances in the delivery of radiotherapy which have been made possible by the development of more powerful computers for treatment planning, delivery and data processing. The integration with better immobilisation of patients and advances in linear accelerator design such as multileaf beam collimators and on-line portal imaging systems, allow more accurate delivery of high radiation doses to the target volume while sparing the normal tissues. These developments imply, however, a more rigorous delineation of target volumes and organs at risk.

The greatest challenge for radiation therapy is to attain the highest probability of cure with the least toxicity. To attain this goal, all cancer cells should be encompassed with sufficient dose of radiation during each fraction, while simultaneously sparing the surrounding normal tissues. Therefore, exact identification of the tumour cells is necessary. Technical improvements in the application of computed tomography scans (CT), magnetic resonance imaging (MRI), ultrasound, positron emission scans (PET) and electronic portal imaging have greatly improved our ability to identify tumours.

Initially, surface anatomy and radiographs were used to delineate the treatment site. This implied large treatment fields, which encompass large amounts of normal tissue. In a second step, thanks to the advent of the simulator, internal bony landmarks could be used by the radiation oncologist to guide the field set-up. Treatment planning was performed in a single plane with doses displayed as isodose lines (Table 18.1). Over the past 10 years, image-guided radiotherapy (IGRT) has come to our attention and CT became routine. Tumours and organs at risk are contoured on the CT images and three-dimensional (3D) images of these structures are reconstructed. Doses are displayed as dose-volume histograms.

Table 18.1. Progress in radiotherapy planning

Evolution	Target definition based on:	Dose calculation:
1D	External anatomy landmarks	At selected points
1950s: 2D	Radiographic anatomy	Planar isodose distribution
1970s: 3D	CT, MRI	3D conformal, IMRT
1990s: Functional imaging	PET scanning, functional MRI	Selective target dose optimisation
Future: Molecular imaging	Biologic, genotypic, phenotypic tumour data	Specific target therapy

MRI is now the standard imaging modality to evaluate nasopharyngeal carcinoma and has complementary value in other localisations of HNC. These modalities still depend on morphologic information for diagnosis. Therefore, the use of (18) F-fluoro-2-deoxy-D-glucose PET (^{18}FDG-PET) has recently drawn attention as a useful and valuable diagnostic tool in tumour delineation which offers the opportunity to obtain functional information about the tumour. However, co-registration to CT in order to maintain geographic accuracy is necessary.

The development of these imaging tools made it possible to target the radiation more conformal to the tumour. High precision 3D-conformal radiotherapy and intensity modulated radiotherapy (IMRT) are nowadays being used to maximally cover the tumoral tissues and to maximally avoid the normal structures. The obvious advantages associated with sparing of the salivary glands have pushed IMRT in the standard treatment of HNC faster than other cancer sites.

Today, the use of functional imaging in radiotherapy is under investigation. Functional images show metabolic, physiologic, genotypic and phenotypic data that may improve target definition for radiation therapy.

This chapter will focus on recent advances in imaging, both anatomical and functional/molecular imaging techniques, as they apply to radiotherapy. Although a comprehensive description of the technical details of the imaging techniques is beyond the scope of this chapter, we will give a brief overview of the advantages/disadvantages of these various imaging modalities. This will be followed by a review of the current and potential applications of these technologies in radiation oncology. But first, a general view of radiotherapy in HNC will be given.

18.2 General Principles of Radiotherapy for Head and Neck Cancer

Radiotherapy plays a very important role in the management of patients with HNC. Most early-stage tumours can be cured by surgery or by irradiation and both treatment modalities produce similar locoregional control rates. The selection of treatment modality depends on results regarding cosmetic and organ function, patient's condition and preference. In advanced tumours, radiation treatment can be given concomitant with chemotherapy or can be complementary to surgery in order to obtain maximal locoregional control.

In radiotherapy, the dose of radiation that can be delivered to a tumour is limited by the damage caused to the surrounding normal tissues and the consequent risk of complications. Although radiation damages both normal and neoplastic cells, most normal tissues have a small advantage over cancers in their ability to recover from radiation injury. In curative treatment, this difference is amplified to obtain a therapeutic advantage by using multiple small dose fractions over a period of several weeks. The higher the dose delivered, the greater the risk of complications. However, the more normal tissue that can be spared, the greater the potential for escalating the tumour dose. Improvement in locoregional tumour control can be obtained by increasing the dose of radiation. This, however, implies physical and biological optimisation to prevent normal tissue damage. To achieve this optimal dose distribution in the tumour, while sparing the normal tissues, it is critical to accurately delineate the target volumes.

In routine practice in many centers, most head and neck cancers are treated with two-dimensional (2D) radiotherapy consisting of two lateral opposed portals encompassing the primary and the nodal areas, with a separate low neck portal for treatment of the supraclavicular nodes (Fig. 18.1). At some time during treatment, the portals are reduced to limit the radiation dose to the spinal cord. An additional boost is given to the primary tumour and to the grossly involved nodes. This technique has several limitations:

- Total radiation dose can not be increased above 70–74 Gy in 2-Gy fractions without severe late toxicity.
- Salivary glands can not be spared, leading to permanent xerostomia.
- Large amounts of mucosa are being irradiated.
- Matching of the fields can be critical especially if the junction lies over gross disease.

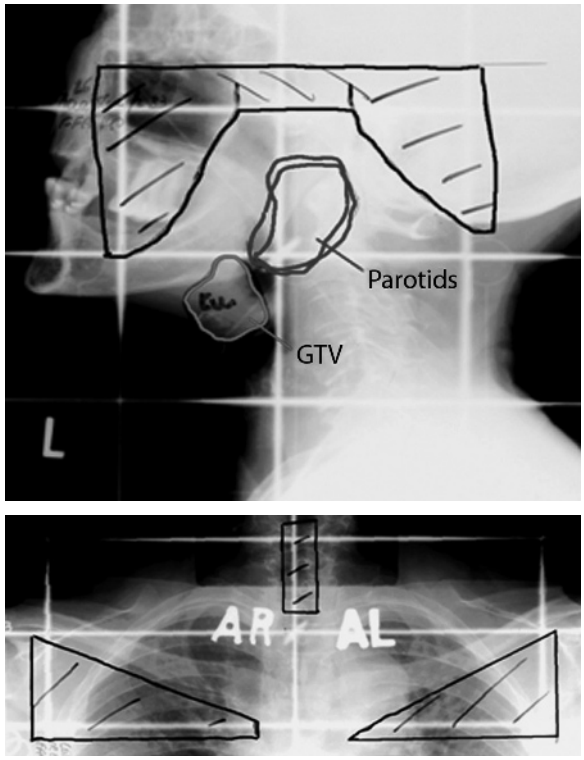

a

b

Fig. 18.1a,b. Standard 2D radiation portals for HNC: two lateral opposed fields (**a**) and a lower anterior field (**b**). In this field setup, both parotid glands receive full dose radiation. *GTV*, gross tumour volume

These issues have led to the development of conformal or CT-based radiotherapy allowing truly 3D dose delivery to the tumour (Fig. 18.2). Planning systems can reconstruct the CT images to a 3D model of the patient. Amongst the software tools available, the 'beam's eye view' display is probably the most used. It consists of a projection of the patient's anatomy as seen from the localisation of the radiation source and thus shows which structures are present in the beam. Beam angles, collimator angles, table angles and field sizes can thus be optimised for each beam. Information on electron densities and tissue depths acquired by CT are necessary for dosimetric computation using appropriate heterogeneity corrections. Following international guidelines concerning dose prescription (ICRU International Commission for Radiation Units 50 & 62), a treatment plan is developed. Dose volume histograms reproduce which radiation doses are delivered to which percentage of the structures (both normal and tumoral) so the treating radiation oncologist can make a prediction of the tumour control probability (TCP) and the normal tissue complication probability (NTCP).

To improve dose distribution to the target even further, IMRT was introduced in clinical practice. As its name implies, IMRT allows us to modulate the intensity of each radiation beam, so each field may have one or more areas of high intensity irradiation, while other areas receive lower doses. By modulating the number of fields and the intensity within each field, radiation dose can be sculpt around the tumour (Fig. 18.2).

High precision 3D-conformal radiotherapy and IMRT present the opportunity to reduce radiation exposure to normal tissues and thereby diminish the extent of toxicity. The head and neck is an ideal site for conformal radiotherapy (3D-CRT and IMRT) due to the complex geometry of this area and the severity of radiation-associated toxicity. Frequently, the distance between either gross tumour volume (GTV) or areas at high risk for microscopic disease (clinical target volume CTV) and critical structures such as optic nerve, spinal cord, brainstem, salivary gland is no more then a few millimetres. In the past, it was extremely difficult to deliver a high radiation dose to the tumour while limiting the dose to an organ at risk just a few millimetres away. The toxicity from head and neck radiotherapy was therefore among the worst seen in radiotherapy. Toxicities are defined as acute or late; acute toxicities are seen during treatment and are usually self-limiting, late toxicities are seen months or years after treatment and are usually permanent. In head and neck radiotherapy most common acute side-effects are mucositis and its accompanying dysphagia and odynophagia, salivary changes and dermatitis. Late toxicities include xerostomia, fibrosis, myelitis and osteonecrosis.

Because of the potential to escalate the dose to the tumour with the aim to improve the locoregional control and to decrease dose to normal tissue and thus reduce toxicity, 3D-CRT and IMRT are introduced in the treatment of HNC, thanks to the progress made in cancer imaging. These new developments, however, imply the risk of geographical misses if tumour delineation is not adequate. Expertise in the knowledge of the anatomy of the head and neck region, clinical examination, knowledge about the regional tumour spread, and interpretation of diagnostic imaging are therefore of major importance.

Another requisite of appropriate dose delivery is optimal patient positioning and immobilisation. In head and neck radiotherapy, masks are used which are fixed to the treatment table to prevent movement of the patient during therapy. This assures the ability to re-establish this position on a daily basis. Planning CT images, taken with the patient in treatment posi-

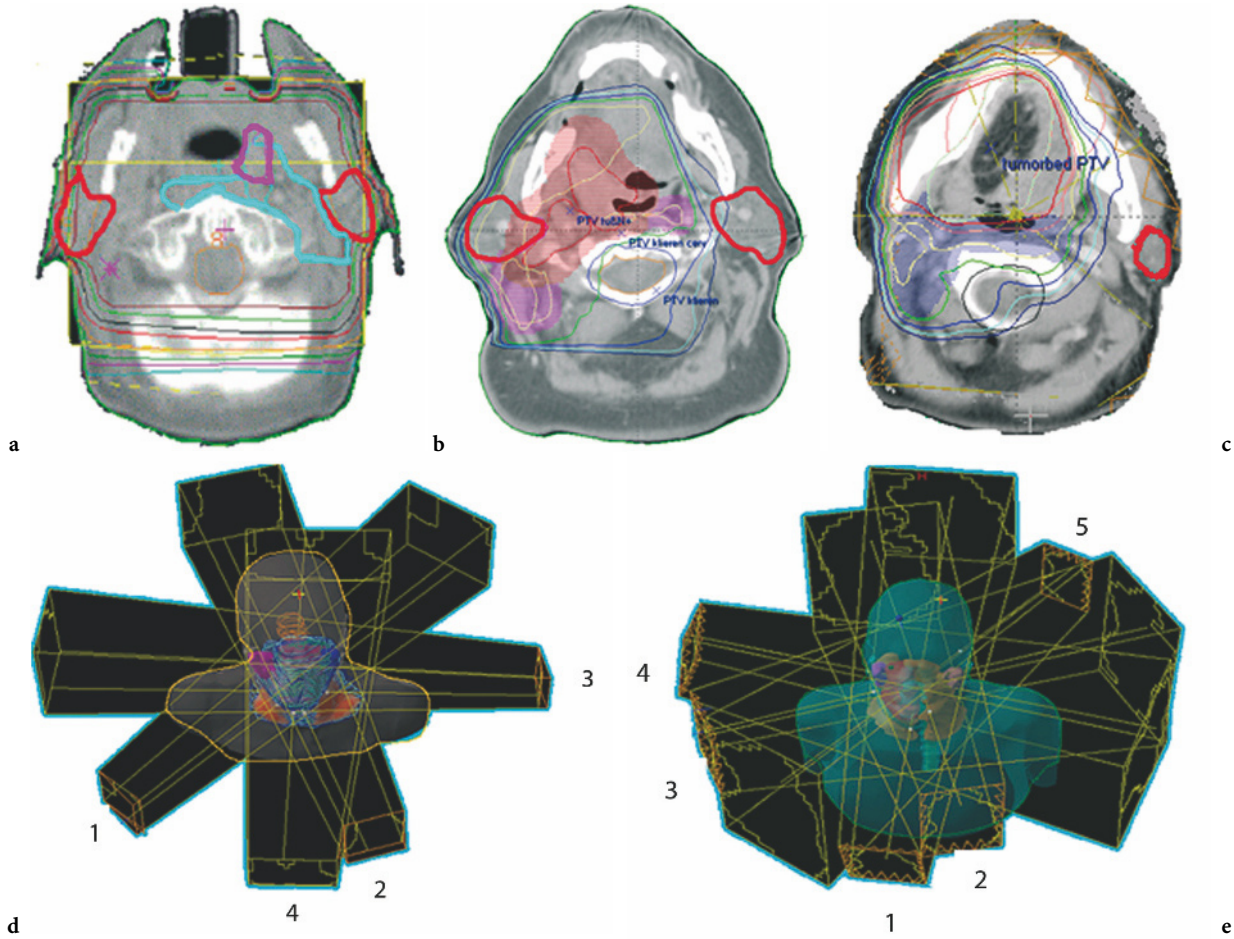

Fig. 18.2a-e. Comparison between isodoses obtained with 2D, 3D and IMRT planning for HNC and field setup for 3D-CRT and IMRT. **a** Isodoses obtained with two lateral opposed fields. **b** Isodoses obtained with three co-planar fields (two oblique anterior and one lateral field). **c** Isodoses obtained with five-field IMRT setup. As shown in the figure, 3D-CRT and IMRT show the capacity to spare the contralateral parotid gland from high doses radiation. **d** 3D-CRT field setup: two upper oblique, one lateral field and a lower anterior field. **e** Five-field IMRT setup

tion, with the patient wearing his or her mask, and on a flat table top are used for delineation of the tumour and organs at risk.

During treatment, target positioning and treatment verification is necessary. The size and shape of the treatment portal can be checked by using the ionising irradiation exiting from the irradiated patient. Adapted radiographic films are commercially available for that purpose. The image quality is less than diagnostic radiographs, but improvements have been made by the development of electronic portal imaging (EPI). Here, fluorescent screens, 2D ion chambers or matrix flat panel imagers are used. These online electronic images have made it possible to check and correct patient positioning before a significant amount of radiation is given (Fig. 18.3).

These recent developments in the use of imaging techniques in head and neck radiotherapy have made it necessary for the radiation oncologist to have excellent knowledge about the use, advantages and disadvantages, as well as interpretation of these different modalities.

18.3 Present Status of Imaging Modalities in Radiotherapy: Overview

The imaging modalities in radiation oncology can be divided into two main categories: anatomical imaging modalities, which provide structural or morphological information, and functional imaging modalities,

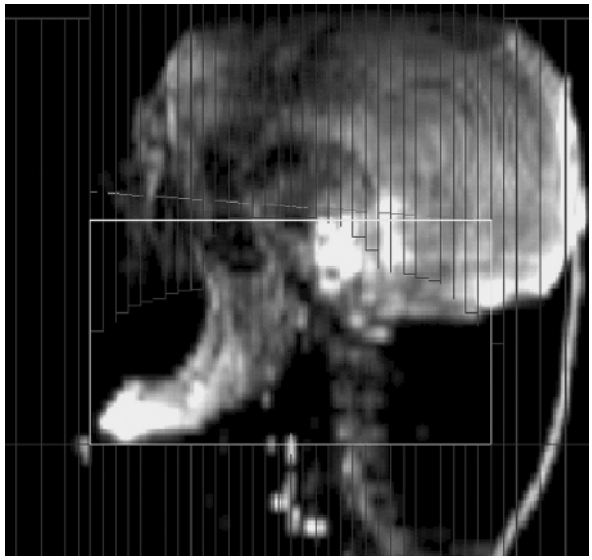

a

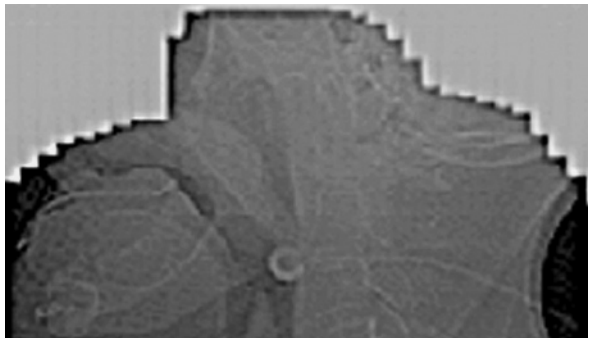

b

Fig. 18.3a,b. Comparison between digitally reconstructed radiograph (**a**) and portal image (**b**). The digitally reconstructed radiograph is reconstructed based on CT images taken in treatment position. The corresponding portal image is obtained during irradiation. Both images are compared to one another to verify patient positioning and size and shape of the treatment portal

which elucidate the biological or molecular features of tissue. The general features of the imaging modalities are summarized in Table 18.2.

Table 18.2. Characteristics of various imaging modalities

Technique	Tumour discrimination	Spatial resolution
Plain radiography	Poor	Poor
CT	Good/average	Excellent
MRI	Excellent/good	Excellent
PET	Good/average	Average

18.3.1 Computed Tomography in Radiotherapy

18.3.1.1 General Considerations

The opportunity to develop more conformal radiotherapy, thanks to the use of CT images, has led to an exponential increase in the use of CT in radiotherapy planning. The development of spiral CT and multi-slice CT leading to reduced examination times, and increased resolution has greatly enhanced the usefulness of CT in tumour detection and delineation. Nowadays, high-quality multiplanar imaging is feasible with CT.

18.3.1.2 Advantages

- Good contrast between air, fat and bone.
- High spatial resolution.
- Widespread availability, (relatively) inexpensive.
- Good geometric accuracy.
- Visualization of bony anatomy for comparison with radiographs.
- Potential for rapid scanning.
- Contrast agents can improve tumour detection and delineation.
- Electronic density mapping availability.

18.3.1.3 Disadvantages

- Differentiation between tumour margins and adjacent normal tissue.
- Contrast agents and scattering caused by for example tooth fillings affect the signal intensity of the tissues and hamper the possibility to convert the signal to true tissue electron density.

18.3.1.4 Special Features

- Patient position must ensure immobilisation and be reproducible.
- The couch top must be the same as the treatment couch.
- Radio-opaque markers used to indicate skin reference marks.
- Between 2- and 10-mm thick slices depending on site.
- Ideally networked to planning computer to enable direct data transfer.
- Accurate calibration of CT numbers for inhomogeneity corrections.
- CT may be used to define a conformal treatment volume from digitally reconstructed radiographs.

18.3.2 Magnetic Resonance Imaging in Radiotherapy

18.3.2.1 General Considerations

MRI provides multi-planar anatomical information with high spatial and contrast resolution.

18.3.2.2 Advantages

- No patient radiation dose
- Excellent soft tissue delineation
- Vast flexibility in imaging protocols allowing optimalisation of image quality according to the tissue of interest
- Functional imaging capabilities
- Molecular imaging capability (e.g. spectroscopy)
- MRI-visible markers (e.g. oil-filled plastic tubes) to indicate skin reference marks
- High spatial resolution (<1 mm)

18.3.2.3 Disadvantages

- No inhomogeneity information available for treatment planning
- Patient positioning may be a problem as scanner aperture is usually small
- Long scan times
- Geometrical distortion must be corrected

18.3.2.4 Use

Today, most treatment planning is based on CT images only. Only for specific sites like nasopharyngeal and paranasal sinus cancers, MRI is used as an adjunct to CT (Fig. 18.4).

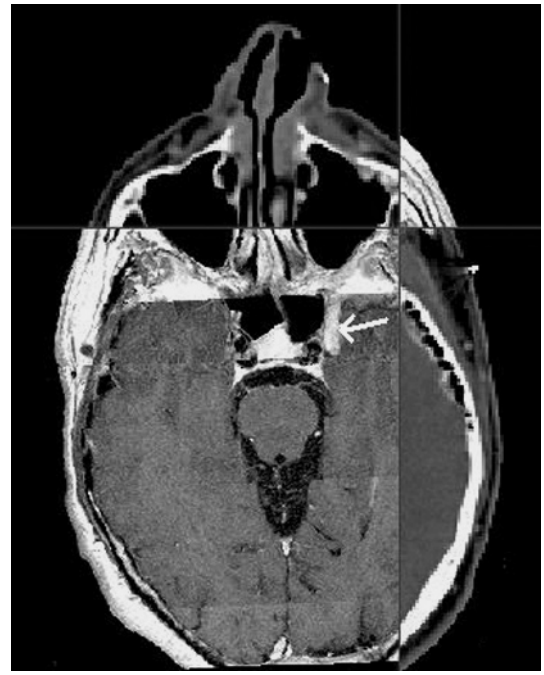

Fig. 18.4. Example of CT/MRI fusion image. A 48-year-old male presented with a tumor recurrence of a squamous cell carcinoma of the facial skin with perineural spread along the infraorbital nerve into the fossa pterygopalatina, with further extension to the lateral wall of the left cavernous sinus (*arrow*). The diagnostic MRI was fused to the CT in treatment position to delineate the perineural spread

18.3.3 Positron Emission Tomography in Radiotherapy

18.3.3.1 General Considerations

Availability of more radionuclides and technological advances in PET scanning have increased the interest in using this modality in radiotherapy treatment planning. PET scanning results in biochemical information. Deoxyglucose labelled with fluorine (FDG) is frequently used to assess functional tumour metabolism.

Several studies have shown that FDG-PET might be better than CT or MRI at detecting cervical involved lymph nodes in HNSCC (Laudenbacher et al. 1995; Adams et al. 1998). The average sensitivity and specificity of PET was 84% and 96%, respectively, compared to 69% and 68%, respectively, for CT/MRI. However, other studies show that FDG-PET offers little additional information over CT and MRI (Stoeckli et al. 2002; Benchaou et al. 1996). These negative studies showed similar sensitivity and specificity for both FDG-PET and CT/MRI. All studies show, however, that the specificity of PET is high, around 90%. The sensitivity for PET to detect small lesions, is however a limitation. Brink et al. (2002) showed a sensitivity of 83% of PET to detect nodes larger than 1 cm^3, but for smaller nodes the sensitivity dropped to 71%.

Many new radiopharmaceuticals are under development.

18.3.3.2 Advantages

- Metabolic/biologic data will be useful to define the biological target volume (BTV).
- Visualize the viable part of tumours.
- Detection of metastasis.
- Differentiate fibrous tissue from the residual mass after radiotherapy or chemotherapy.

18.3.3.3 Disadvantages

- False positive results with FDG-PET (physiological tracer uptake and uptake in inflammatory tissue).
- Lower spatial resolution compared with CT and MRI (about 2–7 mm), leading to false negative results.
- Anatomical localization may be difficult.

18.3.3.4 Use

It is mandatory to register these functional studies with either CT or MR data, in order to define the clinical target volume, that will be used afterwards in radiotherapy planning.

18.4 Applications of Imaging Data in Radiation Oncology

Imaging of tumours and surrounding normal tissues is used for several purposes related to radiation therapy:

- Medical diagnosis, including detection, staging and grading.
- Planning: to determine the treatment fields, we need to delineate the target and organs at risk. Both anatomical and biological imaging modalities are applied.
- Treatment guiding and verification: ensure that the field of irradiation is appropriate throughout the entire treatment period, taking into consideration factors such as:
  - Changes in tumour size and shape
  - Patient positioning variation
  - Variation in anatomy
  - Organ motion
    - All leading to intra- and inter-fraction targeting errors
- Evaluation of response to therapy and follow up:
  - Anatomical changes
  - Functional changes

In the following, we will focus on improved target delineation and treatment verification based on imaging techniques. Combinations of two or more imaging modalities (including 'image fusion') are increasingly important, since complementary information can be provided.

18.4.1 Target Delineation: Anatomical Information

Optimal delineation of the primary tumour and the involved lymph nodes are a prerequisite to perform curative radiotherapy in head and neck cancer. Functional imaging can hereby complement anatomical imaging. In the planning of radiation therapy, it is important to localize the most peripherally located tumour cells, in order to irradiate the tumour tissue as precisely as possible, while sparing the normal, adjacent tissue. Improvement of target definition is therefore one of the most critical steps towards improvement in radiation therapy.

18.4.1.1 CT

CT is at present routinely used for initial delineation of tumour volumes and is considered to be the gold standard. However, both inter- and intraobserver variability in both GTV and CTV delineation exists. Hermans et al. (1998) investigated the inter- and intraobserver variability of CT based volume measurement of 13 laryngeal tumours by five different observers, who repeated the delineation four different times. They found that both interobserver variability and, to a lesser extent, intraobserver variability had a statistically significant effect on volume measurement. They also found that the most experienced observer obtained the most stable mean tumour volume over all sessions. This led them to conclude that variability in the CT-based volume measurements can be reduced by having the measurements done by a single experienced observer. However, this is not evident since not all radiation oncologists are evenly talented in CT image interpretation. Several groups have therefore published guidelines on both delineation of primary tumour CTV and nodal regions, based on CT images (Eisbruch et al. 2002; Gregoire et al. 2003; Chao et al. 2002).

18.4.1.2 MRI

Evidence is growing that complementary information from alternative imaging modalities could help decrease the variability encountered for GTV delineation. MRI shows several potential advantages over CT, such as better discrimination between tumour and normal tissues in many organs. Rash et al. (1997) studied the potential impact of the combined use of CT and MRI on tumour volume delineation in advanced head and neck cancer. Four observers outlined the GTV in six patients with advanced cancers with extension to the base of skull on CT, axial MRI, and coronal or sagittal MRI. They found that MRI-derived GTVs are smaller (difference of 30%) and have less interobserver variation than CT-derived GTVs. The ability to obtain images in any anatomical plane and the superior soft tissue contrast of MRI has led to its use in target delineation in nasopharyngeal carcinoma (NPC). Enami et al. (2003) examined the use of MRI and CT in eight NPC patients. Compared with CT, the MRI-based targets were 74% larger, more irregularly shaped, and did not always include the CTV targets. On average, the composite CT+MRI GTV was 10% larger than the GTV drawn from MRI alone. Therefore, the use of CT-based targets may lead to underdosing of some regions of the tumour. Image fusion allows one to use both CT and MRI information in drawing the target volumes. The authors concluded that fusion of MRI and CT images is recommended in treatment planning for NPC, because it significantly reduces the possibility of missing parts of the tumour volume. This was confirmed by Chung et al. (2004) who studied the impact of MRI versus CT on NPC in 258 patients. They found that MRI was superior to detect intracranial infiltration since in 40.3% of patients this was detected by MRI, whereas CT showed negative findings. Detection of pterygopalatine fossa involvement accompanying intracranial invasion was higher with MRI than CT (96.1% vs. 56.9%).

18.4.1.3 PET

A recent literature survey on the use of ^{18}FDG PET in HNC indicates that when compared with CT, PET has a higher sensitivity (87% vs. 62%) and specificity (89% vs. 73%) for staging cancer, higher sensitivity (93% vs. 54%) and specificity (83% vs. 74%) for imaging recurrences, and higher sensitivity (84% vs. 60%) and specificity (95% vs. 39%) for monitoring effects of therapy (Gambhir et al. 2001). However, ^{18}FDG is not a specific marker for cancer since other normal tissues, including salivary gland, skeletal muscle, brain, and heart can have increased tracer uptake. In addition, activated macrophages and areas of inflammation also show high tracer uptake, which can lead to false-positive examinations.

The impact of PET imaging on target delineation in radiotherapy for HNC has recently been investigated. The utility of PET further improved by the introduction of combination PET/CT scanners. Syed et al. (2005) examined the impact of combined FDG PET/CT in HNC in 24 patients and concluded that PET/CT significantly increases interobserver agreement and improved the confidence in disease localisation of FGD-avid lesions with 51%. However, one crucial remark must be made concerning the interpretation of the PET images. If we want to use PET to delineate volumes, we must define the way the PET images are viewed. For example, changing the window setting changes the interpretation of lesion margins; the optimal window setting for radiotherapy contouring applications has yet to be determined. Until now, every study uses its own threshold, or even does not comment on which threshold was used, which makes it difficult to compare the data.

Scarfone et al. (2004) evaluated the influence and accuracy of FDG-PET in target volume definition as a complementary study to CT. Six HNC patients were studied. Tumours were delineated on CT and modified based on the PET data. The resulting PET-CT GTV was larger than the original CT volume by an average of 15%. The final lymph node volume based on PET+CT was on average 17% larger than the initial CT volume. The authors concluded that PET can act as a complementary modality, providing information on target viability not visible by CT. Koshy et al. (2005) also examined the use of FDG PET in radiotherapy planning for HNC. A total of 36 patients with HNC received PET-CT as part of their treatment planning. In 38% of patients, PET-CT fusion altered the TNM score. Radiotherapy volumes and dose were altered in five patients (14%) and four patients (11%), respectively. Paulino et al. (2005) compared the GTV identified on CT to that obtained from FDG-PET in 40 patients with HNC. They found that the PET-GTV was smaller, the same size, and larger than the CT-GTV in 75%, 8% and 18% of cases, respectively. In approximately 25% of patients, the primary GTV would have been underdosed when the CT-GTV was used for IMRT planning. The authors therefore recommend using both CT- and PET-defined primary tumour in determining the GTV for IMRT. Ciernik

et al. (2003) used integrated PET-CT for target volume definition in 39 patients with various solid tumours, 12 were HNC. They detected an increase in PET-GTV of >=25% compared to CT-GTV in 17% of patients, while the GTV was reduced >=25% in 33% of patients. In patients with nasopharyngeal (*n*, 9) and oropharyngeal (*n*, 12) tumours, Nishioka et al. (2002) found that PET-CT detected 39 positive nodes in contrast to only 28 nodes detected by clinical examination and CT/MRI. In four patients, the nodal status was increased, which impacted on target delineation. Parotid sparing became possible in 71% of patients whose upper neck areas near the parotid glands were tumour free on PET-CT, and, except for one patient, no recurrences were seen at 18 months when the PET-CT defined volumes were used as GTV. In general, all studies conclude that PET adds extra information to both CT and MRI concerning target delineation.

However, we must keep in mind that the majority of FDG-PET findings lack corresponding pathology data. A small study by Schwartz et al. (2005) compared FDG-PET findings with the pathology findings in 20 patients undergoing neck dissection. FDG-PET/CT showed a high nodal staging sensitivity and specificity of 96% and 98.5%, respectively. FDG-PET/CT detected nodal disease in two patients considered to have node-negative disease by CT alone. Daisne et al. (2004) compared CT, MR and FDG-PET in 29 patients with stages II–IV HNC. Nine patients underwent total laryngectomy. PET volumes were delineated based on a specific tumour to background ratio (Daisne et al. 2003). The key finding of this study was that, in comparison with the surgical specimen used as reference, all the imaging modalities tended to result in overestimation of the tumour extension. For anatomical imaging, average GTVs were up to 107% larger, whereas for functional imaging, a 46% overestimation was still observed. Despite this finding, all three imaging modalities failed to depict a small fraction of the subclinical tumour extension, which thereby revealed their insufficient resolution.

Overall, two general questions remain unsolved concerning the use of FDG-PET in radiotherapy treatment planning:

- What is the optimal PET volume for radiation therapy? To the contouring physician, the edges of tumours on PET are fuzzy, unlike CT. As discussed above, some authors arbitrarily define the FDG-avid volume as the region encompassed by the 50% intensity level relative to the tumour maximum (e.g. Paulino et al. 2005; Scarfone et al. 2004; Koshy et al. 2005), others use certain signal-to-background ratio's (e.g. Daisne et al. 2004) as threshold.
- Will treatment of PET-defined tumour improve outcome? In theory, better delineation of the target should mean better tumour coverage and hence better local control. Whether this better treatment planning will have an impact on clinical outcome, either by improving local tumour control or by reducing toxicity remains to be determined.

Clinical studies with optimal follow-up will hopefully bring clarity in these issues.

18.4.2 Target Delineation: Biological Information

Besides the location, size and extent of the tumour, knowledge about biological features of the tumour might be useful in the management of head and neck cancer. Treatment selection may be based on this information, dose-painting can be applied, or response prediction can be extrapolated from these data.

The concept of biological target volume (BTV) was therefore introduced (Ling et al. 2000). This implies the integration of physical and biological conformality, leading to multidimensional conformal radiotherapy. The concept of gross, clinical, and planning target volume (GTV, CTV, and PTV), as proposed by the International Commission on Radiation Units and Measurements Report No. 50 (ICRU 50), is currently used in radiotherapy treatment design. In general, CT, MRI and sometimes FDG-PET are used to delineate the GTV and CTV, and radiation portals are designed to entirely cover the volumes and deliver a uniform dose distribution to it. Recent interest has been developed to create nonuniformity within the targets, more specifically to increase dose to certain tumour subregions in order to increase local control (so-called dose-painting). IMRT has the ability to deliver nonuniform dose distributions, but the question remains how to track the regions of interest. Therefore, there has been a lot of interest in developing imaging modalities to deliver molecular and biological information regarding hypoxia, proliferation, apoptosis, angiogenesis and receptor status of tumours (Chapman et al. 2003). Biological imaging can be of value, but still a lot of research and clinical studies are needed before this can be realized in clinical routine.

18.4.2.1 Hypoxia

Hypoxia is believed to be a major determinant in tumour response to radiation and their subsequent outcome. Hypoxic cells are 2.5–3 times more resistant to ionising irradiation than well-oxygenated cells. Identifying and quantifying tumour hypoxia may predict outcome and identify patients who could benefit from more aggressive radiotherapy to overcome the hypoxic effect. Escalating the dose to these tumour regions might improve outcome. A variety of methods have been used to measure oxygenation of tumours. Clinical studies have been performed using polarographic needle electrodes (Eppendorf, Hamburg, Germany) (e.g. Nordsmark and Overgaard 2004). This, however, is an invasive technique and no discrimination is possible between necrotic tissue and viable hypoxic tissue. Moreover, the presence of tumour heterogeneity prompts the question as to whether these measurements are representative for the entire tumour. An additional drawback is the fact that this technique is only useful for accessible tumours by electrodes. Other noninvasive techniques have gained interest in recent years.

Tumour perfusion and tumoral oxygen concentration are factors that are usually strongly linked, although tumour oxygenation also depends on oxygen consumption by the tumour cells. The tumour perfusion rate can be determined noninvasively by dynamic CT. Hermans et al. (2003) used dynamic CT in 105 patients, treated with radiotherapy, to determine the rate of tumour perfusion. Therefore, a contrast agent bolus was rapidly injected i.v., while during the first pass a dynamic data acquisition was performed at the level of the largest axial tumour slice. The perfusion was calculated by using the time-density curve of the tumour and the maximal value in arterial density. When the patients were stratified according to the median perfusion value, those with lower perfusion rate had a significantly higher local failure rate. The authors concluded that CT-determined tumour perfusion rate was an independent predictor of local outcome in irradiated HNC.

Tissue perfusion can be estimated using MRI from the increase in the T1 signal after the bolus administration of a gadolinium-based contrast medium. Echo-planar dynamic imaging (EPI) can track the uptake of the contrast agent using fast pulse sequences. The derived parametric image can yield pixel by pixel information on blood volume, blood perfusion, diffusion, extravascular space, etc. These techniques can be applied to assess tumour grade and type, treatment response and prognosis. Hoskin et al. (1999) used dynamic contrast enhanced MRI in 13 patients with advanced HNC before and after completion of radiotherapy. The authors found that tumours with diminished tumour perfusion at the end of therapy are those most sensitive to radiotherapy and that those tumours which show greater tumour enhancement after radiotherapy are likely to fail locally. Schmitt et al. (2003) used noninvasive MR spin-labeling techniques to quantify tissue perfusion in HNC patients before and during radiation therapy. Ten patients were examined before radiotherapy, five of them were investigated twice during radiotherapy. In four of five patients studied at the start and end of radiotherapy, perfusion decreased, while in one patient there was an increase. Tumours with high initial perfusion tended to be smaller in size and showed a better response than those showing weak pre-treatment perfusion. Tissue oxygen levels can be assessed noninvasively by blood–oxygen level-dependent (BOLD) fMRI (Krishnan et al. 1988; Taylor et al. 2001; Landuyt et al. 2001) This technique is based on the paramagnetic property of deoxygenated hemoglobin that induces magnetic inhomogeneities, enhances the relaxation of the adjacent water molecules, and thereby decreases the T2* signal adjacent to the blood vessels. Studies by Kaanders et al. (2002) showed that treatment results in advanced HNC can be improved by accelerated radiotherapy with carbogen breathing (a hyperoxic hypercapnic gas mixture) and nicotinamide (ARCON). The mechanism of action of carbogen and nicotinamide is thought to be an increase in tumour oxygenation and thus a reduction of hypoxic regions in the tumour. Rijpkema et al. (2002) investigated tumour vascularity and oxygenation by dynamic gadolinium contrast-enhanced MRI and BOLD MRI, respectively, in 11 HNC patients. Patients were investigated twice, with and without breathing the hyperoxic hypercapnic gas mixture. BOLD MRI revealed a significant increase of the MRI time constant of transverse magnetization decay (T2*) in the tumour during hypercapnic hyperoxygenation, which correlates to a decrease of the deoxyhemoglobin concentration. No changes in overall tumour vascularity were observed, as measured by the gadolinium contrast uptake rate in the tumour. Multiple gradient-echo MRI may thus be an important tool for the assessment of the local oxygenation status of tumours and may assist in the prediction of responses to therapy.

PET scanning can be used to identify and quantify hypoxia in solid tumours. Several tracers have been tested so far, both imidazole and non-imidazole containing agents. ^{18}F fluorinated misonidazole (FMISO)

and ^{123}I-arabinoside act as bioreductive molecules which are reduced and incorporated into the cells under hypoxic conditions (Chapman et al. 1983; Koh et al. 1992). In a study of Rasey et al. (1996), using FMISO-PET, 36 of the 37 patients investigated had hypoxic regions, with fractional hypoxic volumes of 9%. Eschmann et al. (2005) compared the uptake of FMISO of HNC with clinical outcome after treatment. A total of 26 patients with HNC were scanned before radiotherapy and FMISO uptake was quantified using standardized uptake values (SUV) and tumour-to-background ratios. The authors found that patients with local recurrence could be separated from disease-free patients by SUV 4h after injection (all recurrences had SUV>2). All patients with tumour-to-muscle ratio>1.6 presented with tumour recurrence. The authors also found that the activity curve of FMISO was prognostic: tumours with a rapid washout showed no recurrences in contrast to tumours with an accumulation curve. However, FMISO distribution over timed seemed not to be constant. As a consequence, tumour regions defined as hypoxic on the basis of the cutoff values shifted. If one wants to use these data for radiotherapy planning, regional kinetic analysis that takes into account early as well as late FMISO data are needed.

Newer generations of nitroimidazoles have been studied including ^{18}F-labeled fluoroerythronitroimidazole (FETNIM), fluoroetanidazole (FETA) and 2-(2-nitro-1[H]-imidazol-1-yl)-N-(2,2,3,3,3-pentafluoropropyl)-acetamide (EF5). FETNIM and FETA are both more stable to non-oxygen dependent metabolism and have higher tumour-to-background contrast secondary to their increased hydrophilicity (Yang et al. 1995; Lehtio et al. 2001; Rasey et al. 1999). EF5 has already been used for immunohistochemical detection of hypoxia, creating the opportunity to correlate PET findings with immunohistochemistry (Ziemer et al. 2003). A possible drawback of EF5 is the low tumour-to-background ratio due to nonspecific binding caused by its lipophilic nature. FETNIM has already been used clinically to determine the oxygenation status of HNC in patients undergoing radiotherapy. Lehtio et al. (2004) studied 21 patients who underwent multitracer PET scans with FETNIM to evaluate the oxygenation status and [$^{15}O_2$] H_2O to measure the blood flow. PET findings were correlated with the radiotherapy outcome and survival. The authors concluded that tumours with a high blood flow were associated with poor survival. A high FETNIM tumour/plasma ratio or fractional hypoxic volume had no significant relationship with survival in this small series.

Other non-imidazole agents like ^{62}Cu-diacetylbis (N-4-methyl-thiosemicaarbazone; Cu-ATSM) are being evaluated. Cu-ATSM is a potentially good marker for hypoxia because of its rapid uptake, activity ratio, rapid blood clearance and washout from normally oxygenated cells. Chao et al. (2001) examined the feasibility of dose-escalation to hypoxic areas using IMRT by co-registration of Cu-ATSM PET to CT images for treatment planning. This planning study showed that 80 Gy could be delivered in 35 fractions to the hypoxic target volume, with 70 Gy in 35 fractions delivered to the rest of the clinical target volume.

However, temporal stability might be a concern for hypoxia imaging. Intermittent opening and closure of vessels can cause microscopic changes in oxygenation, so-called acute hypoxia (Chaplin et al. 1986). In addition, reoxygenation of hypoxic regions occurs during the 6- to 7-week period of fractionated radiotherapy. Studies on the temporal stability of tumour hypoxia mapping are therefore necessary (Fig. 18.5).

Although these new tracers have promise, much more work remains to be done before they can be used to influence treatment decisions for these patients. The difficult challenge is to validate the correlation with marker uptake and the presence of viable hypoxic cells. This validation is difficult, however, because no gold standard for measuring these tumour properties exists.

18.4.2.2 Proliferation

Uncontrolled proliferation is one of the hallmarks of cancer. Imaging the amount of proliferation may be predictive for tumour response, and regions of high cell proliferation may benefit from dose escalation. Slowly proliferating tumours generally show less FDG uptake than rapidly proliferating tumours. FDG uptake in cells, however, is not an absolutely specific measure of tumour growth or proliferative activity, because regions of inflammation, musculature, are known to take up FDG. Because of this, more specific tracers have been studied. Radiolabeled nucleosides can be used to quantify DNA synthesis and radiolabeled amino acids to infer protein synthesis. The most studied nucleoside tracers is ^{18}F-labeled fluorothymine (FLT), a pyrimidine analogue, which measures indirectly DNA synthesis via the DNA salvage pathway. FLT has high specific activity and good tumour-to-background ratio (Shields et al. 1998). Cobben et al. (2004) studied the use of FLT-PET for visualization of laryngeal cancer in 21 patients and

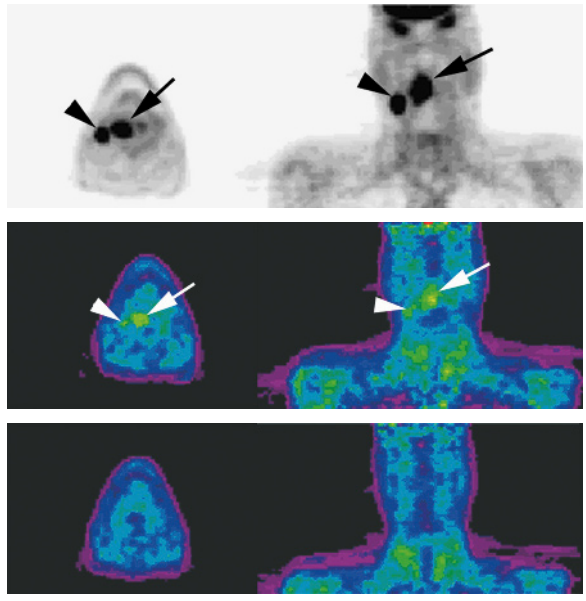

Fig. 18.5a–c. Temporal change in hypoxia. A 57-year-old patient presented with a squamous cell carcinoma of the oropharynx, stage T3N2b. A base-line FDG-PET (**a**) shows uptake at the primary tumour (*black arrow*) and regional adenopathy (*black arrowhead*). A FMISO-PET (**b**) was acquired 1 day later and shows uptake both in the primary tumour (*white arrow*) and the adenopathy (*white arrowhead*), demonstrating the presence of hypoxia. The repeat FMISO-PET after 4 weeks of radiotherapy (**c**) shows a loss in the FMISO uptake suggesting a temporal change in hypoxia

compared these data with FDG-PET. The authors detected an equal amount of tumours with FLT and FDG-PET. In laryngeal cancer, they detected a higher uptake of FDG than FLT. Therefore, the authors concluded that FLT-PET seems less adequate for the detection of laryngeal cancer but further research is warranted. Sensitivity of FLT imaging, however, is not optimal because DNA synthesis is not as robust as glucose uptake and less tracer is taken up (Buck et al. 2003).

The most studied amino acid tracers are ^{11}C-methionine (MET) and ^{11}C-tyrosine. One advantage of using amino acid tracers over FDG is that they can better discriminate between tumour and inflammatory tissue because inflammatory cells have lower protein metabolism than glucose metabolism (Kubota et al. 1995). Geets et al. (2004) studied the role of MET-PET for the delineation of the tumour volume in pharyngolaryngeal squamous cell carcinoma. In all, 23 patients received CT, FDG-PET and MET-PET before treatment (radiotherapy or surgery). The authors found that the MET volumes did not differ from the CT volumes, while the FDG volumes were significantly smaller than CT. They concluded that MET-PET does not have any additional value since MET volumes are not different from CT volumes, probably because of the high uptake of MET by the normal mucosa and salivary glands surrounding the tumour.

Another indicator of proliferation is an increased level of choline in cells. ^{1}H MR-spectroscopy can be used to estimate choline levels in human tumours. This procedure has already been successfully used to localize active disease sites within the prostate (Kurhanewicz et al. 1996), but data on HNC are missing.

18.4.2.3 Apoptosis

Apoptosis can be a marker for radiosensitivity and prognosis for radiotherapy treatment outcome because apoptosis is a major form of cell death after ionising irradiation. Annexin V binds to membrane-bound phosphatidyl serine and is selectively exposed on the surface of cells as they undergo apoptosis. ^{99m}Tc-radiolabeled annexin V is therefore being tested to measure apoptosis (Green and Steinmetz 2002). Annexin accumulation has been imaged successfully using ^{99m}Tc-SPECT and near infrared fluorescence (NIRF) in several tumoral sites. van de Wiele et al. (2003) performed a quantitative tumour apoptosis imaging using ^{99m}Tc-radiolabeled annexin V and SPECT. A total of 20 patients with HNC underwent CT, ^{99m}Tc-radiolabeled annexin V SPECT and subsequent surgical resection. Quantitative ^{99m}Tc-radiolabeled annexin V tumour uptake values correlated well with the number of apoptotic cells derived from TUNEL assays (detects apoptosis-induced DNA fragmentation), if only tumour samples with no or minimal amounts of necrosis are considered. The authors conclude that radiolabeled annexin V can be used to monitor treatment response, if the treatment does not alter the diffusion-related uptake of the peptides. ^{99m}Tc-radiolabeled annexin V scintigraphy has already been used successfully in monitoring radiation-induced apoptotic cell death in follicular lymphoma patients (Haas et al. 2004). Data on HNC are missing.

18.4.2.4 Receptor Status/Molecular Imaging

Proliferation of certain tumours is regulated by growth factors and hormones that bind to membrane or intracellular receptors to activate signal

transduction pathways. In vivo imaging of the receptor status might provide relevant information concerning prognosis and choice of therapy. One example is epidermal growth factor receptor (EGFr) imaging using SPECT and NIRF optical imaging. EGFr is a transmembrane glycoprotein involved in activating several pathways associated with proliferation, migration, stromal invasion, angiogenesis and resistance to cell death-inducing signals (Dancey 2004). EGFR is overexpressed in nearly all HNC (80%–100%) (Grandis et al. 1996), and this overexpression is associated with both increased metastatic potential and poor prognosis (Ang et al. 2002). Optical contrast agents to visualise EGFr are under development.

18.4.3 Treatment Verification

Treatment guiding and verification refer to the use of imaging to ensure that the field of irradiation is appropriate throughout the entire treatment period, taking into consideration factors such as changes in tumour size and shape, patient positioning and organ movement. Today, the treatment fields are routinely verified using the accelerator beam and conventional film or, in modern systems, using 2D electronic portal image detectors (EPID) as detectors (Fig. 18.3). As with portal films, electronic portal images are compared with some reference image. The latter can be a digitized simulator film or a digitally reconstructed radiograph in case of 3D treatment planning. Recently, cone beam CT has been introduced for verification of treatment fields in 3D view. To create these fields, an extra tube is mounted on the accelerator producing a divergent X-ray beam, which is captured using a portal detector, opposed to the CT tube. Both make a 360° rotation around the patient. This allows a 3D visualisation of the treatment field in relation to organs of interest.

Recently, the next generation in radiation oncology has been developed, called four-dimensional (4D) conformal radiotherapy (CRT), a logical regression from 3D-CRT. During a course of radiotherapy, when successful, tumours shrink. Patients may also lose weight which will further alter their geometry and dosimetry (Barker et al. 2004). 4D CRT accounts for these geometrical changes. In radiotherapy, spatio-temporal instability of target and normal structures, and/or geometric uncertainty of patient positioning are one of the reasons for treatment failure. Especially in sophisticated radiotherapy such as IMRT, devices and methods of increasing precision and accuracy are needed. Latest generation linear accelerators are therefore equipped with CT and/or fluoroscopy modes. A CT-based image guidance system can visualize soft-tissue structures while fluoroscopy can be used to track fiducial markers e.g. during breathing. The recent development of megavoltage cone beam CT (MVCT) will allow the reconstruction of the actual daily-delivered dose based on patient's anatomy in real time (Pouliot et al. 2003; Ghilezan et al. 2004). By acquiring a low-dose megavoltage CT image on the treatment machine immediately prior to therapy, the patient position – including soft tissue anatomy – can in principle be verified on-line. The same imaging device can then be used to record the portal dose during treatment. By converting this portal dose to primary fluence at the plane of the detector and back projecting through the MVCT model of the patient, the 3D dose delivered at the time of treatment can be obtained. This may lead to 'adaptive radiotherapy' with modulation of prescription and delivery based on the actual delivered dose, as opposed to planned dose (Welsh et al. 2002). Further studies are ongoing to optimize MVCT imaging and better define its utility in patients.

18.5 Conclusion and Future Challenges

The use of multimodality imaging, both anatomical and functional, has already led in several cancer centers to improved staging of disease, as well as to improved treatment planning, by better dose delivery to GTV while sparing critical normal structures. The development of imaging markers associated with prediction of radioresistance and/or outcome could impact significantly on treatment planning. Such information could be used in the (near) future to design conformal dose distributions, 'paint' additional dose to specific tumour regions, or rationally describe adjuvant therapy targeted to specific tumour phenotype and genotype.

The ability to predict the ultimate outcome early in treatment would have tremendous implications for patients. Functional imaging could identify nonresponders early, which allows for a switch in therapy.

There still remain some hurdles to be overcome, including imaging pathological validation, timing of post-treatment imaging, and accounting for spatial and temporal tumour motion during radiation therapy.

However, we must keep in mind that no single imaging modality can provide us the entire picture of tumour profiling. Anatomical and functional imaging fusion will be essential. Knowledge about the capabilities and especially limitations of all the imaging modalities remains essential in their clinical use.

References

Adams S, Baum RP, Stuckensen T, et al. (1998) Prospective comparison of ^{18}F-FDG PET with conventional imaging modalities (CT, MRI, US) in lymph node staging of head and neck cancer. Eur J Nucl Med 25:1255–1260

Ang KK, Berkey BA, Tu X, et al. (2002) Impact of epidermal growth factor receptor expression on survival and pattern of relapse in patients with advanced head and neck carcinoma. Cancer Res 62:7350–7356

Barker JL Jr, Garden AS, Ang KK,, et al. (2004) Quantification of volumetric and geometric changes occurring during fractionated radiotherapy for head-and-neck cancer using an integrated CT/linear accelerator system. Int J Radiat Oncol Biol Phys 59:960–970

Benchaou M, Lehmann W, Slosman DO, et al. (1996) The role of FDG-PET in the preoperative assessment of N-staging in head and neck cancer. Acta Otolaryngol 116:332–335

Brink I, Kleznr T, Krause T, et al. (2002) Lymph node staging in extracranial head and neck cancer with FDG PET-appropriate uptake period and size-dependence of the results. Nuklearmedizin 41:108–113

Buck AK, Halter G, Schirrmeister H, et al. (2003) Imaging proliferation in lung tumors with PET: ^{18}F-FLT versus ^{18}F-FDG. J Nucl Med 44:1426–1431

Chao C, Bosch WR, Mutic S, et al. (2001) A novel approach to overcome hypoxic tumor resistance: Cu-ATSM-guided intensity-modulated radiation therapy. Int J Radiat Oncol Biol Phys 49:1171–1182

Chao C, Wippold FJ, Ozyigit G, et al. (2002) Determination and delineation of nodal target volumes for head-and-neck cancer based on patterns of failure in patients receiving definitive and postoperative IMRT. Int J Radiat Oncol Biol Phys 53:1174–1184

Chaplin DJ, Durand RE, Olive PL (1986) Acute hypoxia in tumors: implications for modifiers of radiation effects. Int J Radiat Oncol Biol Phys 12:1279–82

Chapman JD, Baer K, Lee J (1983) Characteristics of the metabolism-induced binding of misonidazole to hypoxic mammalian cells. Cancer Res 43:1523–1528

Chapman JD, Bradley JD, Eary JF, et al. (2003) Molecular (functional) imaging for radiotherapy applications: an RTOG symposium. Int J Radiat Oncol Biol Phys 55:294–301

Chung N, Ting L, Hsu W, et al. (2004) Impact of magnetic resonance imaging versus CT on nasopharyngeal carcinoma: primary tumor target delineation for radiotherapy. Head Neck 26:241–246

Ciernik FI, Dizendorf E, Baumert B, et al. (2003) Radiation treatment planning with an integrated positron emission and computer tomography (PET/CT):a feasibility study. Int J Radiat Oncol Biol Phys 57:853–863

Cobben DCP, van der Laan BFAM, Maas B, et al. (2004) ^{18}F-FLT PET for visualization of laryngeal cancer: comparison with ^{18}F-FDG PET. J Nuclear Med 45:226–231

Daisne JF, Sibomana M, Bol A, et al. (2003) Evaluation of a multimodality image (CT, MRI and PET) coregistration procedure on phantom and head and neck cancer patients: accuracy, reproducibility and consistency. Radiother Oncol 69:237–245

Daisne JF, Duprez T, Weynant B, et al. (2004) Tumor volume in pharyngolaryngeal squamous cell carcinoma: comparison at CT, MR imaging, and FDG PET and validation with surgical specimen. Radiology 233:93–100

Dancey J (2004) Epidermal growth factor receptor inhibitors in clinical development. Int J Radiat Oncol Biol Phys 58:1003–1007

Eisbruch A, Foote RL, O'Sullivan B, et al. (2002) Intensity-modulated radiation therapy for head and neck cancer: emphasis on the selection and delineation of the targets. Sem Radiat Oncol 12:238–249

Enami B, Sethi A, Petruzelli GJ (2003) Influence of MRI on target volume delineation and IMRT planning in nasopharyngeal carcinoma. Int J Radiat Oncol Biol Phys 57:481–488

Eschmann S, Paulsen F, Reimold M, et al. (2005) Prognostic impact of hypoxia imaging with ^{18}F-misonidazole PET in non small lung cancer and head and neck cancer before radiotherapy. J Nucl Med 46: 253–260

Geets X, Daisne JF, Gregoire V, et al. (2004) Role of 11-C-methionine positron emission tomography for the delineation of the tumor volume in pharyngo-laryngeal squamous cell carcinoma: comparison with FDG-PET and CT. Radiother Oncol 71:267–273

Gambhir SS, Czernin J, Schwimmer J, et al. (2001) A tabulated summary of the FDG PET literature. J Nucl Med 42:1S–93S

Ghilezan M, Yan D, Liang J, et al. (2004) Online image-guided intensity-modulated radiotherapy for prostate cancer: How much improvement can we expect? A theoretical assessment of clinical benefits and potential dose escalation by improving precision and accuracy of radiation delivery. Int J Radiat Oncol Biol Phys 60:1602–1610

Grandis JR, Melhem MF, Barnes El, et al. (1996) Quantitative immunohistochemical analysis of transforming growth factor-alpha and epidermal growth factor receptor in patients with squamous cell carcinoma of the head and neck. Cancer 78:1284–1292

Green AM, Steinmetz ND (2002) Monitoring apoptosis in real time. Cancer J 8:82–92

Gregoire V, Levendag P, Ang KK, et al. (2003) CT-based delineation of lymph node levels and related CTVs in the node-negative neck: DAHANCA, EORTC, GORTEC, NCIC, RTOG consensus guidelines. Radiother Oncol 69:227–236

Haas RLM, De Jong D, Valdes Olmos R, et al. (2004) In vivo imaging of radiation-induced apoptosis in follicular lymphoma patients. Int J Radiat Oncol Biol Phys 59:782–787

Hermans R, Feron M, Bellon E, et al. (1998) Laryngeal tumor volume measurements determined with CT: a study on intra- and interobserver variability. Int J Radiat Oncol Biol Phys 40:553–557

Hermans R, Meijerink M, Van den Bogaert W, et al. (2003) Tumor perfusion rate determined noninvasively by dynamic computed tomography predicts outcome in head-and-neck cancer after radiotherapy. Int J Radiat Oncol Biol Phys 57:1351–1356

Hoskin PJ, Saunders MI, Goodchild K, et al. (1999) Dynamic contrast enhanced magnetic resonance scanning as a predictor of response to accelerated radiotherapy for advanced head and neck cancer. Br J Radiol 72:1093–1098

Kaanders JHAM, Pop LA, Marres HAM, et al. (2002) ARCON: experience in 215 patients with advanced head-and-neck cancer. Int J Radiat Oncol Biol Phys 52:769–778

Koh WJ, Rasey JS, Evans ML, et al. (1992) Imaging of hypoxia in human tumors with [F-18] fluoromisonidazole. Int J Radiat Oncol Biol Phys 22:1299–212

Koshy M, Paulino AC, Howell R, et al. (2005) F-18 FDG PET-CT fusion in radiotherapy treatment planning for head and neck cancer. Head Neck 27:494–502 (epub ahead of print)

Krishnan L, Krishnan EC, Jewell WR (1988) Immediate effect of irradiation on microvasculature. Int J Radiat Oncol Biol Phys 15:147–50

Kubota R, Kubota K, Yamada S, et al. (1995) Methionine uptake by tumor tissue: a microautoradiographic comparison with FDG. J Nucl Med 36:484–492

Kurhanewicz J, Vigneron DB, Hricak H, et al. (1996) Three-dimensional H-1 MR spectroscopic imaging of the in situ human prostate with high (0.24-0.7-cm^3) spatial resolution. Radiology 198:795–805

Landuyt W, Hermans R, Bosmans H, et al. (2001) BOLD contrast fMRI of whole rodent tumour during air or carbogen breathing using echo-planar imaging at 1.5T. Eur Radiol 11:2332–2340

Laudenbacher C, Saumweber D, Wagner-Manslau C, et al. (1995) Comparison of fluorine-18-deoxyglucose PET, MRI and endoscopy for staging head and neck squamous-cell carcinomas. J Nucl Med 36:1747–1757

Lehtio K, Oikonen V, Gronroos T, et al. (2001) Imaging of blood flow and hypoxia in head and neck cancer: initial evaluation with $^{15}OH_2O$ and ^{18}F fluoroerythonitroimidazole PET. J Nucl Med 42:1643–1652

Lehtio K, Eskola O, Viljanen T, et al. (2004) Imaging perfusion and hypoxia with PET to predict radiotherapy response in head-and-neck cancer. Int J Radiat Oncol Biol Phys 59:971–982

Ling CC, Humn J, Larson S, et al. (2000) Towards multidimensional radiotherapy (MD-CRT): biological imaging and biological conformality. Int J Radiat Oncol Biol Phys 47:551–560

Nishioka T, Shiga T, Shirato H, et al. (2002) Image fusion between ^{18}FDG-PET and MRI/CT for radiotherapy planning of oropharyngeal and nasopharyngeal carcinomas. Int J Radiat Oncol Biol Phys 53:1051–1057

Nordsmark M, Overgaard J (2004) Tumor hypoxia is independent of hemoglobin and prognostic for loco-regional tumor control after primary radiotherapy in advanced head and neck cancer. Acta Oncol 43:396–403

Paulino AC, Koshy M, Howell R, et al. (2005) Comparison of CT- and FDG-PET-defined gross tumor volume in intensity-modulated radiotherapy for head-and-neck cancer. Int J Radiat Oncol Biol Phys 61:1385–1392

Pouliot J, Xia P, Langen K, et al. (2003) Dose-guided radiation therapy using low-dose megavoltage con-beam CT. In 44th Annual AAPM Annual Meeting. San Diego, CA. Med Phys

Rasey JS, Koh WJ, Evans ML, et al. (1996) Quantifying regional hypoxia in human tumors with positron emission tomography of ^{18}F fluoromisonidazole: a pretherapy study of 37 patients. Int J Radiat Oncol Biol Phys 36:417–428

Rasey JS, Hofstrand PD, Chin LK, et al. (1999) Characterization of ^{18}F fluoroetanidazole, a new radiopharmaceutical for detecting tumor hypoxia. J Nucl Med 40:1072–1079

Rash C, Keus R, Pameijer FA, et al. (1997) The potential impact of CT-MRI matching on tumor volume delineation in advanced head and neck cancer. Int J Radiat Oncol Biol Phys 39:841–848

Rijpkema M, Kaanders JHAM, Joosten FBM, et al. (2002) Effects of breathing a hyperoxic hypercapnic gas mixture on blood oxygenation and vascularity of head-and-neck tumors as measured by magnetic resonance imaging. Int J Radiat Oncol Biol Phys 53:1185–1191

Scarfone C, Lavely WC, Cmelak AJ, et al. (2004) Prospective feasibility trial of radiotherapy target definition for head and neck cancer using 3-dimensional PET and CT imaging. J Nucl Med 45:543–552

Schmitt P, Kotas M, Tobermann A, et al. (2003) Quantitative tissue perfusion measurements in head and neck carcinoma patients before and during radiation therapy with a non-invasive MR imaging spin-labeling technique. Radiother Oncol 67:27–34

Schwartz DL, Ford EC, Rajendran J, et al. (2005) FDG-PET/CT imaging for preradiotherapy staging of head-and-neck squamous cell carcinoma. Int J Radiat Oncol Biol Phys 61:129–136

Shields AF, Grierson JR, Dohmen BM, et al. (1998) Imaging proliferation in vivo with ^{18}F FLT and positron emission tomography. Nat Med 4:1334–1336

Stoeckli SJ, Steinert H, Pfaltz M, et al. (2002) Is there a role for positron emission tomography with ^{18}F-fluorodeoxyglucose in the initial staging of nodal negative oral and oropharyngeal squamous cell carcinoma? Head Neck 24:345–349

Syed R, Bomanji JB, Nagabhushan N, et al. (2005) Impact of combined ^{18}F-FDG PET/CT in head and neck tumours. Br J Cancer 92:1046–1050

Taylor NJ, Baddeley H, Goodchild KA, et al. (2001) BOLD MRI of human tumor oxygenation during carbogen breathing. J Magn Reson Imaging 14:156–163

Van de Wiele C, Lahorte C, Vermeersch H, et al. (2003) Quantitative tumor apoptosis imaging using Technetium-99m-HYNIC Annexin V single photon emission computed tomography. J Clin Oncol 21:3483–3487

Welsh JS, Patel RR, Ritter MA, et al. (2002) Helical tomotherapy: an innovative technology and approach to radiation therapy. Technol Cancer Res Treat 1:311–316

Yang DJ, Wallace S, Cherif A, et al. (1995) Development of F-18-labeled fluoroerythonitroimidazole as a PET agent for imaging tumor hypoxia. Radiology 194:795–800

Ziemer LS, Evans SM, Kachur AV, et al. (2003) Noninvasive imaging of tumor hypoxia in rats using 2-nitroimidazole ^{18}F-EF5. Eur J Nucl Med Mol Imaging 30:259–266

Subject Index

List of Contributors

Cathérine Castaigne, MD
Nuclear Medicine Bordet
Positron Emission Tomography IRIS
Institut Jules Bordet
121, Boulevard de Waterloo
1000 Brussels
Belgium

Jonas A. Castelijns, MD, PhD
Professor, VU University Medical Center
Department of Radiology
De Boelelaan 1117
1081 HV Amsterdam
The Netherlands

Vincent F. H. Chong, MD, MBA
Department of Diagnostic Radiology
National University Hospital
Yong Loo Lin School of Medicine
5 Lower Kent Ridge Road
Singapore 119074
Singapore

Emmanuel E. Coche, MD
Department of Radiology
and Medical Imaging
Université Catholique de Louvain
Cliniques Universitaires Saint-Luc
Avenue Hippocrate, 10
1200 Brussels
Belgium

Frederik De Keyzer, MSc
Department of Radiology
University Hospitals Leuven
Herestraat 49
3000 Leuven
Belgium

Pierre Delaere, MD, PhD
Professor, Department of Otorhinolaryngology,
Head and Neck Surgery
University Hospitals Leuven
Herestraat 49
3000 Leuven
Belgium

Frédérique Dubrulle, MD
Plateau Technique d'Imagerie
Hôpital Huriez Sud, CHU Lille
59000 Lille
France

Thierry P. Duprez, MD
Department of Radiology and Medical Imaging
Université Catholique de Louvain
Cliniques Universitaires Saint-Luc
Avenue Hippocrate, 10
1200 Brussels
Belgium

Davide Farina, MD
Department of Radiology
University of Brescia
Piazzale Spedali Civili 1
25123 Brescia, BS
Italy

Patrick Flamen, MD, PhD
Nuclear Medicine Bordet
Positron Emission Tomography IRIS
Institut Jules Bordet
121, Boulevard de Waterloo
1000 Brussels
Belgium

Rick L. M. Haas, MD
Department of Radiotherapy
The Netherlands Cancer Institute
Antoni van Leeuwenhoek Hospital
Plesmanlaan 121
1066 CX Amsterdam
The Netherlands

Robert Hermans, MD, PhD
Professor, Department of Radiology
University Hospitals Leuven
Herestraat 49
3000 Leuven
Belgium

Marc Keberle, MD
Diagnostic Radiology
Medizinische Hochschule Hannover
Carl-Neuberg-Straße 1
30625 Hannover
Germany

Kristoff Muylle, MD
Nuclear Medicine Bordet
Positron Emission Tomography IRIS
Institut Jules Bordet
121, Boulevard de Waterloo
1000 Brussels
Belgium

Sandra Nuyts, MD, PhD
Professor, Department of Radiation Oncology
University Hospitals Gasthuisberg
Herestraat 49
3000 Leuven
Belgium

Frank A. Pameijer, MD, PhD
Department of Radiology
The Netherlands Cancer Institute
Antoni van Leeuwenhoek Hospital
Plesmanlaan 121
1066 CX Amsterdam
The Netherlands

and

Department of Radiology
University Medical Center Utrecht
Heidelberglaan 100
3584 CX Utrecht
The Netherlands

Soraya Robinson, MD
Department of Radiology
Helsinki University Central Hospital
Haartmaninkatu 4
POB 340
00029 HUS Helsinki
Finland

Ilona M. Schmalfuss, MD
Department of Radiology
Malcolm Randall VA Medical Center and
University of Florida College of Medicine
1601 SW Archer Road
Gainesville, FL 32608
USA

Raphaëlle Souillard, MD
Plateau Technique d'Imagerie
Hôpital Huriez Sud, CHU Lille
59000 Lille
France

M.W.M. van den Brekel, MD, PhD
Department of Otolaryngology –
Head & Neck Surgery
The Netherlands Cancer Institute
Antoni van Leeuwenhoek Hospital
Plesmanlaan 121
1066 CX Amsterdam
The Netherlands

Vincent Vandecaveye, MD
Department of Radiology
University Hospitals Leuven
Herestraat 49
3000 Leuven
Belgium

Vincent Vander Poorten, MD, MSc, PhD
Professor, Department of Otorhinolaryngology,
Head and Neck Surgery
University Hospitals Leuven
Herestraat 49
3000 Leuven
Belgium

Medical Radiology Diagnostic Imaging and Radiation Oncology

Titles in the series already published

Diagnostic Imaging

Innovations in Diagnostic Imaging
Edited by J. H. Anderson

Radiology of the Upper Urinary Tract
Edited by E. K. Lang

The Thymus - Diagnostic Imaging, Functions, and Pathologic Anatomy
Edited by E. Walter, E. Willich, and W. R. Webb

Interventional Neuroradiology
Edited by A. Valavanis

Radiology of the Pancreas
Edited by A. L. Baert, co-edited by G. Delorme

Radiology of the Lower Urinary Tract
Edited by E. K. Lang

Magnetic Resonance Angiography
Edited by I. P. Arlart, G. M. Bongartz, and G. Marchal

Contrast-Enhanced MRI of the Breast
S. Heywang-Köbrunner and R. Beck

Spiral CT of the Chest
Edited by M. Rémy-Jardin and J. Rémy

Radiological Diagnosis of Breast Diseases
Edited by M. Friedrich and E.A. Sickles

Radiology of the Trauma
Edited by M. Heller and A. Fink

Biliary Tract Radiology
Edited by P. Rossi, co-edited by M. Brezi

Radiological Imaging of Sports Injuries
Edited by C. Masciocchi

Modern Imaging of the Alimentary Tube
Edited by A. R. Margulis

Diagnosis and Therapy of Spinal Tumors
Edited by P. R. Algra, J. Valk, and J. J. Heimans

Interventional Magnetic Resonance Imaging
Edited by J.F. Debatin and G. Adam

Abdominal and Pelvic MRI
Edited by A. Heuck and M. Reiser

Orthopedic Imaging
Techniques and Applications
Edited by A. M. Davies and H. Pettersson

Radiology of the Female Pelvic Organs
Edited by E. K.Lang

Magnetic Resonance of the Heart and Great Vessels
Clinical Applications
Edited by J. Bogaert, A.J. Duerinckx, and F. E. Rademakers

Modern Head and Neck Imaging
Edited by S. K. Mukherji and J. A. Castelijns

Radiological Imaging of Endocrine Diseases
Edited by J. N. Bruneton in collaboration with B. Padovani and M.-Y. Mourou

Trends in Contrast Media
Edited by H. S. Thomsen, R. N. Muller, and R. F. Mattrey

Functional MRI
Edited by C. T. W. Moonen and P. A. Bandettini

Radiology of the Pancreas
2nd Revised Edition
Edited by A. L. Baert. Co-edited by G. Delorme and L. Van Hoe

Emergency Pediatric Radiology
Edited by H. Carty

Spiral CT of the Abdomen
Edited by F. Terrier, M. Grossholz, and C. D. Becker

Liver Malignancies
Diagnostic and Interventional Radiology
Edited by C. Bartolozzi and R. Lencioni

Medical Imaging of the Spleen
Edited by A. M. De Schepper and F. Vanhoenacker

Radiology of Peripheral Vascular Diseases
Edited by E. Zeitler

Diagnostic Nuclear Medicine
Edited by C. Schiepers

Radiology of Blunt Trauma of the Chest
P. Schnyder and M. Wintermark

Portal Hypertension
Diagnostic Imaging-Guided Therapy
Edited by P. Rossi
Co-edited by P. Ricci and L. Broglia

Recent Advances in Diagnostic Neuroradiology
Edited by Ph. Demaerel

Virtual Endoscopy and Related 3D Techniques
Edited by P. Rogalla, J. Terwisscha Van Scheltinga, and B. Hamm

Multislice CT
Edited by M. F. Reiser, M. Takahashi, M. Modic, and R. Bruening

Pediatric Uroradiology
Edited by R. Fotter

Transfontanellar Doppler Imaging in Neonates
A. Couture and C. Veyrac

Radiology of AIDS
A Practical Approach
Edited by J.W.A.J. Reeders and P.C. Goodman

CT of the Peritoneum
Armando Rossi and Giorgio Rossi

Magnetic Resonance Angiography
2nd Revised Edition
Edited by I. P. Arlart, G. M. Bongratz, and G. Marchal

Pediatric Chest Imaging
Edited by Javier Lucaya and Janet L. Strife

Applications of Sonography in Head and Neck Pathology
Edited by J. N. Bruneton in collaboration with C. Raffaelli and O. Dassonville

Imaging of the Larynx
Edited by R. Hermans

3D Image Processing
Techniques and Clinical Applications
Edited by D. Caramella and C. Bartolozzi

Imaging of Orbital and Visual Pathway Pathology
Edited by W. S. Müller-Forell

Pediatric ENT Radiology
Edited by S. J. King and A. E. Boothroyd

Radiological Imaging of the Small Intestine
Edited by N. C. Gourtsoyiannis

Medical Radiology Diagnostic Imaging and Radiation Oncology

Titles in the series already published

Imaging of the Knee
Techniques and Applications
Edited by A. M. Davies
and V. N. Cassar-Pullicino

Perinatal Imaging
From Ultrasound to MR Imaging
Edited by Fred E. Avni

Radiological Imaging of the Neonatal Chest
Edited by V. Donoghue

Diagnostic and Interventional Radiology in Liver Transplantation
Edited by E. Bücheler, V. Nicolas,
C. E. Broelsch, X. Rogiers,
and G. Krupski

Radiology of Osteoporosis
Edited by S. Grampp

Imaging Pelvic Floor Disorders
Edited by C. I. Bartram
and J. O. L. DeLancey
Associate Editors: S. Halligan,
F. M. Kelvin, and J. Stoker

Imaging of the Pancreas
Cystic and Rare Tumors
Edited by C. Procacci
and A. J. Megibow

High Resolution Sonography of the Peripheral Nervous System
Edited by S. Peer and G. Bodner

Imaging of the Foot and Ankle
Techniques and Applications
Edited by A. M. Davies,
R. W. Whitehouse,
and J. P. R. Jenkins

Radiology Imaging of the Ureter
Edited by F. Joffre, Ph. Otal,
and M. Soulie

Imaging of the Shoulder
Techniques and Applications
Edited by A. M. Davies and J. Hodler

Radiology of the Petrous Bone
Edited by M. Lemmerling
and S. S. Kollias

Interventional Radiology in Cancer
Edited by A. Adam, R. F. Dondelinger,
and P. R. Mueller

Duplex and Color Doppler Imaging of the Venous System
Edited by G. H. Mostbeck

Multidetector-Row CT of the Thorax
Edited by U. J. Schoepf

Functional Imaging of the Chest
Edited by H.-U. Kauczor

Radiology of the Pharynx and the Esophagus
Edited by O. Ekberg

Radiological Imaging in Hematological Malignancies
Edited by A. Guermazi

Imaging and Intervention in Abdominal Trauma
Edited by R. F. Dondelinger

Multislice CT
2nd Revised Edition
Edited by M. F. Reiser, M. Takahashi,
M. Modic, and C. R. Becker

Intracranial Vascular Malformations and Aneurysms
From Diagnostic Work-Up to Endovascular Therapy
Edited by M. Forsting

Radiology and Imaging of the Colon
Edited by A. H. Chapman

Coronary Radiology
Edited by M. Oudkerk

Dynamic Contrast-Enhanced Magnetic Resonance Imaging in Oncology
Edited by A. Jackson, D. L. Buckley,
and G. J. M. Parker

Imaging in Treatment Planning for Sinonasal Diseases
Edited by R. Maroldi and P. Nicolai

Clinical Cardiac MRI
With Interactive CD-ROM
Edited by J. Bogaert,
S. Dymarkowski, and A. M. Taylor

Focal Liver Lesions
Detection, Characterization, Ablation
Edited by R. Lencioni, D. Cioni,
and C. Bartolozzi

Multidetector-Row CT Angiography
Edited by C. Catalano
and R. Passariello

Paediatric Musculoskeletal Diseases
With an Emphasis on Ultrasound
Edited by D. Wilson

Contrast Media in Ultrasonography
Basic Principles and Clinical Applications
Edited by Emilio Quaia

MR Imaging in White Matter Diseases of the Brain and Spinal Cord
Edited by M. Filippi, N. De Stefano,
V. Dousset, and J. C. McGowan

Diagnostic Nuclear Medicine
2nd Revised Edition
Edited by C. Schiepers

Imaging of the Kidney Cancer
Edited by A. Guermazi

Magnetic Resonance Imaging in Ischemic Stroke
Edited by R. von Kummer and T. Back

Imaging of the Hip & Bony Pelvis
Techniques and Applications
Edited by A. M. Davies, K. J. Johnson,
and R. W. Whitehouse

Imaging of Occupational and Environmental Disorders of the Chest
Edited by P. A. Gevenois and
P. De Vuyst

Contrast Media
Safety Issues and ESUR Guidelines
Edited by H. S. Thomsen

Virtual Colonoscopy
A Practical Guide
Edited by P. Lefere and S. Gryspeerdt

Vascular Embolotherapy
A Comprehensive Approach
Volume 1
Edited by J. Golzarian. Co-edited by
S. Sun and M. J. Sharafuddin

Vascular Embolotherapy
A Comprehensive Approach
Volume 2
Edited by J. Golzarian. Co-edited by
S. Sun and M. J. Sharafuddin

Head and Neck Cancer Imaging
Edited by R. Hermans

Vascular Interventional Radiology
Current Evidence in Endovascular Surgery
Edited by M. G. Cowling

Springer

Medical Radiology Diagnostic Imaging and Radiation Oncology

Titles in the series already published

Radiation Oncology

Lung Cancer
Edited by C.W. Scarantino

Innovations in Radiation Oncology
Edited by H. R. Withers
and L. J. Peters

Radiation Therapy
of Head and Neck Cancer
Edited by G. E. Laramore

Gastrointestinal Cancer –
Radiation Therapy
Edited by R.R. Dobelbower, Jr.

Radiation Exposure
and Occupational Risks
Edited by E. Scherer, C. Streffer,
and K.-R. Trott

Radiation Therapy of Benign Diseases
A Clinical Guide
S. E. Order and S. S. Donaldson

Interventional Radiation
Therapy Techniques – Brachytherapy
Edited by R. Sauer

Radiopathology of Organs and Tissues
Edited by E. Scherer, C. Streffer,
and K.-R. Trott

Concomitant Continuous Infusion
Chemotherapy and Radiation
Edited by M. Rotman
and C. J. Rosenthal

Intraoperative Radiotherapy –
Clinical Experiences and Results
Edited by F. A. Calvo, M. Santos,
and L.W. Brady

Radiotherapy of Intraocular
and Orbital Tumors
Edited by W. E. Alberti and
R. H. Sagerman

Interstitial and Intracavitary
Thermoradiotherapy
Edited by M. H. Seegenschmiedt
and R. Sauer

Non-Disseminated Breast Cancer
Controversial Issues in Management
Edited by G. H. Fletcher and
S.H. Levitt

Current Topics in
Clinical Radiobiology of Tumors
Edited by H.-P. Beck-Bornholdt

Practical Approaches to
Cancer Invasion and Metastases
A Compendium of Radiation
Oncologists' Responses to 40 Histories
Edited by A. R. Kagan with the
Assistance of R. J. Steckel

Radiation Therapy in Pediatric Oncology
Edited by J. R. Cassady

Radiation Therapy Physics
Edited by A. R. Smith

Late Sequelae in Oncology
Edited by J. Dunst and R. Sauer

Mediastinal Tumors. Update 1995
Edited by D. E. Wood
and C. R. Thomas, Jr.

Thermoradiotherapy
and Thermochemotherapy
Volume 1:
Biology, Physiology, and Physics
Volume 2:
Clinical Applications
Edited by M.H. Seegenschmiedt,
P. Fessenden, and C.C. Vernon

Carcinoma of the Prostate
Innovations in Management
Edited by Z. Petrovich, L. Baert,
and L.W. Brady

Radiation Oncology
of Gynecological Cancers
Edited by H.W. Vahrson

Carcinoma of the Bladder
Innovations in Management
Edited by Z. Petrovich, L. Baert,
and L.W. Brady

Blood Perfusion and
Microenvironment of Human Tumors
Implications for
Clinical Radiooncology
Edited by M. Molls and P. Vaupel

Radiation Therapy of Benign Diseases
A Clinical Guide
2nd Revised Edition
S. E. Order and S. S. Donaldson

Carcinoma of the Kidney and Testis,
and Rare Urologic Malignancies
Innovations in Management
Edited by Z. Petrovich, L. Baert,
and L.W. Brady

Progress and Perspectives in the
Treatment of Lung Cancer
Edited by P. Van Houtte,
J. Klastersky, and P. Rocmans

Combined Modality Therapy of
Central Nervous System Tumors
Edited by Z. Petrovich, L. W. Brady,
M. L. Apuzzo, and M. Bamberg

Age-Related Macular Degeneration
Current Treatment Concepts
Edited by W. A. Alberti, G. Richard,
and R. H. Sagerman

Radiotherapy of Intraocular
and Orbital Tumors
2nd Revised Edition
Edited by R. H. Sagerman,
and W. E. Alberti

Modification of Radiation Response
Cytokines, Growth Factors,
and Other Biolgical Targets
Edited by C. Nieder, L. Milas,
and K. K. Ang

Radiation Oncology for Cure and Palliation
R. G. Parker, N. A. Janjan,
and M. T. Selch

Clinical Target Volumes in Conformal and
Intensity Modulated Radiation Therapy
A Clinical Guide to Cancer Treatment
Edited by V. Grégoire, P. Scalliet,
and K. K. Ang

Advances in Radiation Oncology
in Lung Cancer
Edited by Branislav Jeremić

New Technologies in Radiation Oncology
Edited by W. Schlegel, T. Bortfeld,
and A.-L. Grosu

Springer